WITS
UNIVERSITY

The synthesis of aryl benzamides as potential HIV-1 non-nucleoside reverse transcriptase inhibitors (NNRTIs).

LIKHOPOTSO C MOHASOA

Supervised by: Prof M.L. Bode

Co-supervised by: Dr. M. Zimuwandeyi

A dissertation submitted to the Faculty of Science, University of the Witwatersrand, Johannesburg, in fulfilment of the requirements for the degree of Master of Science

Submitted 03 July 2023

DECLARATION

I Likhopotso C Mohasoa, hereby declare that this dissertation is my own work which was conducted in the School of Chemistry. It is submitted to the University of the Witwatersrand in Johannesburg for consideration of the Master of Science degree. It has never been submitted to any other university for the purpose of a degree or examination.

……..

Signature

03 July 2023

Abstract

Dihydro-alkoxybenzyloxopyrimidines are heteroaryl-containing compounds that have previously been shown to exhibit excellent activity against HIV-1 reverse transcriptase (RT) enzyme. In our own laboratory, 2-chloro-*N*-(6-(piperidin-1-yl)pyridin-2-yl)benzamide was identified as a compound with activity against wild-type HIV-1. Using these two structural types as a guide, as part of our ongoing studies to search for anti-HIV therapeutic agents that target the RT enzyme, a library of arylbenzamide compounds bearing a pyrimidine ring as a central core was synthesized. These compounds contained an oxygen linker to allow flexible rotation of the molecule in the RT active site, with the aim of achieving activity against wild-type and mutant HIV-1.

As a starting point, in order to first identify a suitable synthetic method and then apply it for our target novel compounds, four different carboxylic acids and two classes of amines were tested. Amidation reactions were carried out on unsubstituted benzoic acid, 3-methoxybenzoic acid, 3-hydroxybenzoic acid, and 3-((2,6-dichloropyrimidin-4-yl)oxy)benzoic acid. In this last case, the 3-hydroxybenzoic acid moiety had already been linked to the pyrimidinyl core in order to test which order of reaction worked best: linking followed by amidation, or the reverse. Reaction of these benzoic acid derivatives with anilines and aminopyridines gave the resulting benzamides in 22-99% yields after optimization. When triethylamine was used as a base in amidation reactions involving 2-amino-3-bromopyridine, 2-amino-5-bromopyridine and 2-amino-5-methylpyridine, diacylation was favoured, while when pyridine was used, monoacylation predominated.

The reactions to link benzoic acid derivatives to the pyrimidinyl core were carried out by displacement of chlorine on 2,4,5-trichloropyrimidine. The displacement of the first chloride was tested using three types of nucleophiles. The first nucleophile was methyl 3-hydroxybenzoate, effectively a protected benzoic acid, which afforded methyl 3-((2,6-dichloropyrimidin-4-yl)oxy)benzoate in 81% yield. Problems with subsequent hydrolysis of the ester made this route impractical. The second nucleophile was 3-hydroxybenzoic acid which provided 3-((2,6-dichloropyrimidin-4-yl)oxy)benzoic acid in 81% yield. The third nucleophile was *N*-(5-bromopyridin-2-yl)-3-hydroxybenzamide, where amidation had already been performed, which transformed into the desired compound *N*-(5-bromopyridin-2-yl)-3-((2,6-dichloropyrimidin-4-yl)oxy)benzamide in 28%. The low yield obtained from reaction of the amidated nucleophile identified the most promising route to be linking of 3-hydroxybenzoic acid to 2,4,5-trichloropyrimidine first, followed by amidation.

After the successful displacement of the first chlorine atom, two of the resulting analogues 3-((2,6-dichloropyrimidin-4-yl)oxy)-*N*-(p-tolyl)benzamide and *N*-(4-bromophenyl)-3-((2,6-dichloropyrimidin-4-yl)oxy)benzamide were functionalized with sulfur and nitrogen nucleophiles by displacement of a

second chlorine atom. Ethanethiol proved to be highly nucleophilic, leading to pyrimidine C-O bond cleavage and sulfur disubstitution, while the nitrogen nucleophiles propylamine and piperidine afforded their corresponding derivatives in good yields without breaking the carbon-oxygen bond. The newly coupled propyl compound was further derivatized by means of hydrolysis with sodium hydroxide to yield the desired novel 3-((6-hydroxy-2-(propylamino)pyrimidin-4-yl)oxy)-*N*-(p-tolyl)benzamide or 3-((6-oxo-2-(propylamino)-1,6-dihydropyrimidin-4-yl)oxy)-N-(p-tolyl)benzamide compound.

DEDICATION

This dissertation is dedicated to my late mother Manthomeng Mahao and my beloved family who unceasingly encouraged and supported me throughout the course of this study.

ACKNOWLEDGEMENTS

To my father Steve Mohasoa, for not only providing me with the tools I need to succeed, but also for instilling in me the desire to do so. I have been able to get to where I am now because of your support and love. I love you daddy.

My sincere gratitude goes to my supervisors, **Prof. Moira L. Bode** and **Dr Memory Zimuwandeyi** accepting me as master student, for their endless support of my MSc study and research, and for their immerse knowledge, patience, motivation, and enthusiasm. Your guidance groomed me throughout the course of this project and writing of this dissertation. I thank you for reading my dissertation and providing me with your insightful comments. I could not have imagined having wonderful supervisors for my MSc study.

Thank you Dr. Kotze and Dr. Zimuwandeyi for your help in the NMR lab. Your assistance is highly appreciated. My appreciation also goes to Dr. Morifi, Thapelo, and Refilwe for the mass spec training and analyses of results. My great thanks go to Prof. Manuel for conducting crystallographic analyses for me. To Dr. Changunda who did the previous work on benzamides and pyrimidines, thank you. A big thanks to the entire organic chemistry group, you gave me a warm welcome on my first day of the MSc enrolment. I thank every one of you for the input and valuable information that I needed. Thank you Lebogang Tefu, Kabelo Zimba, Bianca Davis, Khanya Jaqeni, Nafisa, Edward, Dr. Thabo Peme, and Sandile Mkhize. I really enjoyed every single moment in the lab with your presence. Kabelo Dilebo and Aneesa Ghani, I thank you for your emotional and research support. Bongi and Tshegofatso Maboye, thank you for the funny jokes and laughter. Thank you Khonzisizwe Somnadi for sharing ideas with me. Thank you Nompumelelo Mathebula for being a good sister and a good colleague, I thank you for your willingness to help at all times. Thank you Kamegelo Butsi, the first person to help me with the NMR peak assignments.

Above all, I would like to thank God, the Creator for that He never left nor forsaken me. No weapon formed against me prospered for the greater you are in me. Many thanks to my lovely sister Mamafa Mohasoa for her love, support, guidance, and motivation. To my parents' first born Nthomeng Mohasoa, you are appreciated for your love. To mama Phikiwe Nhlapo, thanks for your love and kindness to get me a medical assistance, and for a warm welcome in your family. I appreciate and love you. Lastly, my appreciation goes to NRF and Wits University for the financial support. To Mr Kalumba Simba for the ADU opportunity to share my chemistry knowledge with the first-year engineering students. Lastly, I would like to thank Wits University for giving me the opportunity to enrol as a master student.

Table of Contents

Abstract 3
LIST OF ABBREVIATIONS AND ACRONYMS 11
CHAPTER 1: INTRODUCTION AND BACKGROUND 14
1.1 HIV-AIDS 14
1.1.1 Global HIV prevalence 14
1.1.2 HIV lifecycle 15
1.1.3 Social and health effects of HIV/AIDS 16
1.1.4 Access, treatment, and care for people living with HIV 17
1.1.5 Newer tools for HIV/AIDS prevention and control 19
1.1.5.1 Provision of prophylactic agents 19
1.1.5.2 Implementation and monitoring of programs 19
1.1.6 HIV-1 reverse transcriptase inhibitors in the treatment of HIV 21
1.1.6.1 NRTIs mechanism of action 22
1.1.6.2 NNRTIs mechanism of action 23
1.1.6.3 Drug resistance to NNRTIs 24
1.2 Synthetic targets with interesting biological activity 25
1.2.1. Benzamides as structural cores 25
1.2.1.1 Biological activity of benzamides 26
1.2.1.2 Amide bond formation 29
1.2.1.5 Amide bond formation from acyl chlorides 35
1.2.2 Pyrimidines as key structural components 42
1.2.2.1 Biological activity of pyrimidines 43
1.2.2.2 Pyrimidine synthesis and reactions 49
1.3 Research aims and objectives 62
1.4 Aims and objectives of the project 65
1.4.1 Proposed overall synthetic approach 65
1.4.2 Proposed methodology 65
CHAPTER 2: RESULTS AND DISCUSSION 68
2.1 Synthesis of benzamides 68
2.1.1 Preparation of benzamides from unsubstituted benzoic acid **152** and aniline derivatives **151a**-**h** 68
2.1.2 Preparation of benzamides from methoxybenzoic acid **153** and anilines **151a**-**h** 74
2.1.2.1 Comparison between the C-8 signals of benzamide analogues derived from unsubstituted benzoic acid **152** and those derived from the methoxy-substituted benzoic acid **153** 77

2.1.3 Preparation of benzamides from unsubstituted benzoic acid **152** and aminopyridines **151**-**o** 77
2.1.4 Preparation of benzamides form methoxybenzoic acid **153** and aminopyridines **151i**-**o** 85
2.1.5 Preparation of benzamides **166** from 3-hydroxybenzoic acid **154** and anilines 94
2.1.5.1 The ^{1}H NMR spectrum comparison between the appearance and disappearance of the hydroxybenzoic acid proton 99
2.1.6 Preparation of benzamides from 3-hydroxybenzoic acid **154** and aminopyridines 101
2.1.7 Synthesis of complex benzamides 103
2.1.7.1 Synthesis of 3-((2,6-dichloropyrimidin-4-yl)oxy)benzoic acid 103
2.1.7.2 Comparison between the carbon signals of 2,4,6-trichloropyrimidine **102** and acid **155** 108
2.1.6.2 Synthesis of complex benzamides from anilines **151a**-**h** 108
2.1.6.3 Synthesis of complex benzamides from aminopyridines **151i**-**o** 113
2.1.6.4 Synthesis of complex benzamides from aminopyrazines **164p**-**q** 116
2.2 Nucleophilic substitution of the second chlorine atom 117
2.3 Third chlorine displacement by hydrolysis 126
2.4 Conclusion 130
Future work 137
CHAPTER 3: EXPERIMENTAL PROCEDURE 143
3.1 Synthesis of benzamides from unsubstituted benzoic acid **152** and aniline derivatives **151a**-**h** 143
*3.1.1 N-(4-bromophenyl)benzamide **157a*** 144
*3.1.2 N-(3-bromophenyl)benzamide **157b*** 145
*3.1.3 N-(4-bromo-2-methylphenyl)benzamide **157c*** 145
*3.1.4 N-(p-tolyl)benzamide **157d*** 145
*3.1.5 N-(4-methoxyphenyl)benzamide **157e*** 146
*3.1.6 N-(2-bromo-4-methylphenyl)benzamide **157f*** 146
*3.1.7 N-(2-bromo-4-methylphenyl)benzamide **157g*** 146
*3.1.8 N-(4-chloro-2-methylphenyl)benzamide **157h*** 147
3.2 Synthesis of benzamides from unsubstituted benzoic acid **152** and aniline derivatives ***151j-o*** 147
*3.2.1 N-(5-bromopyridin-2-yl)benzamide **157j*** 148
*3.2.2 N-(6-methylpyridin-2-yl)benzamide **157k*** 148
*3.2.3 N-(6-bromopyridin-2-yl)benzamide **157l*** 148
*3.2.4 N-(6-chloropyridin-2-yl)benzamide **157m*** 149
*3.2.5 N-(3-bromopyridin-2-yl)benzamide **157n*** 149
*3.2.6 N-(5-chloropyridin-2-yl)benzamide **157h*** 149

*3.2.7 N-benzoyl-N-(5-methylpyridin-2-yl)benzamide **160i*** 150
*3.2.8 N-benzoyl-N-(3-bromopyridin-2-yl)benzamide **160n*** 150
3.3 Synthesis of benzamides from 3-methoxybenzoic acid **153** and aniline derivatives **151a**-**h** ... 150
*3.3.1 N-(4-bromophenyl)-3-methoxybenzamide **158a*** 151
*3.3.2 N-(3-bromophenyl)-3-methoxybenzamide **158b*** 151
*3.3.3 N-(4-bromo-2-methylphenyl)-3-methoxybenzamide **158c*** 152
*3.3.4 3-methoxy-N-(p-tolyl)benzamide **158d*** 152
*3.3.5 3-methoxy-N-(4-methoxyphenyl)benzamide **158e*** 152
*3.3.6 N-(4-chloro-2-methylphenyl)-3-methoxybenzamide **158h*** 153
3.4 Synthesis of benzamides from 3-methoxybenzoic acid **153** and aniline derivatives **151j**-**o** 153
*3.4.1 3-Methoxy-N-(5-methylpyridin-2-yl)benzamide **158i*** 154
*3.4.2 N-(5-bromopyridin-2-yl)-3-methoxybenzamide **158j*** 154
*3.4.3 3-methoxy-N-(6-methylpyridin-2-yl)benzamide **158k*** 154
*3.4.4 N-(6-bromopyridin-2-yl)-3-methoxybenzamide **158l*** 155
*3.4.5 N-(6-chloropyridin-2-yl)-3-methoxybenzamide **158m*** 155
*3.4.6 N-(3-bromopyridin-2-yl)-3-methoxybenzamide **158n*** 156
*3.4.7 N-(5-chloropyridin-2-yl)-3-methoxybenzamide **158o*** 156
*3.4.8 3-methoxy-N-(3-methoxybenzoyl)-N-(5-methylpyridin-2-yl)benzamide **165i*** 156
*3.4.9 N-(5-bromopyridin-2-yl)-3-methoxy-N-(3-methoxybenzoyl)benzamide **165j*** 157
3.5 Sythesis of benzamides from 3-hydroxybenzoic acid **154** and aminopyridines 157
*3.5.1 N-(5-bromopyridin-2-yl)-3-hydroxybenzamide **166j*** 158
*3.5.2 N-(6-bromopyridin-2-yl)-3-hydroxybenzamide **166l*** 158
*3.5.3 N-(6-chloropyridin-2-yl)-3-hydroxybenzamide **166m*** 158
*3.5.4 N-(5-chloropyridin-2-yl)-3-hydroxybenzamide **166o*** 159
3.6 Preparation of methyl 3-hydroxybenzoate **141** 159
3.7 Synthesis of methyl 3-((2,6-dichloropyrimidin-4-yl)oxy)benzoate **174** 159
3.8 Synthesis of 3-((2,6-dichloropyrimidin-4-yl)oxy)benzoic acid **155** 160
3.9 Synthesis of complex benzamides from anilines **151a**-**h** 160
*3.9.1 N-(4-bromophenyl)-3-((2,6-dichloropyrimidin-4-yl)oxy)benzamide **168a*** 161
*3.9.2 N-(3-bromophenyl)-3-((2,6-dichloropyrimidin-4-yl)oxy)benzamide **168b*** 161
*3.9.3 N-(4-bromo-2-methylphenyl)-3-((2,6-dichloropyrimidin-4-yl)oxy)benzamide **168c*** 162
*3.9.4 3-((2,6-dichloropyrimidin-4-yl)oxy)-N-(p-tolyl)benzamide **168d*** 162
*3.9.5 3-((2,6-dichloropyrimidin-4-yl)oxy)-N-(4-methoxyphenyl)benzamide **168e*** 163
*3.9.6 N-(4-chloro-2-methylphenyl)-3-((2,6-dichloropyrimidin-4-yl)oxy)benzamide **168h*** 163
3.10 Synthesis of complex benzamides from aminopyridines **151j**-**o** 163
*3.10.1 N-(5-bromopyridin-2-yl)-3-((2,6-dichloropyrimidin-4-yl)oxy)benzamide **168j*** 164

*3.10.2 3-((2,6-dichloropyrimidin-4-yl)oxy)-N-(6-methylpyridin-2-yl)benzamide **168k*** 164
*3.10.3 N-(6-bromopyridin-2-yl)-3-((2,6-dichloropyrimidin-4-yl)oxy)benzamide **168l*** 165
*3.10.4 N-(6-chloropyridin-2-yl)-3-((2,6-dichloropyrimidin-4-yl)oxy)benzamide **168m*** 165
*3.10.5 N-(5-chloropyridin-2-yl)-3-((2,6-dichloropyrimidin-4-yl)oxy)benzamide **168o*** 166
3.11 Second chlorine displacement 166
*3.11.1 N-(4-bromophenyl)-3-((6-chloro-2-(ethylthio)pyrimidin-4-yl)oxy)benzamide **180a*** 166
*3.11.2 3-((6-chloro-2-(ethylthio)pyrimidin-4-yl)oxy)-N-(p-tolyl)benzamide **180d*** 167
3.11.3 Preparation of 3-((6-chloro-2-(propylamino)pyrimidin-4-yl)oxy)-N-(p-tolyl)benzamide **184d** 167
*3.11.4 3-((6-chloro-2-(piperidin-1-yl)pyrimidin-4-yl)oxy)-N-(p-tolyl)benzamide **185d*** 168
3.12 Third chlorine displacement by hydrolysis 168
*3.12.1 3-((6-hydroxy-2-(propylamino)pyrimidin-4-yl)oxy)-N-(p-tolyl)benzamide **187d*** 168
References 170
Appendix 1: Single X-ray crystallographic data 181
Appendix 2: ^{1}H and ^{13}C NMR data for a selected number of compounds 266

LIST OF ABBREVIATIONS AND ACRONYMS

HIV	human immunodeficiency virus
AIDS	acquired immune deficiency syndrome
UNAIDS	Joint United Nations Programme on HIV/AIDS
ART	antiretroviral therapy
gp41	transmembrane glycoprotein
gp120	docking glycoprotein
CD4	cluster of differentiation 4
RT	reverse transcriptase
IN	integrase
PR	protease
ds DNA	double-stranded DNA
WHO	World Health Organization
STIs	sexually transmitted infections
PEP	post exposure prophylaxis
PrEP	pre-exposure prophylaxis
NRTIs	nucleoside reverse transcriptase inhibitors
PI	protease inhibitor
INI	integrase inhibitor
NNRTIs	non-nucleoside reverse transcriptase inhibitors
HAART	Highly active antiretroviral therapy
RT	reverse transcriptase
NNIBP	NNRTI binding pocket
Å	angstroms
DNA	deoxyribonucleic acid
FDA	Food and Drug Administration
USA	United States of America
DAPYs	diarylpyrimidines
Wt	wild-type
IC_{50}	half-maximum inhibitory concentration
EC_{50}	median effective concentration
CC_{50}	50% cytotoxicity concentration

AZT	azidothymidine
°C	degree Celsius
DMF	*N*,*N*-dimethylformamide
EDC	1-ethyl-3-(3-dimethylaminopropyl)
DCC	*N*,*N*-dicyclohexylcarbodiimide
CDI	1,1'-carbonyldiimidazole
Et_3N/TEA	triethylamine
HOBt	1-hydroxy-7-azabenzotriazole
WT	wild type
SI	selectivity index
DMAP	4-dimethylaminopyridine
PCl_3	phosphorous trichloride
PCl_5	phosphorus pentachloride
$POCl_3$	phosphorus oxychloride
$(COCl)_2$	oxalyl chloride
$SOCl_2$	thionyl chloride
HCl	hydrochloric acid
µM	micromolar
nM	nanomolar
DABO	Dihydro alkoxy benzyl oxopyrimidine
S_NAr	nucleophilic aromatic substitution
THF	tetrahydrofuran
NMR	nuclear magnetic resonance
FTIR	Fourier-transform infrared spectroscopy
HRMS (ES^+)	high resolution mass spectroscopy (electrospray ionisation)
TLC	thin layer chromatography
m/z	mass-to-charge ratio
DMSO-d_6	hexadeuterodimethyl sulfoxide
$CDCl_3$	deuterated chloroform
EtOAc	ethyl acetate
NHD	normal halogen dependence
$AlCl_3$	aluminium chloride

δ	chemical shift
TMS	tetramethylsilane
UV	ultraviolet
rt	room temperature
ppm	parts per million
Hz	hertz
$NaHCO_3$	sodium hydrogen carbonate
K_2CO_3	potassium carbonate
Na_2SO_4	sodium sulphate
NaOH	sodium hydroxide
ml	millilitre(s)
h	hour(s)
KO^tBu	potassium *tert*-butoxide
DMA	dimethylamine
aq.	aqueous

CHAPTER 1: INTRODUCTION AND BACKGROUND

1.1 HIV-AIDS

Human immunodeficiency virus, typified by HIV-1 and HIV-2, is a member of the retroviridae family that spreads widely and causes acquired immune deficiency syndrome.[1,2] While the two HIV types are similar in viral structures and mechanism of transmission, their origins, infection patterns, and ability to develop into chronic disorders and deaths differ.[3–5] Compared to HIV-1, HIV-2 is less contagious and progression to AIDS is delayed, whereas infection with HIV-1 imparts high plasma viral load and deterioration of the immune system resulting in AIDS-related morbidity and mortality. Additionally, the level of viral replication is the main distinction between the two HIV strains, and host immunity is thought to have a significant role in the more effective management of HIV-2 infection.[3]

1.1.1 Global HIV prevalence

The use of epidemiological estimates from the Joint United Nations Programme on HIV/AIDS is considered helpful for countries to report on their data and progress. As such, it is crucial for countries to provide adequate information, sufficient presumptions and interpretation that considers constraints required to generate estimates.[6]

The UNAIDS epidemiological estimates showed that HIV prevalence increased from 30.7 million[7] to 37.7 million between 2010 and 2020 (Fig **1**).[7,8,9] Among the people living with HIV, 36 million were adults and 1.7 million were children below age fifteen.[7] However, since the first reported case of HIV infection in the early 1980s, the HIV response has led to a tremendous success in containing the disease,[6] although the responsive interventions vary between countries. One of the control strategies includes the implementation of antiretroviral therapy that is widely accessible and scaled up[10] to more than 27.5 million people up to 2020.[6] ART uptake has led to significant strides in the treatment of HIV infection.[9] As a result, the global rates of AIDS-related fatalities declined by 47% from the peak in 2010 (Fig **1**).[6,7,9]

However, the prevalence of HIV-related illnesses and deaths is consistently high in the Eastern Europe and Central Asia with noticeable increments of 43% and 32% ,respectively, from 2010 to 2020.[6,7] Additionally, notwithstanding the gradual expansion of HIV testing capacity, approximately 6.1 million of HIV infected individuals were still uninformed about their status, resulting in a failure to be provided with proper care and treatment programs.[7]

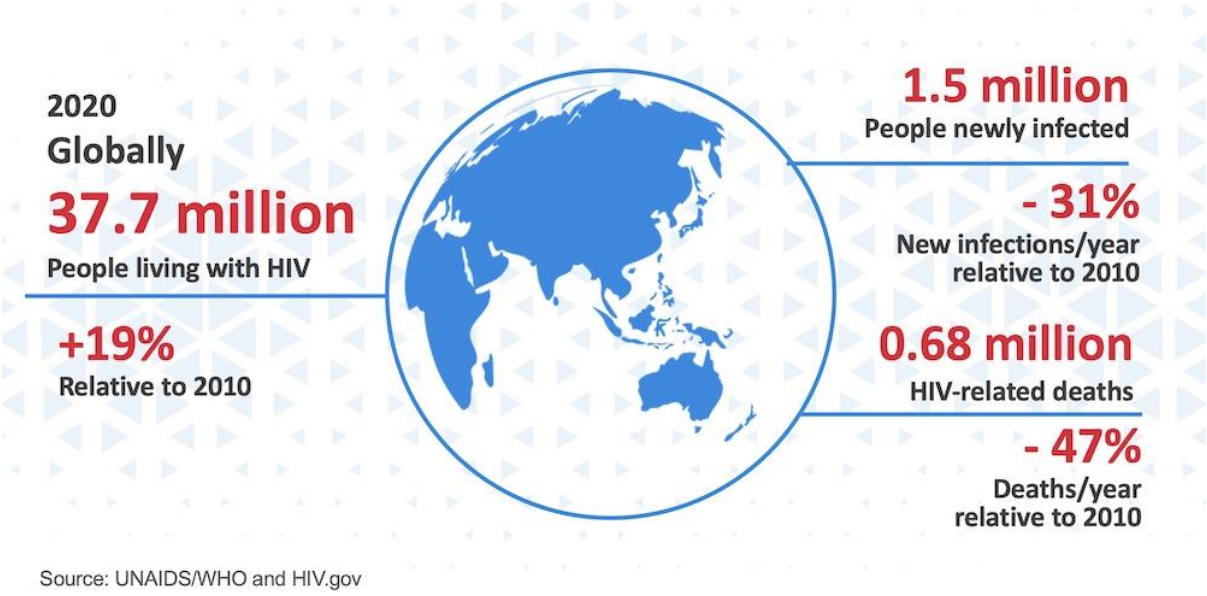

Fig 1 *Global HIV prevalence in 2020*[9]

1.1.2 HIV lifecycle

Due to its relative importance, only the HIV-1 strain will be discussed here. HIV-1 predominantly spreads via certain body fluids and is transmitted through unprotected vaginal or anal sex, sharing contaminated needles with the infected person, and medical procedures involving piercing.[11,12] Upon entry of HIV into the body, the viral envelope protein mediates insertion of the virus into a host cell membrane. This HIV-1 envelope consists of two components, transmembrane glycoprotein and the docking glycoprotein[13] that make up the spikes on surface 49 of the virion.[14] During the entry process, the gp120 connects to the host's CD4 receptor, followed by interactions with one of the chemokine receptors (CCR5 or CXCR4).[15] The co-receptor binding induces irreversible changes in the gp120 shape that enables the gp41 transmembrane protein to penetrate its hydrophobic fusion peptide into the host cell membrane, establishing the initial direct engagements between the virus and its target cell.[16] Thereafter, the fusion of the virus with the host cell membrane occurs, and the viral core is subsequently released into the host cell cytoplasm.

The HIV-1 life cycle is regarded as a concatenation of the steps detailed in Fig **2**, which are controlled by three main enzymatic proteins; reverse transcriptase, integrase and protease. Since the viral genome reverse transcription and integration require both RT and IN, respectively, these enzymes are essential throughout the initial stages of the HIV viral replication cycle.[17] The catalytic activities of RT enzyme that include RNA template-dependent DNA polymerization and DNA template-dependent DNA polymerization allow conversion of the single-stranded viral RNA genome into double-stranded DNA. Following the DNA-RNA hybrid strand creation, degradation of RNA strand by RNase H occurs leaving single-stranded DNA. Here, a complementary RNA strand is reverse transcribed by the viral

enzyme RT, generating the linear double-stranded DNA.[4,13] At this stage, the IN enzyme travels through the nuclear membrane carrying the pre-integrated viral ds DNA and incorporates it into the host DNA. Using the cellular machinery of the host, the integrated viral DNA is now subjected to transcription and translation into viral polyprotein. This polyprotein is broken down into its constituent structural and functional proteins by the viral enzyme PR, resulting in viral maturation and the capacity of the mature virions to infect new host cells.[4,13,17] Left untreated, HIV transitions into AIDS due to the immune system's weakness when the infected individuals become vulnerable to destruction by the virus. Thus, these three enzymes have emerged as critical targets in the development of new drugs for HIV treatment.

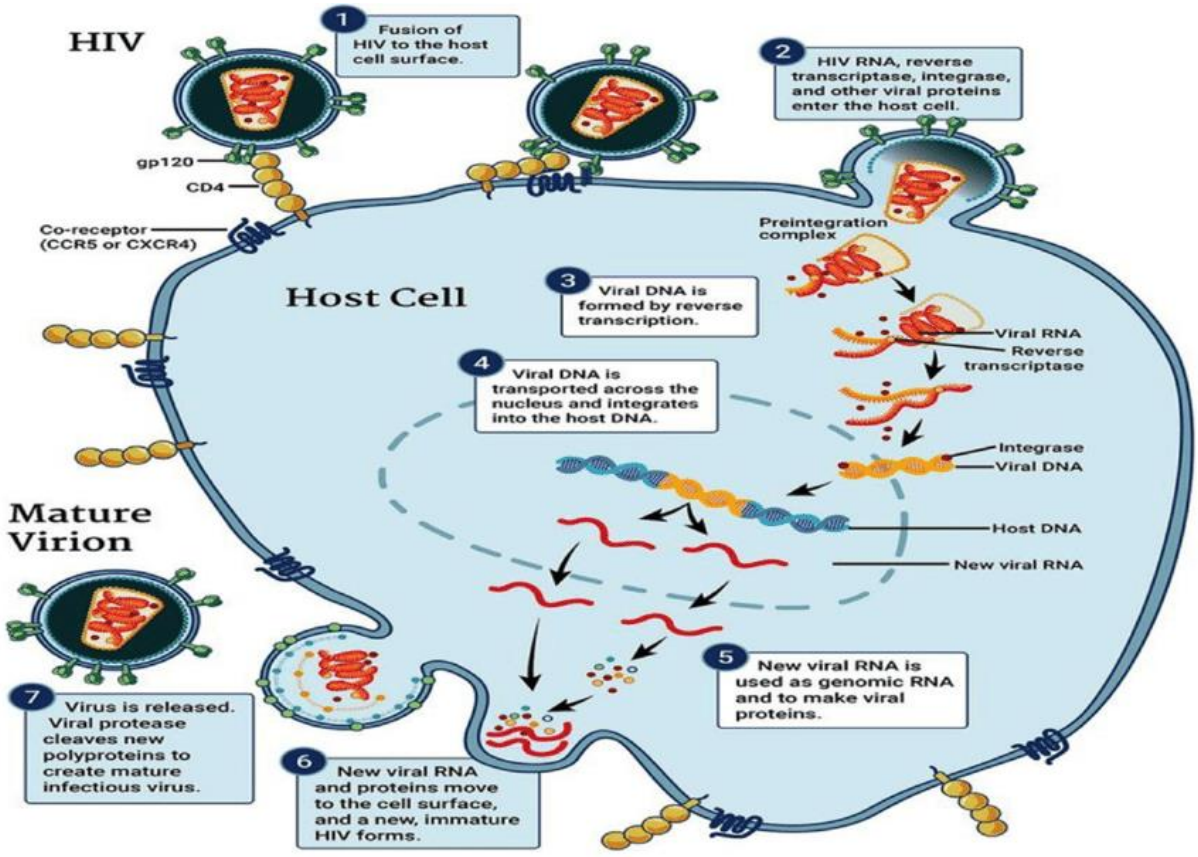

Fig 2 *HIV life cycle*[14]

1.1.3 Social and health effects of HIV/AIDS

The time taken for HIV infection to develop into AIDS is approximately between five months to fifteen years. The first AIDS case was identified in the United States in 1981[18] among homosexual men, and although male-to-male sex is prevalent as a mode of HIV transmission in many parts of the developed countries, heterosexual sex is a primary element of the disease's global transmissions responsible for 75% of infections.[19]

It has been reported that gender inequality also contributed in HIV exposure. Specifically, women are more socially vulnerable than men due to biological disparities in susceptibility, lack of sexual agency, as well as the power and privilege that men enjoy in sexual relationships.[20] These effects are most recognised in sub-Saharan Africa, where women and young girls between fifteen and twenty-four years contributed 25% of infections, although this age group accounted for 10% of global infections recorded in 2020.[7]

Vertical HIV transmission on the other hand, can occur at any point during the pregnancy period increasing the chances of an HIV-positive mother infecting her unborn child, hampered by risk factors that include early delivery, low maternal cell-mediated immunity, prolonged labour, low CD4 counts, high viral loads, premature membrane rupture, delivery method, and untreated STDs.[19,21] HIV can also be transmitted from mother to child through breast milk, although the likelihood of contracting the virus rises with lactation duration[22] A number of methods have been implemented to prevent and reduce mother-to-child transmissions while breast-feeding.[19] These alternative approaches involve premature discontinuation of breast-feeding and adoption of artificial feeding.[23]

1.1.4 Access, treatment, and care for people living with HIV

There are many HIV prevention strategies in place that have not been used nearly enough with respect to the extent to which HIV infection spreads annually.[27] To lower HIV transmission significantly and change the course of the epidemic, HIV typologies, transmission modes, and populations affected need to be well understood to intensify prevention activities as these factors influence how well evidence-based interventions can be combined and adapted.[27]

Prophylactic and antiretroviral therapies are two epidemiological strategies useful for HIV/AIDS control, with ART being appropriate to all HIV-infected individuals, whereas prophylaxis is applicable to all people at the risk of exposure to HIV infection.[28] Prophylaxis shall be covered in the next section.

As of 2015, the World Health Organization advises people living with HIV to begin antiretroviral therapy as soon as a positive test result is obtained for the maximum therapeutic benefits of effective viral suppression to be realized and to avoid additional transmission.[29] ART development has prolonged the lifespan of HIV-infected individuals by controlling viral replication and helps immunological recovery. However, effective treatment needs ART consistency which is difficult for some people and the resulting relapses cause a burden on healthcare systems, especially in resource-constrained settings.[30] Delayed treatment commencement, non-treatment adherence, and early therapy termination result in negative impact on the survival of HIV-infected people.[31] ART discontinuation can either be temporary or permanent, intentional, or unplanned by health professionals or patient. Doctors might advise ART cessation either when underlying illnesses interfere

with oral therapy or surgery prevents oral therapy. In addition, ART discontinuation may be recommended when there is lack of antiretroviral drugs or when the medications are toxic or have severe side effects to patients.[32] On the other hand, patients may decide to cease ART for reasons that include personal beliefs when a patient is virally suppressed and does not see the necessity to continue receiving treatment. Structural obstacles that include imprisonment and lack of money are additional barriers to ART discontinuation.[32]

Research conducted in Botswana indicated that inconsistent ART adherence accelerates the chances of seeing virus resistant to ARVs, requiring a shift to more expensive second- or third-line drug therapies.[33] It was added that ART defaulters might have stopped taking their medication when financial problems made it difficult for them to pay transport to clinics where they could receive monthly treatment.[33] Some participants reported that they started relying more on religion and spirituality as their coping approach.[33] Coping was investigated in HIV-positive individuals in the late 1990s, and was defined as the behavioural and cognitive attempts made by an individual to change or minimize the problems brought on by a particular stressful situation.[34] It was also emphasized that coping mechanisms had a significant impact on psychological effects of HIV infection. Furthermore, it was believed that HIV-infected patients who exhibit signs of psychological stress inhibit their anger by resorting to engagements in drug and alcohol use to ease their discomfort, thus, posing a significant burden to therapists.[34] A decade later, another study in the US Southeast mentioned that alcohol and drug misuse is common among HIV-positive people, and is in turn linked to higher risk behaviours for secondary transmissions and lower ART adherence.[35] These findings were supported by a recent study conducted in South Africa that alcohol use in people infected with HIV increases treatment inconsistency and lowers viral load suppression.[36]

Recently, several countries were heavily burdened by COVID-19, during which adherence to ART was disrupted in compliance to the implemented COVID-19 protocols, posing potential detrimental effects on HIV control efforts. During the COVID-19 pandemic, it was emphasized that barriers like constrained movement, prohibitive transportation costs, and stringent measures implemented to relieve the healthcare facilities and maintain social distance, and the fear of contracting and dying from COVID-19 limited access to healthcare.[30,37,38] As such, many healthcare systems struggled to offer basic health services to patients due to severity of corona-virus disease.[30] However, it was suggested that various medical facilities should assume leadership roles and provide care for individuals who have HIV and other immune-compromised illnesses to continue receiving HIV services.[24]

1.1.5 Newer tools for HIV/AIDS prevention and control

1.1.5.1 Provision of prophylactic agents

Regular evaluation of knowledge, attitudes and behaviours that are considerate of gender roles and cultural norms is essential to help plan and administer prevention programs.[39] Encouraging behaviour change, male circumcision, harm reduction initiatives for injecting substance use and HIV status awareness about testing and effectiveness of condom use are just a few of the comprehensive and successful public health programs. Many other interventions include voluntary counselling and testing, preventing vertical transmission, identifying cases of, and treating STIs and supply of post exposure prophylaxis,[27] and pre-exposure prophylaxis.[39]

PrEP and PEP are two efficient prophylactic techniques currently accessible for use in preventing HIV infection. These methods work best when combined with non-pharmacological awareness tools like safe sex education and other synergistic and syndemic effects of the co-existing risk factors. WHO recommended PEP as a brief antiretroviral medication used to lower the risk of HIV infection after accidental exposure. It is potent if used within a 72-hour time frame, but its effectiveness depends on clinic attendance and adherence to the prescribed 28-day course of treatment.

WHO advised in 2015 that regardless of gender, PrEP should be made available as a preventive measure to all those who have increased chance of HIV acquisition.[40] People on PrEP are HIV negative, often young and have few comorbid conditions, if any, as opposed to those on ART. Furthermore, there are few restrictions to PrEP because it is a short-term control measure that can be stopped at any time depending on the person's preferences and risk levels of acquiring the infection, whereas antiretroviral therapy is continued throughout one's life.[41] PrEP displays 99% effectiveness when following the directed dosage, but poor compliance lowers its potency and the value to public health.[42]

1.1.5.2 Implementation and monitoring of programs

The 2016 Political Declaration on HIV initiated a plan aimed to lower new HIV infections and AIDS-related deaths by 90% from 2010 to 2030 with at least 75% reduction by 2020. Additionally, the developments of the 90-90-90 testing and treatment targets were committed to eradicating the AIDS epidemic by 2030, which was implemented as a 90% decrease from 2010 in the number of new HIV infections and AIDS-related mortalities. This strategy states that 90% of people infected with HIV are aware of their status, 90% of HIV-positive individuals initiate ART and 90% of those on ART should be virally suppressed. The new Global AIDS Strategy and the 2021 Political declaration also incorporated extremely ambitious 95-95-95 targets.[6,7]

Although encouraging from a theoretical perspective, realistically these targets are quite elusive, especially in such a short period of time. The global efforts to lower new HIV infections by 75% failed.[6,7]

Since 2010, the overall number of new infections decreased by just 31% (Fig **1**), far from reaching the 75% objective for the year 2020.[6,7] Despite global gains being achieved by deployment of programs that use treatment as a preventative measure,[43] approximately 1.5 million new infections (Fig **1**) were recorded in 2020,[6,7,9,10] with the majority of the infected people living in sub-Saharan Africa, contributing 67%.[9] Moreover, despite the great advancements in awareness of HIV treatment and prevention to achieve epidemic control, sexual transmission, a key factor in the mode of HIV infection in sub-Saharan Africa, continues to hamper the potential of an HIV/AIDS-free generation.[10] Assefa and Gilks pointed out that when the national overall number of people infected with HIV drops to the levels last observed at the beginning of the HIV pandemic, the disease can be declared over.[44]

Further reviewing the 90-90-90 targets, it was estimated that 84-87-90 testing and treatment targets were accomplished across the world by the end of 2020. Although promising that the third 90 target was achieved, this is only applicable to people who are informed about their HIV status and are receiving treatment. As of 2020, the overall percentage of all HIV-infected individuals with suppressed viral loads was 66% (Fig **3**).[6,7] Moreover, though narrow, there is still a missing gap of people infected with HIV who know their status but do not receive ART. According to literature, ART coverage was predicted to rise at a global rate of 59% in 2017 to 64.8% by 2020, also to 71.9% by 2030. Notwithstanding the significant advancements these predicted gains signify, they however missed the 81% target of the UNAIDS by the year 2020 and reflect slow progress towards 90% coverage by 2030.[43]

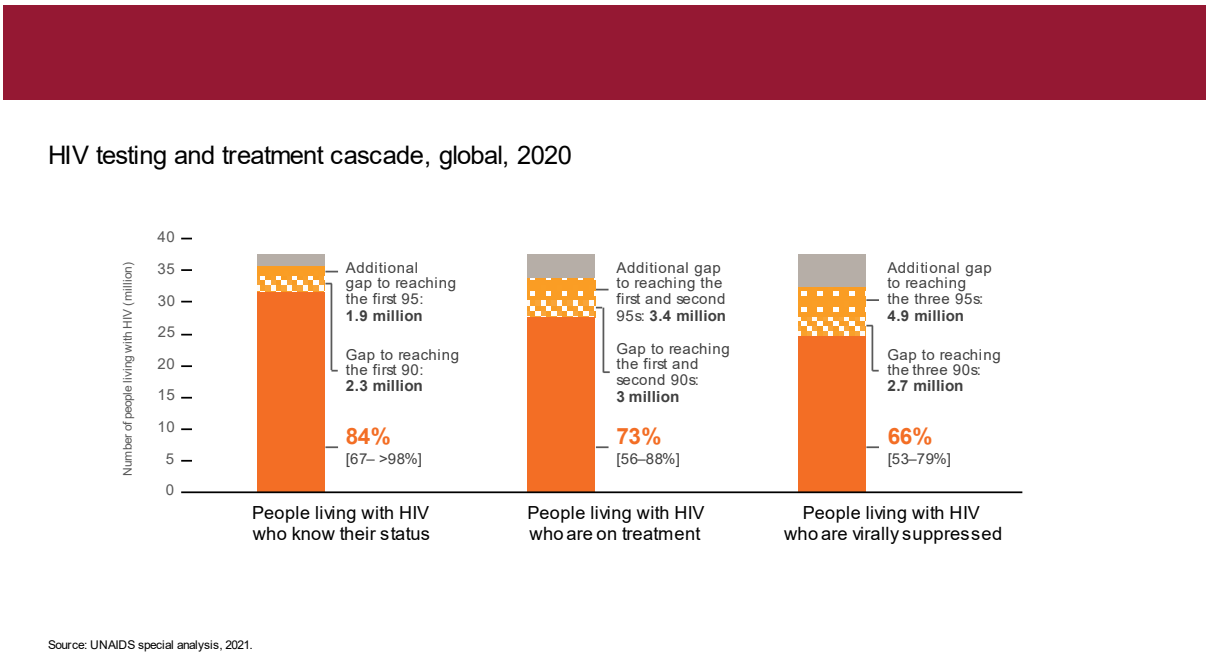

Fig 3 *The 2020 global HIV testing and treatment cascade*[8]

Therefore, the HIV outbreak does not seem close to its end, and it is envisioned to remain a great threat across the world. However, HIV infection may decrease if remedial action is taken, according to the International AIDS Society-Lancet Commission.[44] Reaching project 2030, whilst recognizing the global developments of therapeutic programs as preventive measures, raises concerning questions about additional steps required to encourage those particularly ignorant of their HIV-positive status to initiate ART and ensure its adherence. Again, it is unclear how each country will ensure that the 3rd 90 target is maintained, given risk behaviours arising from ART defaulters.

Another primary uncertainty is associated with the financial demands. Proper planning and allocation of resources will be required for PrEP and ART scale-up to achieve the project 2030 target. Chen and co-workers in their study, estimated that USD 4.7 trillion will be needed annually to fund ART supply for 90% of the global 37 million people infected with HIV.[45] However, the funding for HIV/AIDS is currently stagnating because of the unwillingness to maintain funding for the disease.[44] Avancena and Hutton urged the donors and recipients to alleviate the financing gaps that could jeopardize the disease progress made by contributing additional funds and increasing the impact of existing resources.[46]

HIV/AIDS persists in spreading across the world and there is still no viable vaccine or cure for the disease.[10] Therefore, our research arises as part of the ongoing global campaign to search for novel anti-HIV therapeutic drugs that can have high anti-HIV activity, reduced toxicity, and selectivity features to help combat transmission of the concomitant pandemic.

1.1.6 HIV-1 reverse transcriptase inhibitors in the treatment of HIV

The current standard regimen for HIV/AIDS treatment is a triple therapy combination, which consists of two nucleoside reverse transcriptase inhibitors plus either a protease inhibitor or an integrase inhibitor or non-nucleoside reverse transcriptase inhibitors. Highly active antiretroviral therapy is the term most frequently used to describe this combination therapy. Because monotherapies fall short in their capacity to prevent HIV-1 replication, HAART is used to block numerous viral proteins at various stages in the HIV life cycle. However, HAART does not eradicate the virus completely, but when adhered to effectively, HIV is changed from a deadly condition to a controllable chronic illness.[47–49] Multiple medications can be harmful and ultimately offer health hazards due to prolonged use and drug-drug interactions. [49]

HIV-1 RT is the first enzyme utilized by the virus when it enters the body of a host, and it controls the genetic replication of genetic material of HIV. RT is the most common target in the field of antiretroviral drug development. Structurally, HIV-1 RT is an asymmetric heterodimer containing two subunits (Fig **4**) namely the p66 subunit which is vital for carrying out enzymatic activities and the p51

subunit that gives the structural and conformational support for RT. The catalytic site of HIV-1 RT is situated within the palm subdomain and is the primary target of the NRTIs whereas the hydrophobic pocket is allosterically targeted by NNRTIs.[17,50]

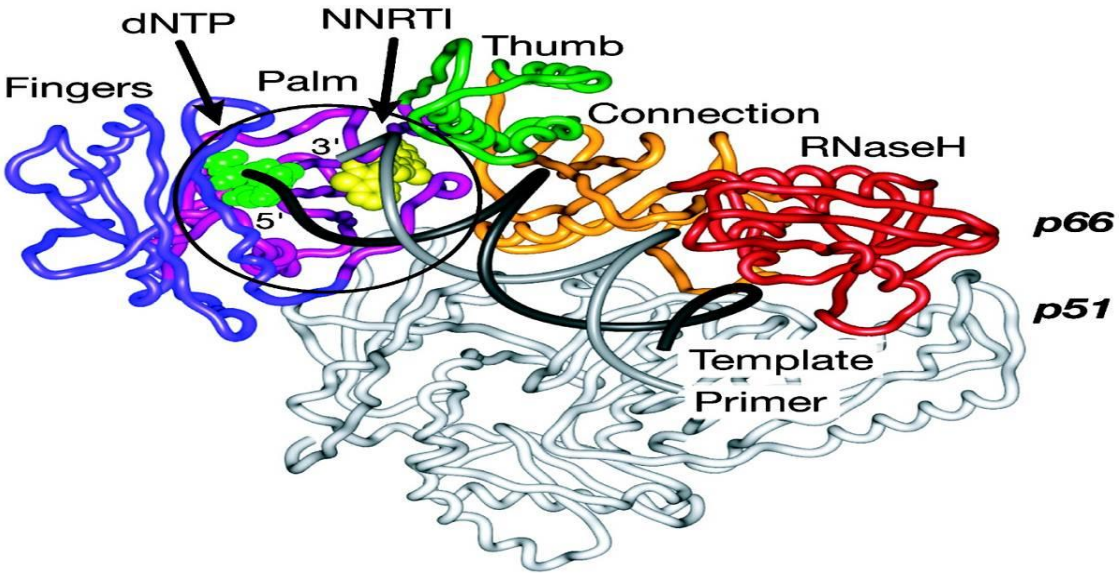

Fig 4 *HIV-1 RT enzyme structure*

1.1.6.1 NRTIs mechanism of action

NRTIs are nucleosides that lack the 3'-hydroxyl group on the deoxyribose moiety.[15] They enable proper base pairing and inclusion into DNA chains after phosphorylation, but a crucial hydroxyl group that is necessary for the insertion of the following nucleotide is missing. These competitive inhibitors act by mimicking the nucleotides that make up the viral DNA, and once incorporated into nascent viral DNA, they prevent the viral DNA chain from growing and thus, terminate the DNA chain extension.[13,15,48] However, their activity depends on the ability of cellular kinases to convert them metabolically into an active triphosphate form. Such NRTIs include tenofovir **1**, lamivudine **2**, and emtricitabine **3** (Fig **5**), which are considered as South Africa's first-line treatment regimens.[13]

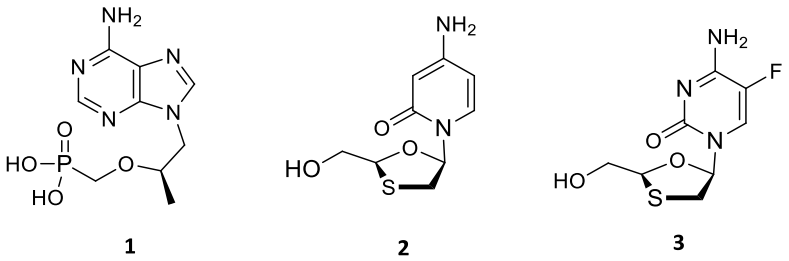

Fig 5 *Some of the approved NRTIs: tenofovir **1**, lamivudine **2**, and emtricitabine **3***

1.1.6.2 NNRTIs mechanism of action

NNRTIs, which also target RT, are one of the most important components in drug combination therapies. They garnered considerable attention among the various types of anti-HIV therapeutic agents because of their low toxicity, high specificity, and high levels of antiviral activity.[51] NNRTIs are non-competitive inhibitors discovered in 1990 that effectively deactivate polymerization of HIV-1 RT without the need for activation through phosphorylation. These drugs act by causing a conformational shift in the RT enzyme, through attachment to a hydrophobic region just outside the RT active site known as the NNRTI binding pocket, located 10 Å away from the DNA polymerase active site.[47,51,52] Using X-ray crystal structures of NNRTIs in association with RT, studies revealed that NNRTIs retain comparable interaction modalities and binding patterns to RT, despite their structural differences. A variety of NNRTI structures could be compared to a butterfly, horseshoe, or U-like shape.[48,53] They appear to be electron rich and have the potential to donate π-electrons to aromatic side chain residues near the binding pocket.[48]

As of September 2019, the Food and Drug Administration had approved six NNRTIs, shown in Fig **6**. Nevirapine **4** was the first NNRTI drug discovered by Boehringer Ingelheim, and was approved by the FDA for use when combined with nucleoside derivatives in USA in June 1996[33,52,53] and in the European Union in 1998.[53] This dipyridodiazepinone NNRTI[15] has strong metabolic stability, excellent biological activity, and is readily able to penetrate the blood-brain barrier,[53] but has unpleasant side effects and a low genetic barrier to resistance.[52] Delavirdine **5** that belongs to a family of bis(heteroaryl)piperazines, was discovered by ViiV Healthcare, and was the second NNRTI to be approved by the FDA in 1997.[15] Its use was however ceased owing to similar drawbacks to those of nevirapine.

Efavirenz **6** is a benzoxazinone second generation NNRTI approved by the FDA in September 1998.[15] It was said to drastically reduce the activity of HIV-1 in cell culture when combined with NRTIs like didanosine, zidovudine and the protease inhibitor indinavir. However, its antiviral effectiveness is often dramatically diminished after two or more mutations in HIV-1 RT. The FDA-approved NNRTIs etravirine **7** and rilpivirine **8** are diarylpyrimidines that share common structures and binding mechanisms in the NNIBP which enables both drugs to be rearranged inside RT, to compensate for the amino acid alterations caused by mutations.[47,48] Doravirine **9** is the most recent NNRTI drug discovered by Merck & Co. to receive approval by the FDA in August 2018. Due to its several benefits including favourable safety profile, substantial efficacy, and low risk of developing resistance, it is currently administered to treatment naïve patients.[15]

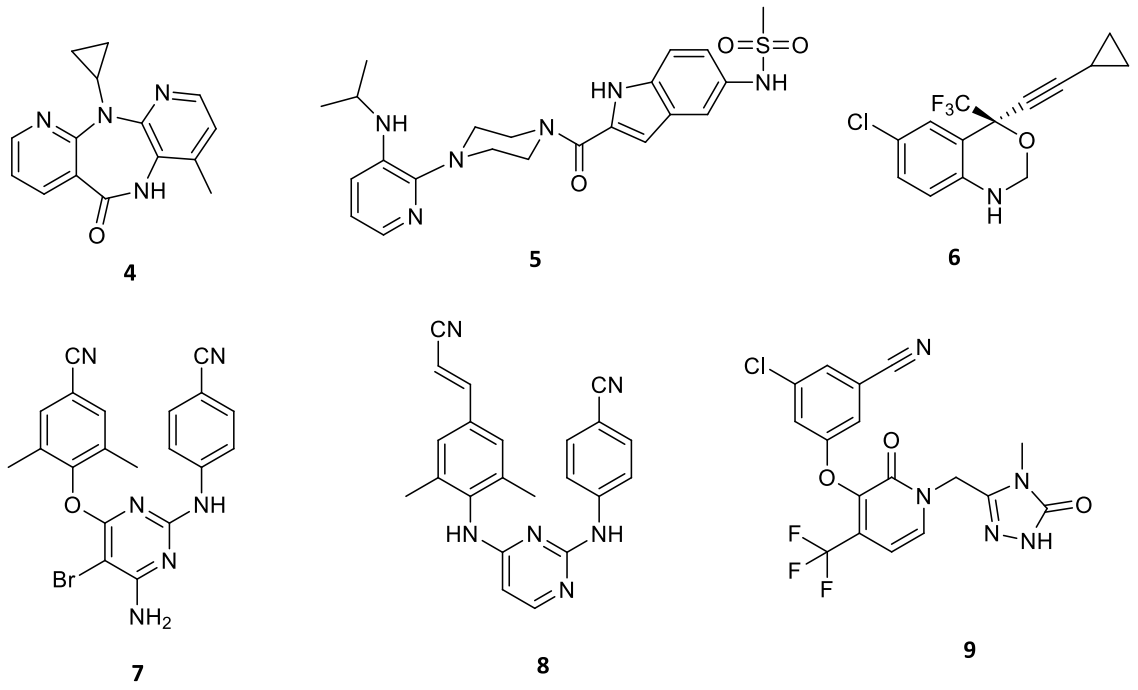

Fig 6 *FDA approved NNRTIs: Nevirapine* ***4****, Delavirdine* ***5****, Efavirenz* ***6****, etravirine* ***7****, rilpivirine* ***8****, and doravirine* ***9***

1.1.6.3 Drug resistance to NNRTIs

During drug therapy, resistance to NNRTIs quickly develops because of the low fidelity of HIV-1 RT and high level of HIV-1 replication[47] that results in mutations that change the amino acids surrounding the NNIBP. This reduces the potency of NNRTIs, leading to treatment failures.[48]

NNRTIs **4**, **5**, and **6** can successfully halt the reproduction of HIV-1 wild-type virus but are less active against several frequently seen mutant viruses which include Y181C, L100I, Y188C, and K103N.[54] Among the reported HIV-1 mutations, K103N is the most prevalent NNRTI resistant mutation. The K103N is a non-polymorphic mutation present on the loop that links β5 and β6 in the p66 subunit of RT situated near the binding pocket, and is positioned farther away from the RT active site.[55] The X-ray crystal structure of a K103N mutant comprising Tyr181 bound to efavirenz in exchangeable positions is represented in Fig **7**.[13] The K103N mutation blocks the entrance of efavirenz to the NNIBP causing the unliganded conformation of NNIBP to remain unchanged. The presence of the K103N mutation also lowers the activity of these first generation NNRTIs, resulting in the IC_{50} values ranging from 20 to 55 times higher.[56] Thus, evaluation of challenges related to the evolving drug resistance is imperative for examining different scaffolds as potential pathways towards the development of alternative NNRTI therapeutic agents.

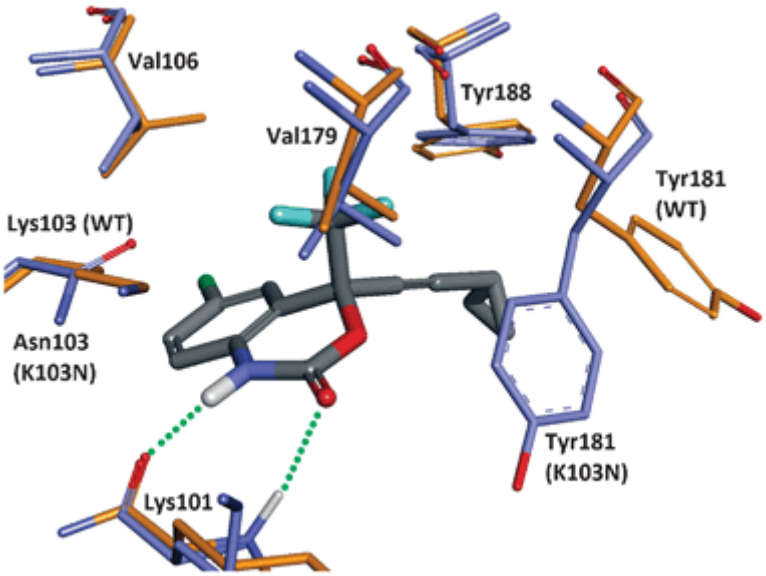

Fig 7 *Efavirenz interacting with Tyr 181 in the wild type*

The DAPY NNRTI drugs etravirine **7** and rilpivirine **8** were developed using structure-based multidisciplinary strategies to prevent the activity of HIV-1 bearing similar NNRTI-resistant mutations. They have a higher genetic barrier to resistance than the former NNRTI drugs **4**, **5**, and **6**.[55] They retain their efficacy against the wild type virus and additionally, unlike the first and second generation NNRTIs **4**, **5**, and **6**, the DAPYs are not sensitive to the K103N mutation, and substantially preserve almost all of their effectiveness.[13] The intrinsic torsional freedom of the DAPYs enables them to shift into various conformational modes through orientation (wiggling) and reposition (jiggling) to fit in the NNIBP alterations induced by different RT resistance mutations.[57,58] Again, compared to nevirapine that is structurally rigid, the inhibitors' relative flexibility may allow the DAPYs to easily adapt to a drug pocket that has undergone mutation.[57]

Despite that, Changunda[59] suggested that caution should be exercised while exploring the idea of more conformational flexibility to preserve the best possible balance between the benefits that could be obtained from either the improved torsional mobility or less constrained rotation. He added that forsaking limited rotation at the expense of increased torsional flexibility might offer excessive amount of entropic energy to the ligand. Consequently, this could restrict the ligand from locking itself inside the enzyme's binding site, and in turn negate the purpose of boosting the ligand binding affinity.[59]

1.2 Synthetic targets with interesting biological activity

1.2.1. Benzamides as structural cores

Continuous efforts made in the development of new NNRTIs in our laboratory led to the identification of benzamide compounds possessing anti-HIV activity.[59] Benzamide compounds are classified as carbonic acid amide derivatives of benzoic acids.[60] An amide (CONR) commonly referred to as

carboxamide or organic amide, is a chemical molecule having a generic formula RC(C=O)NR'R", where R, R', and R" represent the organic groups or hydrogen atoms. Carboxamides in their classical configuration, have a central carbon skeleton attached simultaneously to the nitrogen and oxygen atoms through single and double bonds respectively.[61,62] Based on the number of substituents bonded to the nitrogen atom, amides are categorized into primary, secondary, and tertiary subclasses. The primary amide is obtained when the hydroxyl group (OH) of a carboxylic acid is displaced by the NH_2 amino group. When other groups substitute one or both hydrogen atoms in the primary amides, the resulting molecule is referred to as a secondary or tertiary carboxamide.[60]

1.2.1.1 Biological activity of benzamides

Benzamide-based derivatives have been identified as a valuable class of compounds that inhibit histone deacetylase both in *in vivo* and *in vitro* anticancer studies.[63] Two examples of the benzamide-containing drugs that have undergone clinical trials include entinostat **9** and mocetinostat **10** (Fig **8**). Entinostat **9** is an effective class I selective histone deacetylase (HDAC) inhibitor that can be used alone or in conjunction with other medications due to its high level of tolerability. The combination of entinostat and 13-*cis*-retinoic acid was examined in a phase I trial to ascertain their tolerability, safety, pharmacodynamics/pharmacokinetic characteristics in advanced solid tumours. Despite their lack of activity, the combination therapy was well tolerated, and patients with kidney, pancreatic, and prostate cancer experienced prolonged stable illness. In breast cancer patients, the effects of entinostat alone or in combination with the aromatase inhibitor exemestane were assessed in a placebo-controlled and randomized phase II research. The results highlighted the safety, and clinical efficacy of this combination therapy in ER+ advanced breast cancer patients. Mocetinostat **10** is an HDAC inhibitor that targets both Class I and IV histone deacetylases with high specificity. The safety and antileukaemic efficacy of mocetinostat were both demonstrated in a phase I trial in individuals with myelodysplastic syndrome or leukaemia. An effective treatment with a controllable side effect profile was shown in a phase II trial in individuals infected with chronic lymphocytic leukaemia.[63]

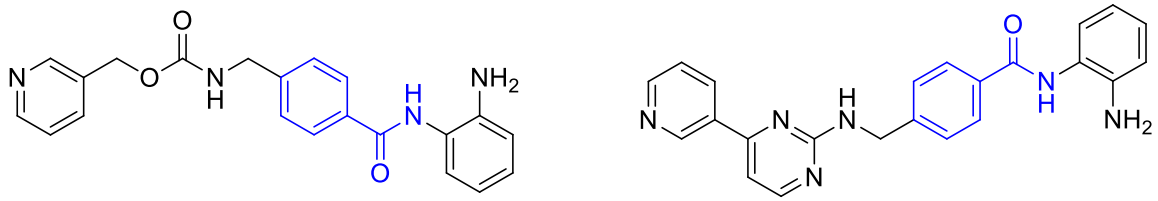

9 **10**

Fig 8 *Structures of entinostat **9** and mocetinostat **10***

Other significant biological characteristics of benzamides are shown by *N*-(4-chlorophenyl)-4-methoxy-3-(methylamino)benzamide, IMB-0523 **11** (Fig **9**), which is a drug candidate for inhibiting Hepatitis B virus (HBV), with a promising selectivity index and anti-HBV profile.[64]

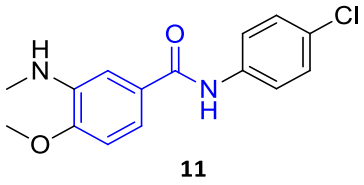

11

Fig 9 *Chemical structure of IMB-0523* ***11***

Sorafenib **12** (Fig **10**) is also a benzamide-containing drug that has pharmacophoric profiles such as H-bond donor/acceptor, terminal lipophilic moiety, central aromatic linker, and heteroatomic ring,[65] which received approval for use in Europe as a treatment for hepatocellular carcinoma.[66]

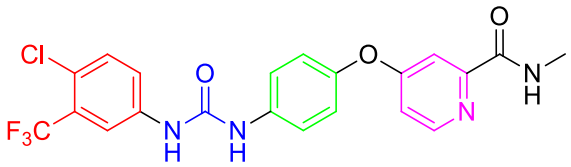

12

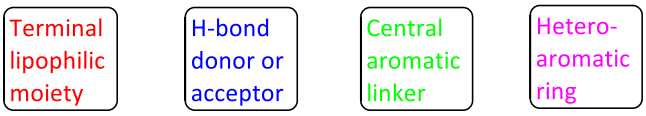

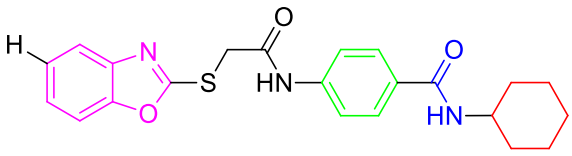

13

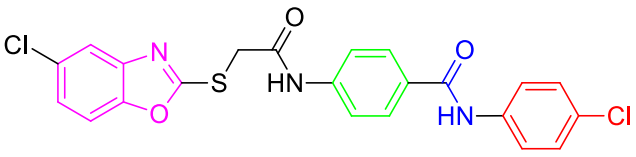

14

Fig 10 *Pharmacophoric features of sorafenib* ***12*** *and related analogues* ***13*** *and* ***14***

Eissa and co-workers assessed benzoxazole benzamide compounds related to sorafenib as potential anti-proliferative inhibitors of VEGFR-2 (vascular endothelial growth factor receptor-2) and apoptotic inducers.[66] Compounds **13** and **14** (Fig **10**), were deemed most effective and displayed pharmacophoric features that are indistinguishable from those of **12**, with superior docking scores

relative to that of **12**. One feature of interest is that of the amide group, which is crucial as a hydrogen-bond donor/acceptor present in both **12** and compounds **13** and **14**. These compounds exhibited different activities against the VEGFR enzyme, with **13** (IC_{50}= 0.268 µM) being more active than **14** (IC_{50}= 0.361 µM) and **12** (IC_{50}= 0.352 µM)**.**[66]

Al-Masoudi and colleagues examined a range of thiazol-2-yliedene-benzamide derivatives for anti-HIV-1 and anti-HIV-2 activities based on a Quantitative Structure-Activity Relationship (QSAR).[67] In reference to their results, twenty of their compounds were deduced to have adopted a butterfly-like conformation, which is significant for RT inhibitory efficacy against HIV-1. Among the twenty compounds, analogues **15** and **16** (Fig **11**) were hypothesized to act as potential NNRTIs because of their extraordinary antiviral effectiveness.[67]

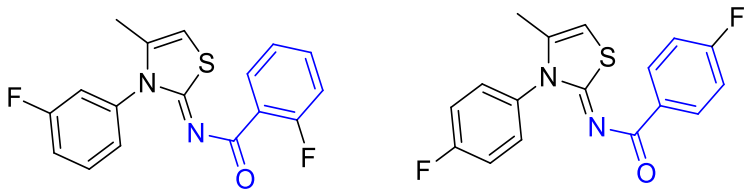

15 **16**

Fig 11 *Structures of compounds* ***15*** *and* ***16***

Scala and co-workers also evaluated the anti-HIV potency of compounds **17** and **18** *in vitro* in a classic MTT-MT4 test.[68] Compound **18** with a benzamide moiety at the *N*1 position of the pyrazole ring was found to be effective at blocking HIV proliferation with low cytotoxicity and a considerable selectivity index (EC_{50}= 2.77 µM, CC_{50}= 116.7 µM, and SI= 68). Even though compound **17** also consists of a benzamide tail, it did not appear to exhibit the antiviral activity in comparison to scaffold **18**, thus, highlighting the crucial role displayed by the position of the benzamide motif present in **18** (Fig **12**). Impressively, it exhibited the RT inhibitor properties, dramatically lowering RT DNA synthesis, albeit to a lesser extent than shown by AZT.[68]

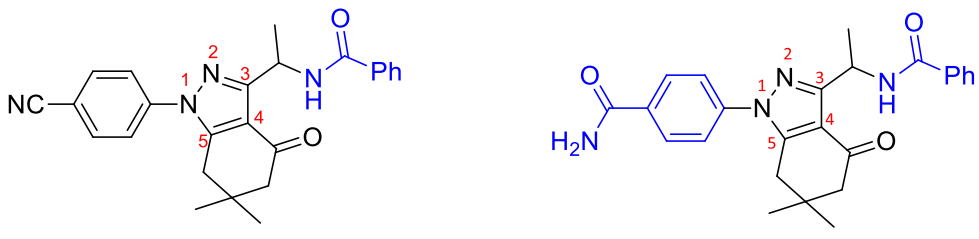

17 **18**

Fig 12 *Structures of compounds* ***17*** *and* ***18***

1.2.1.2 Amide bond formation

One of the most significant organic processes involves the formation of amide bonds since these bonds frequently occur in both natural and industrial products[69] such as plastics, fabrics, insecticides, and fertilizers.[70] The amide functionality is also present in various synthetic structures and serves as the protein's structural backbone. Polymers containing the amide bond are fundamental for use in a vast number of applications from materials that include Kevlar and nylon to more sophisticated uses for biological applications like drug administration.[71] Given that the amide bond is present in 25% of all medications now available on the market,[71,72] amide synthesis is equally important in small scale and large-scale processes,[73] with amidation reactions the most widely employed techniques in medicinal chemistry.[72]

1.2.1.2.1 Induced thermal and microwave-assisted amidation reactions

The amidation reaction is characterized by a condensation process between carboxylic acids **19** and amines **20** (Scheme **1**). Usually, the amidation reactions are nonspontaneous[74] and require conditions like high temperatures above 100 °C to overcome the formation of unreactive carboxylate ammonium salt **21** (Scheme **1**). The benefits of thermal conditions include the ease of use and great atom economy.[71] However, substrates sensitive to high reaction temperatures like amino acids should not be exposed to such harsh conditions.[75] In addition, the reactants must exhibit particular features that include excellent thermal stability, low volatility, and melting points under 200 °C.[74] Furthermore, the preparative utility of thermal amidation can be restricted by the amide's dehydration at increased reaction temperatures to produce a corresponding nitrile or tar.[71]

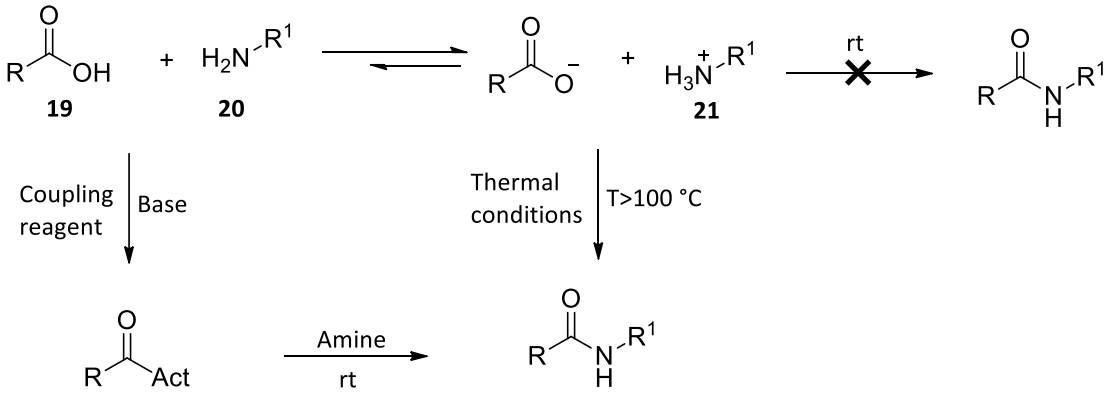

Scheme 1 *Thermal amidation v/s coupling reagent amidation*[75]

Mitchell and Reid were the first authors to publish primary amide synthesis from ammonia and aliphatic carboxylic acids under thermal conditions at approximately 190 °C in 1931.[76] Although good yields were obtained, the products were often contaminated with either nitrile or ammonium salt or both, and in some instances, autoclaving was necessary to dehydrate the ammonium salts.[76] A

commercial production of dimethylacetamide was carried out following the similar method, with the product being isolated as an azeotrope after the reaction of dimethylamine and acetic acid.[77] It appeared that with the optimization of reaction conditions to pressures above 6200 kPa and high temperatures between 250 and 325 ˚C, the formation of azeotrope could be lowered by reacting excess amounts of dimethylamine with acetic acid.[77]

Using 4 Å molecular sieves, a variety of amides synthesized without using catalysts or coupling reagents at 140 ˚C were reported by Cossy and Pale-Grosdemange in 1989.[78] At temperatures ranging from 120 °C to 160 ˚C, amides were formed by reacting neat mixtures of carboxylic acid and amines under 3 Å molecular sieves. Compared to benzylamine which gave 75% yield, the reaction between benzoic acid and *N*-benzylamine only provided trace amounts of the product at 160 ˚C after 24 hours.[79] Thus, direct amide bond formation from uncatalyzed amines and carboxylic acids at temperatures below those previously reported was explored.[80] Conducting the reaction in a sealed vessel in the absence of molecular sieves promoted a favourable equilibrium without the efforts to eliminate water, and the use of non-polar solvents like toluene facilitated the formation of amides at 110 °C for 22 h. Although the conversion rates were unsatisfactory in most cases, at least *N*-benzylpropionamide **22** was isolated in 79% yield under similar conditions (Scheme **2**).[80]

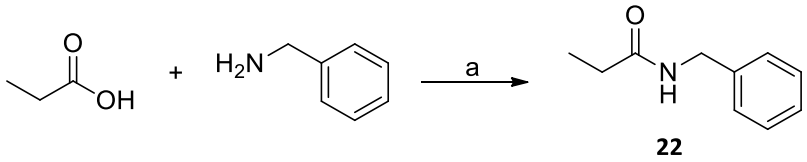

22

Scheme 2 *Reagents and conditions: (a) Toluene (2.0M), 110 °C, 22 h*

In 2008, Herrero and colleagues reported the effects of nonthermal microwave and conventional thermal conditions on the direct amidation reaction of methacrylic acid **23** with (*R*)-1-phenylethylamine **24** in the absence of activating or coupling reagents (Scheme **3**).[81] In a single mode microwave reactor, placing equivalent amounts of the starting materials at 180 °C monitored by a calibrated IR sensor, and applying simultaneous cooling afforded methacrylamide **25** in 90% yield after 15 minutes. The calibrated technique used estimated the real internal temperature to be around ca. 200 °C. Carrying out a similar experiment at the same reaction temperature and time by applying conventional heating afforded only 12% of **25**, while increasing the reaction time two-fold proved ineffective in improving the yields. It was further demonstrated that at the same temperature range, different product distributions were isolated when comparing the results from the microwave reactions and conventional heating.[81]

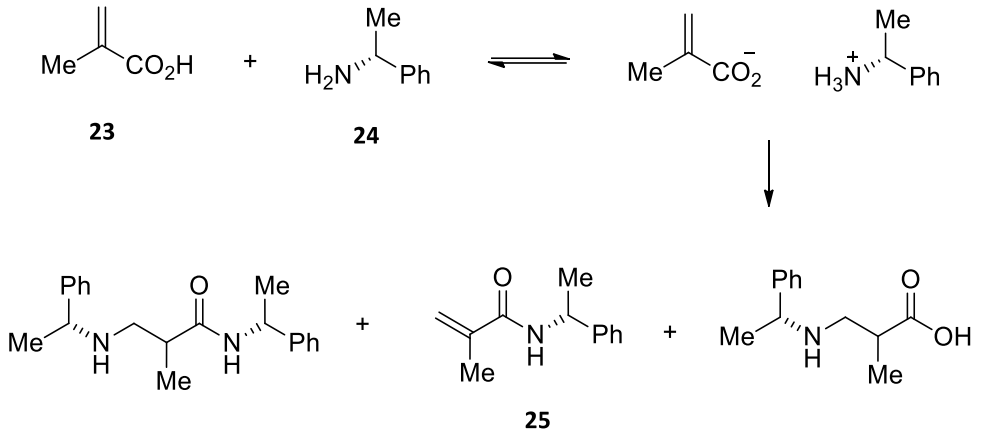

*Scheme **3** Amidation reaction between **23** and **24** by thermal and microwave energy*

Khadse and co-workers outlined the ring opening of dimethylaminobenzylidene oxazolone **26** (Scheme **4**), based on thermal effects, by employing conventional heating and induced microwave-assisted irradiation for the synthesis of benzamides.[82] It was reported that the conventional method was time consuming and resulted in decomposition of materials in the reaction vessel. Additionally, getting the desired product was difficult even when different solvents were used. Furthermore, a variety of by-products were obtained when performing similar reactions using polar solvents like dimethylsulfoxide or dimethylformamide, resulting in failure to separate the target compounds from the resultant mixtures. In contrast, when repeating similar reactions using microwave conditions, the reaction time was significantly decreased without decomposition and co-products, while minimal work-up was necessary for the product purity. Although direct interaction of the microwave energy with the reaction mixture accelerates the reaction, this method, however, suffers if the energy penetration depth is poor, thus, impeding the reaction scale-up.[82]

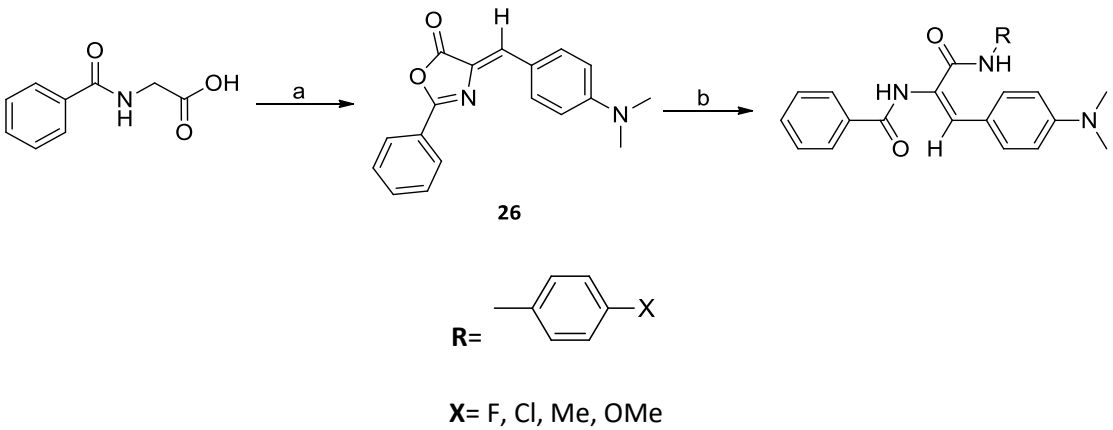

***Scheme 4** Reagents and conditions: (a) p-Dimethylaminobenzaldehyde, $(CH_3CO)_2O$, CH_3COONa, heat; (b) R-NH_2, acetonitrile, triethylamine, MW, 420-560 Watt, 8-20 min, 65%*

1.2.1.2.2 Amide synthesis using peptide coupling reagents

Direct amide synthesis can easily be performed from various commercially available reagents under mild reaction conditions.[74] The OH^- group is a strong base and a poor leaving group, so the OH^- from carboxylic acid needs to be converted into a reactive intermediate to create a better leaving group.[75] To circumvent the high energy barrier for making amides, these activating agents are commonly used to promote efficient amide bond formation, though the selection of an effective coupling reagent is imperative. As demonstrated by library-based synthesis in medicinal chemistry, a wide variety of substrates with different reactivities such as bulky substrates, secondary amines and anilines are often employed to produce amides. This broad range of reactivity would need to be well tolerated by the coupling reagents.[83] Forty-five percent of amidation reactions are reportedly conducted by employing carbodiimides that include 1-ethyl-3-(3-dimethylaminopropyl) carbodiimide **27**, *N*,*N*-dicyclohexylcarbodiimide **28**, and uronium salts like (2-(1*H*-benzotriazol-1-yl)-1,1,3,3-tetramethyluronium hexaflurophosphate **29**, and 1-[Bis(dimethylamino)methylene]-1*H*-1,2,3-triazolo[4,5-*b*]-pyridinium 3-oxide hexafluorophosphate **30**, while 4% are performed by using 1,1'-carbonyldiimidazole **31** and *n*-propylphosphonic acid anhydride **32** (Fig **13**).[73]

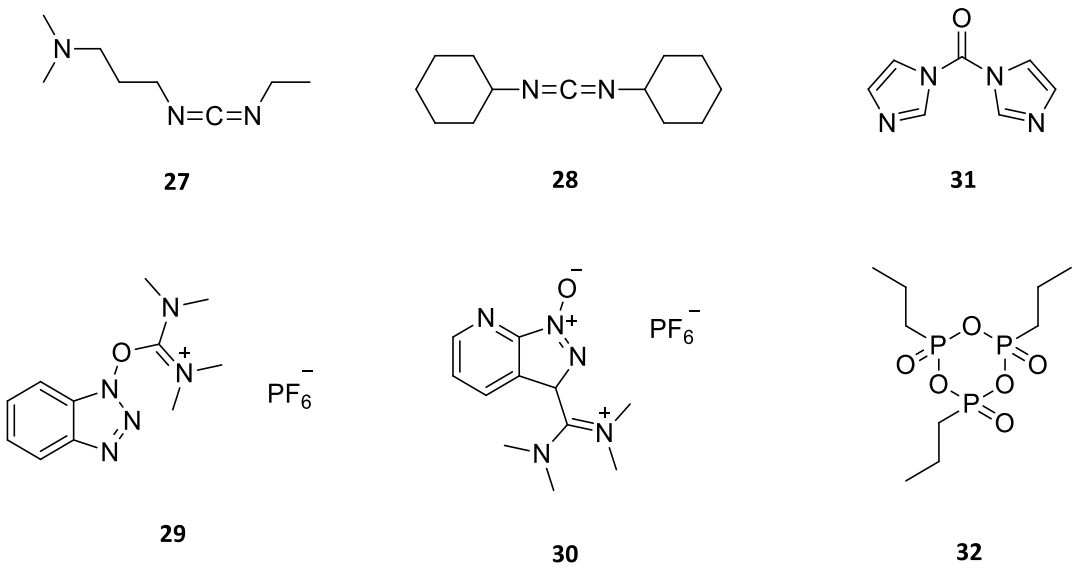

Fig 13 *Structures of carbodiimides and uronium salts*

DCC **28** was first documented in 1955 by Sheehan and Hess for coupling reactions of carboxylic acids and amines.[84a] Scheme **5** illustrates the coupling mechanism for which the two reagents combine. In the first step, carboxylic acid interacts with **28** to produce an active *O*-acylisourea intermediate **33** which in turn reacts readily with nucleophiles such as amines. Following the formation of this intermediate, a variety of products are produced;

(i) the amide formation through the amine coupling resulting in the establishment of dicyclohexylurea **34**. This by-product is a precipitate that can be eliminated by filtration.

(ii) a by-product referred to as *N*-acylurea **35**.[83] Ideally, the temperature should be low to prevent its production.[84a]

(iii) the carboxylic acid anhydride production, which upon interaction with the amine (often requires 2 equivalents of acid) provides the amide.[83] The reaction is usually carried out at equal stoichiometric amounts of all the necessary reagents which would need to be dissolved in various aprotic solvents that include but are not limited to DMF and chloroform.

For the formation of the desired amide product, the mixture is then subjected to ice-cold conditions and left overnight to reach room temperature. Where relevant, to lower the broad racemization that is observed with DCC alone in peptide and protein synthesis, *N*-hydroxysuccinimide (HOSu) is normally introduced to mediate the DCC coupling process[84a] due to its high nucleophilicity towards the carbonyl carbon of the carboxylic acid.[84c] The resulting HOSu ester rapidly reacts with the amino group of the protein[84b] preserving the chirality of the peptide activated compounds susceptible to racemization.[84c]

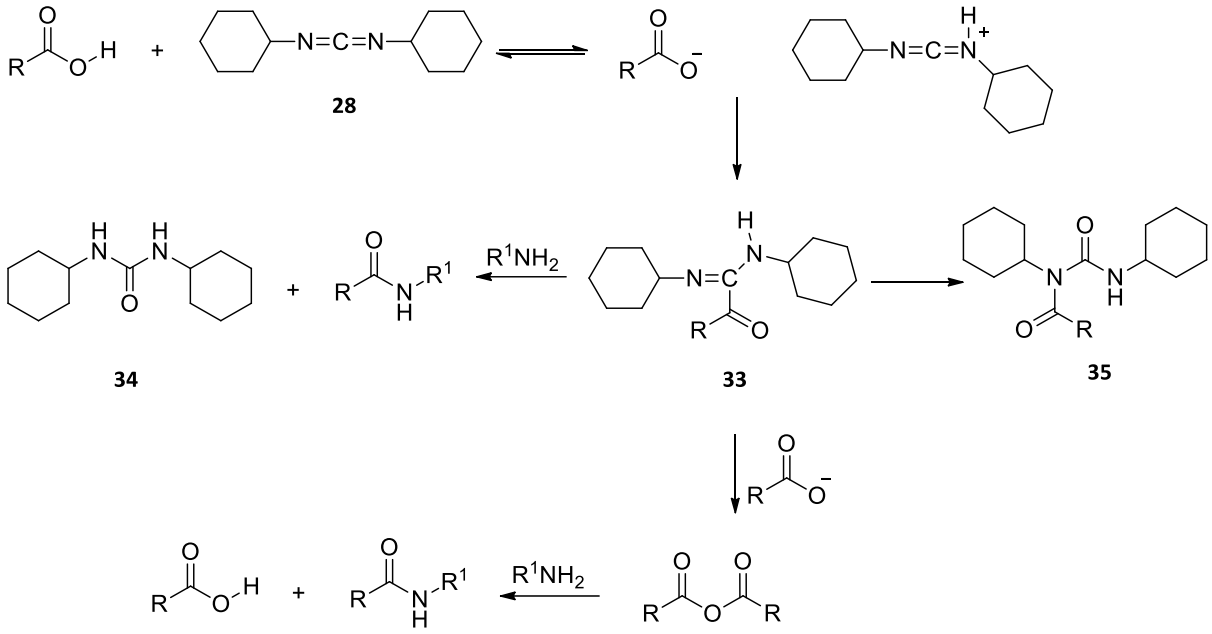

Scheme 5 *Mechanism of amide synthesis using DCC*[83,85]

For the synthesis of amide prodrugs **36**, Makhija *et al*[86] examined the reactivity of various nonsteroidal anti-inflammatory drugs and sulfonamides exemplified by ibuprofen **37** and suphamethoxazole **38**, respectively, employing DCC **28** in the absence of additives (Scheme **6**). To reduce the levels of *N*-acylurea **35**, the reaction of carboxylic acid **37** and **28** was allowed to proceed for 2 hours under the pre-cold conditions and left stirring overnight at ambient temperature. Once the reaction was

complete, elimination of dicyclohexylurea by filtration was applicable to afford derivative **36** in 76% yield.[86]

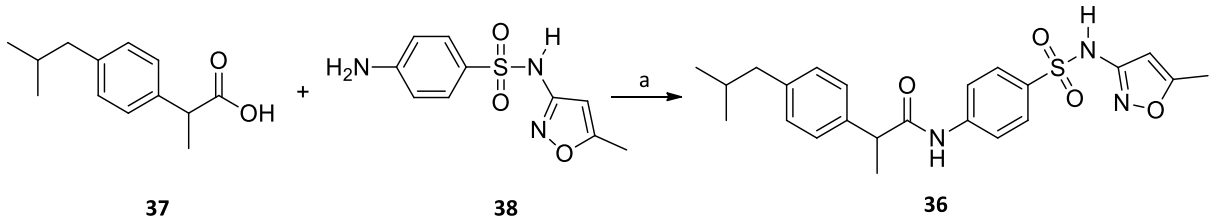

Scheme 6 *Reaction conditions: (a) DCC **28**, DCM, 0 °C, 2h, rt, overnight, 76%*

Since the unveiling of DCC **28** as a coupling agent in amidation reactions, several other carbodiimides such as CDI **31** have also been studied. For instance, Lee and Kim presented the efficient coupling of ammonium acetate (NH_4OAc) and carboxylic acid in the presence of **31** in ionic liquid medium for the preparation of primary amides **39** (Scheme **7**).[87] It was reported that the amide bond was successfully formed by one-pot sequential addition of the various carboxylic acids (Represented by **40**) and **31** in 1-butyl-3-methylimidazolium tetrafluoroborate ([BMIM]BF_4. Subsequent treatment with NH_4OAc and triethylamine (Et_3N) at 80 °C yielded the corresponding amide **39** in 92%.

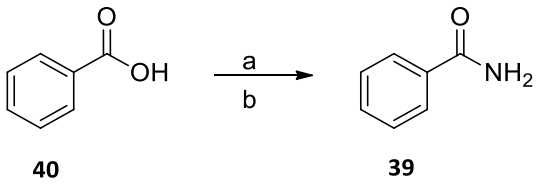

Scheme 7 *Reaction conditions: (a) **31**, [BMIM]BF_4, 80 °C, 2h; (b) NH_4OAc, Et_3N, 80 °C, 3 h, 92%*

Another popular peptide coupling reagent EDC **27**, also attracted a great deal of attention due to the ease with which its side product, dimethylaminopropyl-3-ethylurea is separable from the product. This urea is highly soluble and can effortlessly be removed during aqueous extraction.[88] In 1993, Desai and Stramiello performed amidation reactions using a polymer-bound EDC, where single coupled products with yields ranging from 77-97% were isolated. Chloroform was selected as a solvent of choice since performing the reactions in the presence of either tetrahydrofuran or ether led to insufficient swelling of reagents, resulting in slow reaction.[89] In 1995, Nakajima and Ikanda examined the function of **27** in an aqueous system to study the impact of dissociation and pH of the amino and carboxyl groups in amidation reactions.[90] In this study, hydrogels (Gel-A and Gel-B) containing carboxyl groups were used to simply separate the products from the reaction batch. In comparison to Gel-A, the amide formation was substantially elevated in Gel-B due to different positions where the carboxyl groups were situated along the polymer chains.[90]

Recently, Ghosh and Shahabi demonstrated that EDC **27** can effectively promote the coupling of *Boc*-protected acid **41** and electron deficient amine **42** in the presence of both the HOBt and DMAP coupling reagents.[91] It was shown that 0.1 equivalents of DMAP and HOBt were insufficient to promote the reaction since only 38% yield of **43** could be obtained. Instead, excess molar quantities of DMAP (1 equiv) were required to enhance the reaction yield to 72%. The general reaction mechanism to which both additives mediate the coupling is illustrated in Scheme **8**. The reactive HOBt ester **44** is produced during the interaction of acid **41** and **27** together with HOBt, followed by the acyl transfer formation of the highly reactive acyl iminium ion **45** driven by DMAP. The reaction between **44** and less reactive amines like aniline was anticipated to proceed slowly. In the last step, the reaction between **42** and intermediate **45** ought to proceed more rapidly, allowing the generation of DMAP and the formation of product **43**.

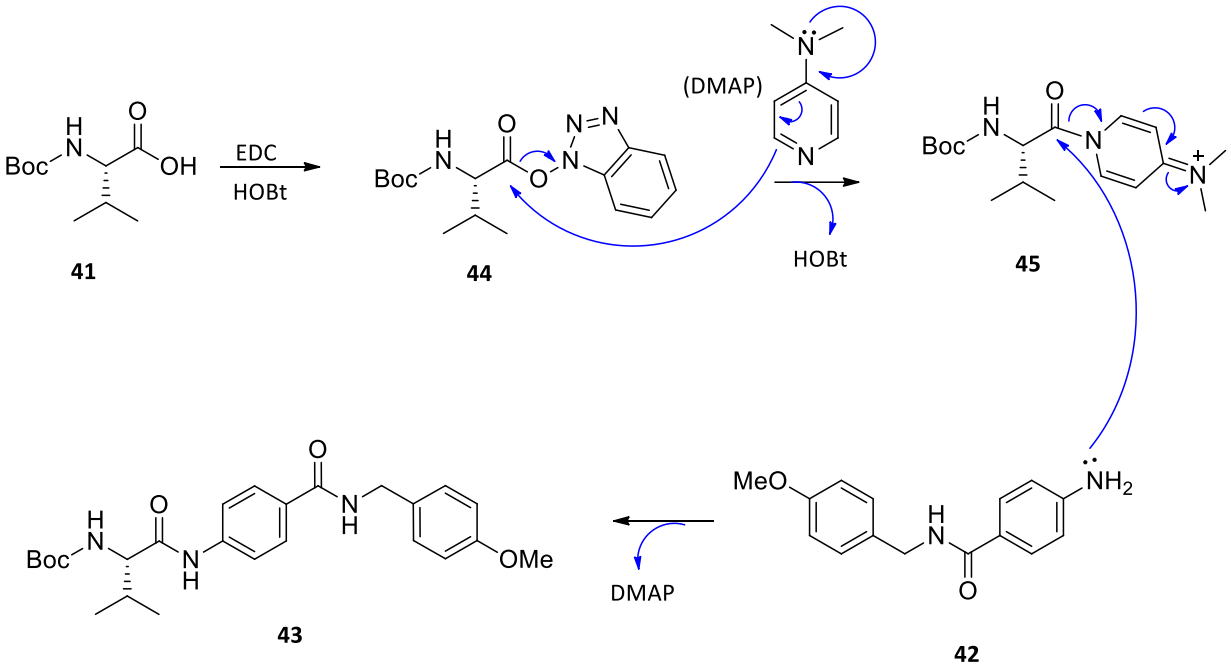

Scheme 8 *Mechanism of amide formation using EDC/HOBt coupling*

Despite the significance of the peptide coupling reagents to improve the yields and allow mild reaction conditions, excess stoichiometric quantities of these substances are needed. Consequently, each product molecule generates at least one comparable amount of waste, which is rendered strenuous and is time-consuming to eliminate from the reaction mixture, thus, raising transformation costs.[70,71,73,74,75,92]

1.2.1.5 Amide bond formation from acyl chlorides

The preparation of therapeutic agents by three pharmaceutical companies was examined in 2006, and it was discovered that out of 128 inspected compounds 65% contained a minimum of one amide unit.

It was reported that 36% of these compounds were synthesized through the application of coupling reagents, whilst 44% were made by employing acyl chloride precursors.[71] Acyl chlorides also known as acid chlorides, are one of the most common and straightforward intermediates convenient for the production of amide bonds which do not involve peptides, and are usually used when there is no risk for racemization, hydrolysis, or cleavage of the protecting groups. Acid chlorides are normally prepared using a vast array of chlorinating reagents such as phosphorous trichloride, phosphorus pentachloride, phosphorus oxychloride, oxalyl chloride, thionyl chloride,[88,93] or cyanuric chloride[75] (Fig **14**). The phosphorus, carbon, or sulphur atoms of these reagents activate the carbonyl carbon from the carboxylic acid[93] by providing the chloride which substitutes the hydroxyl group.

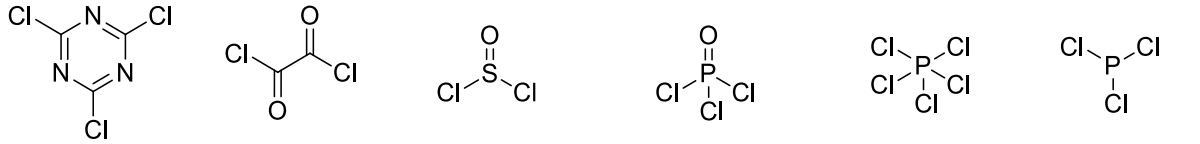

Fig 14 *Structures of chlorinating reagents*

$(COCl)_2$ is often used for the production of acyl chlorides in process chemistry. Its application is advantageous due to its low boiling point (61 °C) that makes it easier to remove from the reaction mixture by distillation.[94] However, owing to the stoichiometric liberation of three gases, carbon monoxide, carbon dioxide, and hydrochloric acid, the use of oxalyl chloride is somewhat toxic and potentially harmful. The phosphorus-containing reagents are often used in circumstances where the acid is incompatible with the thionyl chloride. [93] Although the phosphorus chlorinating reagents are relatively affordable and easily accessible, they are less frequently utilized on large-scale for the synthesis of the acid chlorides.[94] The most frequently reported methods involve the small-scale syntheses. For example, Boyer and co-workers reported the formation of picryl chloride using $POCl_3$ on a milligram scale.[95] Zeng and colleagues synthesized itaconyl chloride from itaconic acid and PCl_5 on a milliliter scale.[96] Various benzoyl chlorides were also produced on a millimole scale by Xiao and Han employing PCl_3.[97]

Cyanuric chloride is readily accessible on the market, non-expensive,[98] and can be used on large-scale processes. Its advantages include functional group tolerance, and reduced side-product generation. Additionally, the insoluble cyanuric acid by-product can be easily eliminated by filtration.[99] Senier heated cyanuric chloride together with sodium salts of the carboxylic acid at 100 °C for eight hours to prepare benzoyl and acetyl chlorides in 1886.[100] Venkataraman and Wagle performed similar reactions at room temperature for three hours. The acid chloride rapidly formed upon treating cyanuric chloride with two equivalents of the acid and triethylamine, through the sigma complex **46** (Scheme **9**),

occurring from a nucleophilic attack by the oxygen atom of the acid on cyanuric chloride. The resulting insoluble precipitate **47** described as a corresponding monoanilino or dianilino derivative, is termed chlorodihydroxy-s-triazine or dichlorohydroxytriazine.[100]

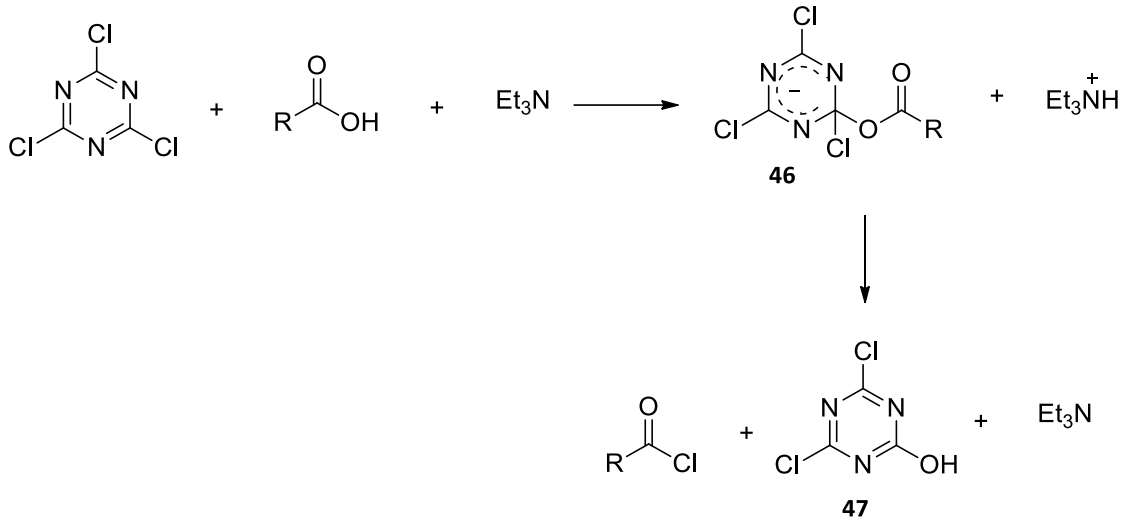

Scheme 9 *Acyl chloride formation from cyanuric chloride*

In 2002, Luo and colleagues prepared amino resin-bound dichlorotriazine (DCT) from a reaction of cyanuric chloride with the Wang alcohol resin as a chlorinating agent for the synthesis of acyl chlorides (Scheme **10**).[101] In 2008, Betti and co-workers demonstrated that cyanuric chloride can be used in ionic liquids for the Beckmann rearrangement of oximes to prepare amides.[102] Recently, Yadav and Awashthi prepared a triazine-linked covalent organic polymer from cyanuric chloride and *p*-aminophenol to effectively promote the coupling of carboxylic acids with amines.[103]

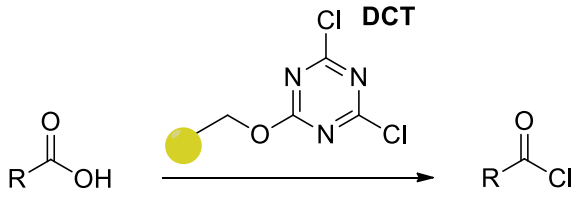

Scheme 10 *Acid chloride synthesis through DCT*

Thionyl chloride is the most popular reagent employed for the activation of carboxylic acids because it is volatile, inexpensive, and among the most cost-effective methods for making acyl chlorides.[93] The conversion of carboxylic acids into acyl chlorides through $SOCl_2$ can be done neat or using a solvent.[88] The most frequently reported solvents employed when carrying out reactions following the thionyl chloride route include *n*-heptane, acetonitrile, dichloromethane, toluene, and tetrahydrofuran.[94] Additionally, the application of thermal energy is required, and in some instances, pyridine can be added to speed up the process.[88] The thionyl chloride approach liberates sulfur dioxide and

hydrochloric acid gases as the only by-products present in the reaction vessel. These gases are considered non-carcinogenic although $SOCl_2$ and the generated HCl can practically pose significant challenges due to high corrosive nature of the acid. Owing to their low molecular masses can effortlessly be eliminated through distillation.[71] A schematic representation of amide bond formation is detailed below in Scheme **11**, where the carboxylic acid attacks thionyl chloride **47** to yield unstable and highly electrophilic intermediate **48**. Subsequently, protonation of **48** by the generated HCl gives rise to carbonium ion **49** which is attacked by a weakly nucleophilic chloride ion. The resulting intermediate **50** is a tetrahedral structure that can disintegrate into the acid chloride **51**, sulfur dioxide, and HCl.

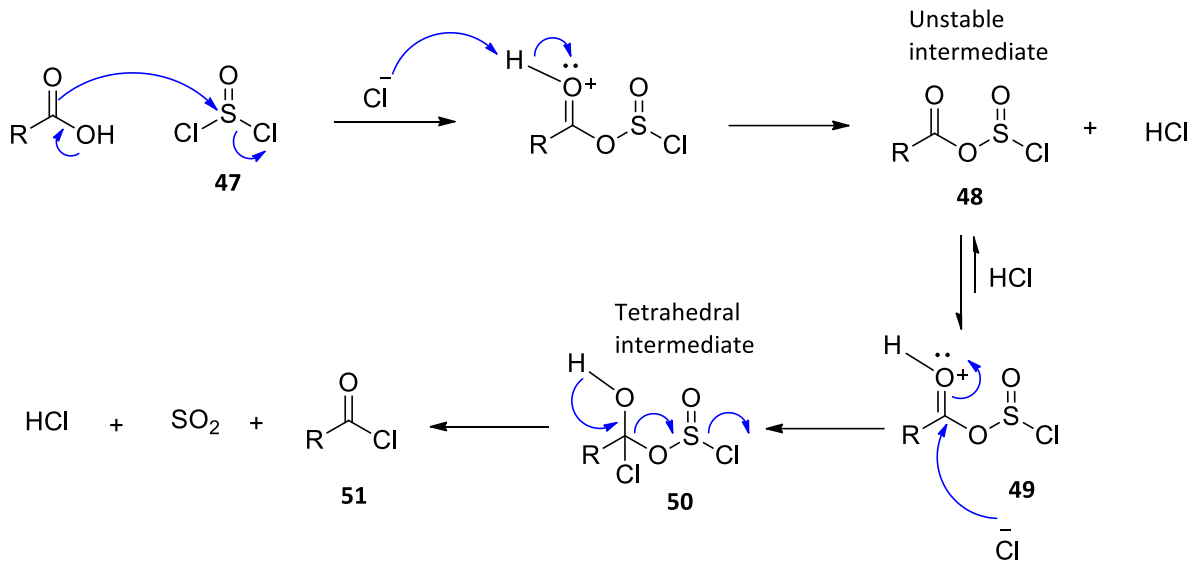

Scheme 11 *Mechanism of the acyl chloride formation*[104]

Upon the formation of the acid chloride **51**, subsequent *in situ* aminolysis can be carried out while using an organic base to prevent the deprotonation of an amine into its unreactive HCl salt and absorb the resultant HCl. Inert anhydrous solvents are typically used for the couplings with non-nucleophilic tertiary amines such as diisopropylmethylamine (Hunig' base), triethylamine, *N*-methylmorpholine,[88] or pyridine **52**. In rare instances, pyridine can be employed as a solvent to enhance solubility and accelerate the reaction. Since **52** reacts more effectively with **51** than amine **20**, it functions as an acyl transfer catalyst in the amination process via nucleophilic acyl substitution reaction resulting in the formation of acyl-pyridinium salt adduct **53** (Scheme **12**).[93] This behavior is attributable to the robust Lewis basic nature and comparative soft character of the nitrogen atom on **52**. Relative to the acyl chloride, the resulting ionic complex **53** is highly electrophilic and susceptible to nucleophilic attack by an amine, exacerbated by the nitrogen's positive charge.[93] Although acid chlorides are water sensitive, they can react with amines under aqueous conditions in the presence of sodium hydrogen carbonate,

potassium carbonate, potassium phosphate, or sodium hydroxide.[94] This transformation is commonly known as the Schotten-Baumann reaction.[70,71]

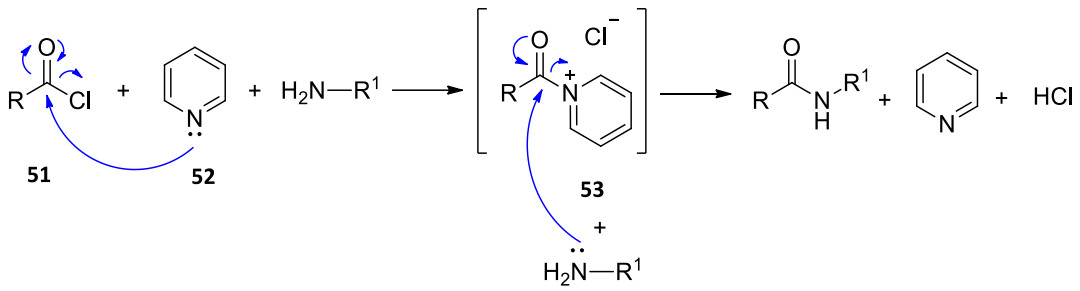

Scheme 12 *Mechanism amide bond formation by acyl-transfer with pyridine*

Kwolek and colleagues outlined the synthesis of poly(1.4-benzamide) **54** starting from the reaction of *p*-aminobenzoic acid with two equivalents of thionyl chloride under reflux for 3 h (Scheme **13**). [105] The resulting acyl chloride **55** was obtained in 95% yield and used for further derivatization to afford polymer **54**.

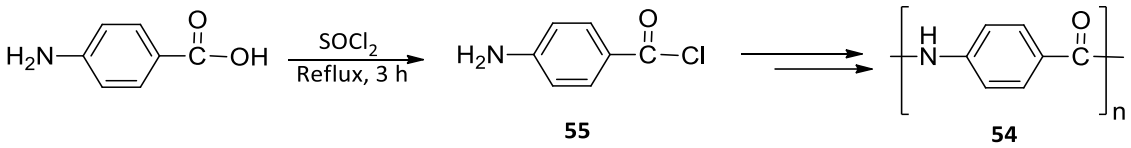

Scheme 13 *Synthesis of **54** via thionyl chloride route*

Acrylol chloride was prepared by reacting acrylic acid with thionyl chloride, and reacted without prior isolation with stoichiometric quantities of anilines using *N*,*N*-dimethylacetamide (DMAC) as a solvent in the presence of aqueous NaOH to give corresponding acrylamides in 88-98%.[106] It was observed that the use of DMAC offered benefits over DMF in terms of stability and conversion rates. However, because DMAC appeared to react with thionyl chloride, cautious addition was necessary to circumvent the reactivity problem. Similar reactions were carried out by heating acyl chlorides with stoichiometric amounts of benzylamine without the presence of a base resulting in 80-90% yields of benzylamides exemplified by **56** (Scheme **14**).[106]

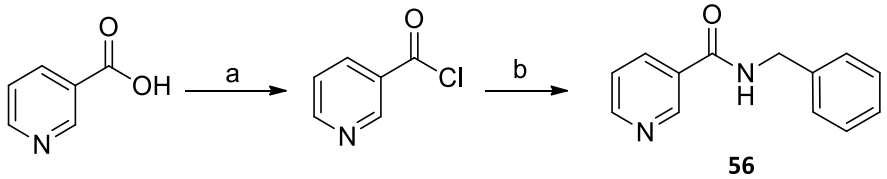

Scheme 14 *Reagents and conditions: (a) $SOCl_2$, DMAC, -5 °C; (b) benzylamine, 0-60 °C, 80-90%*

The synthesis of benzamides **57** as possible antiprofiliferative agents was reported by Asaki and colleagues.[107] In this experiment, various carboxylic acids were first esterified by ethanol, α-brominated, and coupled with *N*-bromosuccinimide. The resultant esters were hydrolyzed, and subsequently chlorinated with thionyl chloride under reflux. Successive amination of the corresponding acyl chlorides resulted in the formation of the desired benzamides **57** (Scheme **15**).[107]

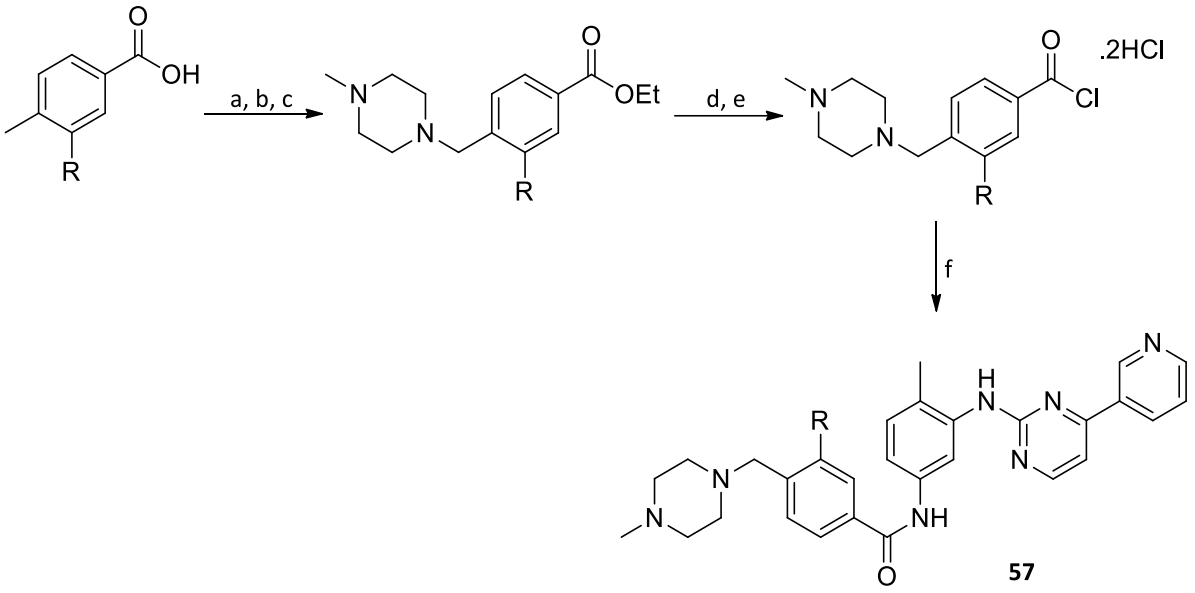

R= F, Cl, Br, I, CF_3

Scheme 15 *Reagents and conditions: (a) EtOH, H_2SO_4, reflux; (b) NBS (N-bromosuccinamide), CCl_4, cat. $(PhCO)_2O_2$, reflux; (c) K_2CO_3, 1-methylpiperazine, THF, rt; (d) 1 N NaOH, reflux, then aq. HCl; (e) $SOCl_2$, reflux; (f) 6-methyl-N1-(4-(pyridin-3-yl)pyrimidin-2-yl)benzene-1,3-diamine,* ***52****, rt,*

The antibacterial *N*-(3-hydroxy-2pyridinyl)benzamides **58** with the electron withdrawing R-groups, were synthesized by Mobinikhaledi and co-workers through the activation of carboxylic acids **59** with thionyl chloride (Scheme **16**).[108] A drop-wise addition of the resultant acid chlorides **60** to an ice-cold solution of 2-amino-3-pyridinol, sodium carbonate, diethyl ether, and water afforded benzamide derivatives **58** in 40-65% yields.

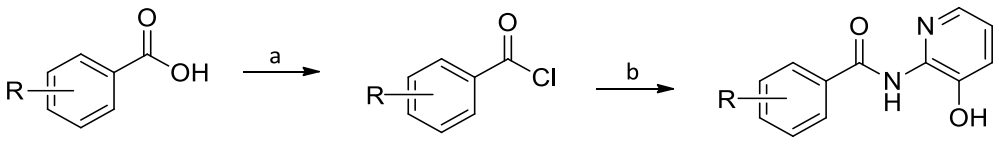

59 **60** **58**

R= 4-nitro, 3,5-dinitro, 4-chloro-3-nitro

Scheme 16 *Reagents and conditions: $SOCl_2$, benzene, reflux, 1-2 h; (b) 2-amino-3-pyridinol, K_2CO_3, diethyl ether, H_2O, rt, overnight, 40-65%*

Davi and colleagues reported the preparation of mono-amide ligands through the conversion of picolinic acid and pyridine-2,6-dicarboxlic acid into their corresponding acid chlorides using thionyl chloride.[109] During the picolinic acid activation, a pair of products **61** (31-54% yield) was isolated after the *in situ* reaction of picolinoyl chlorides with the corresponding anilines. Each pair contains a minor product **62** (10-13% yield) substituted with a chlorine atom at the *para*-position to the ring nitrogen (Scheme **17**).[109] It was assumed that the ring was chlorinated when the pyridine ring was activated during a nucleophilic attack by the chloride anion. This was suggested to have occurred either at the time of the coupling process or during the acid chloride formation.

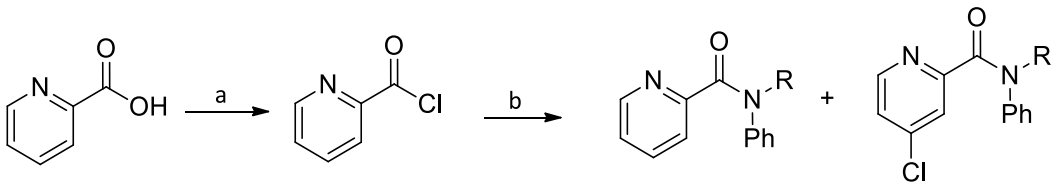

61
major

62
minor

R= Me, Et, Ph

Scheme 17 *Reagents and conditions: (a) $SOCl_2$, reflux, 16 h; (b) N-methylaniline or N-ethylaniline or N-diphenylaniline, DCM, rt, 16 h, 10-54%*

Jagtap and colleagues reported a one-pot synthesis of benzamides by combining benzoic acid **63** with different amines induced by thionyl chloride under catalyst, solvent, and ligand free conditions at room temperature.[110] The reaction proceeded for 2-4 hours, and the products were isolated in 80-94% yields. The reaction shown below (Scheme **18**) proceeds in a similar manner as previously described.

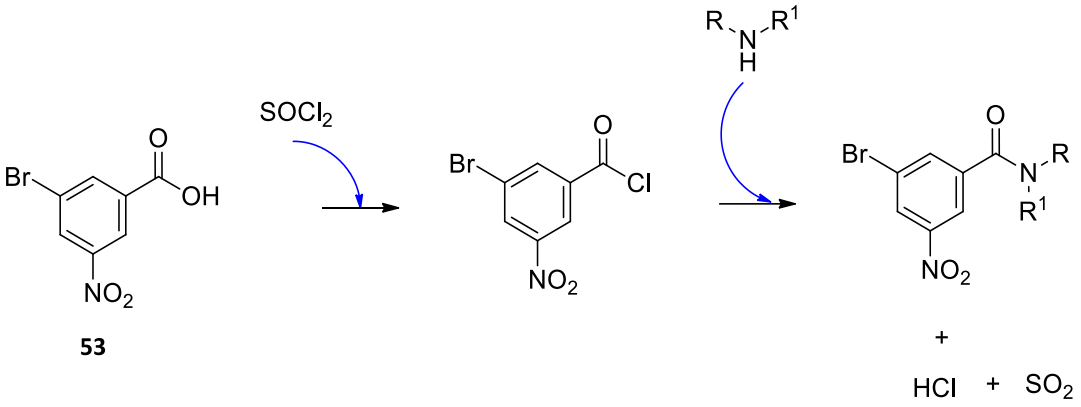

*Scheme **18** Reported formation of the amide bond*[118]

Leggio and co-workers also outlined a one-pot synthesis of amides from various benzoic acids and amines employing thionyl chloride.[111] Initially, the reaction between benzoic acid and diethylamine was put to test in the presence of triethylamine as a base, and thionyl chloride as a promoter (Scheme **19**). A complete reaction conversion was realized within 5 minutes, the corresponding *N*,*N*-diethylbenzamide **54** was isolated in 86% yield. A second experiment was carried out to examine how the reaction would proceed without the use of triethylamine. The reaction was conducted by combining equimolar amounts of all the reagents involved in the reaction such as thionyl chloride, benzoic acid, and diethylamine in dichloromethane at room temperature. The reaction did not go to completion after 20 minutes in the absence of a base resulting in the recovery of benzoic acid **40** in 65 % and isolation of **54** in 31% yield. The order in which the reagents were added also was shown to have a significant impact on the reaction's outcome. A series of analogues were therefore synthesized using triethylamine, which occurred according to the reaction scheme illustrated below (Scheme **19**).[111]

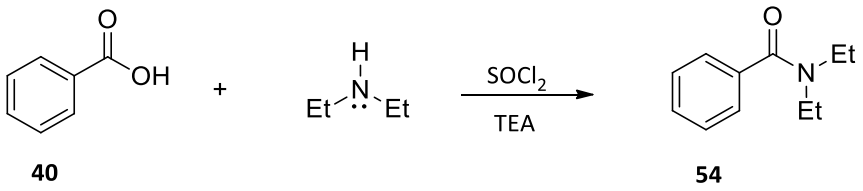

***Scheme 19** One-pot amide bond formation*

1.2.2 Pyrimidines as key structural components

The pyrimidine nucleus is an azaheterocyclic structure[112] related to the benzene ring, which is characterized by the replacement of two ring carbons in the first and third positions of its six-membered ring with electronegative heteroatoms nitrogen atoms. This results in an increased electron density on the nitrogen atom, accompanied by greater electron deficiency on the remaining carbon atoms. Due to this lack of electron density, the carbon atoms are susceptible to nucleophilic

attack, followed by nucleophilic displacement of a suitable leaving group, particularly at the α- and y-positions to the ring nitrogens.[113] Pyrimidine-containing heterocycles are of tremendous interest because they present a vital class of both natural and synthetic compounds.[114] These aza-substituted arenes are also useful as electron donating ligands in coordination chemistry that serve as suitable substitutes for pyridines.[112]

1.2.2.1 Biological activity of pyrimidines

In a wide array of natural products and biologically active scaffolds, heteroatoms and heterocyclic compounds are typically found as familiar cores. According to statistics, 85% of all bioactive substances contain heterocycles or are heterocyclic compounds themselves, with nitrogen-based heterocycles constituting the most common backbone in these complex structures.[115] The pyrimidine moiety can be found in a broad range of commercially marketed medications with adenine **55** and thiamine **56** amongst the most popular examples of biological or pharmaceutical molecules (Fig **15**).[112] Thymine **57**, uracil **58**, and cytosine **59** are other relevant pyrimidine-based compounds which are vital as components of DNA and RNA nucleic acids.[114]

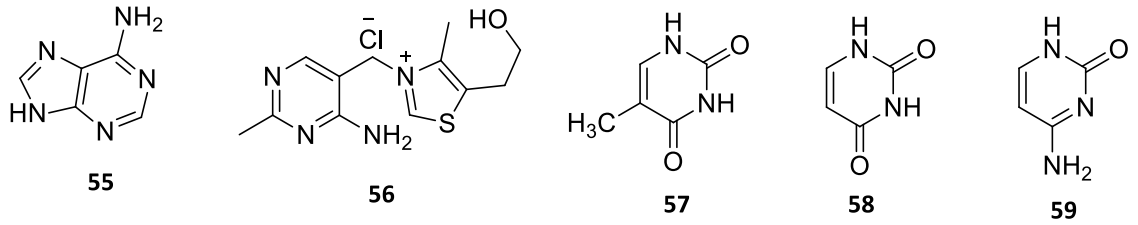

Fig 15 *Structures of pyrimidine-containing substances*

The pyrimidine skeleton has additional significant chemical and pharmacological activities as a compound of veterinary and agrochemical products.[116] It was discovered to possess antihistaminic, antioxidant, anticonvulsant, antidiabetic, antipyretic, antihypertensive, analgesic, anti-inflammatory, antileishmanial, antifungal, herbicidal and antibacterial properties.[114,117] A number of pyrimidine derivatives some of which are shown in Fig **16**, are said to exhibit anticancer (Compounds **60**-**63**) and antiviral (Compounds **64**-**67**) characteristics.[116] For this reason, pyrimidine synthesis is a crucial area of attention to synthetic chemists and novel approaches are reported.[112]

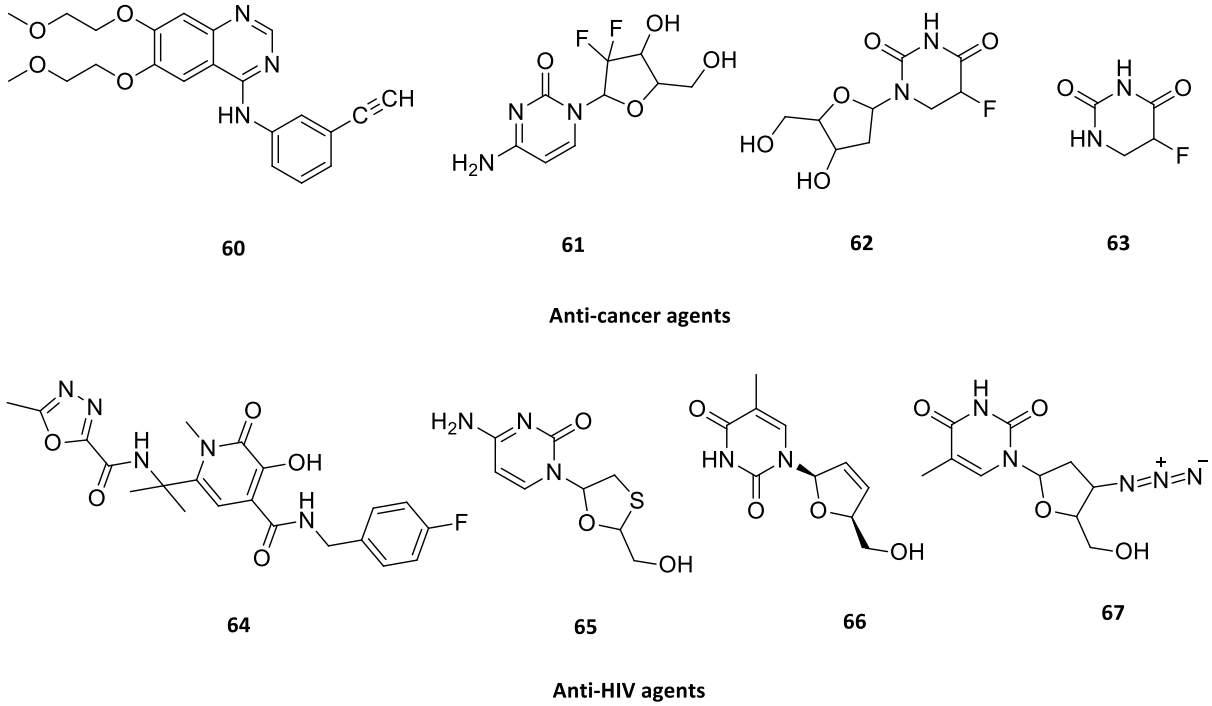

Fig 16 *Anti-cancer and anti-HIV drugs containing the pyrimidine pharmacophore*

Adding to the antiviral activity of the pyrimidine derivatives, dihydrothiopyrano[4,3-*d*]pyrimidine **68**[118] and dihydrofuro[3,4-*d*]pyrimidine compounds **69** and **70** have been evaluated as potential NNRTIs with promising antiviral properties.[119] Kang and colleagues designed a library of thiophene[3,2-*d*]pyrimidine compounds as possible HIV-1 NNRTI drugs (Fig **17**).[120] All the compounds were proven to show moderate or superior activity against the wild-type virus in MT-4 cells. The sulphonamide derivatives **71** (Fig **17**), were particularly found to be active against the entire viral panel, excluding REFS056. Both compounds demonstrated excellent antiviral effectiveness against the K103N mutant at EC_{50} values of 0.032 and 0.070 µM respectively, and potent against the E138K with EC_{50} values up to 0.035 and 0.045 µM respectively. Moreover, they functioned as conventional NNRTIs and displayed substantial affinity for the wild-type virus at IC_{50} values of 1.041 and 1.138 µM respectively. Wang and co-workers assessed a range of hydrazone-substituted thiophene[3,2-*d*] compounds and tested them for their anti-HIV-1 potential .[121] The results indicated that compound **72** (Fig **17**), exhibited the best anti-HIV potency (EC_{50}= 21.2 nM), with more than 10-fold increased effectiveness over nevirapine (EC_{50}= 281 nM). Furthermore, compared to nevirapine, etravirine, and azidothymidine, **72** displayed significantly less cytotoxicity (CC_{50}= 183 M) with a high selectivity index (8632).

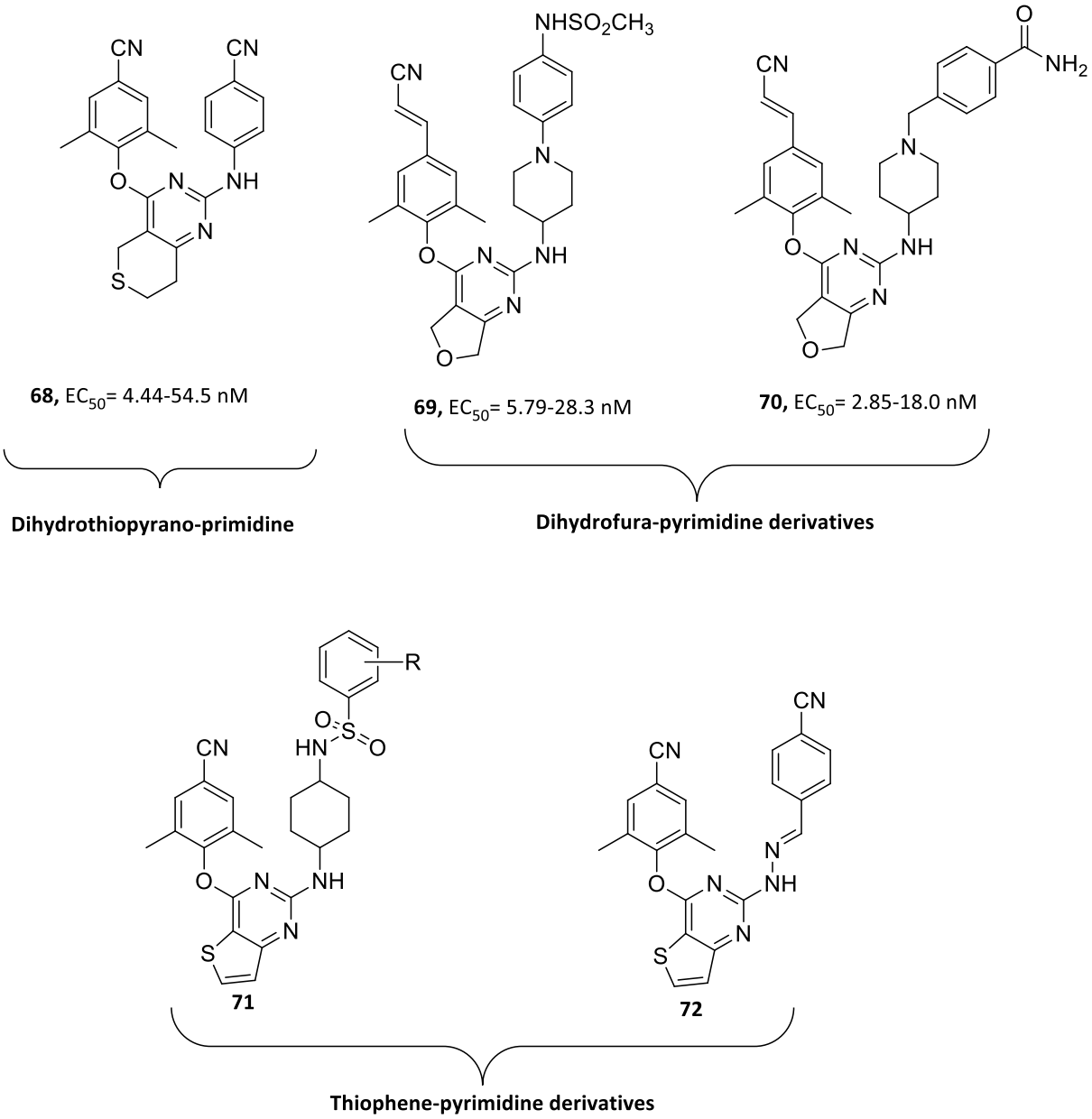

Fig 17 *Reported pyrimidine derivatives potent against HIV*

Dihydro alkoxy benzyl oxopyrimidine **73** (Fig **18**) compounds were identified as an intriguing class of NNRTI agents introduced over the past three decades.[48,51,58] DABOs belong to a family of heterocyclic compounds that share the pyrimidine backbone as a prevalent structural feature with the HEPTs **74** and DAPYs (represented by **7**, Fig **18**), that allows them to directly interact with the NNIBP.[58] The 4-pyrimidinone-based DABOs are structurally related to HEPTs when the N-1 substituent on the HEPTs is shifted to the second carbon atom of the pyrimidine ring, resulting in considerable anti-HIV potency.[48]

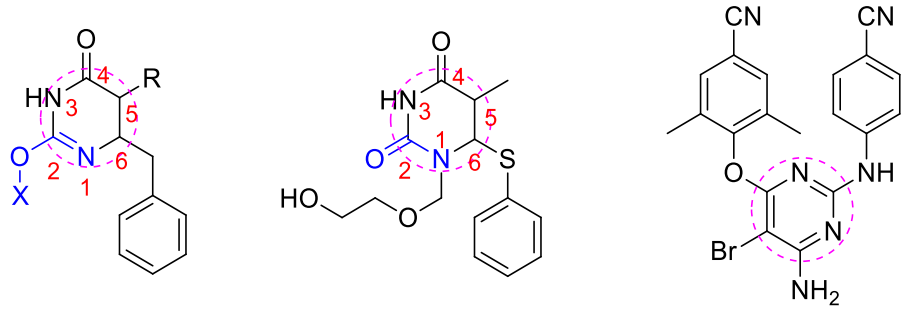

Fig 18 *Structural similarities of DAPY* ***7****, DABO* ***73*** *and HEPT* ***74***[48]

Following the initial publication of the DABO compounds in 1992, several structural modifications have been made throughout the years leading to the discovery of numerous DABO analogues which include N-DABOs, S-DABOs, and other similar derivatives to improve their antiviral efficacy.[51] 2-Alkylthio-6-benzylpyrimidin-4(3*H*)-ones (S-DABOs) have since then sparked the extensive curiosity of researchers, resulting in the revelation of various novel analogues with outstanding antiviral activities as NNRTIs.[51] Modifications on S-DABO compounds **75** (Fig **19**), led to the synthesis of various analogues based on SAR for the purpose of enhancing their antiviral activity.[122] It was revealed that the alkylthio side chains of S-DABOs are essential structural features necessary for anti-HIV-1 efficacy of these compounds, whereas eliminating the C-2 linker resulted in reduced antiviral activity. Displacing a benzyl moiety at the C-6 position of the pyrimidine ring with the phenyl or *n*-propyl (derivatives **76** and **77** respectively), resulted in substantial loss of the anti-HIV-1 activity. While the introduction of the bulkier groups like 1-naphthylmethyl and 2-naphthylmethyl motifs afforded compounds (**78** and **79** respectively) with reduced activity concentrations, reasonable anti-HIV-1 potencies were observed in systematic modifications with the phenylethyl, phenoxymethyl, and (phenylthio)methyl (**80**) substituents at the 6-position. It was further emphasized that the antiviral activity was lost when exchanging the substituents at the C_5 and C_6 positions as represented by scaffolds **75** and **81**.[122]

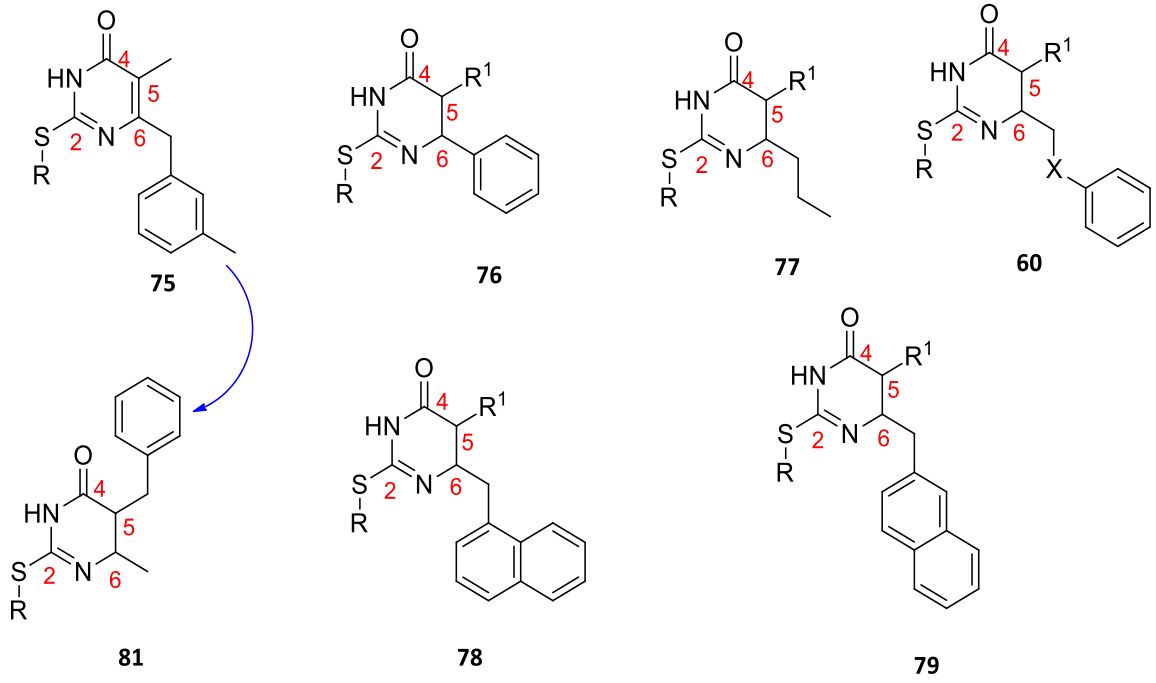

R= *sec*-butyl, cyclopentyl, cyclohexyl; **R**^{1}= H, Me; **X**= CH_2, O, S

Fig 19 *S-DABO lead compounds*

Vig and colleagues reported structural alterations by introducing alkyl groups on the 6-benzyl ring and C-5 position of the thymine ring, while keeping the C-2 linker fixed.[123] In cell-free inhibition, compounds with bulkier substituents displayed superior IC_{50} values with better composite binding pocket filling. A good agreement was demonstrated by the improvement in the inhibitory efficacy that occurred as isopropyl, ethyl, and methyl groups were introduced to the thymine ring at the C-5 position (Table **1**). Compound **82** bearing the methyl motifs at the 6-benzyl ring improved hydrophobic interaction with the NNIBP and was marginally more active against recombinant HIV RT than its related analogues **93**-**85** containing hydrogen atoms at the same position. Despite the lower IC_{50} concentrations in recombinant RT in cell free tests, compound **82** lacked the capacity to reduce the replication of HIV in cells infected with HTLVIIIB, presumably due to their distinct intracellular metabolism and cellular absorption.[123]

Table 1: The results of S-DABO effects on p24 synthesis in peripheral blood mononuclear cells infected with HIV, purified recombinant HIV RT enzymatic potency, and peripheral blood mononuclear cells feasibility.[123]

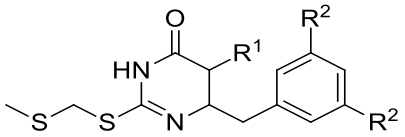

Compound Number	R^1	R^2	IC_{50} [rRT] (µM)
82	*i*-Pr	Me	4.8
83	*i*-Pr	H	6.1
84	Me	H	18.8
85	Et	H	9.7

Manetti and co-workers explored the role played by the expansion of the alkylarylthio linker on anti-HIV efficacy, given that this type of substitution at the second position of the S-DABO compounds is rarely studied.[124] Therefore, while maintaining 2,6-dichlorobenzyl at the 6-position and *p*-methoxyphenyl attached to the S-alkyl n-linker, the antiviral activity of compounds **86** varied depending on the length of the extension (n= 1, n= 2, and n= 3 respectively) of the C-2 alkyl chain. The scaffold linked by an ethyl core was the most effective S-DABO derivative with respect to its shortened n= 1 and lengthened n= 3 analogues and showed superior anti-HIV activity in cell assays infected with pluriresistant (IRLL98) and WT viruses. However, a shortened linker gave a compound with the improved activity against the WT-RT, with notable efficacy against IRLL98. The reduced activity of the expanded derivatives against the WT virus was attributed to diminished hydrophobic contact of the benzyl motif at C-2, including the solvent and the methyl group adverse interactions. Molecular modelling calculations demonstrated that the Leu234, Leu100, Trp229, Phe227, and Tyr188 aromatic side chains that construct the hydrophobic region, allow the 6-benzyl ring of **86** (n= 1) to fit properly within the location (Fig **20**). Conversely, expansion of the benzyl group, caused the 4-methoxy moiety to exceed the Pro225 and Pro236 apertures, leading to undesirable interactions with the solvent, thus, resulting in restricted hydrophobic engagements between the phenyl ring and Val106.[124]

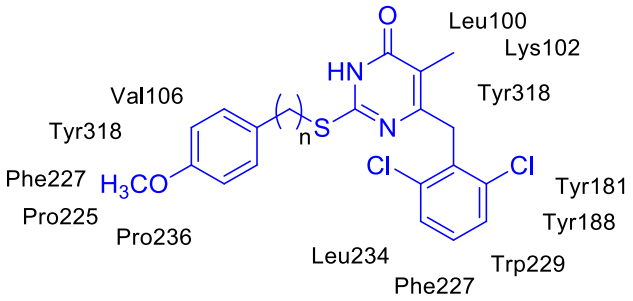

86

Fig 20 *Structure for S-DABO derivative* ***106*** *and surrounding reported mutations*

1.2.2.2 Pyrimidine synthesis and reactions

1.2.2.2.1 Pyrimidine core formation

Gabriel and Colman have been widely acknowledged by various researchers for their breakthrough in isolating the parent compound **87** in 1899[112,125,126] through decarboxylation of pyrimidine-4-carboxylic acid **88** (Fig **21**).[112]

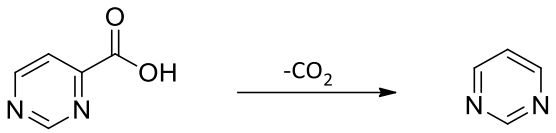

88 **87**

Fig ***21*** *Formation of* ***87*** *via decarboxylation of* ***88***

Oostveen *et al*[127] published a paper on the synthesis of unsubstituted pyrimidine **87** by dissolving 1-methylpyridinium methyl sulfate in liquid ammonia under extremely cold conditions (-33 °C) for one hour. After the second process of ring opening and ring closure, 6-amino-1-methyl-1,6-dihydropyrimidine **88** transformed into 2-methylamino-1,2-dihydropyrimidine **89**, which then aromatized to afford pyrimidine **87** in 55-60% yield (Scheme **20**).

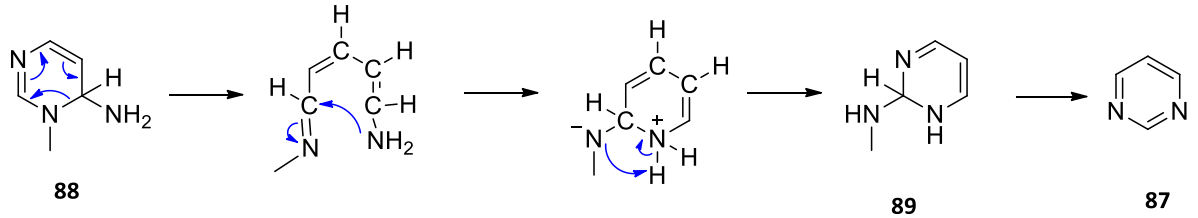

88 **89** **87**

Scheme 20 *Formation of unsubstituted pyrimidine*

1.2.2.2.2 Synthesis of simple pyrimidine derivatives

A quest for a quick transformation to produce more substituted pyrimidines remains fundamental among organic chemists since these templates can be employed to synthesise important intermediates or final compounds. Brugnatelli[128] prepared the first pyrimidine derivative, alloxan **90** in 1818 through the oxidative degradation of uric acid by nitric acid (Scheme **21**).[128]

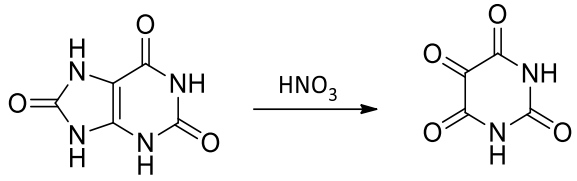

90

Scheme 21 *Brugnatelli synthesis of alloxan* ***90***

The Frankland and Kolbe synthesis is also a popular method known[112,129] for the preparation of a pyrimidine derivative, cyanalkine **91** (Scheme **22**) is obtained via treatment of propionitrile with potassium metal under thermal conditions.[129]

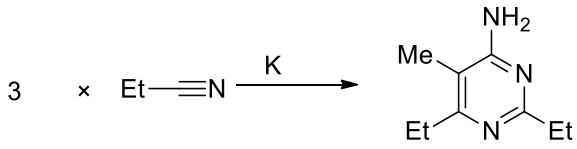

91

Scheme 22 *Frankland and Kolbe synthesis of cyanalkine* ***91***

The Pinner reaction evolved as the preferred method for making pyrimidine derivatives.[130] This method entails the condensation reaction of amidine **92** and 1,3-dicarbonyl **93** (Scheme **23**), which enables the synthesis of several substituted pyrimidines **94**. However, this strategy is frequently impeded by harsh reaction conditions and occasionally results in low yields.[112]

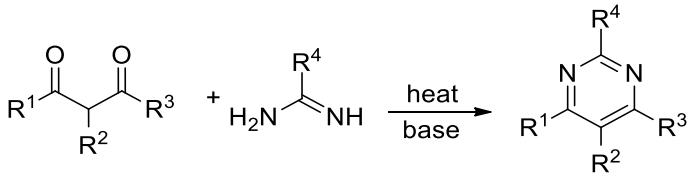

93 **92** **94**

Scheme 23 *Pinner synthesis*

Consequently, a variety of techniques have also been researched to broaden the application and increase the chemical effectiveness of the pyrimidine syntheses. Several of the widely used methods rely on the nitrogen-containing fragments starting from either urea, guanidine, or thiourea. Acetyl

acetone is a great illustration of this approach since it reacts well with the nitrogen-based fragments for the synthesis of dimethyl-substituted pyrimidines (Scheme **24**).[131]

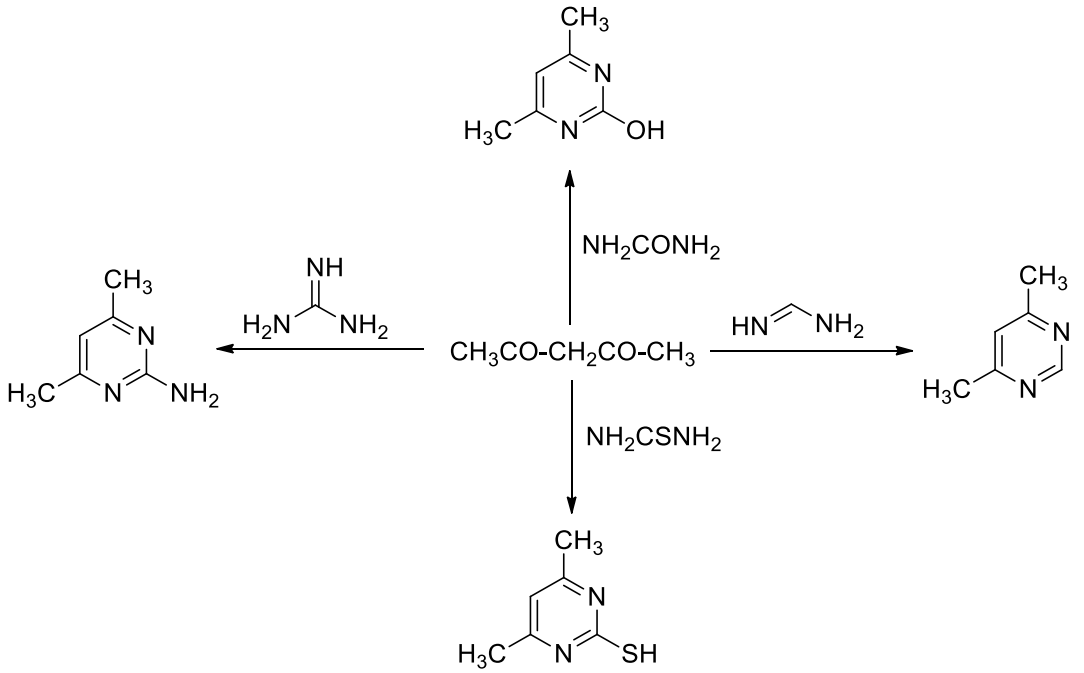

Scheme 24 *Production of dimethylpyrimidines*

Nitriles are considered as valuable nitrogen units of the nitrogen-containing fragments to create various pyrimidine derivatives. Cyanamide **95** (Scheme **25**) is specifically a helpful nitrile source that allows the formation of the pyrimidines.[129]

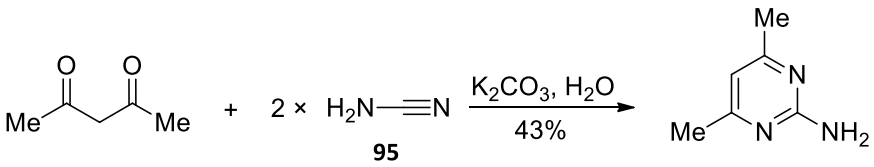

Scheme 25 *Synthesis of pyrimidine derivatives from nitriles*

The synthesis of several pyrimidine compounds, 6-methylthiouracils was published by Tominaga and colleagues using *N*-bis(methylthio)methylenecyanamide **96** as a nitrogen source. Subsequent reaction of **96** with various methylene derivatives employing potassium carbonate or potassium hydroxide at room temperature provided pyrimidine derivatives **97** in 15 to 80% yields (Scheme **26**).[132]

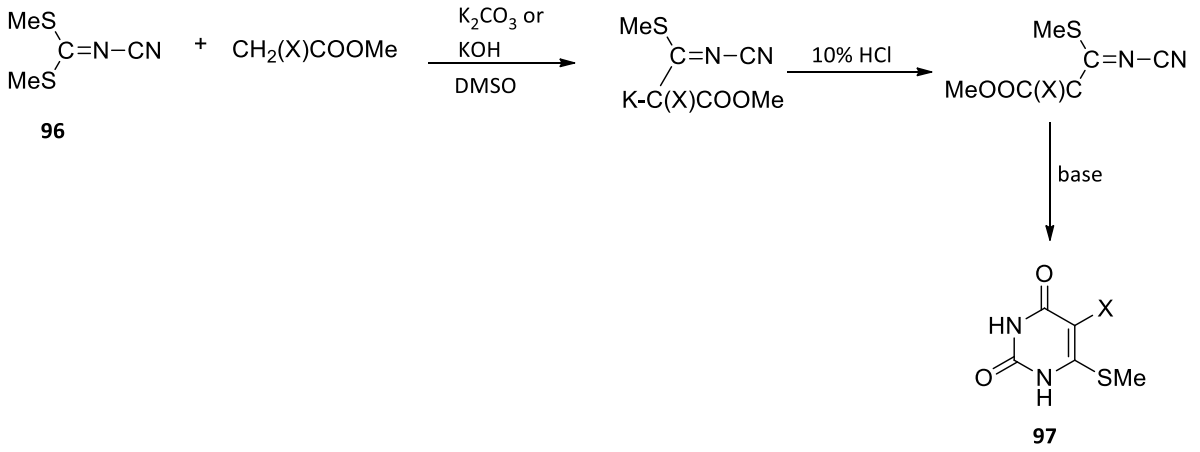

X= CN, COOMe, COMe, C_6H_5

Scheme 26 *Synthesis of pyrimidines from N-bis(methylthio)methylenecyanamide* ***96***

Within biological synthesis, the pyrimidine ring is naturally formed by the reactions of aspartate, bicarbonate, and glutamine. Four enzymatic processes transform these initial ingredients into orotate **97** (Scheme **27**), which is a ribonucleotide biosynthesis precursor.[129,133] Glutamine and bicarbonate are converted by carbamoyl phosphate synthetase II into carbamoyl phosphate, which is successively condensed with aspartate through catalysis by aspartate transcarbamoylase, resulting in the formation of *N*-carbamoyl-aspartate **98**. The elimination of water results in ring closure to form dihydroorotate **99** which is in turn oxidized to provide orotate **97**.[129,133]

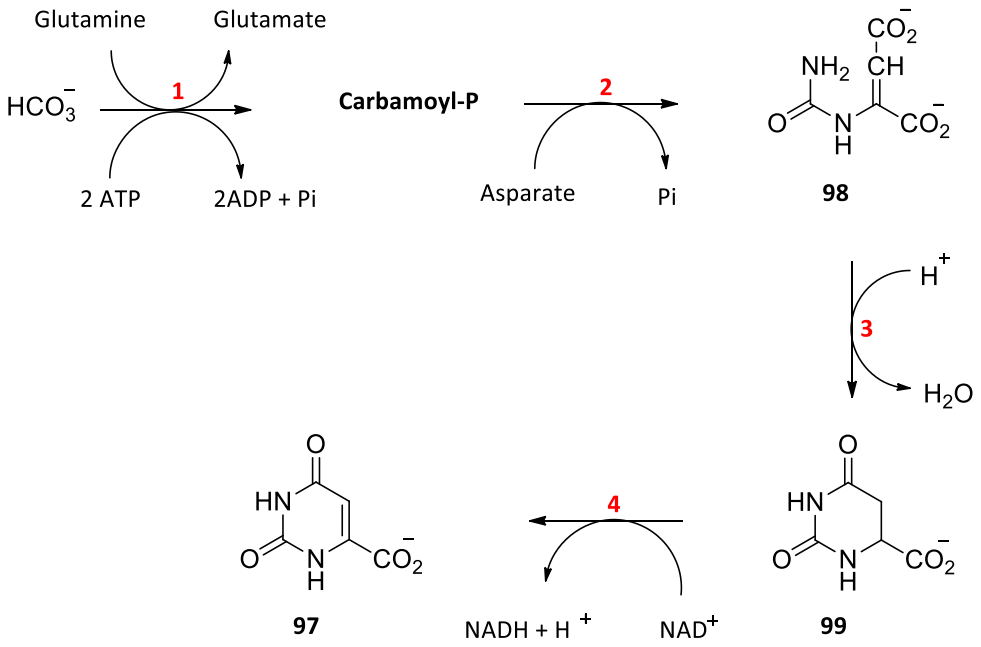

Scheme ***27*** *Mechanism of formation of orate* ***97*** [141]

Methyl 2-cyano-3,3-bis(methylthio)acrylate **100**, was treated with a variety of amides employing sodium hydride in a 1:1 ratio of benzene and DMAC at ambient temperature for 30 hours to give pyrimidine analogues **101** in 90 to 98% yields. The mechanism of formation of the pyrimidine is depicted in Scheme **28**.[134]

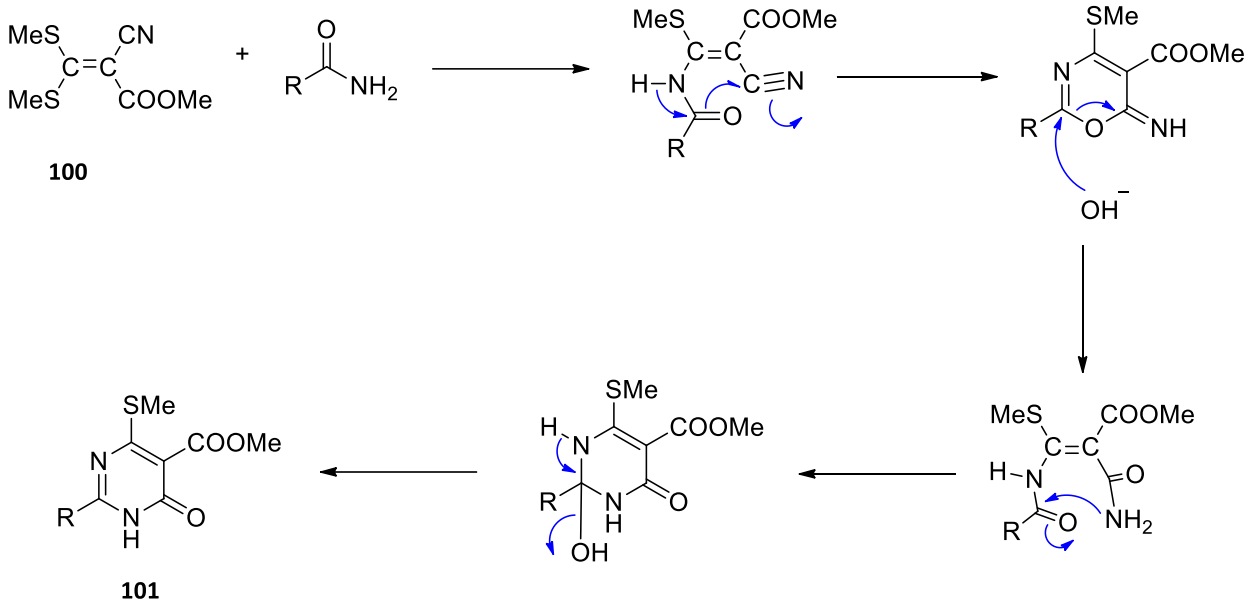

R= C_6H_5, *p*-O_2N-C_6H_4, *p*-Me-C_6H_4, *p*-MeO-C_6H_4, styryl, Cl-CH_2

Scheme 28 *Synthesis of pyrimidines from Ketene dithioacetal* ***100***

1.2.2.2.3 Synthesis of more complex pyrimidine derivatives

The pyrimidine motif largely exists as a component of more complex structures and is extensively studied.[125] Apart from the versatility of the previously reported techniques for the formation of simple pyrimidine derivatives, the innovative novel approaches to synthesize complex pyrimidine compounds have attracted the attention of researchers. In particular, pyrimidine halides (Fig **22**), have reportedly served as core intermediates to a wide array of substituted pyrimidines owing to their pi-electron deficiency and tri-halide functionality.[135] Additionally, their halogen atoms are good leaving groups and susceptible to nucleophilic displacement reactions.[136] One of the favoured techniques for derivatizing aromatic compounds is a nucleophilic aromatic substitution reaction which can function through a plethora of different chemical pathways.[135] The S_NAr process is inexpensive and simple as opposed to the commonly employed metal mediated coupling reactions[137] like Suzuki-Miyaura, Heck and Buchwald-Hartwig. Three fundamental factors that govern the extent of this reaction are (i) the lack of electrons at the electrophilic carbon in a heterocyclic system, (ii) the type of a leaving group to be replaced, and (iii) the nucleophile's reactivity. The most effective substrates for this process have turned out to be halogen-substituted aromatics. Considering that the order of reactivity for aliphatic

nucleophilic substitution generally increases with the size of a halide anion (I- > Br- > Cl- >> F-), this pattern is typically inverted for S_NAr reactions.[135] Therefore, 2,4,6-trifluoropyrimidine **101** is deemed more reactive to undergo aromatic nucleophilic substitutions than its related trihalogenated pyrimidines like 2,4,6-trichloropyrimidine **102** and 2,4,6-triiodopyrimidine **103**.[17] However, electrophile **102** is considered useful for enabling possible incorporation of several substituents onto the pyrimidine ring system.[136] Three chlorine atoms on azaheterocyclic compound **102** readily replaced by a variety of oxygen, mercapto, and nitrogen nucleophiles.

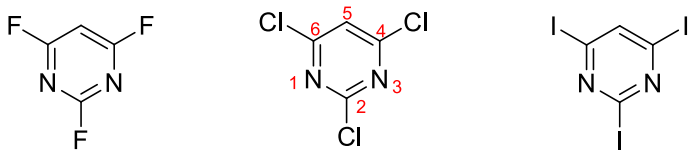

101 **102** **103**

Fig 22 *Trihalogenated pyrimidines*

The positional replacement of the halogen atoms in halopyrimidines generally occurs in the following order: 4>2>6.[138] Pyrimidine nucleophilic displacement is predicted on the idea that, excluding some *ortho*-directing effects, the reactivity increases *para* to the activating ring nitrogen. The most reactive locations for nucleophilic attack are either C-2, the region between the ring nitrogens, or C-4/6, the region *ortho* and *para* to the ring nitrogen. The transition states in which the nucleophile and ring-nitrogen are furthest away (C-4/6 > C-2) are predicted to have a significantly lower activation energy.

In comparison to a triazine precursor, the selectivity in the order of nucleophilic chlorine displacements in trichloropyrimidine, poses some dificulties.[139] For instance, **102** was used in the synthesis of other pyrimidine-halogenated systems like **101** and **103** (Fig **22**), which were used to study the preferred nucleophilic site of attack for direct arylation by the Suzuki coupling process relative to the trihalogenated precursor **102**. It was observed that arylation of **103** under Suzuki coupling reaction conditions with one equivalent of phenylboronic acid heated at 70 °C resulted in a mixture of low yielding di- and tri-substituted products, while arylation of tri-fluoropyrimidine was completely impossible. Conversely, although trace amounts of di- and tri-functionalized pyrimidines appeared when **102** was treated with one equivalent under similar conditions, the desired mono-substituted product was obtained in 88 % yield. Noticeably, increasing the stoichiometric quantities of phenylboronic acid increased the frequency of chlorine displacements, and C-4/6 was the second preferred site of nucleophilic attack over C-2 when using two equivalents (Scheme **29**).[140]

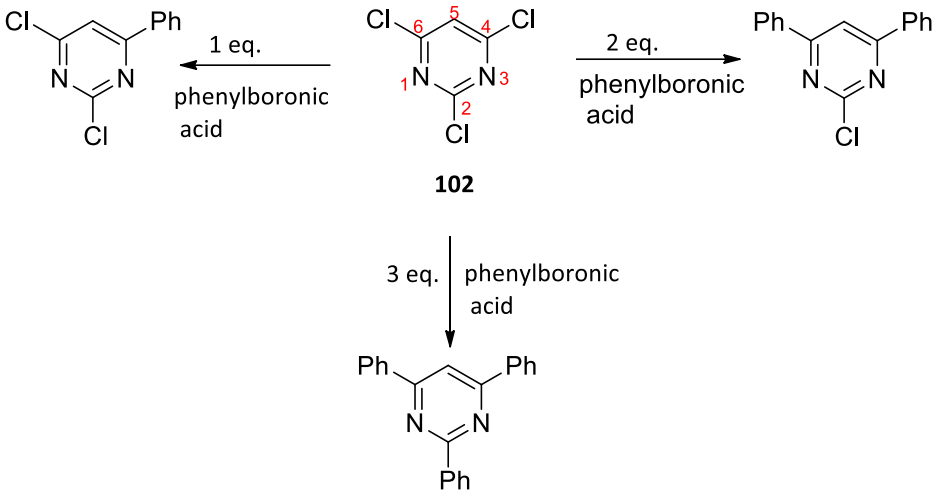

Scheme 29 *Arylation of* ***102*** *with phenylboronic acid*

Delia and Nagarajan investigated the possibility of attaining selectivity and sequential replacements of the chlorine atoms when treating **102** with various *para*-substituted aryloxides.[141] It was shown that **102** reacted well with one equivalent of phenoxide nucleophiles **104** at ambient temperature in the presence of an equimolar amount of sodium hydroxide. A mixture of isomeric monosubstituted products **105** and **106** was obtained in ratios ranging from 8:2 to 9:1 respectively (Fig **23**). Noticeably, these reactions were highly dependent of the thermal energy used and molar quantities of bases and nucleophiles. For example, intermediates **105** and **106** were not used for further derivatization, instead, a mixture of diaryloxypyrimidines **107** and **108** (obtained in approximately 1:1 ratio) appeared when **102** was heated to reflux with two equivalents of **104** and excess sodium carbonate. Even the final product **109** was achievable by reacting **102** and **104** with three equivalents of sodium hydroxide at approximately 50 °C.[141] These observations are in good agreement with the idea that selectivity can be obtained by adjusting the type of phenoxide ion, quantity, concentration, and reaction conditions when substituting a chlorine atom on pyrimidine with O-nucleophiles.[138]

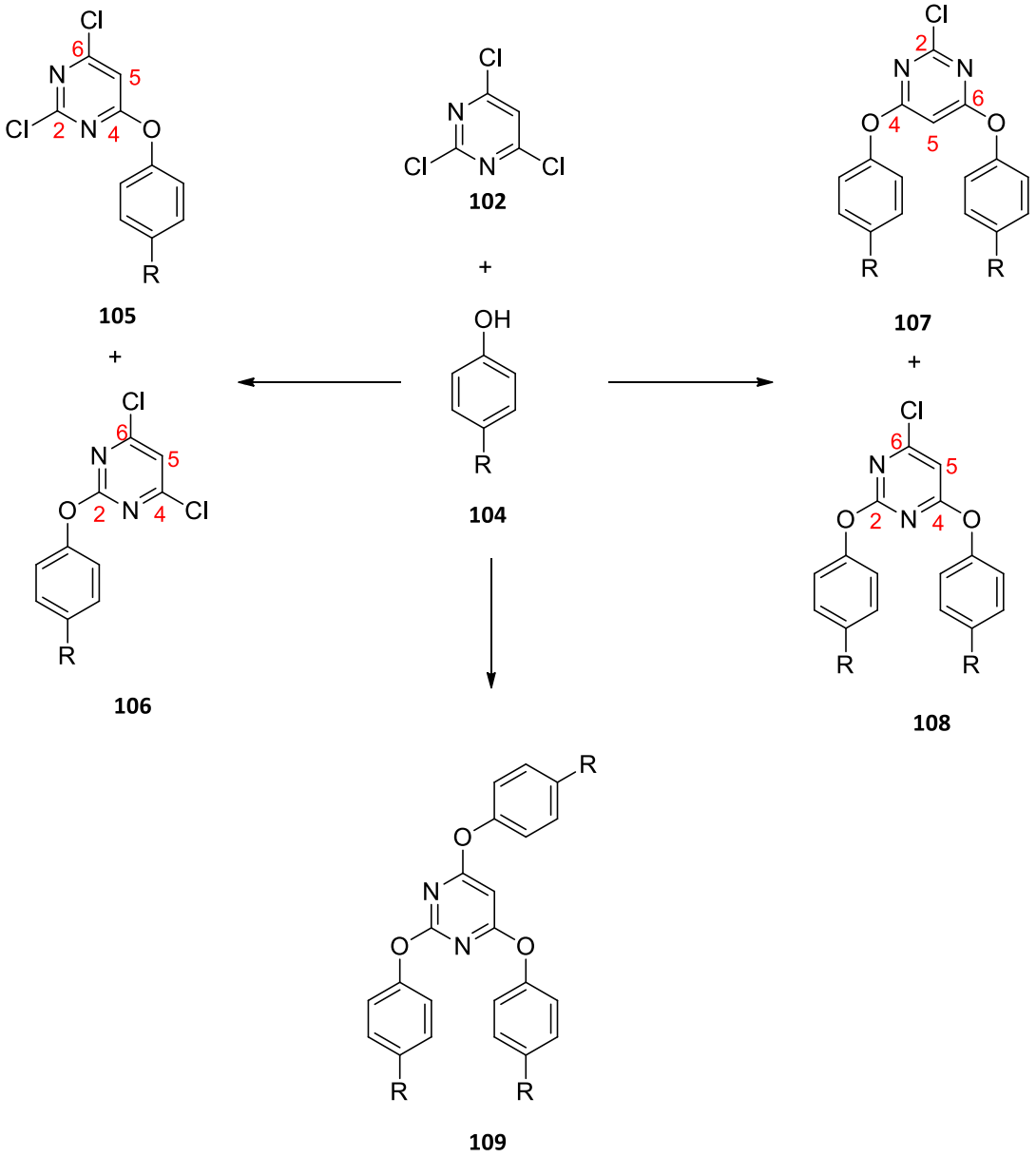

Fig 23 *Replacement of chlorine atoms on* ***102***

These reactions were believed to undergo S_NAr (addition-elimination), and the Meisenheimer intermediate provides an excellent explanation for the difference in reactivity between the C_2-Cl and C_4-Cl bonds. In the *para*-quinoid structure **110**, the ring nitrogen that is opposite to the tetrahedral carbon can tolerate a negative charge better as opposed to the nitrogen atom in the *ortho*-quinoid structure **111** (Fig **24**).[141]

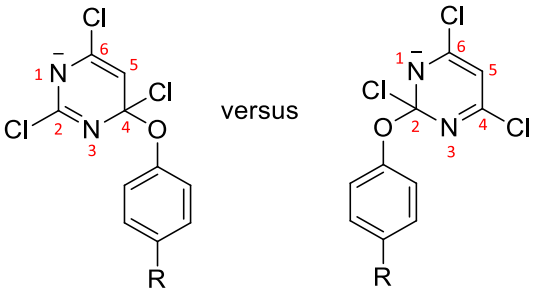

110 preferred **111**

Fig 24 *Structures of para-quinoid* ***110*** *and ortho-quinoid* ***111*** *intermediates*

Compounds prepared by sequential halogen displacements of **102** were assessed as PI_3 kinase inhibitors. Nucleophilic aromatic substitutions of the first two chlorine atoms were followed by displacement of the third chlorine atom through a cross-coupling reaction (Cross-coupling not shown) (Scheme **30**).[139] Although the first chlorine substitution with morpholine proceeded more readily than replacement with primary amino alcohols, subsequent treatment with a primary amine required long reaction times with low product yields. Furthermore, the mixtures of monosubstituted intermediates **112**:**113** and **115**:**114** were obtained where the 4-Cl was the favoured position for nucleophilic attack compared to the 2-Cl position in both reactions. A good yield of 76% for product **116** was achievable when amino alcohol was added first, followed by the second chlorine displacement on intermediate **114** by morpholine (Scheme **29**). [139]

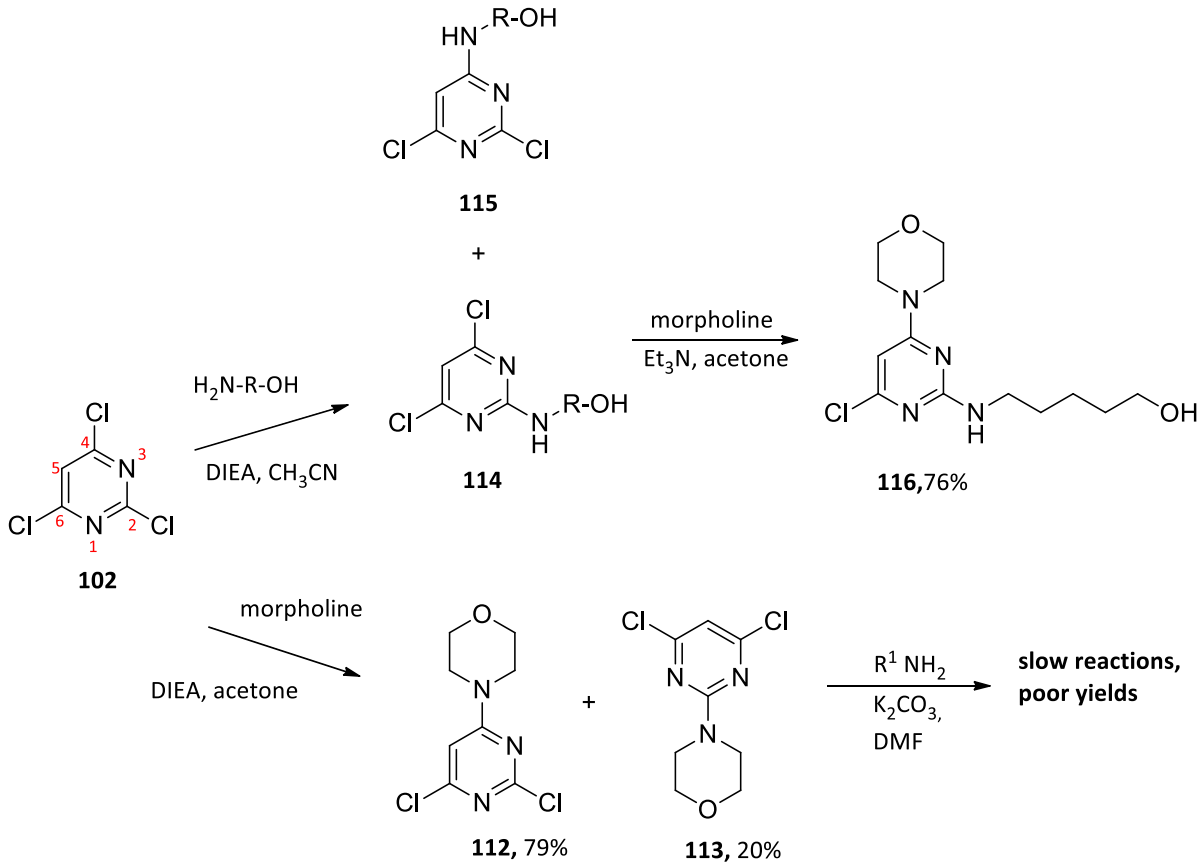

114, R= $(CH_2)_6$ (37%), CH_2PhCH_2 (13%)

115, R= $(CH_2)_6$ (55%), CH_2PhCH_2 (35%)

Scheme 30 *Nucleophilic displacement reactions of chlorines on* ***102***

2,4,6-Trichloropyrimidine **102** was evaluated for the preparation of HIV-1 inhibitor **7**, given that the known synthetic approaches pose certain drawbacks like slow reactions and low conversion rates, thus contributing to the high cost of etravirine **7**.[142] The reaction of **102** with equimolar quantities of 4-hydroxy-3,5-dimethylbenzonitrile **117** in the presence of a weak base such as potassium carbonate yielded intermediate **118** and its isomer **119**. The percentage yield of **118** was higher compared to that of **120** due to the currently known selectivity differences between the 2-Cl and 4/6-Cl bonds. Treatment of dichloropyrimidines **118** with 4-aminobenzonitrile **121** gave rise to the monochloropyrimidine **122** and isomer **123**. Finally amination of **122** by microwave-assistance and bromination of **123** resulted in the formation of **7** (Scheme **31**). Among the reported synthetic routes thus far, the 2,4,6-trichloropyrimidine route is the most efficient process to produce etravirine since the product yield was improved from 30.4 to 38.5%.[142]

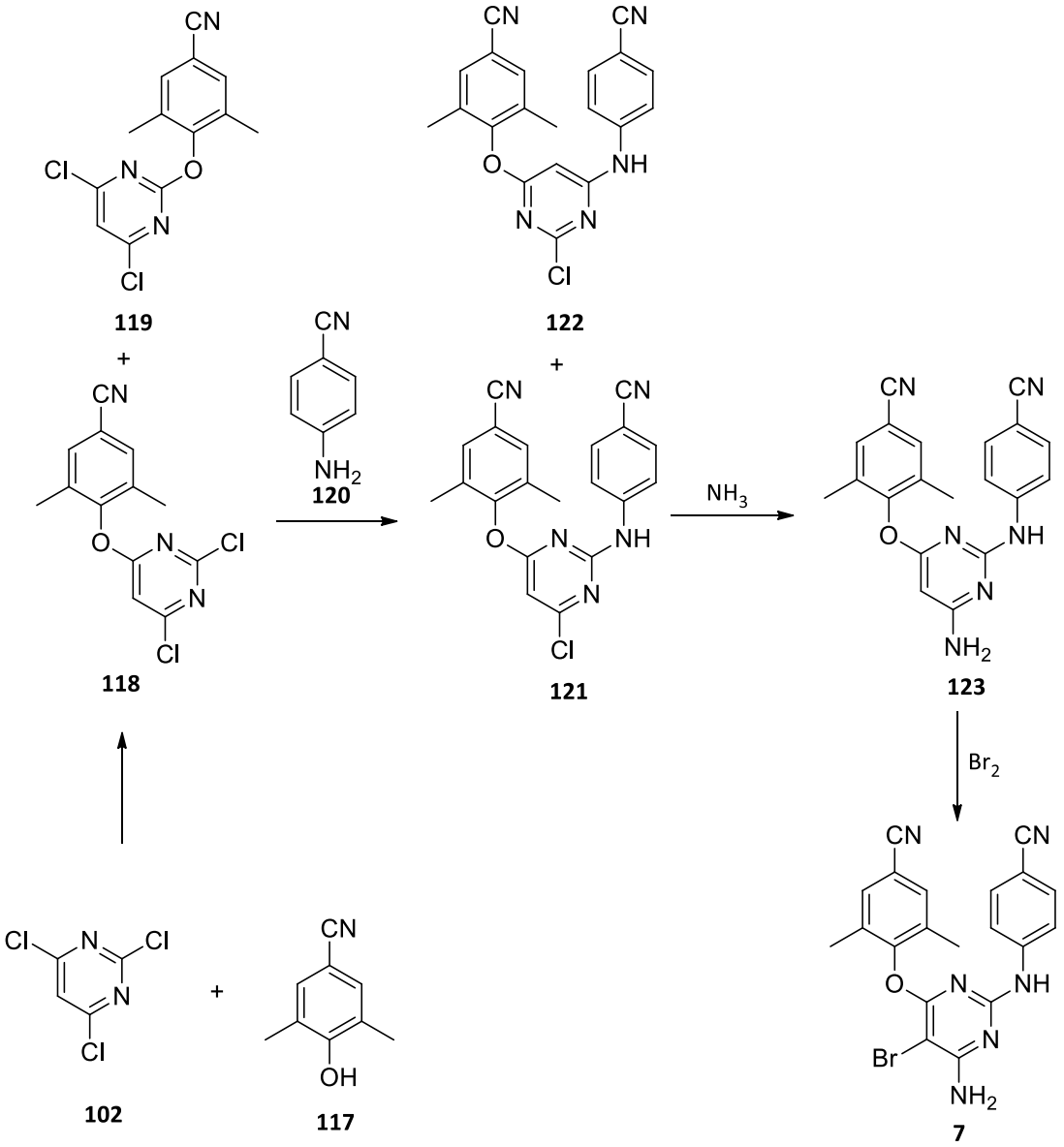

Scheme 31 *The synthesis of* ***7*** *starting from* ***102***

Work done in our laboratory identified etravirine-related analogues exemplified by compounds **124** (Scheme **32**) derived from 2,4,6-trichloropyrimidine **102** for synthesis and anti-HIV activity testing. The reaction of **102** with 4-chlorophenolate ion **125** under prolonged ice-conditions favoured the *para*-position, and subsequent addition of various amine nucleophiles **126** at room temperature displaced the second chloride in the 2-position of the pyrimidine ring to give the corresponding analogues **124**.[59]

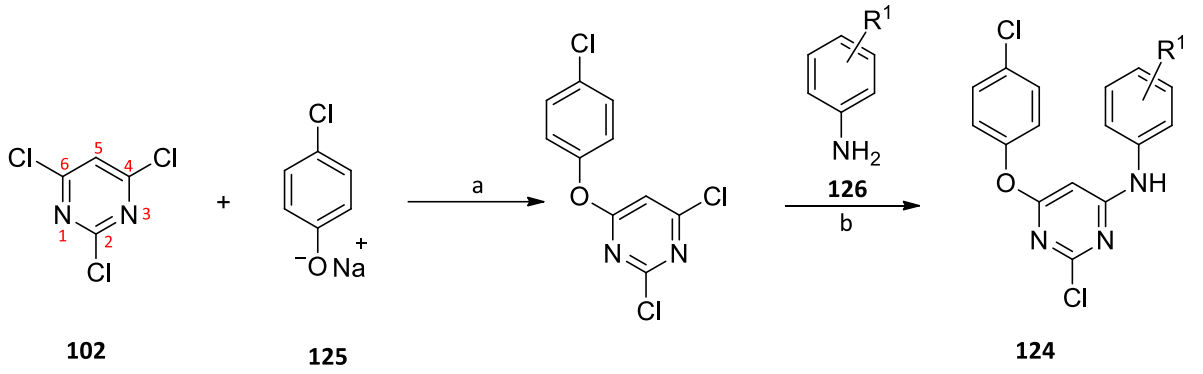

102 **125** **124**

R[1]= Me, Br, Cl, CN

Scheme 32 *Reagents and conditions: (a) acetone, 0 °C-rt, 2 h, 90%, (b) THF, KO[t]Bu, rt, 47-73%*

From these observations, it becomes apparent that the order of the chlorine substitutions on **102** are dependent on the type of nucleophile and the conditions used to drive the reaction. A considerable body of literature has illustrated the significance of the C-4/6 position for nucleophilic aromatic substitution reactions when treating 2,4,6-trichloropyrimidine with different nucleophiles.

With all that being said, the sulfur-based pyrimidines have also been extensively investigated.[143] They comprise a closely connected category of substances of enormous significance, and are useful intermediates that can be used for the synthesis of other compounds.[143] Alkyl- or aryl-thio groups can replace halogens substituted at any pyrimidine ring position even though the mostly preferred methodologies involve S-alkylation of the appropriate thione. Although halogens at position 5 can be replaced by S-nucleophiles, the reaction is simpler at the *ortho* or *para* positions to the ring nitrogens.[143] However, substitution of the first chlorine atom by the sulfur-containing nucleophiles is rarely studied. Consequently, this provides little information about the preferred position when introducing the thio-nucleophiles. One example reported for the thiolation of trichloropyrimidine **102** includes the reaction with thiourea in hot alcohol upon which intractable products were obtained.[144]

While alternative pathways for the synthesis of thiopyrimidines are performed by S-arylation of the already substituted chloropyrimidines,[145,146] other valuable synthetic approaches can be instigated from mercaptopyrimidines **127** (Scheme **33a**)[147] or **128** (Scheme **33b**)[148] as a starting material, followed by S-alkylation.

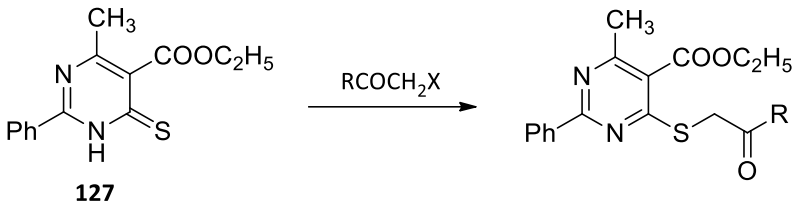

127

(a) Ethyl 4-methyl-2-phenyl-6-thioxo-1,6-dihydropyrimidine-5-carboxylate **127** as a starting material

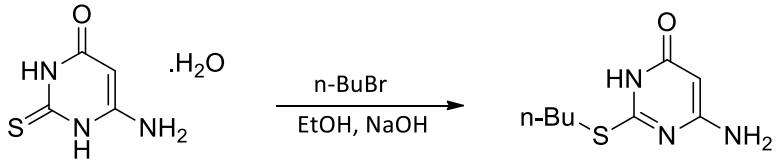

128

(b) 6-amino-2-thioxo-2,3-dihydropyrimidin-4(1*H*)-one hydrate **128** as a starting material

Scheme 33 *S-alkylation of mercaptopyrimidine **127** and **128***

In some instances, the sulfur-based pyrimidine compounds like S-DABOs have been widely prepared according to the Clay procedure for the formation of the β-oxo esters **129** that are required for subsequent steps (Scheme **34**).[122,124,149]

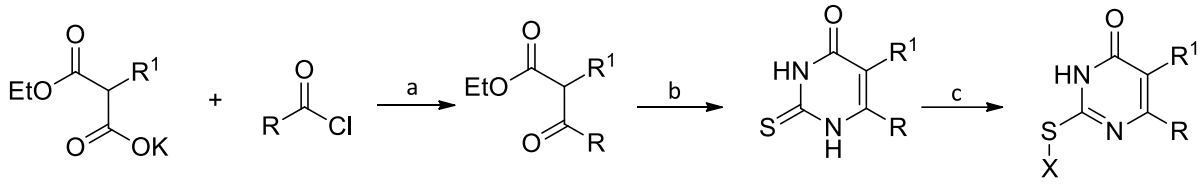

129

R= 1-/2-naphthylmethyl, phenoxymethyl; **R[1]**= H, Me; **X**= cyclopentyl, cyclohexy, *sec*-butyl

Scheme 34 *Reagents and conditions: (a) Et_3N, $MgCl_2$, MeCN; (b) $CS(NH_2)_2$, EtOH, EtONa; (c) K_2CO_3, X-hal, DMF*

Hydrolysis of halogenated pyrimidines can be carried out under acidic or basic conditions.[138] Basic hydrolysis of trichloropyrimidine **102** (Scheme **35**) with aqueous sodium hydroxide was reported by El-Eman in 2004[145] and Goudgaon in 2013.[146]

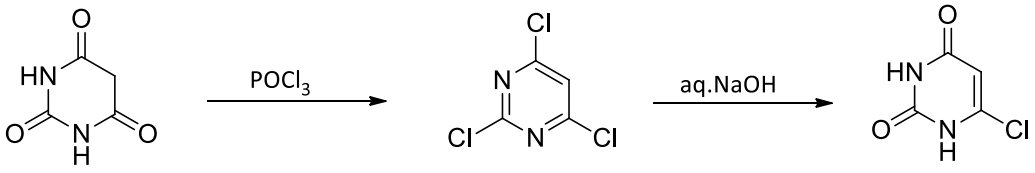

102

*Scheme **35** Alkaline hydrolysis of **102***

1.3 Research aims and objectives

The primary goal of this project is to construct aryl benzamide derivatives as possible NNRTI therapeutic agents. The antiviral activity of imidazo-[1,2-*a*]-pyridin-3-amines as NNRTI drugs was previously investigated in our laboratory by Bode.[150] The results of this study demonstrated that compound **130** with R=cyclohexyl, R^1=Cl and R^2=CN was among the most active scaffolds. This derivative was proven to exhibit antiviral inhibitory activity against the wild-type virus, but lost potency against the mutant viral strains. Therefore, a "virtual ring opening" of the effective compounds was envisaged to identify possible new compounds with NNRTI activity, but which would possess intrinsic torsional flexibilities compared to the original rigid imidazopyridines **130**. This strategy was applied and resulted in the synthesis of a series of pyridinylbenzamide derivatives **131** (Scheme **35**).

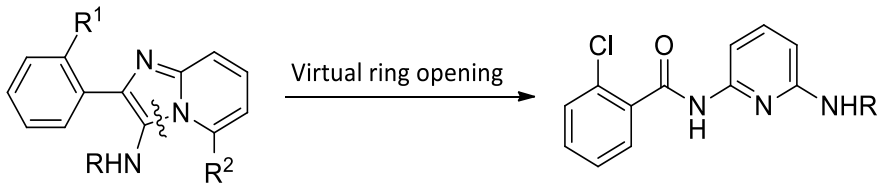

130 **131**

Scheme 36 *Synthesis of pyridinylbenzamides* ***131***

Of the library of compounds tested, compound **132** (Fig **25**) was found to show the best anti-HIV properties and exhibited superior activity (0.7 µM) against HIV-1 WT in an *in vitro* single-cycle test and antimicrobial activity (39 µg ml^{-1}) against *S. aureus*. [59]

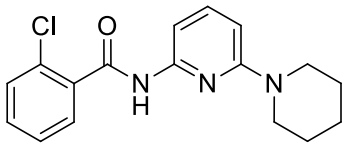

132

Fig 25 *Structure of compound* ***132***

On the other hand, Zhang and co-workers used S-DABO **133** (Fig **26**) as a lead compound for the synthesis of potential NNRTIs that exhibit favourable interactions with the NNBIP that is composed of amino acids like Tyr 188 and Trp 229 residues. The existence of *N*-3-H in S-DABOs is vital for the formation of the H-bond with the Lys 101 within the hydrophobic binding pocket. Thus, their preliminary work identified novel compound **134** as potential NNRTIs, with analogue **135** possessing significant activity against HIV-RT (IC_{50}= 0.71 µM), although moderately active against HIV_{SF33} (EC_{50} 1.06 µM) .[151]

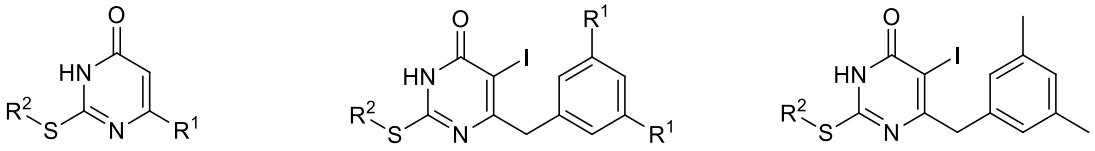

133 **134** **135**

R²= (p-CH_3CO)$C_6H_5CH_2$

Fig 26 *Structures of S-DABO compounds*

Therefore, considering the moderate activity of **135**, we thought it would be useful to modify this compound by moving the position of the pyrimidine ring (Fig **27**) and introducing a benzamide moiety, as found in compound **132**.

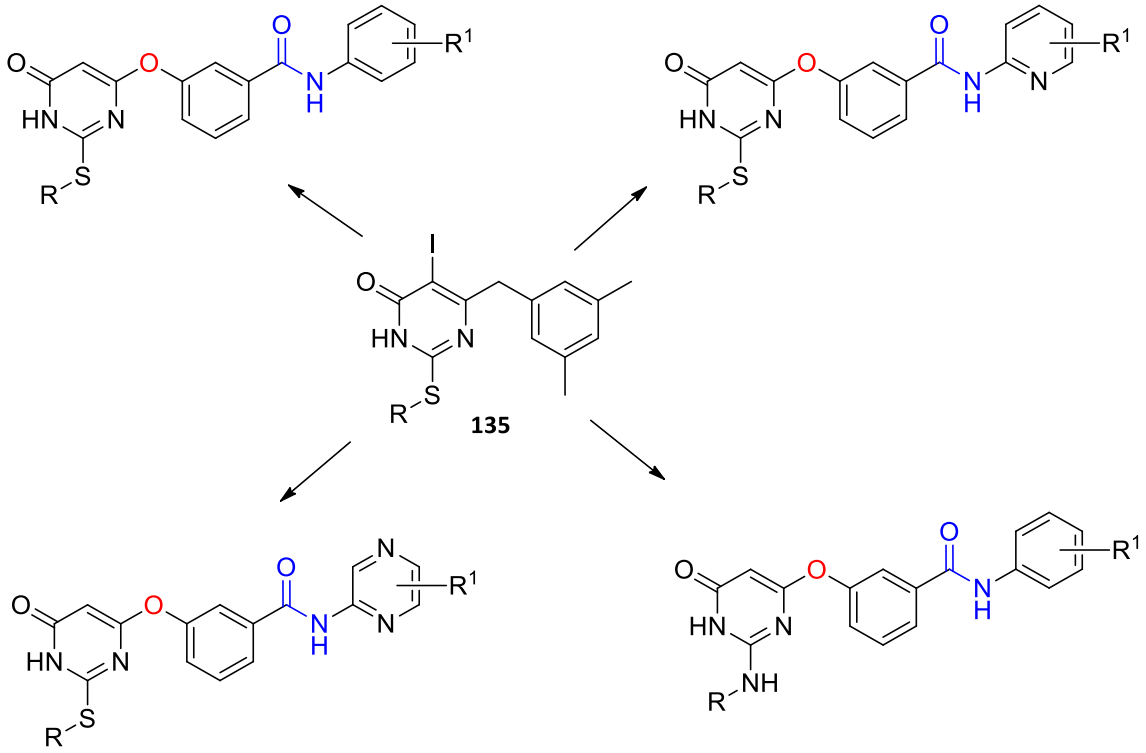

*Fig **27** Combining pyrimidinyl and benzamide moieties in design of possible NNRTIs*

Thus, through the adoption of a scaffold hopping technique, compounds **132** and **135** will be used as the starting point for the design of new aryl benzamides. This strategy has been successfully applied in the development of NNRTIs. For example, Li and colleagues put this approach to use to develop cyclo-arylpyrimidines, biphenyldiarylpyrimidines, and thiophenyl-DAPYs with excellent antiviral activities relative to their lead compounds.[152] Etravirine **7**, bearing an oxygen linker, was used to synthesize a library of DAPY analogues containing cyano and methyl groups of compound **136** (Scheme **37**). Among the scaffolds synthesized, novel derivative **137** was significantly potent against the WT

HIV-1 strain, hence, the scaffold-hopping strategy is considered advantageous in anti-HIV drug development.[152]

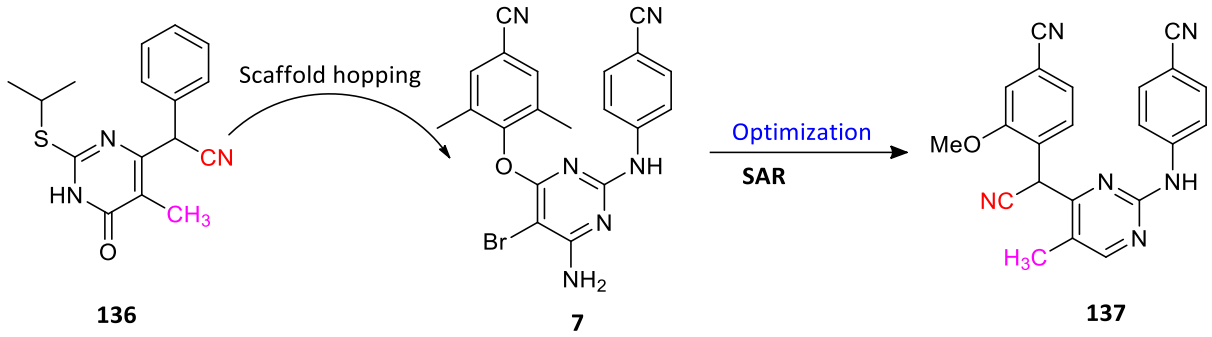

Scheme 37 *Scaffold-hopping approach by Li et al*[152]

Considering these encouraging discoveries, phenylbenzamides **138**, pyridinylbenzamides **139**, and pyrazinylbenzamides **140** (Fig **30**) will be examined for the possible alterations on the 6-benzyl ring of the DABO molecule **135** linked by an oxygen atom via a scaffold hopping method. The goal of designing such compounds was to produce a more adaptable collection of new analogues that could have improved binding interactions and enhanced antiviral activity than their lead compounds. These compounds are further expected to demonstrate low toxicity and establish a barrier to development of resistance. We thought it would be important to functionalize our scaffolds with groups possessing good hydrogen bond donating or hydrogen bond accepting properties to enable favourable interactions with HIV-1 RT mutant strains. In addition, we assume that the presence of an oxygen linker could be essential for the increased torsional flexibility, allowing the molecules to fit in the RT active site through various conformational modes. NNRTI drug adaption to torsional flexibility is tolerant of the structural variations and fundamental for targeting HIV-1 RT mutants. However, as previously indicated, a drawback of such free rotation is that the ligand might have extreme entropic energy that could counteract the advantages of increased ligand binding affinity by preventing the ligand from locking itself in place within the enzyme's active site. [59] Interestingly, the molecules consist of an amide functionality that has a restricted rotation, which could be compatible with and enable the ligand locking.

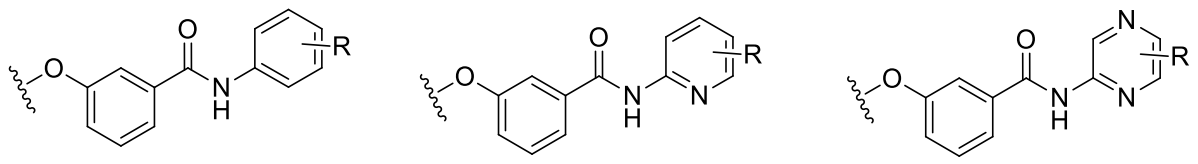

Fig 28 *Potential replacements of the 6-benzyl ring of* ***135***

1.4 Aims and objectives of the project

Acknowledging the significant role played by the benzamide and DABO compounds in medicinal chemistry, this study is aimed at synthesizing aryl benzamide analogues as potential NNRTIs that may prevent HIV-RT activity in wild-type virus and mutant strains. The objective is to prepare a series of different compound libraries based on the scaffold hopping strategy by coupling the pyrimidine nucleus to various benzamides linked by an oxygen atom to prepare a series of scaffolds for biological testing.

1.4.1 Proposed overall synthetic approach

The proposed overall synthetic approach is shown in Scheme **38**. Through the S_NAr reaction, the first step involves etherification of 2,4,6-trichloropyrimidine **102** with methyl 3-hydroxybenzoate **141** using a strong base for deprotonation of the hydroxyl group.

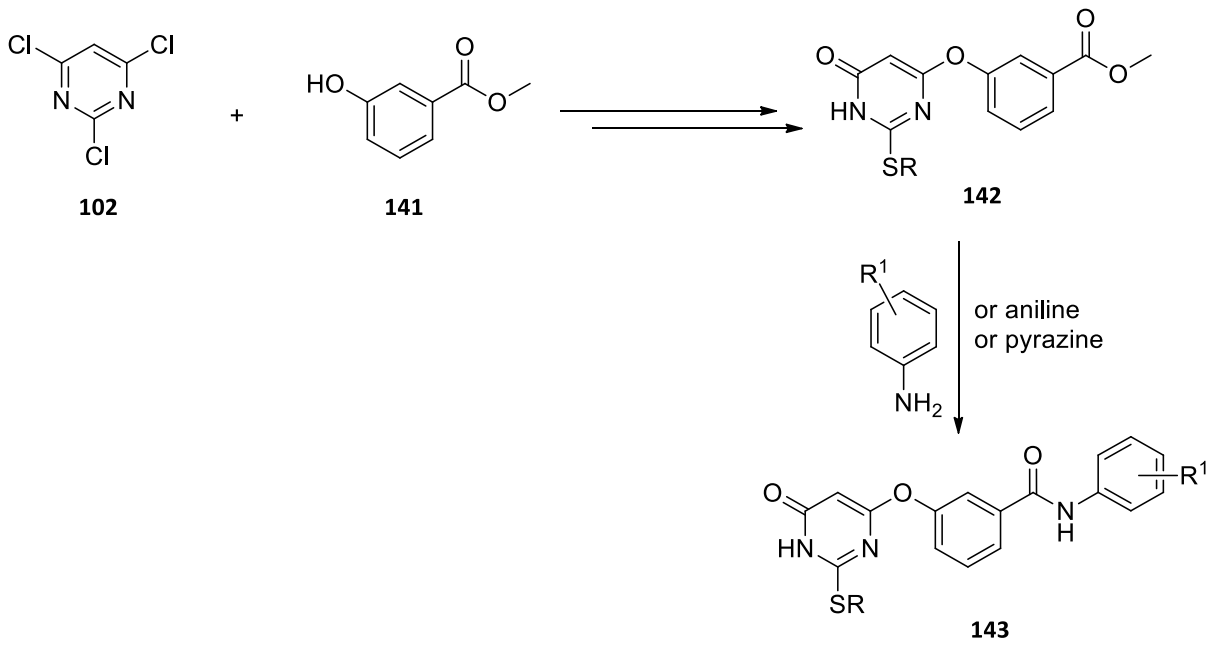

Scheme ***38*** *Proposed synthetic approach*

This step will be followed by thiolation which will displace a second chloride. Finally, the third chloride will be replaced by a hydroxyl group under aqueous acidic conditions to give compound **142**. Reaction of a suitable nitrogen nucleophile will give aryl benzamide **143**. Subsequent steps will be outlined in the next section.

1.4.2 Proposed methodology

2,4,6-Trichloropyrimidine **102** will be obtained through a reaction of barbituric acid **144** with $POCl_3$ in the presence of a catalytic amount of *N*,*N*-dimethylaniline (Scheme **39**). Intermediate **102** will be

treated with sodium hydride and reacted with **141** to afford 2,4-dichloro-6-(3-methoxyphenoxy)pyrimidine **145** which will in turn be reacted with an appropriate thioalkyl compound in pyridine to form compound **146**. Subsequent hydrolysis of **146** with aqueous hydrochloric acid will provide **147** which is expected to tautomerise to compound **148**. Similar methods for aminating the C_2-Cl of the pyrimidine ring will also be explored to examine the reactivity of the nitrogen nucleophiles compared to that of sulfur nucleophiles.

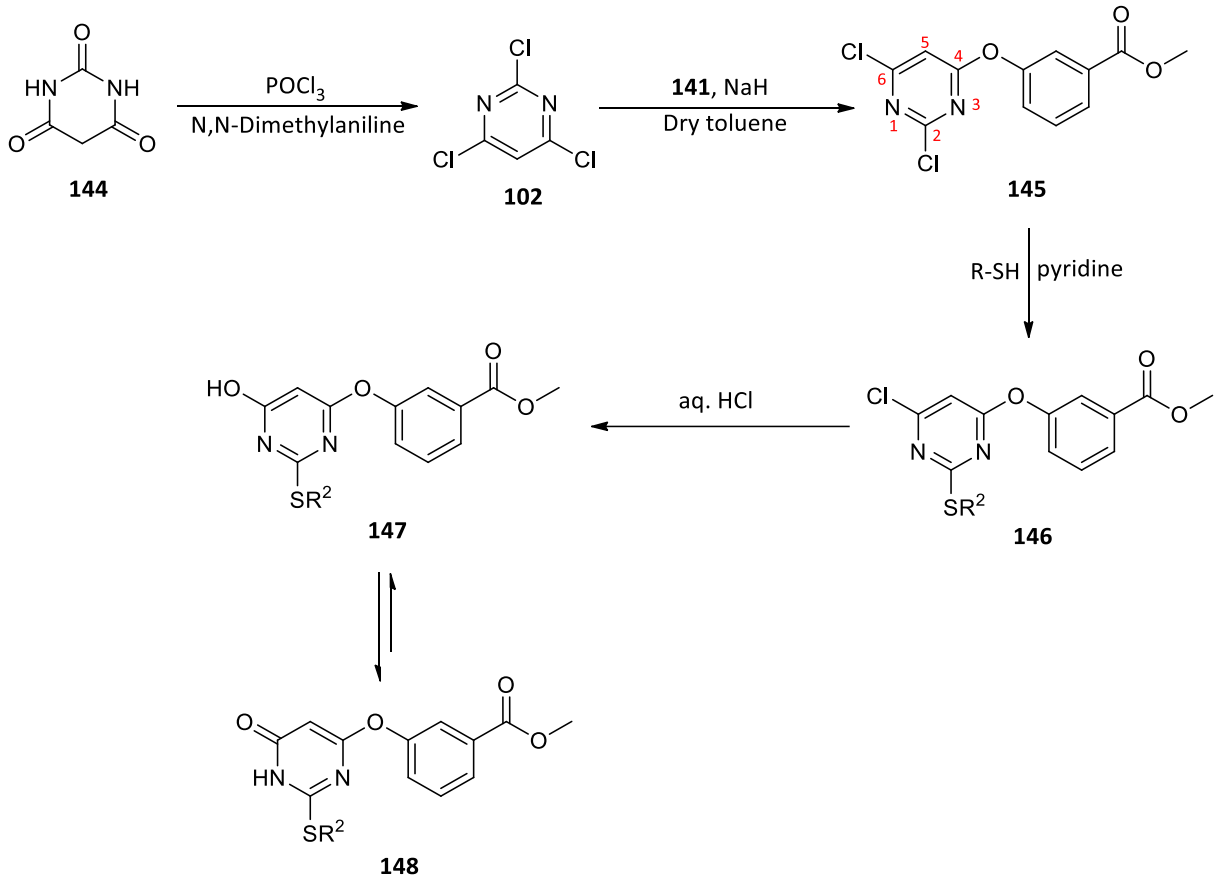

*Scheme **39** Proposed synthetic route*

Acid- or base-catalyzed hydrolysis of an ester **148** will form carboxylic acid **149** which will be activated with thionyl chloride to afford a highly reactive electrophilic acyl chloride **150**. Reaction of **150** with aniline **151a-h** *in situ* will then produce compound **143a-h** (Scheme **40**). Similar methods can be used to prepare compound libraries using either aminopyridine or aminopyrazines to give corresponding derivatives **143i-o** and **143p-q** respectively.

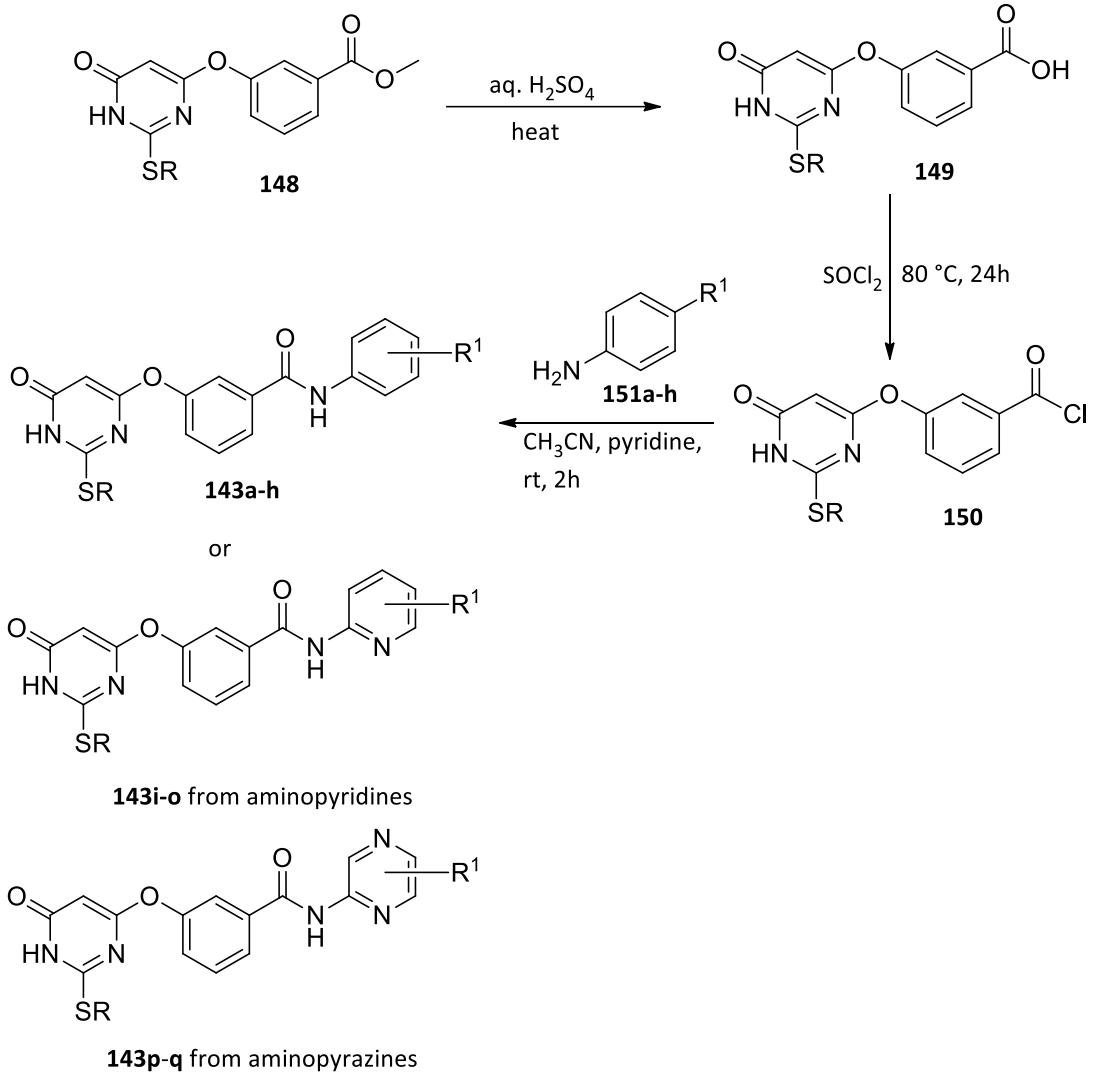

*Scheme **40** Hydrolysis of **174***

Anilines	**Aminopyridines**	**Aminopyrazines**
151a= 4-Br	**151i**= 6-Br	**151p**= 5-Br
151b= 3-Br	**151j**= 6-Cl	**151q**= 5-Cl
151c= 4-Br-2Me	**151k**= 5-Br	
151d= 4-Me	**151l**= 5-Cl	
151e= 4-OMe	**151m**= 5-Me	
151f= 2,4,6-TriBr	**151n**= 6-Me	
151g= 2-Br-4-Me	**151o**= 3-Br	
151h= 4-Cl-2-Me		

CHAPTER 2: RESULTS AND DISCUSSION

This section describes strategic approaches employed to synthesize our novel potential NNRTI analogues. As indicated in the introductory chapter, the scaffold hopping strategy is useful for improving antiviral properties when new fragments are introduced onto the lead compounds. Using the same technique, a library of arylbenzamide derivatives are reported herein. Because the proposed compounds contain relatively complex benzamides, our starting point was to investigate methodology for the synthesis of simple benzamides first. The reactivity of different anilines and amines with benzoic acids **152**-**155** (Fig **29**), was examined in order to establish a suitable synthetic route to our target compounds. While three benzoic acids (**152**-**154**) were commercially available, acid **155** was prepared and the synthesis is detailed in section **2.1.6.1**.

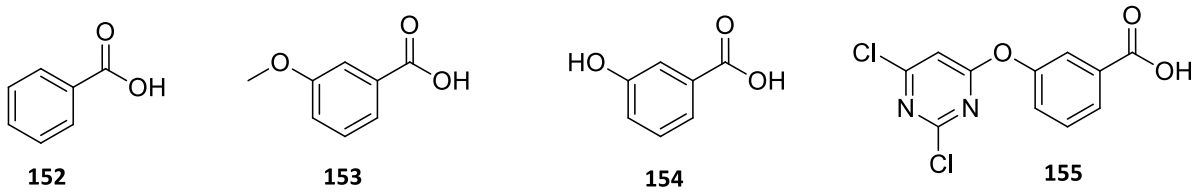

Fig 29 *Benzoic acids used for amidation reactions*

2.1 Synthesis of benzamides

2.1.1 Preparation of benzamides from unsubstituted benzoic acid **152** and aniline derivatives **151a-h**

Benzamides were identified in our laboratory as targets for the synthesis of NNRTIs.[59] A number of approaches for amide bond formation were attempted through the activation of benzoic acid, and the thionyl chloride route was found most effective in facilitating the amidation reactions.[59] Thus, inspired by the ease with which benzamides were accessed, this method was adopted for our further studies. Anilines **151a**-**h** depicted in Fig **30** were commercially available and were used without further purification for amidation reactions.

The methodology was first tested using simple unsubstituted benzoic acid **152** which was heated under reflux for 24 h in the presence of $SOCl_2$. After removal of excess $SOCl_2$, the corresponding acyl chloride **156** was reacted without purification with an equimolar amount of 4-bromoaniline **151a** in dry acetonitrile using pyridine as a base. During this time a precipitate started forming upon cautious addition of the acid chloride to a pre-cooled solution of **151a**, and stirring was continued for 30 minutes at low temperature (Scheme **41**). The reaction mixture was stirred for a further 24 h, while gradually warming to ambient temperature. The desired product **157a** was obtained in 83% yield as a white solid. Ahmadi and colleagues obtained 71% of product **157a** by performing an amidation reaction under ultrasonic irradiation employing diatomic earth@IL/$ZrCl_4$.[153] While Liang and

colleagues obtained 85% yield also starting from benzoic acid **152** and using triethylamine in THF as a solvent,[154] Das and co-workers recently demonstrated that the synthesis of derivative **157a** can be achieved from a reaction of thiobenzoic acid with 4-bromoaniline **151a** in the presence of 3,6-di(pyridin-2-yl)-1,2,4,5-tetrazine in THF.[155]

The structure of compound **157a** was verified by NMR and FTIR spectroscopic techniques. The IR spectroscopic data showed the broad and stretching signals absorbing at 3331 cm^{-1} and 1645 cm^{-1} representing the presence of amide NH and carbonyl C=O, respectively. The ^{1}H NMR spectrum showed an overall of ten expected protons with a deshielded singlet signal of an amide proton at 10.40 ppm. Due to symmetry, the ^{13}C NMR spectrum showed nine carbon signals with the carbonyl carbon at 166.2 ppm and aromatic signals at chemical shifts ranging from 115.8 to 139.0 ppm (C8).

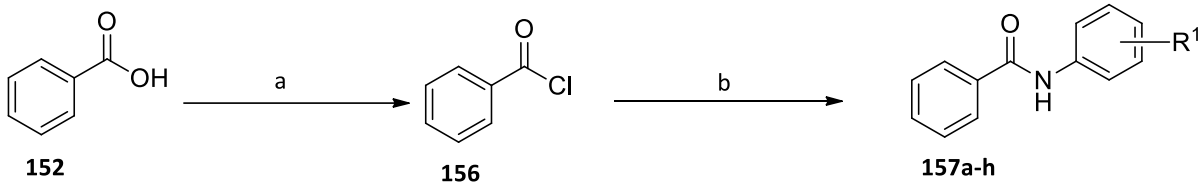

Scheme 41 *Reagents and conditions: (a) $SOCl_2$, reflux, 24 h; (b)* ***151a-h****, CH_3CN, pyridine or triethylamine, 0 °C-rt, 14-24 h, 29-93%*

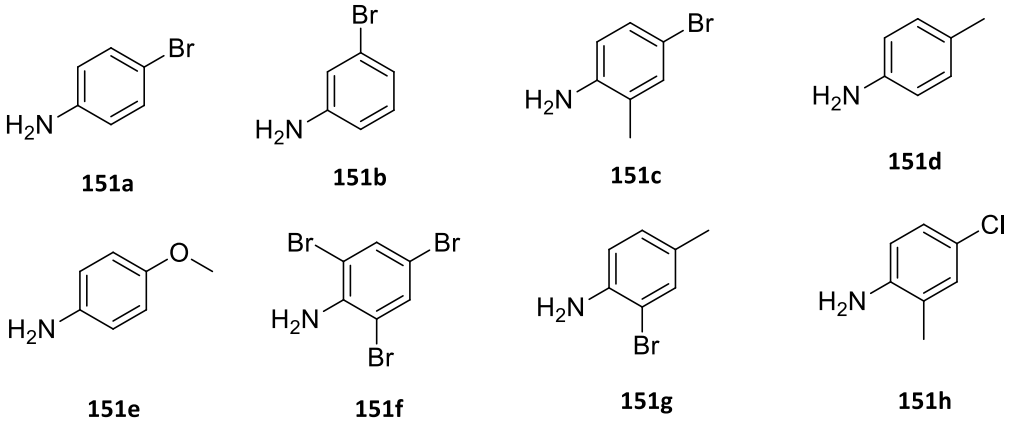

Fig 30 *Anilines used for amidation reactions*

We next examined the substrate scope and versatility of this methodology by varying substituents on the aniline. The structures of all the synthesised *N*-phenylbenzamides derived from **151a**-**h** are shown below in Fig **31**. The yields shown in Fig **31** for compounds **157a** and **157c** were obtained from the pyridine method while those shown for compounds **175b** and **157d**-**h** were obtained in the presence of triethylamie.

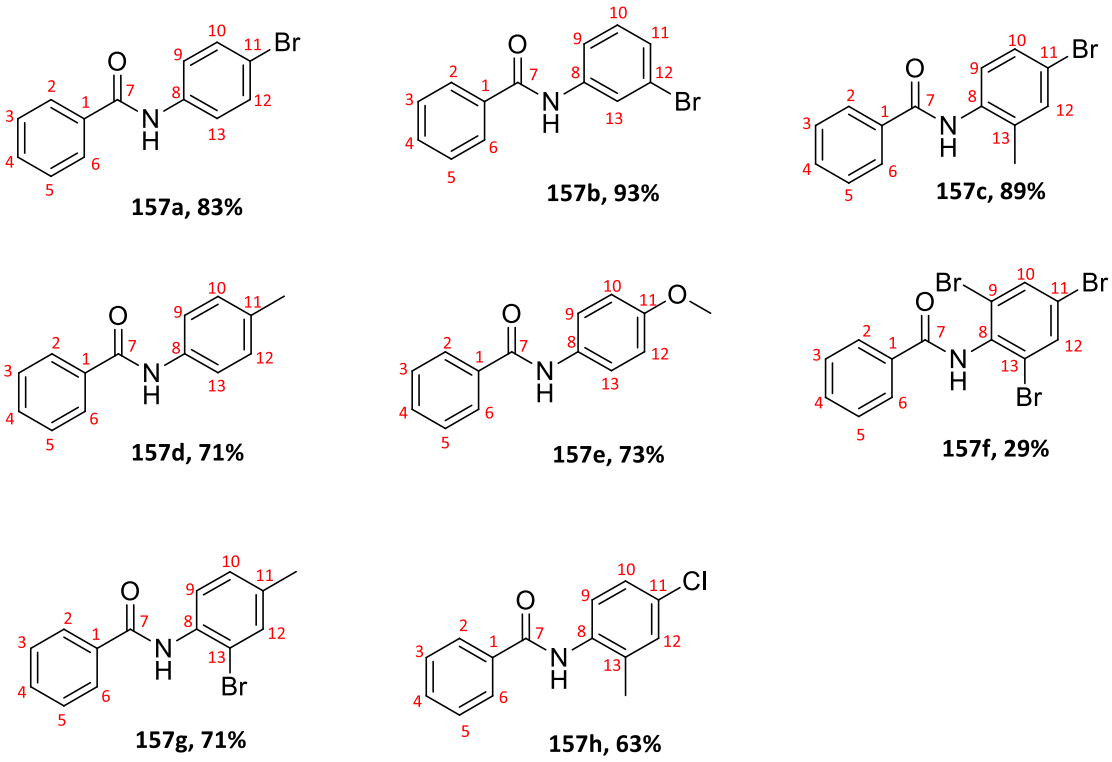

Fig 31 *Structures of the synthesised aniline-derived benzamides*

The results indicated that with the bromo-substituent shifted to the 3-position (**151b**), the reaction did not go to completion after 24 h. Additionally, longer reaction times probably resulted in product decomposition as evidenced by many spots observed on the thin layer chromatography plate. Column chromatography purification was also difficult because the starting materials and product **157b** co-eluted. An impure solid product was collected, and further purification was achieved by recrystallization using hot ethyl acetate and cold hexane yielding 42% of the product **157b**.

The IR spectroscopic data confirmed the formation of an amide bond by showing amide signals at 3282 cm^{-1} (broad for NH) and 1649 cm^{-1} (stretching for C=O). The ^{1}H NMR spectrum showed an overall of ten proton signals. The amide NH signal was deshielded at 8.00 ppm. The ^{13}C NMR spectroscopic data displayed ten aromatic carbon signals with the C8 signal appearing at 139.2 ppm while the carbonyl carbon was at 165.5 ppm.

During the reaction of benzoyl chloride **156** with aniline bearing a bromine atom in the 4-position and methyl group in the 2-position (**151c**), the product also precipitated out of solution. Because the product was contaminated after filtration, column chromatography purification was performed starting with 20% ethyl acetate/hexane as an eluent. However, co-elution of the desired product and starting material occurred due to similar polarities. Unfortunately, either increasing the solvent system polarity to 30-50% or decreasing to 10% did not improve the separation. Intriguingly, after

collecting the impure product and performing recrystallization with hot ethyl acetate and cold hexane, a pure product **157c** was obtained in excellent yield of 89%.

The IR spectroscopic data showed the key functional groups; NH signal at 3257 cm^{-1} and C=O signal at 1651 cm^{-1}. The ^{1}H NMR spectroscopic results displayed six distinct aromatic signals and a downfield amide signal at 9.99 ppm as an indication that the amide bond was successfully formed. The ^{13}C NMR spectrum also showed an overall ten aromatic carbon signals. The C8 signal was more shielded at 136.0 ppm probably due to both the *ortho*-electron donating effects caused by the methyl substituent and *para*-directing effects by the bromo group on **157c**. The carbonyl carbon signal was also observed at 165.4 ppm.

The amination of benzoic acid **152** with anilines **151d** and **151e** afforded corresponding benzamides **157d** and **157e** in 37% and 40% yields, respectively. The low yields are attributed to the loss of material after recrystallization. The acylation of aniline **151f** and **151g** gave the desired compounds **157f** and **157g** in 3% and 22%, respectively, with the low yields probably a result of the steric hindrance caused by the bromine atom. In each instance, the starting materials were recovered in significant amounts (53% of **151f** and 48% of **151g**). For benzoylation of **151h**, the product precipitated out of solution, and 49% of the desired compound **157h** was isolated after column chromatography purification.

For structural determinations, compounds **157d** and **157e** integrated for nine aromatic protons in the ^{1}H NMR spectrum. Compound **157f** integrated for seven aromatic protons, while **157g** and **157h** both integrated for eight aromatic protons. The ^{13}C NMR spectrum showed nine distinct carbon signals for derivatives **157d** and **157e**. Nine aromatic carbon signals were observed for compound **157f** and eleven aromatic carbon signals for **157g**.

The reactions in the presence of pyridine afforded low yields and difficult purification for some compounds, and triethylamine is another suitable tertiary base that is more basic than pyridine, that has the potential to mediate the C-N amide coupling reaction. Under similar conditions, the utility of triethylamine was first tested in reactions between the acyl chloride **156** and anilines possessing electron donating groups like *p*-methylaniline **151d** and *p*-methoxyaniline **151e** giving **157d** and **157e** in 72% and 73%, respectively.

This protocol was extended in the cases where use of pyridine gave low yields and where purifications were not possible. In particular, while several trials with the *meta*-substituted aniline **151b** resulted in difficult purification when using pyridine, a similar approach with triethylamine slightly increased the yield of **157b** to 53% after 12 h. Gratifyingly, increasing the reaction time to 24 h increased the yield to 93% (Table **3**) without the need for column chromatography purification. In relation to the pyridine

method that offered 3% yield of product **157f**, steric effects probably influenced the reaction outcome since 2,4,6-tribromoaniline **151f** still gave a low percentage yield (29%) when using triethylamine. Aniline **151g** bearing a bromine atom in the 2-position and methyl group in the 4-position reacted well, affording **157g** in 71% yield.

In the preparation of derivative **157h**, the mixture formed a clay-like slurry upon addition of the acyl chloride at 0°C, resulting in improper stirring. Despite several variations in solvent composition being tested, the same problem was encountered, however, 63% yield of the product was recoverable. Since the number of carbon signals was doubled in the ^{13}C NMR spectrum, single X-ray crystallographic analysis was conducted which revealed the structure of the *N*-(4-chloro-2-methylphenyl)benzamide **157h** with different orientations (Fig **32**).

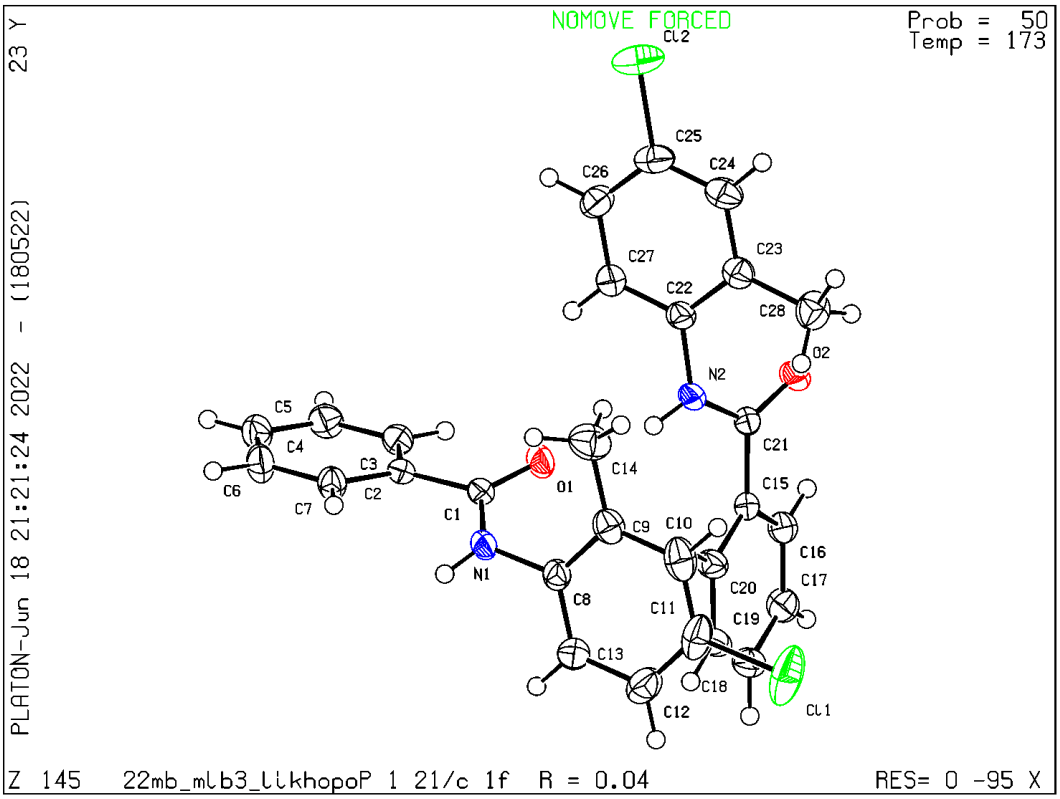

Fig 32 *Crystal structure of product* ***157h*** *showing the atom numbering, hydrogen atoms shown as small spheres arbitrary radius, oxygen atoms in red, chlorine atoms in green, and nitrogen atoms in blue*

The phenyl ring of the molecule on the right-hand side flipped while the chlorophenyl motifs are parallel to each other with their *trans*-substituents, thus allowing the amide C-O⋯H-N interactions

through intermolecular hydrogen bonding. Mass spectroscopic data (m/z) was found for $C_{14}H_{13}ClNO^+$ $[M+H]^+$: 246.0676, which was consistent with the mass-to-charge calculated $[M+H]^+$: 246.0681.

The improvement in the yields when using triethylamine can best be explained by the strength of the base used. The pK_b of triethylamine is 3.01 and that of pyridine is 8.75. This means that TEA is more basic than pyridine and can more easily start removing a proton from the amino group, making the nitrogen more nucleophilic for the attack on the carbonyl carbon.[156] Although it was impressive that the yields improved when using triethylamine, in some instances the yield was still low and starting materials were recovered. A short summary of the yields obtained with the use of pyridine compared to triethylamine is shown in Table **2**.

Table 2: Yields obtained using pyridine as base versus yields obtained using triethylamine as base

Compound number	**Pyridine Yield (%)**	**Triethylamine Yield (%)**
157b	42	93
157d	37	72
157e	40	73
157f	3	29
157g	22	71
157h	49	63

Compound IR and NMR characterizations are summarized with key data shown in Table **3** and **4**. For all derivatives, the IR spectroscopic data confirmed the presence of broad amide NH signals absorbing beyond the frequency of 3100 cm^{-1}, while the stretching signals from the carbonyl carbons were observed at approximately 1640 cm^{-1}. All the anticipated peaks were observed with the easily distinguishable groups like amide H, C-8, and C=O signals in ^1H NMR and ^{13}C NMR spectra being shown in Table **4**. The chemical shifts for the tabulated compounds **157a**-**h** varied based on the substituent effects and NMR solvent used. The ^1H NMR spectra showed a consistent frequency of absorption for the amide proton of derivatives **157a**, **157d**, and **157e** with their substituents in the *para* position relative to the amino group at 10.40, 10.19, and 10.16 ppm, respectively. The halogen effects were pronounced in the chemical shifts of compounds **157c** and **157h** at the C10, C11, and C12 positions in ^{13}C NMR spectra.

Table 3: IR spectroscopic results for aniline-derived benzamides **157a**-**h**

Compound Number	**157a**	**157b**	**157c**	**157d**	**157e**	**157f**	**157g**	**157h**
C=O (cm^{-1})	1645	1649	1651	1645	1646	1652	1647	1648
NH (cm^{-1})	3331	3282	3257	3310	3330	3227	3247	3249

Table 4: ^{1}H and ^{13}C NMR spectroscopic results showing similar chemical shifts for derivatives **157a**-**h**

Compound Number	**Amide H (s) ^{1}H NMR (δ: ppm)**	**C-8 ^{13}C NMR (δ: ppm)**	**C=O ^{13}C NMR (δ: ppm)**	**NMR Solvent**
157a	10.40	138.5	165.6	DMSO-d_6
157b	8.00	139.2	165.9	$CDCl_3$
157c	9.99	136.0	165.4	DMSO-d_6
157d	10.19	137.1	165.8	DMSO-d_6
157e	10.16	132.7	165.6	DMSO-d_6
157f	10.38	136.3	165.5	DMSO-d_6
157g	9.96	136.8	165.9	$CDCl_3$
157h	8.39	135.4	165.2	DMSO-d_6

2.1.2 Preparation of benzamides from methoxybenzoic acid **153** and anilines **151a-h**

To further extend the versatility of the previously reported methods for preparing benzamides **157a**-**h**, similar approaches were assessed using *meta*-methoxy substituted benzoic acid to give benzamides **158a**-**h**. Using the same method previously described this acid **153** was converted into its corresponding acid halide **159** (Scheme **42**) and used without purification. The reactions were carried out employing triethylamine and proceeded well with the yields ranging from moderate to excellent. In certain circumstances, it was difficult to compare the role played by the position of the substituents in conversion rates due to the difficulties encountered in column chromatography purification, necessitating the need for recrystallization. The structures of the isolated methoxy-based *N*-phenylbenzamides are shown in Fig **33**.

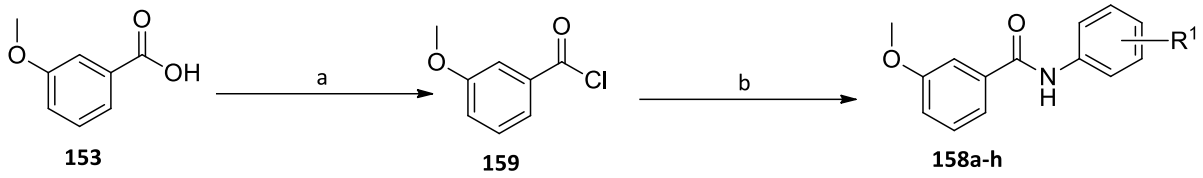

Scheme 42 *Reagents and conditions: (a) $SOCl_2$, reflux, 24 h; (b)* ***151a-h****, CH_3CN, triethylamine, 0 °C-rt, 14-24 h, 49-83%*

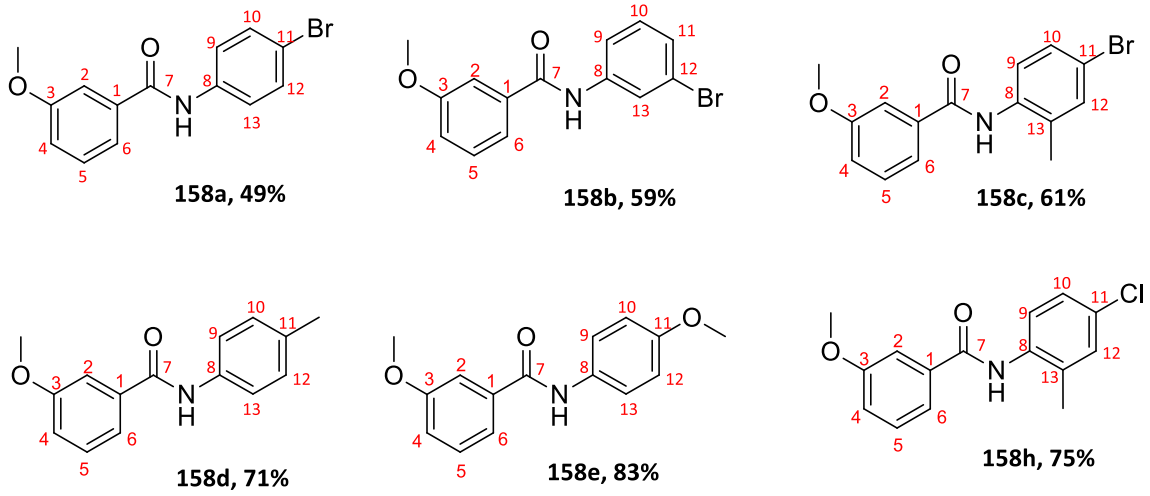

Fig 35 *Structures of methoxy-containing N-phenylbenzamides isolated when using triethylamine*

The 4-bromo substituted aniline **151a** only gave derivative **158a** in 49% owing to the loss of the material during the additional purification by recrystallization. The 3-bromo-aniline **151b** offered product **158b** in a reasonable yield of 59%. Compound **158c** was also isolated in a moderate yield of 61%. Anilines with methyl (**151d**) and methoxy (**151e**) groups in the 4-position furnished corresponding amides **158d** and **158e** in excellent yields (71% and 83%, respectively). As with the case of compound **158f**, the steric effects induced by the three bromine atoms had a significant impact on the reaction since only trace amounts of impure product **158f** were recovered. Derivative **158g** could not be isolated pure and 85% of the starting material was recovered. Compound **158h** was obtained in a good yield of 75% compared to derivative **158c** bearing bromine and methyl groups in the same position.

From the IR spectroscopic information, the isolated compounds **158a-e** and **158h** (Table **5**) showed the presence of broad amide NH signals appearing at frequencies between 3200 cm^{-1} and 3330 cm^{-1}. The stretching C=O signals were observed beyond the frequency of 1640 cm^{-1}.

Table 5: IR spectroscopic results for methoxybenzamide series of analogues

Compound Number	**158a**	**158b**	**158c**	**158d**	**158e**	**158h**
C=O (cm^{-1})	1647	1647	1644	1645	1643	1644
NH (cm^{-1})	3293	3274	3217	3312	3302	3211
C-O (cm^{-1})	1259	1243	1250	1247	1243	1251

For NMR spectroscopic results (Table **6**), the chemical shifts varied based on the solvent used for preparing the NMR sample. Deuterated chloroform was used to dissolve compounds **158**-**b** and **158e** whereas deuterated DMSO was used to dissolve **158c**-**d** and **158h**. The ^{1}H NMR spectroscopic data showed a slight difference in chemical shifts (~0.03 ppm) of the amide NH signals appearing at 7.98 ppm, 7.96 ppm, and 8.01 ppm for compounds **158a**, **158b** and **158e**, respectively. The NH signal of derivative **158d** was more deshielded at 10.16 ppm compared to those for compounds **158c** and **158h** appearing at 9.89 ppm and 9.93 ppm, respectively. The ^{13}C NMR spectroscopic results showed that the chemical shifts of the C-8 nuclei for derivatives **158a**, **158b**, and **158e** were substantially influenced by the inductive effects. An increase in electron density of the C8 nucleus increased with the *para*-donating strength of the substituent. In particular, the C8 signal of compound **158e** at 131.0 ppm was more shielded than that of **158a** at 137.0 ppm. Despite the NMR solvent used the chemical shifts of the carbonyl carbon nuclei were observed from 165.0 ppm and 165.6 ppm for all the compounds.

Table 6: ^{1}H and ^{13}C NMR spectroscopic results showing similar chemical shifts for the methoxy benzamide series of analogues

Compound Number	**Amide H (s) ^{1}H NMR (δ: ppm)**	**C-8 ^{13}C NMR (δ: ppm)**	**C=O ^{13}C NMR (δ: ppm)**	**NMR solvent**
158a	7.98	137.0	165.7	$CDCl_3$
158b	7.96	138.7	165.2	$CDCl_3$
158c	9.89	136.5	165.0	DMSO-d_6
158d	10.16	137.0	165.5	DMSO-d_6
158e	8.01	131.0	165.6	$CDCl_3$
158h	9.93	135.9	165.6	DMSO-d_6

2.1.2.1 Comparison between the C-8 signals of benzamide analogues derived from unsubstituted benzoic acid **152** and those derived from the methoxy-substituted benzoic acid **153**

The IR spectroscopic results showed analogous NH and C=O signal absorptions of compounds **158a**-**e** and **158h** to those of derivatives **157a**-**e** and **157h** with additional C-O signals absorbing at frequencies ranging from 1243 cm^{-1} to 1251 cm^{-1}. For the NMR spectroscopic results, the C8 signals of derivatives **158a**-**b** and **158e** are incomparable to those of **157a**-**b** and **157e** since they were analysed in different deuterated solvents. For compounds **158b**-**d** and **158h**, similar NMR spectroscopic patterns to those observed for *N*-phenylbenzamides **157b**-**d** and **157h** were obtained, with the additional methoxy CH_3 signals appearing in the aliphatic region in ^1H NMR and ^{13}C NMR spectra.

2.1.3 Preparation of benzamides from unsubstituted benzoic acid **152** and aminopyridines **151**-**o**

The amidation reactions were carried out by treating benzoyl chloride **156** with aminopyridines **151i**-**o** following the procedures discussed for the previously reported analogues. To further extend the utility of the triethylamine protocol, a series of *N*-pyridinylbenzamides **157i**-**o** was prepared (Scheme **43**). Aminopyridines **151i**-**o** (Fig **34**) were commercially available and were used for amidation reactions without further purification.

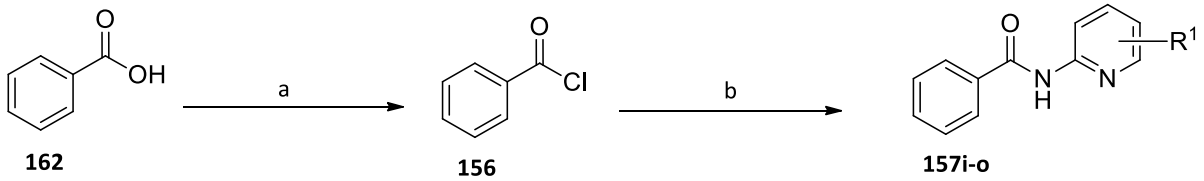

Scheme 43 *Reagents and conditions: (a) $SOCl_2$, reflux, 24 h; (b)* ***151i-o****, CH_3CN, pyridine or triethylamine, 0 °C-rt, 8-24 h, 3-76%*

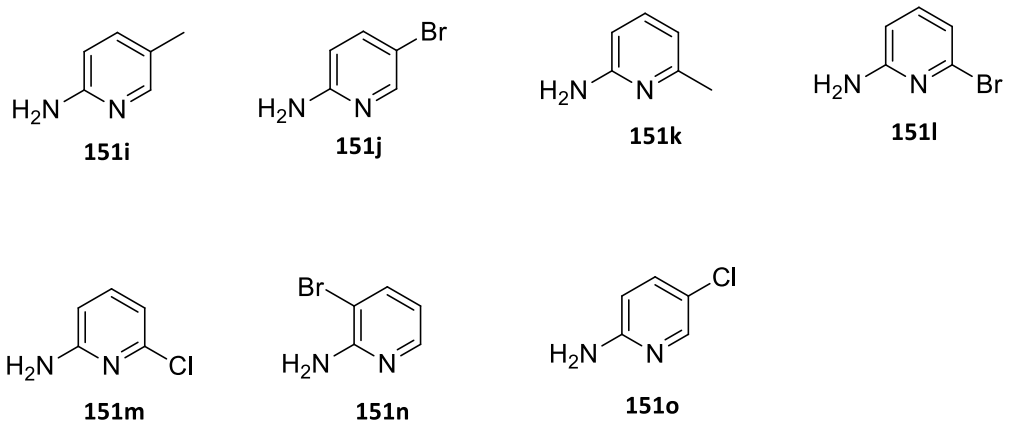

Fig 34 *Aminopyridines used for amidation reactions*

The structures of all the isolated *N*-pyridinylbenzamides **157j**-**o** with the yields ranging from poor to excellent are shown below (Fig **35**). The yields shown in Fig **35** for compounds **157k** and **157m** were obtained employing TEA while those shown for derivatives **157j**, **157l**, and **157n**-**o** were obtained through the pyridine method.

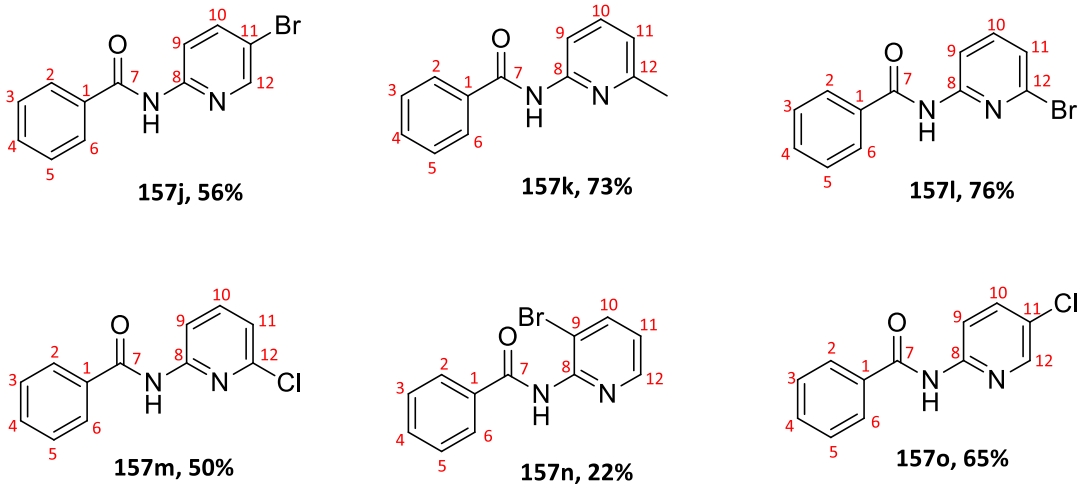

Fig 35 *N-pyridinylbenzamides derived from aminopyridines*

The reaction between benzoic acid **152** and aminopyridine **151i** substituted with a methyl group in the *para*-position to the amino group afforded an apparent 73% yield. After purification, it was clear that there was a problem because the compound integrated for thirteen aromatic protons in the ^{1}H NMR spectrum while the expected number was eight. However, the ^{13}C NMR spectrum showed ten aromatic carbon nuclei as anticipated. TLC analysis after purification by column chromatography had indicated the presence of a single product, therefore the unexpected integration could not be attributed to contamination by either of the starting materials. Similar spectroscopic results were observed even after recrystallization, after which the sample was analysed by single crystal X-ray diffraction. The results obtained gave us the information that substitution of both hydrogen atoms of the amino moiety of aminopyridine had occurred. The crystal structure (Fig **36**) shows that the phenyl motifs are *syn* to the oxygen atoms of the amidic group, while the carbonyl groups are *anti* to each other. The pyridine nitrogen is synclinal to the carbonyl C8 and *anti* to the C1 (Fig **36**), but *cis* to one phenyl ring and *syn* to the other ring.

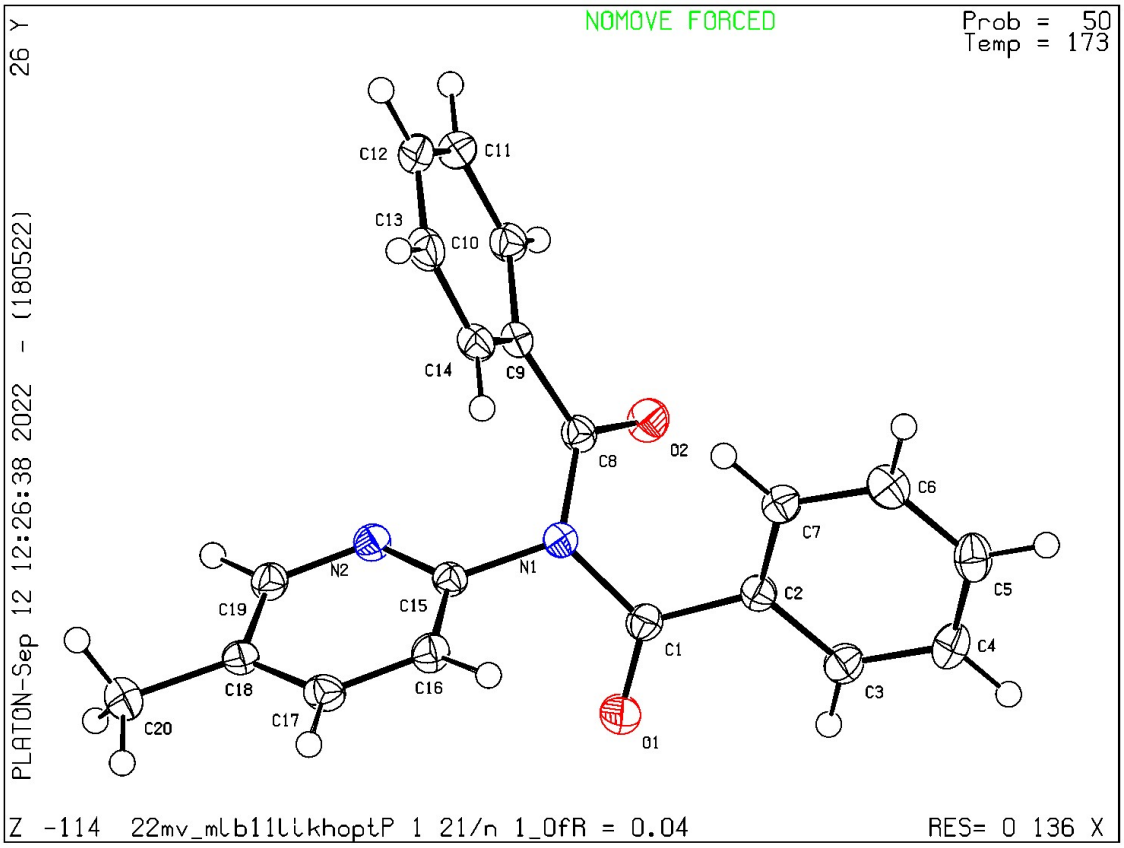

Fig 36 *Crystal structure of the N,N-diacylated product* ***160i*** *showing the atom numbering, hydrogen atoms shown as small spheres arbitrary radius, oxygen atoms in red, and nitrogen atoms in blue*

The mechanism by which triethylamine mediated the C-N coupling of carboxylic acid and amine was also documented by Putra and colleagues in 2017.[156] According to this mechanism, it becomes apparent that the first step of our reaction involved nucleophilic attack by the amino NH_2 group of **151i** to the electrophilic carbonyl carbon of **156**. After this nucleophilic attack, triethylamine deprotonated the NH_2 of intermediate **161i**. The resulting adduct **162i** loses a chloride ion affording the desired compound **157i**. After the formation of the secondary amide **157i**, the nitrogen atom uses its lone pair of electrons for nucleophilic attack of the carbonyl carbon of **156** forming intermediate **163i**. Another molecule of triethylamine removed the amide proton from **163i** resulting in the formation of adduct **164i**. This intermediate also collapsed upon the removal of the chloride ion to produce the *N*,*N*-diacylated product **160i** (Scheme **44**). As amides are acidic, it is also possible that triethylamine may directly deprotonate amide **157i** to make the nitrogen considerably more nucleophilic.

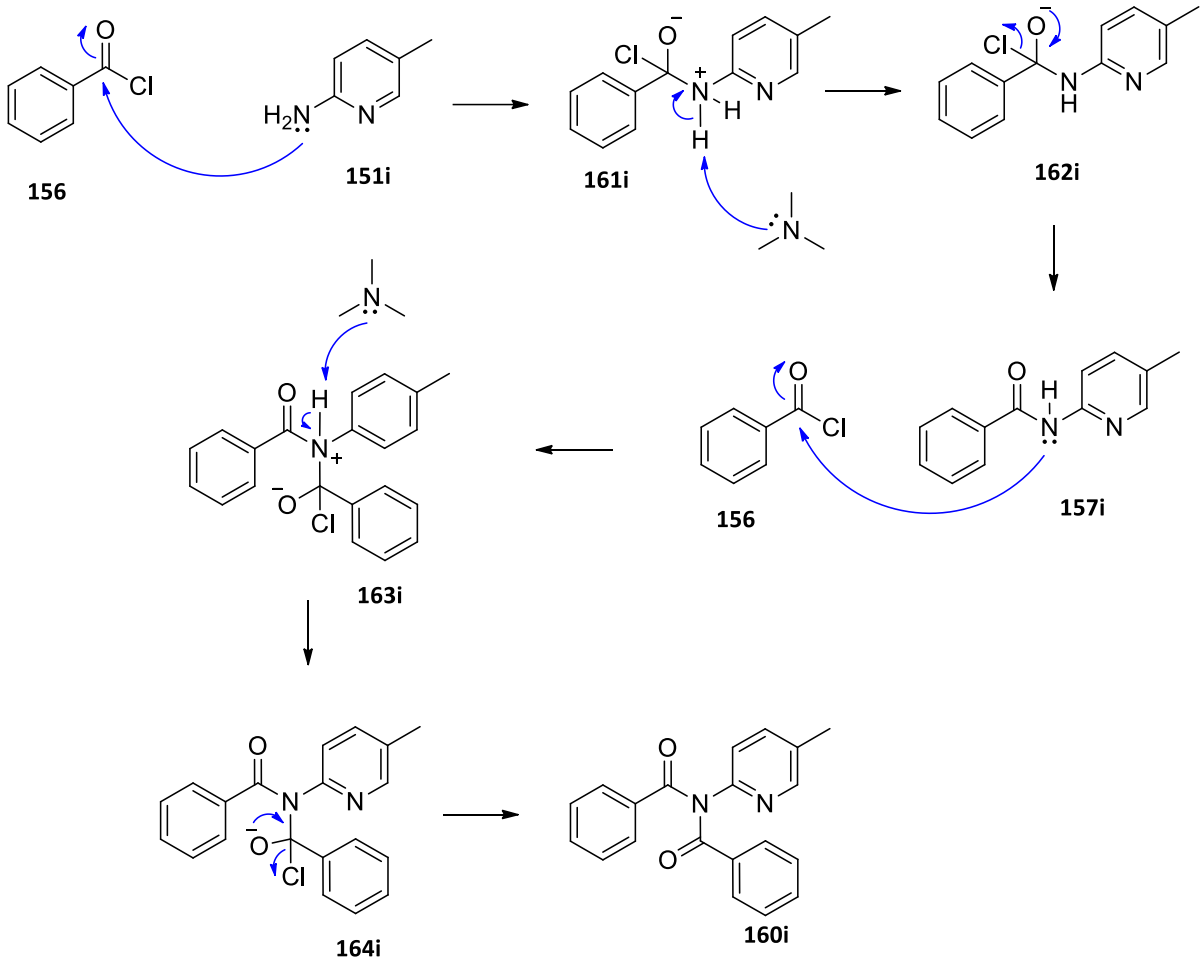

Scheme 44 *Mechanism of formation of product* ***160i***

Sylvie and co-workers synthesised compound **157i** from carboxylic acid **152** and aminopyridine **151i** using triethylamine without an indication of disubstitution.[157] However, in their case, 1,2-dichloroethane was used as a solvent and the reaction mixture was stirred for one hour at room temperature and heated at 60 °C for 3 h to give **157i** in 70% yield.[157] Apart from that, various reports have demonstrated that this compound can be obtained in high yields by oxidative amidation of aminopyridine **151i** with benzaldehyde[158,159] or phenylmethanol .[160]

The probability of di-substitution occurring with other substrates was examined by reacting benzoyl chloride **156** with aminopyridine **151k** containing the same methyl substituent, but in the 6-position. The mono-substituted product **157k** was obtained in 73% yield. For structural determination, the NH signal on the IR spectrum was unclear and therefore the structure of this compound was further analysed by single crystal X-ray diffraction. The results displayed multiple conformations that included π-π stacking interactions and hydrogen bonding between the amide hydrogen and the ring nitrogen (Fig **37**). The ^{1}H NMR spectrum integrated for eight aromatic protons as expected, and the ^{13}C NMR spectrum showed ten different chemical environments for aromatic carbon nuclei due to symmetry.

The DEPT NMR results also confirmed the presence of six distinct CH signals and four quaternary signals.

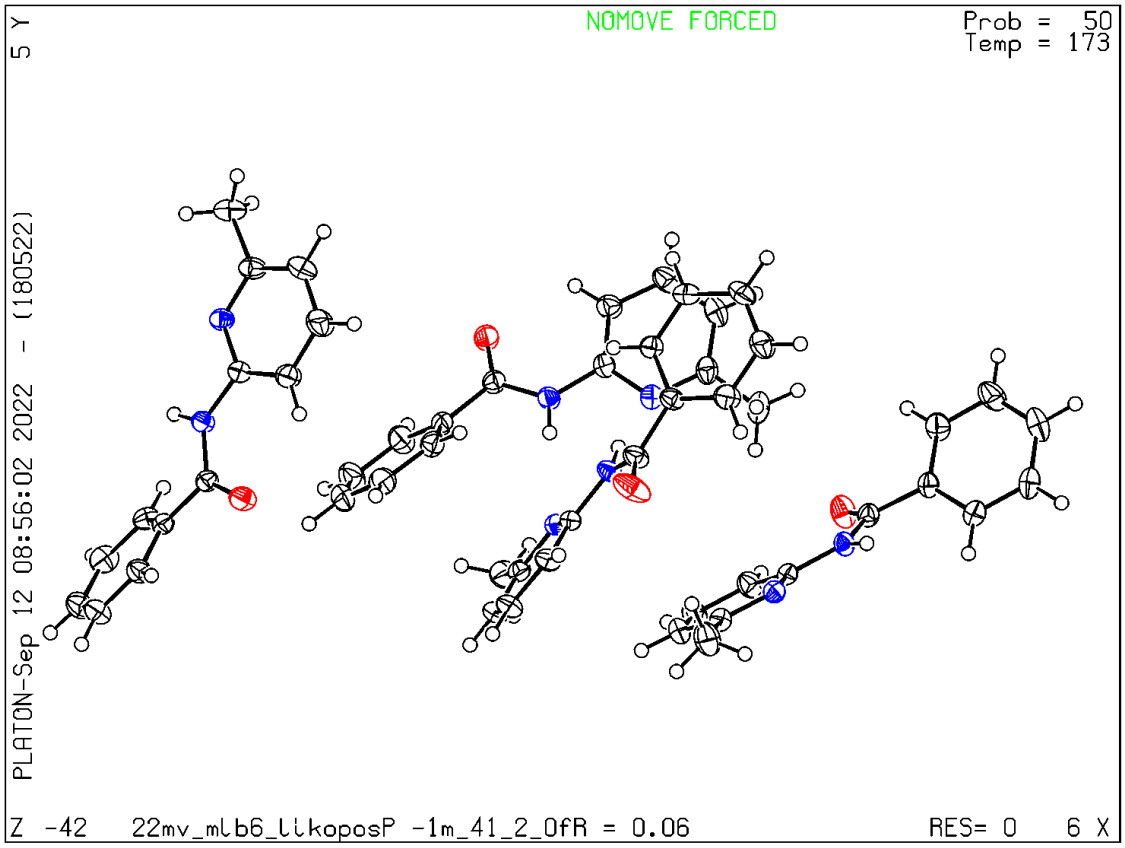

Fig 37 *Crystal structure of the N,N-diacylated product* ***157k*** *showing the atom numbering, hydrogen atoms shown as small spheres arbitrary radius, oxygen atoms in red, and nitrogen atoms in blue*

Heterocyclic amines **151l** and **151m** with the bromo and chloro substituents in the 6-position were also successfully converted into their corresponding *N*-pyridinylbenzamide **157l** and **157m** in yields of 35%, and 50%, respectively. Because the IR spectrum of **157m** showed two broad signals at 3408 cm^{-1} and 3325 cm^{-1}, it was difficult to assign the signal for the amide NH and the compound structure was analysed by single crystal X-ray diffraction where different orientations were seen (Fig **38**). The NMR results showed similar spectra for both compounds **157l** and **157m**. The ^{1}H NMR spectrum integrated for eight aromatic protons and the ^{13}C NMR spectrum showed ten aromatic carbon signals. The NH signal of derivative **157l** appeared at 8.59 ppm while that of **157m** at 8.73 ppm. The C-12 signal of **157m** was more deshielded at 148.9 ppm than that of **157l** at 134.2 ppm from the ^{13}C NMR spectrum.

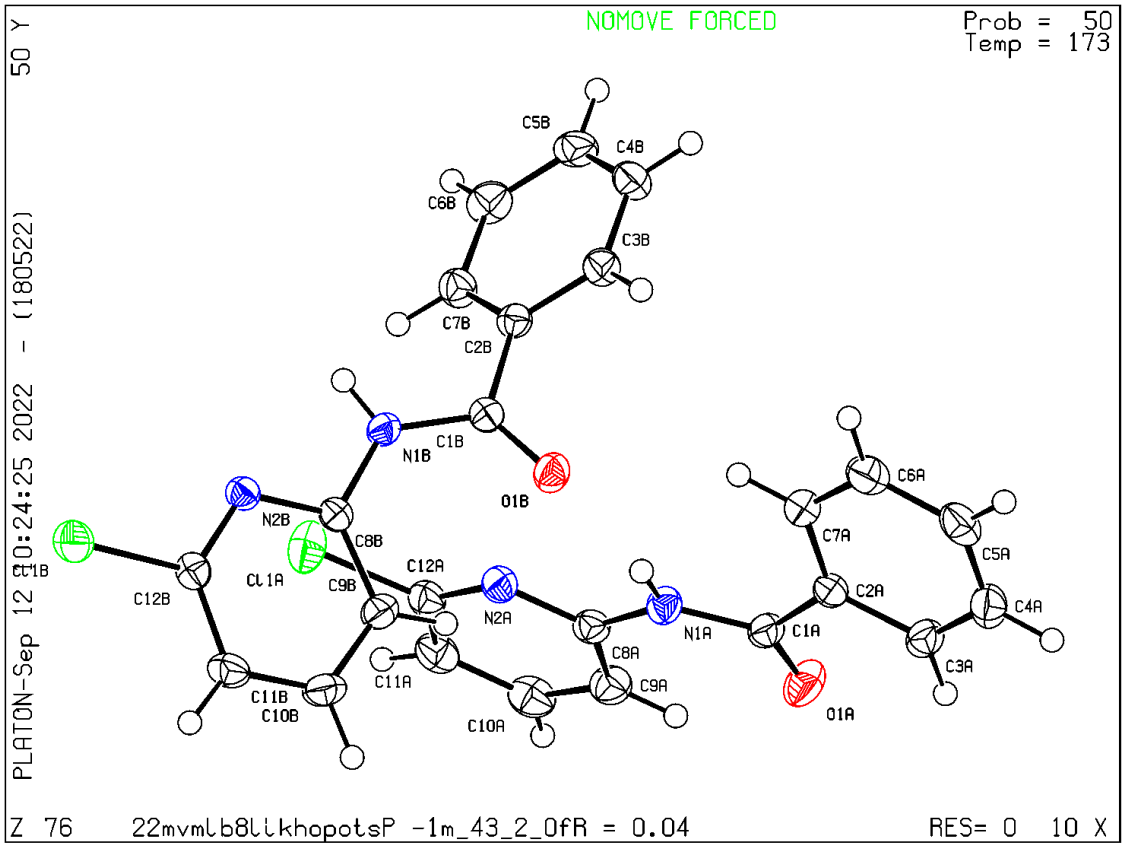

Fig 38 *Crystal structure of product* ***157m*** *showing the atom numbering, hydrogen atoms shown as small spheres arbitrary radius, oxygen atoms in red, chlorine atoms in green, and nitrogen atoms in blue*

The reaction between benzoic acid **152** and amine **151n** with a bromo-substituent in the 3-position gave undesirable results. The ^{1}H NMR spectrum showed five additional aromatic protons without the amide proton being seen. Based on the previously observed diacylation of aminopyridine **151i**, it was clear that disubstitution had also taken place and the diamide product **160n** was isolated in 11% yield. The compound could not be analysed by single crystal X-ray diffraction because it was isolated as a fine solid that did not form crystals despite solvent variations. However, further structural determinations will be detailed shortly after discussing the successful preparation of the desired compound **157n**.

Theodorou reported that *N*,*N*-diacylation occurs in heterocyclic amines like 2-aminopyrimidine, aminopyrazine, aminopyridine, and related amines, and is dependent on the strength of the base used.[161] To confirm these findings, Zitko and colleagues performed amidation reactions from various benzoyl chlorides and aminopyrazines.[162] Their results complemented Theodorou's observations that

pyridine offers mono-substituted products as the major products while triethylamine furnishes *N*,*N*-disubstituted derivatives.

Thus, taking this information into consideration, the amination of benzoic acid **152** with amine **151n** was repeated using pyridine and the monoacylated product **157n** was obtained in 22% yield due to steric hindrance effect caused by the bromine substituent. The formation of the desired product **157n** was confirmed by the presence of eight aromatic protons and an amide proton appearing at 9.03 ppm on the ^{1}H NMR spectrum. Due to the symmetric phenyl ring, the ^{13}C NMR spectrum showed ten distinct carbon signals. The DEPT NMR data showed the presence of six CH signals and absence of four quaternary carbon signals on the spectrum. The HMBC NMR spectrum demonstrated the ^{3}J coupling between the carbonyl carbon and the H2 and H6 nuclei. Another long-range coupling was realised between the C8 nucleus and H12.

As previously indicated, the structure of compound **160n** was reviewed. The absence of the amide proton and the presence of five extra aromatic signals on the ^{1}H NMR spectrum verified the idea that diacylation had occurred. Because of symmetric benzoyl moieties, the ^{13}C NMR spectrum showed ten different carbon nuclei, and six CH signals were observed on the DEPT NMR spectrum.

Dibenzoylation of **151n** was further confirmed by comparing signal absorptions of **157n** and **160n** on both the proton and carbon NMR spectra. The ^{1}H NMR spectrum revealed that the H10, H11, and H12 signals of derivative **157n** were more shielded at 7.71, 6.83, and 8,17 ppm, respectively, than those of compound **160n** appearing at 7.98, 7.12, and 8.31 ppm, respectively. Even the phenyl signals of compound **160n** were less shielded at chemical shifts ranging from 7.37-7.82 ppm than those of **157n** in the ranges of 7.28-7.80 ppm. The ^{13}C NMR data showed the major C=O and C8 signals for compound **157n** highly shielded at 165.4 ppm and 148.9 ppm, respectively, compared to those of **160n** at 172.5 and 152.3 ppm, respectively. The structures of the N,N-diacylated products **160i** and **160n** from obtained from acid **152** in the presence of triethylamine are shown in Fig **39**.

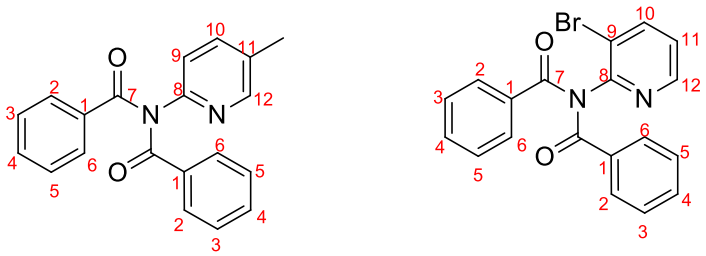

Fig 39 *N,N-diacylated products obtained using benzoic acid* ***152***

We next evaluated the preparation of the previously synthesised compound **157l** in our laboratory in the presence of pyridine and the resultant monoacylated product was obtained in 76%, albeit, lower than the originally reported yield (92%).[59] Despite that, it was interesting that the yield obtained when using pyridine improved by 41% compared to the one catalysed by TEA. Benzoylation of **151j** and **151o** was also performed employing pyridine, and the desired compounds **157j** and **157o** were isolated in 56% and 65% yields, respectively. It is worth noting that acylation of **151i** was not repeated using pyridine, and that of **151j** and **151o** were not performed using triethylamine.

Characteristic signals for compounds **157**-**m**, and **157o** for the amide H, C=O and C8 in the ^{1}H and ^{13}C NMR spectra are shown in Table **7**. Deuterated DMSO was used only for derivatives **157j** and **157o**. The ^{1}H NMR spectrum showed uniform amide NH signals between 8.50 ppm and 8.90 ppm for the compounds dissolved in deuterated chloroform, except for compounds **157k** and **157n** in which case the amide protons were more deshielded at 9.13 ppm and 9.03 ppm, respectively. The NH signals for compounds **157j** and **157o** were seen with negligible absorption difference (0.01 ppm) at 11.00 ppm and 11.01 ppm, respectively. The ^{13}C NMR spectroscopic results indicate that the C8 signals of the carbon nuclei directly bonded to the amide nitrogen for the *N*-pyridinylbenzamides **157k**-**m** were highly deshielded compared to the C8 signal of **157n** possibly because of the *ortho*-directing effects of the bromo substituent. The C-8 signal of derivative **157k** was highly deshielded at 156.8 ppm compared to the C2 signals of **157l** and **157m** as an indication of the electron withdrawing effects increasing with the electron withdrawing strength of substituents. The C8 signals for compounds **157j** and **157o** were consistent at 151.7 ppm and 151.3 ppm, respectively.

Table 7: ^{1}H and ^{13}C NMR spectroscopic results for compounds **157j**-**m**

Compound Number	**Amide H (s) ^{1}H NMR (δ: ppm)**	**C-8 ^{13}C NMR (δ: ppm)**	**C=O ^{13}C NMR (δ: ppm)**	**NMR Solvent**
157j	11.00	151.7	166.6	DMSO-d_6
157k	9.13	156.8	165.9	$CDCl_3$
157l	8.59	151.6	165.5	$CDCl_3$
157m	8.73	151.4	165.7	$CDCl_3$
157n	9.03	148.9	165.4	$CDCl_3$
157o	11.01	151.3	166.6	DMSO-d_6

2.1.4 Preparation of benzamides from methoxybenzoic acid **153** and aminopyridines **151i-o**

Following the methods discussed for the preparation of the previously synthesised analogues **157i-o**, a series of the methoxy-containing *N*-pyridinylbenamides **158i-o** (Fig **40**) was prepared keeping the variability in the pyridine core unchanged. Due to the observed *N*,*N*-diacylated products that formed when benzoic acid **152** was reacted with aminopyridines **151i** and **151n** in the presence of triethylamine, we became interested in first assessing the behaviour of TEA when methoxybenzoic acid **153** was used (Scheme **45**). The yields shown in Fig **40** for compounds **158i-j** and **158l-o** were isolated from the pyridine method whereas the yield shown for derivative **158k** was obtained when triethylamine was used.

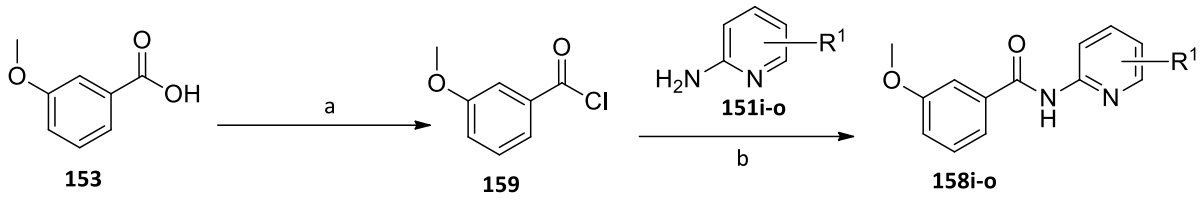

Scheme 45 *Reagents and conditions: (a) $SOCl_2$, reflux, 24 h; (b)* ***151i-0****, CH_3CN, pyridine or triethylamine, 0 °C-rt, 10-24 h, 10-99%*

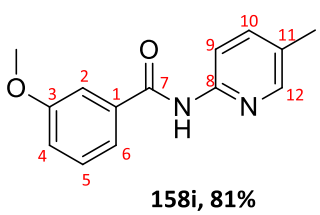
158i, 81%

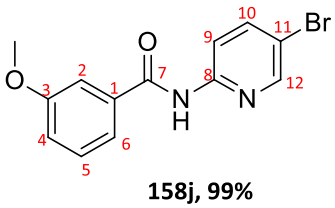
158j, 99%

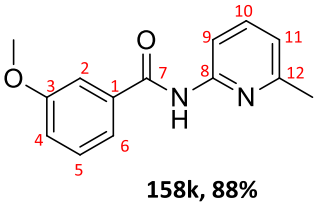
158k, 88%

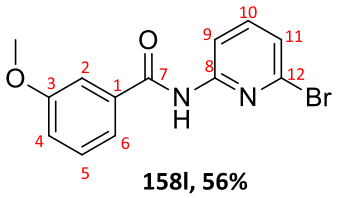
158l, 56%

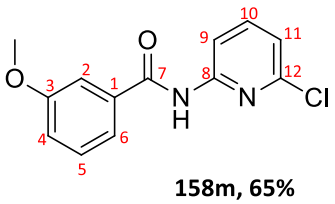
158m, 65%

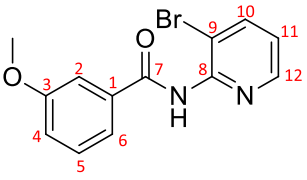
158n, 48%

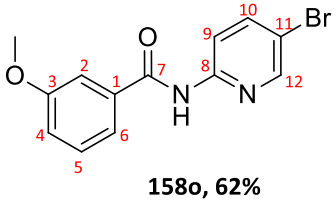
158o, 62%

Fig 40 *N-pyridinylbenzamides from methoxybenzoic acid* ***153***

The amidation reaction was performed by treating carboxylic acid **153** with amine **151i** in the presence of triethylamine. As expected, the *N*,*N*-diacylated product **165i** was recovered in 39% yield as the only constituent. To understand the tendency of *N*,*N*-diacylated products to form, the reaction between **153** and aminopyridine **151j** bearing a bromo substituent in the same position was conducted. Not surprisingly, the *N*-diamide product **165j** was obtained in 62% yield. Compound structures were verified based on the IR and NMR spectroscopic results. The NH signals were not observed on the IR spectra, while the ^{1}H NMR spectra showed four extra protons in the aromatic region. The ^{13}C NMR spectra showed ten expected aromatic carbon signals due to symmetry. Further structural determinations were conducted by single crystal X-ray diffraction. Similar crystallographic structural configurations reported for the compound **160i** were observed for the compounds **165i** (Fig **41a**) and **165j** (Fig **41b**, resolution was poor because the structure was disordered). The phenyl motifs are *syn* to the oxygen atoms of the amidic groups, while the carbonyl groups are *anti* to each other.

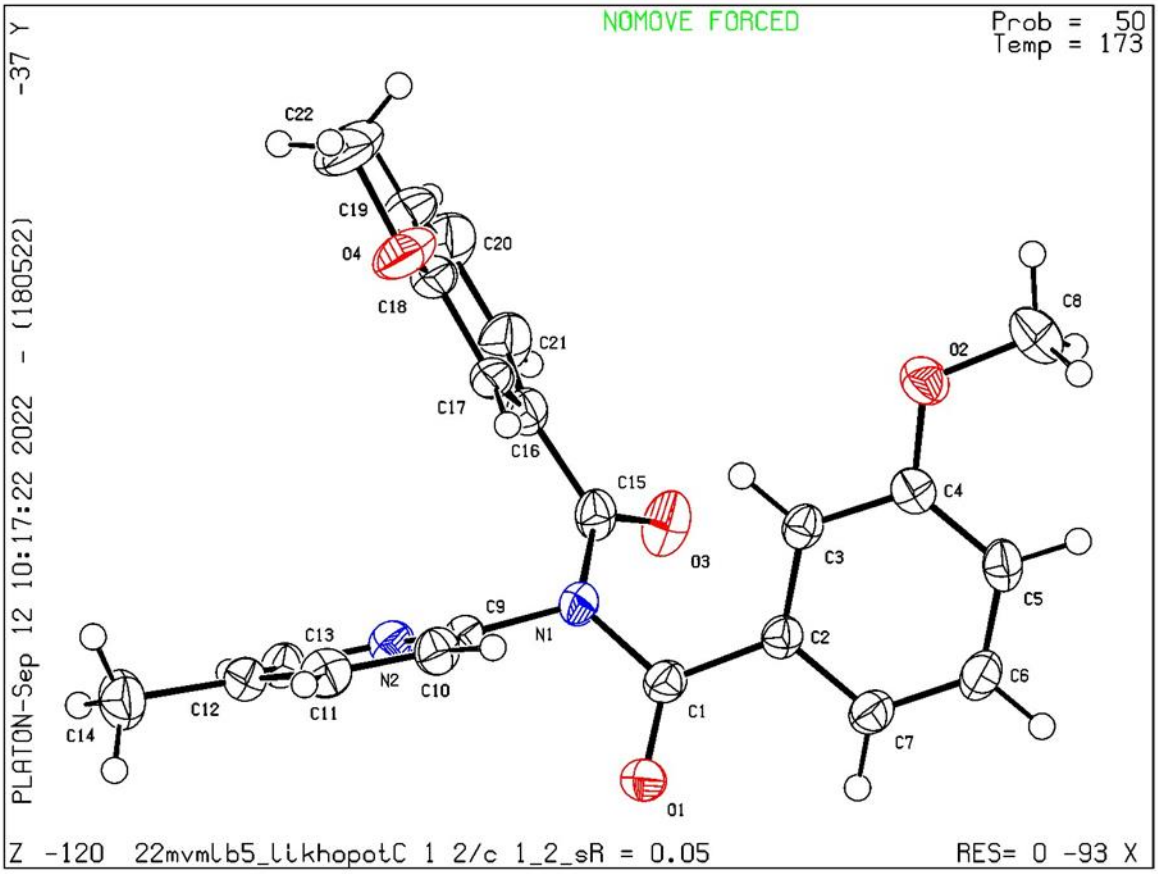

(a) *Crystal structure of the N,N-diacylated product **165i** showing the atom numbering*

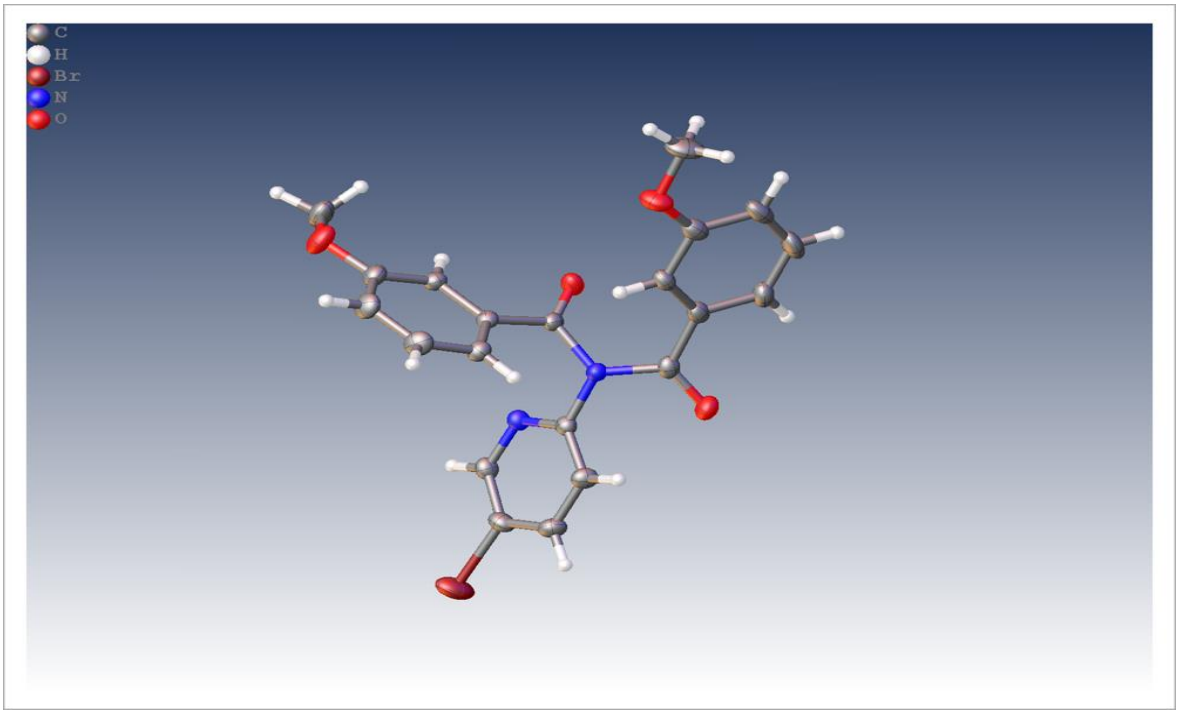

(b) Crystal structure of compound **165j**

Fig 41 *Single X-ray crystal structures of compounds* ***165i*** *and* ***165j*** *showing hydrogen atoms in white, oxygen atoms in red, carbon atoms in grey, nitrogen atoms in blue, and bromine atom in maroon*

The occurrence of *N*,*N*-diacylated products derived from the 5-substituted aminopyridines can be attributed to the *para*- electron donating effects caused by the substituents, specifically the methyl group. Although halogens are electron withdrawing through the inductive effects (-*I*), they have non-bonding valence electrons that contribute to p-π conjugation, and they usually direct electron density to *ortho*- and *para*-positions of the unsaturated ring system. Table **8** shows a comparison between the products obtained with the use of pyridine and triethylamine.

Table 8 *N*-diacylated products from meta-methoxybenzoic acid

Amine	Isolated product with Pyridine	Isolated product with Triethylamine
151i	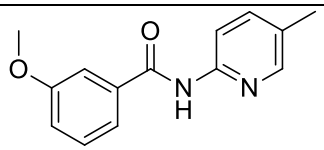 **158i**	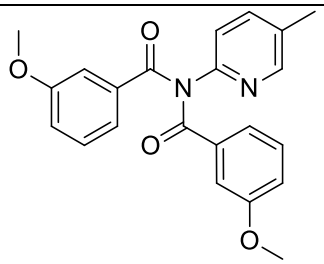 **165i**
151j	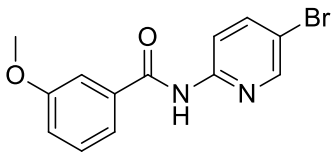 **158j**	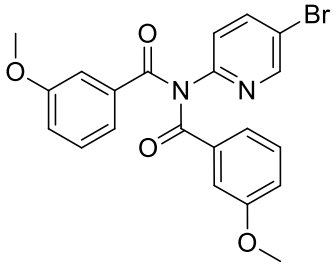 **165j**

To further extend our explorations, aminopyridines **151k**, **151l**, and **151m** bearing the methyl, bromo, and chloro substituents in the 6-position were assessed, all transforming into the desired monoacylated products **158k**, **158l**, and **158m** in 88%, 10%, and 23% respectively. However, in the case of **158l** and **158m**, the integrated protons exceeded the expected number. The single crystal X-ray diffraction revealed the hydrogen bonding interactions between the oxygen atom of a water molecule and the amide proton (Fig **42a** and **b** respectively). Although unverified, it is possible that this bonding occurred during the workup process.

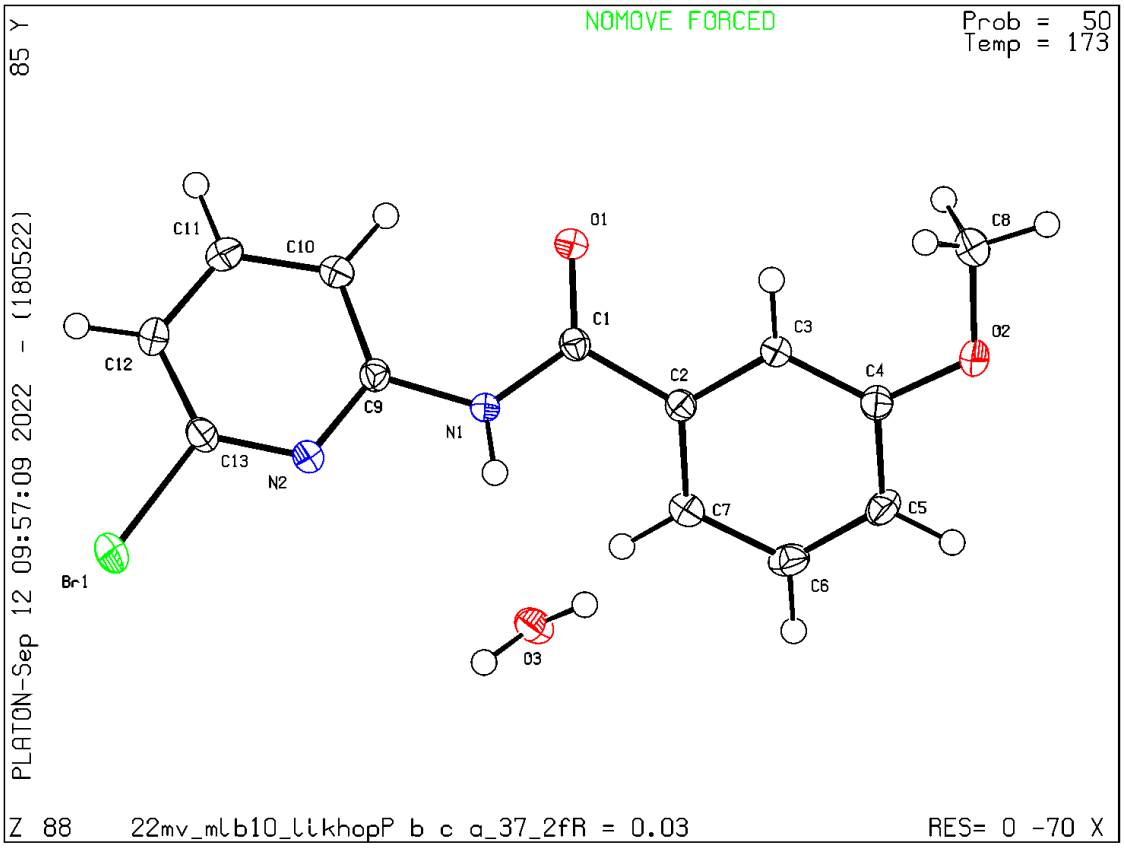

(a) Crystal structure of compound **158l**

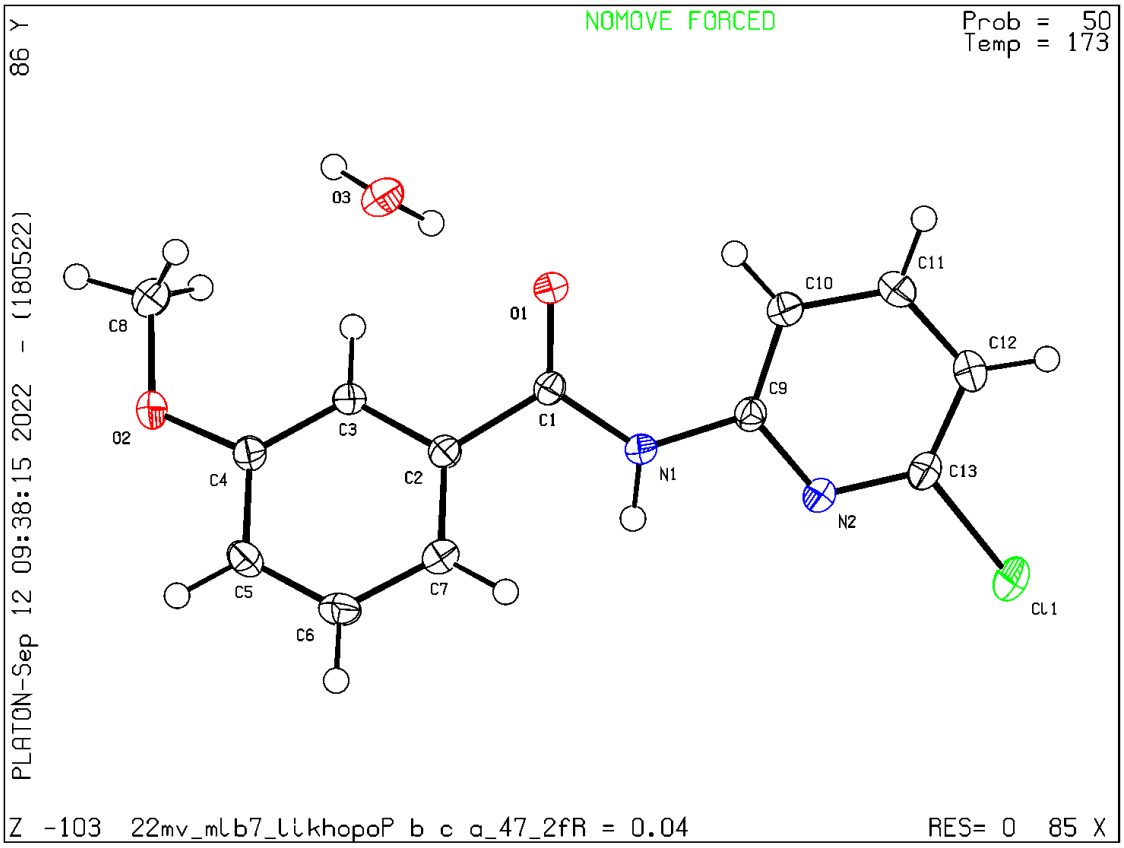

(b) Crystal structure of compound **158m**

Fig 42 *Single X-ray crystal structures of compounds* ***158l*** *and* ***158m*** *showing hydrogen atoms in white, oxygen atoms in red, carbon atoms in grey, nitrogen atoms in blue, chlorine atom in green, and bromine atom in maroon*

Although disubstitution was expected in the reaction of the methoxybenzoic acid **153** and 2-amino-3-bromopyridine **151n**, the monobenzoylated product **158n** was isolated in 22 % yield as the only constituent after purification by column chromatography. The low yield is suspected to have occurred as a result of steric hindrance by the bromine atom. The crystal structure showing the mono-substituted product **158n** is depicted below (Fig **43**).

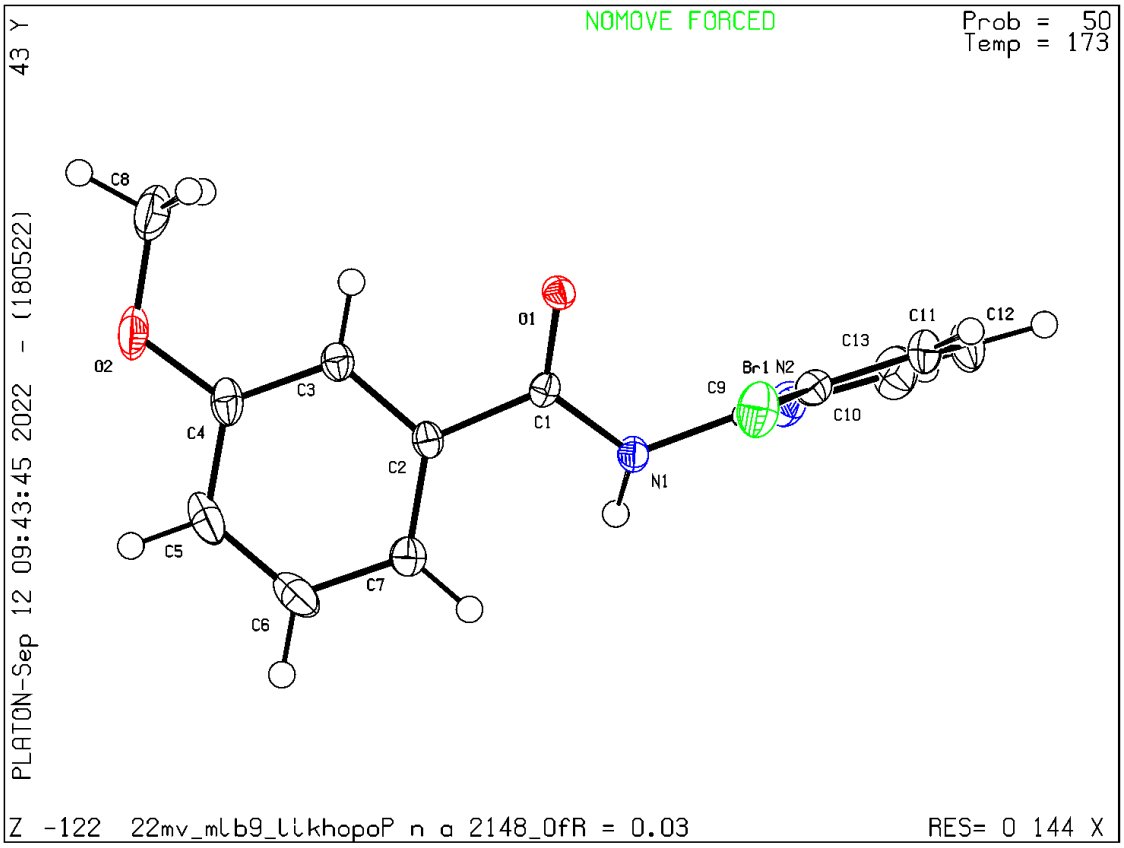

Fig 43 *Crystal structure of product* ***158n*** *showing the atom numbering, hydrogen atoms shown as small spheres arbitrary radius, oxygen atoms in red, bromine atom in green, and nitrogen atoms in blue*

After exploring the poor yields and *N*,*N*-diacylation for some of the products, triethylamine was replaced by pyridine. Repeating acylation of **151i** and **151j** under pyridine conditions furnished the *N*-pyridinylbenzamides **158i** and **158j** in 81% and 99% respectively, which were the highest yields reported for the entire series of the methoxybenzamides synthesised. The overlaid ^{1}H NMR spectra of compounds **158i** and **165i** is depicted in Fig **44** where the amide proton appears at around 9.00 ppm for compound **158i**. Aminopyridines **151l**, **151m**, and **157n** also proved the effectiveness of pyridine by enhancing the yields of their corresponding analogues **158l**, **158m**, **158n** to 56%, 65%, and 48% yields respectively. Derivative **164o** was only synthesised in the presence of pyridine and was afforded in 62% yield.

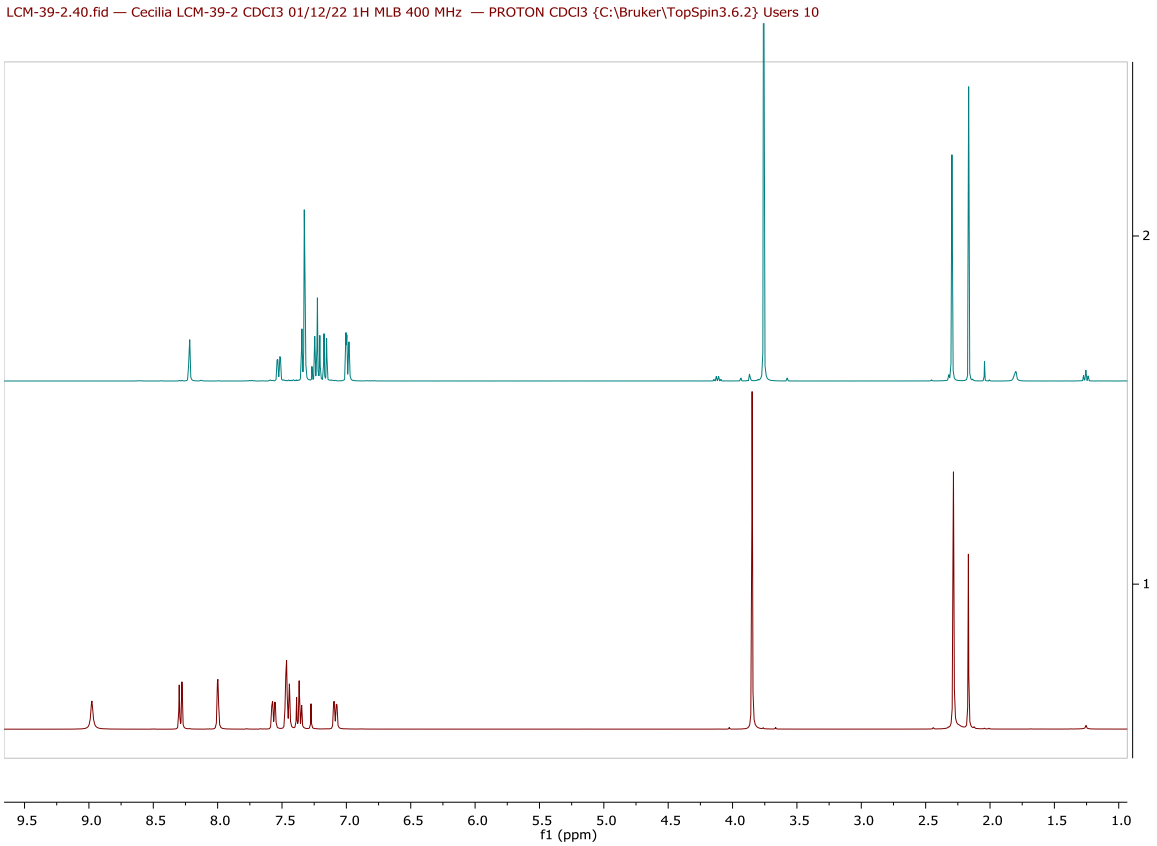

Fig 44 *^{1}H NMR representation showing the presence of amide H in **158i** (red) and absence of amide H in **165i** (green)*

Characteristic signals of the derivatives **158i**-**o** for the amide H, C=O and C-8 in the ^{1}H and ^{13}C NMR spectra are shown in Table **9**. The ^{1}H NMR spectra showed uniform amide NH absorptions between 8.65 ppm and 8.90 ppm for the compounds.

Table 9: Selected ^{1}H and ^{13}C NMR spectroscopic data for derivatives **158i**-**o**

Compound Number	**Amide H (s) ^{1}H NMR (δ: ppm)**	**C-8 ^{13}C NMR (δ: ppm)**	**C=O ^{13}C NMR (δ: ppm)**	**NMR Solvent**
158i	8.89	150.0	165.6	$CDCl_3$
158j	8.85	151.5	165.4	$CDCl_3$
158k	8.76	156.8	165.6	$CDCl_3$
158l	8.74	151.6	165.5	$CDCl_3$
158m	8.73	151.4	165.5	$CDCl_3$
158n	8.66	148.7	164.8	$CDCl_3$
158o	8.76	149.8	165.5	$CDCl_3$

The ^{13}C NMR spectroscopic results indicate that the C-8 signals of the carbon nuclei directly bonded to the amide nitrogen for the *N*-pyridinylbenzamides are highly deshielded. The C-8 value of derivative **158k** is predominantly downfield at 156.8 ppm owing to the methyl substituent being *meta* to C-8 and therefore not being able to release electron density to that position. The C-8 values for compounds **158n** and **158o** were more shielded at 148.7 ppm and 149.8 ppm respectively due the known electron donating effects by resonance of the halogens.

Our experiments were consistent with the literature results that the use of pyridine provides monosubstituted products in acylation of heterocyclic amines, while triethylamine yields diacylated product.[161,162] It was mentioned earlier that the pK_b of pyridine is higher than the pK_b of triethylamine. As a result, pyridine is less basic and therefore less likely to deprotonate the amidic proton formed, which favours monoacylation (Scheme **46**).

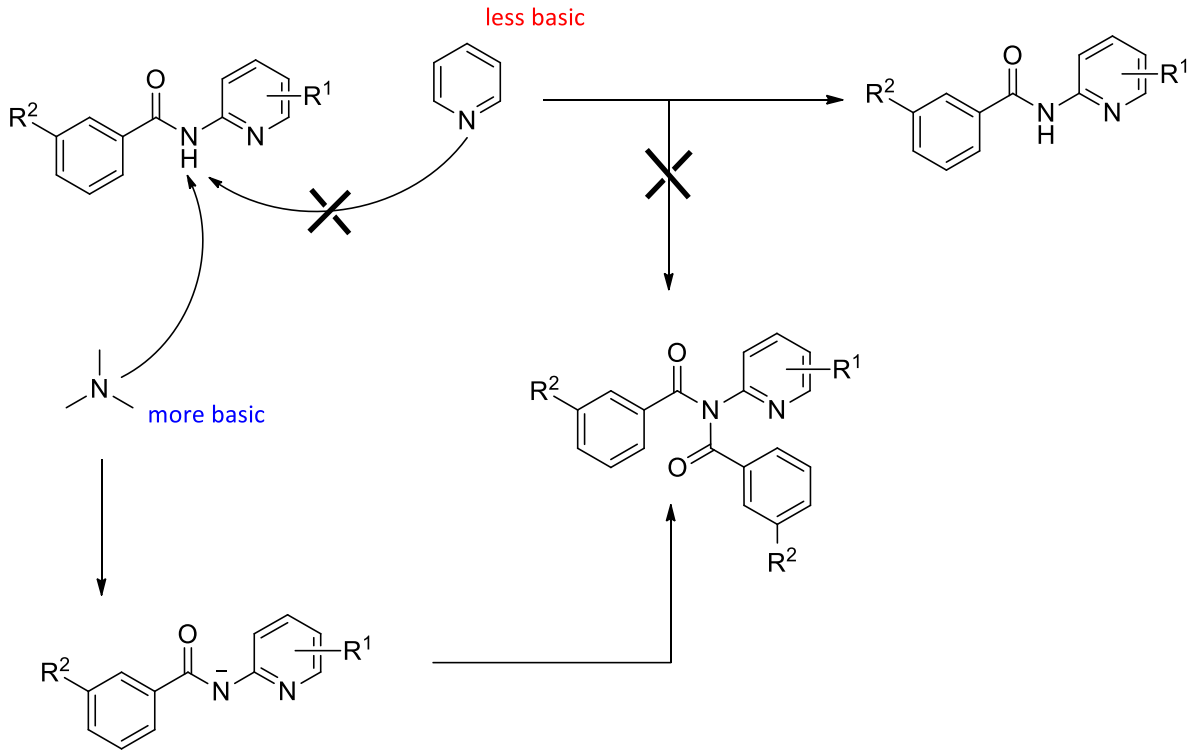

R[1]= Me, Br, **R**[2]= H, OMe

Scheme 46 *Generic representation of the major difference in basicity between triethylamine and pyridine in acylation reactions*

In our case the observed *N*,*N*-dibenzoylations were specifically for those compounds derived from heterocyclic amines substituted with the bromo and methyl groups in the *meta*-positions relative to the ring nitrogen. Monoacylation was favoured in aminopyridines containing the same substituents in the 6-position. Lastly, Putra and co-workers reported that when pyridine was used to catalyse

their amidation reactions, the product percentage yield was four times higher than the yield they obtained when using triethylamine.[156] In our case the enhanced yields were particularly observed for the compounds re-synthesised from aminopyridines. As with the case of anilines the yields improved with the employment of triethylamine.

2.1.5 Preparation of benzamides **166** from 3-hydroxybenzoic acid **154** and anilines

Our next strategy was to conduct the amidation reactions starting from 3-hydroxybenzoic acid **154** following a similar approaches to those described in the previous sections. The aim was to test amidation to obtain compounds **166**, which could then be linked to 2,4,6-trichloropyrimidine **102** through forming the phenolate ion **167** from the hydroxy-based benzamide **166** under basic conditions, and then using this to displace the first chlorine atom to form dichloro-substituted product **168** (Scheme **47**). This would represent an amidation first, linking second approach to the preparation of the final desired products.

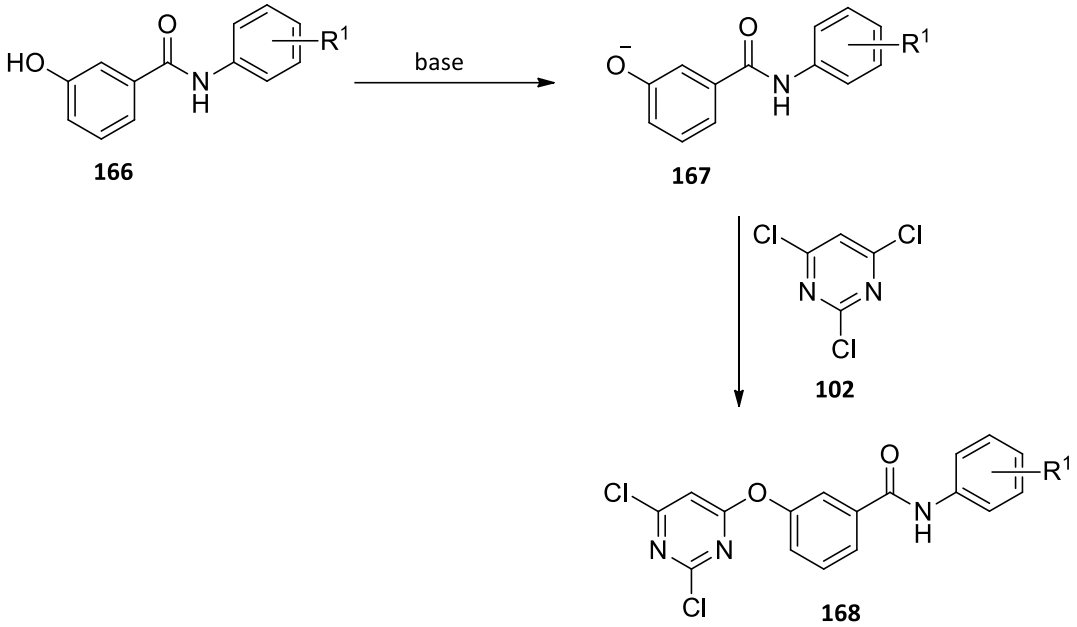

Scheme 47 *First chlorine displacement representation*

The synthesis of 3-hydroxybenzoyl chloride **169** from benzoic **154** acid was reported in the literature and was obtained in 73.6-76.3% yields, where *meta*-hydroxybenzoic acid was reacted with thionyl chloride employing DMF as a solvent (Scheme **48**).[163]

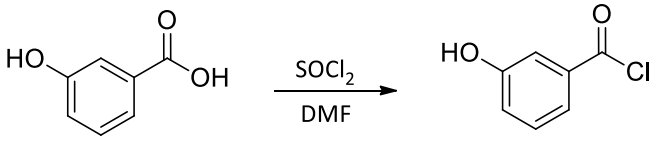

154 **169**

Scheme 48 *Literature synthesis of meta-hydroxybenzoyl chloride* ***169***

This method was put to the test, however, converting the 3-hydroxybenzoic acid to its acyl chloride came with numerous synthetic challenges. Firstly, since DMF is non-volatile it could not be removed *in vacuo* as previously done with the already reported acyl chlorides. Instead, the residue was directly added as a thick and sticky paste to the ice-cold mixture of 4-bromoaniline and pyridine in acetonitrile. Secondly, the presence of DMF in the mixture made it difficult for us to monitor the reaction progress because the mixture was viscous, resulting in extremely difficult stirring. For this reason, the reaction was stopped after 24 h.

Upon evaporating acetonitrile, the contents of the reaction were dissolved in ethyl acetate and washed several times with saturated brine solution to remove DMF. Thirdly, after column chromatography purification with 30% ethyl acetate/hexane, it appeared that DMF was not completely removed from the mixture as per observations from the ^{1}H NMR spectrum, as the DMF residual signal was observed at 3.92 ppm. Lastly, we could not verify if the product was formed because of the small signal intensities in the aromatic region. Although increasing the concentration increased the intensities, there were multiple unidentified signals in the spectrum. Recrystallization was also not helpful as the spectrum appeared the same thereafter.

As an alternative, the use of peptide coupling reagents like DCC **28** for direct amide bond formation came to our attention (Scheme **49**). Screening a range of solvents for dissolving the acid proved effective as THF particularly stood out to be an excellent solvent for dissolution. Adding two equivalents of **28** to a solution of **154** in THF for one hour at room temperature and adding an equimolar amount of aniline **151a** while stirring for a further 4 h resulted in depletion of the carboxylic acid as seen by TLC analysis. However, there were many spots on the TLC plate that made purification challenging even with the use of different solvent systems and after filtering off the DCC side-product. As indicated in the introductory chapter, it is possible that a variety of products were formed, or either **28** simultaneously deprotonated both the carboxyl and hydroxyl hydrogens to afford 3-oxidobenzoate **170** according to the proposed mechanism below (Scheme **49**).

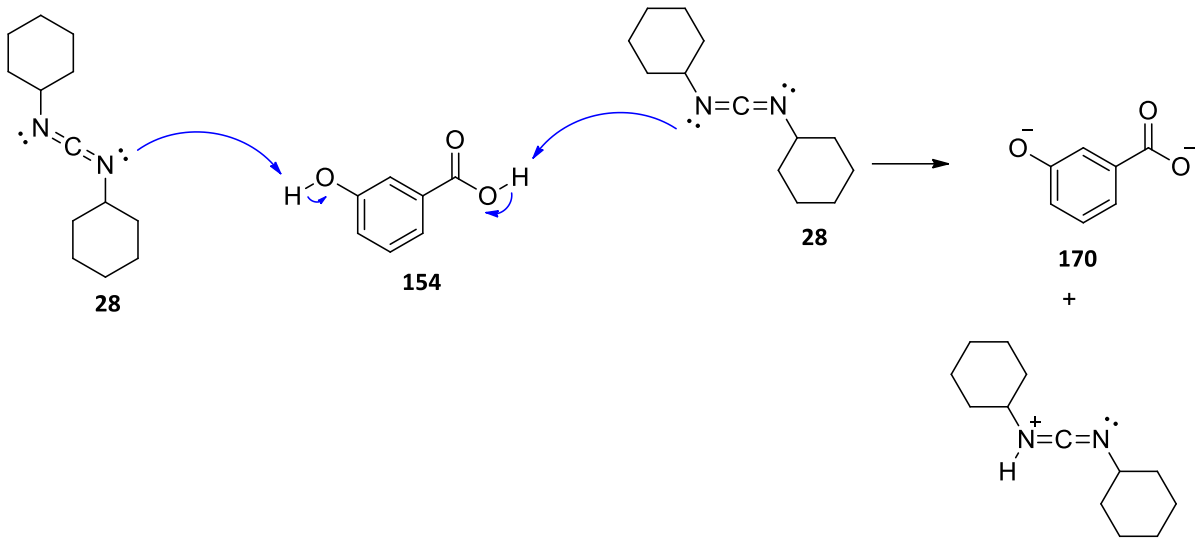

Scheme 49 *Plausible mechanism for the formation of* ***170***

We next wanted to investigate the direct condensation reaction between **154** and aniline under solvent free microwave irradiation without the use of a base to assess if the product would be formed. The utility of this technique was first tested by reacting benzoic acid **152** with **151a** in a microwave reactor at 100 °C for 5 minutes, where compound **157a** was obtained in 28%. The low yield is attributed to the reaction not going to completion owing to the widespread assumption that lack of interaction between the carboxylic acid and amine occurs as a result of the presence of an unreactive ammonium carboxylate salt **171** produced in the reaction (Scheme **50**). As such, the reaction needs to be conducted under relatively forcing conditions.[164] It is worth noting that because our focus was on obtaining the target compound, the reaction conditions were not optimized.

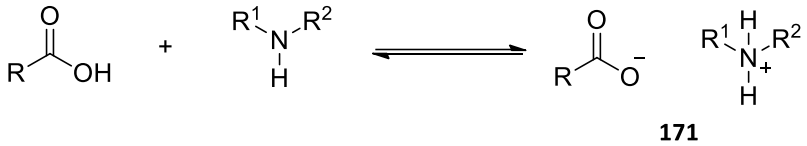

Scheme 50 *Formation of ammonium carboxylate salt*

A similar approach was applied using stoichiometric amounts of aniline **151a** and **154** in attempts get to the target compound **166a** (Scheme **51**), where new spots were observed on the TLC plate. It is worth mentioning that before workup the reaction mixture was monitored by TLC whilst comparing with the product obtained from the DCC method, but no correlating spots were observed.

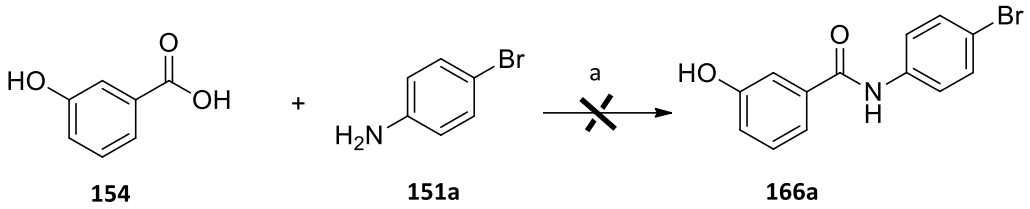

154 **151a** **166a**

Scheme 51 *Reagents and conditions (a) MW, 150 Watt, 10 min*

Considering that the reaction is reversible leading to the recovery of the starting materials, the acidic and basic workup were necessary to remove both starting materials. However, from the ^{1}H NMR spectrum it wasn't clear that the desired product had been obtained (Fig **45**). Analysis of certain amide products by NMR is also hindered by the fact that these amides can adopt different conformations in solution, and it is sometimes difficult to distinguish between impure products and products that are pure, but which adopt different solution conformations.

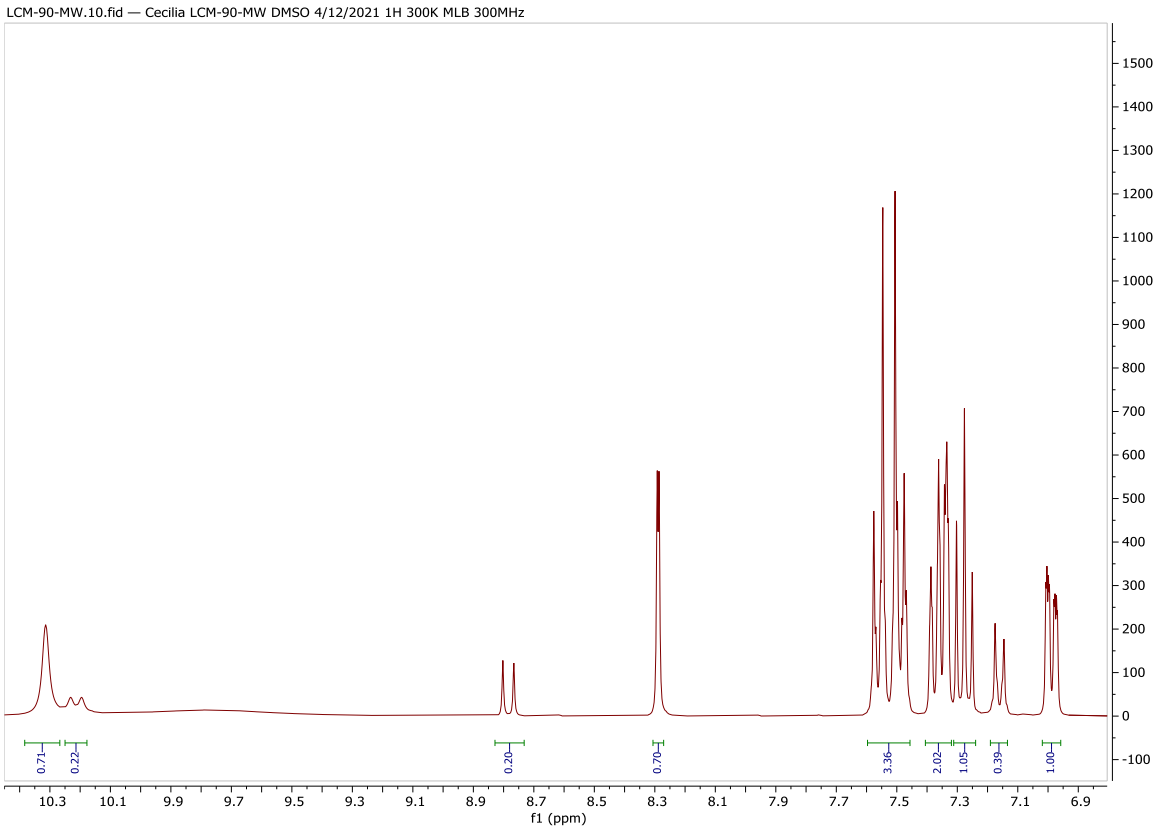

Fig 45 *^{1}H NMR of the unidentified product*

The reaction between **154** and thionyl chloride was reattempted omitting the solvent. Impressively, although the acid initially seemed difficult to dissolve in thionyl chloride, it was able to dissolve upon refluxing for overnight. After the amidating with aniline **151a**, the TLC analysis showed a few new spots. Column chromatography purification was done using 30% ethyl acetate/hexane. Based on the

NMR spectroscopic results (Fig **46**), extra signals with small intensities were seen which led to an assumption that the starting materials were not fully converted. The signals remained unchanged even after recrystallization and repeated acidic workup. Overlaying the proton spectra of the starting materials against the one of the reaction mixture demonstrated that neither the carboxylic acid nor amine was present because the signals appeared at distinct chemical environments.

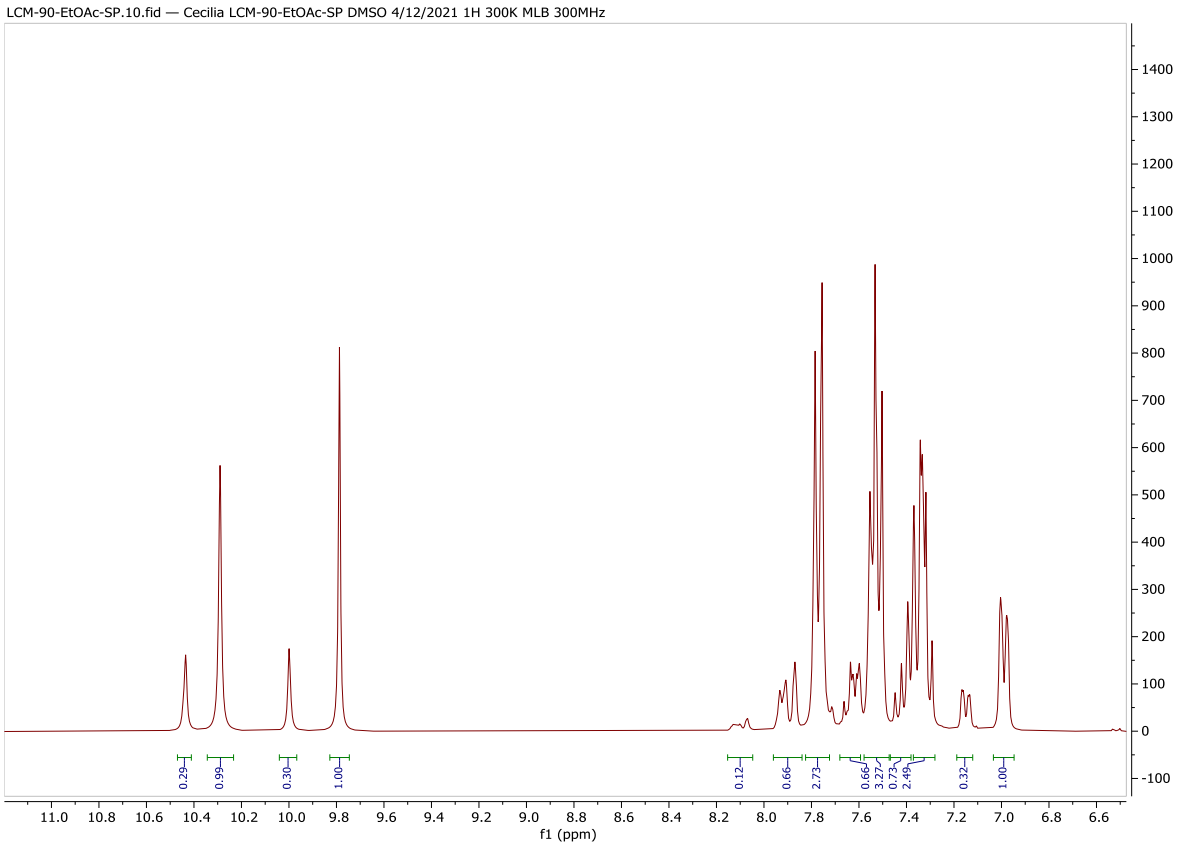

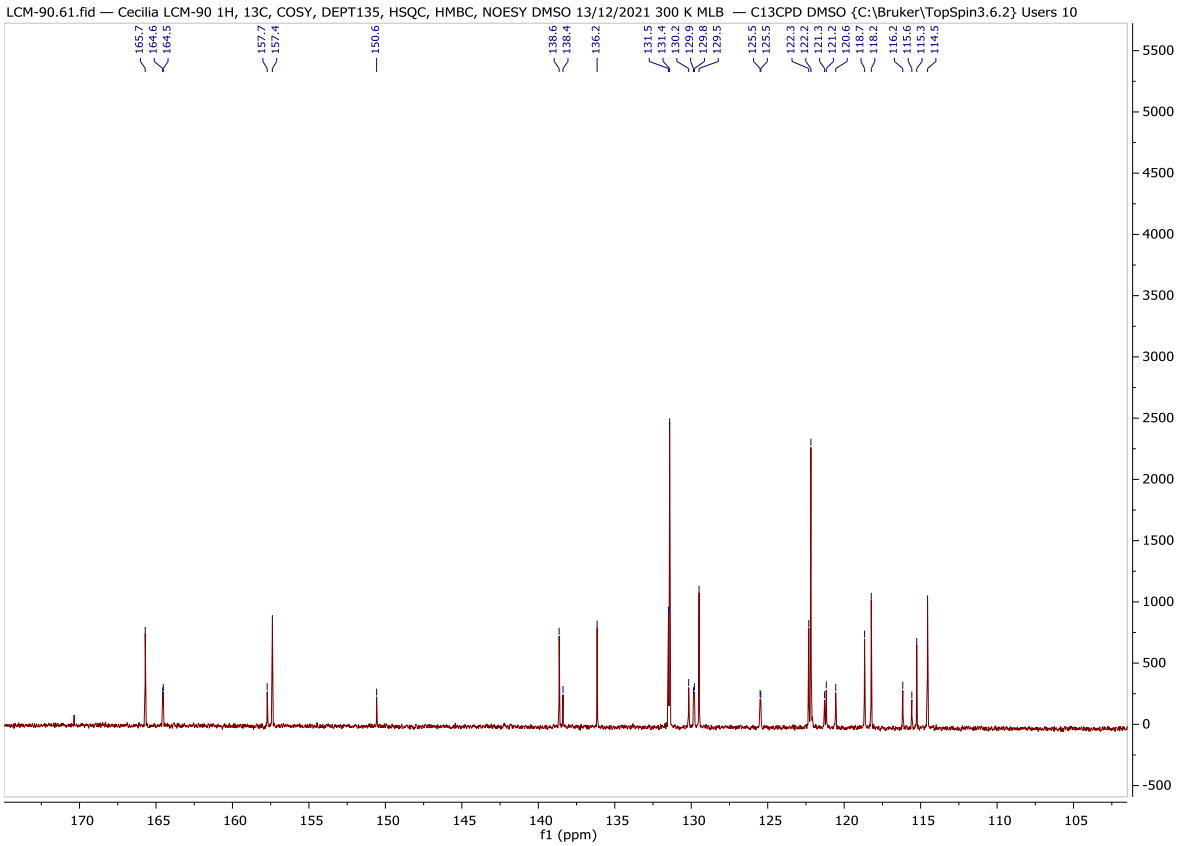

Fig 46 *^{1}H and ^{13}C NMR spectroscopic results for the reaction between acid 154 and aniline 151a using thionyl chloride*

2.1.5.1 The ^{1}H NMR spectrum comparison between the appearance and disappearance of the hydroxybenzoic acid proton

Considering that 3-hydroxybenzoyl chloride is unstable upon its preparation, we were prompted to repeat the chlorination step to investigate if the acyl chloride was the only component present. After analysing the crude mixture by proton NMR, the overlaid spectra showed disappearance of the carboxyl proton and multiple signals in the aromatic region were observed as depicted in Fig **47** (Blue spectrum at the top is for carboxylic acid, and the red one underneath is for the reaction mixture). As a result of the overlapping signals, it was difficult to verify the formation of the desired *meta*-hydroxybenzoyl chloride.

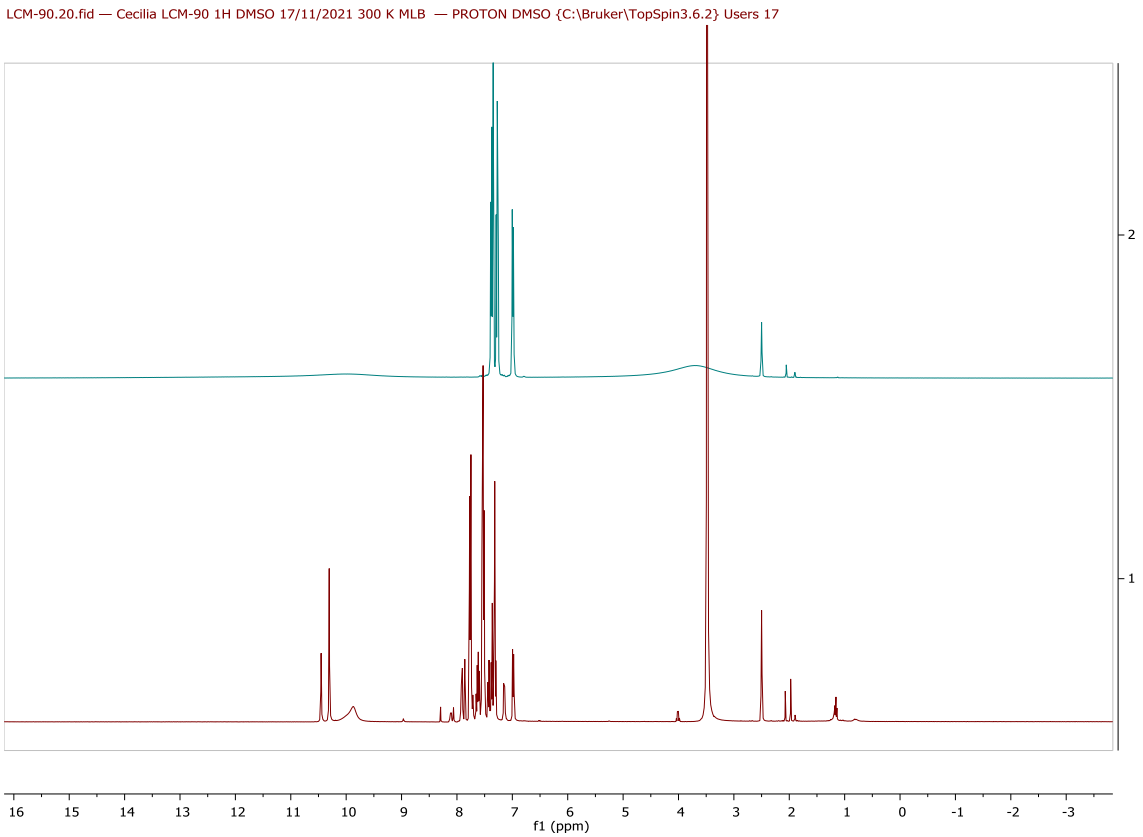

Fig 47 *^{1}H NMR spectra of the reaction between acid **154** and thionyl chloride*

There is a possibility that the hydroxyl oxygen of intermediate **169** was involved in a nucleophilic attack on the carbonyl carbon of another molecule of **160**, resulting in the formation of an ester-acyl chloride **172** (Scheme **52**) which can react further leading to polymerization. The involvement of the hydroxyl group is likely considering the successful chlorination of the protected methoxybenzoic acid **153** discussed in section **2.1.2** and **2.1.4**, where the corresponding acid chloride gave the desired compounds without polymerization.

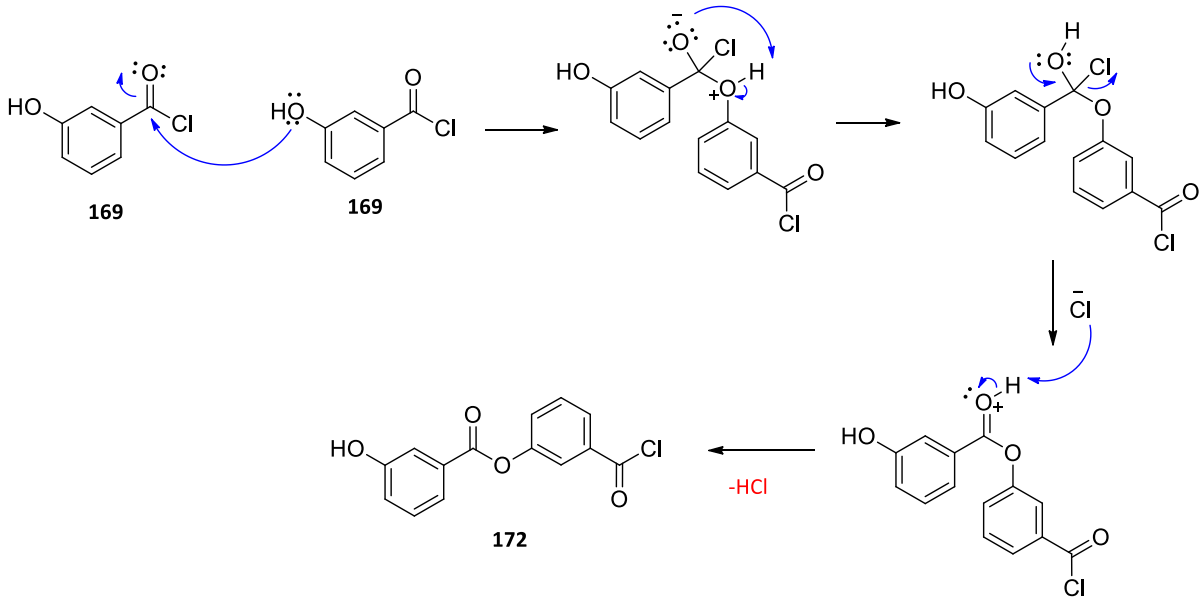

Scheme 52 *Proposed mechanism for polymerization of* ***169***

2.1.6 Preparation of benzamides from 3-hydroxybenzoic acid **154** and aminopyridines

After several failures to obtain the desired compound **166a**, we next wanted to evaluate the reactivity of the hydroxybenzoyl chloride using a different class of amines. Based on the previously discussed diacylation problems encountered when heterocyclic reagents were used in amidation reactions catalysed by triethylamine, similar reactions involving the *meta*-hydroxybenzoic acid **154** and aminopyridines **151i-o** were conducted employing pyridine (Scheme **53**). The structures of the isolated hydroxyl-based pyridinylbenzamides are shown in Fig **48**.

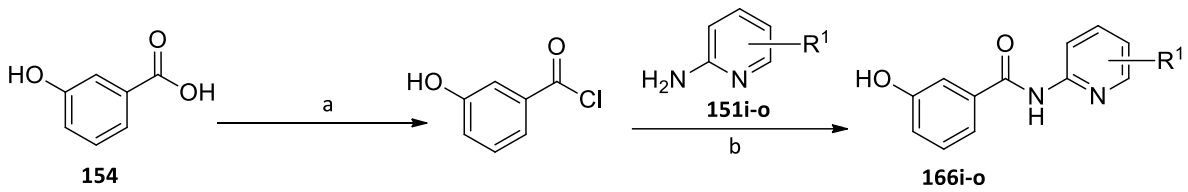

Scheme 53 *Reagents and conditions: (a) $SOCl_2$, reflux, 24 h; (b) CH_3CN, pyridine, 0 °C-rt, 3-24 h, 28-53%*

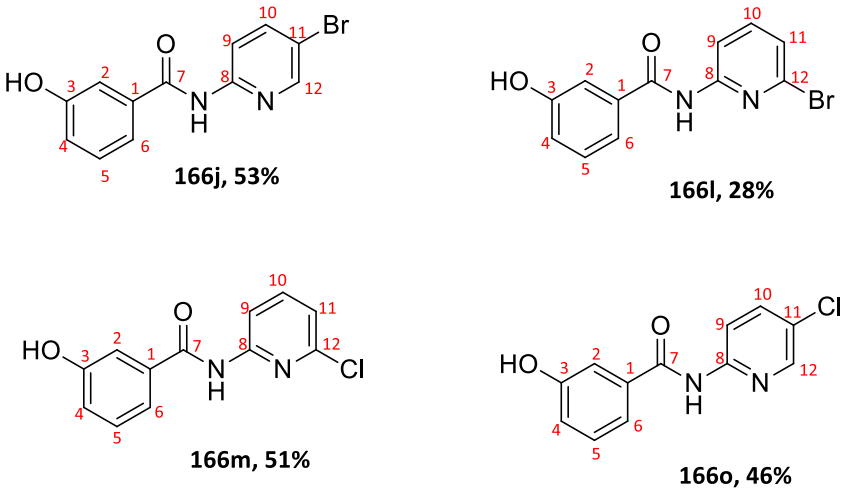

Fig 48 *Structures of the synthesised N-pyridinylbenzamides derived from 3-hydroxybenzoic acid* ***154***

The reaction between acid **154** and aminopyridine **151j** was first tested during which depletion of starting materials was observed on the TLC plate after 21 hours. After purification by column chromatography, similar NMR spectroscopic results described in the previous section were seen as expected. Further purification by recrystallization was not possible because the impure product was a fine solid. Fortunately, since the product was partially soluble in ethyl acetate, several washes with ethyl acetate enabled the recovery of product **166j** in 53% with negligible traces of undesirable impurity. Similar analogues synthesised from aminopyridines with varying substitution (**151l**, **151m**, and **151o**) also afforded the expected compounds. Likewise, successive washing with EtOAc was required to afford analogues **166l**, **166m** and **166o** in 28%, 51%, and 46% yields respectively. Unfortunately, the isolation of derivatives **166i**, **166k**, and **166n** was impossible, even after multiple washes with ethyl acetate.

The ^{1}H NMR spectroscopic data indicated that each of the analogues **166j**, **166l**, **166m**, and **166o** had seven aromatic protons and the most downfield signals were phenolic and amide protons. The ^{13}C NMR spectra showed that the position at which the halogens were bonded was the main difference between these compounds. The C12 carbon in the *meta*-position to the amide nitrogen was the common feature between **166l** and **166m** with their signals appearing at 138.8 and 148.0 ppm, respectively. Compound **166j** and **166o** had C11 *para* to the amide NH in common appearing at 113.9 and 125.9 ppm, respectively. The ^{13}C signal in the NMR spectrum for the bromo-attached carbon for derivatives **166j** and **166l** signals were more shielded at 113.9 ppm and 138.8 ppm, respectively when compared to the analogous chloro-containing compounds **166m** and **166o** which were observed at 148.0 ppm and 125.9 ppm respectively. This observation is as a result of the normal halogen dependence effects rather than electronegativity effects. The NHD effects were recently described by Viesser and co-workers as relativistic effects caused by a phenomenon called spin-orbit (SO) coupling,

which increases with the nuclear charge of halogens.[165] Halogen undergoes spin polarization due to the SO coupling, which is brought on by the external magnetic field and transferred to adjacent nucleus through covalent bonds. Specifically for the atom covalently bonded to the halogen, the magnetic field generated by the induced electron spin density may have a considerable shielding effect. This effect is noticeable for the bromine substituted compounds. The observed chemical shift differences for the carbon bound to bromine when compared to carbon attached to chlorine for the synthesised analogues agrees with the proposed explanation. H12 nuclei of **166m** and **166o** (7.26 and 8.37 ppm respectively) were more shielded than the H11 nuclei of **166j** and **166l** (8.51 and 7.39 ppm respectively).

Aside from the differences in the chemical shifts of the H11, H12, C11, and C12, the primary nuclei from the NMR spectra that determined the formation of the products are the amide NH, C-8, and C=O and their signal absorptions are summarised below (Table **10**). As can be seen from the table, similar patterns are observed for all the key nuclei identified. For the analogues substituted *meta* to the amide on the pyridine ring (**166l** and **166m**), the amide NH signals appeared at 10.98 ppm and 10.97 ppm respectively, and NH signals of the compounds with *para* substituents relative to the amide (**166j** and **166m**) appeared at 10.85 ppm and 10.81 ppm respectively. The C-8 signals for **166l** and **166m** appeared downfield, while those for **166j** and **166o** were upfield. Identical carbonyl carbon absorptions were observed for derivatives **166j**, **166l**, and **166m** at 166.2 ppm.

Table 10: ^{1}H and ^{13}C NMR spectroscopic results for the isolated compounds **166j**, **166l**, **166m** and **166n**

Compound Number	**Amide H (s) ^{1}H NMR (δ: ppm)**	**C-8 ^{13}C NMR (δ: ppm)**	**C=O ^{13}C NMR (δ: ppm)**	**NMR Solvent**
166j	10.85	151.2	166.2	DMSO-d_6
166l	10.98	152.5	166.2	DMSO-d_6
166m	10.97	152.3	166.2	DMSO-d_6
166o	10.81	151.3	166.6	DMSO-d_6

2.1.7 Synthesis of complex benzamides

2.1.7.1 Synthesis of 3-((2,6-dichloropyrimidin-4-yl)oxy)benzoic acid

After several difficulties encountered with purification of compounds **166j**, **166l**, **166m**, and **166o**, and with the possibility that the free hydroxyl group was interfering in the reaction, the proposed synthetic approach was revisited in an attempt to find a suitable route to get to the target compounds **168**. At this stage, there was some evidence to support the possibility that coupling the 3-hydroxybenzoic acid derivative to 2,4,6-trichloropyrimidine **102** first, followed by amidation, would be a preferred route.

According to the proposed approach, in order to prepare intermediate **155** (Scheme **54**), the synthesis of ester **141**, pyrimidine **102**, and complex ester **173** would be required. We considered the C-O coupling reaction more likely to succeed using an ester rather than the free carboxylic acid.

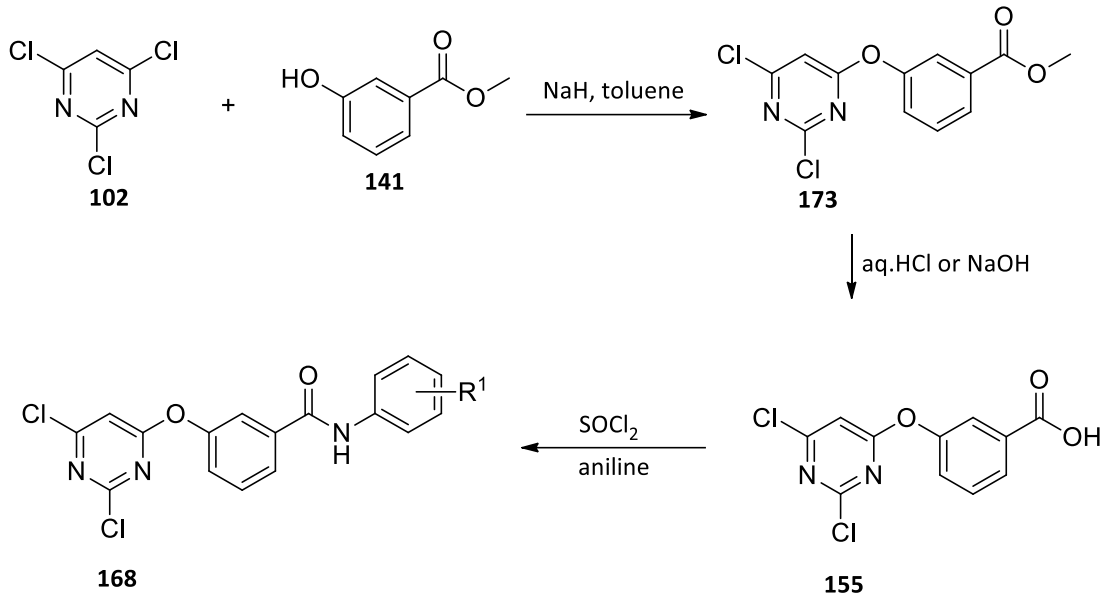

Scheme 54 *Proposed synthetic route to the target compounds* ***168***

Intermediate **141** (Scheme **55**) was prepared from a reaction of carboxylic acid **154** and thionyl chloride using methanol as a methylating agent under ice-cold conditions, followed by overnight room temperature stirring. A cream-white solid product **141** (97%) was isolated, and the structure was confirmed by the disappearance of the carboxylic acid proton and appearance of the methyl ester protons at around 3.93 ppm in the ^{1}H NMR spectrum. The key starting material 2,4,6-trichloropyrimidine **102** appropriate for this study was prepared from barbituric acid **174** (Scheme **55**) according to literature reports.[59] Initially, the product was obtained in a reasonable yield of 57%. After extensive optimizations of increasing the reaction temperature from 130 °C to 150 °C, 76% was the highest yield obtained compared to an excellent yield of 86% previously reported.[59] The ^{1}H NMR spectroscopic data revealed the appearance of a singlet H-5 proton signal at 7.38 ppm. Because the C-4 and C-6 carbon nuclei are chemically equivalent, the ^{13}C NMR spectrum showed the presence of three aromatic peaks at 163.0, 160.3, and 120.1 ppm, which was consistent with literature results.[59]

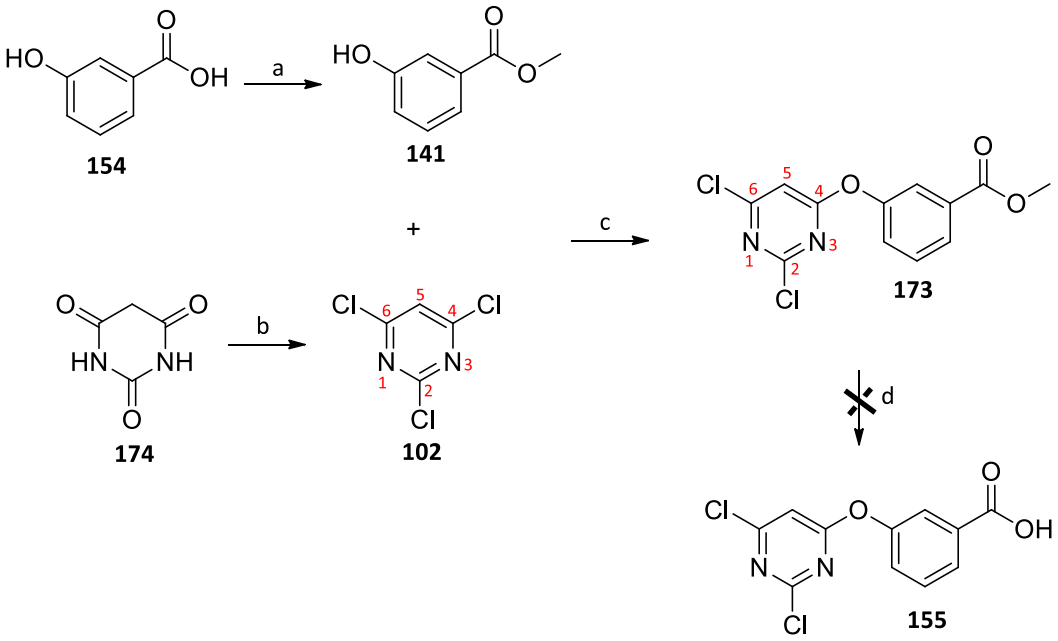

Scheme 55 *Reagents and conditions (a) $SOCl_2$, MeOH, 0 °C-rt, 97%; (b) $POCl_3$, tetraethylammonium chloride, reflux, 24 h, 57-76%; (c) K_2CO_3, acetone, overnight, 81% (d) aq. HCl or NaOH, DMF, heat, 24 h (no product)*

The complex ester **173** was obtained from a reaction between **102** and **141** employing potassium carbonate as a base and acetone as a solvent (Scheme **59**). After column chromatography purification, a white amorphous solid product was obtained in 81% yield. The ^{1}H NMR spectrum for this compound integrated for eight protons as expected, with three shielded protons for the methoxy group at 3.94 ppm, and the remaining protons were observed in the aromatic region. One upfield aromatic proton singlet peak at 6.87 ppm is for the H5 proton. Four protons from 7.35-8.00 ppm belong to the phenyl motif, and their splitting patterns vary based on their neighbouring protons. Applying the 2n+1 rule, two protons H12 and H10 at 7.35 and 8.00 ppm gave doublet signals (d, *J*= 8.1 Hz and d, *J*= 7.8 Hz, respectively). The H8 proton at 7.81 ppm was a singlet peak because of the adjacent quaternary carbons, while the H11 proton at 7.54 ppm split into a triplet (t, *J*= 8.0 Hz) owing to spin-spin coupling caused by its two neighbouring protons, which although not equivalent gave rise to very similar coupling constants. The ^{13}C NMR spectrum presented a total of twelve chemically distinct signals; four in the pyrimidine ring, six from a phenyl ring, one carbon nucleus in the aliphatic region, and one carbonyl carbon. DEPT NMR confirmed the presence of the CH_3 and five CH signals, and six quaternary aromatic peaks, also counting the carbonyl carbon.

After the successful synthesis of compound **173**, acidic hydrolysis in methanol was attempted with dilute HCl or H_2SO_4 (1 M) under refluxing conditions. However, compound **155** did not form even after prolonging the reaction time to three days. Doubling the concentration of the acid was also ineffective

as there was no indication of the product formation by TLC analysis. The reaction was anticipated to proceed according to a hydrolytic mechanism detailed by Yates and McClelland.[163] The carbonyl oxygen atom of **173** was expected to take a proton from the hydroxonium ion (H_3O^+) to form an electrophilic intermediate **175**. Nucleophilic attack by one lone pair on the oxygen atom of the water molecule would result in the formation of a tetrahedral intermediate **176**. Consecutive proton transfers would then lead to elimination of CH_3OH giving rise to carboxylic acid **155** as depicted in Scheme **56**. The failure of the reaction to occur could be explained by the reversible nature of this mechanism. It is worth noting that the starting material was also recovered when the reaction was repeated under base-catalysed conditions.

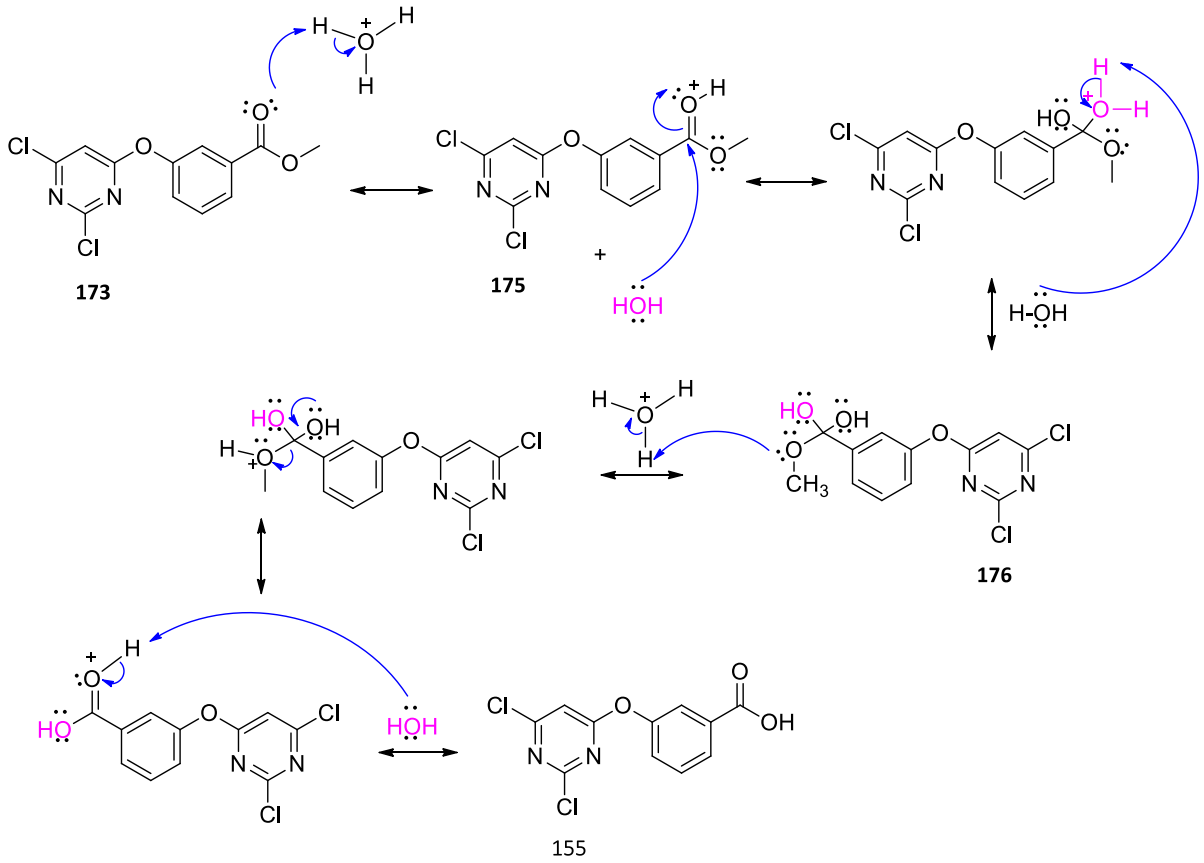

Scheme 56 *Possible hydrolytic reaction mechanism under acidic conditions*

The direct coupling of **102** with 3-hydroxybenzoic acid **154** became the alternative approach to the formation of **155** (Scheme **57**). The synthesis of aryl carboxylic acid **155** was initially attempted by reaction of **102** directly with carboxylic acid **154** in the presence of potassium carbonate. Unfortunately, the reaction did not proceed as anticipated because the starting materials were recovered and increasing the molar amounts of K_2CO_3 to three equivalents was also ineffective. Although the intention was to deprotonate the hydroxyl hydrogen because the carboxylic acid

hydrogen is more acidic, potassium carbonate could have been too weak for deprotonating both protons on **154** and might only deprotonate the carboxylic acid proton.

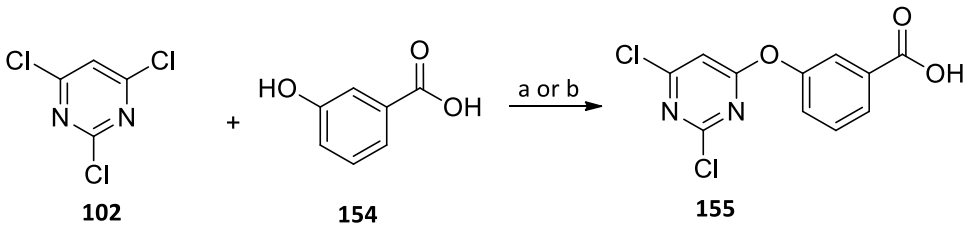

Scheme 57 *Reagents and conditions: (a) K_2CO_3, acetone, 0 °C-rt, 24 h (no product); (b) 1 M NaOH, acetone, 0 °C-rt, 24 h, 48-81%*

Previous approaches employed NaOH as a suitable base for establishing the Meisenheimer inermediate.[59] Fortunately, repeating the reaction using 1 M NaOH proved effective as the product **155** was isolated in 48% yield. The possible reaction mechanism is shown in Scheme **58**. The first step involves the deprotonation of acid intermediate **154**. Subsequent cautious addition of the phenolate ion **170** to a solution of **102** in acetone provides the *para*-quinoid structure **177**. Chloride can act as a leaving group, resulting in the formation of the C-O coupled ionic intermediate **178**. At first, saturated ammonium chloride was used during the workup as a protonating agent of the ionic complex **178**, and an unsatisfactory yield (48%) of product **155** was obtained.

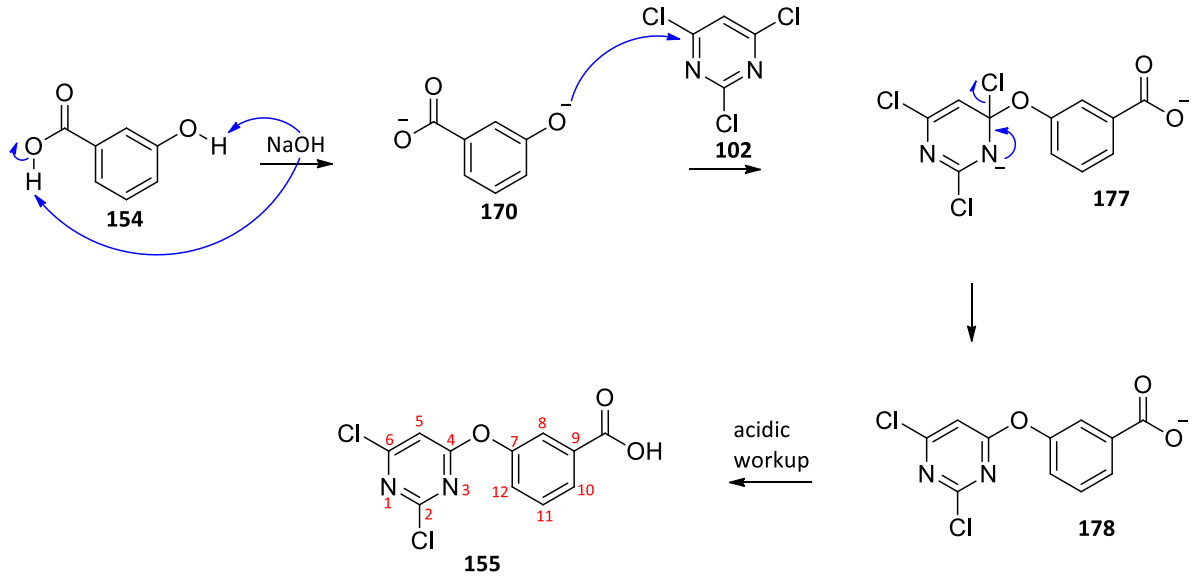

Scheme 58 *Plausible reaction mechanism for the formation of acid **155***

After several trials to improve the reaction yields, it became apparent that aqueous ammonium chloride was moderately acidic even after increasing its concentration for the neutralization of excess sodium hydroxide and protonation. Hydrochloric acid is undoubtedly a strong enough alternative acid

that can facilitate the protonation of **178**. However, caution should be exercised when sensitive substrates like heteroatom-containing compounds are involved. Adjusting the reaction mixture to pH 4 during workup improved the yield to 63%. Gratifyingly, decreasing the pH to 3 offered 81% yield without the need for column chromatographic purification.

Even though there are two possible positions for substitution of the chloride (C-2 or C-6), the 4/6-substituted intermediate **155** was the only isolated product. Additionally, there was no indication of a nucleophilic attack at the C2 position. This reaction outcome complements literature reports which state that nucleophilic attack of these systems occurs at C4/6 preferentially. [59,141]

The structure of the compound **155** was confirmed based on spectroscopic data. Surprisingly, the ^{1}H NMR spectrum showed the absence of a carboxylic acid proton, and a total integration of five aromatic protons. A resonance peak from the H-5 pyrimidine ring proton appeared at δ 7.50 ppm. Four phenyl protons were indicated by the presence of signals at 7.91 ppm (d, *J*= 7.7 Hz, 1H, H-10), 7.79 ppm (s, 1H, H-8), 7.63 ppm (t, *J*= 7.9 Hz, 1H, H-11), and 7.55 ppm (dd, *J*= 7.6 Hz, 1H, H-12). The ^{13}C NMR spectrum demonstrated an overall of eleven carbon nuclei which was consistent with DEPT135 analysis showing six quaternary signals and five CH signals. Quaternary C-2, and C-6 of the pyrimidine motif appeared at 158.2 and 161.7 ppm, respectively.

2.1.7.2 Comparison between the carbon signals of 2,4,6-trichloropyrimidine **102** and acid **155**

The C-O coupled carbon nucleus of acid **155** at 170.9 ppm was the most deshielded signal in comparison to that of **102** at 163.0 ppm. The C-5 signal at 107.6 ppm was the most shielded compared to 120.1 ppm recorded for precursor **102**. The C-8 and C-12, and C-10 which were *ortho* and *para* to the oxygen appeared at 122.1, 126.1, and 127.3 ppm, respectively. They were relatively upfield owing to the electron donating effects caused by an oxygen atom increasing the electron density in those positions. Taking the inductive effects into consideration, the C7 at 151.5 ppm was downfield because it is directly bonded to a more electronegative oxygen atom which pulls the electron density towards itself leaving that carbon electron deficient. The carbonyl carbon appeared at 166.3 ppm due to the latter effects. Obviously, the remaining quaternary carbon C-9 belonged to a signal at 132.9 ppm, while the C-11 nucleus in the *meta*-position to the electron donating group appeared at 130.4 ppm.

2.1.6.2 Synthesis of complex benzamides from anilines **151a**-**h**

The aforementioned C-O coupling breakthrough enabled a quick access to the synthesis of complex benzamides. As had been done with benzoic acids **152**-**154**, the complex acid **155** was converted into its corresponding acid chloride **179** by heating at 70 °C in the presence of thionyl chloride, and the reaction was complete within an hour (Scheme **59**). Despite the fact that triethylamine enhanced the yields for the *N*-phenylbenzamide derivatives, we wanted to suppress the risk of amine diacylation

and the preparation of the target compounds **168a**-**h** was performed under the previously described pyridine conditions. The isolated compounds **168a**-**e** and **168h** are shown in Fig **49** and the yields for compounds **168b** and **168d**-**h** were isolated from the TEA method.

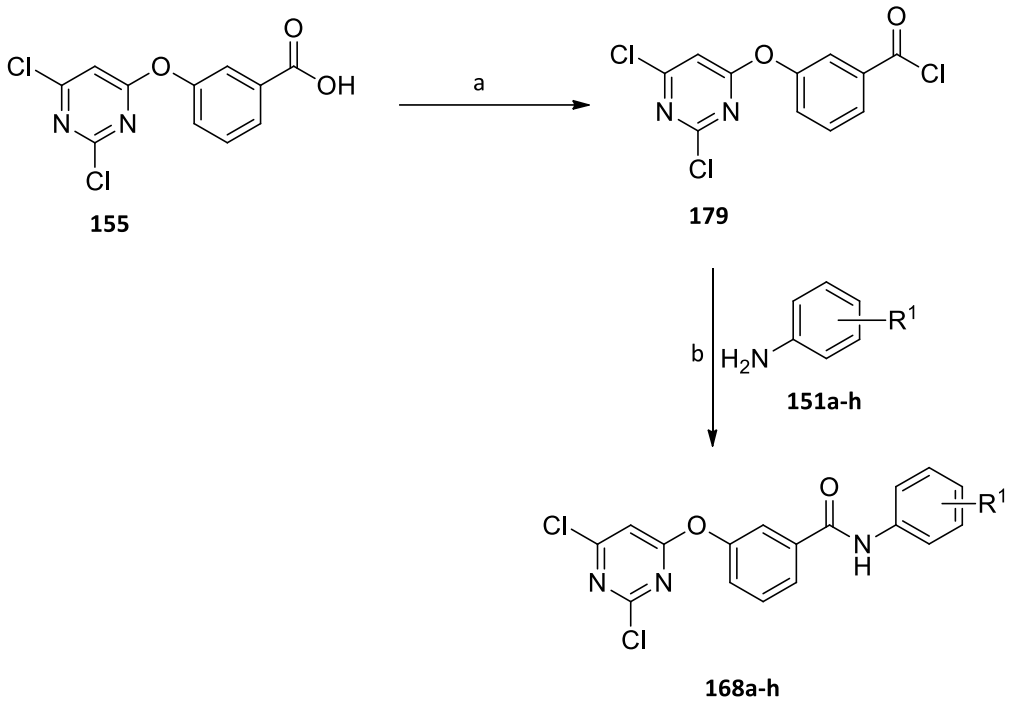

Scheme 59 *Reagents and conditions: (a) $SOCl_2$, 70 °C, 1 h; (b) pyridine or triethylamine, CH_3CN/THF, 0 °C-rt, 13-24 h, 16-93%*

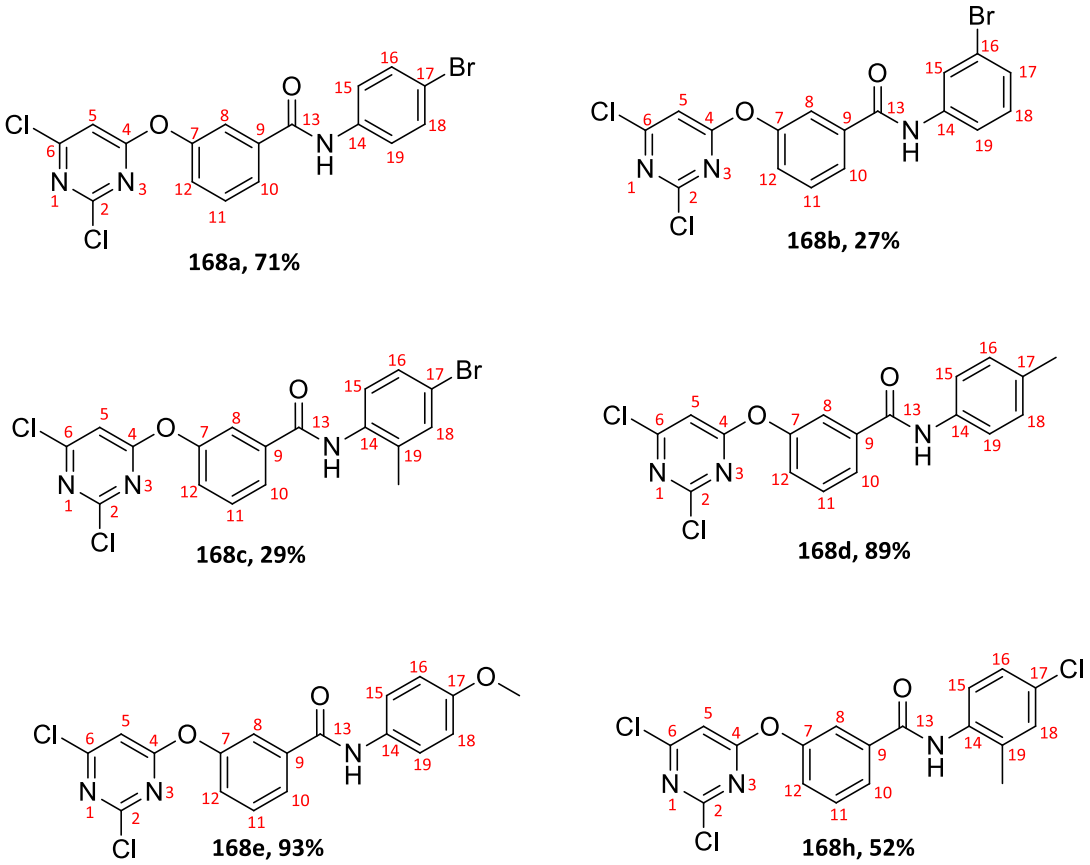

Fig 49 *Complex benzamides derived from acid* ***155***

The amination of acid chloride **179** with 4-bromoaniline **151a** was achieved without any synthetic problems and resulted in 71% yield of compound **168a**. The product formation was confirmed by the appearance of nine aromatic protons on the ^{1}H NMR spectrum. The presence of a broad deshielded NH signal at 10.46 ppm and an additional four aromatic protons observed at 7.75 ppm (H15 and H19) and 7.57 ppm (H16 and H18), confirmed the successful formation of the product. A pyrimidinyl H5 signal was observed at 7.56 ppm which was quite different to that of a starting material at 7.49 ppm. The proton signals of the phenyl ring were observed as multiplets at 7.54-7.93 ppm, and they were slightly distinguishable from those of **155** at 7.55-7.91 ppm. The ^{13}C NMR data complemented the proton NMR data by displaying fifteen distinct carbon signals. The most significant carbon signal that revealed the presence of a different functional group was that of the amide carbonyl carbon appearing at 164.3 ppm. Four supplementary carbon nuclei represented by two CH signals with high intensities were also observed at 122.3 and 131.5 ppm showing the inclusion of 4-bromoaniline in the final structure. DEPT135 NMR showed seven CH signals because of the symmetric bromo-phenyl ring and eight quaternary carbon signals.

The efforts to extend this protocol to effect the condensation reaction between **179** and 3-bromoaniline **151b** provided the product **168b** in only 17% yield. Attempts to drive the reaction

without the pre-cooling conditions failed as evidenced by the TLC analysis. The recovered complex mixture of products could not be separated or characterised. There is a possibility that the exclusion of ice-cooling resulted in spontaneous heating during the addition of **151b** as higher reaction temperatures could favour the formation of *N*-diacylated products according to Zitko.[162] Thompson indicated that the factors determining the feasibility of either monoacylation, amide dehydration to a nitrile, or diacylation are reaction conditions, the impact of a substituent on the acyl chloride, and rarely the amide structure being acylated.[166]

The ^{1}H NMR spectrum of compound **168b** showed nine aromatic protons, with singlet H-5, H-8, and H-15 protons being observed at 6.87 ppm, 7.63 ppm, and 7.84 ppm, respectively whilst the NH peak appeared at 8.31 ppm. The H-11 and H-17 signals overlapped and appeared as multiplets at 7.48 ppm (m, 2H). The H-18 signal appeared as a triplet at 7.16 (*J*= 8.0 Hz, 1H) while H-10 appeared as a doublet at 7.71 ppm (*J*= 7.7 Hz, 1H). The H-12 and H-19 signals were observed as multiplets (m, 2H) from 7.22-7.31 ppm. The ^{13}C NMR data demonstrated that there were seventeen overall carbon signals as expected. The DEPT NMR spectrum agreed by showing nine CH signals and eight quaternary carbon signals. Of significance was the amide carbonyl C-13 appearing at 164.7 ppm and C-14 signal at 138.9 ppm as an indication of successful amide bond formation.

The reaction with 4-bromo-2-methylaniline **151c** only offered **168c** in 29% yield, and similar low yields were obtained for more nucleophilic anilines, *p*-toluidine **151d** and *p*-anisidine **151e** which afforded **168d** and **168e** in 16% and 19% respectively. Notably, since amides are normally polar, they have the potential to get adsorbed onto the silica gel during the column chromatography purification leading to the loss of the material. In each case, the mixture was allowed to react for less than 24 h because exceeding that reaction time gave undesirable results as multiple products were formed as evidenced by the TLC analysis. Furthermore, emulsions occurred during workup and a lumpy-like slurry was recovered after removal of excess solvent. For column chromatography purification, the slurry required a dry loading approach which often interferes with separation when the column is not properly packed.

^{1}H and ^{13}C NMR results for **168c**, **168d**, and **168e** showed similar patterns to those assigned for **168b** in chemical shifts except for the phenyl ring attached to the amide nitrogen atom. The key difference in compound **168c** was that the ^{13}C NMR spectrum showed C-17 more shielded at 118.8 ppm relative to the C-17 of **168b** at 119.0 ppm. The C-19 of **168c** was more deshielded at 131.9 ppm than that of **168b** at 127.8 ppm. C-17 signals of **168d** and **168e** were more deshielded compared to those of **168b** both appearing at 133.3 ppm, whereas their C-19 peaks were more shielded at 121.1 and 122.5 ppm respectively.

Poor yields of **168d** and **168e** led to an assumption that complex acid chloride **179** was either incompatible with pyridine or intolerant of the reaction conditions. Thus, considering this probability, the amidation reactions involving anilines **151f**, **151g**, and **151h** were not performed with the use of pyridine. The amidation reaction using Et_3N was first reattempted by acylating **151d** and **151e** with **179** to evaluate the scope of the reaction. Gratifyingly, using *p*-toluidine and *p*-anisidine as nucleophiles in the presence of TEA proved effective in facilitating the formation of analogue **168d** and **168e** with the yields of 89% and 93%, respectively. Pleased by the excellent yields, derivative **168h** was successfully synthesised and obtained in reasonable yield of 52%. The acylation reactions of **151f** and **151g** were completely impossible, seemingly, due to steric effects caused by the bromo substituents. Below is the summary of the yields isolated for compounds **168b**-**e** using pyridine versus triethylamine (Table **11**).

Table 11: Comparison between the yields obtained using pyridine and triethylamine

Compound number	**Pyridine** **Yield (%)**	**Trriethylamine** **Yield (%)**
168b	17	27
168c	29	89
168d	16	93

The structure of **168h** was confirmed by the presence of the amide NH overlapping with H-10 and H-15 at 7.74-7.80 ppm on the ^{1}H NMR spectrum. The ^{13}C NMR spectrum showed that the C-17 (C-Cl) of **168h** appearing at 130.8 ppm was highly deshielded compared to the C17 (C-Br) of **168c** at 118.8 ppm, highlighting the impact of the NHD effects. In contrast, the *ortho* C-16 and 18 of **168h** seen at 126.9 ppm and 130.4 ppm, respectively were more shielded than those of **168b** at 130.0 ppm and 133.4 ppm, respectively. This could have occurred possibly because of mesomeric effects, because generally these effects are inversely proportional to the size of a halogen.

Compound NMR characterizations summarized with key data; amide NH, C-14, and C=O signals are shown in Table **12**. The ^{1}H NMR spectroscopic data demonstrated consistency in the chemical shifts of the amide protons for compounds **168a**, **168d**, and **168d** appearing at 10.45, 10.27, 10.23 ppm, respectively. The amide protons of compounds **168c** and **168h** overlapped with the aromatic signals appearing between 7.79 – 7.66 ppm and 7.80-7.74 ppm, respectively. In addition, their chemical shifts had a negligible difference between 0.21-0.08 ppm. The ^{13}C NMR spectrum showed that the C-2 signal of derivative **168e** is more shielded than the C-2 signals of **168a** and **168d**, presumably due to the strength of a *para*-directing methyl group.

Table 12: ^{1}H and ^{13}C NMR results for the isolated derivatives **168a**-**e** and **168h**

Compound Number	Amide H (s) ^{1}H NMR (δ: ppm)	C-14 ^{13}C NMR (δ: ppm)	C=O ^{13}C NMR (δ: ppm)	NMR Solvent
168a	10.45	138.3	164.4	DMSO-d_6
168b	8.31	138.9	164.7	$CDCl_3$
168c	7.79 – 7.66	134.7	164.5	$CDCl_3$
168d	10.27	136.8	164.5	DMSO-d_6
168e	10.23	132.4	164.3	DMSO-d_6
168h	7.80-7.74	134.0	164.4	$CDCl_3$

2.1.6.3 Synthesis of complex benzamides from aminopyridines **151i-o**

For the next set of analogues, the two possible synthetic routes were assessed. The first approach, amidation then linking, involved replacing one of the chlorine atoms by treating the trichlorinated intermediate **102** with the *N*-pyridinylbenzamides **166j**, **166l**-**m**, and **166o** (Scheme **60**). Following the procedure previously described for the preparation of aryl ester **173**, the reaction was initially tested by reacting **102** with **166j** in the presence of potassium carbonate. The desired compound **168j** was isolated in 28% yield together with unreacted starting materials even after allowing the mixture to react for over 24 h. The reaction optimizations could not be performed due to insufficient starting materials that required several synthetic steps to prepare.

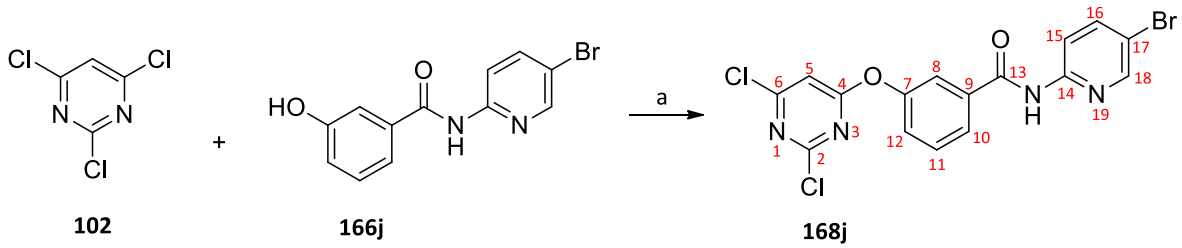

102 **166j** **168j**

Scheme 60 *Reagents and conditions: (a) acetone, K_2CO_3, 24 h, 28%*

The product formation was verified by the appearance of a broad NH signal at 11.06 ppm on the ^{1}H NMR spectrum. A singlet H-5 signal from the pyrimidinyl moiety was observed at 7.53 ppm. Four phenyl protons were observed at 8.00 ppm (d, *J*= 7.8 Hz, 1H, H-10), 7.92 ppm (s, 1H, H-8), 7.64 ppm (t, *J*= 7.9 Hz, 1H, H-11), and 7.54 ppm (d, J= 6.1 Hz, 1H, H-12). The pyridinyl signals appeared downfield at 8.52 ppm (d, *J*=2.2 Hz, 1H, H-18), 8.18 ppm (d, *J*= 8.9 Hz, 1H, H-15), and 8.08 ppm (dd, *J*= 8.9 Hz, 2.4 Hz, 1H, H-16). The ^{13}C NMR spectrum showed sixteen non-equivalent carbon nuclei. The DEPT NMR

spectroscopic data revealed eight CH signals and eight quaternary signals with a significant amide carbonyl nucleus at 164.9 ppm.

The second approach, linking then amidation, involves the acylation of aminopyridines **151i**-**o** as done with the previously synthesized compounds. The amidation reaction between the complex carboxylic acid **155** and **151j** was reattempted in the presence of pyridine under the similar acylation conditions reported for synthesizing simple benzamides. However, multiple spots were observed on the TLC plate without the indication of product formation. Even though triethylamine resulted in diacylation for amidation reactions involving some of the heterocyclic amines, it was used in place of pyridine to mediate the C-N coupling of acid **155** and amines **151i**-**o** (Scheme **61**). The assigned structures of aryl benzamides **168k**-**m** and **168o** are shown below (Fig **50**).

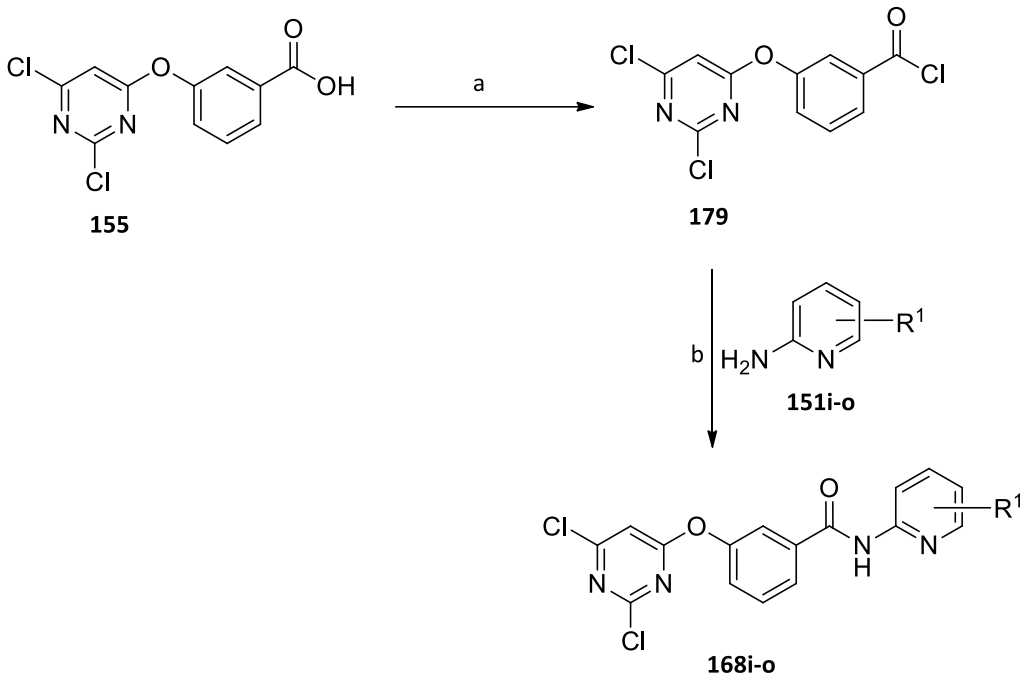

Scheme 61 *Reagents and conditions: (a) $SOCl_2$, 70 °C, 1 h; (b) pyridine, CH_3CN/THF, 0 °C-rt, 13-24 h, 28-63%*

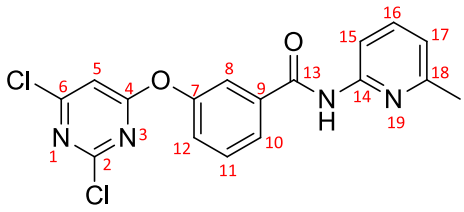

168k, 63%

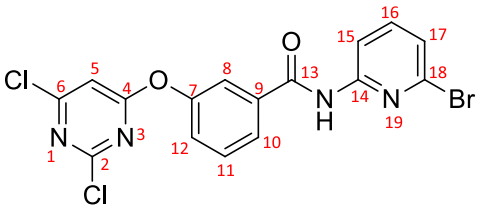

168l, 56%

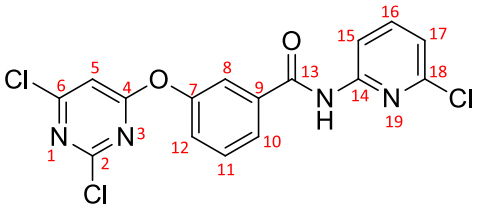

168m, 50%

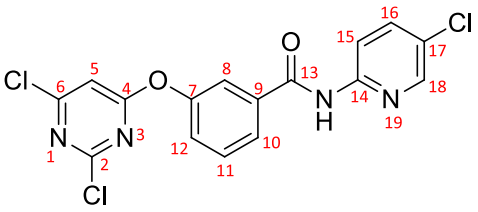

168o, 28%

Fig 50 *Assigned structures of* ***168k-l*** *and* ***168o***

Thus, the synthesis of **168j** was repeated by aminating **179** with **151j**, and product **168j** was obtained in a moderate yield of 50%. The aryl *N*-pyridinylbenzamide analogues **168k**, **168l**, **168m**, and **168o** were prepared under similar conditions and isolated in poor to modest yields (63%, 56%, 50%, and 28% respectively) due to recrystallization being necessary for their purification. Acylation of **151i** afforded a product with inseparable impurities even after recrystallization, or else *N*-disubstitution occurred, supporting the idea that heterocyclic amines are intolerant of triethylamine. Lastly, modifying the reaction conditions to improve the yields of the former compounds was not the area of attention since we had enough material of the arylated *N*-phenylbenzamides and *N*-pyridinylbenzamides to use in the next step. Based on the results obtained, the reaction sequence of linking the benzoic acid derivative to the pyrimidine nucleus prior to amidation is favoured over the amidation followed by linking reaction sequence

Structure assignments for aryl *N*-pyridinylbenzamides **168k-m** and **168o** were determined in a similar fashion to their previously assigned related analogues based on the ^{1}H NMR and ^{13}C NMR spectroscopic information. Like compound **168j**, the C-17 of derivative **168o** was also a quaternary carbon found in the *para*-position to the amide nitrogen at 127.2 ppm, which was however significantly different from the chemical shift of **168j** at 114.2 ppm. The same trend was observed in analogues **168k**, **168l** and **168m** where their quaternary C-18 carbons in the *meta*-position to the amide nitrogen appeared at 157. Ppm, 138.8 ppm and 148.0 ppm, respectively.

The tabulated values in Table **13** are an indication of the successful C-N amide bond formation showing the presence of the key signals; amide H, C-14, and C=O. These signals were identified in the ^{1}H and ^{13}C NMR spectra. Except for compound **168o** that was dissolved in deuterated chloroform for preparing the NMR sample, analogues **168j**-**m** were dissolved in deuterated DMSO. For derivatives **168l** and **168m** bearing the halogen atoms in the 6-position, the amide protons appeared at 11.18 ppm and 11.13 ppm, respectively and were more deshielded than that of compound **168k** at 10.80 ppm. The halogen effects did not have an impact on the C-14 chemical shifts of **168l** and **168m**. Mesomeric effects were prevalent for the C-14 signal of derivative **168k**.

Table 13: ^{1}H and ^{13}C NMR spectroscopic data showing the key signals for compounds **168j**-**m** and **168o**

Compound Number	**Amide H (s) ^{1}H NMR (δ: ppm)**	**C-14 ^{13}C NMR (δ: ppm)**	**C=O ^{13}C NMR (δ: ppm)**	**NMR Solvent**
168j	11.06	151.0	164.9	DMSO-d_6
168k	10.80	151.8	165.1	DMSO-d_6
168l	11.18	152.3	165.0	DMSO-d_6
168m	11.13	152.0	164.9	DMSO-d_6
168o	8.84	149.6	154.3	$CDCl_3$

2.1.6.4 Synthesis of complex benzamides from aminopyrazines **164p**-**q**

Since aminopyrazinyl-containing benzamides are among the proposed class of compounds, the amidation reactions involving acylation of aminopyrazines **151p** and **151q** with carboxylic acid **155** were attempted in the presence of triethylamine (Scheme **62**). Unfortunately, neither pyrazine derivative participated successfully in the reaction and the desired compounds **168p** and **168q** were not obtained.

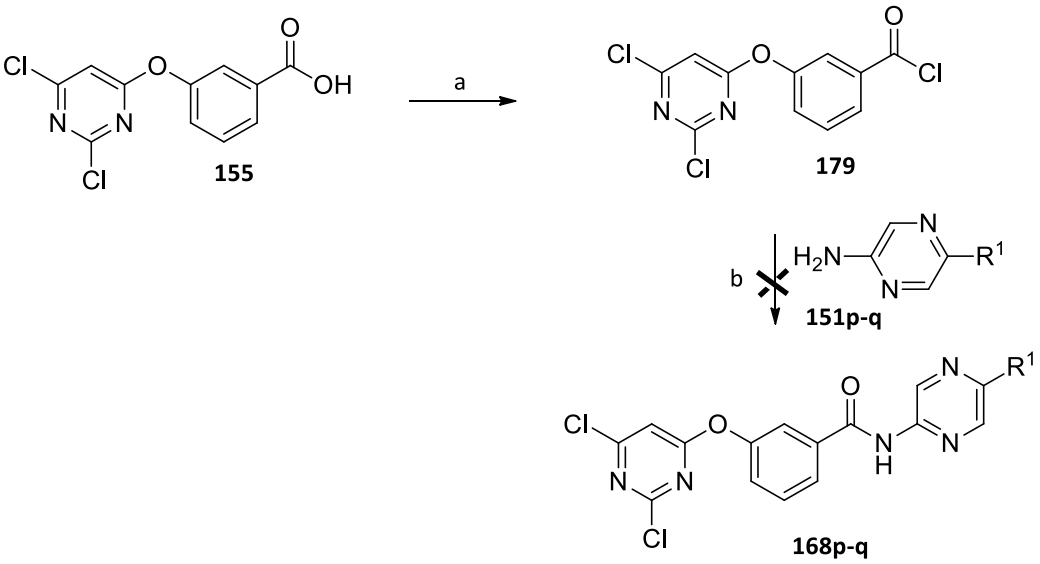

Scheme 62 *Reagents and conditions: (a) $SOCl_2$, 70 °C, 1 h; (b) triethylamine, CH_3CN/THF, 0 °C-rt, 24 h, (no product)*

2.2 Nucleophilic substitution of the second chlorine atom

The next step required in the preparation of the target compounds **180** was substitution of the second chlorine atom. The second chlorine substitution on **168a** was carried out at room temperature by treatment with ethanethiol in the presence of aqueous sodium hydroxide dissolved in acetone or THF (Scheme **63**).

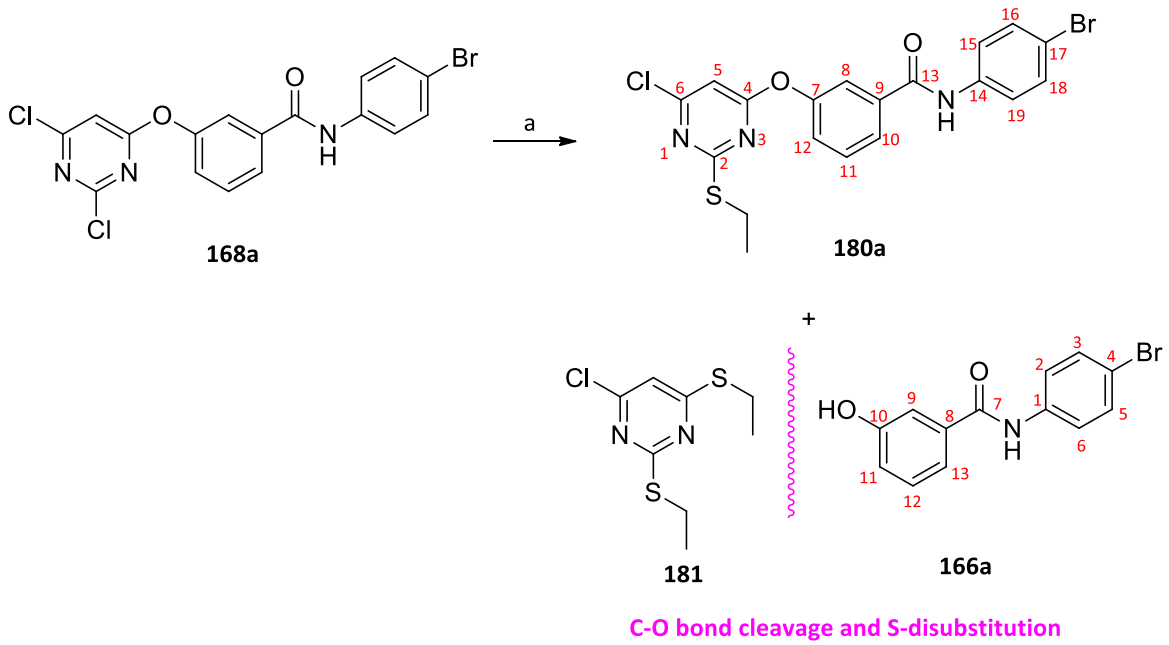

Scheme 63 *Reagents and conditions: (a) Ethanethiol, 1 M NaOH, acetone or THF, rt, 1 h, 43%*

After column chromatography purification, three products from fractions of different polarities were analysed by proton NMR spectroscopy. The assigned structure of the most polar product eluted using 30% ethyl acetate/hexane is shown in Fig **51**. The ^{1}H NMR spectrum showed eight aromatic protons and two singlet signals appearing at 9.80 and 10.31 ppm with no aliphatic signals being observed. The ^{13}C NMR spectroscopy also demonstrated the absence of aliphatic carbon signals and the presence of ten distinct aromatic signals appearing at 115.0-157.8 ppm and the carbonyl carbon at 166.1 ppm. HMBC NMR spectroscopy showed correlations between the C-10 signal at 157.8 ppm and the C9 and C11 signals at 115.0 and 119.1 ppm, respectively, through ^{2}J coupling. The C9 and C11 signals including the C-13 signal at 118.7 ppm were the most shielded in the hydroxyphenyl ring due to the *ortho* and *para* electron donating effects arising from the oxygen atom. The quaternary C-8 signal at 136.6 ppm correlated with the CH signal at 129.9 ppm through ^{3}J coupling. Symmetrical signals at 122.6 ppm and 131.9 ppm belong to the bromo-phenyl motif. DEPT NMR displayed the existence of six CH signals due to symmetry and five quaternary peaks. Thus, it was clear that this fraction did not contain the expected product **180a**. HRMS (ES*) analysis gave the mass of 291.9956, which matched the expected mass of 291.9966 for compound **166a**.

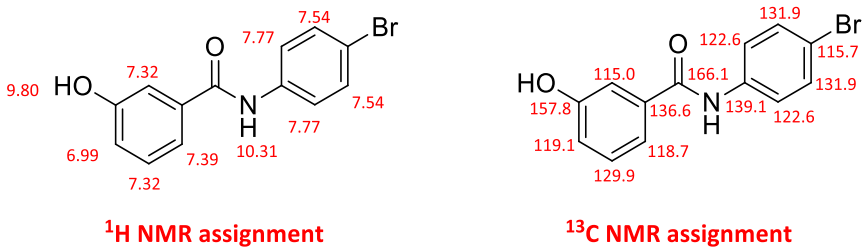

^{1}H NMR assignment **^{13}C NMR assignment**

Fig 51 *^{1}H and ^{13}C NMR assignment for* ***166a***

Fortunately, the second fraction was more promising and gave the desired compound **180a** in 43% yield after recrystallization. The ^{1}H NMR spectroscopic results showed the nine expected aromatic protons and five aliphatic protons coming from a quartet and the most shielded triplet signal which integrated for two and three protons respectively. In comparison to **166a**, minor shifts were seen for both the amide and aromatic signals. ^{13}C NMR data revealed the appearance of two aliphatic signals at 14.7 and 25.3 ppm, and the DEPT NMR spectrum was consistent with the presence of the CH_3 and CH_2 at these chemical environments. Clear correlations were observed between H-5 at 7.11 ppm and C-4 and C-6 at 161.2 and 169.7 ppm respectively from HMBC NMR spectrum. There was a noticeable change in the chemical shift of the C-2 confirming the success of nucleophilic substitution at this position of the pyrimidine ring.

We were also interested in knowing the identity of the third constituent present with the hopes of being able to improve the yield of the desired compound. Therefore, the proton NMR analysis of the

least polar product was conducted and the ^{1}H NMR spectroscopic data showed approximately eleven protons with a ratio of 1:4:6 (Fig **52a**). Taking this into consideration, the predicted structure was that of **181** (Fig **52b**), which gave an indication of how the C-O bond cleaved giving rise to **166a** had occurred in this reaction.

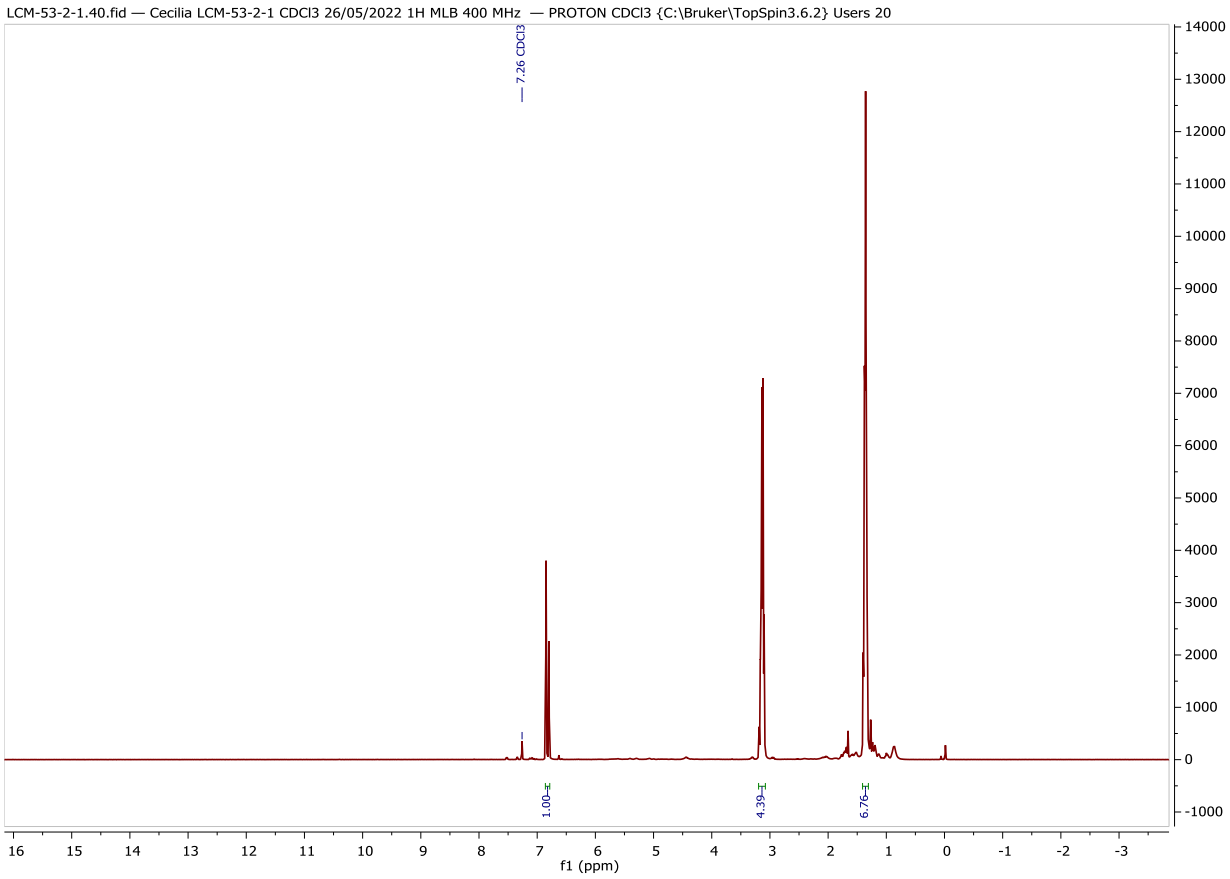

(a) ^{1}H NMR spectrum for compound **181**

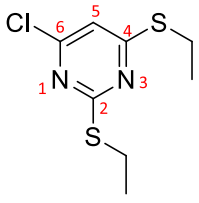

181

(b) Proposed structure of **181**

Fig 52 *NMR proton spectrum and proposed structure of compound* ***181***

The ^{13}C NMR spectrum (Fig **53**) showed eight different chemical environments with three downfield quaternary signals appearing in the ranges of 170.0-172.3 ppm, and one upfield signal at 113.2 ppm belonging to the aromatic region. Two carbon signals appearing at 14.4-24.2 ppm reside in the

aliphatic region. Their adjacent signals and their intensities indicate that the molecule has adopted different conformations.

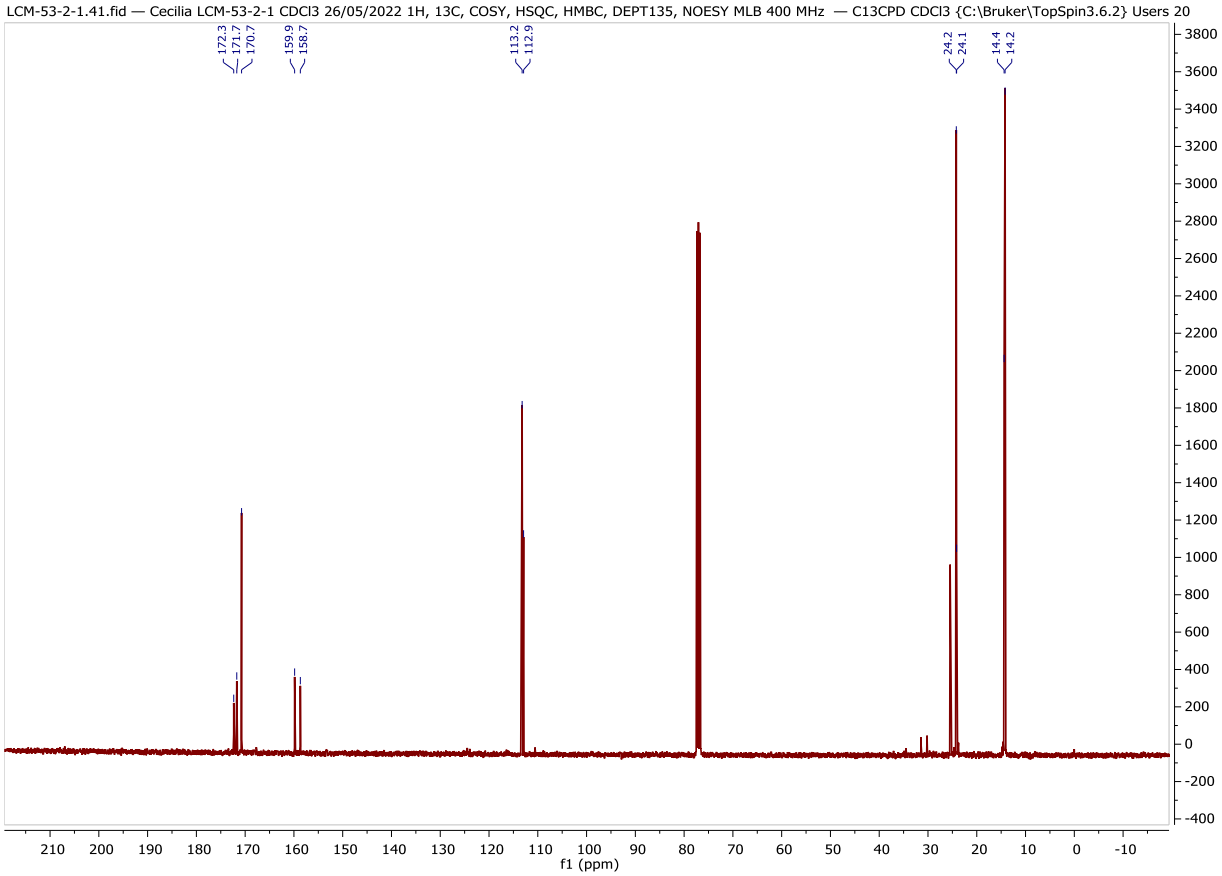

Fig 53 *^{13}C NMR spectrum of compound* ***181***

DEPT NMR spectroscopic data (Fig **54**) was in agreement with the results from the carbon NMR spectrum by showing the presence of two aromatic CH signals, two CH_2 signals and CH_3 signals.

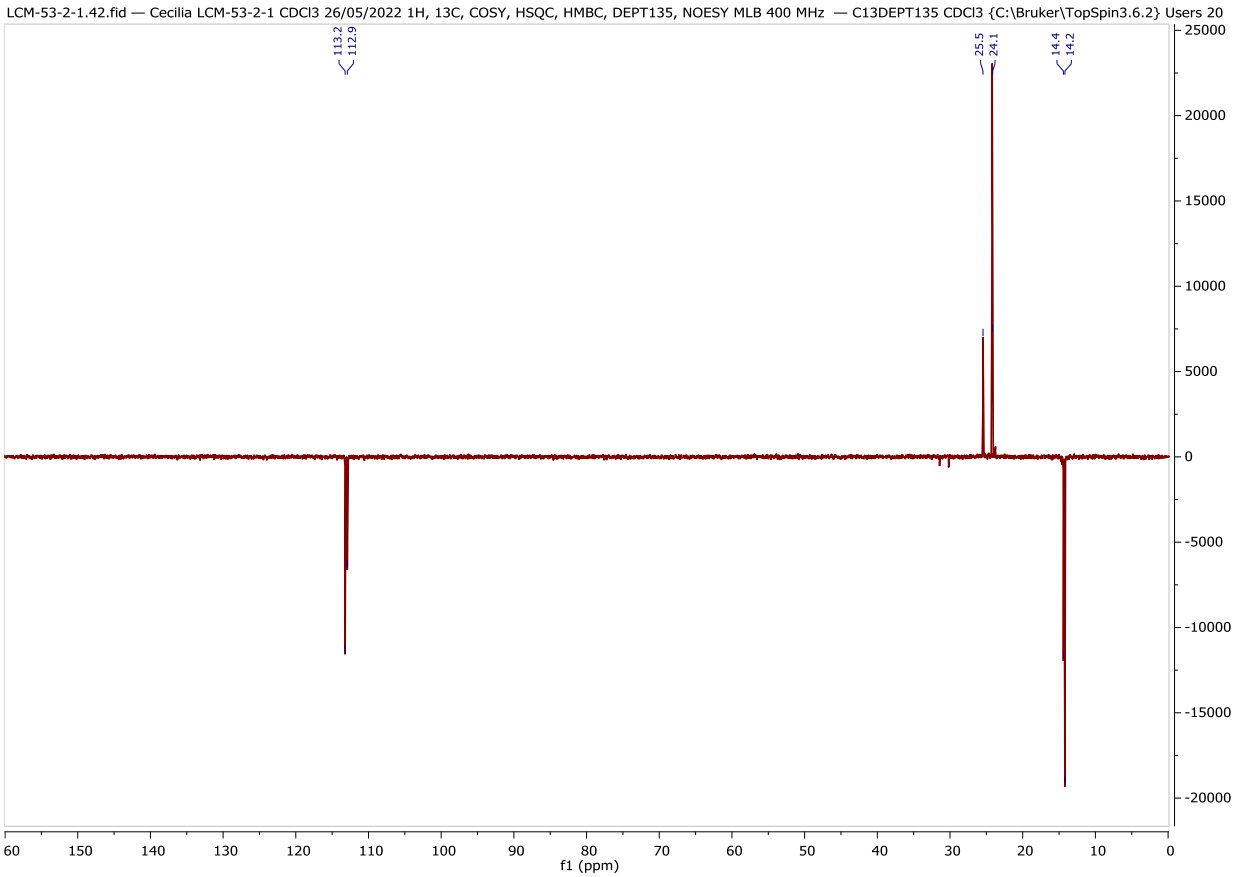

Fig 54 *DEPT NMR spectrum of compound* ***181***

HSQC NMR spectroscopic information (Fig **55**) demonstrated correlations between 112.9-113.2 ppm and 6.87-6.95 ppm as well as the methyl interactions between 14.2-14.4 ppm and 1.12-1.50 ppm. Additionally, the CH_2 pair of signals at 24.1-24.2 ppm correlated with proton signals at 1.12-1.50 ppm.

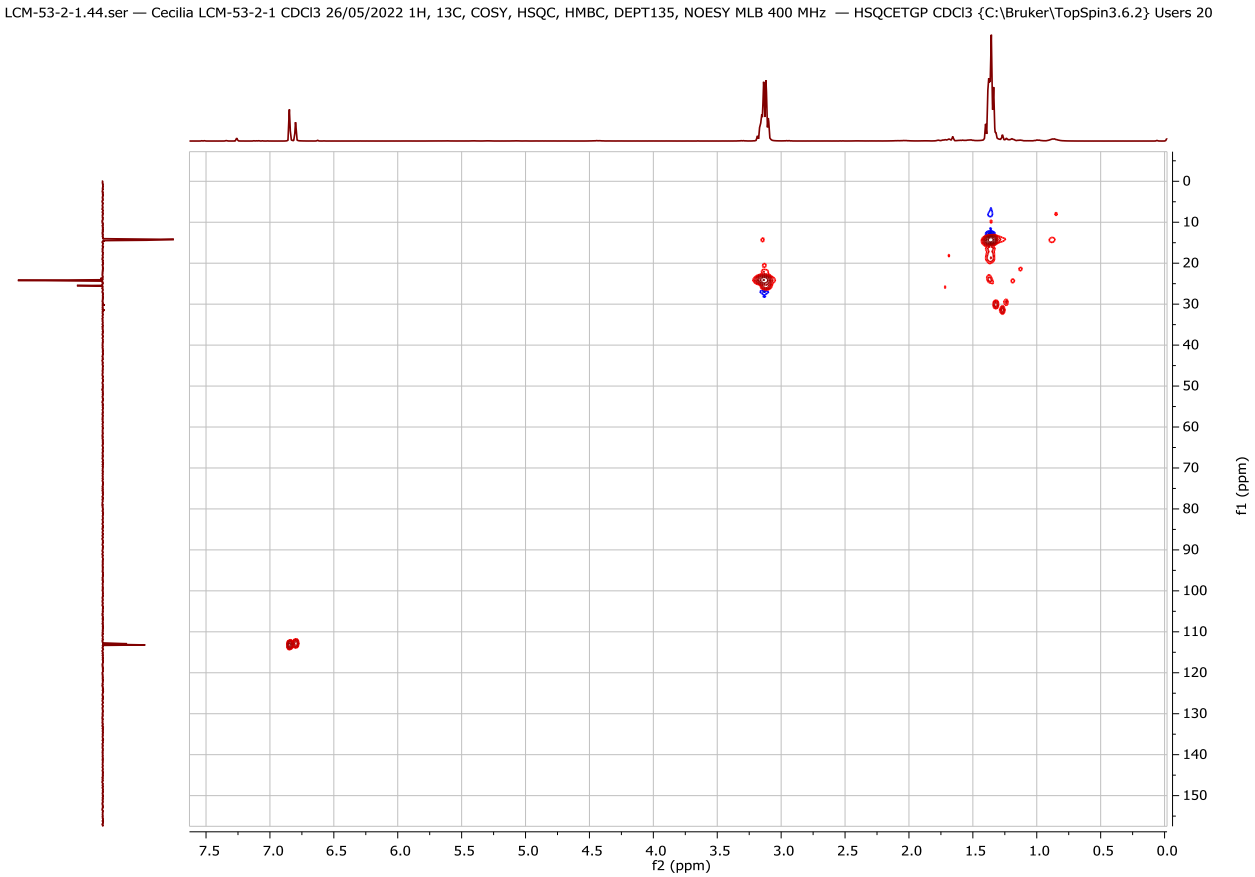

Fig 55 *HSQC NMR spectrum of compound* ***181***

The HMBC NMR spectrum (Fig **56**) showed that the carbon signal at 172.3 ppm is highly deshielded and correlates through ^{3}J coupling with a CH_2 proton that is adjacent to the methyl carbon at 14.2 ppm. The ^{13}C signal at 112.9 ppm was shown to be a neighbour of quaternary carbons at 158.7 and 171.7 ppm owing to the ^{2}J link with a proton signal at 6.95 ppm. A signal at 170.7 ppm was seen with a higher intensity representing the presence of two nuclei at that environment. This peak displayed concurrent *ortho* correlation with a proton at 6.87 ppm and long-range coupling with the ethyl proton at 24.2 ppm.

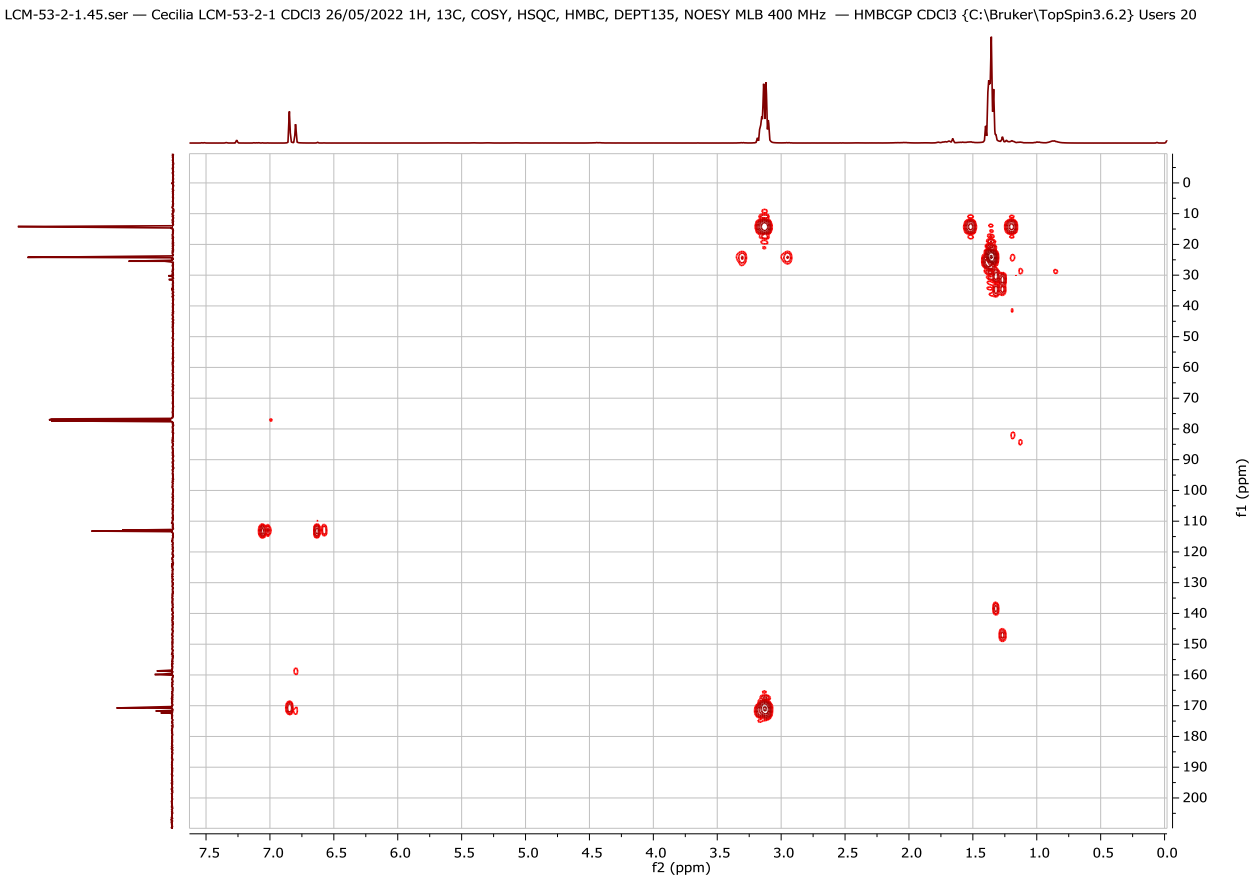

Fig 56 *HMBC NMR spectrum correlations*

In line with this spectroscopic information, we suspected that because the C-O carbon on the pyrimidine ring of **168a** is highly deshielded (170.8 ppm), the decreased electron density could allow for a nucleophilic attack by certain nucleophiles. Thus, it can be postulated that the C-O bond cleavage occurred according to the proposed mechanism below (Scheme **64**). Intermediate **182a** could have possibly formed upon nucleophilic attack by ethanethiol on the C-O carbon of the pyrimidine ring. This intermediate was suggested in connection with the Meisenheimer complex involving the *para*-quinoid structure.[141] The cleaved compound **183** is predicted to have formed during the removal of 3-((4-bromophenyl)carbamoyl)phenolate that was in turn protonated during acidic workup forming compound **166a**, being isolated in 20% yield. Another molecule of ethanethiol could have displaced the C-2 chlorine atom of **183** leading to the formation of the proposed compound **181**.

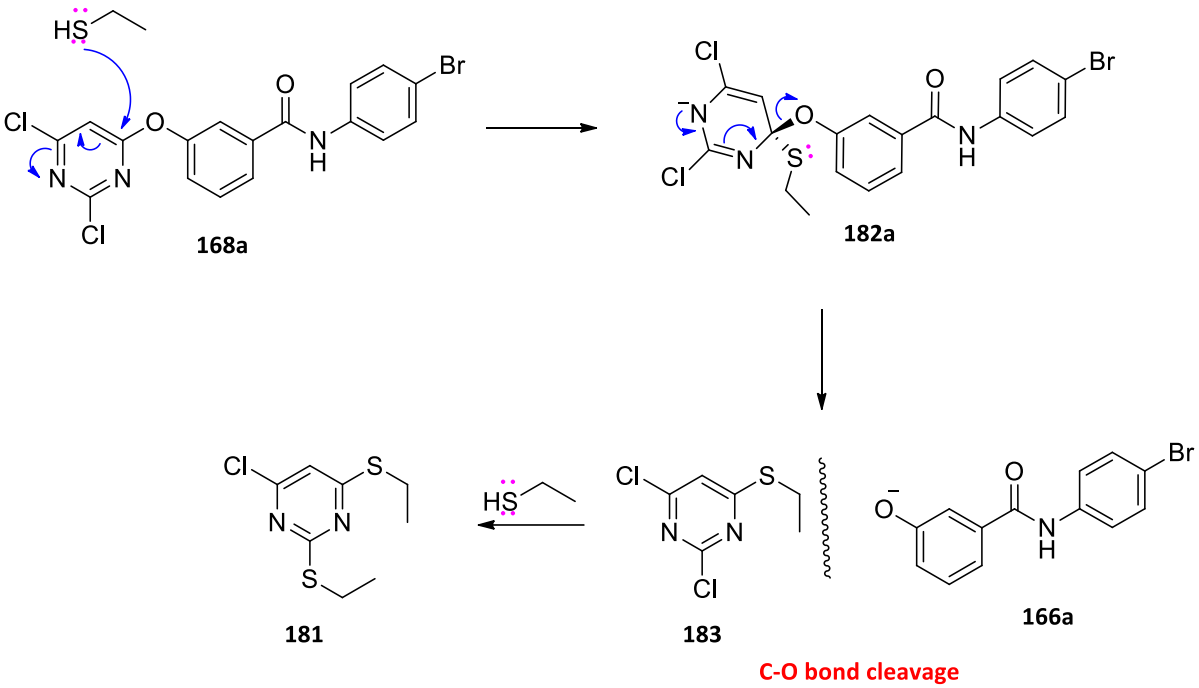

Scheme 64 *Proposed reaction mechanism showing the cleavage of pyrimidine C-O bond*

The reaction between **168d** and ethanethiol (Scheme **65**) was also assessed under similar conditions during which 38% yield of **180d** was recovered after purification by recrystallization, and similar **168a** C-O cleavage was observed giving rise to **181** (18%) and **166d** (20%). Repeating the reaction by changing from a strong inorganic base (aq. NaOH) to a strong organic base (triethylamine) was not effective as a contaminated unidentified side product appeared instead of **181**. Just like NaOH, the rationale behind the use of TEA was to serve the purpose of neutralizing the HCl generated during the displacement. Reaction with a longer-chained butanethiol still offered similar bond breaking results and unfavourable trace impurities in the aliphatic region despite the quantitative amounts of a base used. Due to the presence of these impurities, proper characterisation of the products from the butanethiol reaction was not possible.

To test if the C-O bond cleavage occurred with other nucleophiles, nucleophilic substitutions by aliphatic and cyclic nitrogen-based nucleophiles were performed. Treatment of **168d** (Scheme **65**) with *n*-propylamine efficiently transformed into the desired derivative **184d** in 66% without the C-O bond cleavage. Piperidine (Scheme **65**) was also a competent nucleophile providing the desired compound **185d** in 64% without breaking the C-O bond.

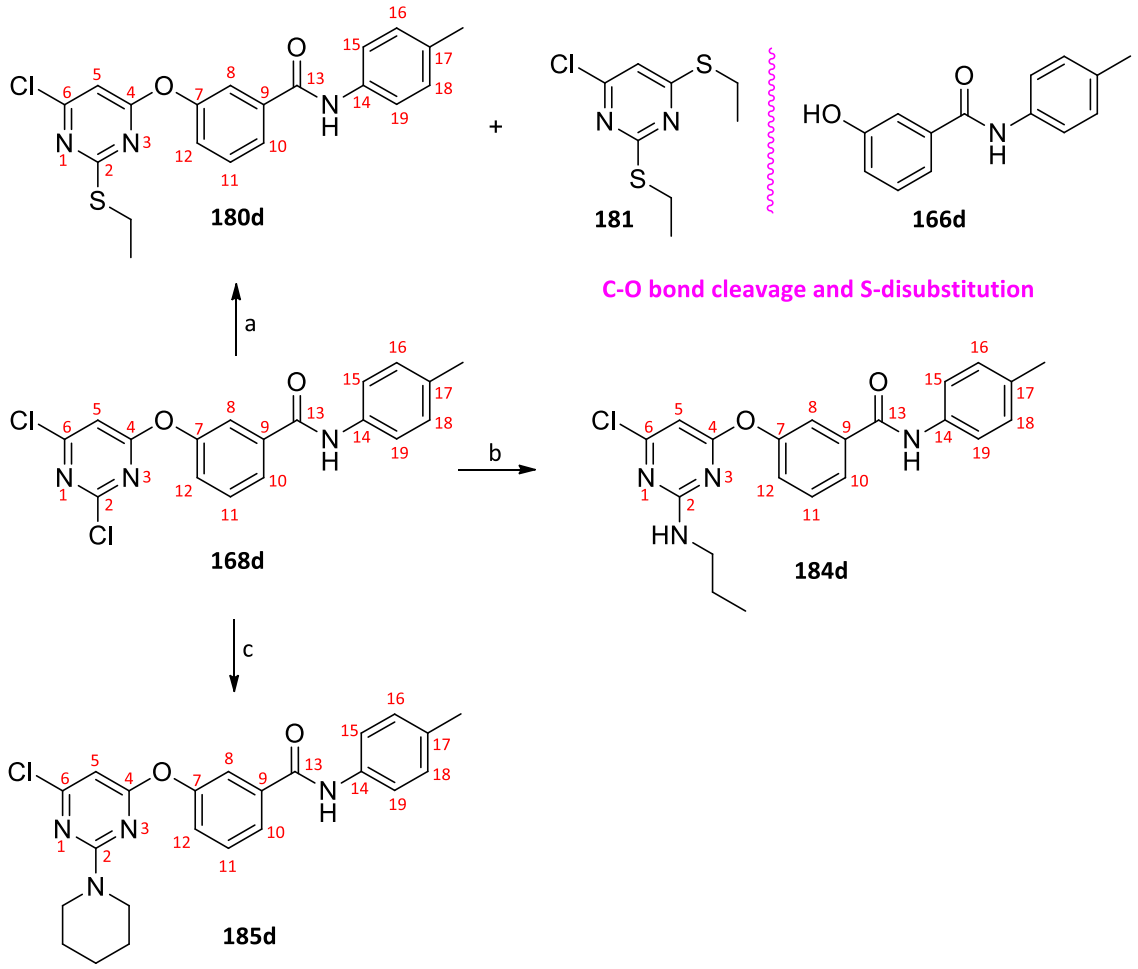

Scheme 65 *Reagents and conditions: (a) Ethanethiol, aq. NaOH, acetone, rt, 1 h, 43%; (b) n-propylamine, aq. NaOH, acetone, rt, 1 h, 66%; (c) Piperidine, aq. NaOH, acetone, rt, 5 h, 64%*

For structural determinations, compounds **180d** and **185d** provided similar NMR trends to those of **168d**, where the H-5 proton in both compounds showed the ^{2}J coupling interactions with the C-4 and C-6 nuclei in the HMBC NMR spectrum. The C-2 signals of **180d** and **185d** were more shielded at 173.1 ppm and 170.1 ppm, respectively in the ^{13}C NMR spectra.

For compound **184d**, deuterated DMSO was used to dissolve the NMR sample. The ^{1}H NMR spectrum demonstrated that the desired compound had been obtained, and the following signals were observed; the amide NH signal at 10.19 ppm, nine aromatic protons at 7.88-7.15 ppm, propyl NH signal at 6.34-6.26 ppm, propyl CH_2 signal at 2.91-2.90 ppm, tolyl CH_3 signal at 2.28 ppm, and propyl CH_2-CH_3 signals at 1.49-1.31 ppm and 0.85-0.65 ppm. Because unusual patterns were observed for the propyl chain in the ^{1}H NMR spectrum, with two separate sets of signals being observed, the sample was further analysed by single crystal X-ray diffraction for confirmation that the correct structure had been obtained (Fig **57**), the resolution for the X-ray crystallography was not good). The results demonstrated the correct compound had clearly been prepared, and different conformations adopted in solution

must have given rise to the unusual pattern observed in the spectrum run in deuterated DMSO. The methyl-substituted phenyl motif of one molecule was synclinal to the amidic group while perpendicular to the same group on the other molecule.

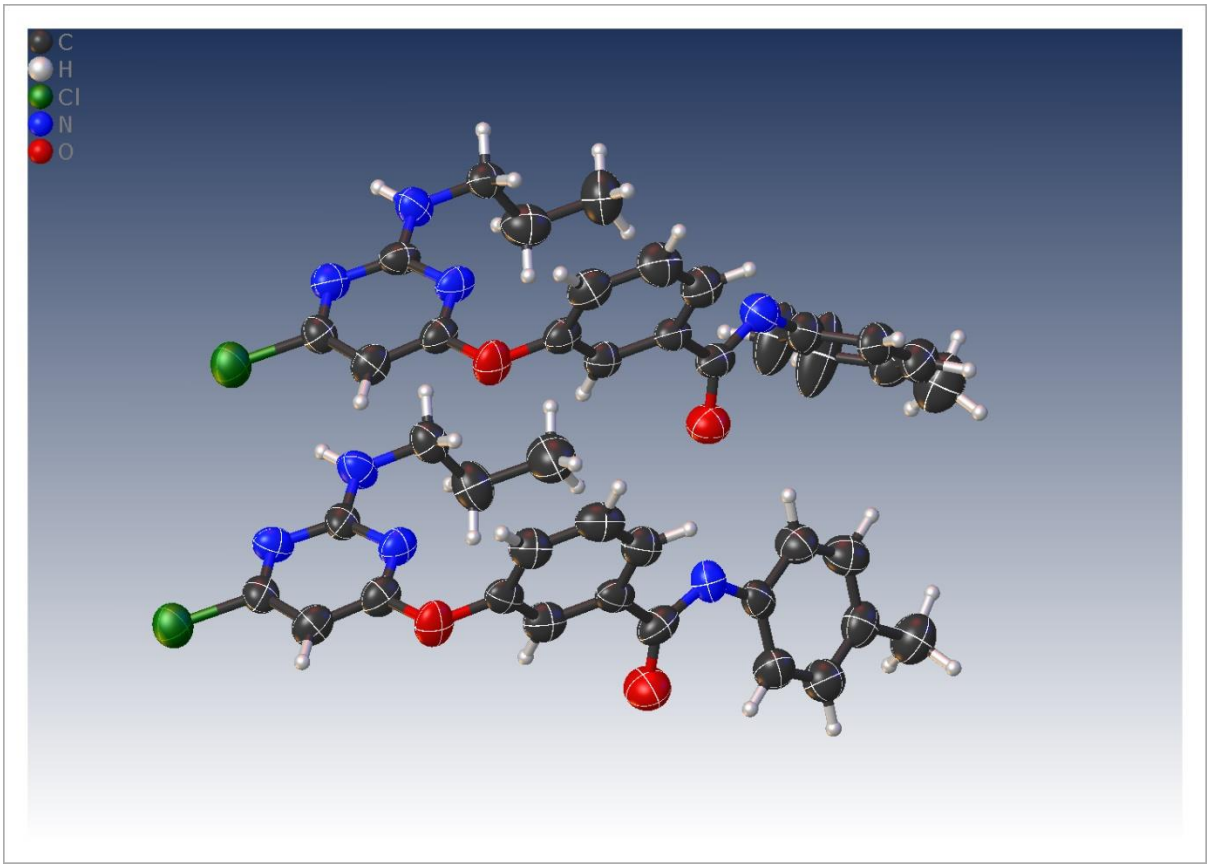

Fig 57 *Single X-ray crystal structure of compound* ***184d*** *showing hydrogen atoms in white, oxygen atoms in red, carbon atoms in grey, nitrogen atoms in blue, and chlorine atoms in green*

The results from the crystal structure analysis of compound **184d** and the NMR spectroscopic data for compounds **180d** and **185d** indicate that the substitution of the second chloride had occurred at the C2 position of the pyrimidine ring. These observations were highly supportive of the widespread consensus that the halogen substituted C-2 carbon is the second preferred position for aromatic nucleophilic attack.[138]

2.3 Third chlorine displacement by hydrolysis

The conversion of chloropyrimidines to hydroxypyrimidines can be achieved through hydrolysis under acidic or basic conditions.[138] One example of the acid hydrolysis reported in literature includes the treatment of dichloro-substituted pyrimidines with 8 M hydrochloric acid under reflux. [167] Following this method, compound **184d** was treated with 6 M HCl at refluxing temperature for over 24 hours (Scheme **66**). New faint spots were observed on TLC analysis under UV light visualization. Despite the

fact that the reaction was not given enough time to go to completion, the reaction was stopped, and the products purified by column chromatography in order to determine if one of the spots belonged to the desired product **186d**. Minor differences in the polarity of the spots required the use of flash silica gel to facilitate proper separation, but co-elusion still occurred. Apart from that, extending the reaction time to sixty hours or increasing the concentration of HCl to 8 M was not productive as trace amounts of the impure product were isolated while recovering the starting material in approximately 72%. Padilla and Pearlman emphasised that the proton or water concentrations do not often determine the rates of hydrolysis reactions in strong aqueous acid given that a rise in proton concentration results in progressive desolvation of the proton thereby elevating the acidity.[168]

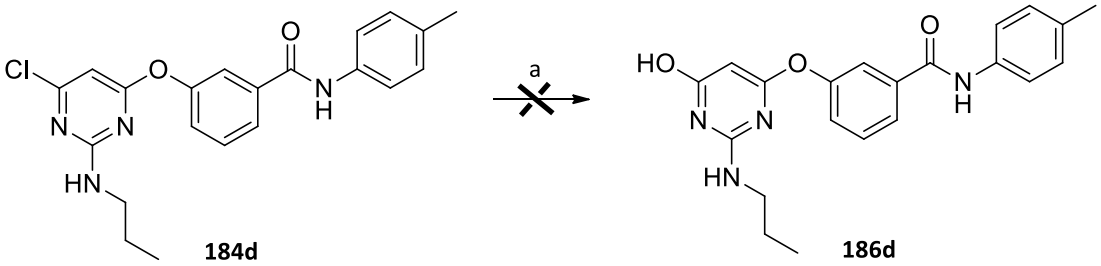

184d **186d**

Scheme 66 *Reagents and conditions: (a) aq. HCl/, DMF, heat or reflux, 24 h (no product)*

Another alternative hydrolytic approach to synthesise hydroxypyrimidines involves the use of aqueous NaOH. Examples of alkaline hydrolysis include the conversion of various 2-chloropyrimidines into their corresponding 2-hydroxypyrimidines by means of heating in 0.5 M NaOH.[168] A method for the hydrolysis of 2,4,6-trichloropyrimidine **102** by means of refluxing in dilute sodium hydroxide was reported to afford 6-chloropyrimidine-2,4(1*H*,3*H*)-dione. [145,146]

Thus, guided by these findings, the hydrolysis reaction of **184d** was repeated switching from aqueous HCl to dilute NaOH. Initially, 10% NaOH was cautiously added to a solution of **184d** at room temperature and heated at 130 °C while stirring for 24 h (Scheme **67**). Since DMF was used as a solvent, a mini workup was necessary to enable proper TLC plate separation when monitoring the reaction progress. The TLC visualization under UV light showed new faint spots and allowing the mixture to react for a further 24 hours had no effect. Elevating the percentage of sodium hydroxide by 10% intervals proved 50% w/v molar concentration effective in conversion rates within a short duration. Although traces of the starting material were seen on the TLC plate, a more concentrated new spot was convincing that the product could be obtained in significant quantities, particularly when the mixture was reacted for five hours. The overlapping of spots required the use of a combiflash column for purification during which a substantial amount (35%) of unidentified product was separable.

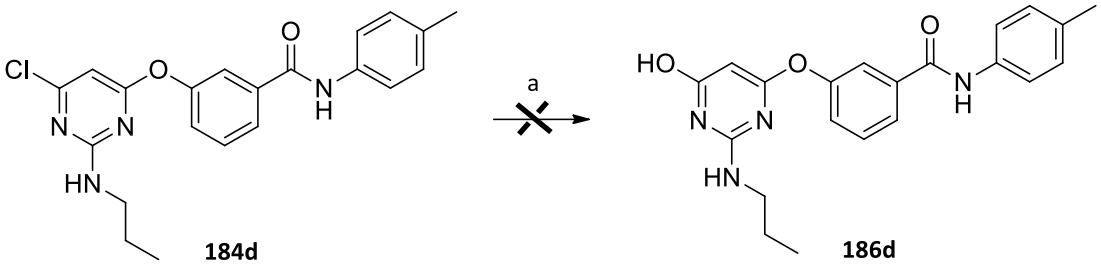

Scheme 67 *Reagents and conditions: (a) 50% w/v NaOH, 130 °C, 5 h, 35%*

Based on the ^{1}H NMR spectroscopic data which showed clear splitting patterns and a slight shift in product signals compared to those of a starting material when overlaying the spectra (Fig **58**), it was encouraging that the remaining chlorine atom could have been hydrolysed. For the preparation of the NMR samples, both compounds were dissolved in deuterated chloroform.

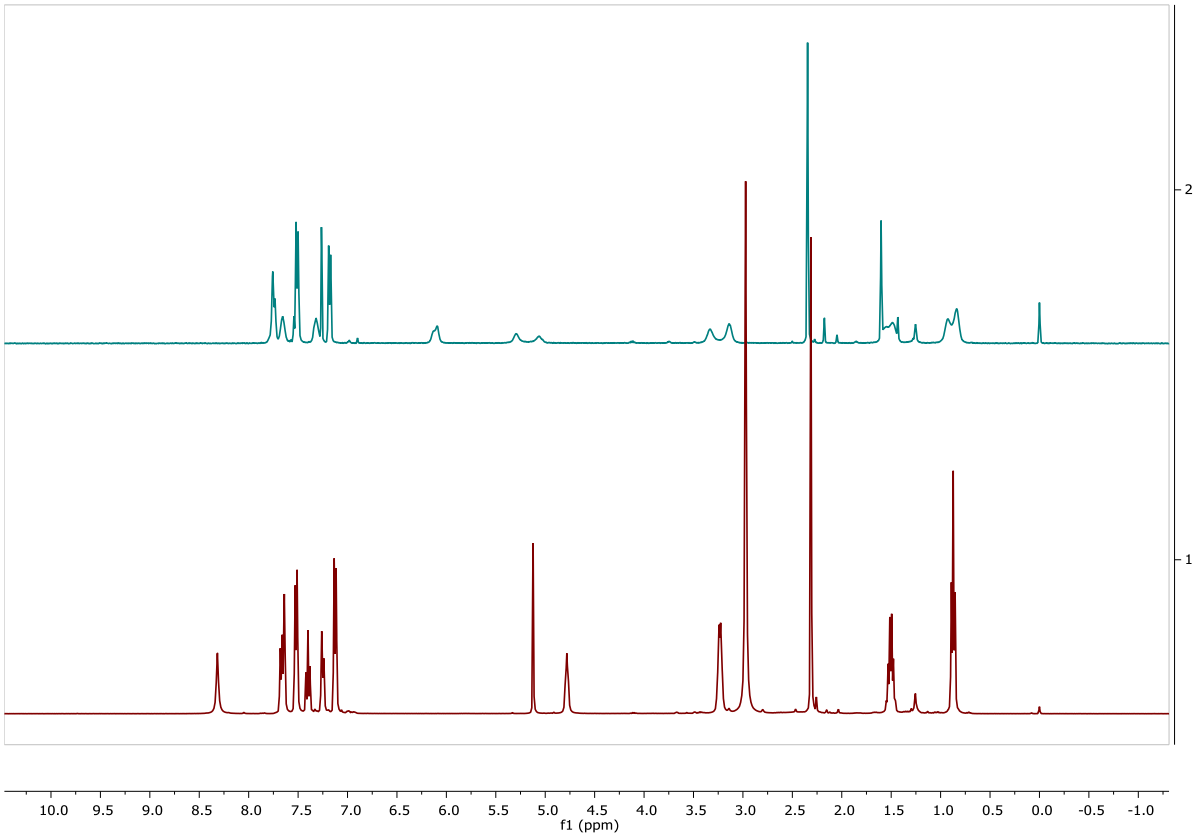

Fig 58 *Overlaid spectra of* ***184d*** *(green) and unidentified product (red)*

Although the chlorine atom was successfully substituted, disappointingly, the formation of the desired product **186d** was not achieved. Initially, the signal at 2.97 ppm on proton NMR was thought to be coming from DMF methyl groups and was neglected. The hydroxyl proton was believed to have overlapped with the 2.97 ppm signal considering the successful formation of **186d**. It was later discovered after the mass spectroscopic analysis that what was thought to be the DMF signal was

actually part of the molecule. The actual mass of 406.2252 on HRMS (ES^+) did not match the expected mass of 379.1765 for the desired compound **186d**. In fact, the detected mass matched the calculated mass of 406.2238 that is linked to the proposed compound **187d** shown in Fig **59**.

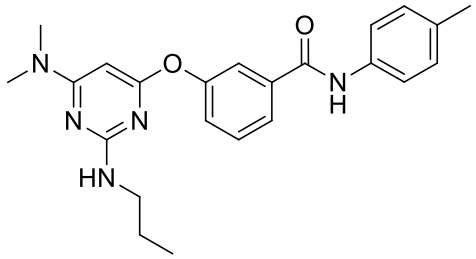

Fig 59 *Structure of the proposed product* ***187d***

The above compound **187d** was suggested given that DMF is prone to decarbonylation and converts into formate **188** and DMA **189** (Scheme **68**) at high temperatures close to its boiling point in the presence of strong bases like sodium hydroxide.[169] Therefore, it becomes apparent that in our reaction under the latter conditions NaOH rather catalysed decomposition of DMF than serving the intended purpose of acting as a hydrolysing agent.

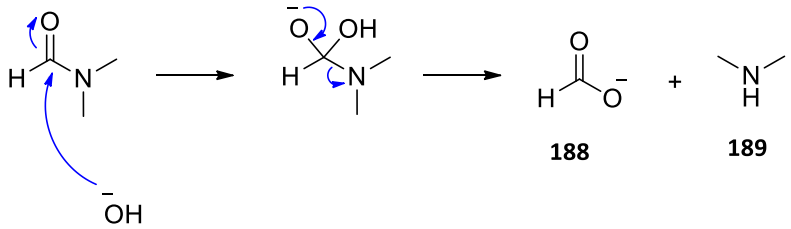

Scheme 68 *Decomposition of DMF*

Consequently, the resulting DMA was predominant in participating in the S_NAr reaction and displaced the chlorine atom to afford compound **187d** as shown in Scheme **69**.

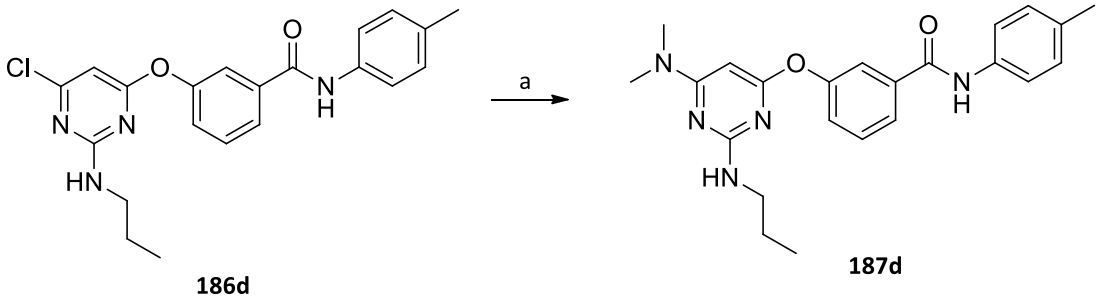

Scheme 69 *Reagents and conditions: (a) 50% w/v NaOH, 130 °C, 5 h, 35%*

After identifying the possible structure of the isolated product, the NMR peak assignment was re-evaluated. The ^1H NMR spectrum showed that there were nine aromatic protons, sixteen aliphatic

protons, and two NH protons from the amino and amide functional groups. Each pair of chemically equivalent nuclei at 7.13 and 7.52 ppm from a methylphenyl ring integrated for two protons. The ether phenyl signals at chemical environments in the ranges of 7.25-7.67 ppm had a ratio of 1:1:2. The pyrimidine proton was the most shielded aromatic nucleus appearing at 5.12 ppm. The chemically equivalent Me_2N protons appeared at 2.97 ppm and the methyl protons from a tolyl moiety were observed at 2.31 ppm, while the CH_3 protons of the propylamino tail were highly shielded at 0.89 ppm. The amide proton was deshielded at 8.32 ppm whereas the amino proton was seen upfield at 4.78 ppm. Due to symmetrical Me_2N and tolyl motif, the ^{13}C NMR spectrum displayed fourteen aromatic carbon signals and five signal absorptions from the aliphatic carbons. The C=O carbon was also observed at 165.1 ppm. The DEPT NMR spectrum showed the presence of three CH_3, two CH_2, and seven CH signals. The HMBC NMR spectrum demonstrated the ^3J coupling between the proton signal at 2.97 ppm and the pyrimidine carbon signal at 165.3 ppm. These results were in good agreement with the mass spectroscopic data, thus, confirming the formation of compound **187d**.

2.4 Conclusion

The overall aim of this project was to synthesise a library of novel potential NNRTIs with more flexible structures to improve or halt development of resistance by the HIV-1 RT enzyme. The scaffold hopping approach has demonstrated that these compounds can be designed by various alterations on the lead compounds for the possibility of obtaining enhanced binding affinities at the RT binding site. Thus, encouraged by these findings we explored the synthesis of different classes of benzamides.

The first class of compounds that was successfully synthesised include derivatives **157a**-**o** (Fig **60**) derived from unsubstituted benzoic acid **152** and anilines **151a**-**h**. Compounds **157b**, **157d**, and **157e**-**h** were obtained in low yields when pyridine was used as a base and obtained in good to excellent yields when triethylamine was used.

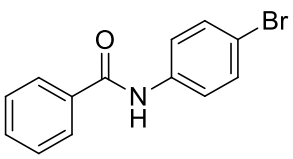

157a, 83%

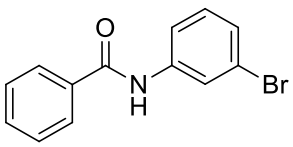

157b, 93%

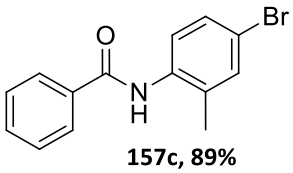

157c, 89%

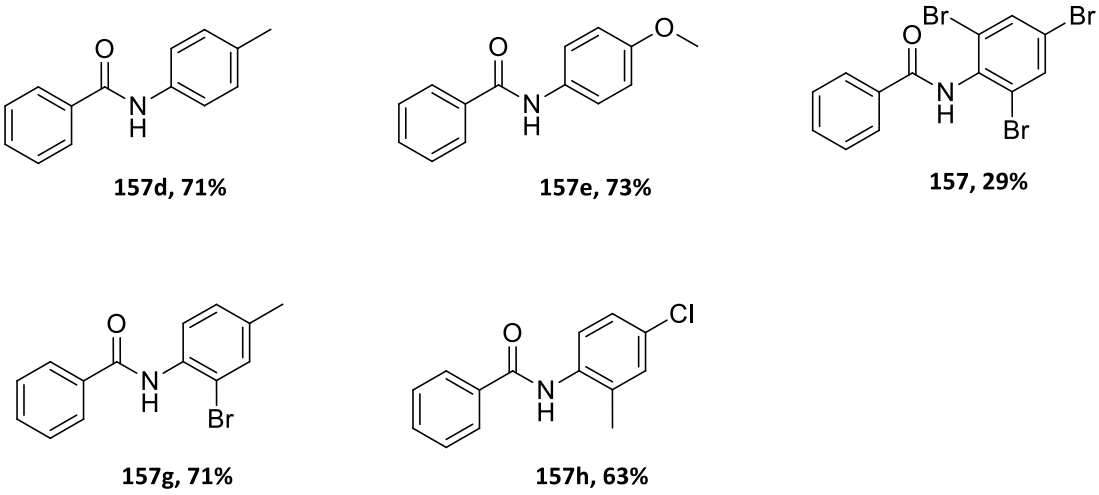

Fig 60 *N-phenylbenzamides successfully synthesised*

A series of the *N*-pyridinylbenzamide analogues **157j**-**o** (Fig **61**) was successfully synthesised employing either pyridine or triethylamine.

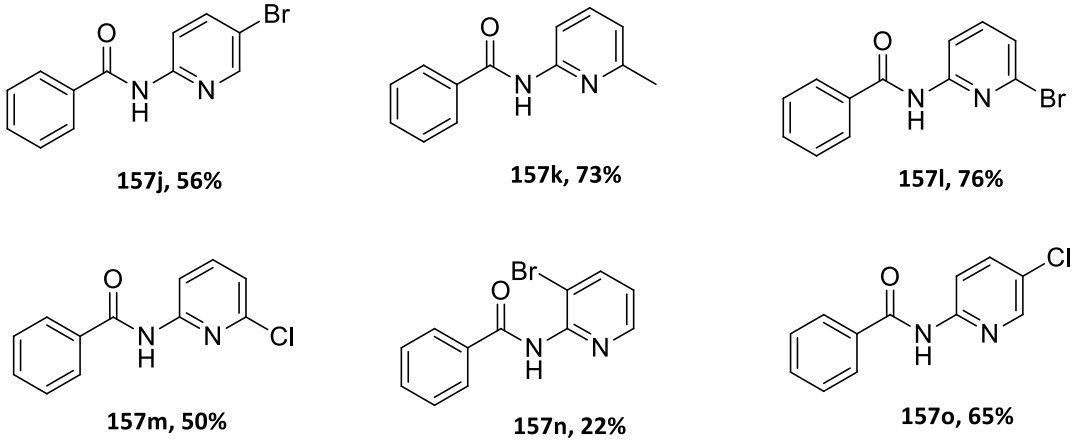

Fig 61 *N-pyridinylbenzamides successfully synthesized*

The amidation reactions between benzoic acid **152** and aminopyridines **151i** and **151n** favoured diacylated products **160i** and **160n** (Fig **62**) in the presence of triethylamine while monoacylation was favoured with the use of pyridine.

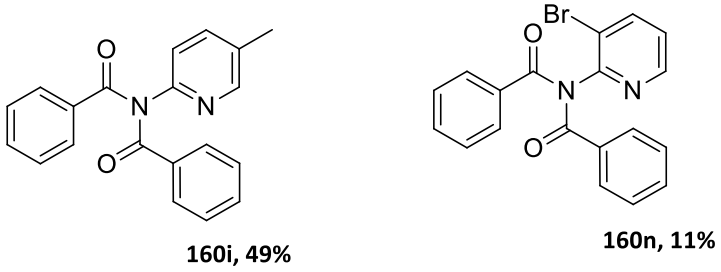

Fig 62 *N-diamide products obtained from benzoic acid **152***

The second class of compounds **158a**-**e** and **158h** (Fig **63**) were achieved by reacting 3-methoxybenzoic acid **153** with anilines **151a**-**e** and **151h** employing triethylamine and were isolated in reasonable to good yields. For some compounds further purification by recrystallization was required resulting in the loss of material and difficult comparisons in substituent effects.

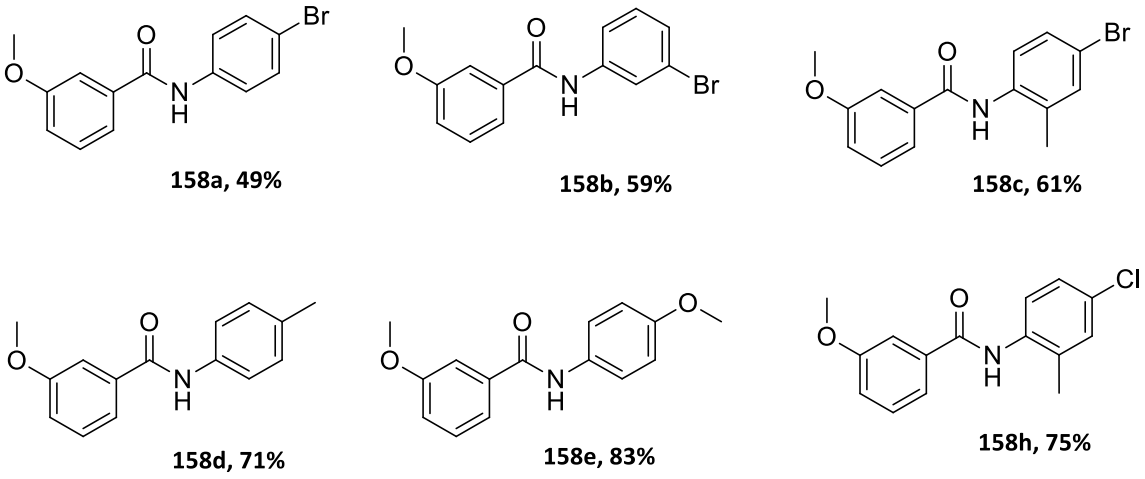

Fig 63 *Successfully synthesised N-phenylbenzamides derived from 3-methoxybenzoic acid*

Another library of compounds **158i**-**o** (Fig **64**) derived from **153** and amines **151i**-**o** was successfully prepared and isolated in modest to excellent yields with the use of pyridine.

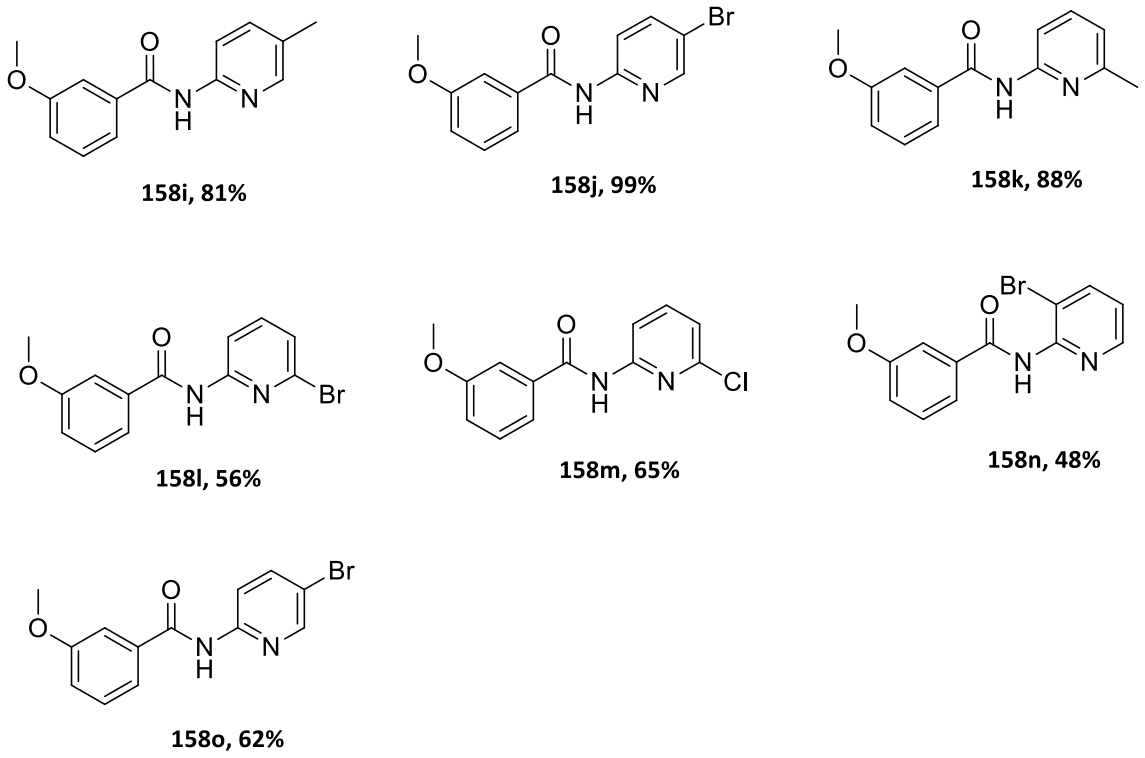

Fig 64 *Successfully synthesised N-pyridinylbenzamides derived from meta-methoxybenzoic acid*

The *N*,*N*-diacylation (**165i** and **165j**) was observed in amidation reactions involving **153** and aminopyridines **151i** and **151j** when using triethylamine (Fig **65**). The repeated reactions with the use of pyridine afforded the desired monosubstituted products **158i** and **158j** in excellent yields. Derivative **158n** that was only prepared in the presence of triethylamine did not undergo further acylation and was obtained in poor yield possibly because of the steric effects.

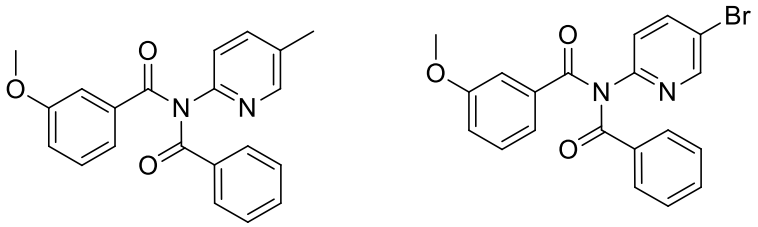

165i, 39% **165j, 62%**

Fig 65 *N-diamide products obtained from acid **153***

The third class of benzamide analogues that were successfully isolated include **166j**, **166l**, **166m**, and **166o** (Fig **66**) derived from the 3-hydroxybenzoic acid **154** using pyridine. In each instance the conversion of **154** into the corresponding acid chloride gave undesirable results as observed from the NMR spectra. Pure compounds were achieved following successive washing with ethyl acetate after column chromatography purification.

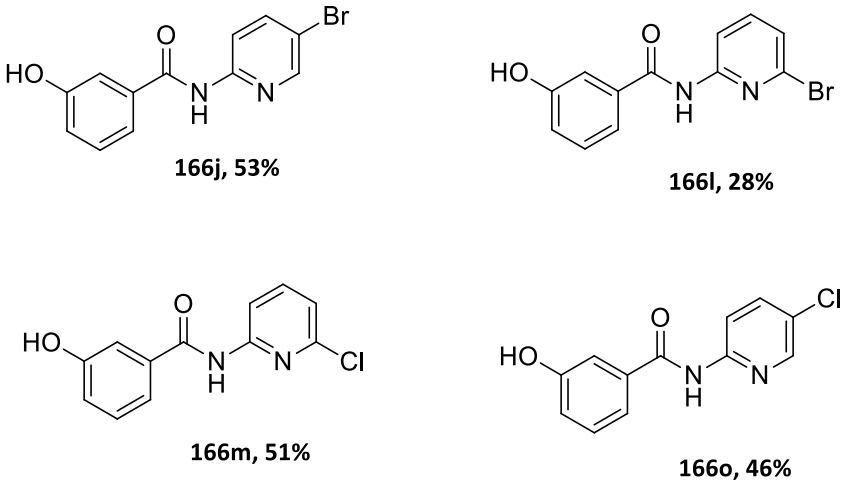

166j, 53% **166l, 28%**

166m, 51% **166o, 46%**

Fig 66 *N-pyridinylbenzamides successfully synthesised from meta-hydroxybenzoic acid*

Moving on to the first chloride displacement on **102**, it was discovered that substitution of chlorine atoms was possible, and selectivity could be achieved by controlling the stoichiometric amount of reagents and reaction conditions as suggested by Dillender.[138] Methyl 3-hydroxybenzoate **141** (Scheme **70**), was the first example to demonstrate possible nucleophilic substitution of a chlorine atom on **102** during which the product **173** was isolated in excellent yield.

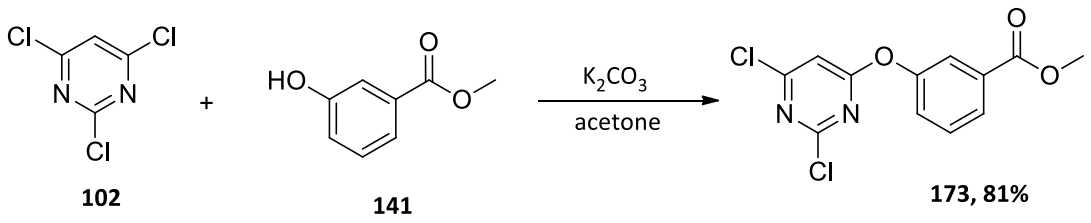

Scheme 70 *Displacement of the first chloride by methyl 3-hydroxybenzoate* ***141***

3-((2,6-Dichloropyrimidin-4-yl)oxy)benzoic acid **155** (Scheme **71**) was also formed by replacing the first chlorine atom in the presence of aq. NaOH and was obtained in excellent yield after protonation by adjusting the pH to 3 with aqueous HCl during workup. The product failed to form when potassium carbonate was used as a base, highlighting the significance of quantifying basicity when strongly acidic reagents are involved.

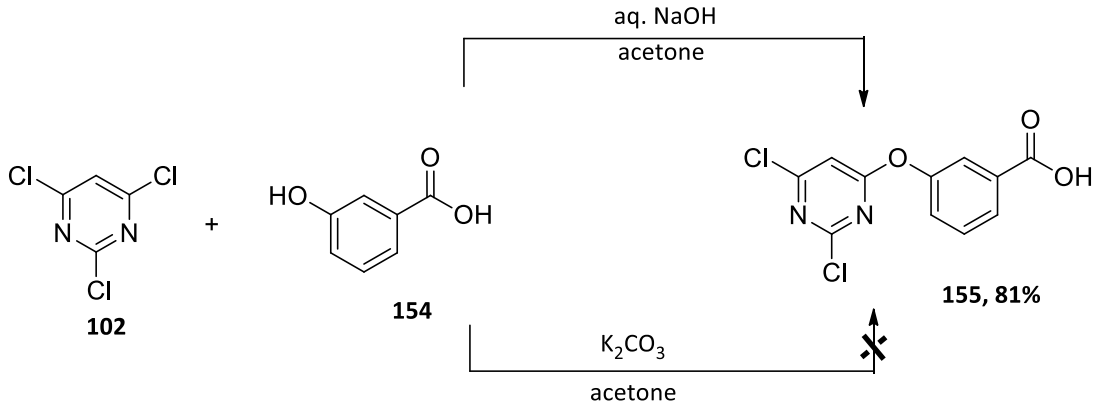

Scheme 71 *Displacement of the first chloride by 3-hydroxybenzoic acid* ***154***

N-(5-bromopyridin-2-yl)-3-hydroxybenzamide **166j** also successfully coupled to the chlorinated pyrimidine **102** (Scheme **72**), although low yield of **168j** was obtained due to the reaction not going to completion.

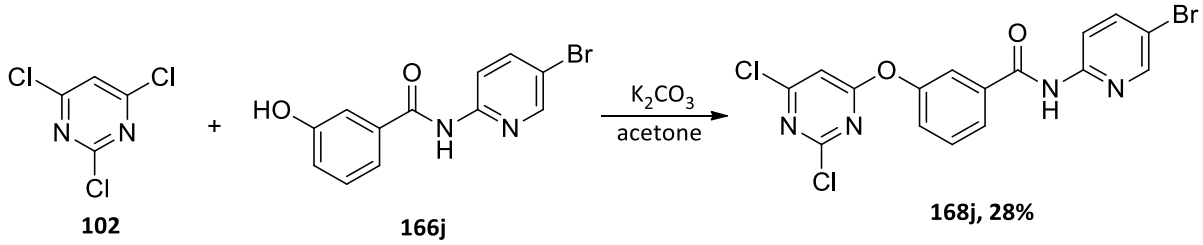

Scheme 72 *First chlorine displacement by N-(5-bromopyridin-2-yl)-3-hydroxybenzamide* ***166j***

Interestingly, when **155** was reacted with **151j**, the yield was better for compound **168j** (Fig **67**), than when **102** was directly coupled with **166j**. Unlike for simple *N*-pyridinylbezamide derivatives where pyridine worked better in amidation reactions than triethylamine, it was in fact incompatible with the

entire panel of the aryl benzamides offering poor yields and many unidentifiable products. Triethylamine offered better yields for both series of the complex benzamides derived from anilines and aminopyridines.

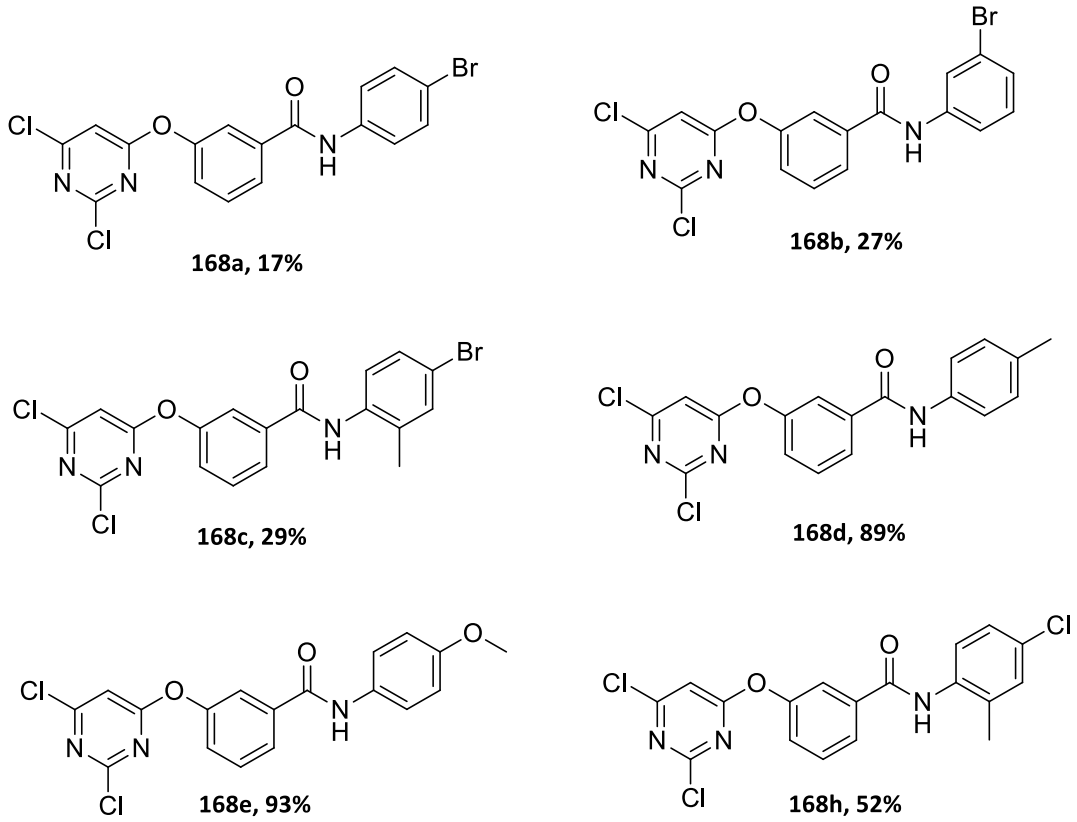

Fig 67 *Complex benzamides successfully synthesised from anilines*

Another range of the successfully synthesised complex benzamides through the amination of complex acid **155** with amines **151j**-**k** are shown below (Fig **68**).

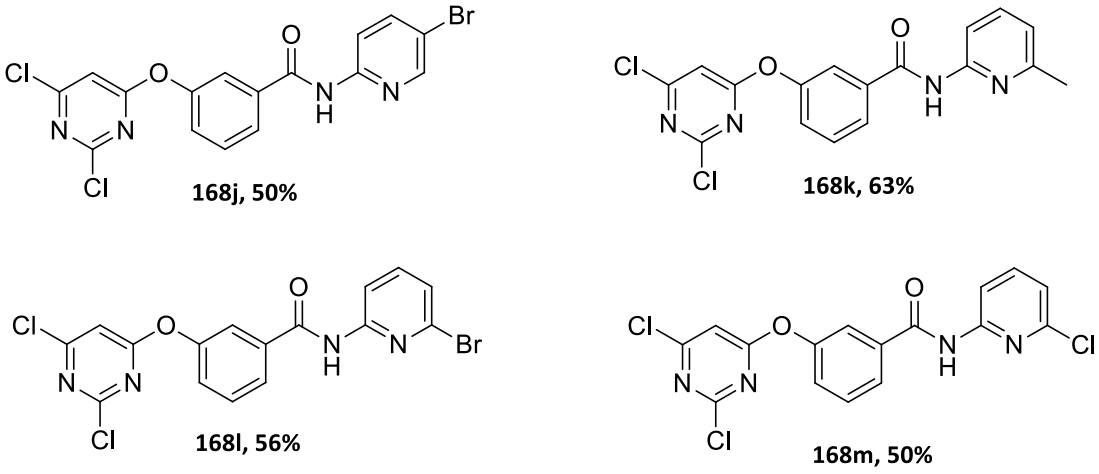

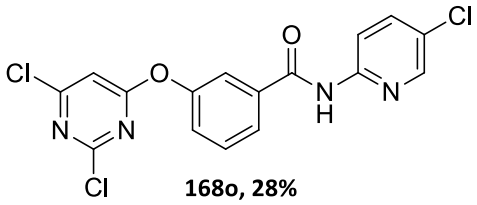

168o, 28%

Fig 68 *Complex benzamides successfully derived from aminoypridines*

During the second chlorine substitution with the sulphur-containing nucleophiles, the pyrimidine ring C-O bond cleavage occurred, no matter the nature of the base used, but that was not true for the nitrogen-based nucleophiles. For this reason, it can be concluded that the C-O cleavage was directly proportional to the strength of the nucleophile used. The successfully synthesised compounds from the second functionalization of the chloropyrimidine **102** are shown below (Fig **69**).

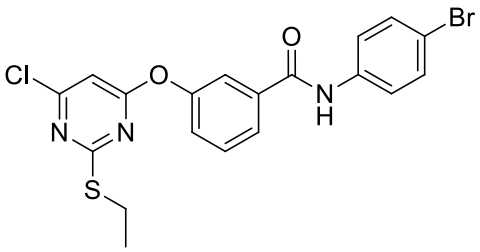

180a, 43%

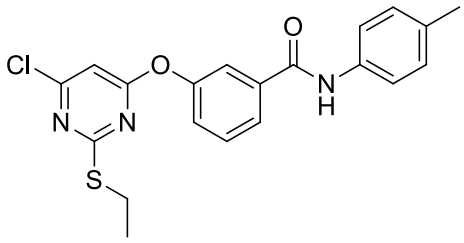

180d, 38%

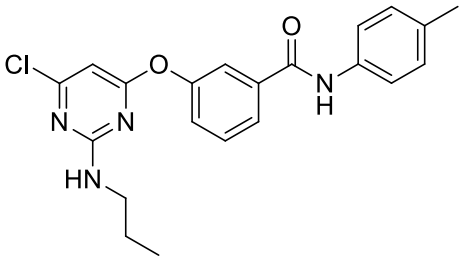

184d, 66%

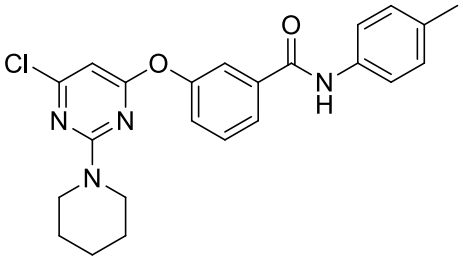

185d, 64%

Fig 69 *Compounds successfully synthesised from the second chloride displacement*

The third chlorine replacement was carried out in strong basic medium although hydrolysis of **184d** to compound **186d** failed. Instead, decomposition of DMF to DMA occurred which in turn acted as a nucleophile during the substitution of the chlorine atom giving rise to unexpected derivative **187d** (Scheme **73**).

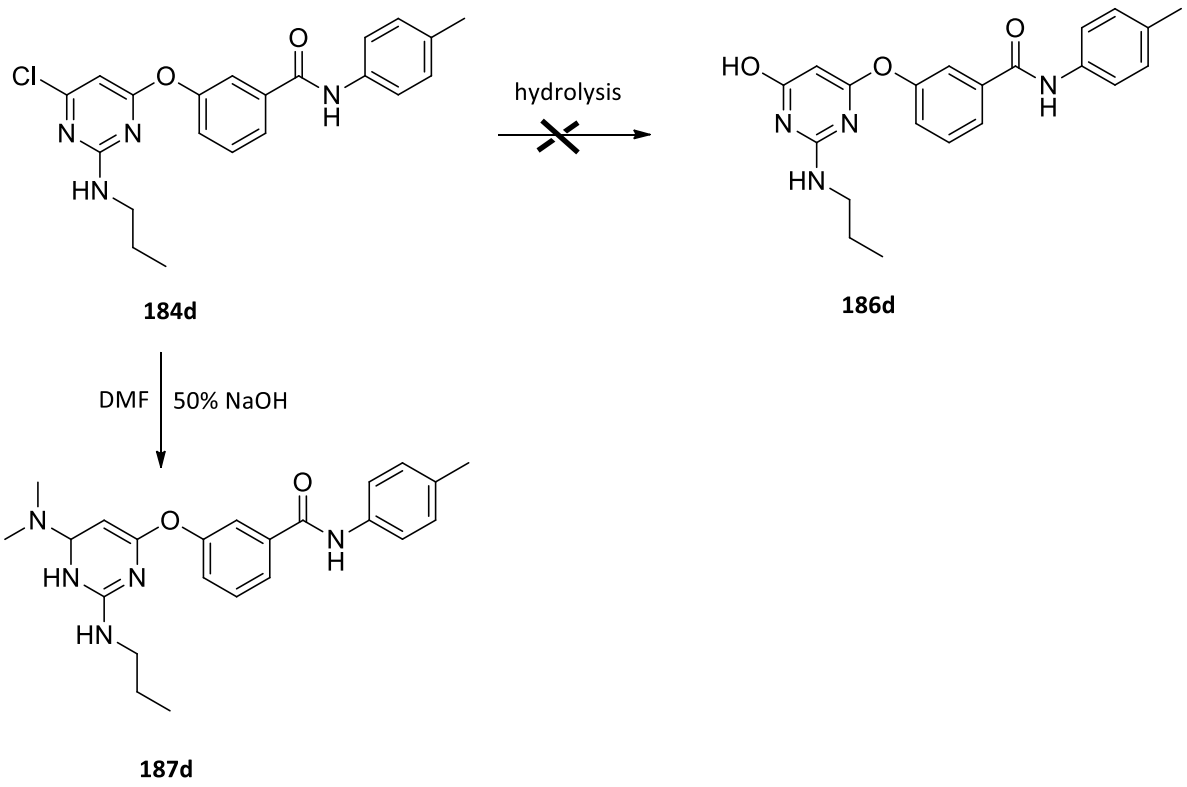

Scheme 73 *Unexpected formation of compound* ***187d***

Overall, the first aim of this project achieved was the successful synthesis of simple benzamides derived from benzoic acid, 3-methoxybenzoic acid, and 3-hydroxybenzoic acid. The second aim achieved was the replacement of chlorine atoms on 2,4,6-trichloropyrimidine with various nucleophiles. Even though the attempts to displace the third chlorine atom by means of hydrolysis gave undesirable results, it was encouraging to find out that it is replaceable. It was also discovered that the pyrimidine ring system became less electrophilic upon the introduction of a nucleophile thus necessitating the forcing conditions by either quantifying the molar concentrations or elevating the reaction temperature. The final aim was unfortunately not achieved because time restrictions did not allow us to evaluate the biological efficacy of the novel compounds. Most significantly, it would be exciting to examine their effectiveness against the wild-type virus and the most prevalent K103N mutant strain of HIV-1 RT.

Future work

Mikroyannidis *et al*[170] have shown that 3-hydroxybenzoyl chloride **169** can be obtained by treating 3-hydroxybenzoic acid **154** with two equivalents of $SOCl_2$ in the presence of $AlCl_3$ and petroleum ether heating at 55 °C for five hours to afford 30% yield. Inspired by the author's successful chlorination of **154** (Scheme **74**), the versatility of this protocol will be evaluated following the same approach to either complement or disagree with the author's results. Again, considering that most of the yields

obtained in this project were reasonable, improving the reaction yields by either varying bases or solvent composition will be our priority.

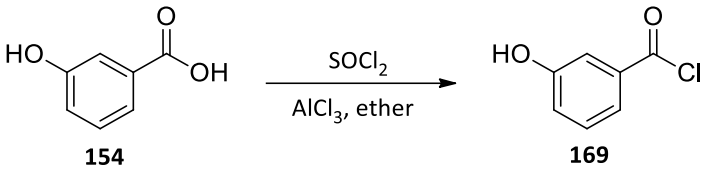

154 **169**

Scheme 74 *Preparation 3-hydroxybenzoyl chloride* ***169***

The attempted synthesis or synthesis of compounds **166a**-**o**, which are hydroxyl version of derivatives **158a**-**o** was initiated by chlorination of 3-hydroxybenzoic acid **154** followed by the amination step, which proved to be difficult to transform into the desired compounds. The alternative route to access **166** series of compounds will be through deprotection of derivatives **158a**-**o** using BBr_3 as a demethylation agent. Another attractive approach is the use of iodocyclohexane which stood out to be efficient in facilitating the conversion of 4-methoxyphenol into its corresponding 4-hydroxyphenol according to Zuo's results.[171] These methods will possibly give the desired hydroxy counterparts **166a**-**o** in one step as shown below (Scheme **75**).

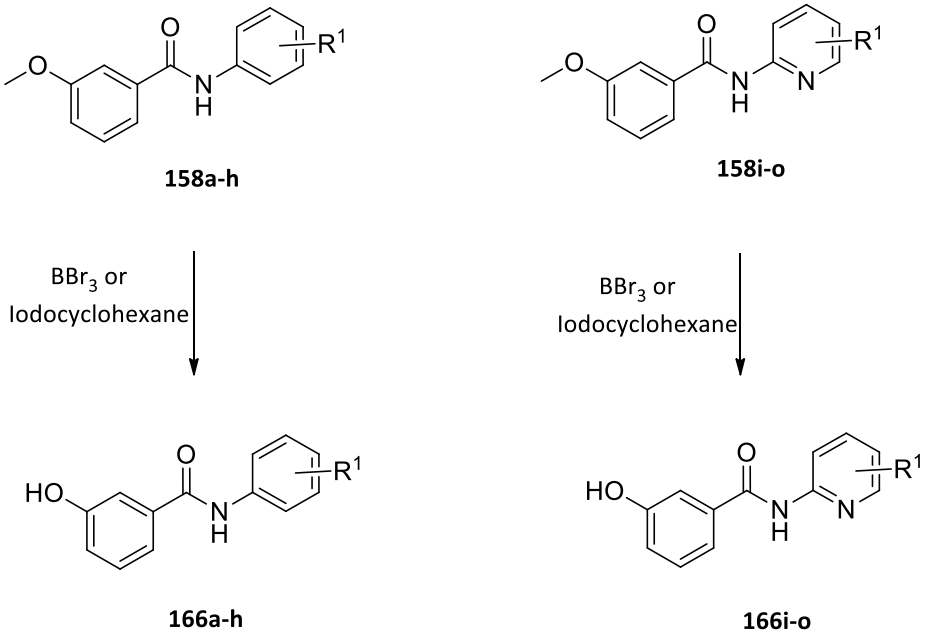

Scheme 75 *Considered demethylation of aryl methyl ethers* ***158a*****-*****o***

Since hydrolysis of compound **184d** was not achieved under both acidic and basic conditions, we will look into alternative approaches to synthesise compound **186d**. One of our options includes the screening of solvents composition and stability, and to optimize reaction conditions. Once compound **186d** is formed and considering its ability to tautomerize because of rapid hydrogen exchange, it will

be crucial to identify its form of existence (enol or keto form). Oxygen and carbon atoms will share a single pair of electrons if the molecule adopts the hydroxy form (**186d**) or be doubly bonded to each other in the oxo form (**190d**) (Fig **70**).

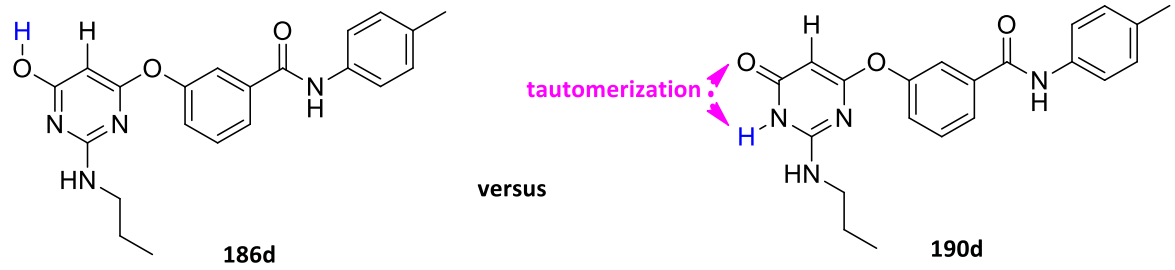

186d **190d**

Fig 70 *Tautomeric representation of* ***186d***

Considering that the nucleophilic aromatic substitution reaction was instigated by etherification followed by thiolation, the order of reactions will change. The first chlorine displacement will be tested by thiolation followed by the second chlorine replacement through etherification, and the last displacement by hydrolysis (Scheme **76**). This will enable a suitable comparison to be made in terms of the preferred sequence of introducing the nucleophiles onto the pyrimidine ring system.

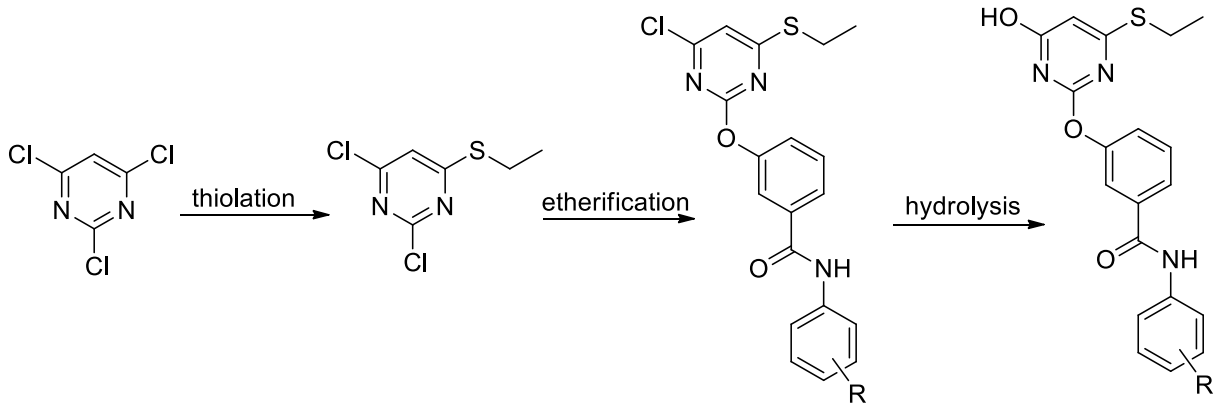

Scheme 76 *Initiating the synthesis by thiolation*

Hydrolysis can also be performed first although minimal selectivity can be attained because of di- or tri-hydrolysed products or even a mixture of both. However, as previously mentioned, the reaction conditions will need to be controlled in such a way that monosubstitution can be maximized while depressing di- or tri-substitution. It would also be interesting to perform hydrolysis reactions of the S-coupled compounds, *N*-(4-bromophenyl)-3-((6-chloro-2-(ethylthio)pyrimidin-4-yl)oxy)benzamide **180a** and 3-((6-chloro-2-(ethylthio)pyrimidin-4-yl)oxy)-*N*-(p-tolyl)benzamide **180d** in order to compare them to that of the N-coupled derivative 3-((6-chloro-2-(propylamino)pyrimidin-4-yl)oxy)-*N*-(p-tolyl)benzamide **184d** in respect of its response to harsh NaOH conditions, the yields, and the form of the resulting molecule (Scheme **77**).

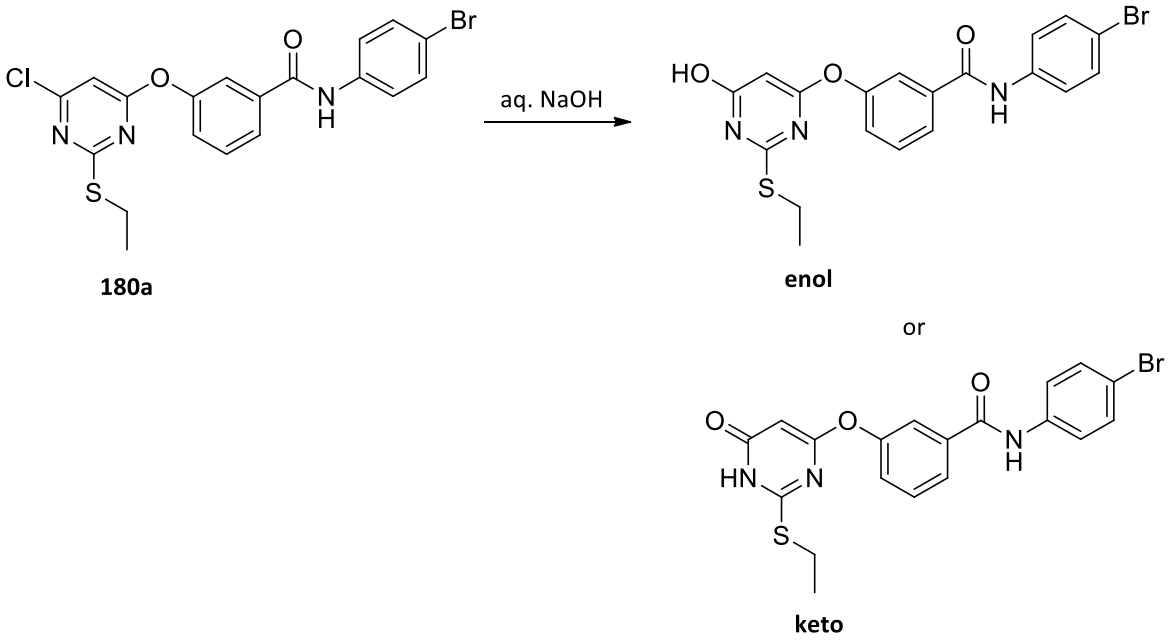

180a **enol** **keto**

Scheme 77 *Planned hydrolysis of* ***180a***

3-((2,6-Dichloropyrimidin-4-yl)oxy)-*N*-(p-tolyl)benzamide and *N*-(4-bromophenyl)-3-((2,6-dichloropyrimidin-4-yl)oxy)benzamide have demonstrated that the formation of the pyrimidine C-S bond is indeed feasible in spite of the surprising emergence of the C-O bond cleavage problems. Thus, another tempting approach to be undertaken is the thiolation of carboxylic acid **155**, which can be followed by an amidation reaction, then hydrolysis or vice versa (Scheme **78**). Although it seems possible to thiolate, it is concerning that many unfavourable side reactions may take place. Still on the sulphur coupling, it is imperative to investigate the reactivity of the aromatic S-nucleophiles such as thiophenol.

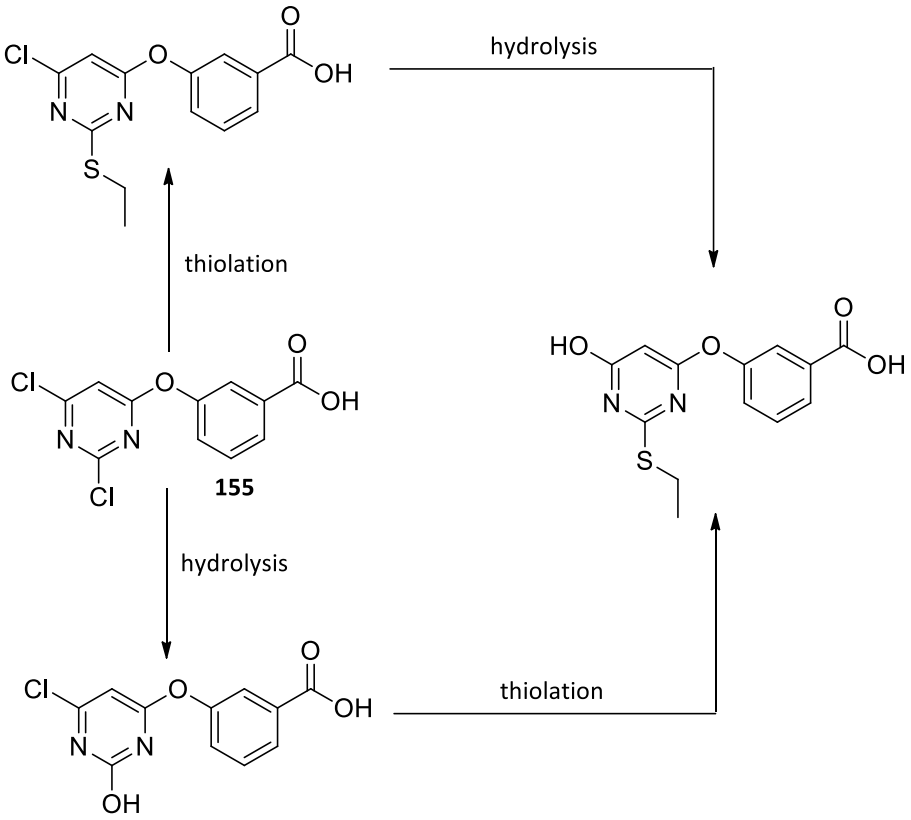

Scheme 78 *Second chloride displacement on acid* ***155***

This project can also be extended to other interesting, chlorinated heterocycles like 2,4,6-trichloropyridine **191** and 2,4,6-trichloro-1,3,5-triazine **192** (Fig **71**). However, such reactions are rarely studied, most publications deal with consecutive displacements of two ring chlorides leaving the other unsubstituted.

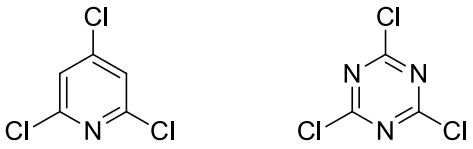

191 **192**

Fig 71 *Structures of other trichlorinated heterocycles*

To validate the feasibility of amidation reactions in chlorinated pyridines, 2,6-dichloroisonicotinic and 2,6-dichloronicotinic acids were first converted into amides through the *in situ* reaction between their acyl chlorides and cyclopropylamine. The resulting 2,6-dichloro-*N*-cyclopropylnicotinamide and 2,6-dichloro-*N*-cyclopropylisonicotinamide were furnished in 99% yield and further used in the S_NAr reactions to replace the first chloride by treatment with 4-chlorophenol employing palladium/*rac*-BINAP catalyst. The second chlorine displacement was found possible by amination with piperidine

through the application of both Pd/*rac*-BINAP catalyst giving **193** (53% yield) and Pd/Xantphos affording **194** in 54% yield (Fig **72**).[63]

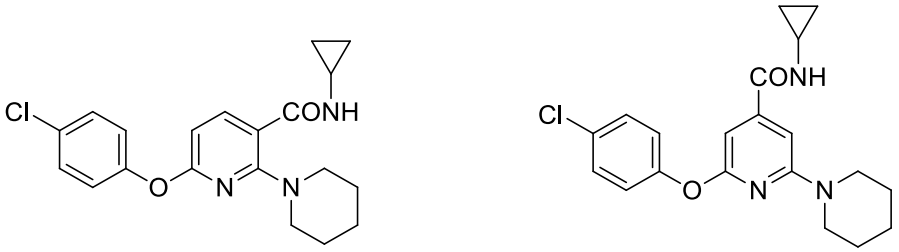

193 **194**

Fig 72 *Literature compounds* ***193*** *and* ***194*** *synthesised from* ***191***

Thus, the reported possibility of replacing the ring chlorides on both 2,4,6-trichloropyridine and cyanuric chloride means that another series of potential NNRTIs is possible to prepare from these precursors following the nucleophilic substitution sequence reported for 2,4,6-trichloropyrimidine. It will be exciting to learn about the susceptibility or resistance of the latter electrophiles to the C-O bond cleavage occurring as a result of the attack by S-nucleophiles. Above all, not forgetting the significance of our project, the novel synthesised compounds will need to be subjected to biological testing for the evaluation of their antiviral inhibitory activity against HIV-1 RT.

CHAPTER 3: EXPERIMENTAL PROCEDURE

All solvents used in this project for reactions and column chromatography separation were purified by distillation. Ethyl acetate and hexane that were used in chromatographic separation were distilled prior to use. Acetonitrile was distilled from anhydrous calcium hydride whereas tetrahydrofuran was distilled from a sodium wire using benzophenone as an indicator. All other solvents and reagents used for reactions were purchased commercially from Merck and Sigma-Aldrich and were used without further purification.

TLC plates used for monitoring reactions progress were coated with 0.25mm silica gel 60 and backed with aluminium Macherey-Nagel AlugramSil G/UV254. The TLC plates were visualized under UV light using a TLC visualizer operating at λ=254 nm or λ=366 nm. Column chromatography purification was performed on Merck or silica gel 60 with particle size of 0.063-0.200 mm for normal silica or flash silica with particle size of 0.040-0.063 mm. All the melting points were measured using a Stuart SMP10 melting point apparatus and are uncorrected. FT-IR spectra were recorded using a Bruker Vector 22 Spectrometer and all the signals are reported on the wavenumber scale of v/cm^{-1}.

NMR spectra were recorded on a Bruker Avance-300, Bruker Advance-400, or Bruker Avance-500 spectrometer with ^{1}H NMR operating at a frequency of 300 MHz, 400 MHz, or 500 MHz respectively, and ^{13}C NMR at 75 MHz, 101 MHz, and 125 MHz respectively. Deuterated chloroform ($CDCl_3$) or deuterated dimethyl sulfoxide (DMSO-d_6) were used as solvents while trimethyl silane (TMS) as a reference internal standard. Chemical shift (δ) values are reported in parts per million (ppm) relative to TMS (δ=0). Spin multiplicities like singlet, doublet, triplet, quartet, and multiplet are abbreviated as s, d, t, and m respectively, and coupling constants (*J*) reported in Hertz (Hz). High resolution mass spectroscopic data was recorded using a Waters Synapt G2 and data for all novel compounds is reported in relative abundance (m/z).

3.1 Synthesis of benzamides from unsubstituted benzoic acid **152** and aniline derivatives **151a-h**

General procedure

Benzoic acid **152** (1.00 g, 8.20 mmol) was placed in a round-bottomed flask, followed by addition of excess thionyl chloride (2 ml). The mixture was stirred and refluxed at 80 °C in an oil bath for 24 h. After cooling the mixture to room-temperature, excess thionyl chloride was evaporated leaving a pale yellow benzoyl chloride residue which was dissolved in distilled acetonitrile (4 ml), followed by slow addition of an ice-cold mixture of the appropriate aniline (**157a-h**) and pyridine or triethylamine (3 ml) in dry acetonitrile (10 ml). The mixture was stirred at 0 °C for 30 min, warmed to room temperature and stirred for 10-24 h. Excess solvent was removed *in vacuo* and the residue dissolved in ethyl acetate

(50 ml). The organic mixture was washed with aqueous saturated $NaHCO_3$ or aqueous K_2CO_3 (2× 50 ml), saturated brine solution (50 ml) and the organic layer was separated and dried over anhydrous Na_2SO_4. The solvent was removed under reduced pressure and the crude product purified by normal silica gel chromatography eluting with 20-30% EtOAc/hexane. Recrystallization was performed using hot ethyl acetate and cold hexane where necessary to afford compounds **157a**-**h**. Only compound **157f** is novel.

*3.1.1 N-(4-bromophenyl)benzamide **157a***

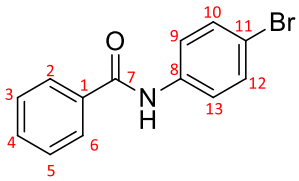

(i) 4-bromoaniline **151a** (1. 02 g, 8.20 mmol) was reacted with benzoyl chloride **156** (8.20 mmol) for 18 h forming a precipitated which was filtered to recover compound **157a** as a white solid (1.17 g, 83% yield).

(ii) In a round-bottomed flask was added benzoic acid **152** (1.03 g, 8.20 mmol) and DCC **28** (1.70 g, 1.64 mmol) in DMF (5 ml). The mixture was stirred and heated at 80 ˚C in an oil bath for 40-60 min. After quantitative consumption of the acid, 4-bromoaniline **151a** (1.43 g, 8.20 mmol) was cautiously added and contents of the reaction proceeded for 24h. After cooling the reaction mixture to room temperature, ethyl acetate (50 ml) was added, and the mixture was washed successively with water (50 ml × 7) to remove DMF. The organic layer was dried over anhydrous Na_2SO_4 and the solvent removed *in vacuo* leaving a crude mixture which was purified by normal silica gel chromatography eluting with 30% EtOAc/hexane to give a white solid **157a** (0.520 g, 23% yield)

(iii) Benzoic acid **152** (1.00 g, 8.20 mmol) and 4-bromoaniline **151a** (1.38 g, 8.20 mmol) were added in a microwave tube, and irradiated in a closed vessel microwave reactor at 140 ˚C and 150 W, for 10 min. The reaction was monitored by TLC plate comparing against the reference product **157a** obtained in the previous reactions. A spot corresponding to the desired product was observed. The reaction mixture was dissolved in ethyl acetate (50 ml), washed several times with aqueous K_2CO_3 (5 × 50 ml) and dilute HCl (5 × 50 ml). The organic layer was separated, and excess solvent was evaporated leaving pure cream-white solid **157a** (0.630 g, 28% yield). Rf= 0.4 (7:3 EtOAc/hexane); M.p= 209-211 ˚C; IR (ν/cm^{-1}) 3331 (NH, br), 1545 (C=O, str); ^{1}H NMR (300 MHz, DMSO-d_6) δ_H 10.38 (s, 1H, NH), 7.98 – 7.93 (m, 2H, H2 and H6), 7.81 – 7.75 (m, 2H, H9 and H13), 7.64 – 7.51 (m, 5H, H3, H4, H5, H10, and H12); ^{13}C NMR (75 MHz, DMSO-d_6) δ_C 165.6 (C7), 138.5 (C8), 134.7 (C1), 131.7 (C3 and C5), 131.4 (C4), 128.4 (C2 and C6) , 127.6 (C10 and 12), 122.2 (C9 and C13), 115.3 (C11).

*3.1.2 N-(3-bromophenyl)benzamide **157b***

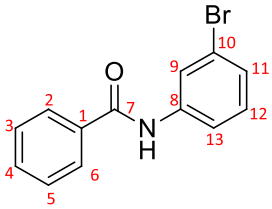

3-bromoaniline and pyridine **151b** (0.900 ml, 8.20 mmol) was reacted with benzoyl chloride **156** (8.20 mmol) for 24 h. Compound **157b** was obtained as a white solid product (0.951 g, 42% yield when pyridine was used and 2.10 g, 93% yield when triethylamine was used). Rf= 0.4 (7:3 EtOAc/hexane); M.p= 124-126 °C; IR (ν/cm^{-1}) 3282 (NH, br), 1649 (C=O, str); ^{1}H NMR (300 MHz, $CDCl_3$) δ_H 8.00 (s, 1H, NH), 7.90 (t, J = 1.9 Hz, 1H, H9), 7.84-7.82 (m, 2H, H2 and H6), 7.58 – 7.51 (m, 2H, H4 and H11), 7.49 – 7.42 (m, 2H, H3 and H5), 7.29 – 7.16 (m, 2H, H12 and H13); ^{13}C NMR (75 MHz, $CDCl_3$) δ_C 165.9 (C7), 139.2 (C8), 134.5 (C1), 132.1 (C4), 130.3 (C12), 128.8 (C3 and C5), 127.5 (C13), 127.1 (C3 and C5), 123.2 (C9), 122.7 (C10), 118.7 (C11).

*3.1.3 N-(4-bromo-2-methylphenyl)benzamide **157c***

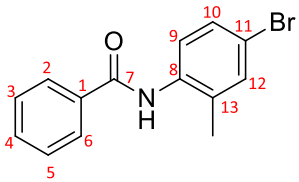

4-bromo-2-methylaniline **151c** (1.350 g, 8.20 mmol) was reacted with benzoyl chloride **156** (8.20 mmol) for 24 h resulting in a precipitate. Purification of the desired product was afforded by column chromatography and recrystallization using hot EtOAc and cold hexane. Compound **157c** was obtained as a white solid product (1.22 g, 89% yield). Rf= 0.2 (7:3 EtOAc/hexane); M.p= 174-176 °C; IR (ν/cm^{-1}) 3257 (NH, br), 1587 (C=O, str), ^{1}H NMR (300 MHz, DMSO-d_6) δ_H 10.00 (s, 1H, NH), 8.03 – 7.96 (m, 2H, H2 and H6), 7.64 – 7.49 (m, 4H, H3, H4, H5, and H12), 7.41 (dd, J = 2.2, 8.5 Hz, 1H, H10), 7.32 (d, J = 8.5 Hz, 1H, H9), 2.24 (s, 3H, H-CH_3); ^{13}C NMR (75 MHz, DMSO-d_6) δ_C 165.3 (C7), 136.5 (C8), 135.9 (C13), 134.2 (C1), 132.7 (C12), 131.6 (C4), 128.7 (C9), 128.4 (C3 and C5), 127.7 (C2 and C6), 118.2 (C11), 17.6 (C-CH_3).

*3.1.4 N-(p-tolyl)benzamide **157d***

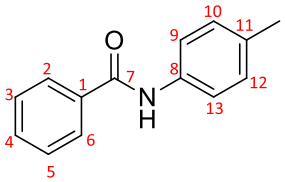

4-methylaniline **151d** (0.880 g, 8.20 mmol) was reacted with benzoyl chloride **156** (8.20 mmol) for 14 h. Compound **157d** was obtained as a white solid (pyridine, 1.24 g, 72% yield and triethylamine, 1.31 g, 72% yield). Rf= 0.4 (7:3 EtOAc/hexane); M.p= 162-164 °C; IR (ν/cm^{-1}) 162-167 °C; 3310 (NH, br), 1645 (C=O, str); ^{1}H NMR (400 MHz, DMSO-d_6) δ_H 10.19 (s, 1H, NH), 7.98 – 7.94 (m, 2H, H2 and H6), 7.68 (d, J = 8.4 Hz, 2H, H9 and H13), 7.61 – 7.50 (m, 3H, H3, H4, and H5), 7.16 (d,

J = 8.3 Hz, 2H, H10 and H12), 2.29 (s, 3H, H-CH_3); ^{13}C NMR (101 MHz, DMSO-d_6) δ_C 165.8 (C7), 137.1 (C8), 135.5 (C1), 133.1 (C11), 131.9 (C4), 129.4 (C10 and C12), 128.8 (C3 and C5), 128.1 (C2 and C6), 120.8 (C9 and C13), 21.0 (C-CH_3).

*3.1.5 N-(4-methoxyphenyl)benzamide **157e***

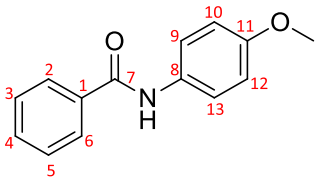

4-methoxyaniline **151e** (0.990 g, 8.20 mmol) was reacted with benzoyl chloride **156** (8.20 mmol) for 22 h. Compound **157e** was obtained as a white solid (pyridine, 1.36 g, 73% yield and tiethylamine, 1.36 g, 73% yield). Rf= 0.4 (7:3 EtOAc/hexane); M.p= 162-164 °C; IR (ν/cm^{-1}) 3330 (NH, br), 1646 (C=O, str), 1174 (C-O); ^{1}H NMR (400 MHz, DMSO-d_6) δ_H 10.16 (s, 1H, NH), 7.98 – 7.93 (m, 2H, H2 and H6), 7.70 (d, *J* = 12.1 Hz, 2H, H9 and H13), 7.61 – 7.50 (m, 3H, H3, H4, and H5), 6.93 (d, *J* = 9.0 Hz, 2H, H10 and H12), 3.75 (s, 3H, H-OCH_3); ^{13}C NMR (101 MHz, DMSO-d_6) δ_C 165.6 (C7), 156.0 (C11), 135.5 (C1), 132.7 (C8), 131.8 (C4), 128.8 (C3 and C5), 128.0 (C2 and C6), 122.4 (C9 and C13), 114.2 (C10 and C12), 56.6 (C-OCH_3).

*3.1.6 N-(2-bromo-4-methylphenyl)benzamide **157f***

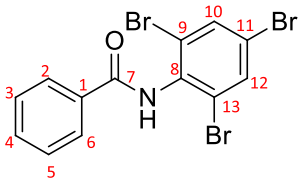

2,4,6-tribromoaniline **151g** (2.72 g, 8.20 mmol) was reacted with benzoyl chloride **156** (8.20 mmol) for 10 h. Compound **157g** was obtained as a white solid (pyridine, 0.110 g, 3% yield and tiethlamine, 1.04 g, 29% yield). Rf= 0.3 (7:3 EtOAc/hexane); M.p= 207-209°C; IR (ν/cm^{-1}) 3227 (NH, br), 1652 (C=O, str) ; ^{1}H NMR (400 MHz, DMSO-d_6) δ_H 10.38 (s, 1H, NH), 8.09 – 7.98 (m, 4H, H2, H6, H10, and H12), 7.58 (dt, *J* = 30.4, 7.3 Hz, 3H, H3, H4, and H5); ^{13}C NMR (101 MHz, DMSO-d_6) δ_C 165.5 (C7), 136.3 (C8), 134.8 (C10 and C12), 133.8 (C1), 132.6 (C4), 129.0 (C3 and C5), 128.2 (C2 and C6), 126.1 (C9 and C13), 121.7 (C11); HRMS (ES$^+$) calculated for $C_{13}H_9Br_3NO$ $[M+H]^+$: 431.8229, found: 431.8219.

*3.1.7 N-(2-bromo-4-methylphenyl)benzamide **157g***

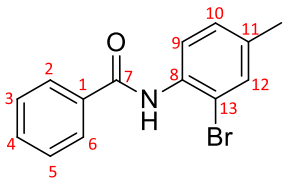

2-bromo-4-methylaniline **151g** (1.52 g, 8.20 mmol) was reacted with benzoyl chloride **156** (8.20 mmol) for 24 h. Compound **157g** was obtained as a white solid (pyridine, 0.521 g, 22% and triethylamine, 1.88 g, 74% yield). Rf= 0.3 (7:3 EtOAc/hexane); M.p= 150-152 °C; IR (ν/cm^{-1})

3247 (NH, br), 1647 (C=O); ^{1}H NMR (300 MHz, $CDCl_3$) δ_H 8.40 – 8.37 (m, 2H, H9 and NH), 7.93 (dt, *J*= 6.8, 1,4 Hz, 2H, H2 and H6), 7.60 – 7.52 (m, 4H, H3, H4, H5, H12), 7.19 – 7.16 (m, 1H, H10), 2.32 (s, 3H, H-CH_3); ^{13}C NMR (75 MHz, $CDCl_3$) δ_C 162.5 (C7), 135.4 (C10), 134.7 (C1), 133.2 (C8), 132.5 (C12), 132.1 (C4), 129.1 (C10), 128.9 (C3 and C5), 127.1 (C1 and C6), 121.6 (C9), 113.7 (C13), 20.6 (C-CH_3).

*3.1.8 N-(4-chloro-2-methylphenyl)benzamide **157h***

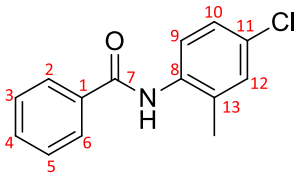

4-chloro-2-methyloaniline **151h** (1.16 g, 8.2 mmol) was reacted with benzoyl chloride **156** (8.20 mmol) resulting in a precipitate after 16 h. The reaction mixture was purified by column chromatography. Compound **157h** was obtained as a white solid (pyridine, 0.980 g, 49% yield and triethylamine, 1.26 g, 63% yield). Rf= 0.2 (7:3 EtOAc/hexane); M.p= 170-173 ˚C; IR (ν/cm^{-1}) 3249 (NH, br), 1648 (C=O, str); ^{1}H NMR (400 MHz, DMSO-d_6) δ_H 9.96 (s, 1H, NH), 7.99 (d, *J* = 7.2 Hz, 2H, H2 and H6), 7.57 (dt, *J* = 7.2, 27.4 Hz, H4, H5, and H6), 7.40 (d, *J* = 8.4 Hz, 2H, H10 and H12), 7.29 (dd, *J* = 2.4, 8.4 Hz, 1H, H9), 3.41 (s, 3H, H-CH_3); ^{13}C NMR (101 MHz, DMSO-d_6) δ_C 165.9 (C7), 136.6 (C8), 135.9 (C11), 134.7 (C1), 132.1 (C4), 130.3 (C12), 128.9 (C3 and C5), 128.6 (C2 and C6), 128.1 (C10), 126.3 (C9), 18.2 (C-CH_3).

3.2 Synthesis of benzamides from unsubstituted benzoic acid **152** and aniline derivatives ***151j-o***

General procedure

Benzoic acid **152** (1.00 g, 8.20 mmol) was placed in a round-bottomed flask, followed by addition of excess thionyl chloride (2 ml). The mixture was stirred and refluxed at 80 °C in an oil bath for 24 h. After cooling the mixture to room-temperature, excess thionyl chloride was evaporated leaving a pale-yellow benzoyl chloride residue which was dissolved in distilled acetonitrile (4 ml), followed by slow addition of an ice-cold mixture of the appropriate aminopyridine (**151j-o**) and pyridine or triethylamine (3 ml) in dry acetonitrile (10 ml). The mixture was stirred at 0 °C for 30 min, warmed to room temperature and stirred for 8-24 h. Excess solvent was removed *in vacuo* and the residue dissolved in ethyl acetate (50 ml). The organic mixture was washed with aqueous saturated $NaHCO_3$ or aqueous K_2CO_3 (2× 50 ml), saturated brine solution (50 ml) and the organic layer was separated and dried over anhydrous Na_2SO_4. The solvent was removed under reduced pressure and the crude product purified by normal silica gel chromatography eluting with 20-30% EtOAc/hexane. Recrystallization was performed using hot ethyl acetate and cold hexane where necessary to afford compounds **157j**-**o**. All compounds are not novel.

3.2.1 N-(5-bromopyridin-2-yl)benzamide ***157j***

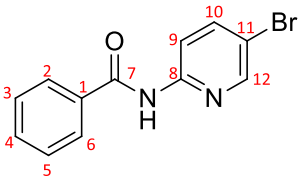

2-amino-5-bromopyridine **151j** (1.38 g, 8.20 mmol g) was reacted with benzoyl chloride **156** (8.20 mmol) for 22 h. Compound **157j** was obtained as a white solid (1.28 g, 56% yield). Rf= 0.3 (7:3 EtOAc/hexane); M.p= 123-128 °C; ; IR (ν/cm^{-1}) 3230 (NH, br), 1676 (C=O, str); ^{1}H NMR (400 MHz, DMSO-d_6) δ_H 11.00 (s, 1H, NH), 8.52 (d, J = 2.0 Hz, 1H, H12), 8.20 (d, J = 8.9 Hz, 1H, H9), 8.07 (dd, J = 8.9, 2.5 Hz, 1H, H10), 8.05 – 8.00 (m, 2H, H2 and H6), 7.63 – 7.57 (m, 1H, H4), 7.52 (t, J = 7.5 Hz, 2H, H3 and H5); ^{13}C NMR (101 MHz, DMSO-d_6) δ_C 166.6 (C7), 151.7 (C8), 148.9 (C12), 141.0 (C10), 134.3 (C1), 132.5 (C4), 128.8 (C3 and C5), 128.5 (C2 and C6), 116.8 (C9), 114.4 (C11).

3.2.2 N-(6-methylpyridin-2-yl)benzamide ***157k***

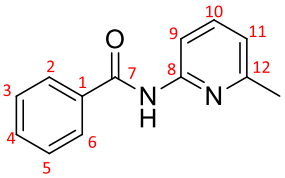

2-amono-6-methylpyridine **151k** (0.890 g, 8.20 mmol) was reacted with benzoyl chloride **156** for 9 h. Compound **157k** was obtained as a white solid (1.27 g, 73% yield). Rf= 0.3 (7:3 EtOAc/hexane); M.p= 97-99 °C; IR (ν/cm^{-1}) 3321 (NH, br), 1670 (C=O, str); ^{1}H NMR (400 MHz, $CDCl_3$) δ_H 9.13 (s, 1H, NH), 8.22 (d, J = 8.3 Hz, 1H, H9), 7.91 (d, J = 7.5 Hz, 2H, H2 and H6), 7.62 (t, J = 7.9 Hz, 1H, H10), 7.51 (t, J = 7.3 Hz, 1H, H4), 7.43 (t, J = 7.4 Hz, 2H, H3 and H5), 2.35 (s, 3H, H-CH_3); ^{13}C NMR (101 MHz, $CDCl_3$) δ_C 165.9 (C7), 156.8 (C8), 151.0 (C12), 138.8 (C10), 134.4 (C1), 132.1 (C4), 128.7 (C3 and C5), 127.3 (C2 and C6), 119.4 (C11), 111.1 (C9), 23.8 (C-CH_3); HRMS (ES$^+$) calculated for $C_{13}H_{12}N_2O$ $[M+H]^+$: 213.1023, found: 213.1036.

3.2.3 N-(6-bromopyridin-2-yl)benzamide ***157l***

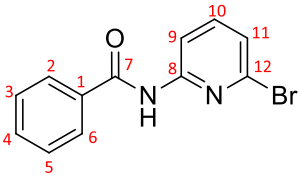

2-amino-6-bromopyridine **151l** (1.42 g, 8.20 mmol) was reacted with benzoyl chloride **156** (8.20 mmol) for 8 h and recrystallized with hot ethyl acetate and cold hexane after column chromatography purification. Compound **157l** was obtained as a white solid (0.79 g, 35% yield when triethylamine was used and 1.73 g, 76% yield, when pyridine was used). Rf= 0.3 (7:3 EtOAc/hexane); M.p= 98-100°C; IR (ν/cm^{-1}) 3416 (NH, br), 1673 (C=O, str); ^{1}H NMR (400 MHz, $CDCl_3$) δ_H 8.60 (s, 1H, NH), 8.38 (d, J = 8.2 Hz, 1H, H9), 7.92 (d, J = 7.4 Hz, 2H, H2 and H6), 7.66 – 7.57 (m, 2H, H4 and H10), 7.52 (t, J = 7.5 Hz, 2H, H3 and H5), 7.27 (d, J = 7.7 Hz, 1H, H11); ^{13}C NMR (101 MHz, $CDCl_3$)

δ_C 165.5 (C7), 151.6 (C8), 140.7 (C10), 139.2 (C12), 133.7 (C1), 132.6 (C4), 128.9 (C3 and C5), 127.2 (C2 and C6), 123.7 (C11), 112.5 (C9).

*3.2.4 N-(6-chloropyridin-2-yl)benzamide **157m***

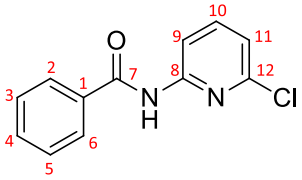

2-amino-6-chloropyridine **151m** (1.05 g, 8.20 mmol) was reacted with benzoyl chloride **156** (8.20 mmol) for 16 h. Compound **157m** was obtained as a white solid product (0.960 g, 50%). Rf= 0.3 (7:3 EtOAc/hexane); M.p= 99-101 °C; IR (ν/cm^{-1}) 3408 (NH, br) 1674 (C=O, str); ^{1}H NMR (400 MHz, $CDCl_3$) δ_H 8.73 (s, 1H NH), 8.31 (d, *J* = 8.2 Hz, 1H, H9), 7.92 – 7.87 (m, 2H, H2 and H6), 7.68 (t, *J* = 8.0 Hz, 1H, H10), 7.54 (t, *J* = 7.4 Hz, 1H, H4), 7.46 (t, *J* = 7.5 Hz, 2H, H3 and H5), 7.06 (d, *J* = 7.7 Hz, 1H, H11); ^{13}C NMR (101 MHz, $CDCl_3$) δ_C 165.7 (C7), 151.4 (C8), 148.9 (C12), 141.0 (C10), 133.7 (C1), 132.5 (C4), 128.9 (C3 and C5), 127.3 (C2 and C6), 119.8 (C11), 112.2 (C3).

*3.2.5 N-(3-bromopyridin-2-yl)benzamide **157n***

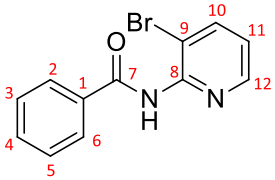

2-amino-3-bromopyridine **151n** (1.40 g, 8.20 mmol) was reacted with benzoyl chloride **156** (8.20 mmol) for 24 h. Compound **157n** was obtained as a dark brown solid product (0.0400 g, 3% yield). Rf= 0.3 (7:3 EtOAc/hexane); M.p= 117-119 °C; IR (ν/cm^{-1}) 3284 (NH, str), 1641 (C=O, str); ^{1}H NMR (400 MHz, $CDCl_3$) δ_H 9.03 (s, 1H, NH), 8.18 (d, *J* = 3.9 Hz, 1H, H12), 7.76 (dd, *J* = 7.7, 36.8 Hz, 3H, H2, H6, and H10), 7.38 (dt, *J* = 7.4, 36.7 Hz, 3H, H3, H4, and H5), 6.83 (dd, *J* = 4.7, 7.9 Hz, 1H, H9); ^{13}C NMR (101 MHz, $CDCl_3$) δ_C 165.4 (C7), 148.9 (C8), 147.3 (C12), 141.6 (C10), 133.9 (C1), 132.2 (C4), 128.7 (C3 and C5), 127.6 (C2 and C6), 122.0 (C11), 114.2 (C9).

*3.2.6 N-(5-chloropyridin-2-yl)benzamide **157h***

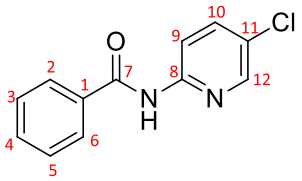

2-amino-5-chloropyridine **151h** (1.01 g, 8.2 mmol) was reacted with benzoyl chloride **156** (8.20 ooml) for 22 h. Compound **157h** was obtained as a white solid product (1.25 g, 65% yield). Rf= 0.3 (7:3 EtOAc/hexane); M.p= 128-130 °C; IR (ν/cm^{-1}) 3231 (NH, br), 1675 (C=O, str); ^{1}H NMR (400 MHz, DMSO-d_6) δ_H 11.01 (s, 1H, NH), 8.46 – 8.44 (m, 1H, H12), 8.27 – 8.23 (m, 1H, H9), 8.05 – 8.01 (m, 2H, H2 and H6), 7.97 (dd, *J* = 8.9, 2.7 Hz, 1H, H10), 7.63 – 7.58 (m, 1H, H4), 7.52 (t, *J* = 7.5 Hz,

2H, H3 and H5); ^{13}C NMR (101 MHz, DMSO-d_6) δ_C 166.6 (C7), 151.3 (C8), 146.7 (C12), 138.3 (C10), 134.3 (C1), 132.5 (C4), 128.8 (C3 and C5), 128.5 (C2 and C6), 126.0 (C11), 116.3 (C9).

*3.2.7 N-benzoyl-N-(5-methylpyridin-2-yl)benzamide **160i***

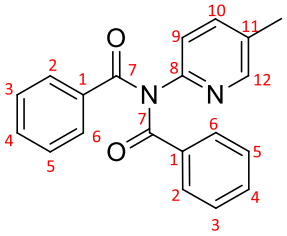

2-amno-5-methylpyridine **151i** (0.890 g, 8.20 mmol) was reacted with benzoyl chloride **156** (8.20 mmol) in the presence of triethylamine for 10 h. Compound **160i** was obtained as a white solid (1.27 g, 49% yield). Rf= 0.3 (7:3 EtOAc/hexane); M.p= 167-172 °C; IR (ν/cm^{-1}) 1689 (C=O, str); ^{1}H NMR (400 MHz, $CDCl_3$) δ_H 8.22 (d, J = 2.1 Hz, 1H, H12), 7.80 – 7.75 (m, 4H, H2 and H6), 7.51 (dd, J = 8.1, 2.0 Hz, 1H, H10), 7.45 (t, J = 7.4 Hz, 2H, H4), 7.34 (t, J = 7.7 Hz, 4H, H3 and H5), 7.15 (d, J = 8.1 Hz, 1H, H9), 2.29 (s, 3H, H-CH_3); ^{13}C NMR (101 MHz, $CDCl_3$) δ_C 173.1 (C7), 151.3 (C8), 149.6 (C12), 138.9 (C10), 134.7 (C1), 132.4 (C4), 132.2 (C11), 129.3 (C3 and C5), 128.5 (C2 and C6), 121.6 (C9), 18.0 (C-CH_3); HRMS (ES$^+$) calculated for $C_{20}H_{17}N_2O_2$ $[M+H]^+$: 317.1285, found: 317.1275.

*3.2.8 N-benzoyl-N-(3-bromopyridin-2-yl)benzamide **160n***

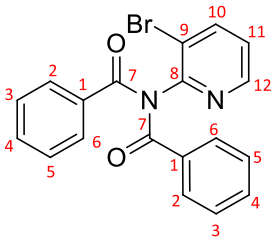

2-amino-3-bromopyridine **151n** (1.40 g, 8.20 mmol) was reacted with benzoyl chloride **156** (8.20 mmol) in the presence of triethylamine for 24 h. Compound **160n** was obtained as a dark brown solid (0.0344 g, 11% yield). Rf= 0.3 (7:3 EtOAc/hexane); M.p= 197-199 °C; IR (ν/cm^{-1}) 1680 (C=O, str); ^{1}H NMR (300 MHz, $CDCl_3$) δ_H 8.31 (dd, J = 4.7, 1.5 Hz, 1H, H12), 7.98 (dd, J = 8.0, 1.5 Hz, 1H, H10), 7.85 – 7.79 (m, 4H, H2 and H6), 7.50 – 7.43 (m, 2H, H4), 7.40 – 7.32 (m, 4H, H3 and H5), 7.13 – 7.08 (m, 1H, H11); ^{13}C NMR (75 MHz, $CDCl_3$) δ_C 172.5 (C7), 152.3 (C8), 148.1 (C12), 142.4 (C10), 134.5 (C1), 132.6 (C4), 129.1 (C3 and C5), 128.6 (C2 and C6), 124.2 (C11), 119.0 (C9); HRMS (ES$^+$) calculated for $C_{19}H_{14}BrN_2O_2$ $[M+H]^+$: 381.0233, found: 381.0233.

3.3 Synthesis of benzamides from 3-methoxybenzoic acid **153** and aniline derivatives **151a-h**

General procedure

3-methoxybenzoic acid **153** (1.00 g, 6.60 mmol) was placed in a round-bottomed flask, followed by addition of excess thionyl chloride (2 ml). The mixture was stirred and refluxed at 80 °C in an oil bath

for 24 h. After cooling the mixture to room-temperature, excess thionyl chloride was evaporated leaving a pale-yellow benzoyl chloride residue which was dissolved in distilled acetonitrile (4 ml), followed by slow addition of an ice-cold mixture of the appropriate aniline (**151a-h**) and pyridine or triethylamine (3 ml) in dry acetonitrile (10 ml). The mixture was stirred at 0 °C for 30 min, warmed to room temperature and stirred for 15-24 h. Excess solvent was removed *in vacuo* and the residue dissolved in ethyl acetate (50 ml). The organic mixture was washed with aqueous saturated $NaHCO_3$ or aqueous K_2CO_3 (2× 50 ml), saturated brine solution (50 ml) and the organic layer was separated and dried over anhydrous Na_2SO_4. The solvent was removed under reduced pressure and the crude product purified by normal silica gel chromatography eluting with 20-30% EtOAc/hexane. Recrystallization was performed using hot ethyl acetate and cold hexane where necessary to afford compounds **158a**-**h**. Only compound **158c** is novel.

*3.3.1 N-(4-bromophenyl)-3-methoxybenzamide **158a***

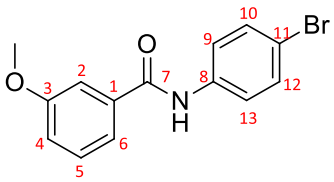

4-bromoaniline **151a** (1.34 g, 6.60 mmol) was reacted with 3-methoxybenzoyl chloride **159** (6.60 mmol) for 24 h and recrystallized with hot ethyl acetate and cold hexane after column chromatography purification. Compound **158a** was obtained a white solid (1.05 g, 52% yield). Rf= 0.3 (7:3 EtOAc/hexane); M.p= 136-138 °C; IR (ν/cm^{-1}) 3293 (NH), 1585 (C=O); ^{1}H NMR (300 MHz, $CDCl_3$) δ_H 7.98 (s, 1H, NH), 7.56 – 7.50 (m, 2H, H9 and H13), 7.48 – 7.41 (m, 2H, H10 and H6), 7.41 – 7.33 (m, 3H, H2, H5, and H6), 7.10 – 7.03 (m, 1H, H4), 3.84 (s, 3H, H-OCH3); ^{13}C NMR (75 MHz, $CDCl_3$) δ_C 165.7 (C7), 160.0 (C3), 137.0 (C8), 136.0 (C1), 132.0 (C10 and C12), 129.8 (C5), 121.8 (C9 and C13), 118.7 (C6), 118.2 (C4), 117.2 (C11), 112.5 (C2), 55.5 (C-OCH_3).

*3.3.2 N-(3-bromophenyl)-3-methoxybenzamide **158b***

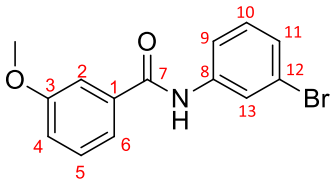

3-bromoaniline **151b** (3.00 ml, 6.60 mmol) was reacted with 3-methoxybenzoyl chloride **159** (6.60 mmol) for 24 h. Compound **158b** was obtained as a white solid (1.19, 59% yield). Rf= 0.3 (7:3 EtOAc/hexane); M.p= 110-112 °C; IR (ν/cm^{-1}) 3074 (NH, br), 1647 (C=O, str); ^{1}H NMR (300 MHz, $CDCl_3$) δ_H 7.96 (s, 1H NH), 7.90 (t, J = 1.8 Hz, 1H, H13), 7.57 – 7.52 (m, 1H, H9), 7.42 – 7.39 (m, 1H, H11), 7.36 (d, J = 5.1 Hz, 1H, H6), 7.27 (d, J = 7.4 Hz, 1H, H10), 7.20 (t, J = 7.9 Hz, 1H, H5), 7.07 (td, J = 4.6, 2.7 Hz, 1H, H4), 3.84 (s, 3H, H-OCH_3); ^{13}C NMR (75 MHz, $CDCl_3$) δ_C 165.2 (C7),

159.5 (C3), 138.7 (C8), 135.5 (C1), 129.9 (C5), 129.4 (C10), 127.1 (C11), 122.7 (C13), 122.2 (C12), 118.2 (C4 and C6), 117.8 (C9), 112.0 (C6), 55.0 (C-OCH_3).

*3.3.3 N-(4-bromo-2-methylphenyl)-3-methoxybenzamide **158c***

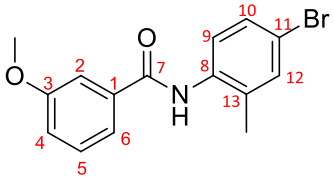

4-bromo-2-methylaniline **151c** (1.14 g, 6.60 mmol) was reacted with 3-methoxybenzoyl chloride **159** (6.60 mmol) for 24 h, purified by column chromatography and recrystallized. Compound **158c** was obtained as a white solid (1.58, 75% yield). Rf= 0.3 (7:3 EtOAc/hexane); M.p= 156-158 °C; IR (ν/cm^{-1}) 3217 (NH, br), 1644 (C=O, str); ^{1}H NMR (300 MHz, DMSO-d_6) δ_H 9.90 (s, 1H, NH), 7.56 (dt, *J* = 7.7, 1.3 Hz, 1H, H2), 7.53 – 7.49 (m, 2H, H4 and H12), 7.48 – 7.39 (m, 2H, H5 and H9), 7.31 (d, *J* = 8.5 Hz, 1H, H10), 7.17 (ddd, *J* = 8.2, 2.6, 1.0 Hz, 1H, H6), 3.84 (s, 3H, H-OCH_3), 2.23 (s, 3H, H-CH_3); ^{13}C NMR (75 MHz, DMSO-d_6) δ_C 165.0 (C7), 159.2 (C3), 136.5 (C8), 135.8 (C1), 135.6 (C13), 132.7 (C12), 129.6 (C10), 128.8 (C5), 128.5 (C9), 119.8 (C6), 118.3 (11), 117.5 (C4), 112.8 (C2), 55.3 (C-OCH_3), 17.6 (C-CH_3); HRMS (ES^+) calculated for $C_{15}H_{15}BrNO_2$ $[M+H]^+$: 320.0281, found: 320.0283.

*3.3.4 3-methoxy-N-(p-tolyl)benzamide **158d***

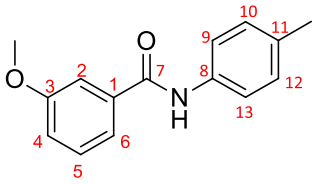

4-methylaniline **151d** (0.730 g, 6.60 mmol) was reacted with 3-methoxybenzoyl chloride **159** (6.60 mmol) for 18 h. Compound **158d** was obtained as a white solid (1.12, 71% yield). Rf= 0.3 (7:3 EtOAc/hexane); M.p= 136-138°C, IR (ν/cm^{-1}) 3312 (NH, br), 1645 (C=O, str), 1225 (C-O, str); ^{1}H NMR (400 MHz, DMSO-d_6) δ_H 10.16 (s, 1H, NH), 7.66 (d, *J* = 8.4 Hz, 2H, H9 and H13), 7.54 (d, *J* = 7.7 Hz, 1H, H6), 7.50 – 7.42 (m, 2H, H2 and H5), 7.15 (dd, *J* = 7.7, 4.7 Hz, 3H, H4, H10, and H12), 3.84 (s, 3H, H-OCH_3), 2.28 (s, 3H, H-CH_3); ^{13}C NMR (101 MHz, DMSO-d_6) δ_C 165.5 (C7), 159.6 (C3), 137.0 (C8), 136.9 (C1), 133.1 (C11), 130.0 (C5), 129.4 (C10 and C12), 120.9 (C9 and C13), 120.3 (C6), 117.7 (C4), 113,3 (C2), 55,8 (C-OCH_3), 21.0 (C-CH_3).

*3.3.5 3-methoxy-N-(4-methoxyphenyl)benzamide **158e***

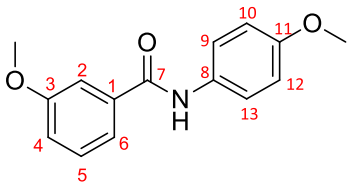

4-methoxyaniline **151e** (0.800 g, 6.60 mmol) was reacted with 3-mthoxybenzoyl chloride **159** (6.60 mmol) for 18 h. Compound **158e** was obtained as a light-yellow

solid (1.38, 83% yield). Rf= 0.3 (7:3 EtOAc/hexane); M.p= 117-119 °C; IR (ν/cm^{-1}) 3302 (NH, br), 1643 (C=O, str), (1243 (C-O, str); ^{1}H NMR (400 MHz, $CDCl_3$) δ_H 8.01 (s, 1H, NH), 7.53 (d, J = 8.9 Hz, 2H, H9 and H13), 7.42 – 7.29 (m, 3H, H2, H5, and H6), 7.04 (ddd, J = 7.9, 2.5, 1.1 Hz, 1H, H4), 6.89 – 6.84 (m, 2H, H10 and H12), 3.80 (2s 6H, H-OCH_3); ^{13}C NMR (101 MHz, $CDCl_3$) δ_C 165.6 (C7), 159.9 (C3), 156.6 (C11), 136.5 (C1), 131.0 (C8), 129.7 (C5), 122.2 (C9 and C13), 118.8 (C6), 117.9 (C4), 114.2 (C10 and C12), 112.4 (C2), 55.5 (C-OCH_3).

*3.3.6 N-(4-chloro-2-methylphenyl)-3-methoxybenzamide **158h***

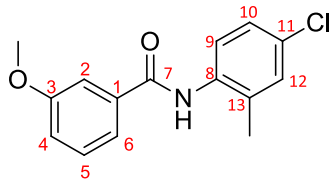

2-chloro-2-methylaniline **151h** (0.920 g, 6.60 mmol) was reacted with 3-methoxybenzoyl chloride **159** (6.60 mmol) for 15 h. Compound **158h** was obtained as a white solid (1.09 g, 61% yield). M.p= 172-174 °C; IR (ν/cm^{-1}) 3211 (NH, br), 1644 (C=O, str), 1251 (C-O, str); ^{1}H NMR (400 MHz, DMSO-d_6) δ_H 9.93 (s, 1H, NH), 7.57 (d, J = 7.7 Hz, 1H, H6), 7.52 (s, 1H, H2), 7.45 (t, J = 7.9 Hz, 1H, H5), 7.40 – 7.35 (m, 2H, H9 and H12), 7.28 (dd, J = 8.5, 2.3 Hz, 1H, H10), 7.17 (dd, J = 8.1, 2.4 Hz, 1H, H4), 3.84 (s, 3H, H-OCH_3), 2.24 (s, 3H, H-CH_3); ^{13}C NMR (101 MHz, DMSO-d_6) δ_C 165.6 9 (C8), 159.7 (C3), 136.6 (C13)), 136.1 (C1), 135.9 (C8), 130.4 (C11), 130.3 (C12), 130.1 (C5), 128.7 (C9), 126.3 (C10), 120.3 (C6), 118.0 (C4), 113.3 (C2), 55.8 (C-OCH_3), 18.2 (C-CH_3).

3.4 Synthesis of benzamides from 3-methoxybenzoic acid **153** and aniline derivatives **151j-o**

General procedure

3-methoxybenzoic acid **153** (1.00 g, 6.60 mmol) was placed in a round-bottomed flask, followed by addition of excess thionyl chloride (2 ml). The mixture was stirred and refluxed at 80 °C in an oil bath for 24 h. After cooling the mixture to room-temperature, excess thionyl chloride was evaporated leaving a pale-yellow benzoyl chloride residue which was dissolved in distilled acetonitrile (4 ml), followed by slow addition of an ice-cold mixture of the appropriate aminopyridine (**151j-o**) and pyridine or triethylamine (3 ml) in dry acetonitrile (10 ml). The mixture was stirred at 0 °C for 30 min, warmed to room temperature and stirred for 11-18 h. Excess solvent was removed *in vacuo* and the residue dissolved in ethyl acetate (50 ml). The organic mixture was washed with aqueous saturated $NaHCO_3$ or aqueous K_2CO_3 (2× 50 ml), saturated brine solution (50 ml) and the organic layer was separated and dried over anhydrous Na_2SO_4. The solvent was removed under reduced pressure and the crude product purified by normal silica gel chromatography eluting with 20-30% EtOAc/hexane. Recrystallization was performed using hot ethyl acetate and cold hexane where necessary to afford compounds **158i**-**o**. Compounds **158j**, **158l**, and **158n** are novel.

*3.4.1 3-Methoxy-N-(5-methylpyridin-2-yl)benzamide **158i***

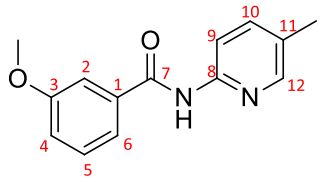

2-amono-5-methylpyridine **158i** (0.710 g, 6.60 mmol) was reacted with 3-methoxybenzoyl chloride **159** (6.60 mmol) for 13 h. Compound **158i** was obtained as a white solid (1.30 g, 81% yield). Rf= 0.2 (7:3 EtOAc/hexane); M.p= 100-102°C; IR (ν/cm^{-1}) 3225 (NH, br), 1670 (C=O, str), 1213 (C-O, str); ^{1}H NMR (400 MHz, $CDCl_3$) δ_H 8.98 (s, 1H, NH), 8.29 (d, J = 8.5 Hz, 1H, H9), 8.00 (d, J = 2.4 Hz, 1H, H12), 7.57 (dd, J = 2.4, 8.6 Hz, 1H, H10), 7.49 – 7.42 (m, 2H, H2 and H6), 7.37 (t, J = 7.9 Hz, 1H, H5), 7.09 (ddd, J = 1.1, 2.6, 8.2 Hz, 1H, H4), 3.85 (s, 3H, H-OCH_3), 2.28 (s, 3H, H-CH_3); ^{13}C NMR (101 MHz, $CDCl_3$) δ_C 165.6 (C7), 159.9 (C3), 149.4 (C8), 147.8 (C12), 139.0 (C10), 135.9 (C1), 129.7 (C5), 129.3 (C11), 119.1 (C6), 118.5 (C4), 113.8 (C9), 112.3 (C2), 55.5 (C-OCH_3), 17.8 (C-CH_3); HRMS (ES^+) calculated for $C_{14}H_{15}N_2O_2$ $[M+H]^+$: 243.1128, found: 243.1141.

*3.4.2 N-(5-bromopyridin-2-yl)-3-methoxybenzamide **158j***

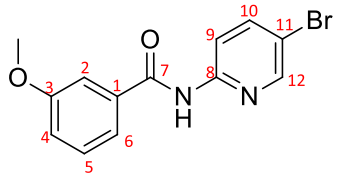

2-amino-5-bromopyridine **151j** (1.12 g, 6.60 mmol) was reacted with 3-methoxybenzoyl chloride **159** (6.60 mmol) for 18 h. Compound **158j** was obtained as a white solid (1.66 g, 99% yield). Rf= 0.2 (7:3 EtOAc/hexane); M.p= 61-63°C; IR (ν/cm^{-1}) 3232 (NH, br), 1671 (C=O, str), 1213 (C-O, str); ^{1}H NMR (500 MHz, $CDCl_3$) δ_H 8.75 (s, 1H, NH), 8.35 – 8.33 (m, 1H, H9), 8.29 – 8.26 (m, 1H, H12), 7.84 (dd, J = 2.4, 8.9 Hz, 1H, H10), 7.47 – 7.36 (m, 3H, H2, H5, and H6), 7.11 (ddd, J = 1.2, 2.6, 8.1 Hz, 1H, H4), 3.87 (s, 3H, H-OCH_3); ^{13}C NMR (125 MHz, $CDCl_3$) δ_C 165.6 (C7), 160.1 (C3), 150.3 (C8), 148.8 (C12), 140.9 (C10), 135.4 (C1), 129.9 (C5), 119.0 (C6), 118.7 (C4), 115.4 (C9), 114.8 (C11), 112.5 (C2), 55.5 (C-OCH_3); HRMS (ES^+) calculated for $C_{13}H_{12}BrN_2O_2$ $[M+H]^+$: 307.0077, found: 307.0088.

*3.4.3 3-methoxy-N-(6-methylpyridin-2-yl)benzamide **158k***

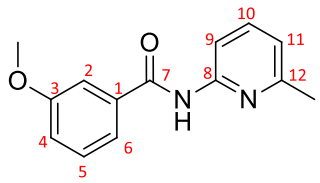

2-amono-6-methylpyridine **151k** (0.710 g, 6.60 mmol) was reacted with 3-methxybenzoyl chloride **159** (6.60 mmol) for 13 h. Compound **158k** was obtained as a white solid (1.38 g, 88% yield). Rf= 0.2 (70:30 EtOAc/hexane); M.p= 57-59 °C; IR (ν/cm^{-1}) 3182 (NH, br), 1666 (C=O, str), 1227 (C-O); ^{1}H NMR (400 MHz, $CDCl_3$) δ_H 8.76 (s, 1H, NH), 8.12 (d, J = 8.2 Hz, 1H, H9), 7.56 (t, J = 7.9 Hz, 1H, H10), 7.41 – 7.36 (m, 2H, H2 and H6), 7.28 (t, J = 7.9 Hz, 1H, H5), 7.00 (dd, J = 8.1, 2.4 Hz, 1H,

H4), 6.84 (d, *J* = 7.5 Hz, 1H, H11), 3.76 (s, 3H, H-OCH_3), 2.34 (s, 3H, H-CH_3); ^{13}C NMR (101 MHz, $CDCl_3$) δ_C 165.6 (C7), 159.9 (C3), 156.8 (C8), 150.8 (12), 138.8 (C10), 135.8 (C1), 129.7 (C5), 119.5 (C6), 119.0 (C11), 118.6 (C4), 112.3 (C2), 111.1 (C9), 55.5 (C-OCH_3), 23.9 (C-CH_3).

*3.4.4 N-(6-bromopyridin-2-yl)-3-methoxybenzamide **158l***

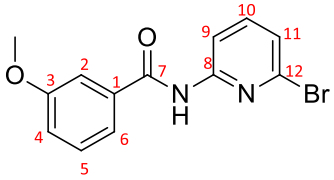

2-amono-6-bromopyridine **151l** (1.10 g, 6.60 mmol) was reacted with 3-methoxybenzoyl chloride **159** (6.60 mmol) for 12 h and recrystallized with hot toluene and cold hexane after column chromatography purification. Compound **158l** was obtained as a white solid (pyridine, 1.13 g, 65% yield and triethylamine, 0.19, 10% yield). Rf= 0.2 (7:3 EtOAc/hexane); M.p= 95-97 °C, IR (ν/cm^{-1}) 3394 (NH, br), 1644 (C=O,str), 1166 (C-O, str); ^1H NMR (300 MHz, $CDCl_3$) δ_H 8.74 (s, 1H, NH), 8.34 (d, *J* = 8.2 Hz, 1H, H11), 7.58 (t, *J* = 8.0 Hz, 1H, H10), 7.46 – 7.40 (m, 2H, H2 and H6), 7.39 – 7.32 (m, 1H, H5), 7.25 – 7.19 (m, 1H, H9), 7.11 – 7.05 (m, 1H, H4), 3.84 (s, 3H, H-OCH_3); ^{13}C NMR (75 MHz, $CDCl_3$) δ_C 165.5 (C7), 160.0 (C3), 151.6 (C8), 140.7 (C10), 139.3 (C12), 135.0 (C1), 129.8 (C5), 123.7 (C9), 119.1 (C6), 118.9 (C4), 112.5 (C2), 112.4 (C11) , 55.5 (C-OCH_3); HRMS (ES^+) calculated for $C_{13}H_{12}BrN_2O_2$ $[M+H]^+$: 307.0077, found: 307.0070.

*3.4.5 N-(6-chloropyridin-2-yl)-3-methoxybenzamide **158m***

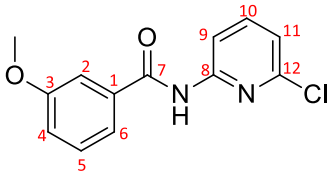

2-amono-6-chloropyridine **151m** (0.86 g, 6.60 mmol) was reacted with 3-methoxybenzoyl chloride **159** (6.60 mmol) for 11 h, purified by column chromatography and recrystallized with hot toluene and cold hexane. Compound **158m** was obtained as a white solid (pyridine, 1.13 g, 65% yield and triethylamine, 0.40 g, 23% yield). Rf= 0.2 (7:3 EtOAc/hexane); M.p= 100-102 °C, IR (ν/cm^{-1}) 3390 (NH, br), 1640 (C=O, str), 1188 (C-O, str); ^1H NMR (400 MHz, $CDCl_3$) δ_H 8.73 (s, 1H, NH), 8.28 (d, *J* = 8.2 Hz, 1H, H9), 7.65 (t, *J* = 8.0 Hz, 1H, H10), 7.43 – 7.38 (m, 2H, H2 and H6), 7.32 (t, *J* = 7.9 Hz, 1H, H5), 7.07 – 7.01 (m, 2H, H4 and H11), 3.80 (s, 3H, H-OCH_3); ^{13}C NMR (101 MHz, $CDCl_3$) δ_C 165.5 (C7), 159.9 (C3), 151.4 (C8), 148.9 (C12), 141.0 (C10), 135.1 (C1), 129.8 (C5), 119.8 (C11), 119.1 (C6), 118.8 (C4), 112.4 (C2), 112.2 (C9), 55.4 (C-OCH_3); HRMS (ER^+) Calculated for $C_{13}H_{11}ClN_2O_2$ $[M+H]^+$: 263.0582, found: 263.0580.

*3.4.6 N-(3-bromopyridin-2-yl)-3-methoxybenzamide **158n***

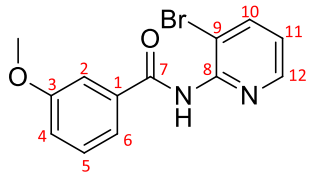

2-amono-3-bromopyridine **151n** (1.12 g, 6.60 mmol) was reacted with 3-methoxybenzoyl chloride **159** (6.60 mmol) for 14 h. Compound **158n** was obtained as a cream white solid (0.44 g, 22% yield when triethylamine was used, and 0.97 g, 48% when pyridine was used). Rf= 0.2 (7:3 EtOAc/hexane); M.p= 136-138 °C; IR (ν/cm^{-1}) 3183 (NH, br), 1651 (C=O, str); ^{1}H NMR (400 MHz, $CDCl_3$) δ_H 8.66 (s, 1H, NH), 8.46 (s, 1H, H12), 7.93 (d, J = 7.8 Hz, 1H, H10), 7.53 – 7.46 (m, 2H, H2 and H6), 7.40 (t, J = 7.9 Hz, 1H, H5), 7.13 – 7.01 (m, 2H, H4 and H11), 3.87 (s, 3H, H-OCH_3); ^{13}C NMR (101 MHz, $CDCl_3$) δ_C 164.8 (C7), 160.0 (C3), 148.7 (C8), 147.5 (C12), 141.5, 135.6 (C1), 129.9 (C5), 121.6 (C9), 119.2 (C6), 118.6 (C4), 112.9 (C2), 55.5 (C-OCH_3); HRMS (ES^+) calculated for $C_{13}H_{12}BrN_2O_2$ $[M+H]^+$: 307.0077, found: 307.0077.

*3.4.7 N-(5-chloropyridin-2-yl)-3-methoxybenzamide **158o***

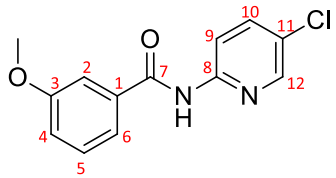

2-amino-5-chloropyridine **151o** (0.840 g, 6.60 mmol) was reacted with 3-methoxybenzoyl chloride **159** (6.60 mmol) for 24 h and recrystallized after column chromatography purification. Compound **158o** was obtained as a white solid (1.07 g, 62% yield). Rf= 0.2 (7:3 EtOAc/hexane); M.p= 84-86 °C; IR (ν/cm^{-1}) 3218 (NH, br), 1674 (C=O str), 1218 (C-O); ^{1}H NMR (400 MHz, $CDCl_3$) δ_H 8.76 (s, 1H, NH), 8.38 (d, J = 8.9 Hz, 1H, H9), 8.18 (d, J = 1.8 Hz, 1H, H12), 7.71 (dd, J = 8.9, 2.0 Hz, 1H, H10), 7.48 – 7.35 (m, 3H, H2, H5, and H6), 7.13 – 7.08 (m, 1H, H4), 3.86 (s, 3H, H-OCH_3). ^{13}C NMR (101 MHz, $CDCl_3$) δ_C 165.5 (C7), 160.0 (C3), 149.8 (C8), 146.5 (C12), 138.1 (C10), 135.3 (C1), 129.9 (C5), 126.9 (C11), 119.0 (C6), 118.7 (C5), 114.8 (C9), 112.5 (C2), 55.5 (C-OCH_3).

*3.4.8 3-methoxy-N-(3-methoxybenzoyl)-N-(5-methylpyridin-2-yl)benzamide **165i***

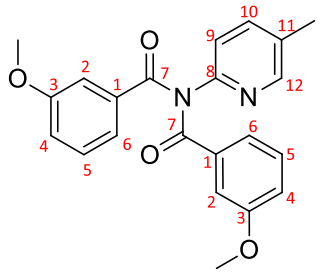

2-amono-5-methylpyridine **151i** (0.71 g, 6.5 mmol) was reacted with 3-methoxybenzoyl chloride **159** (6.60 mmol) for 13 h. Compound **165i** was obtained as a white solid (0.97 g, 39% yield). Rf= 0.2 (7:3 EtOAc/hexane); M.p= 128-130 °C; IR (ν/cm^{-1}) 1681 (C=O, str), 1207 (C-O, str); ^{1}H NMR (400 MHz, $CDCl_3$) δ 8.23 – 8.21 (m, 1H, H12), 7.53 (dd, J = 8.1, 2.1 Hz, 1H, H10), 7.34

(d, *J* = 7.3 Hz, 4H, H2 and H6), 7.23 (t, *J* = 7.9 Hz, 2H, H5), 7.16 (d, *J* = 8.1 Hz, 1H, H9), 6.99 (dd, *J* = 8.0, 2.9 Hz, 2H, H4), 3.76 (s, 6H, H-OCH_3), 2.30 (s, 3H, H-CH_3); ^{13}C NMR (101 MHz, $CDCl_3$) δ 172.9 (C7), 159.6 (C3), 151.3 (C8), 149.6 (C12), 138.9 (C10), 136.0 (C1), 132.1 (C11), 129.5 (C5), 121.6 (C9), 121.4 (C6), 119.0 (C4), 113.9 (C2), 55.4 (C-OCH_3), 18.0 (CCH_3); HRMS (ES^+) calculated for $C_{22}H_{21}N_2O_4$ $[M+H]^+$: 377.1496, found: 377.1505.

*3.4.9 N-(5-bromopyridin-2-yl)-3-methoxy-N-(3-methoxybenzoyl)benzamide **165j***

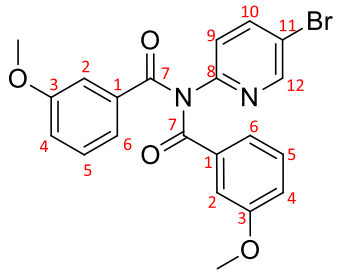

2-amino-5-bromopyridine **151j** (1.12 g, 6.60 mmol) was reacted with 3-methoxybenzoyl chloride **159** (6.60 mmol) for 18 h. Compound **165j** was obtained as a white solid (1.66 g, 99% yield). Rf= 0.2 (7:3 EtOAc/hexane); M.p= 138-140 °C; IR (ν/cm^{-1}) 1678 (C=O, str), 1208 (C-O, str); ^{1}H NMR (400 MHz, DMSO-d_6) δ_H 8.47 (d, *J* = 2.3 Hz, 1H, H12), 8.20 (dd, *J* = 8.6, 2.5 Hz, 1H, H10), 7.68 (d, *J* = 8.6 Hz, 1H, H9), 7.37 (d, *J* = 7.3 Hz, 4H, H5 and H6), 7.28 (d, *J* = 2.6 Hz, 2H, H2), 7.14 (dt, *J* = 7.3, 2.3 Hz, 2H, H4), 3.73 (s, 1H, H-OCH_3); ^{13}C NMR (101 MHz, DMSO-d_6) δ_C 172.6 (C7), 159.6 (C3), 152.6 (C8), 149.9 (C12), 141.9 (C10), 135.8 (C1), 130.5 (C5), 124.4 (C9), 121.8 (C11), 119.0 (C4), 118.9 (C6), 114.6 (C2), 55.8 (C-OCH_3); HRMS (ES^+) calculated for $C_{21}H_{18}BrN_2O_4$ $[M+H]^+$: 441.0444, found: 441.0439.

3.5 Sythesis of benzamides from 3-hydroxybenzoic acid **154** and aminopyridines

General procedure

3-methoxybenzoic acid **154** (1.00 g, 7.20 mmol) was placed in a round-bottomed flask, followed by addition of excess thionyl chloride (2 ml). The mixture was stirred and refluxed at 80 °C in an oil bath for 24 h. After cooling the mixture to room-temperature, excess thionyl chloride was evaporated leaving a pale-yellow benzoyl chloride residue which was dissolved in distilled acetonitrile (4 ml), followed by slow addition of an ice-cold mixture of the appropriate aminopyridine (**151j, 151l, 151m,** and **151o**) and pyridine or triethylamine (3 ml) in dry acetonitrile (10 ml). The mixture was stirred at 0 °C for 30 min, warmed to room temperature and stirred for 21-24 h. Excess solvent was removed *in vacuo* and the residue dissolved in ethyl acetate (50 ml). The organic mixture was washed with aqueous saturated $NaHCO_3$ or aqueous K_2CO_3 (50 × 2 ml), saturated brine solution (50 ml) and the organic layer was separated and dried over anhydrous Na_2SO_4. The solvent was removed under reduced pressure and the crude product purified by normal silica gel chromatography eluting with 30% EtOAc/hexane. The impure product was washed several times (50 ml × 7) to afford compounds **166j**, **166l**, **166m**, and **166o**. All compounds are novel.

3.5.1 N-(5-bromopyridin-2-yl)-3-hydroxybenzamide ***166j***

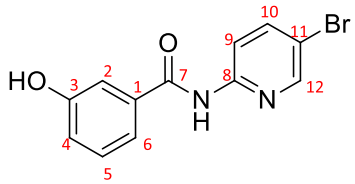

2-amino-5-bromopyridine **151j** (1.25 g, 7.20 mmol) was reacted with 3-hydroxybenzoyl chloride **169** (7.20 mmol) for 21 h. Compound **166j** was isolated as brown solid (1.21 g, 53% yield). Rf= 0.2 (7:3 EtOAc/hexane); M.p= 225-227 ˚C; IR (ν/cm^{-1}) 3397 (NH, br), 3065 (OH, br), 1686 (C=O, str), 1292 (C-O, str); ^{1}H NMR (400 MHz, DMSO-d$_6$) δ_H 10.85 (s, 1H, NH), 9.78 (s, 1H, H-OH), 8.51 (s, 1H, H12), 8.22 – 8.01 (m, 2H, H9 and H10), 7.51 – 7.26 (m, 3H, H2, H5, and H6), 7.02 – 6.95 (m, 1H, H4); ^{13}C NMR (101 MHz, DMSO-d$_6$) δ_C 166.2 (C7), 157.4 (C3), 151.2 (C8), 148.5 (C12), 140.5 (C10), 135.3 (C1), 129.4 (C5), 119.1 (C4), 118.6 (C6), 116.4 (C2), 114.9 (C9), 113.9 (C11); HRMS (ES$^+$) calculated for $C_{12}H_{10}BrN_2O_2$ [M+H]$^+$: 292.9920, found: 292.9923.

3.5.2 N-(6-bromopyridin-2-yl)-3-hydroxybenzamide ***166l***

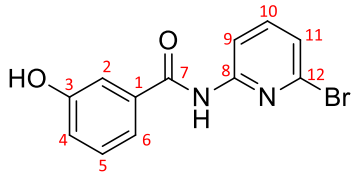

2-amino-6-bromopyridine **151l** (1.25 g, 7.20 mmol) was reacted with 3-hydroxybenzoyl chloride **169** (7.20 mmol) for 23 h. Compound **166l** was isolated as brown solid (0.60g, 28% yield). Rf= 0.2 (7:3 EtOAc/hexane); M.p= 243-245 ˚C; IR (ν/cm^{-1}) 3393 (NH, br), 3115 (OH, br), 1689 (C=O str), 1289 (C-O); ^{1}H NMR (400 MHz, DMSO-d_6) δ_H 10.98 (s, 1H, NH), 9.75 (s, 1H, H-OH), 8.19 (d, J = 8.1 Hz, 1H, H9), 7.78 (t, J = 7.9 Hz, 1H, H10), 7.47 (d, J = 7.7 Hz, 1H, H6), 7.41 – 7.35 (m, 2H, H2 and H11), 7.29 (t, J = 7.9 Hz, 1H, H5), 7.00 – 6.96 (m, 1H, H4); ^{13}C NMR (101 MHz, DMSO-d$_6$) δ_C 166.2 (C7), 157.3 (C3), 152.5 (C8), 141.2 (C10), 138.8 (C12), 135.0 (C1), 129.4 (C5), 123.4 (C11), 119.2 (C6), 118.7 (C4), 115.0 (C2), 113.7 (C9); HRMS (ES$^+$) calculated for $C_{12}H_{10}BrN_2O_2$ [M+H]$^+$: 292.9920, found: 292.9919.

3.5.3 N-(6-chloropyridin-2-yl)-3-hydroxybenzamide ***166m***

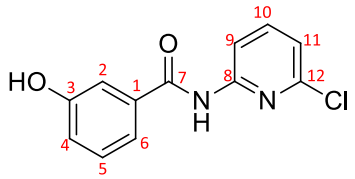

2-amino-6-chloropyridine **151m** (0.930 g, 7.20 mmol) was reacted with 3-hydroxybenzoyl chloride **169** (7.20 mmol) for 24 h. Compound **166m** was isolated as light brown solid (0.92 g, 51% yield). Rf= 0.2 (7:3 EtOAc/hexane); M.p= 232-234 ˚C; IR (ν/cm^{-1}) 3392 (NH, br), 3118 (OH, br), 1690 (C=O, str), 1290 (C-O, str); ^{1}H NMR (400 MHz, DMSO-d$_6$) δ_H 10.98 (s, 1H, NH), 9.76 (s, 1H, H-OH), 8.17 (d, J = 8.2 Hz, 1H, H9), 7.89 (t, J = 8.0 Hz, 1H, H10), 7.47 (d, J = 7.7 Hz, 1H, H6), 7.37 (s,

1H, H2), 7.32 – 7.23 (m, 2H, H5 and H11), 6.98 (dd, *J* = 8.0, 1.9 Hz, 1H, H4); ^{13}C NMR (101 MHz, DMSO-d_6) δ_C 166.2 (C7), 157.3 (C3), 152.3 (C8), 148.0 (C12), 141.6 (C10), 135.1 (C1), 129.4 (C5), 119.5 (C11), 119.2 (C4), 118.7 (C6), 115.0 (C2), 113.4 (C9); HRMS (ES$^+$) calculated for $C_{12}H_{10}ClN_2O_2$ $[M+H]^+$: 249.0425, found: 249.0427.

*3.5.4 N-(5-chloropyridin-2-yl)-3-hydroxybenzamide **166o***

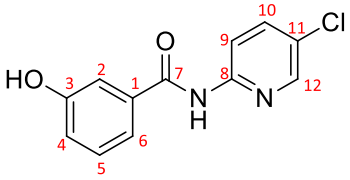

2-amino-5-chloropyridine **151o** (0.930 g, 7.20 mmol) was reacted with 3-hydroxybenzoyl chloride **169** (7,2 mmol) for 21 h. Compound **166o** was isolated as brown solid (0.82 g, 46% yield). Rf= 0.2 (7:3 EtOAc/hexane); M.p= 215-217 ˚C; IR (ν/cm^{-1}) 3396 (NH, br), 1689 (C=O, str), 1293 (C-O, str); ^{1}H NMR (400 MHz, DMSO-d_6) δ_H 10.81 (s, 1H, NH), 9.71 (s, 1H, H-OH), 8.37 (d, *J* = 2.4 Hz, 1H, H12), 8.15 (d, *J* = 8.9 Hz, 1H, H9), 7.89 (dd, *J* = 8.9, 2.6 Hz, 1H, H10), 7.40 (d, *J* = 7.9 Hz, 1H, H6), 7.32 – 7.28 (m, 1H, H2), 7.24 (t, *J* = 7.9 Hz, 1H, H5), 6.92 (dd, *J* = 8.0, 1.8 Hz, 1H, H4); ^{13}C NMR (101 MHz, DMSO-d_6) δ_C 166.6 (C7), 157.8 (C3), 151.3 (C8), 146.7 (C12), 138.2 (C10), 135.7 (C1), 129.9 (C5), 125.9 (C11), 119.5 (C4), 119.0 (C6), 116.3 (C9), 115.3 (C2); HRMS (ES$^+$) calculated for $C_{12}H_{10}ClN_2O_2$ $[M+H]^+$: 249.0425, found: 249.0426.

3.6 Preparation of methyl 3-hydroxybenzoate **141**

In a round-bottomed flask was added 3-hydroxybenzoic acid **154** (1.00 g, 7.20 mmol) which was dissolved in methanol (20.0 ml) and cooled to 0˚C. Thionyl chloride (4.00 ml, 2.80 mol) was added dropwise to the stirring solution for 1 h. The reaction was allowed to proceed for 12 h whilst the temperature gradually increased to room temperature. The solvent and excess thionyl chloride were evaporated under reduced pressure and the residue was dissolved in ethyl acetate (20 ml), washed successively with saturated aqueous $NaHCO_3$ (20 ml × 3). The organic layer was separated and dried over anhydrous Na_2SO_4. Excess solvent was removed *in vacuo* and yielding a cream white solid methyl 3-hydroxybenzoate product **141** (97%).

3.7 Synthesis of methyl 3-((2,6-dichloropyrimidin-4-yl)oxy)benzoate **174**

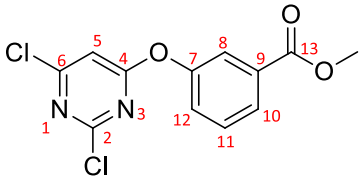

2,4,6-trichloropyrimidine **102** (0.180 g, 1.00 mmol) and potassium carbonate (0.280 g, 2.00 mmol) in acetone (5 ml) were added in a round-bottomed flask and the solution stirred for 5 min. To the stirring mixture was added **141** (0.150 g, 1.00 mmol) and the reaction was allowed to proceed for 1 h. Thereafter, the mixture was gradually to warm to room temperature

while left overnight. After evaporating the solvent, the residue was dissolved in ethyl acetate (20 ml), washed successively with aqueous saturated $NaHCO_3$ (20 ml×3) and water (20 ml). The organic layer was separated and dried over anhydrous Na_2SO_4. The solvent removed under reduced pressure and product was purified by normal silica gel chromatography eluting with 20% EtOAc/hexane. A white solid product **173** (0.240 g, yield= 81%) was obtained. Rf= 0.4; M.p= 127-129 ˚C; (7:3 EtOAc/hexane); IR (ν/cm^{-1}) 1720 (C=O, str), 1261-1262 (C-O, str); ^{1}H NMR (400 MHz, $CDCl_3$) δ_H 8.00 (d, J = 7.8 Hz, 1H, H10), 7.81 (s, 1H, H8), 7.54 (t, J = 8.0 Hz, 1H, H11), 7.35 (d, J = 8.1 Hz, 1H, H12), 6.87 (s, 1H, H5), 3.94 (s, 3H, H-CH_3); ^{13}C NMR (101 MHz, $CDCl_3$) δ_C 170.8 (C4), 166.0 (C13), 163.0 (C6), 160.2 (C2), 151.7 (C7), 132.5 (C9), 130.2 (C11), 127.8 (C10), 126.0 (C12), 122.6 (C8), 106.4 (C5), 52.6 (C-CH_3); HRMS (ES$^+$) calculated for $C_{12}H_9Cl_2N_2O_3$ $[M+H]^+$: 298.9985, found: 298.9981.

3.8 Synthesis of 3-((2,6-dichloropyrimidin-4-yl)oxy)benzoic acid **155**

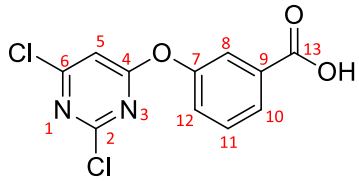

In a round-bottomed flask was added 3-carboxyphenol **154** (5.04 g, 36.0 mmol) and 1 M NaOH (2.73 g, 68.3 mmol) dissolved in 500 ml round-bottomed flask. The mixture was stirred at room temperature for 30 min to give 3-carboxyphenoxide. In a separate flask chilled in ice was placed 2,4,6-trichloropyrimidine **102** (6.62 g, 36.0 mmol) dissolved in acetone (70.0 ml) and a solution of 3-carboxyphenoxide was slowly added. The mixture was stirred under similar conditions for 1h. Thereafter, the mixture was allowed to proceed for 24 h whilst the temperature gradually increased to room temperature. The solvent was evaporated under reduced pressure and the residue adjusted to pH 3 with aqueous 1 M HCl. This aqueous mixture was extracted several times with ethyl acetate (7 × 100 ml) and the organic layer dried over anhydrous Na_2SO_4. The solvent was evaporated and product **155** (8.31 g, 81% yield) was obtained. Rf= 0.2 (7:3 EtOAc/hexane); M.p= 187-189 °C; IR (ν/cm^{-1}) 2800-3200 (OH, br), 1682 (C=O, str), 1262 (C-O, str) ^{1}H NMR (500 MHz, DMSO-d_6) δ_H 13.34 (s, 1H, H-OH), 7.91 (d, J = 7.7 Hz, 1H, H10), 7.79 (s, 1H, H8), 7.63 (t, J = 7.9 Hz, 1H, H11), 7.55 (dd, J = 7.6, 2.2 Hz, 1H, H12), 7.50 (s, 1H, H5); ^{13}C NMR (126 MHz, DMSO-d_6) δ_C 170.7(C4), 166.4 (C13), 161.7 (C6), 158.2 (C2), 151.5 (C7), 132.9 (C9), 130.4 (C11), 127.3 (C10), 126.1 (C12), 122.2 (C8), 107.6 (C5); HRMS (ES$^+$) calculated for $C_{11}H_7Cl_2N_2O_3$ $[M+H]^+$: 284.9828, found: 284.9821.

3.9 Synthesis of complex benzamides from anilines **151a-h**

General procedure

3-((2,4-dichloropyrimidin-4-yl)oxo)benzoic acid **155** (1.00 g, 3.50 mmol) was placed in a round-bottomed flask, and thionyl chloride (2 ml) was added. The mixture was stirred and heated at 70 °C in an oil bath for overnight. After cooling the mixture to room-temperature, excess thionyl chloride was

removed *in vacuo* leaving a pale yellow 3-(2,4-dichloropyrimidin-4-yl)oxo)benzoyl chloride residue **179** which was dissolved in distilled acetonitrile (4 ml) and cautiously added to an ice-cold mixture of amine (**151a**-**h**) and pyridine or triethylamine (2 ml) in distilled acetonitrile or THF (15 ml). The mixture was stirred at 0 °C for 30 min, warmed to room temperature and stirred for 3-22 h. Excess solvent was removed under reduced pressure and the residue dissolved in ethyl acetate (50 ml). The organic mixture was washed with aqueous saturated K_2CO_3 (50 ml × 2), saturated brine solution (50 ml), and followed by separation of organic layer which was dried over anhydrous Na_2SO_4. The solvent was removed under reduced pressure and the crude product purified by normal silica gel chromatography eluting with 30% EtOAc/hexane to obtain derivatives **168a**-**e** and **168h**. All compounds are novel.

*3.9.1 N-(4-bromophenyl)-3-((2,6-dichloropyrimidin-4-yl)oxy)benzamide **168a***

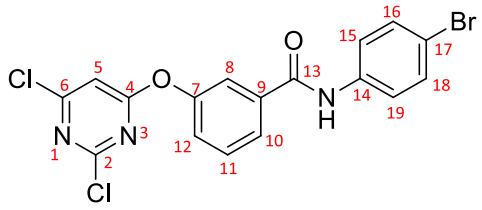

4-bromoaniline **151a** (0.600 g, 3.50 mmol) was reacted with 3-((2,6-dichloropyrimidin-4-yl)oxy)benzoyl chloride **179** (3.50 mmol) for 5 h. Compound **168a** was obtained as a light brown solid (1.07 g, 76% yield). Rf= 0.4 (7:3 EtOAc/hexane); M.p= 178-180 ^{o}C; IR (ν/cm^{-1}) 3341 (NH, br), 1661 (C=O, str), 1259 (C-O, str); ^{1}H NMR (300 MHz, DMSO-d$_6$) δ_H 10.45 (s, 1H, NH), 7.93 (d, *J* = 7.8 Hz, 1H, H10), 7.84 – 7.81 (m, 1H, H8), 7.76 (d, *J* = 8.9 Hz, 2H, H15 and H19), 7.67 (t, *J* = 7.9 Hz, 1H, H11), 7.64 – 7.55 (m, 4H, H5, H12, H16, and H18); ^{13}C NMR (75 MHz, DMSO-d$_6$) δ_C 170.8 (C4), 164.4 (C13), 161.7 (C2), 158.2 (C6), 151.5 (C7), 138.3 (C14), 136.7 (C9), 131.5 (C16 and C18), 130.2 (C11), 125.8 (C10), 124.9 (C12), 122.3 (C15 and C19), 120.7 (C8), 115.6 (C17), 107.8 (C5); HRMS (ES$^+$) calculated for $C_{17}H_{11}BrCl_2N_3O_2$ $[M+H]^+$: 437.9406, found: 437.9396.

*3.9.2 N-(3-bromophenyl)-3-((2,6-dichloropyrimidin-4-yl)oxy)benzamide **168b***

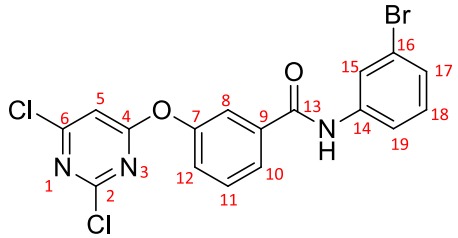

3-bromoaniline **151b** (0.380 ml, 3.50 mmol) was reacted with 3-((2,6-dichloropyrimidin-4-yl)oxy)benzoyl chloride **179** (3.50 mmol) for 22 h. Compound **168b** was obtained as a light brown solid (0.260 g, 17%). Rf= 0.5 (7:3 EtOAc/hexane). M.p=150-152°C; IR (ν/cm^{-1}) 3301 (NH, br), 1655 (C=O, str), 1275 (C-O, str); ^{1}H NMR (400 MHz, $CDCl_3$) δ_H 8.31 (s, 1H, NH), 7.84 (s, 1H, H15), 7.71 (d, *J* = 7.7 Hz, 1H, H10), 7.64 (s, 1H, H8), 7.49 (q, *J* = 7.9, 7.4 Hz, 2H, H11 and H17), 7.31 – 7.22 (m, 2H, H12 and H19), 7.16 (t, *J* = 8.0 Hz, 1H, H18), 6.86 (s, 1H, H5); ^{13}C NMR (101 MHz, $CDCl_3$) δ_C 170.5 (C4), 164.7 (C13), 162.9 (C2), 159.8 (C6), 151.8 (C7), 138.9 (C14), 136.5 (C9), 130.4 (C11),

127.8 (C19), 124.9 (C10 and C12), 123.4 (C15), 122.7 (C16), 120.4 (C8), 119.0 (C17), 106.5 (C5); HRMS (ES^+) calculated for $C_{17}H_{11}BrCl_2N_3O_2$ $[M+H]^+$: 437.9406, found: 437.9400.

*3.9.3 N-(4-bromo-2-methylphenyl)-3-((2,6-dichloropyrimidin-4-yl)oxy)benzamide **168c***

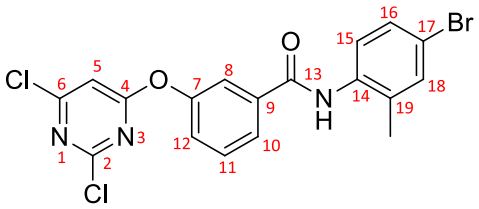

4-bromo-2-methylaniline **151c** (0.650 g, 3.50 mmol) was reacted with 3-((2,6-dichloropyrimidin-4-yl)oxy)benzoyl chloride **179** (3.50 mmol) for 22 h. Compound **168c** was obtained as a cream-white solid product (0.520 g, 21%). Rf= 0.5 (7:3 EtOAc/hexane); M.p= 138-140 °C; IR (ν/cm^{-1}) 3086 (NH), 1634 (C=O, str), 1261 (C-O, str) ^{1}H NMR (400 MHz, $CDCl_3$) δ_H 7.77 – 7.69 (m, 4H, H8, H12, H15, and NH), 7.56 (t, *J* = 7.9 Hz, 1H, H11), 7.35 (d, *J* = 8.2 Hz, 3H, H10, H16, and H18), 6.91 (s, 1H, H5), 2.29 (s, 3H, H-CH_3); ^{13}C NMR (101 MHz, $CDCl_3$) δ_C 170.6 (C4), 164.5 (C13), 163.1 (C2), 160.1 (C6), 152.1 (C7), 136.8 (C9), 134.7 (C14), 133.4 (C18), 131.9 (C19), 130.6 (C11), 130.0 (C16), 125.1 (C10 and C15), 124.8 (C12), 120.7 (C8), 118.8 (C17), 106.7 (C5), 17.8 (C-CH_3); HRMS (ES^+) calculated for $C_{18}H_{13}BrCl_2N_3O_2$ $[M+H]^+$: 451.9563, found: 451.9542.

*3.9.4 3-((2,6-dichloropyrimidin-4-yl)oxy)-N-(p-tolyl)benzamide **168d***

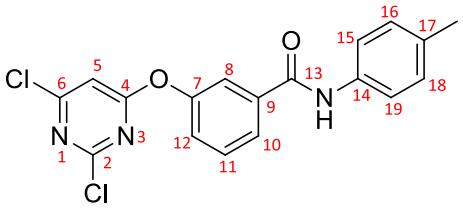

4-methylaniline **151d** (0.380 g, 3.50 mmol) was reacted with 3-((2,6-dichloropyrimidin-4-yl)oxy)benzoyl chloride **179** (3.50 mmol) for 14 h. Compound **168d** was obtained as a white solid product (1.17 g, 89% yield). Rf= 0.5 (7:3 EtOAc/hexane); M.p= 168-170 °C; IR (ν/cm^{-1}) 3282 (NH, br), 1662(C=O, str); ^{1}H NMR (400 MHz, DMSO-d_6) δ_H 10.27 (s, 1H, NH), 7.94 (d, *J* = 7.9 Hz, 1H, H10), 7.85 – 7.81 (m, 1H, H8), 7.69 – 7.63 (m, 3H, H11, H15, and H19), 7.56 – 7.50 (m, 2H, H5 and H12), 7.17 (d, *J* = 8.3 Hz, 2H, H16 and H18), 2.28 (s, 3H, H-CH_3); ^{13}C NMR (101 MHz, DMSO-d_6) δ_C 171.3 (C4), 164.5 (13), 162.2 (C2), 158.7 (C6), 151.9 (C7), 137.5 (C14), 136.8 (C9), 133.3 (C17), 130.6 (C11), 129.5 (C16 and C18), 126.1 (C10), 125.1 (C12), 121.1 (C15 and C19), 120.9 (C8), 108.0 (C5), 21.0 (C-CH_3); HRMS (ES^+) calculated for $C_{17}H_{13}Cl_2N_4O_2$ $[M+H]^+$: 375.0410, found: 375.0417.

*3.9.5 3-((2,6-dichloropyrimidin-4-yl)oxy)-N-(4-methoxyphenyl)benzamide **168e***

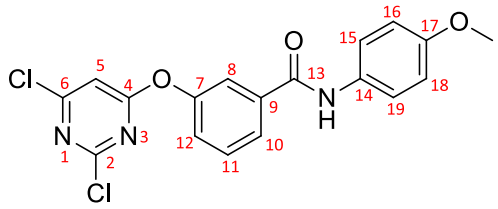

4-methoxyaniline **151e** (0.430 g, 3.50 mmol) was reacted with 3-((2,6-dichloropyrimidin-4-yl)oxy)benzoyl chloride **179** (3.50 mmol) for 3 h and the impure product washed successively with 10% EtOAc. Compound **168e** was obtained as a white solid product (1.28 g, 93%). Rf= 0.5 (7:3 EtOAc/hexane); M.p= 169-171°C; IR (ν/cm^{-1}) 3297 (NH, br), 1637 (C=O, str), 1248 (C-O, str); ^{1}H NMR (400 MHz, DMSO-d$_6$) δ_H 10.23 (s, 1H, NH), 7.94 (d, J = 7.8 Hz, 1H, H10), 7.83 (s, 1H, H8), 7.70 – 7.63 (m, 3H, H12, H15 and H19), 7.56 – 7.50 (m, 2H, H5 and H11), 6.94 (d, J = 9.0 Hz, 2H, H16 and H18), 3.75 (s, 3H, H-OCH$_3$); ^{13}C NMR (101 MHz, DMSO-d$_6$) δ_C 171.3 (C4), 164.3 (C13), 162.2 (C6), 158.7 (C2), 156.1 (C17), 151.9 (C7), 137.5 (C9), 132.4 (C14), 130.6 (C11), 126.1 (C10), 125.0 (C12), 122.5 (C8), 121.0 (C15 and C19), 114.2 (C16 and C18), 108.0 (C5), 55.6 (C-OCH$_3$); HRMS (ES$^+$) calculated for $C_{18}H_{14}Cl_2N_3O_3$ [M+H]$^+$: 390.0407, found: 390.0407.

*3.9.6 N-(4-chloro-2-methylphenyl)-3-((2,6-dichloropyrimidin-4-yl)oxy)benzamide **168h***

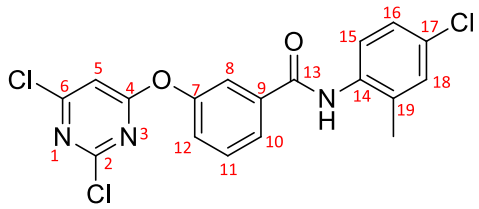

4-chloro-2-methylaniline **151h** (0.500 g, 3.50 mmol) was reacted with 3-((2,6-dichloropyrimidin-4-yl)oxy)benzoyl chloride **179** (3.50 mmol) for 14 h. Compound **168h** was obtained as a white solid (0.740 g, 52% yield). Rf= 0.3 (7:3 EtOAc/hexane); M.p= 83-85^{o}C; IR (ν/cm^{-1}) 3260 (NH, br), 1647 (C=O, str); ^{1}H NMR (400 MHz, CDCl$_3$) δ_H 7.80 – 7.74 (m, 3H, NH, H10, H15), 7.70 – 7.67 (m, 1H, H8), 7.56 (t, J = 8.0 Hz, 1H, H11), 7.35 (ddd, J = 8.2, 2.3, 0.8 Hz, 1H, H12), 7.20 (d, J = 7.5 Hz, 2H, H18), 6.91 (s, 1H, H5), 2.28 (s, 3H, methyl H); ^{13}C NMR (101 MHz, CDCl$_3$) δ_C 170.5 (C4), 164.4 (C13), 163.0 (C2), 159.9 (C6), 151.9 (C7), 136.7 (C9), 134.0 (C14), 131.7 (C19), 130.8 (C17), 130.5 (C18), 130.4 (C11), 126.9 (C16), 124.9 (C10), 124.7 (C12), 120.5 (C8), 106.6 (C5), 17.8 (C-methyl); HRMS (ES$^+$) calculated for $C_{18}H_{13}Cl_3N_3O_2$ [M+H]$^+$: 408.0068, found: 408.0055.

3.10 Synthesis of complex benzamides from aminopyridines **151j-o**

General procedure

3-((2,4-dichloropyrimidin-4-yl)oxo)benzoic acid **155** (1.00 g, 3.50 mmol) was placed in a round-bottomed flask, and thionyl chloride (2 ml) was added. The mixture was stirred and heated at 70 °C in an oil bath for overnight. After cooling the mixture to room-temperature, excess thionyl chloride was removed *in vacuo* leaving a pale yellow 3-(2,4-dichloropyrimidin-4-yl)oxo)benzoyl chloride residue **179**

which was dissolved in distilled acetonitrile (4 ml) and cautiously added to an ice-cold mixture of aminopyridine (**151j**-**o**) and pyridine or triethylamine (2 ml) in distilled acetonitrile or THF (15 ml). The mixture was stirred at 0 °C for 30 min, warmed to room temperature and stirred for 3-13 h. Excess solvent was removed under reduced pressure and the residue dissolved in ethyl acetate (50 ml). The organic mixture was washed with aqueous saturated K_2CO_3 (50 ml × 2), saturated brine solution (50 ml), and followed by separation of organic layer which was dried over anhydrous Na_2SO_4. The solvent was removed under reduced pressure and the crude product purified by normal silica gel chromatography eluting with 30% EtOAc/hexane to obtain derivatives **168j**-**m** and **168o**. All the compounds are novel.

*3.10.1 N-(5-bromopyridin-2-yl)-3-((2,6-dichloropyrimidin-4-yl)oxy)benzamide **168j***

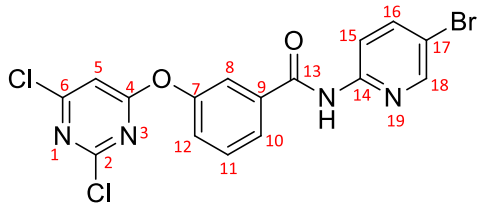

2-amino-5-bromopyridine **151j** (0.620 g, 3.50 mmol) was reacted with 3-((2,6-dichloropyrimidin-4-yl)oxy)benzoyl chloride **179** (3.50 mmol) for 3 h. Compound **168j** was obtained as a white solid product (0.770 g, 50% yield). Rf= 0.3 (7:3 EtOAc/hexane); M.p= 168-176˚C; IR (ν/cm^{-1}) 3228 (NH, br), 1668 (C=O, str), 1272 (C-O); ^{1}H NMR (300 MHz, DMSO-d$_6$) δ_H 11.06 (s, 1H, NH), 8.52 (d, *J* = 2.2 Hz, 1H, H18), 8.18 (d, *J* = 8.9 Hz, 1H, H15), 8.08 (dd, *J* = 8.9, 2.4 Hz, 1H, H16), 8.00 (d, *J* = 7.8 Hz, 1H, H10), 7.92 (s, 1H, H8), 7.64 (t, *J* = 7.9 Hz, 1H, H11), 7.54 (d, *J* = 6.1 Hz, 2H, H5 and H12); ^{13}C NMR (75 MHz, DMSO-d$_6$) δ_C 170.8 (C4), 164.9 (13), 161.7 (C6), 158.2 (C2), 151.5 (C7), 151.0 (C14), 148.5 (C18), 140.6 (C16), 135.8 (C9), 130.2 (C11), 126.1 (C10), 125.2 (C12), 121.1 (C8), 116.3 (C15), 114.2 (C17), 107.5 (C5); HRMS (ES$^+$) calculated for $C_{16}H_{10}BrCl_2N_4O_2$ [M+H]$^+$: 438.9359, found: 438.9361.

*3.10.2 3-((2,6-dichloropyrimidin-4-yl)oxy)-N-(6-methylpyridin-2-yl)benzamide **168k***

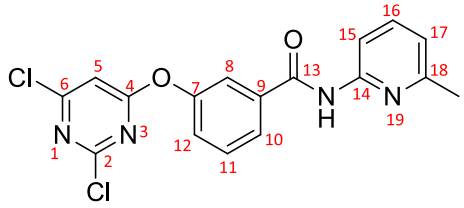

2-amino-6-methylpyridine **151k** (0.380 g, 3.50 mmol) was reacted with 3-((2,6-dichloropyrimidin-4-yl)oxy)benzoyl chloride **179** (3.50 mmol) for 13 h. Compound **168k** was obtained as a white solid (0.830 g, 63% yield); Rf= 0.3 (7:3 EtOAc/hexane); M.p= 162-164 °C IR (ν/cm^{-1}) 3385 (NH, br), 1676 (C=O, str), 1265 (C-O, str); ^{1}H NMR (400 MHz, DMSO-d$_6$) δ_H 10.80 (s, 1H, NH), 8.04 – 7.98 (m, 2H, H10 and H15), 7.97 – 7.93 (m, 1H, H8), 7.73 (t, *J* = 7.9 Hz, 1H, H16), 7.63 (t, *J* = 7.9 Hz, 1H, H11), 7.56 – 7.50 (m, 2H, H5 and H12), 7.04 (d, *J* = 7.4 Hz, 1H, H17), 2.45 (s, 3H, H-

CH_3); ^{13}C NMR (101 MHz, DMSO-d_6) δ_C 171.3 (C4), 165.1 (C13), 162.2 (C6), 158.7 (C2), 151.9 (C7), 151.8 (C18), 138.9 (C16), 136.5 (C9), 130.6 (C11), 126.5 (C10), 125.4 (C12), 121.5 (C8), 119.7 (C17), 112.2 (C15), 108.0 (C5), 24.0 (C-CH_3); HRMS (ES^+) calculated for $C_{17}H_{13}Cl_2N_4O_2$ $[M+H]^+$: 375.0410, found: 375.0419.

*3.10.3 N-(6-bromopyridin-2-yl)-3-((2,6-dichloropyrimidin-4-yl)oxy)benzamide **168l***

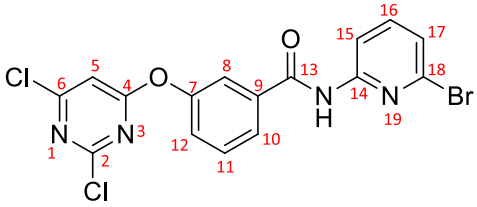

2-amino-6-bromopyridine **151l** (0.620 g, 3.50 mmol) was reacted with 3-((2,6-dichloropyrimidin-4-yl)oxy)benzoyl chloride **179** (3.50 mmol) for 3 h and the impure product washed with 10% EtOAc/hexane. Compound **168l** was obtained as a white solid product (0.590 g, 38% yield). Rf= 0.3 (7:3 EtOAc/hexane); M.p=185-187˚C; IR (ν/cm^{-1}) 3374 (NH, br), 1682 (C=O, str), 1299 (C-O); ^1H NMR (400 MHz, DMSO-d_6) δ_H 11.19 (s, 1H, NH), 8.21 (d, *J* = 8.1 Hz, 1H, H15), 8.00 (d, *J* = 7.8 Hz, 1H, H10), 7.92-7.95 (m, 1H, H8), 7.80 (t, *J* = 8.0 Hz, 1H, H16), 7.64 (t, *J* = 7.9 Hz, 1H, H11), 7.54 (q, *J* = 2.4 Hz, 2H, H12), 7.41 (d, *J* = 7.6 Hz, 1H, H17); ^{13}C NMR (101 MHz, DMSO-d_6) δ_C 170.8 (C4), 165.0 (C13), 161.8 (C6), 158.2 (C2), 152.3, (C14), 151.4 (C7), 141.4 (C16), 138.8 (C18), 135.6 (C9), 130.2 (C11), 126.3 (C10), 125.3 (C11)), 123.6 (C17), 121.2 (C8), 113.7 (C15), 107.5 (C5); HRMS (ES^+) calculated for $C_{16}H_{10}BrCl_2N_4O_2$ $[M+H]^+$: 438.9359, found: 438.9352.

*3.10.4 N-(6-chloropyridin-2-yl)-3-((2,6-dichloropyrimidin-4-yl)oxy)benzamide **168m***

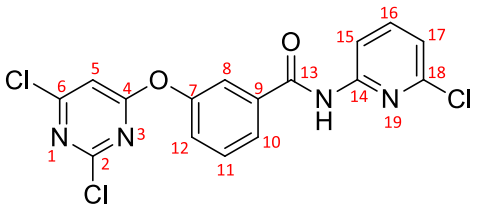

2-amino-6-chloropyridine **151m** (0.460 g, 3.50 mmol) was reacted with 3-((2,6-dichloropyrimidin-4-yl)oxy)benzoyl chloride **179** (3.50 mmol) for 3 h. Compound **168m** was obtained as a white solid product (0.670 g, 50% yield). Rf= 0.3 (7:3 EtOAc/hexane); M.p= 168-170 ˚C; IR (ν/cm^{-1}) 3377 (NH, br), 1681 (C=O, str), 1262 (C-O); ^1H NMR (500 MHz, DMSO-d_6) δ_H 11.14 (s, 1H, NH), 8.19 (d, *J* = 8.2 Hz, 1H, H15), 8.01 (d, *J* = 7.8 Hz, 1H, H10), 7.92 (dd, *J* = 15.8, 7.8 Hz, 2H, H8 and H16), 7.55 – 7.51 (m, 2H, H5 and H12), 7.28 (d, *J* = 7.7 Hz, 1H, H17); ^{13}C NMR (125 MHz, DMSO-d_6) δ_C 170.8 (C4), 164.9 (C13), 161.7 (C6), 158.2 (C2), 152.0 (C14), 151.4 (C7), 148.0 (C18), 141.6 (C16), 135.6 (C9), 130.2 (C11), 126.2 (C10), 125.3 (C12), 121.1 (C17), 119.7 (C8), 113.3 (C15), 107.5 (C5); HRMS (ES^+) calculated for $C_{16}H_{10}Cl_3N_4O_2$ $[M+H]^+$: 394.9864, found: 394.9856.

*3.10.5 N-(5-chloropyridin-2-yl)-3-((2,6-dichloropyrimidin-4-yl)oxy)benzamide **168o***

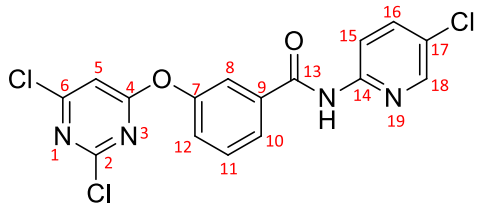

2-amino-5-chloropyridine **151o** (0.450 g, 3.50 mmol) was reacted with 3-((2,6-dichloropyrimidin-4-yl)oxy)benzoyl chloride **179** (3.50 mmol) for 4 h. Compound **168o** was obtained as a white solid product (0.410 g, 28% yield). Rf= 0.3 (7:3 EtOAc/hexane); M.p= 132-137 °C; IR (ν/cm^{-1}) 3326 (NH, br) 1671 (C=O, str), 1298 (C-O, str); ^{1}H NMR (400 MHz, $CDCl_3$) δ_H 8.84 (s, 1H, NH), 8.35 (d, J = 8.9 Hz, 1H, H15), 8.18 (d, J = 2.3 Hz, 1H, H18), 7.82 (d, J = 7.8 Hz, 1H, H10), 7.72 (dd, J = 8.7, 2.3 Hz, 2H, H8 and H16), 7.58 (t, J = 8.0 Hz, 1H, H11), 7.40 – 7.34 (m, 1H and H12), 6.92 (s, 1H, H5); ^{13}C NMR (101 MHz, $CDCl_3$) δ_C 170.5 (C4), 164.3 (C13), 162.9 (C6), 160.0 (C2), 152.0 (C7), 149.6 (C14), 146.6 (C18), 138.2 (C16), 136.1 (C9), 130.5 (C11), 127.2 (C17), 125.4 (C12), 124.9 (C10), 120.8 (C8), 115.0 (C15), 106.5 (C5); HRMS (ES$^+$) calculated for $C_{16}H_{10}Cl_3N_4O_2$ $[M+H]^+$: 394.9864, found: 394.9865.

3.11 Second chlorine displacement

*3.11.1 N-(4-bromophenyl)-3-((6-chloro-2-(ethylthio)pyrimidin-4-yl)oxy)benzamide **180a***

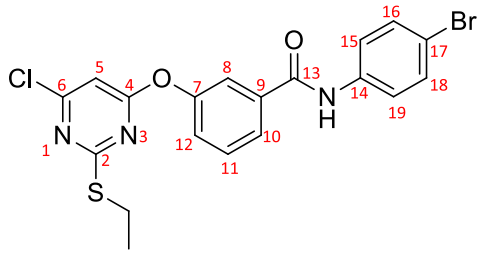

To a round-bottomed flask was added N-(4-bromophenyl)-3-((2,6-dichloropyrimidin-4-yl)oxy)benzamide **168a** (0.50 g, 1.1 mmol) in acetone (15 ml) and ethanethiol (0.10 ml, 1.3 mmol). To the stirring mixture was added 1 M NaOH (0.044 g, 1.1 mmol) in water (4.4 ml) and the reaction proceeded for 1 h. Excess solvent was removed under reduced prssure and the residue dissolved in ethyl acetate (20 ml), washed successively with aqueous saturated $NaHCO_3$ (20 ml × 2) and saturated brine solution (20 ml). The organic layer was separated and dried over anhydrous Na_2SO_4. The solvent was evaporated, and the crude mixture (0.49 g) purified by normal silica gel (60.07 g) chromatography eluting with 30% ethyl acetate/hexane. The main two products were isolated, and the impure desired product was recrystallized with hot ethyl acetate and cold hexane. A white solid product **180a** (0.22 g, 43% yield). Rf= 0.4 (7:3 EtOAc/hexane); M.p= 174-176 °C; IR (ν/cm^{-1}) 3294 (NH, br) 1665 (C=O, str), 1288 (C-O, str); ^{1}H NMR (400 MHz, DMSO-d_6) δ_H 10.42 (s, 1H, NH), 7.92 (d, J = 7.7 Hz, 1H, H10), 7.85 (s, 1H, H8), 7.76 (d, J = 8.7 Hz, 2H, H15 and H19), 7.64 (t, J = 7.9 Hz, 1H, H11), 7.54 (t, J = 8.4 Hz, 3H, H12, H16, and H18), 7.11 (s, 1H, H5), 2.85 (q, J = 7.3 Hz, 2H, H-ethyl), 1.11 (t, J = 7.2 Hz, 3H, H-ethyl); ^{13}C NMR (101 MHz, DMSO-d_6) δ_C 172.2 (C2), 169.7 (C4), 164.8

(C13), 161.2 (C6), 152.1 (C7), 138.8 (C14), 136.7 (C9), 131.9 (C16 and C18), 130.4 (C11), 125.9 (C10), 125.6 (C12), 122.7 (C15), 121.4 (C8), 116.0 (C17), 103.4 (C5), 25.3 (C-ethyl), 14.7 (C-ethyl); HRMS (ES^+) calculated for $C_{19}H_{16}BrClN_3O_2S$ $[M+H]^+$: 463.9830, found: 463.9789.

*3.11.2 3-((6-chloro-2-(ethylthio)pyrimidin-4-yl)oxy)-N-(p-tolyl)benzamide **180d***

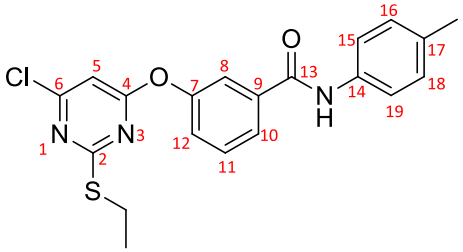

In a round-bottomed flask was added the 3-((2,6-dichloropyrimidin-4-yl)oxy)-N-(p-tolyl)benzamide **168d** (0.50 g, 1.3 mmol) and ethanethiol (0.12 ml, 1.6 mmol) in THF (10 ml) and the mixture was stirred at room temperature. To the stirring mixture was added 0.2 M NaOH (0.068 g, 1.7 mmol) in water (8.5 ml) or KO^tBu (0.10 g, 0.5 eq) or triethylamine (0.36 ml, 2 eq). The reaction mixture was stirred for further 1 h. The solvent was evaporated under reduced pressure and the residue dissolved in ethyl acetate (20 ml), washed with aqueous K_2CO_3 (20 ml × 2) and saturated brine solution (20 ml). The organic layer was separated and dried over anhydrous Na_2SO_4 and excess solvent removed under reduced pressure. The crude product was purified by normal silica gel chromatography eluting with 30% EtOAc/hexane. The product was recrystallized with hot ethyl acetate and cold hexane to obtain a white solid product **180d** (0.20 g, 38%) was obtained. M.p= °C; Rf= 0.4 (7:3 EtOAc/hexane); M.p= 168-170˚C; IR (ν/cm^{-1}) 3319 (NH, br), 1669 (C=O, str), 1218 (C-O, str); ^{1}H NMR (400 MHz, $CDCl_3$) δ_H 8.01 (s, 1H, NH), 7.73 (d, J = 7.6 Hz, 1H, H10), 7.65 (s, 1H, H8), 7.53 – 7.45 (m, 3H, H11, H15, and H19), 7.28 (d, J = 8.6 Hz, 1H, H12), 7.15 (d, J = 7.8 Hz, 2H, H16 and H18), 6.54 (s, 1H, H5), 2.89 (q, J = 7.2 Hz, 2H, H-ethyl), 2.33 (s, 3H, H-CH_3), 1.20 (t, J = 7.3 Hz, 3H, H-ethyl); ^{13}C NMR (101 MHz, $CDCl_3$) δ_C 173.1 (C2), 169.2 (C4), 164.4 (C13), 161.7 (C6), 152.2 (C7), 136.8 (C9), 135.1 (C14), 134.5 (C17), 129.9 (C11), 129.6 (C16 and C18), 125.0 (C12), 124.4 (C10), 120.6 (C8), 120.4 (C15), 102.3 (C5), 25.6 (C-ethyl), 20.9 (C-CH_3), 14.2 (C-ethyl); HRMS (ES^+) calculated for $C_{20}H_{19}ClN_3O_2S$ $[M+H]^+$: 400.0881, found: 400.0865.

3.11.3 Preparation of 3-((6-chloro-2-(propylamino)pyrimidin-4-yl)oxy)-N-(p-tolyl)benzamide **184d**

In a round-bottomed flask was added 3-((2,6-dichloropyrimidin-4-yl)oxy)-N-(p-tolyl)benzamide **168d** (0.52 g, 1.3 mmol) and n-propylamine (0.11 ml, 1.3 mmol) in THF (10 ml). The mixture was stirred at room temperature and 0.2 M NaOH (0.052 g, 1.3 mmol) was added dropwise. The reaction mixture continued stirring under similar conditions for 1 h. Excess solvent was removed under reduced pressure and the residue dissolved in ethyl acetate (20 ml), washed with aqueous K_2CO_3 (20 ml × 2) and saturated brine solution (20 ml). The organic layer was separated and dried over anhydrous

Na_2SO_4 and the solvent evaporated. The crude product (0.40 g) was purified by normal silica gel (120.5 g) chromatography eluting with 30% EtOAc/hexane. A white solid amorphous product **184d** (0.31 g, 66%) yield was obtained. HRMS (ES^+) calculated for $C_{21}H_{22}ClN_4O_2$ $[M+H]^+$: 397.1426, found: 397.1412.

*3.11.4 3-((6-chloro-2-(piperidin-1-yl)pyrimidin-4-yl)oxy)-N-(p-tolyl)benzamide **185d***

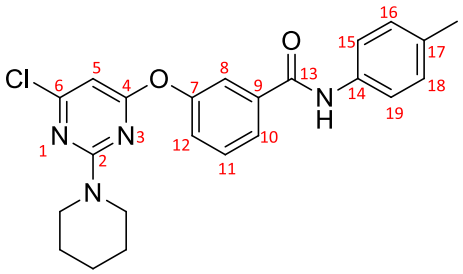

In a round-bottomed flask was added 3-((2,6-dichloropyrimidin-4-yl)oxy)-N-(p-tolyl)benzamide **168d** (0.50 g, 1.3 mmol) dissolved in THF (10 ml) and piperidine (0.13 ml, 1.3 mmol). The mixture was stirred at room temperature and 1M NaOH (0.052 g, 1.3 mmol) in water (1.3 ml) was added dropwise. The mixture continued stirring under similar conditions for 5 h. The solvent was removed under reduced pressure and the residue dissolved in ethyl acetate (20 ml), washed successively with aqueous K_2CO_3 (2 × 20 ml) and saturated brine solution (20 ml). The organic layer was separated and dried over anhydrous Na_2SO_4. The crude product was purified by normal silica gel chromatography eluting with 20% EtOAc/hexane. Compound **185d** was obtained as a white solid (0.35 g, 64%) was obtained. Rf= 0.4 (7:3 EtOAc/hexane); M.p: 155-160 °C ; IR (ν/cm^{-1}) 3353 (NH, br), 1647 (C=O, str), 1246 (C-O, str); ^{1}H NMR (400 MHz, $CDCl_3$) δ_H 7.91 (s, 1H, NH), 7.72 (d, *J* = 7.8 Hz, 1H, H10), 7.65 (s, 1H, H8), 7.53 – 7.44 (m, 3H, H11, H15 and H19), 7.30 (d, *J* = 8.3 Hz, 1H, H12), 7.15 (d, *J* = 8.0 Hz, 2H, H16 and H18), 5.97 (s, 1H, H5), 3.74 – 3.46 (m, 4H, H-piperidinyl), 2.33 (s, 3H, H-CH_3), 1.66 – 1.45 (m, 6H, H-piperidinyl); ^{13}C NMR (101 MHz, $CDCl_3$) δ_C 170.1 (C2), 164.6 (C13), 162.0 (C4), 160.4 (C6), 152.8 (C7), 136.6 (C1), 135.1 (C14), 134.5 (C17), 129.8 (C11), 129.6 (C16 and C18), 125.1 (C12), 123.9 (C10), 120.5 (C8), 120.4 (C15 and C19), 44.9 (C-piperidinyl), 25.6 (C-piperidinyl), 24.6 (C-piperidinyl), 20.9 (C-CH_3); HRMS (ES^+) calculated for $C_{23}H_{24}ClN_4O_2$ $[M+H]^+$: 463.9830, found: 463.9789.

3.12 Third chlorine displacement by hydrolysis

*3.12.1 3-((6-hydroxy-2-(propylamino)pyrimidin-4-yl)oxy)-N-(p-tolyl)benzamide **187d***

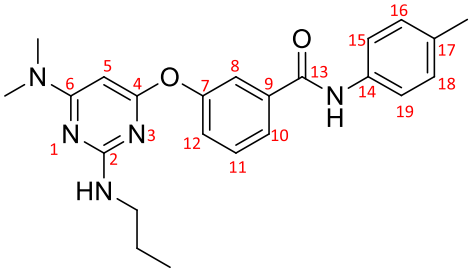

In a round bottomed flask was added 3-((6-chloro-2-(propylamino)pyrimidin-4-yl)oxy)-N-(p-tolyl)benzamide **184d** (0.20 g, 0.50 mmol) dissolved in DMF (10

ml) and 50% w/v NaOH (1 ml). The mixture was heated at 130 °C in an oil bath for 5 h. After cooling the reaction mixture to room temperature, excess solvent was evaporated. The residue was dissolved in ethyl acetate and washed several times (20 ml × 7) with saturated brine solution and with warm water to remove excess DMF. The organic layer was separated and dried over anhydrous Na_2SO_4, and the removed *in vacuo*. The crude product (0.12 g) was purified by combiflash column chromatography eluting with 10-40% EtOAc/hexane. A white solid product **187d** (0.070 g, 37% yield) was obtained. Unfortunately, the melting point was not recorded due to insufficient material. Rf= 0.3 (7:3 EtOAc/hexane); IR (ν/cm^{-1}) 3289 (NH, br), 1660 (C=O, weak str), 1237 (C-O, str); ^{1}H NMR (400 MHz, $CDCl_3$) δ_H 8.32 (s, 1H, H-amide), 7.70 – 7.61 (m, 2H, H8 and H10), 7.52 (d, *J* = 7.8 Hz, 2H, H15 and H19), 7.40 (t, *J* = 7.8 Hz, 1H, H11), 7.25 (d, *J* = 8.1 Hz, 1H, H12), 7.13 (d, *J* = 7.8 Hz, 2H, H16 and H18), 5.12 (s, 1H, H5), 4.81 – 4.75 (m, 1H, H-amine), 3.28 – 3.19 (m, 2H, H-ethyl), 2.97 (s, 6H, H-Me_2N), 2.31 (s, 3H, CH_3), 1.50 (h, *J* = 7.0 Hz, 2H, H-ethyl), 0.87 (t, *J* = 7.3 Hz, 3H, H-ethyl); ^{13}C NMR (101 MHz, $CDCl_3$) δ_C 170.5 (C4), 165.3 (C6), 165.1 (C13), 161.8 (C2), 153.8 (C7), 136.6 (C9), 135.4 (C14), 134.1 (C17), 129.7 (C11), 129.5 (C16 and C18), 124.7 (C12), 123.4 (C10), 120.4 (C15 and C19), 120.1 (C8), 76.2 (C5), 43.2 (C-ethyl), 37.1 (C-Me_2N), 23.0 (C-ethyl), 20.9 (C-CH_3), 11.5 (C-ethyl); HRMS (ES+) calculated for $C_{23}H_{28}N_5O_2$ [M+H]+: 406.2238, found: 406.2252.

References

1. Himathongkham S and Luciw PA. Restriction of HIV-1 (Subtype B) replication at the entry step in Rhesus Macaque cells. *Virology*, **1996**, 219, 485-488.

2. Rezaei T, Khalili S, Baradaran B, Mosafer J, Rezaei S, Mokhtarzadeh A, and de la Guardia M. Recent advances on HIV DNA vaccines development: stepwise improvements to clinical trials. *Journal of Controlled Release*, **2019**, 316, 116-137.

3. Zheng NN, Kiviat NB, Sow PS, Hawes SE, Wilson A, Diallo-Agne H, Critchlow CW, Gottlieb GS, Musey L, and McElrath MJ. Comparison of human immunodeficiency virus (HIV)-specific T-Cell responses in HIV-1- and HIV-2-infected individuals in Senegal. *Journal of Virology*, **2004**, 78, 13934-13942.

4. Gill MSA, Hassan SS, and Ahemad N. Evolution of HIV-1 reverse transcriptase and integrase dual inhibitors: Recent advances and developments. *European Journal of Medicinal Chemistry*, **2019**, 179, 423-448.

5. Sharp PM and Hahn BH. The evolution of HIV-1 and the origin of AIDS. *Philosophical Transactions of the Royal Society B*, **2010**, 365, 2487-2494.

6. Mahy MI, Sabin KM, Feizzadeh A, and Wanyeki I. Progress towards 2020 global HIV impact and treatment targets. *Journal of the International AIDS Society*, **2021**, 24, 5779.

7. Unaids. UNAIDS 2021 epidemiological estimates. Unaids. Published online **2021**. (https://aidsinfo.unaids.org/).

8. UNAIDS/WHO and HIV.org: global HIV prevalence in 2020 (https://asm.org/Resource-Page/HIV-AIDS-Resources).

9. Bertagnolio S, Thwin SS, Silva R, Nagarajan S, Jassat W, Fowler R, Haniffa R, Reveiz L, Fordd N, Doherty M, and Diaz J . Clinical features of, and risk factors for, severe or fatal COVID-19 among people living with HIV admitted to hospital: analysis of data from the WHO Global Clinical Platform of COVID-19. *Lancet HIV*, **2022**, 9, 486-495.

10. Kharsaney ABM and Karim QA. HIV infection in sub-Saharan Africa: current status, challenges and opprotunities. *The Open AIDS Journal*, **2016**, 10, 34-48.

11. Kabapy AF, Shatat HZ, and El-Wahab EWA. Attributes of HIV infection over decades (1982–2018): a systematic review and meta-analysis. *Transboundary and Emergency Disease*, **2020**, 67, 2372-2388.

12. Lahey KE. The New Line of defense: Criminal HIV transmission Laws. *Syracuse Journal of Legislation & Policy*, **1995**, 1, 85.

13. Reynolds C, de Koning CB, Pelly SC, van Otterlo WAL, and Bode ML. In search of a treatment for HIV – current therapies and the role of non-nucleoside reverse transcriptase inhibitors (NNRTIs). *Chemical Society Reviews*, **2012**, 41, 4657-4670.

14. Elkodous AM, El-Sayyad GS, Nasser HA, elshamy AA, Morsi M, Abdelrahman IY, Kodous AS, Mosallam FM, Gobara M, and El-Batal AI. Engineered nanomaterials as potential candidates for HIV treatment: between opportunities and challenges: *Journal of Cluster Science*, **2019**, 30, 531-540.

15. Popović-Djordjević J, Quispe C, Giordo R, Kostic A, Stankovic JSK, Fokou PVT, Carbone K, Martorell M, Kumar M, Pintus G, Sharifi-Rad J, Docea AO, and Calina D. Natural products and synthetic analogues against HIV: a perspective to develop new potential anti-HIV drugs: *European Journal of Medicinal Chemistry*, **2022**, 233, 114217.

16. Kirchhoff F. HIV life cycle: Overview. *Encyclopedia of AIDS*, **2013**, 1-9

17. Chen L, Ao Z, Jayappa KD, Kobinger G, Liu S, Wu G, Wainberg MA, and Yao X. Characterization of antiviral activity of benzamide derivative AH0109 against HIV-1 infection. *Antimicrobial Agents and Chemotherapy*, **2013**, 57, 3547-3554.

18. Goyal M, Baskonus HM, and Prakash A. Regarding new positive, bounded and convergent numerical solution of nonlinear time fractional HIV/AIDS transmission model. *Chaos, Solitons & Fractals*. **2020**, 139, 110096.

19. Gayle HD and Hill GL. Global impact of human immunodeficiency virus and AIDS. *Clinical Microbiology Reviews*, **2001**, 14, 327-335.

20. Higgins JA, Hoffman S, and Dworkin SL. Rethinking gender, heterosexual men, and women's vulnerability to HIV/AIDS. *American Journal of Public Health*, **2010**, 100, 435-445.

21. Dreyfuss ML and Fawzi WW. Micronutrients and vertical transmission of HIV-1. *American Journal of Clinical Nutrition*, **2002**, 75, 959-970.

22. John-Stewart G, Mbori-Ngacha D, Ekpini R, Janoff EN, Nkengasong J, Read JS, Van de Perre P, and Newell M. Breast-feeding and transmission of HIV-1. *Journal of Acquired Immune Deficiency Syndromes (1999)*, **2004**, 35, 196-202.

23. Rollins N, Meda N, Becquet R, Coutsoudis A, Humphrey J, Jeffrey B, Kanshana S, Kuhn L, Leroy V, Mbori-Ngacha D, Mcintyre J, and Newell M. Preventing postnatal transmission of HIV-1 through breast-feeding: modifying infant feeding practices. *Journal of Acquired Immune Deficiency Syndromes (1999)*, **2004**, 35, 188-195.

24. Aborode AT, Olotu TM, Oyetunde OB, Ajagbe AO, Mustapha MA, and Oko CI. COVID-19 outcomes in HIV patients: a review. *Annals of Medicine and Surgery*, **2022**, 78, 103768

25. Sayles JN, Ryan GW, Silver JS, Sarkisian CA, and Cunningham WE. Experiences of social stigma and implications for healthcare among a diverse population of HIV positive adults. *Journal of Urban Health*, **2007**, 84, 814-828.

26. Hsieh E, Polo R, Qian HZ, Fuster-RuizdeApodaca MJ, and del Amo J. Intersectionality of stigmas and health-related quality of life in people ageing with HIV in China, Europe, and Latin America. *The Lancet Healthy Longevity*, **2022**, 3, 206-215.

27. Kharsany ABM and Karim QA. HIV Infection and AIDS in Sub-Saharan Africa: Current Status, Challenges and Opportunities. *The Open AIDS Journal*, **2016**, 10, 34-48.

28. Chen X, Yu B and Zhao L. The evaluation of global epidemic of HIV/AIDS with a novel approach using country-specific counts of HIV infections and three rates controlled for population and geographic area. *Global Health Journal*, **2019**, 3, 66-67.

29. Bekker LG, Alleyne G, Baral S, Cepeda J, Daskalakis D, Dowdy D, Dybul M, Eholie S, Esom K, Garnett G, Grimsrud A, Hakim J, Havlir D, Isbell MT, Johnson L, Kamarulzaman A, Kasaie P, Kazatchkine M, Kilonzo N, Klag M, Klein M, Lewin SR, Luo C, Makofane K, Martin NK, Mayer K, Millett G, Ntusi N, Pace L, Pike C, Piot P, Pozniak A, Quinn TC, Rockstroh J, Ratevosian J, Ryan O, Sippel S, Spire B, Soucat A, Starrs A, Strathdee SA, Thomson N, Vella S, Schechter M, Vickerman P, Weir B, and Beyer C. Advancing global health and strengthening the HIV response in the era of the sustainable development goals: the international AIDS society—Lancet Commission. *The Lancet*, **2018**, 392, 312-358.

30. Fidler S, Lewin S, Deeks S, Sogaard OS, Vandekerckhove L, Collins S, Kelly D, Singh J, Caskey M, and Frater J. HIV cure research in the time of COVID-19 - Antiretroviral therapy treatment interruption trials: a discussion paper. *Journal of Virus Eradication*, **2021**, 7, 100025.

31. Losina E, Schackman BR, Sadownik SN, Gebo KA, Walensky RP, Chiosi JJ, Weinstein MC, Hicks PL, Aaronson WH, Moore RD, Paltiel AD, and Freedberg KA. Racial and sex disparities in life expectancy

losses among HIV-infected persons in the United States: impact of risk behavior, late initiation, and early discontinuation of antiretroviral therapy. *Clinical Infectious Diseases*, **2009**, 49, 1570-1578.

32. Hughes AJ, Mattson CL, Scheer S, Beer L, and Skarbinski J. Discontinuation of antiretroviral therapy among adults receiving HIV care in the United States. *Journal of Acquired Immune Deficiency Syndromes (1999)*, **2014**, 66, 80-89.

33. Ndubuka NO, Lim HJ, van der Wal DM, and Ehlers VJ. Health-related quality of life of antiretroviral treatment defaulters in Botswana. *Southern African Journal of HIV Medicine*, **2016**, 17, 475.

34. Grassi L, Righi R, Sighinolfi L, Makoui S, and Ghinelli F. Coping Styles and Psychosocial-Related Variables in HIV-Infected Patients. *Psychosomatics*, **1998**, 39, 350-359.

35. Pence BW, Thielman NM, Whetten K, Ostermann J, Kumar V, and Mugavero MJ. Coping strategies and patterns of alcohol and drug use among HIV-infected patients in the United States southeast. *AIDS Patient Care STDs*, **2008**, 22, 869-877.

36. Regenauer KS, Kleinman MB, Belus JM, Myers B, Joska JA, and Magidson JF. Effects of intersecting internalized stigmas and avoidance on HIV and alcohol-related outcomes among people living with HIV in South Africa. *Drug and Alcohol Dependence*, **2022**, 233, 109364.

37. Palattiyil G, Kisaakye P, Mwenyango H, Katongole S, Mulekya F, Sidhva D, Nair H, and Bukuluki P. Access to HIV/AIDS or TB care among refugees in Kampala, Uganda: exploring the enablers and barriers during the COVID-19 pandemic. *Journal of Migration and Health*, **2022**, 5, 100098.

38. Okoli C, van de Velde N, Allan B, Hardy WD, Corberlli GM, Muchenje M, Castellanos E, Brough G, Young B, Eremin A, Ramothwala P, McBritton M, and de Los Rios P. Regional differences in perceived treatments needs and priorities in relation to antiretroviral therapy among people living with HIV in 25 countries. *Previntive Medicine*, **2021**, 142, 106372.

39. Terry PE, Mhloyi M, Masvaure T, and Adlis S. An examination of knowledge, attitudes and practices related to HIV/AIDS prevention in Zimbabwean university students: Comparing intervention program participants and non-participants. *International Journal of Infectious Diseases*, **2006**, 10, 38-46.

40. Moseholm E, Gilleece Y, Collins B, Kowalska JD, Cairns, and Aebi-Popp K. Achievements and gaps to provide pre-exposure prophylaxis (PrEP) for women across the European Region – Results from a European survey study. *Journal of Virus Eradication*, **2021**, 7, 100026.

41. Schmidt HMA, Schaefer R, Radebe M, Sued O, Rodolph M, Ford N, and Baggaley R. Scaling up access to HIV pre-exposure prophylaxis (PrEP): should nurses do the job? *The Lancet HIV*. **2022**, 9, 363-366.

42. Massud I, Ruone S, Zlotorzynska M, Haaland R, Mills P, Cong M, Kelley K, Johnson R, Holder A, Dinh C, Khalil G, Pan Y, Kelley CF, Sanchez T, Heneine W, and Garcia-Lerma JG. Single oral dose for HIV pre or post-exposure prophylaxis: user desirability and biological efficacy in macaques. *EBioMedicine*, **2020**, 58, 102894.

43. Stanley TL, Fourman LT, Feldpausch MN, Purdy J, Zheng I, Buckless C, Tsao A, Pan CS, Aepfelbacher J, Kellogg A, Branch K, Lee H, Liu C, Corey KE, Chung RT, Torriani M, Kleiner DE, Hadigan CM, and Grinspoon SK. Effects of tesamorelin on non-alcoholic fatty liver disease in HIV: a randomised, double-blind, multicentre trial. *The Lancet HIV*, **2019**, 6, 821-830.

44. Assefa Y and Gilks CF. Ending the epidemic of HIV/AIDS by 2030: will there be an endgame to HIV, or an endemic HIV requiring an integrated health systems response in many countries? *International Journal of Infectious Diseases*, **2020**, 100, 273-277.

45. Chen X, Yu B, and Zhao L. The evaluation of global epidemic of HIV/AIDS with a novel approach using country-specific counts of HIV infections and three rates controlled for population and geographic area. *Global Health Journal*, **2019**, 3, 66-67.

46. Avanceña ALV and Hutton DW. Systematic Literature review optimization models for HIV/AIDS resource allocation: A Systematic review. *Value in Health*, **2020**, 23, 1509-1521.

47. Asahchop EL, Wainberg MA, Sloan RD, and Tremblay CL. Antiviral drug resistance and the need for development of new HIV-1 reverse transcriptase inhibitors. *Antimicrobial Agents and Chemotherapy*, **2012**, 56, 5000-5008.

48. Zhuang C, Pannecouque C, de Clercq E, and Chen F. Development of non-nucleoside reverse transcriptase inhibitors (NNRTIs): our past twenty years. *Acta Pharmaceutica Sinica B*, **2020**, 10, 961-978.

49. Qian K, Morris-Natschke SL, and Lee K. HIV entry inhibitors and their potential in HIV therapy. *Medicinal Research Reviews*, **2009**, 29, 369-393.

50. Esposito F, Corona A, and Tramontano E. HIV-1 Reverse transcriptase still remains a new drug target: structure, function, classical inhibitors, and new inhibitors with innovative mechanisms of actions. *Molecular Biology International*, **2012**, 2012, 586401.

51. Khalifa NM and Al-Omar MA. Synthesis and biological evaluation of 2-thioxopyrimidin-4(1H)-one derivatives as potential non-nucleoside HIV-1 reverse transcriptase inhibitors. *International Journal of Molecular Sciences*, **2014**, 15, 20723-20735.

52. Wang Y, de Clercq E, and Li G. Current and emerging non-nucleoside reverse transcriptase inhibitors (NNRTIs) for HIV-1 treatment. *Expert Opinion on Drug Metabolism & Toxicology*, **2019**, 15, 813-829.

53. Pedersen OS and Pedersen EB. Non-nucleoside reverse transcriptase inhibitors: the NNRTI boom. *Antiviral Chemistry Chemotherapy*, **1999**, 10, 285-314.

54. Zhan P, Liu X, Li Z, Pannecouque C, and de Clercq E. Design Strategies of Novel NNRTIs to Overcome Drug Resistance. *Current Medicinal Chemistry*, **2009**, 16, 3903-3917.

55. Liu X, Chen P, Li X, Ba M, Jiao X, Guo Y, and Xie P. Design, synthesis and biological evaluation of substituted (+)-SG-1 derivatives as novel anti-HIV agents. *Bioorganic & Medicinal Chemistry Letters*, **2018**, 28, 1699-1703.

56. Pata JD, Stirtan WG, Goldstein SW, and Steitz TA. Structure of HIV-1 reverse transcriptase bound to an inhibitor active against mutant reverse transcriptases resistant to other nonnucleoside inhibitors. *Proceedings of the National Academy of Sciences*, **2004**, 101, 10548-10553.

57. Das K and Arnold E. HIV-1 reverse transcriptase and antiviral drug resistance. Part 1. *Current Opinion in Virology*, **2013**, 3, 111-118.

58. Meng G, Liu Y, Zheng A, Chen F, Chen W, De Clercq E, Pannecouque C, and Balzarini J. Design and synthesis of a new series of modified CH-diarylpyrimidines as drug-resistant HIV non-nucleoside reverse transcriptase inhibitors. *European Journal of Medicinal Chemistry*, **2014**, 82, 600-611.

59. Changunda RCK. Synthesis and evaluation of novel pyridine-, pyrimidine-and triazine derivatives as potential HIV-1 non-nucleoside reverse transcriptase inhibitors (NNRTIs). University of the Witwatersrand. Thesis. **2018**.

60. Asif M. Pharmacological potential of benzamide analogues and their uses in medicinal chemistry. *Modern Chemistry & Applications*, **2016**, 4, 1-10.

61. Santosh KS. Method of synthesis of amides and its biological significance. *Journal of Emerging Technologies and Innovative Research*, **2017**, 4, 241-251.

62. Kaiser D, Bauer A, Lemmerer M, and Maulide N. Amide activation: an emerging tool for chemoselective synthesis. *Chemical Society Reviews*, **2018**, 47, 7899-7925.

63. Mottamal M, Zheng S, Huang TL, and Wang G. Histone deacetylase inhibitors in clinical studies as templates for new anticancer agents. *Molecules*, **2015**, 20, 3898-3941.

64. Cui AL, Sun WF, Zhong Z, Jin J, Xue S, Wu S, Li Y, and Li Z. Synthesis and bioactivity of n-(4-chlorophenyl)-4-methoxy-3-(methylamino) benzamide as a potential anti-HBV agent. *Drug Design, Development and Therapy*, **2020**, 14, 3723-3729.

65. Keating GM, Santoro A, Galle PR, and Raoul JL. Sorafenib: a review of its use in advanced hepatocellular carcinoma. *Targeted Oncology*, **2017**, 12, 243-253.

66. Eissa IH, El-Haggar R, Dahab MA, Ahmed MF, Mahdy HA, Alsantali RI, Masurier N, and Fatahala SS. Design, synthesis, molecular modeling and biological evaluation of novel Benzoxazole-Benzamide conjugates via a 2-Thioacetamido linker as potential anti-proliferative agents, VEGFR-2 inhibitors and apoptotic inducers. *Journal of Enzyme Inhibition and Medicinal Chemistry*, **2022**, 37, 1587-1599.

67. Al-Masoudi NA, Salih B, Jassim J, and Saeed A. Quantitative structure-activity relationship (QSAR) on new substituted thiazol-2-yliedene-benzamides as potential anti-HIV agents. *Journal of Computational and Theoretical Nanoscience*, **2012**, 9, 752-756.

68. Scala A, Piperno A, Micale N, Christ F, and Debyser Z. Synthesis and anti-HIV profile of a novel tetrahydroindazolylbenzamide derivative obtained by oxazolone chemistry. *ACS Medicinal Chemistry Letters*, **2018**, 10, 398-401.

69. Guo Y, Wang RY, Kang JX, Ma Y, Xu C, Li J, and Chen X. Efficient synthesis of primary and secondary amides via reacting esters with alkali metal amidoboranes. *Nature Communications*, **2021**, 12, 1-9.

70. Chhatwal AR, Lomax HV, Blacker AJ, Williams JMJ, and Marcé P. Direct synthesis of amides from nonactivated carboxylic acids using urea as nitrogen source and Mg(NO3)2 or imidazole as catalysts. *Chemical Science*, **2020**, 11, 5808-5818.

71. Lundberg H. Group (IV) metal-catalyzed direct amidation synthesis and mechanistic considerations. Department of Organic Chemistry, Stockholm University; **2015**.

72. Lanigan RM, Starkov P, and Sheppard TD. Direct synthesis of amides from carboxylic acids and amines using B(OCH2CF3)3. *Journal of Organic Chemistry*, **2013**, 78, 4512-4523.

73. Sabatini MT, Boulton LT, Sneddon HF, and Sheppard TD. A Green chemistry perspective on catalytic amide bond formation. *Nature Catalysis*, **2019**, 2, 10-17.

74. Pawelski D, Delgado OF, Wilczewska AZ, Strawa JW, and Plonska-Brzezinska ME. Nanostructured carbon catalyst for amide coupling reactions under microwave heating in the absence of a solvent. *ACS Applied Nano Material*, **2022**, 5, 16376-16387.

75. de Figueiredo RM, Suppo JS, and Campagne JM. Nonclassical Routes for Amide Bond Formation. *Chemical Reviews*, **2016**, 116, 12029-12122.

76. Mitchell JA and Reid EE. The preparation of aliphatic amides. *Journal of the American Chemical Society*, **1931**, 53, 1879-1883.

77. Grosjean C, Parker J, Thirsk C, and Wright AR. Intensifying azeotropic distillation: a strategy ofr optimizing direct amidation. *Organic Process Research & Development*, **2012**, 16, 781-787.

78. Cossy J and Pale-Grosdemange C. A convenient synthesis of amides from carboxylic acids and primary amines. *Tetrahedron Letters*, **1989**, 30, 2771-2774.

79. Goobsen LJ, Ohlmann DM, and Lange PP. The thermal amidation of carboxylic acids revisited. *Synthesis*, **2009**, 2009, 160-164.

80. Allen CL, Chhatwal AR, and Williams MJ. Direct amide formation from carboxylic acids and amines. *Chemical Communications Journal*, **2012**, 48, 666-668.

81. Herrero MA, Kremsner JM, and Kapper CO. Nonthermal microwave effects revisited: on the important internal temperature monitoring and agitation to microwave chemistry. *Journal of Organic Chemistry*, **2008**, 73, 36-47.

82. Khadse SC, and Chatpalliwar VA. Synthesis of benzamides by microwave assisted ring opening of less reactive dimethylaminobenzylidene oxazolone. *Arabian Journal of Chemistry*, **2017**; 10: S859-S863.

83. Valeur E and Bradley. Amide bond formation: beyond the myth of coupling reagents. *Chemical Society Reviews*, **2009**, 38, 606-631.

84a. Shah TR and Misra A. Challenges in delivery of therapeutic genomics and proteomics: eBook ISBN 9780123849656, 1st edition *Elsivier Inc*. **2010**.

84b. Ireland RE, Marshall DR, and Tilley JW. Racemization during peptide coupling using the mixed anhydride, *N*-hydroxysuccinimide ester, 8-hydroxyquinoline ester, and acyl azide methods. *Jorunal of the American Society*, **1970**, 92, 4756-4757.

84c. Lee NA and Kennedy IR. Immunoassays: Food toxicants analysis. *Techniques, Strategies and Developments,* **2007**, 91-145.

85. Allen CL. Catalytic approaches to the synthesis of amide bonds. University of Bath. Thesis. **2012**.

86. Makhija DT, Somani RR, and Chavan AV. Synthesis and pharmacological evaluation of antiinflamatory mutual amide prodrugs. *Indian Journal of Pharmaceutical Sciences*, **2013**, 75, 353-357.

87. Lee KS and Kim KD. Efficient synthesis of primary amides from carboxylic acids using N,N-carbonyldiimidazole and ammonium acetate in ionic liquid. *Synthetic Communications*, **2011**, 41, 3497-3500.

88. Montalbetti CAGN and Falque V. Amide bond formation and peptide coupling. *Tetrahedron*, **2005**, 61, 10827-10852.

89. Desai MC and Stramiello LMS. Polymer bound (P-EDC): Convenient reagent for formation of an amide bond. *Tetrahedron Letters*, **1993**, 34, 7685-7688.

90. Nakajima N and Ikada Y. Mechanism of amide formation by carbodiimide for bioconjungation in aqueous media. *Bioconjugate Chemistry*, **1995**, 6, 123-130.

91. Ghosh AK and Shahabi D. Synthesis of amide derivative for electron deficient amines and functionalized carboxylic acids using EDC and DMAP and a catalytic amount of HOBt as th coupling reagents. *Tetrahedron Letters*, **2021**, 63, 152719.

92. Mkhonazi BD, Shandu M, Tshinavhe R, Simelani SB, and Moshapo PT. Solvent-free iron (III) catalyzed direct amidation of esters. *Molecules*, **2020**, 25, 1040.

93. Wicht K. Discover of benzamides and triarylimidazoles active against Plasmodium falciparum via Haemozoin inhibition: high throughput screening, synthesis and structure-activity relationships. University of Cape Town. Thesis. **2015**.

94. Dunetz JR, Magano J, and Weisenburger GA. Large-scale applications of amide coupling reagents for the synthesis of pharmaceuticals. *Organic Process Research & Development*, **2016**, 20, 140-177.

95. Boyer R, Spencer EY, and Wright GF. Preparation of picryl chloride. *Canadian Journal of Research*, **1946**, 24, 200-203.

96. Zeng X, Xu G, Wang P, and Wang C. Synthesis and characterization of itaconyl chloride. *Materials Science and Engineering*, **2019**, 490, 022052.

97. Xiao J and Han L. Atom-efficient chlorination of benzoic acids with PCl_3, generating acyl chloride. *Journal of Chemical Research*. **2019**, 43, 205-210.

98. Kangani CO and Day BW. Mild, efficient Friedel-Crafts acylation from carboxylic acids using cyanuric chloride and $AlCl_3$. *Organic Letters*, **2008**, 10, 2645-2648.

99. Rayle HL and Fellmeth L. Development of a process for triazine-promoted amidation of carboxylic acids. *Organic Process Research & Development*, **1999**, 3, 172-176.

100. Venkataraman K and Wagle DR. Cyanuric chloride: A useful reagent for converting carboxylic acids into chlorides, esters, amides, and peptides, *Tetrahedron Letters*. **1979**, 20, 3037-3040.

101. Luo G, Xu L, and Poindexter GS. A novel solid-phase chlorinating reagent for the synthesis of acyl chlorides. *Tetrahedron Letters*, **2002**, 43, 8909-8912.

102. Betti C, Landinini D, Maia A, and Pasi M. Beckmann rearrangement of oximes catalyzed by cyanuric chloride in ionic liquids. *Synlett*, **2008**, 2008, 908-910.

103. Yadav D and Awasthi SK. An unsymmetrical covalent organic polymer for catalytic amide synthesis. *Dalton Transactions*, **2020**, 49, 179-186.

104. Wassei JK, Cha KC, Tung VC, Yang Y, and Kaner RB. The effects of thionyl chloride on the properties of graphene and graphene-carbon nanotube composites. *Journal of Materials Chemistry*, **2011**, 21, 3391-3396.

105. Kwolek SL, Morgan PW, Schaefgen JR, and Gulrich LW. Synthesis of anisotropic solutions, and fibers of poly(1,4-benzamide. *Macromolecules*, **1977**, 10, 1390-1396.

106. Cvetovich R and DiMichele. Formation of acrylanilides, acrylamides, and amides directly from carboxylic acids using thionyl chloride in dimethylacetamide in the absence of a base. *Organic Process Research & Developmen*t, **2006**, 10, 944-946.

107. Asaki T, Sigiyama Y, Hamamoto T, Higashioka M, Umehara M, Naito H, and Niwa T. *Bioorganic & Medicinal Chemistry Letters*, **2006**, 16, 1421-1425.

108. Mobinikhaledi A, Forughafar N, Shariatzadeh SM, and Fallah M. Synthesis and andtibacterial activity of some N-(3-hydroxy-2-pyridyl)benzamide. *Heterocyclic Communications*, **2006**, 12, 427-430.

109. Devi P, Barry SM, Houlihan KM, Murphy HM, Turner P, Jensen P, and Rutledge P. Synthesis and structural characterization of amides from picolinic acid and pyridine-2,6-dicarboxylic acid. *Scientific Reports*, **2015**, 5, 9950.

110. Jagtap SD, Sarkate AP, Khandare AL, Narula IK, Karnik KS, Pansare DN, and Shelke RN. Thionyl chloride induced convenient synthesis of benzamides from 3-bromo-5-nitrobenzoic acid and amines under solvent free conditions. *European Chemical Bulletin*, **2019**, 8, 123-127.

111. Leggio A, Belsito EL, De Luca D, Di Gioia ML, Leotta V, Romio E, Siciliano C, and Liguori A. One-pot synthesis of amides from carboxylic acids activated using thionyl chloride. *RSC Advances*, **2016**, 6, 34468-34475.

112. Mahfoudh M, Abderrahim R, Leclerc E, and Campagne J. Recent approaches to the synthesis of pyrimidine derivatives. *European Journal of Organic Chemistry*, **2017**, 2017, 2856-2865.

113. Terrier F. Modern nucleophilic aromatic substitution; Wiley-VCH: Weinheim, **2013**

114. Sharma V, Chitranshi N, and Agarwal AK. Significance and biological importance of pyrimidine in the microbial world. *International Journal of Medicinal Chemistry*, **2014**, 2014, 1-31.

115. Hevari MM and Adsirjan. Prescribed drugs containing nitrogen heterocyycles: an overview. *Royal Society of Chemistry advances*, **2020**, 10, 44247-44311

116. Sahu M and Siddiqui N. A review on biological importance of pyrimidines in the new era. *International Journal of Pharmacy and Pharmaceutical Science*, **2016**, 8, 8-21.

117. Elkanzi NAA. Synthesis and biological activities of some pyrimidine derivatives: (A-Review). *Oriental Journal of Chemistry*, **2020**, 36, 1001-1015.

118. Wang Z, Zalloum WA, Wang W, Jiang X, De Clercq E, Pannecouque C, Kang D, Zhan P, and Liu X. Discovery of novel dihydrothiopyrimidine[4,3-*d*]pyrimidine derivatives as potential HIV-1 NNRTIs with significantly reduced hERG inhibitory activity and improved resistance profiles. *Journal of Medicinal Chemistry*, **2021**, 64, 13658-13675.

119. Kang D, Sun , Feng D, Gao S, Wang Z, Jing L, Zhang T, Jiang X, Lin H, De Clercq E, Pannecouque C, Zhan P, and Liu X. Development of novel dihydrofuro[3,4-*d*]pyrimidine derivatives as HIV-1 NNRTIs to overcome the highly resistant mutant strains F227L/V106A and K103N/Y181C. *Journal of Medicinal Chemistry*, **2021**, 65, 2458-2470.

120. Kang D, Ding X, Wu G, Huo Z, Zhou Z, Zhao T, Feng D, Wang Z, Tian Y, Daelemans D, De Clercq E, Pannecouque C, Zhan P, and Liu X. Discovery of thiophene[3,2-*d*]pyrimidine derivatives as potent HIV-1 NNRTIs targeting the tolerant region I of NNIBP. *ACS Medicinal Chemistry Letters*, **2017**, 8, 1188-1193.

121. Wang Z, Kang D, Chen M, Wu G, Feng D, Zhao T, Zhou Z, Jing L, Zuo X, Daelemans D, De Clercq E, Pannecouque C, Zhan P, and Liu X. Design, synthesis, and antiviral evaluation of novel hydrazine substituted thiophene[3,2-*d*]pyrimidine derivatives as potent HIV-1 inhibitors. *Chemical Biology & Drug Design*, **2018**, 92, 2009-2021.

122. Mai A, Artico M, Sbardella G, Quartarone S, Massa S, Loi AG, De Montis A, Scintu F, Putzolu M, and La Colla P. Dihydro(Alkylthio)(Naphthylmethyl)Oxopyrimidines: novel non-nucleoside reverse transcriptase inhibitors of the S-DABO series.; *Journal of Medicinal Chemistry,* **1997**, 40, 1447-1454.

123. Vig R, Mao C, Venkatachalam TK, Tuel-Ahlgren L, Sudbeck EA, and Uckun FM. 5-alkyl-2-[(methylthiomethyl) thio]-6-(benzyl)-pyrimidin-4-(1*H*)-ones as potent non-nucleoside reverse transcriptase inhibitors of S-DABO series. *Bioorganic & Medicinal Chemistry Letters*, **1998**, 8, 1461-1466.

124. Manetti F, Esté JA, Clotet-Codina I, Armand-Ugon M, Maga G, Crespan E, Cancio R, Mugnaini C, Bernardini C, Togninelli A, Carmi C, Alongi M, Petricci E, Massa S, Corelli F, and Botta M. Parallel solution-phase and microwave-assisted synthesis of new S-DABO derivatives endowed with subnanomolar anti-HIV-1 activity. *Journal of Medicinal Chemistry*, **2005**, 48, 8000-8008.

125. Kidwai M, Saxena S, Rastogi S, and Venkataramanan R. Pyrimidines as anti-infective agents. *Current Medicinal Chemistry-Anti-Infective Agents*, **2003**, 2, 269-286.

126. Mosby WL. Introduction to the pyrimidines. *Chemistry of Heterocyclic Compounds*, **1962**, 16, 1-30.

127. OOsteveen EA. Ring transformations in reactions of pyrimidine and N-alkylpyridinium salts with nucleophiles. *ProQuest Dissertations & Theses Global*, Thesis. **1977**.

128. Brugnatelli L. On a new acid obtained by treating uric acid with nitric acid. *Annales de Chimie et de Physique*, 1818, 8, 201-206.

129. Hill MD and Movassaghi M. New strategies for the synthesis of pyrimidine derivatives. *Chemistry - A European Journal*, **2008**, 14, 6836-6844.

130. Pinner A. On the action of acetoacetic acid ether on amidines. *Reports of the German Chemical Society*, **1884**, 17, 2519-2520.

131. Gupta JK, Chaudhary A, Dudhe R, Varuna K, Sharma PK, and Verma PK. A review on the synthesis and therapeutic potential of pyrimidine derivatives. *International Journal of Pharmaceutical Sciences and Research*, **2010**, 1, 34-49.

132. Tominaga Y, Ohno S, Kohra S, Fujito H, and Mazume H. Synthesis of pyrimidine derivatives using *N*-Bis(methylthio)methylenecyanamide. *Journal of Heterocyclic Chemistry*, **1991**, 28, 1039-1042.

133. Lagoja IM. Pyrimidine as constituent of natural biologically active compouns. *Chemistry & Biodiversity*, **2005**, 2, 1-50.

134. Kohra S, Tominaga Y, and Hosomi A. Synthesis of pyrimidine derivatives by the reaction of ketene dithioacetals with amides. *Journal of Heterocyclic Chemistry*, **1988**, 25, 959-968.

135. Caron S and McInturff. Nucelophilic aromatic substitution. *Practical Synthetic Organic Chemistry: Reactions, Principles, and Techniques*, **2020**, 231-246

136. Delia TJ, Anderson DP, and Schomaker JM. 2,4,6-Trifluoropyrimidine: reactions with nitrogen nucleophiles. *Journal of Heterocyclic Chemistry*, **2004**, 41, 991-993.

137. Schomaker JM and Delia TJ. 2,4,6-Trichloropyrimidine. Reaction with anilines. *Journal of Heterocyclic Chemistry*, **2000**, 37, 1457-1462.

138. Dillender SC. Reactions of 4-chloro-2,6-dimethoxypyrimidine and 2-chlorothiazol with carbanion nucleophiles. Virginia Polytechnic Institute and State University. Dissertation. **1984**.

139. Wright EW, Nelson RA, Karpova Y, Kulik G, and Welker ME. Synthesis and PI3 kinase inhibition activity of some novel trisubstituted morpholinopyrimidines. *Molecules*, **2018**, 23, 1675.

140. Schomaker JM, and Delia TJ. Arylation of halogenated pyrimidines via a Suzuki coupling reaction. *The Journal of Organic Chemistry*, **2001**, 66, 7125-7128.

141. Delia TJ and Nagarajan A. 2,4,6-Trichloropyrimidine. Reaction with 4-substituted phenolate ions. *Journal of Heterocyclic Chemistry*, **1998**, 35, 269-273.

142. Feng D, Wei F, Wang Z, Kang D, Zhan P, and Liu X. Development of a practical synthesis of etravirine via a microwave-promoted amination. *Chemistry Central Journal*, **2018**, 12, 1-6.

143. Walker RT. Pyrimidines and quinaolines. *Rodd's Chemistry of Carbon compounds*, **1964**, 155-239

144. Boarland MPV and McOmie JFW. Monosubstituted pyrimidines, and action of thiourea on chloropyrimidines, *Journal of the Chemical Society (Resumed)*, **1951**, 1218-1221

145. El-Emam AA, Massoudj MAM, El-Bendary ER, and El-Sayed MA. Synthesis of certain 6-(arylthio) uracils and related derivatives as potential antiviral agents. *Bulletin of the Korean Chemical Society*, **2004**, 25, 991-996.

146. Goudgaon NM, and Sheshikant BU. Synthesis of novel 2,4-bis(substituted phenoxy)-6-(phenylthio)pyrimidine analogs and their antimicrobial activities. *Journal of Pharmacy Research*, **2013**, 7, 75-79.

147. Khalifa M and Metwally M. Utility of alkylthiopyrimidines in heterocyclic chemistry. *Journal of Chemica Acta*, **2012**, 1, 14-21.

148. Parks EL. Polyfunctionalised pyrimidines and pyrazines from perhalogenated precursors. Durham University. Thesis. **2008**.

149. Mai A, Artico M, Sbardella G, Massa S, Novellino E, Greco G, Loi AG, Tramontano E, Marongiu ME, and La Colla P. 5-alkyl-2-(alkylthio)-6-(2,6-dihalophenylmethyl)-3,4-dihydropyrimidin- 4(3H)-ones: novel potent and selective dihydro-alkoxy-benzyl-oxopyrimidine derivatives. *Journal of Medicinal Chemistry*. **1999**, 42, 619-627.

150. Bode ML, Gravestock D, Moleele SS, van der Westhuyzen CW, Pelly SC, Steenkamp PA, Hoppe HC, Khan T, and Nkabinde LA. Imidazo[1,2-a]pyridin-3-amines as potential HIV-1 non-nucleoside reverse transcriptase inhibitors. *Bioorganic & Medical Chemistry*, **2011**, *19*, 4227-4237.

151. Zhang L, Tang X, Cao Y, Wu S, Zhang Y, Zhao J, Guo Y, Tian C, Zhang Z, Liu J, and Wang X. Synthesis and biological evaluation of novel 2-Arylalkylthio-5-iodine-6- substituted-benzyl-pyrimidine-4(3H)-ones as Potent HIV-1 Non-Nucleoside reverse transcriptase inhibitors. *Molecules*, **2014**, *19*, 7104-7121.

152. Li T, Pannecouque C, De Clerq E, Zhuang C, and Chen F. Scaffold hopping in discovery of HIV-1 non-nucleoside reverse transcriptase inhibitors: from CH(CN)-DABOs to CH(CN)-dapys. *Molecules*, **2020,** *25*, 1581.

153. Ahmadi M, Moradi L, and Sadeghzadeh M. Synthesis of benzamides through direct condensation of carboxylic acids and amines in the presence of diatomic earth@IL/$ZrCl_4$ under ultrasonic irradiation. *Research on Chemical Intermediates*, **2018**, 44, 7873-7889.

154. Liang J, Tang Y, Tang X, Liang H, Gao Y, Fang c, Zhang T, and Yan M. Discovery of meta-amido bromophenols as new antitubercular agents. *Chemical and Pharmaceutical Bulletin Advance Publication*, **2019**, 67, 372-381.

155. Das S, Ray S, Ghosh AB, Samanta PK, Samanta S, Adhikary B, and Biswas P. Visible light driven amide synthesis from thioacid and amine using CdS nanoparticle as heterogeneous photocatalyst. *Applied Organometallic Chemistry*, **2017**, 32, 4199.

156. Putra GS, Wadiyana AP, Muchlashi WL, Sulistyowaty MI, Ekowati J, and Budiati.The influence of ratio pyrimidine and triethylamine catalysts on synthesis 2-phenyl-benzo[D][1.3] oxaine-4-on derivative. *Journal of Chemical and Pharmaceutical Research*, **2017**, 9, 73-80.

157. Robert-Piessard S, Le Baut G, Courant J, Brion J, Sparfel L, Bouhayat S, Petit J, Sanchez R, Jude M, Grimaud N, and Welin L. Non-acidic anti-inflammatory compounds: activity of N-(4,6-dimethyl-2-pyridinyl)benzamide and derivatives. *European Journal of Medicinal Chemistry*. **1990**, 25, 9-19.

158. Devi ES, Alanthadka A, Tamilselvi A, nagarajan S, Sridharan V, and Maheswari CU. Metal-free oxidative amidation of aldehydes with aminopyridines employing aqueous hydrogen peroxide. *Organic & Biomolecular Chemistry*, **2016**, 14, 8228-8231.

150. Fu R, Yang Y, Jin W, Zeng X, Chai W, Ma Y, Wang Q, Yi J, and Yuan R. Microwave-assisted heteropolyanion-based ionic liquid promoted sustainable protocol to N-heteroaryl amides via N-directing dual catalyzed oxidative amidation of aldehydes. *Royal Society of Chemistry advances*, **2016**, 107699-107707.

160. Dong D, Hao S, Zhang H, and Wang Z. Transformation of aldehydes or alcohols to amides at room temperature under aqueous conditions. *Chinese Chemical Letters*, **2017**, 28, 1597-1599.

161. Theodorou V, Gogou M, Giannoussi A, and Skobridis K. Insights into the N,N-diacylation of 2-aminopyridines and deactivated anilines: an alternative *N*-monoacylation reaction. *Archive for Organic Chemistry*, **2014**, 11-23.

162. Zitko J, Mindlova A, Valasek O, Jand'ourek O, Paterova P, Janousek J, Konecna K, and Dolezal M. Design, synthesis and evaluation of *N*-pyrazinylbenzamides as potential antimycobacterial agents. *Molecules*, **2018**, 23, 2390.

163. Shanghai Hua Zi Biological Technology Co Ltd. https://patents.google.com.

164. Charville H, Jackson DA, Hodges G, Whiting A, and Wilson MR. The uncatalyzed direct amide formation reaction-mechanism studies and the key role of carboxylic acid H-bonding. *European Journal of Organic Chemistry*, **2011**, 2011, 5981-5990.

165. Viesser RV, Ducati LC, Tormena CF, and Autschbach J. The halogen effect on the ^{13}C NMR chemical shift in substituted benzenes. *Physical Chemistry Chemical Physics*, **2018**, 20, 11247-11259.

166. Thompson QE. The diacylation of amides by acyl chloride-pyridine compounds. *Journal of the American Chemical Society,* **1951**, 73, 5841-5846.

167. Loksha YM. Novel synthetic route for 5-substituted 6-arylmethylluracils from 2,4,6-trichloropyrimidines. *Journal of Heterocyclic Chemistry*, **2009**, 46, 1296-1301.

168. Padilla AG and Pearlman BA. Highly selective hydrolysis of chloropyrimidines to pyrimidinones in 12N hydrochloric acid. *Organic Process Research & Development*, **2006**, 10, 921-926.

169. Yang Q, Sheng M, and Huang Y. Potential safety hazards associated with using *N*,*N*-dimethylformamide in chemical reactions. *Organic Process Research & Development*, **2020**, 24, 1586-1601.

170. Mikroyannidis JA. Synthesis and characterization of polycarbonates derived from N,N-m-phenylenebis(3-hydroxybenzamide) an 4,4-bis(4-hydroxyphenyl)pentanoic acid analide. *European Polymer Journal*, **1985**, 21, 1031-1034.

171. Zuo L, Yao S, Wang W, and Duan W. An efficient method for demethylation of aryl methyl ethers. *Tetrahedron Letters*, **2008**, 49, 4054-4056.

Appendix 1: Single X-ray crystallographic data

1. **Crystallographic data for *N*-(4-chloro-2-methylphenyl)benzamide 157h**

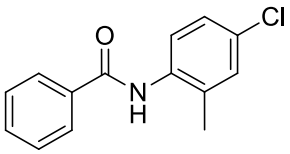

Table 1 Crystal data and structure refinement for 22mB_MLB3_Likhopotso_44_2_0f.

Identification code	22mB_MLB3_Likhopotso_44_2_0f
Empirical formula	$C_{14}H_{12}ClNO$
Formula weight	245.70
Temperature/K	173.00
Crystal system	Monoclinic
Space group	$P2_1/c$
a/Å	9.4254(8)
b/Å	29.145(2)
c/Å	8.9907(7)
α/°	90
β/°	90.168(3)
γ/°	90
Volume/Å^3	2469.8(3)
Z	8
ρ_{calc}g/cm^3	1.322
μ/mm^{-1}	0.291
F(000)	1024.0
Crystal size/mm^3	0.268 × 0.262 × 0.088
Radiation	MoKα (λ = 0.71073)
2Θ range for data collection/°	4.322 to 56.65
Index ranges	-12 ≤ h ≤ 12, -38 ≤ k ≤ 38, -12 ≤ l ≤ 11
Reflections collected	60046
Independent reflections	6132 [R_{int} = 0.0433, R_{sigma} = 0.0227]

Data/restraints/parameters	6132/0/317
Goodness-of-fit on F^2	1.039
Final R indexes [I>=2σ (I)]	R_1 = 0.0397, wR_2 = 0.1076
Final R indexes [all data]	R_1 = 0.0432, wR_2 = 0.1115
Largest diff. peak/hole / e $Å^{-3}$	0.41/-0.54

Table 2 Fractional Atomic Coordinates (×10^4) and Equivalent Isotropic Displacement Parameters ($Å^2$×10^3) for 22mB_MLB3_Likhopotso_44_2_0f. U_{eq} is defined as 1/3 of the trace of the orthogonalised U_{IJ} tensor.

Atom	*X*	*Y*	*Z*	U(eq)
Cl1	3755.9(5)	4532.7(2)	-2283.2(5)	68.85(16)
O1	3688.4(8)	3459.0(3)	4027.5(10)	32.90(19)
N1	5868.8(10)	3692.5(3)	3282.5(11)	27.4(2)
C1	4985.5(11)	3466.1(4)	4206.1(12)	24.3(2)
C2	5655.7(10)	3207.3(4)	5457.4(11)	23.8(2)
C3	4871.4(12)	2852.1(4)	6082.2(13)	29.7(2)
C4	5435.2(13)	2590.4(4)	7224.9(14)	35.1(3)
C5	6777.3(13)	2687.9(5)	7775.5(15)	36.6(3)
C6	7558.7(13)	3044.4(5)	7166.6(15)	36.6(3)
C7	7008.7(12)	3302.7(4)	6003.4(13)	29.8(2)
C8	5361.7(11)	3910.4(4)	1962.9(12)	27.5(2)
C9	4478.1(13)	4293.3(4)	2042.1(15)	33.0(2)
C10	3990.4(15)	4481.9(5)	702.2(18)	41.7(3)
C11	4405.3(15)	4295.5(5)	-638.8(16)	42.2(3)
C12	5319.0(15)	3928.3(5)	-716.5(15)	41.1(3)
C13	5796.6(13)	3734.9(5)	599.9(14)	34.3(3)
C14	4063.1(17)	4506.4(5)	3501.6(18)	45.2(3)
Cl2	-1150.4(5)	4538.6(2)	8896.2(4)	59.44(13)
O2	-1313.2(8)	3451.6(3)	2568.5(10)	31.69(18)

Table 2 Fractional Atomic Coordinates (×10^4) and Equivalent Isotropic Displacement Parameters (Å^2×10^3) for 22mB_MLB3_Likhopotso_44_2_0f. U_{eq} is defined as 1/3 of the trace of the orthogonalised U_{IJ} tensor.

Atom	*X*	*Y*	*Z*	U(eq)
N2	861.5(9)	3694.8(3)	3305.7(10)	26.63(19)
C21	-19.8(11)	3463.7(4)	2386.4(12)	23.9(2)
C15	651.5(10)	3206.5(4)	1137.6(11)	23.3(2)
C16	-128.0(12)	2848.7(4)	513.0(13)	29.5(2)
C17	439.2(13)	2587.4(4)	-624.9(14)	35.0(3)
C18	1776.5(13)	2686.1(4)	-1170.1(14)	35.6(3)
C19	2554.7(13)	3043.7(4)	-562.8(14)	35.4(3)
C20	2002.5(11)	3302.9(4)	595.1(13)	28.9(2)
C22	360.3(11)	3909.1(4)	4631.8(12)	26.4(2)
C23	-540.9(12)	4290.3(4)	4559.1(13)	29.6(2)
C24	-1004.5(14)	4477.7(4)	5901.7(15)	36.1(3)
C25	-560.6(14)	4294.7(5)	7243.7(14)	37.2(3)
C26	359.0(14)	3926.6(5)	7310.2(14)	36.5(3)
C27	814.1(12)	3734.1(4)	5985.8(13)	32.3(2)
C28	-988.0(15)	4502.0(4)	3104.4(16)	39.6(3)

Table 3 Anisotropic Displacement Parameters (Å^2×10^3) for 22mB_MLB3_Likhopotso_44_2_0f. The Anisotropic displacement factor exponent takes the form: $-2\pi^2[h^2a^{*2}U_{11}+2hka^*b^*U_{12}+\ldots]$.

Atom	U_{11}	U_{22}	U_{33}	U_{23}	U_{13}	U_{12}
Cl1	73.5(3)	78.6(3)	54.3(3)	35.0(2)	-29.2(2)	-18.5(2)
O1	18.5(4)	45.6(5)	34.6(4)	6.1(4)	-1.2(3)	0.5(3)
N1	18.3(4)	36.9(5)	26.9(5)	4.7(4)	0.6(3)	2.7(3)
C1	19.9(4)	29.1(5)	23.8(5)	-2.0(4)	0.6(4)	1.7(4)
C2	20.6(4)	28.5(5)	22.3(5)	-1.9(4)	2.2(4)	2.3(4)
C3	23.2(5)	36.3(6)	29.7(5)	1.5(4)	1.8(4)	-2.8(4)
C4	31.6(6)	37.4(6)	36.4(6)	8.9(5)	5.5(5)	-1.4(5)

Table 3 Anisotropic Displacement Parameters ($Å^2×10^3$) for 22mB_MLB3_Likhopotso_44_2_0f. The Anisotropic displacement factor exponent takes the form: $-2π^2[h^2a^{*2}U_{11}+2hka^*b^*U_{12}+…]$.

Atom	U_{11}	U_{22}	U_{33}	U_{23}	U_{13}	U_{12}
C5	31.3(6)	43.2(7)	35.3(6)	11.7(5)	0.0(5)	5.6(5)
C6	25.6(5)	44.9(7)	39.3(7)	9.5(5)	-6.6(5)	-0.3(5)
C7	23.6(5)	33.9(5)	31.9(6)	4.5(4)	-2.2(4)	-2.2(4)
C8	21.5(5)	33.6(5)	27.5(5)	4.1(4)	-0.9(4)	-1.7(4)
C9	28.7(5)	31.4(5)	38.9(6)	3.4(5)	-0.4(5)	-0.6(4)
C10	36.8(6)	34.2(6)	54.1(8)	12.3(6)	-7.5(6)	0.9(5)
C11	39.7(7)	48.7(7)	38.1(7)	17.4(6)	-12.5(5)	-12.5(5)
C12	39.8(7)	55.1(8)	28.4(6)	4.7(5)	-0.2(5)	-8.5(6)
C13	29.7(6)	43.0(6)	30.1(6)	2.2(5)	2.2(4)	1.1(5)
C14	51.1(8)	34.0(6)	50.7(8)	-4.3(6)	6.5(6)	6.7(5)
Cl2	74.6(3)	64.6(3)	39.3(2)	-18.68(17)	18.55(18)	2.19(19)
O2	18.6(3)	43.1(5)	33.4(4)	-6.1(3)	1.5(3)	0.2(3)
N2	17.5(4)	36.2(5)	26.1(5)	-4.6(4)	0.1(3)	1.8(3)
C21	20.9(4)	27.8(5)	23.2(5)	1.8(4)	-0.5(4)	1.7(4)
C15	20.6(4)	27.5(5)	21.8(5)	1.1(4)	-1.7(4)	2.6(4)
C16	22.9(5)	35.8(6)	29.9(5)	-2.5(4)	-1.8(4)	-2.6(4)
C17	31.1(6)	37.3(6)	36.7(6)	-10.3(5)	-5.6(5)	-0.9(5)
C18	31.5(6)	42.2(6)	33.2(6)	-11.7(5)	0.0(5)	6.2(5)
C19	25.7(5)	43.8(6)	36.9(6)	-8.2(5)	6.2(5)	0.9(5)
C20	22.9(5)	33.2(5)	30.6(6)	-4.0(4)	2.2(4)	-1.7(4)
C22	20.7(5)	32.3(5)	26.3(5)	-4.2(4)	1.0(4)	-1.4(4)
C23	27.3(5)	28.9(5)	32.7(6)	-2.0(4)	0.7(4)	-1.6(4)
C24	36.1(6)	30.7(6)	41.4(7)	-7.5(5)	5.4(5)	2.8(4)
C25	38.2(6)	41.4(6)	32.0(6)	-10.8(5)	8.9(5)	-5.7(5)
C26	37.2(6)	46.2(7)	26.2(6)	-2.1(5)	-1.0(5)	-2.6(5)
C27	27.5(5)	38.8(6)	30.6(6)	-2.1(5)	-2.1(4)	3.1(4)

Table 3 Anisotropic Displacement Parameters ($Å^2×10^3$) for 22mB_MLB3_Likhopotso_44_2_0f. The Anisotropic displacement factor exponent takes the form: $-2π^2[h^2a^{*2}U_{11}+2hka*b*U_{12}+…]$.

Atom	U_{11}	U_{22}	U_{33}	U_{23}	U_{13}	U_{12}
C28	46.6(7)	31.6(6)	40.4(7)	3.5(5)	-5.0(6)	4.7(5)

Table 4 Bond Lengths for 22mB_MLB3_Likhopotso_44_2_0f.

Atom	Atom	Length/Å	Atom	Atom	Length/Å
Cl1	C11	1.7416(13)	Cl2	C25	1.7397(13)
O1	C1	1.2328(13)	O2	C21	1.2310(13)
N1	C1	1.3499(14)	N2	C21	1.3500(14)
N1	C8	1.4269(14)	N2	C22	1.4277(14)
C1	C2	1.4929(14)	C21	C15	1.4923(14)
C2	C3	1.3916(15)	C15	C16	1.3931(15)
C2	C7	1.3931(15)	C15	C20	1.3935(15)
C3	C4	1.3844(17)	C16	C17	1.3840(16)
C4	C5	1.3865(18)	C17	C18	1.3840(18)
C5	C6	1.3871(18)	C18	C19	1.3856(17)
C6	C7	1.3878(16)	C19	C20	1.3887(16)
C8	C9	1.3945(16)	C22	C23	1.3999(15)
C8	C13	1.3907(17)	C22	C27	1.3864(16)
C9	C10	1.4005(18)	C23	C24	1.3961(17)
C9	C14	1.5045(19)	C23	C28	1.5052(17)
C10	C11	1.380(2)	C24	C25	1.383(2)
C11	C12	1.376(2)	C25	C26	1.3803(19)
C12	C13	1.3849(18)	C26	C27	1.3855(17)

Table 5 Bond Angles for 22mB_MLB3_Likhopotso_44_2_0f.

Atom	Atom	Atom	Angle/˚	Atom	Atom	Atom	Angle/˚
C1	N1	C8	121.56(9)	C21	N2	C22	121.67(9)

Table 5 Bond Angles for 22mB_MLB3_Likhopotso_44_2_0f.

Atom	Atom	Atom	Angle/˚	Atom	Atom	Atom	Angle/˚
O1	C1	N1	122.77(10)	O2	C21	N2	122.73(10)
O1	C1	C2	120.46(10)	O2	C21	C15	120.52(10)
N1	C1	C2	116.75(9)	N2	C21	C15	116.72(9)
C3	C2	C1	117.12(9)	C16	C15	C21	117.07(9)
C3	C2	C7	119.54(10)	C16	C15	C20	119.41(10)
C7	C2	C1	123.34(10)	C20	C15	C21	123.51(10)
C4	C3	C2	120.42(10)	C17	C16	C15	120.36(10)
C3	C4	C5	120.00(11)	C16	C17	C18	120.11(11)
C4	C5	C6	119.84(11)	C17	C18	C19	119.89(11)
C5	C6	C7	120.40(11)	C18	C19	C20	120.36(11)
C6	C7	C2	119.79(11)	C19	C20	C15	119.85(10)
C9	C8	N1	120.82(11)	C23	C22	N2	120.70(10)
C13	C8	N1	118.04(10)	C27	C22	N2	118.05(10)
C13	C8	C9	121.13(11)	C27	C22	C23	121.24(10)
C8	C9	C10	117.69(12)	C22	C23	C28	122.29(11)
C8	C9	C14	122.13(11)	C24	C23	C22	117.48(11)
C10	C9	C14	120.18(12)	C24	C23	C28	120.23(11)
C11	C10	C9	120.26(12)	C25	C24	C23	120.59(11)
C10	C11	Cl1	119.05(11)	C24	C25	Cl2	119.40(10)
C12	C11	Cl1	118.97(12)	C26	C25	Cl2	118.87(11)
C12	C11	C10	121.98(12)	C26	C25	C24	121.72(11)
C11	C12	C13	118.37(13)	C25	C26	C27	118.27(12)
C12	C13	C8	120.50(12)	C26	C27	C22	120.66(11)

Table 6 Torsion Angles for 22mB_MLB3_Likhopotso_44_2_0f.

A	B	C	D	Angle/˚	A	B	C	D	Angle/˚
Cl1	C11	C12	C13	-178.24(10)	Cl2	C25	C26	C27	179.65(10)

Table 6 Torsion Angles for 22mB_MLB3_Likhopotso_44_2_0f.

A	B	C	D	Angle/˚	A	B	C	D	Angle/˚
O1	C1	C2	C3	20.47(15)	O2	C21	C15	C16	-20.10(15)
O1	C1	C2	C7	-160.08(11)	O2	C21	C15	C20	160.79(11)
N1	C1	C2	C3	-157.87(10)	N2	C21	C15	C16	158.19(10)
N1	C1	C2	C7	21.58(15)	N2	C21	C15	C20	-20.92(15)
N1	C8	C9	C10	-178.32(11)	N2	C22	C23	C24	179.09(10)
N1	C8	C9	C14	2.44(17)	N2	C22	C23	C28	-2.00(16)
N1	C8	C13	C12	178.96(11)	N2	C22	C27	C26	-179.74(11)
C1	N1	C8	C9	67.70(15)	C21	N2	C22	C23	-68.10(14)
C1	N1	C8	C13	-113.52(12)	C21	N2	C22	C27	113.11(12)
C1	C2	C3	C4	178.59(10)	C21	C15	C16	C17	-178.42(10)
C1	C2	C7	C6	-179.69(11)	C21	C15	C20	C19	179.38(11)
C2	C3	C4	C5	1.41(19)	C15	C16	C17	C18	-1.27(19)
C3	C2	C7	C6	-0.26(17)	C16	C15	C20	C19	0.29(17)
C3	C4	C5	C6	-0.8(2)	C16	C17	C18	C19	0.8(2)
C4	C5	C6	C7	-0.4(2)	C17	C18	C19	C20	0.3(2)
C5	C6	C7	C2	0.88(19)	C18	C19	C20	C15	-0.79(19)
C7	C2	C3	C4	-0.88(17)	C20	C15	C16	C17	0.73(17)
C8	N1	C1	O1	-5.01(17)	C22	N2	C21	O2	5.51(17)
C8	N1	C1	C2	173.28(9)	C22	N2	C21	C15	-172.74(9)
C8	C9	C10	C11	-1.26(19)	C22	C23	C24	C25	1.11(18)
C9	C8	C13	C12	-2.26(18)	C23	C22	C27	C26	1.48(18)
C9	C10	C11	Cl1	178.97(10)	C23	C24	C25	Cl2	179.62(10)
C9	C10	C11	C12	-1.2(2)	C23	C24	C25	C26	0.6(2)
C10	C11	C12	C13	1.9(2)	C24	C25	C26	C27	-1.37(19)
C11	C12	C13	C8	-0.18(19)	C25	C26	C27	C22	0.31(19)
C13	C8	C9	C10	2.94(17)	C27	C22	C23	C24	-2.16(17)
C13	C8	C9	C14	-176.30(12)	C27	C22	C23	C28	176.76(11)

Table 6 Torsion Angles for 22mB_MLB3_Likhopotso_44_2_0f.

A	B	C	D	Angle/˚	A	B	C	D	Angle/˚
C14	C9	C10	C11	178.00(12)	C28	C23	C24	C25	-177.83(12)

Table 7 Hydrogen Atom Coordinates (Å×10^4) and Isotropic Displacement Parameters (Å^2×10^3) for 22mB_MLB3_Likhopotso_44_2_0f.

Atom	*X*	*Y*	*Z*	U(eq)
H3	3943.1	2788.81	5722.43	36
H4	4902.64	2344.02	7631.65	42
H5	7160.75	2511.01	8567.89	44
H6	8475.98	3112.19	7548.26	44
H7	7553.11	3543.76	5580.7	36
H10	3371.55	4739.11	716.49	50
H12	5615.13	3810.23	-1650.3	49
H13	6426.05	3480.54	571.7	41
H14A	3254.65	4339.32	3919.06	68
H14B	3798.19	4827.87	3341.5	68
H14C	4865.96	4490.96	4194.77	68
H16	-1054.03	2783.57	870.13	35
H17	-90.3	2339.91	-1032.4	42
H18	2160.29	2508.93	-1959.37	43
H19	3470.95	3111.91	-940.7	43
H20	2544.59	3545.25	1016.41	35
H24	-1630.4	4733.14	5893.24	43
H26	671.63	3808.43	8239.69	44
H27	1443.48	3479.53	6005.77	39
H28A	-187.27	4498.1	2411.59	59
H28B	-1289.38	4819.55	3272.84	59
H28C	-1778.37	4326.2	2681.55	59

Table 7 Hydrogen Atom Coordinates (Å×10^4) and Isotropic Displacement Parameters (Å^2×10^3) for 22mB_MLB3_Likhopotso_44_2_0f.

Atom	*X*	*Y*	*Z*	U(eq)
H1	6727(18)	3621(6)	3280(18)	39(4)
H2	1722(17)	3631(5)	3296(17)	37(4)

2. Crystallographic data for compound *N*-benzoyl-*N*-(5-methylpyridin-2-yl)benzamide 160i

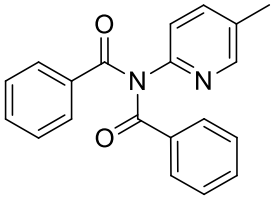

Table 1 Crystal data and structure refinement for 22mv_MLB11LikhoptsoLCM_42_2_0f.

Identification code	22mv_MLB11LikhoptsoLCM_42_2_0f
Empirical formula	$C_{20}H_{16}N_2O_2$
Formula weight	316.35
Temperature/K	173.00
Crystal system	Monoclinic
Space group	$P2_1/n$
a/Å	10.1691(3)
b/Å	9.0510(2)
c/Å	17.3180(5)
α/°	90
β/°	92.6950(10)
γ/°	90
Volume/Å^3	1592.19(7)
Z	4
ρ_{calc}g/cm^3	1.320
μ/mm^{-1}	0.086

F(000)	664.0
Crystal size/mm^3	0.312 × 0.269 × 0.152
Radiation	MoKα (λ = 0.71073)
2Θ range for data collection/°	6.028 to 56.61
Index ranges	-13 ≤ h ≤ 13, -12 ≤ k ≤ 12, -23 ≤ l ≤ 23
Reflections collected	47552
Independent reflections	3961 [R_{int} = 0.0466, R_{sigma} = 0.0206]
Data/restraints/parameters	3961/0/218
Goodness-of-fit on F^2	1.033
Final R indexes [I>=2σ (I)]	R_1 = 0.0417, wR_2 = 0.1012
Final R indexes [all data]	R_1 = 0.0515, wR_2 = 0.1079
Largest diff. peak/hole / e Å^{-3}	0.26/-0.24

Table 2 Fractional Atomic Coordinates (×10^4) and Equivalent Isotropic Displacement Parameters (Å^2×10^3) for 22mv_MLB11LikhoptsoLCM_42_2_0f. U_{eq} is defined as 1/3 of the trace of the orthogonalised U_{IJ} tensor.

Atom	*X*	*Y*	*Z*	U(eq)
O1	3467.8(9)	5575.0(12)	3070.7(6)	32.9(2)
O2	5857.3(9)	8613.3(10)	3254.1(6)	26.7(2)
N1	5668.1(10)	6109.8(11)	3190.2(6)	20.1(2)
N2	6316.4(10)	5156.9(11)	4416.9(6)	20.7(2)
C1	4397.8(12)	6191.0(14)	2800.7(7)	21.0(2)
C2	4302.3(12)	6935.3(13)	2033.6(7)	19.6(2)
C3	3047.5(13)	7270.8(15)	1724.1(8)	25.1(3)
C4	2881.7(13)	7862.1(15)	987.3(8)	28.1(3)
C5	3970.0(14)	8118.4(15)	552.5(7)	27.4(3)
C6	5226.7(13)	7777.1(15)	854.3(7)	26.4(3)
C7	5397.3(12)	7188.5(14)	1591.4(7)	21.9(2)
C8	6405.0(12)	7419.8(13)	3293.4(7)	19.6(2)

Table 2 Fractional Atomic Coordinates (×10^4) and Equivalent Isotropic Displacement Parameters (Å^2×10^3) for 22mv_MLB11LikhoptsoLCM_42_2_0f. U_{eq} is defined as 1/3 of the trace of the orthogonalised U_{IJ} tensor.

Atom	*X*	*Y*	*Z*	U(eq)
C9	7862.5(12)	7283.0(13)	3398.7(7)	19.3(2)
C10	8555.0(13)	8478.0(14)	3728.3(7)	22.8(3)
C11	9918.6(13)	8445.5(15)	3796.3(7)	26.3(3)
C12	10600.4(13)	7229.4(15)	3524.8(8)	27.1(3)
C13	9919.4(13)	6050.8(15)	3185.7(8)	25.6(3)
C14	8550.0(12)	6068.6(13)	3124.4(7)	22.1(2)
C15	5910.2(11)	4865.0(13)	3691.5(7)	18.1(2)
C16	5695.1(12)	3449.8(14)	3403.1(7)	22.3(3)
C17	5883.5(12)	2270.1(14)	3902.7(8)	23.4(3)
C18	6297.4(11)	2523.7(14)	4670.3(7)	21.4(2)
C19	6509.5(12)	3988.6(14)	4886.9(7)	21.9(2)
C20	6515.2(15)	1276.1(16)	5238.1(9)	32.8(3)

Table 3 Anisotropic Displacement Parameters (Å^2×10^3) for 22mv_MLB11LikhoptsoLCM_42_2_0f. The Anisotropic displacement factor exponent takes the form: $-2\pi^2[h^2a^{*2}U_{11}+2hka^*b^*U_{12}+\ldots]$.

Atom	U_{11}	U_{22}	U_{33}	U_{23}	U_{13}	U_{12}
O1	21.2(5)	41.9(6)	35.7(5)	14.8(5)	2.1(4)	-3.0(4)
O2	27.8(5)	19.1(4)	32.7(5)	-2.6(4)	-2.5(4)	3.7(4)
N1	19.9(5)	18.2(5)	21.9(5)	2.0(4)	-1.3(4)	-0.9(4)
N2	21.4(5)	21.1(5)	19.7(5)	-1.2(4)	0.5(4)	-0.3(4)
C1	18.5(5)	20.8(6)	23.7(6)	0.7(5)	0.7(4)	1.6(4)
C2	21.0(6)	17.2(5)	20.6(5)	-0.9(4)	0.2(4)	0.8(4)
C3	20.4(6)	27.2(6)	27.8(6)	1.9(5)	1.3(5)	2.4(5)
C4	25.5(6)	30.4(7)	27.7(6)	0.9(5)	-5.0(5)	5.4(5)
C5	36.2(7)	26.5(6)	19.5(6)	-0.6(5)	-0.6(5)	4.0(5)
C6	29.4(7)	27.5(7)	22.7(6)	-1.0(5)	6.7(5)	1.2(5)

Table 3 Anisotropic Displacement Parameters ($Å^2×10^3$) for 22mv_MLB11LikhoptsoLCM_42_2_0f. The Anisotropic displacement factor exponent takes the form: $-2π^2[h^2a^{*2}U_{11}+2hka^*b^*U_{12}+…]$.

Atom	U_{11}	U_{22}	U_{33}	U_{23}	U_{13}	U_{12}
C7	20.6(6)	21.3(6)	23.8(6)	-1.8(5)	0.9(4)	1.6(4)
C8	23.1(6)	17.4(5)	18.2(5)	0.0(4)	0.7(4)	-0.2(4)
C9	21.1(6)	18.6(5)	18.1(5)	3.7(4)	0.2(4)	-0.7(4)
C10	26.1(6)	20.5(6)	21.7(6)	0.3(5)	-0.7(5)	-1.2(5)
C11	26.5(6)	26.9(6)	25.0(6)	2.7(5)	-4.5(5)	-5.6(5)
C12	20.3(6)	32.4(7)	28.2(6)	9.2(5)	-2.3(5)	-0.3(5)
C13	25.5(6)	23.4(6)	28.1(6)	6.0(5)	3.9(5)	4.9(5)
C14	24.4(6)	17.5(5)	24.3(6)	2.2(5)	2.2(5)	-0.4(4)
C15	17.3(5)	18.0(5)	19.2(5)	0.9(4)	2.4(4)	0.4(4)
C16	26.1(6)	21.2(6)	19.5(5)	-2.9(5)	-1.4(5)	-0.6(5)
C17	23.9(6)	17.4(6)	28.9(6)	-1.9(5)	1.1(5)	-1.4(5)
C18	16.2(5)	23.4(6)	24.7(6)	3.8(5)	1.6(4)	-0.7(4)
C19	21.3(6)	25.4(6)	18.9(5)	0.5(5)	0.0(4)	-0.7(5)
C20	35.4(7)	28.3(7)	34.1(7)	10.4(6)	-5.5(6)	-5.0(6)

Table 4 Bond Lengths for 22mv_MLB11LikhoptsoLCM_42_2_0f.

Atom	Atom	Length/Å	Atom	Atom	Length/Å
O1	C1	1.2105(15)	C6	C7	1.3865(18)
O2	C8	1.2158(15)	C8	C9	1.4900(17)
N1	C1	1.4308(15)	C9	C10	1.3978(17)
N1	C8	1.4095(15)	C9	C14	1.3977(17)
N1	C15	1.4365(15)	C10	C11	1.3864(18)
N2	C15	1.3305(15)	C11	C12	1.394(2)
N2	C19	1.3432(16)	C12	C13	1.3872(19)
C1	C2	1.4887(17)	C13	C14	1.3917(18)
C2	C3	1.3941(17)	C15	C16	1.3884(17)

Table 4 Bond Lengths for 22mv_MLB11LikhoptsoLCM_42_2_0f.

Atom	Atom	Length/Å	Atom	Atom	Length/Å
C2	C7	1.3996(17)	C16	C17	1.3818(18)
C3	C4	1.3866(18)	C17	C18	1.3945(18)
C4	C5	1.387(2)	C18	C19	1.3920(18)
C5	C6	1.3925(19)	C18	C20	1.5068(18)

Table 5 Bond Angles for 22mv_MLB11LikhoptsoLCM_42_2_0f.

Atom	Atom	Atom	Angle/˚	Atom	Atom	Atom	Angle/˚
C1	N1	C15	116.77(10)	C10	C9	C8	117.70(11)
C8	N1	C1	118.64(10)	C10	C9	C14	119.79(11)
C8	N1	C15	120.54(10)	C14	C9	C8	122.30(11)
C15	N2	C19	116.48(11)	C11	C10	C9	120.06(12)
O1	C1	N1	119.92(11)	C10	C11	C12	119.96(12)
O1	C1	C2	122.26(11)	C13	C12	C11	120.24(12)
N1	C1	C2	117.61(10)	C12	C13	C14	120.08(12)
C3	C2	C1	117.50(11)	C13	C14	C9	119.86(12)
C3	C2	C7	119.43(11)	N2	C15	N1	116.85(10)
C7	C2	C1	122.83(11)	N2	C15	C16	124.02(11)
C4	C3	C2	120.49(12)	C16	C15	N1	119.12(10)
C3	C4	C5	119.90(12)	C17	C16	C15	118.22(11)
C4	C5	C6	120.05(12)	C16	C17	C18	119.76(11)
C7	C6	C5	120.25(12)	C17	C18	C20	121.82(12)
C6	C7	C2	119.88(11)	C19	C18	C17	116.72(11)
O2	C8	N1	120.06(11)	C19	C18	C20	121.46(12)
O2	C8	C9	122.08(11)	N2	C19	C18	124.77(11)
N1	C8	C9	117.74(10)				

Table 6 Torsion Angles for 22mv_MLB11LikhoptsoLCM_42_2_0f.

A	B	C	D	Angle/˚	A	B	C	D	Angle/˚
O1	C1	C2	C3	17.53(19)	C8	N1	C1	C2	52.10(15)
O1	C1	C2	C7	-156.86(13)	C8	N1	C15	N2	31.39(16)
O2	C8	C9	C10	22.95(17)	C8	N1	C15	C16	-149.49(12)
O2	C8	C9	C14	-151.76(12)	C8	C9	C10	C11	-176.08(11)
N1	C1	C2	C3	-167.80(11)	C8	C9	C14	C13	175.04(11)
N1	C1	C2	C7	17.81(17)	C9	C10	C11	C12	0.97(19)
N1	C8	C9	C10	-161.00(11)	C10	C9	C14	C13	0.45(18)
N1	C8	C9	C14	24.29(17)	C10	C11	C12	C13	0.08(19)
N1	C15	C16	C17	-177.47(11)	C11	C12	C13	C14	-0.87(19)
N2	C15	C16	C17	1.58(19)	C12	C13	C14	C9	0.60(18)
C1	N1	C8	O2	20.11(17)	C14	C9	C10	C11	-1.23(18)
C1	N1	C8	C9	-156.02(10)	C15	N1	C1	O1	24.44(17)
C1	N1	C15	N2	-125.71(12)	C15	N1	C1	C2	-150.36(10)
C1	N1	C15	C16	53.42(15)	C15	N1	C8	O2	-136.56(12)
C1	C2	C3	C4	-175.13(12)	C15	N1	C8	C9	47.31(15)
C1	C2	C7	C6	174.69(12)	C15	N2	C19	C18	-0.97(18)
C2	C3	C4	C5	0.2(2)	C15	C16	C17	C18	-0.91(18)
C3	C2	C7	C6	0.40(18)	C16	C17	C18	C19	-0.52(18)
C3	C4	C5	C6	0.2(2)	C16	C17	C18	C20	179.91(12)
C4	C5	C6	C7	-0.4(2)	C17	C18	C19	N2	1.55(19)
C5	C6	C7	C2	0.05(19)	C19	N2	C15	N1	178.42(10)
C7	C2	C3	C4	-0.54(19)	C19	N2	C15	C16	-0.66(18)
C8	N1	C1	O1	-133.10(13)	C20	C18	C19	N2	-178.89(12)

Table 7 Hydrogen Atom Coordinates (Å×10^4) and Isotropic Displacement Parameters (Å^2×10^3) for 22mv_MLB11LikhoptsoLCM_42_2_0f.

Atom	*X*	*y*	*Z*	U(eq)
H3	2300.45	7093.07	2020.16	30
H4	2023.99	8091.28	780.64	34
H5	3857.97	8527.07	48.43	33
H6	5969.95	7948.07	554.12	32
H7	6255.91	6957.54	1795.99	26
H10	8090.88	9313.14	3906.01	27
H11	10388.11	9251.4	4027.62	32
H12	11534.73	7207.92	3572.21	33
H13	10388.37	5230.44	2995.05	31
H14	8083.5	5257.16	2896.6	26
H16	5425.63	3296.54	2876.56	27
H17	5731.69	1289.87	3723.73	28
H19	6813.02	4175.68	5404.86	26
H20A	6135.61	365.18	5017.83	49
H20B	6089.94	1512.99	5718.96	49
H20C	7461.8	1138.64	5346.74	49

3. Crystallographic data for *N*-(6-methylpyridin-2-yl)benzamide 157k

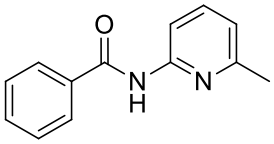

Table 1 Crystal data and structure refinement for 22mv_MLB6_Likoposo_LCM_41_2_0f.

Identification code	22mv_MLB6_Likoposo_LCM_41_2_0f
Empirical formula	$C_{13}H_{12}N_2O$
Formula weight	212.25
Temperature/K	173.00
Crystal system	Triclinic

Space group	P-1
a/Å	11.7887(7)
b/Å	13.8259(8)
c/Å	14.5433(8)
α/°	89.523(2)
β/°	77.410(2)
γ/°	75.932(2)
Volume/Å^3	2241.5(2)
Z	8
ρ_{calc}g/cm^3	1.258
μ/mm^{-1}	0.082
F(000)	896.0
Crystal size/mm^3	0.315 × 0.174 × 0.066
Radiation	MoKα (λ = 0.71073)
2Θ range for data collection/°	5.404 to 56.72
Index ranges	-15 ≤ h ≤ 15, -18 ≤ k ≤ 18, -19 ≤ l ≤ 19
Reflections collected	137386
Independent reflections	11185 [R_{int} = 0.0588, R_{sigma} = 0.0245]
Data/restraints/parameters	11185/0/581
Goodness-of-fit on F^2	1.102
Final R indexes [I>=2σ (I)]	R_1 = 0.0574, wR_2 = 0.1315
Final R indexes [all data]	R_1 = 0.0714, wR_2 = 0.1393
Largest diff. peak/hole / e Å^{-3}	0.30/-0.28

Table 2 Fractional Atomic Coordinates (×10^4) and Equivalent Isotropic Displacement Parameters (Å^2×10^3) for 22mv_MLB6_Likoposo_LCM_41_2_0f. U_{eq} is defined as 1/3 of the trace of the orthogonalised U_{IJ} tensor.

Atom	*X*	*Y*	*Z*	U(eq)
O1A	5117.6(10)	2286.5(9)	5765.8(9)	33.3(3)
N1A	5548.2(11)	820.2(10)	6513.7(9)	26.4(3)
C1A	4788.9(14)	1631.9(11)	6246.4(11)	26.0(3)
N2A	7304.5(12)	-289.1(10)	6607.4(9)	26.4(3)
C2	9221.1(15)	81.3(14)	6172.0(12)	34.9(4)
C2A	3484.8(14)	1667.2(11)	6581.4(12)	27.9(3)
C3A	2997.0(15)	1463.6(12)	7500.1(12)	30.9(3)
C4A	1772.6(16)	1532.0(14)	7775.3(14)	39.2(4)
C5A	1047.0(16)	1799.5(14)	7142.6(16)	44.0(5)
C6A	1523.0(17)	2009.2(16)	6236.1(16)	46.9(5)
C7A	2743.8(16)	1948.5(14)	5954.0(14)	39.1(4)
C8A	6806.3(13)	624.1(11)	6359.0(10)	24.1(3)
C9A	7462.6(15)	1313.3(13)	6014.0(12)	30.7(3)
C10A	8688.6(16)	1025.0(14)	5933.1(13)	36.3(4)
C12A	8504.3(14)	-561.3(12)	6504.1(11)	29.4(3)
C13A	9020.2(17)	-1595.1(14)	6782.4(15)	43.4(4)
O1B	5663.9(13)	-1390.0(12)	9906.8(9)	48.1(4)
N1B	5659.2(11)	-856.0(10)	8408.4(9)	26.0(3)
C1B	6113.8(14)	-1012.4(12)	9202.1(12)	28.9(3)
N2B	4429.7(11)	-863.8(9)	7393.0(9)	24.2(3)
C2B	7248.6(14)	-689.5(12)	9136.1(11)	25.4(3)
C3B	7413.5(14)	195.3(11)	8730.7(11)	25.2(3)
C4B	8483.3(15)	464.7(12)	8687.8(11)	29.5(3)
C5B	9390.0(15)	-152.1(14)	9037.4(12)	33.9(4)
C6B	9222.6(16)	-1025.8(14)	9458.4(13)	37.0(4)

Table 2 Fractional Atomic Coordinates (×10^4) and Equivalent Isotropic Displacement Parameters (Å^2×10^3) for 22mv_MLB6_Likoposo_LCM_41_2_0f. U_{eq} is defined as 1/3 of the trace of the orthogonalised U_{IJ} tensor.

Atom	*X*	*Y*	*Z*	U(eq)
C7B	8150.2(16)	-1288.2(13)	9516.3(12)	33.6(4)
C8B	4578.7(13)	-1024.8(11)	8274.2(11)	23.0(3)
C9B	3738.4(14)	-1306.8(12)	8984.9(11)	27.9(3)
C10B	2709.0(15)	-1442.1(13)	8753.8(13)	33.3(4)
C11B	2556.6(15)	-1311.1(13)	7842.8(13)	32.6(4)
C12B	3430.1(14)	-1017.5(11)	7177.5(11)	26.9(3)
C13B	3300.0(18)	-845.2(15)	6181.3(13)	39.6(4)
O1C	-1014.9(11)	2750.1(9)	9321.3(9)	34.0(3)
N1C	-900.6(11)	4172.4(9)	8525.0(9)	24.6(3)
C1C	-1388.9(13)	3387.1(11)	8796.0(10)	23.9(3)
N2C	338.5(12)	5230.0(10)	8385.9(9)	25.4(3)
C2C	-2457.2(13)	3361.2(11)	8406.3(11)	23.6(3)
C3C	-2562.1(15)	3663.9(12)	7503.5(11)	28.2(3)
C4C	-3592.2(17)	3639.7(13)	7199.2(12)	35.7(4)
C5C	-4503.8(17)	3307.3(14)	7777.8(14)	38.9(4)
C6C	-4388.0(15)	2978.4(14)	8661.5(13)	35.7(4)
C7C	-3369.1(14)	3007.4(12)	8975.0(12)	29.3(3)
C8C	127.4(13)	4376.2(11)	8739.8(10)	24.2(3)
C9C	848.1(15)	3760.7(13)	9260.0(13)	33.4(4)
C10C	1834.4(17)	4059.2(15)	9406.9(14)	40.3(4)
C11C	2060.0(16)	4943.6(14)	9058.8(13)	36.8(4)
C12C	1285.2(15)	5516.5(12)	8557.3(11)	28.6(3)
C13C	1461.6(18)	6497.6(14)	8187.3(13)	38.8(4)
O1D	9827.9(11)	-3690.8(10)	5064.9(8)	37.6(3)
N1D	9332.4(11)	-4188.4(9)	6577.1(9)	24.2(3)

Table 2 Fractional Atomic Coordinates (×10^4) and Equivalent Isotropic Displacement Parameters (Å^2×10^3) for 22mv_MLB6_Likoposo_LCM_41_2_0f. U_{eq} is defined as 1/3 of the trace of the orthogonalised U_{IJ} tensor.

Atom	*X*	*Y*	*Z*	U(eq)
C1D	10119.3(14)	-4049.9(11)	5773.6(11)	25.1(3)
N2D	7550.2(11)	-4078.8(9)	7634.0(9)	25.1(3)
C2D	11403.6(13)	-4338.8(11)	5845.3(10)	24.7(3)
C3D	11883.0(15)	-5213.6(12)	6247.5(11)	28.6(3)
C4D	13081.5(15)	-5444.4(13)	6297.7(12)	35.3(4)
C5D	13787.5(15)	-4794.9(16)	5964.7(13)	41.1(4)
C6D	13316.0(16)	-3922.1(16)	5556.0(13)	40.6(4)
C7D	12130.3(15)	-3705.0(13)	5482.0(12)	33.4(4)
C8D	8069.9(13)	-3953.3(11)	6741.2(11)	23.6(3)
C9D	7432.6(15)	-3628.2(13)	6049.9(12)	31.2(3)
C10D	6192.1(16)	-3402.5(14)	6321.4(13)	37.1(4)
C11D	5639.6(15)	-3504.9(13)	7242.5(13)	33.9(4)
C12D	6345.5(14)	-3853.3(12)	7882.4(12)	28.5(3)
C13D	5797.2(17)	-4003.8(16)	8889.1(13)	43.3(4)

Table 3 Anisotropic Displacement Parameters (Å^2×10^3) for 22mv_MLB6_Likoposo_LCM_41_2_0f. The Anisotropic displacement factor exponent takes the form: $-2\pi^2[h^2a^{*2}U_{11}+2hka^*b^*U_{12}+\ldots]$.

Atom	U_{11}	U_{22}	U_{33}	U_{23}	U_{13}	U_{12}
O1A	29.4(6)	29.3(6)	40.2(7)	13.6(5)	-5.3(5)	-7.8(5)
N1A	22.2(6)	26.0(6)	31.4(7)	9.3(5)	-5.3(5)	-7.6(5)
C1A	26.6(7)	24.7(7)	26.3(7)	4.4(6)	-5.6(6)	-6.1(6)
N2A	25.1(6)	26.6(6)	26.2(6)	1.2(5)	-5.2(5)	-4.4(5)
C2	21.9(7)	47.6(10)	31.4(8)	-0.3(7)	-2.5(6)	-4.7(7)
C2A	24.5(7)	22.7(7)	34.9(8)	6.9(6)	-5.1(6)	-4.6(6)
C3A	30.2(8)	27.8(8)	31.4(8)	1.1(6)	-3.2(6)	-4.5(6)
C4A	34.1(9)	35.5(9)	42.0(10)	-0.3(8)	5.6(8)	-9.5(7)

Table 3 Anisotropic Displacement Parameters ($Å^2×10^3$) for 22mv_MLB6_Likoposo_LCM_41_2_0f. The Anisotropic displacement factor exponent takes the form: $-2π^2[h^2a^{*2}U_{11}+2hka*b*U_{12}+…]$.

Atom	U_{11}	U_{22}	U_{33}	U_{23}	U_{13}	U_{12}
C5A	24.0(8)	36.8(10)	67.5(13)	6.9(9)	-3.5(8)	-6.7(7)
C6A	32.0(9)	46.7(11)	67.9(14)	26.1(10)	-21.4(9)	-12.1(8)
C7A	32.1(9)	41.1(10)	47.2(10)	21.9(8)	-13.1(8)	-11.3(8)
C8A	22.5(7)	27.8(7)	21.0(7)	1.2(6)	-3.8(5)	-4.9(6)
C9A	29.2(8)	31.3(8)	32.7(8)	7.0(7)	-5.9(6)	-10.7(7)
C10A	29.4(8)	45.7(10)	36.4(9)	8.7(8)	-4.7(7)	-16.6(8)
C12A	25.8(8)	32.8(8)	25.5(7)	-3.7(6)	-4.1(6)	-0.7(6)
C13A	32.6(9)	35.2(9)	55.3(12)	1.7(8)	-10.1(8)	5.1(7)
O1B	46.1(8)	75.6(10)	40.5(7)	33.3(7)	-21.3(6)	-39.1(7)
N1B	23.6(6)	32.8(7)	26.1(6)	9.7(5)	-7.5(5)	-13.9(5)
C1B	27.8(8)	32.9(8)	31.6(8)	11.2(7)	-11.2(6)	-14.0(6)
N2B	24.6(6)	22.6(6)	27.0(6)	2.6(5)	-7.5(5)	-7.2(5)
C2B	25.5(7)	29.3(8)	24.8(7)	5.3(6)	-8.9(6)	-10.8(6)
C3B	26.8(7)	25.6(7)	24.8(7)	2.9(6)	-7.2(6)	-7.7(6)
C4B	33.1(8)	29.4(8)	29.1(8)	0.3(6)	-5.6(6)	-14.5(7)
C5B	26.2(8)	45.2(10)	35.0(9)	-3.7(7)	-8.2(7)	-16.3(7)
C6B	31.1(9)	42.1(10)	42.2(10)	5.1(8)	-18.6(7)	-8.3(7)
C7B	35.6(9)	33.3(8)	38.1(9)	11.4(7)	-17.5(7)	-12.2(7)
C8B	21.6(7)	20.8(7)	28.1(7)	2.3(6)	-6.8(6)	-6.9(5)
C9B	27.5(8)	31.3(8)	26.9(7)	4.0(6)	-4.3(6)	-12.6(6)
C10B	25.8(8)	36.6(9)	39.3(9)	3.9(7)	-3.0(7)	-15.0(7)
C11B	26.4(8)	32.6(8)	44.3(10)	0.0(7)	-13.2(7)	-12.6(7)
C12B	28.1(8)	21.1(7)	33.3(8)	-1.5(6)	-11.6(6)	-4.9(6)
C13B	44.7(10)	44.3(10)	36.4(9)	0.7(8)	-20.0(8)	-13.7(8)
O1C	35.5(6)	32.3(6)	42.2(7)	17.9(5)	-19.2(5)	-14.3(5)
N1C	25.3(6)	24.9(6)	27.2(6)	9.0(5)	-10.5(5)	-8.9(5)

Table 3 Anisotropic Displacement Parameters ($Å^2×10^3$) for 22mv_MLB6_Likoposo_LCM_41_2_0f. The Anisotropic displacement factor exponent takes the form: $-2π^2[h^2a^{*2}U_{11}+2hka^*b^*U_{12}+…]$.

Atom	U_{11}	U_{22}	U_{33}	U_{23}	U_{13}	U_{12}
C1C	25.3(7)	22.5(7)	24.8(7)	4.3(6)	-6.0(6)	-7.1(6)
N2C	27.5(6)	26.4(6)	23.3(6)	2.0(5)	-3.9(5)	-9.9(5)
C2C	25.1(7)	20.3(7)	26.1(7)	2.3(5)	-6.5(6)	-6.0(6)
C3C	35.9(8)	24.9(7)	26.0(7)	3.2(6)	-8.3(6)	-10.4(6)
C4C	46.8(10)	35.7(9)	29.5(8)	2.4(7)	-19.3(8)	-10.0(8)
C5C	34.1(9)	43.2(10)	45.1(10)	-3.8(8)	-19.5(8)	-10.5(8)
C6C	27.9(8)	39.7(9)	42.0(10)	1.8(8)	-7.1(7)	-13.6(7)
C7C	28.7(8)	32.1(8)	29.3(8)	7.1(6)	-7.4(6)	-10.7(6)
C8C	24.1(7)	25.5(7)	24.3(7)	1.8(6)	-5.3(6)	-8.4(6)
C9C	33.8(9)	30.1(8)	42.2(9)	10.6(7)	-17.1(7)	-11.7(7)
C10C	36.8(9)	42.4(10)	49.7(11)	10.8(8)	-24.0(8)	-12.5(8)
C11C	32.7(9)	45.2(10)	39.9(9)	0.7(8)	-13.0(7)	-19.3(8)
C12C	32.5(8)	31.1(8)	23.8(7)	-1.2(6)	-2.1(6)	-14.6(7)
C13C	47.4(11)	36.8(9)	38.8(10)	3.8(7)	-8.5(8)	-24.0(8)
O1D	30.5(6)	51.0(8)	29.9(6)	16.0(5)	-9.5(5)	-5.5(5)
N1D	21.4(6)	26.0(6)	25.2(6)	7.5(5)	-7.6(5)	-3.8(5)
C1D	24.7(7)	23.5(7)	25.6(7)	5.2(6)	-5.0(6)	-4.0(6)
N2D	23.9(6)	23.4(6)	27.7(6)	3.3(5)	-5.7(5)	-5.6(5)
C2D	22.9(7)	27.8(7)	20.4(7)	2.1(6)	-2.5(5)	-2.7(6)
C3D	29.6(8)	25.7(7)	27.4(8)	1.9(6)	-5.1(6)	-2.4(6)
C4D	31.1(8)	34.9(9)	34.3(9)	1.8(7)	-9.7(7)	4.6(7)
C5D	21.4(8)	58.2(12)	37.9(9)	0.8(8)	-3.9(7)	-1.4(8)
C6D	27.9(8)	54.5(11)	39.0(10)	9.8(8)	-0.5(7)	-15.7(8)
C7D	28.7(8)	36.1(9)	32.0(8)	11.2(7)	-1.3(7)	-6.5(7)
C8D	23.1(7)	19.2(6)	28.5(7)	1.8(5)	-7.8(6)	-3.8(5)
C9D	28.3(8)	37.2(9)	30.3(8)	7.0(7)	-10.7(6)	-8.8(7)

Table 3 Anisotropic Displacement Parameters ($Å^2×10^3$) for 22mv_MLB6_Likoposo_LCM_41_2_0f. The Anisotropic displacement factor exponent takes the form: $-2π^2[h^2a^{*2}U_{11}+2hka*b*U_{12}+…]$.

Atom	U_{11}	U_{22}	U_{33}	U_{23}	U_{13}	U_{12}
C10D	29.1(8)	42.4(10)	43.9(10)	9.5(8)	-17.6(7)	-7.9(7)
C11D	21.4(7)	33.5(9)	46.3(10)	2.5(7)	-8.8(7)	-4.5(6)
C12D	24.8(7)	24.1(7)	34.7(8)	-0.2(6)	-4.0(6)	-4.6(6)
C13D	30.7(9)	55.6(12)	36.4(10)	2.4(8)	1.6(7)	-5.3(8)

Table 4 Bond Lengths for 22mv_MLB6_Likoposo_LCM_41_2_0f.

Atom	Atom	Length/Å	Atom	Atom	Length/Å
O1A	C1A	1.2246(19)	O1C	C1C	1.2249(18)
N1A	C1A	1.3667(19)	N1C	C1C	1.3651(19)
N1A	C8A	1.4085(19)	N1C	C8C	1.4066(19)
C1A	C2A	1.497(2)	C1C	C2C	1.497(2)
N2A	C8A	1.339(2)	N2C	C8C	1.3406(19)
N2A	C12A	1.347(2)	N2C	C12C	1.343(2)
C2	C10A	1.381(3)	C2C	C3C	1.397(2)
C2	C12A	1.384(3)	C2C	C7C	1.393(2)
C2A	C3A	1.390(2)	C3C	C4C	1.388(2)
C2A	C7A	1.387(2)	C4C	C5C	1.383(3)
C3A	C4A	1.391(2)	C5C	C6C	1.383(3)
C4A	C5A	1.378(3)	C6C	C7C	1.384(2)
C5A	C6A	1.374(3)	C8C	C9C	1.391(2)
C6A	C7A	1.390(3)	C9C	C10C	1.382(2)
C8A	C9A	1.393(2)	C10C	C11C	1.382(3)
C9A	C10A	1.381(2)	C11C	C12C	1.387(2)
C12A	C13A	1.501(2)	C12C	C13C	1.500(2)
O1B	C1B	1.2218(19)	O1D	C1D	1.2206(18)
N1B	C1B	1.3695(19)	N1D	C1D	1.3684(19)

Table 4 Bond Lengths for 22mv_MLB6_Likoposo_LCM_41_2_0f.

Atom	Atom	Length/Å	Atom	Atom	Length/Å
N1B	C8B	1.4032(19)	N1D	C8D	1.4102(19)
C1B	C2B	1.494(2)	C1D	C2D	1.496(2)
N2B	C8B	1.3405(19)	N2D	C8D	1.339(2)
N2B	C12B	1.3475(19)	N2D	C12D	1.344(2)
C2B	C3B	1.391(2)	C2D	C3D	1.387(2)
C2B	C7B	1.393(2)	C2D	C7D	1.393(2)
C3B	C4B	1.388(2)	C3D	C4D	1.389(2)
C4B	C5B	1.384(2)	C4D	C5D	1.383(3)
C5B	C6B	1.387(3)	C5D	C6D	1.387(3)
C6B	C7B	1.383(2)	C6D	C7D	1.384(2)
C8B	C9B	1.392(2)	C8D	C9D	1.391(2)
C9B	C10B	1.382(2)	C9D	C10D	1.386(2)
C10B	C11B	1.380(2)	C10D	C11D	1.379(3)
C11B	C12B	1.387(2)	C11D	C12D	1.388(2)
C12B	C13B	1.501(2)	C12D	C13D	1.501(2)

Table 5 Bond Angles for 22mv_MLB6_Likoposo_LCM_41_2_0f.

Atom	Atom	Atom	Angle/˚	Atom	Atom	Atom	Angle/˚
C1A	N1A	C8A	127.20(13)	C1C	N1C	C8C	127.80(13)
O1A	C1A	N1A	124.32(15)	O1C	C1C	N1C	124.31(14)
O1A	C1A	C2A	121.10(14)	O1C	C1C	C2C	121.24(14)
N1A	C1A	C2A	114.58(13)	N1C	C1C	C2C	114.44(12)
C8A	N2A	C12A	118.34(14)	C8C	N2C	C12C	118.19(14)
C10A	C2	C12A	118.88(15)	C3C	C2C	C1C	122.77(14)
C3A	C2A	C1A	122.24(15)	C7C	C2C	C1C	117.71(13)
C7A	C2A	C1A	118.04(15)	C7C	C2C	C3C	119.52(14)
C7A	C2A	C3A	119.67(15)	C4C	C3C	C2C	119.45(15)

Table 5 Bond Angles for 22mv_MLB6_Likoposo_LCM_41_2_0f.

Atom	Atom	Atom	Angle/˚	Atom	Atom	Atom	Angle/˚
C2A	C3A	C4A	119.54(16)	C5C	C4C	C3C	120.52(16)
C5A	C4A	C3A	120.31(17)	C4C	C5C	C6C	120.22(16)
C6A	C5A	C4A	120.38(17)	C5C	C6C	C7C	119.73(16)
C5A	C6A	C7A	119.86(18)	C6C	C7C	C2C	120.52(15)
C2A	C7A	C6A	120.23(17)	N2C	C8C	N1C	112.48(13)
N2A	C8A	N1A	112.70(13)	N2C	C8C	C9C	123.65(14)
N2A	C8A	C9A	123.39(14)	C9C	C8C	N1C	123.87(14)
C9A	C8A	N1A	123.89(14)	C10C	C9C	C8C	117.06(16)
C10A	C9A	C8A	117.23(15)	C9C	C10C	C11C	120.25(16)
C2	C10A	C9A	120.24(16)	C10C	C11C	C12C	118.76(16)
N2A	C12A	C2	121.90(15)	N2C	C12C	C11C	122.06(15)
N2A	C12A	C13A	116.30(15)	N2C	C12C	C13C	116.70(15)
C2	C12A	C13A	121.79(15)	C11C	C12C	C13C	121.23(15)
C1B	N1B	C8B	127.37(13)	C1D	N1D	C8D	127.28(12)
O1B	C1B	N1B	124.63(15)	O1D	C1D	N1D	124.64(14)
O1B	C1B	C2B	121.52(14)	O1D	C1D	C2D	121.50(14)
N1B	C1B	C2B	113.85(13)	N1D	C1D	C2D	113.81(12)
C8B	N2B	C12B	118.05(13)	C8D	N2D	C12D	118.23(13)
C3B	C2B	C1B	122.04(14)	C3D	C2D	C1D	122.10(14)
C3B	C2B	C7B	119.63(14)	C3D	C2D	C7D	119.86(15)
C7B	C2B	C1B	118.31(14)	C7D	C2D	C1D	118.03(14)
C4B	C3B	C2B	119.91(14)	C2D	C3D	C4D	119.70(16)
C5B	C4B	C3B	120.03(15)	C5D	C4D	C3D	120.11(16)
C4B	C5B	C6B	120.32(15)	C4D	C5D	C6D	120.47(16)
C7B	C6B	C5B	119.78(16)	C7D	C6D	C5D	119.44(17)
C6B	C7B	C2B	120.27(16)	C6D	C7D	C2D	120.34(16)
N2B	C8B	N1B	112.79(13)	N2D	C8D	N1D	112.75(13)

Table 5 Bond Angles for 22mv_MLB6_Likoposo_LCM_41_2_0f.

Atom	Atom	Atom	Angle/˚	Atom	Atom	Atom	Angle/˚
N2B	C8B	C9B	123.56(14)	N2D	C8D	C9D	123.59(14)
C9B	C8B	N1B	123.64(14)	C9D	C8D	N1D	123.67(14)
C10B	C9B	C8B	117.44(15)	C10D	C9D	C8D	117.16(16)
C11B	C10B	C9B	119.86(15)	C11D	C10D	C9D	120.10(16)
C10B	C11B	C12B	119.16(15)	C10D	C11D	C12D	118.91(15)
N2B	C12B	C11B	121.88(15)	N2D	C12D	C11D	121.98(15)
N2B	C12B	C13B	116.69(15)	N2D	C12D	C13D	116.61(15)
C11B	C12B	C13B	121.43(15)	C11D	C12D	C13D	121.41(15)

Table 6 Torsion Angles for 22mv_MLB6_Likoposo_LCM_41_2_0f.

A	B	C	D	Angle/˚	A	B	C	D	Angle/˚
O1A	C1A	C2A	C3A	-135.75(17)	O1C	C1C	C2C	C3C	-145.13(16)
O1A	C1A	C2A	C7A	41.9(2)	O1C	C1C	C2C	C7C	34.1(2)
N1A	C1A	C2A	C3A	44.8(2)	N1C	C1C	C2C	C3C	35.6(2)
N1A	C1A	C2A	C7A	-137.51(16)	N1C	C1C	C2C	C7C	-145.11(15)
N1A	C8A	C9A	C10A	177.61(15)	N1C	C8C	C9C	C10C	179.54(16)
C1A	N1A	C8A	N2A	-172.59(15)	C1C	N1C	C8C	N2C	-177.97(14)
C1A	N1A	C8A	C9A	9.4(3)	C1C	N1C	C8C	C9C	2.2(3)
C1A	C2A	C3A	C4A	178.47(15)	C1C	C2C	C3C	C4C	-178.55(15)
C1A	C2A	C7A	C6A	-178.90(17)	C1C	C2C	C7C	C6C	179.04(15)
N2A	C8A	C9A	C10A	-0.2(2)	N2C	C8C	C9C	C10C	-0.3(3)
C2A	C3A	C4A	C5A	0.0(3)	C2C	C3C	C4C	C5C	-0.8(3)
C3A	C2A	C7A	C6A	-1.2(3)	C3C	C2C	C7C	C6C	-1.7(2)
C3A	C4A	C5A	C6A	-0.5(3)	C3C	C4C	C5C	C6C	-1.1(3)
C4A	C5A	C6A	C7A	0.2(3)	C4C	C5C	C6C	C7C	1.7(3)
C5A	C6A	C7A	C2A	0.7(3)	C5C	C6C	C7C	C2C	-0.3(3)
C7A	C2A	C3A	C4A	0.8(3)	C7C	C2C	C3C	C4C	2.2(2)

Table 6 Torsion Angles for 22mv_MLB6_Likoposo_LCM_41_2_0f.

A	B	C	D	Angle/˚	A	B	C	D	Angle/˚
C8A	N1A	C1A	O1A	5.3(3)	C8C	N1C	C1C	O1C	3.7(3)
C8A	N1A	C1A	C2A	-175.31(14)	C8C	N1C	C1C	C2C	-177.11(14)
C8A	N2A	C12A	C2	1.5(2)	C8C	N2C	C12C	C11C	2.0(2)
C8A	N2A	C12A	C13A	-179.37(15)	C8C	N2C	C12C	C13C	-177.35(14)
C8A	C9A	C10A	C2	1.2(3)	C8C	C9C	C10C	C11C	1.2(3)
C10A	C2	C12A	N2A	-0.5(3)	C9C	C10C	C11C	C12C	-0.4(3)
C10A	C2	C12A	C13A	-179.63(17)	C10C	C11C	C12C	N2C	-1.2(3)
C12A	N2A	C8A	N1A	-179.17(13)	C10C	C11C	C12C	C13C	178.14(17)
C12A	N2A	C8A	C9A	-1.1(2)	C12C	N2C	C8C	N1C	178.86(13)
C12A	C2	C10A	C9A	-0.9(3)	C12C	N2C	C8C	C9C	-1.3(2)
O1B	C1B	C2B	C3B	-139.38(18)	O1D	C1D	C2D	C3D	-138.52(17)
O1B	C1B	C2B	C7B	39.0(3)	O1D	C1D	C2D	C7D	40.7(2)
N1B	C1B	C2B	C3B	41.4(2)	N1D	C1D	C2D	C3D	44.0(2)
N1B	C1B	C2B	C7B	-140.19(16)	N1D	C1D	C2D	C7D	-136.74(15)
N1B	C8B	C9B	C10B	179.64(15)	N1D	C8D	C9D	C10D	-178.50(15)
C1B	N1B	C8B	N2B	-175.56(15)	C1D	N1D	C8D	N2D	-173.20(14)
C1B	N1B	C8B	C9B	5.8(3)	C1D	N1D	C8D	C9D	6.9(2)
C1B	C2B	C3B	C4B	179.84(15)	C1D	C2D	C3D	C4D	-179.86(15)
C1B	C2B	C7B	C6B	179.02(16)	C1D	C2D	C7D	C6D	178.03(16)
N2B	C8B	C9B	C10B	1.2(2)	N2D	C8D	C9D	C10D	1.7(2)
C2B	C3B	C4B	C5B	0.8(2)	C2D	C3D	C4D	C5D	1.3(3)
C3B	C2B	C7B	C6B	-2.6(3)	C3D	C2D	C7D	C6D	-2.7(3)
C3B	C4B	C5B	C6B	-2.0(3)	C3D	C4D	C5D	C6D	-1.7(3)
C4B	C5B	C6B	C7B	0.9(3)	C4D	C5D	C6D	C7D	-0.1(3)
C5B	C6B	C7B	C2B	1.4(3)	C5D	C6D	C7D	C2D	2.3(3)
C7B	C2B	C3B	C4B	1.5(2)	C7D	C2D	C3D	C4D	0.9(2)
C8B	N1B	C1B	O1B	4.8(3)	C8D	N1D	C1D	O1D	0.1(3)

Table 6 Torsion Angles for 22mv_MLB6_Likoposo_LCM_41_2_0f.

A	B	C	D	Angle/˚	A	B	C	D	Angle/˚
C8B	N1B	C1B	C2B	-175.99(14)	C8D	N1D	C1D	C2D	177.44(14)
C8B	N2B	C12B	C11B	1.5(2)	C8D	N2D	C12D	C11D	0.4(2)
C8B	N2B	C12B	C13B	-179.11(14)	C8D	N2D	C12D	C13D	-179.98(15)
C8B	C9B	C10B	C11B	0.9(2)	C8D	C9D	C10D	C11D	-0.1(3)
C9B	C10B	C11B	C12B	-1.8(3)	C9D	C10D	C11D	C12D	-1.2(3)
C10B	C11B	C12B	N2B	0.5(2)	C10D	C11D	C12D	N2D	1.0(3)
C10B	C11B	C12B	C13B	-178.84(16)	C10D	C11D	C12D	C13D	-178.53(17)
C12B	N2B	C8B	N1B	179.01(13)	C12D	N2D	C8D	N1D	178.32(13)
C12B	N2B	C8B	C9B	-2.4(2)	C12D	N2D	C8D	C9D	-1.8(2)

Table 7 Hydrogen Atom Coordinates (Å×10^4) and Isotropic Displacement Parameters (Å^2×10^3) for 22mv_MLB6_Likoposo_LCM_41_2_0f.

Atom	*X*	*y*	*z*	U(eq)
H1A	5214	370.3	6815.95	32
H2	10065.13	-123.62	6109.53	42
H3A	3496.32	1279.09	7936.88	37
H4A	1435.13	1393.57	8402.39	47
H5A	212.71	1839.09	7334.36	53
H6A	1018.73	2195.28	5803.08	56
H7A	3071.93	2100.28	5329.15	47
H9A	7082.95	1954.94	5841.55	37
H10A	9167.18	1477.74	5712.21	44
H13A	8883.59	-1606.41	7471.24	65
H13B	9883.87	-1790.52	6506.96	65
H13C	8630.02	-2063.47	6550.78	65
H1B	6093.99	-623.24	7928.24	31
H3B	6794.73	614.59	8483.61	30

Table 7 Hydrogen Atom Coordinates (Å×10^4) and Isotropic Displacement Parameters (Å^2×10^3) for 22mv_MLB6_Likoposo_LCM_41_2_0f.

Atom	*X*	*y*	*z*	U(eq)
H4B	8593.06	1072.82	8418.21	35
H5B	10130.69	23.76	8988.84	41
H6B	9842.53	-1442.57	9706.13	44
H7B	8027.81	-1878.96	9816.52	40
H9B	3867.45	-1402.65	9605.21	33
H10B	2107.61	-1624.99	9220.97	40
H11B	1862.18	-1420.57	7673.51	39
H13D	2634.91	-262.47	6174.02	59
H13E	3136.02	-1434.4	5919.01	59
H13F	4044.24	-726.23	5800.41	59
H1C	-1273.83	4602.75	8173.61	30
H3C	-1933.58	3884.6	7101.16	34
H4C	-3671.99	3853.12	6588.82	43
H5C	-5211.66	3304.85	7567.54	47
H6C	-5005.42	2733.75	9051.45	43
H7C	-3290.96	2784.18	9582.91	35
H9C	670.08	3161.64	9503.45	40
H10C	2359.05	3655.19	9748.3	48
H11C	2733.35	5154.79	9161.18	44
H13G	1996.13	6386.58	7558.78	58
H13H	1819.25	6812.84	8613.85	58
H13I	684.79	6934.35	8147.51	58
H1D	9649.62	-4453.85	7043.47	29
H3D	11393.64	-5652.88	6487.59	34
H4D	13417.12	-6049.22	6561.09	42
H5D	14600.91	-4947.72	6016.36	49

Table 7 Hydrogen Atom Coordinates (Å×10^4) and Isotropic Displacement Parameters (Å^2×10^3) for 22mv_MLB6_Likoposo_LCM_41_2_0f.

Atom	*X*	*y*	*z*	U(eq)
H6D	13802.75	-3477.11	5328.75	49
H7D	11810.62	-3120.91	5182	40
H9D	7830.79	-3563.58	5418.6	37
H10D	5721.69	-3176.83	5871.97	45
H11D	4789.52	-3339.68	7436.17	41
H13J	5777.47	-3427.86	9285.88	65
H13K	6277.82	-4610.07	9101.61	65
H13L	4978.16	-4071.67	8937.15	65

4. Crystallographic data for *N*-(6-chloropyridin-2-yl)benzamide 157m

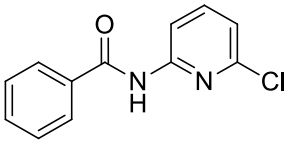

Table 1 Crystal data and structure refinement for 22mvMLB8Likhopotso_LCM_43_2_0f.

Identification code	22mvMLB8Likhopotso_LCM_43_2_0f
Empirical formula	$C_{12}H_9ClN_2O$
Formula weight	232.66
Temperature/K	173.00
Crystal system	Triclinic
Space group	P-1
a/Å	7.9799(4)
b/Å	12.0047(7)
c/Å	12.9895(6)
α/°	108.4629(17)
β/°	98.4142(15)
γ/°	106.8478(15)
Volume/Å^3	1090.09(10)

Z	4
ρ_{calc}g/cm^3	1.418
μ/mm^{-1}	0.328
F(000)	480.0
Crystal size/mm^3	0.471 × 0.271 × 0.148
Radiation	MoKα (λ = 0.71073)
2Θ range for data collection/°	5.482 to 56.83
Index ranges	-10 ≤ h ≤ 10, -16 ≤ k ≤ 16, -17 ≤ l ≤ 17
Reflections collected	63540
Independent reflections	5464 [R_{int} = 0.0560, R_{sigma} = 0.0249]
Data/restraints/parameters	5464/0/297
Goodness-of-fit on F^2	1.048
Final R indexes [I>=2σ (I)]	R_1 = 0.0351, wR_2 = 0.0712
Final R indexes [all data]	R_1 = 0.0518, wR_2 = 0.0788
Largest diff. peak/hole / e Å^{-3}	0.26/-0.27

Table 2 Fractional Atomic Coordinates (×10^4) and Equivalent Isotropic Displacement Parameters (Å^2×10^3) for 22mvMLB8Likhopotso_LCM_43_2_0f. U_{eq} is defined as 1/3 of the trace of the orthogonalised U_{IJ} tensor.

Atom	*X*	*Y*	*z*	U(eq)
Cl1A	-784.7(5)	1757.0(4)	5781.9(4)	38.72(11)
O1A	4128.4(15)	6653.4(11)	4699.2(9)	35.9(3)
N1A	3638.9(16)	5599.1(11)	5872.3(10)	24.0(2)
C1A	4526.8(19)	6603.9(13)	5625.9(12)	24.7(3)
N2A	1453.0(15)	3776.2(11)	5695.1(10)	23.9(2)
C2A	6039.9(19)	7665.4(13)	6552.8(12)	23.6(3)
C3A	7280.2(19)	8504.2(14)	6242.6(13)	27.9(3)
C4A	8722(2)	9506.0(14)	7050.3(14)	31.9(3)
C5A	8919(2)	9698.2(14)	8176.1(14)	32.5(3)

Table 2 Fractional Atomic Coordinates (×10^4) and Equivalent Isotropic Displacement Parameters (Å^2×10^3) for 22mvMLB8Likhopotso_LCM_43_2_0f. U_{eq} is defined as 1/3 of the trace of the orthogonalised U_{IJ} tensor.

Atom	*X*	*Y*	*z*	U(eq)
C6A	7679(2)	8886.4(15)	8495.3(13)	33.4(3)
C7A	6249(2)	7865.0(14)	7689.4(13)	29.5(3)
C8A	2098.6(18)	4553.7(13)	5177.6(12)	23.1(3)
C9A	1298(2)	4329.6(15)	4065.5(12)	29.9(3)
C10A	-254(2)	3275.6(15)	3496.1(13)	32.6(3)
C11A	-959(2)	2471.8(14)	4014.8(13)	30.2(3)
C12A	-18.1(19)	2779.6(13)	5104.6(12)	26.0(3)
Cl1B	3589.4(6)	-103.4(4)	8786.1(3)	33.52(10)
O1B	4402.5(13)	5281.0(9)	8157.4(9)	26.7(2)
N1B	2566.4(16)	3591.7(11)	8407.4(10)	23.8(2)
C1B	3045.9(18)	4782.1(12)	8415.5(11)	20.7(3)
N2B	3160.2(15)	1855.1(10)	8492.7(9)	20.9(2)
C2B	1798.8(18)	5456.8(13)	8786.4(11)	21.3(3)
C3B	2560(2)	6740.8(13)	9425.8(12)	26.1(3)
C4B	1453(2)	7408.8(14)	9770.8(13)	32.2(3)
C5B	-414(2)	6800.9(15)	9456.5(13)	32.0(3)
C6B	-1182(2)	5523.4(16)	8810.0(14)	32.1(3)
C7B	-77.1(19)	4844.6(14)	8482.6(12)	26.7(3)
C8B	3411.8(17)	2718.0(12)	8025.0(11)	20.4(3)
C9B	4356(2)	2729.6(14)	7207.0(12)	26.7(3)
C10B	5096(2)	1805.3(15)	6876.5(13)	30.3(3)
C11B	4885(2)	910.6(14)	7356.6(12)	27.7(3)
C12B	3896.6(18)	992.2(13)	8147.0(11)	22.0(3)

Table 3 Anisotropic Displacement Parameters ($Å^2×10^3$) for 22mvMLB8Likhopotso_LCM_43_2_0f. The Anisotropic displacement factor exponent takes the form: $-2π^2[h^2a^{*2}U_{11}+2hka^*b^*U_{12}+…]$.

Atom	U_{11}	U_{22}	U_{33}	U_{23}	U_{13}	U_{12}
Cl1A	36.3(2)	33.1(2)	43.8(2)	19.82(18)	8.88(17)	3.25(16)
O1A	40.2(6)	40.5(6)	29.7(6)	21.1(5)	10.7(5)	8.7(5)
N1A	27.0(6)	24.2(6)	22.1(6)	11.3(5)	5.8(5)	8.5(5)
C1A	27.4(7)	26.4(7)	28.3(7)	14.1(6)	13.8(6)	13.4(6)
N2A	25.0(6)	23.2(6)	26.0(6)	10.4(5)	7.8(5)	10.1(5)
C2A	26.5(7)	22.4(7)	29.4(7)	12.2(6)	12.9(6)	14.0(6)
C3A	28.6(7)	30.3(8)	34.8(8)	18.0(6)	15.5(6)	15.1(6)
C4A	27.6(7)	26.6(8)	47.4(9)	17.6(7)	15.4(7)	11.3(6)
C5A	30.1(8)	23.8(7)	41.1(9)	6.8(7)	8.5(7)	12.6(6)
C6A	41.5(9)	29.4(8)	29.2(8)	8.1(6)	11.3(7)	15.0(7)
C7A	37.4(8)	24.6(7)	30.2(8)	11.7(6)	15.9(6)	11.3(6)
C8A	24.8(7)	24.3(7)	23.9(7)	9.6(6)	8.5(5)	12.5(6)
C9A	36.4(8)	32.2(8)	24.2(7)	12.1(6)	8.6(6)	14.8(7)
C10A	37.0(8)	35.2(8)	23.1(7)	7.5(6)	2.7(6)	15.9(7)
C11A	26.8(7)	27.7(8)	30.1(8)	4.6(6)	4.2(6)	9.7(6)
C12A	26.0(7)	23.9(7)	31.0(8)	10.2(6)	9.7(6)	12.0(6)
Cl1B	48.6(2)	32.7(2)	34.0(2)	20.41(16)	15.97(17)	24.42(17)
O1B	23.3(5)	26.1(5)	33.7(6)	14.0(4)	10.7(4)	8.3(4)
N1B	27.0(6)	23.9(6)	30.0(6)	14.6(5)	16.0(5)	13.3(5)
C1B	22.0(6)	21.0(7)	18.5(6)	7.3(5)	3.4(5)	7.9(5)
N2B	22.5(5)	20.8(6)	20.3(5)	7.8(4)	5.8(4)	8.9(4)
C2B	23.8(6)	23.3(7)	19.9(6)	10.3(5)	6.4(5)	10.5(5)
C3B	27.8(7)	24.4(7)	25.0(7)	8.8(6)	6.8(6)	8.5(6)
C4B	45.8(9)	24.3(7)	30.8(8)	10.1(6)	14.7(7)	16.6(7)
C5B	41.5(9)	37.7(9)	34.0(8)	19.6(7)	19.6(7)	27.3(7)
C6B	26.2(7)	40.3(9)	37.1(8)	18.5(7)	10.7(6)	16.8(7)

Table 3 Anisotropic Displacement Parameters ($Å^2×10^3$) for 22mvMLB8Likhopotso_LCM_43_2_0f. The Anisotropic displacement factor exponent takes the form: $-2π^2[h^2a^{*2}U_{11}+2hka*b*U_{12}+…]$.

Atom	U_{11}	U_{22}	U_{33}	U_{23}	U_{13}	U_{12}
C7B	25.2(7)	25.0(7)	30.1(8)	10.1(6)	7.3(6)	9.5(6)
C8B	20.8(6)	19.7(6)	21.2(6)	7.4(5)	5.2(5)	8.2(5)
C9B	31.7(7)	28.8(8)	27.0(7)	14.6(6)	14.2(6)	13.8(6)
C10B	33.2(8)	35.7(8)	29.5(8)	13.4(6)	18.1(6)	17.0(7)
C11B	29.7(7)	28.8(8)	29.0(8)	9.2(6)	11.2(6)	17.0(6)
C12B	23.6(6)	21.8(7)	20.7(6)	8.7(5)	2.8(5)	8.8(5)

Table 4 Bond Lengths for 22mvMLB8Likhopotso_LCM_43_2_0f.

Atom	Atom	Length/Å	Atom	Atom	Length/Å
Cl1A	C12A	1.7497(15)	Cl1B	C12B	1.7446(14)
O1A	C1A	1.2238(17)	O1B	C1B	1.2249(16)
N1A	C1A	1.3693(18)	N1B	C1B	1.3642(17)
N1A	C8A	1.4014(18)	N1B	C8B	1.4072(17)
C1A	C2A	1.497(2)	C1B	C2B	1.4963(18)
N2A	C8A	1.3448(18)	N2B	C8B	1.3402(17)
N2A	C12A	1.3187(18)	N2B	C12B	1.3250(17)
C2A	C3A	1.3971(19)	C2B	C3B	1.3905(19)
C2A	C7A	1.395(2)	C2B	C7B	1.3937(19)
C3A	C4A	1.384(2)	C3B	C4B	1.386(2)
C4A	C5A	1.384(2)	C4B	C5B	1.386(2)
C5A	C6A	1.385(2)	C5B	C6B	1.386(2)
C6A	C7A	1.388(2)	C6B	C7B	1.389(2)
C8A	C9A	1.397(2)	C8B	C9B	1.3906(18)
C9A	C10A	1.383(2)	C9B	C10B	1.384(2)
C10A	C11A	1.382(2)	C10B	C11B	1.386(2)
C11A	C12A	1.379(2)	C11B	C12B	1.3801(19)

Table 5 Bond Angles for 22mvMLB8Likhopotso_LCM_43_2_0f.

Atom	Atom	Atom	Angle/˚	Atom	Atom	Atom	Angle/˚
C1A	N1A	C8A	126.99(12)	C1B	N1B	C8B	126.95(12)
O1A	C1A	N1A	122.75(14)	O1B	C1B	N1B	123.34(12)
O1A	C1A	C2A	120.46(13)	O1B	C1B	C2B	121.79(12)
N1A	C1A	C2A	116.79(12)	N1B	C1B	C2B	114.85(11)
C12A	N2A	C8A	116.65(12)	C12B	N2B	C8B	116.24(11)
C3A	C2A	C1A	117.03(13)	C3B	C2B	C1B	117.99(12)
C7A	C2A	C1A	123.79(13)	C3B	C2B	C7B	119.98(13)
C7A	C2A	C3A	119.17(14)	C7B	C2B	C1B	122.01(12)
C4A	C3A	C2A	120.48(14)	C4B	C3B	C2B	119.99(14)
C5A	C4A	C3A	119.97(14)	C5B	C4B	C3B	119.93(14)
C4A	C5A	C6A	120.06(15)	C6B	C5B	C4B	120.35(14)
C5A	C6A	C7A	120.35(15)	C5B	C6B	C7B	119.93(14)
C6A	C7A	C2A	119.94(14)	C6B	C7B	C2B	119.80(14)
N2A	C8A	N1A	112.83(12)	N2B	C8B	N1B	113.60(11)
N2A	C8A	C9A	122.86(13)	N2B	C8B	C9B	123.68(12)
C9A	C8A	N1A	124.30(13)	C9B	C8B	N1B	122.68(12)
C10A	C9A	C8A	117.65(14)	C10B	C9B	C8B	117.64(13)
C11A	C10A	C9A	120.57(14)	C9B	C10B	C11B	120.14(13)
C12A	C11A	C10A	116.21(14)	C12B	C11B	C10B	116.51(13)
N2A	C12A	Cl1A	115.68(11)	N2B	C12B	Cl1B	115.47(10)
N2A	C12A	C11A	126.03(14)	N2B	C12B	C11B	125.78(13)
C11A	C12A	Cl1A	118.27(12)	C11B	C12B	Cl1B	118.74(11)

Table 6 Torsion Angles for 22mvMLB8Likhopotso_LCM_43_2_0f.

A	B	C	D	Angle/˚	A	B	C	D	Angle/˚
O1A	C1A	C2A	C3A	-18.3(2)	O1B	C1B	C2B	C3B	-35.69(19)
O1A	C1A	C2A	C7A	160.65(14)	O1B	C1B	C2B	C7B	142.44(14)
N1A	C1A	C2A	C3A	161.71(12)	N1B	C1B	C2B	C3B	143.31(13)
N1A	C1A	C2A	C7A	-19.4(2)	N1B	C1B	C2B	C7B	-38.57(18)
N1A	C8A	C9A	C10A	-178.01(13)	N1B	C8B	C9B	C10B	-178.48(13)
C1A	N1A	C8A	N2A	-174.63(13)	C1B	N1B	C8B	N2B	155.45(13)
C1A	N1A	C8A	C9A	5.2(2)	C1B	N1B	C8B	C9B	-26.9(2)
C1A	C2A	C3A	C4A	-179.66(13)	C1B	C2B	C3B	C4B	178.83(13)
C1A	C2A	C7A	C6A	-179.00(14)	C1B	C2B	C7B	C6B	-177.38(13)
N2A	C8A	C9A	C10A	1.8(2)	N2B	C8B	C9B	C10B	-1.1(2)
C2A	C3A	C4A	C5A	-1.5(2)	C2B	C3B	C4B	C5B	-1.4(2)
C3A	C2A	C7A	C6A	-0.1(2)	C3B	C2B	C7B	C6B	0.7(2)
C3A	C4A	C5A	C6A	0.3(2)	C3B	C4B	C5B	C6B	0.8(2)
C4A	C5A	C6A	C7A	1.0(2)	C4B	C5B	C6B	C7B	0.6(2)
C5A	C6A	C7A	C2A	-1.1(2)	C5B	C6B	C7B	C2B	-1.3(2)
C7A	C2A	C3A	C4A	1.4(2)	C7B	C2B	C3B	C4B	0.7(2)
C8A	N1A	C1A	O1A	-5.7(2)	C8B	N1B	C1B	O1B	-5.8(2)
C8A	N1A	C1A	C2A	174.32(12)	C8B	N1B	C1B	C2B	175.24(12)
C8A	N2A	C12A	Cl1A	177.94(10)	C8B	N2B	C12B	Cl1B	178.82(10)
C8A	N2A	C12A	C11A	-0.7(2)	C8B	N2B	C12B	C11B	0.0(2)
C8A	C9A	C10A	C11A	-0.8(2)	C8B	C9B	C10B	C11B	0.0(2)
C9A	C10A	C11A	C12A	-0.8(2)	C9B	C10B	C11B	C12B	1.0(2)
C10A	C11A	C12A	Cl1A	-177.02(11)	C10B	C11B	C12B	Cl1B	-179.79(11)
C10A	C11A	C12A	N2A	1.6(2)	C10B	C11B	C12B	N2B	-1.0(2)
C12A	N2A	C8A	N1A	178.77(12)	C12B	N2B	C8B	N1B	178.71(12)
C12A	N2A	C8A	C9A	-1.1(2)	C12B	N2B	C8B	C9B	1.1(2)

Table 7 Hydrogen Atom Coordinates (Å×10^4) and Isotropic Displacement Parameters (Å^2×10^3) for 22mvMLB8Likhopotso_LCM_43_2_0f.

Atom	*X*	*y*	*z*	U(eq)
H3A	7133.03	8386.26	5471.78	33
H4A	9576.01	10061.3	6831.74	38
H5A	9905.36	10387.74	8730.61	39
H6A	7807.43	9029.07	9269.8	40
H7A	5414.22	7302.63	7911.91	35
H9A	1801.32	4881.77	3712.87	36
H10A	-840.07	3102.54	2741.88	39
H11A	-2031.06	1748.33	3641.71	36
H3B	3837.17	7160.15	9626.3	31
H4B	1973.73	8282.25	10222.1	39
H5B	-1171.16	7262.34	9685.34	38
H6B	-2462.7	5112.6	8591.07	39
H7B	-598.49	3965.7	8052.98	32
H9B	4487.95	3349.8	6886.41	32
H10B	5748.93	1784.18	6319.36	36
H11B	5395.48	274.54	7152.32	33
H1B	1770(20)	3362(16)	8740(15)	33(5)
H1A	4020(20)	5602(16)	6525(15)	34(5)

5. Crystallographic data for *N*-(6-bromopyridin-2-yl)-3-methoxybenzamide 158l

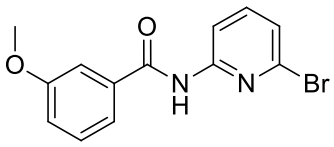

Table 1 Crystal data and structure refinement for 22mv_MLB10_LikhopotsoLCM_37_2f.

Identification code	22mv_MLB10_LikhopotsoLCM_37_2f
Empirical formula	$C_{13}H_{13}BrN_2O_3$

Formula weight	325.16
Temperature/K	173.00
Crystal system	Orthorhombic
Space group	Pbca
a/Å	7.30320(10)
b/Å	13.7187(3)
c/Å	25.8817(5)
α/°	90
β/°	90
γ/°	90
Volume/Å^3	2593.10(8)
Z	8
ρ_{calc}g/cm^3	1.666
μ/mm^{-1}	3.176
F(000)	1312.0
Crystal size/mm^3	0.302 × 0.28 × 0.266
Radiation	MoKα (λ = 0.71073)
2Θ range for data collection/°	5.94 to 56.592
Index ranges	-9 ≤ h ≤ 8, -18 ≤ k ≤ 18, -34 ≤ l ≤ 34
Reflections collected	55908
Independent reflections	3220 [R_{int} = 0.0307, R_{sigma} = 0.0121]
Data/restraints/parameters	3220/0/180
Goodness-of-fit on F^2	1.078
Final R indexes [I>=2σ (I)]	R_1 = 0.0250, wR_2 = 0.0627
Final R indexes [all data]	R_1 = 0.0317, wR_2 = 0.0663
Largest diff. peak/hole / e Å^{-3}	0.39/-0.69

Table 2 Fractional Atomic Coordinates (×10^4) and Equivalent Isotropic Displacement Parameters (Å^2×10^3) for 22mv_MLB10_LikhopotsoLCM_37_2f. U_{eq} is defined as 1/3 of the trace of the orthogonalised U_{IJ} tensor.

Atom	*X*	*Y*	*Z*	U(eq)
Br1	7476.8(3)	4817.7(2)	7145.0(2)	28.29(7)
O1	5100.0(15)	8547.9(7)	5482.8(4)	19.7(2)
N1	5882.3(18)	6963.3(9)	5651.1(5)	16.4(2)
C1	5471(2)	7718.5(10)	5331.1(5)	15.4(3)
O2	6330.7(17)	8684.8(8)	3519.4(4)	25.2(3)
N2	6510.2(17)	6110.4(9)	6384.7(5)	17.3(2)
C2	5465.2(19)	7473.0(10)	4768.3(6)	15.1(3)
C3	5971(2)	8206.3(10)	4419.3(5)	16.0(3)
C4	5867(2)	8025.3(11)	3892.8(6)	18.5(3)
C5	5244(2)	7121.8(12)	3713.7(6)	22.2(3)
C6	4738(2)	6404.7(11)	4060.6(6)	21.6(3)
C7	4855(2)	6571.5(11)	4591.4(6)	18.2(3)
C8	6806(3)	9643.0(12)	3686.0(6)	29.8(4)
C9	5855(2)	6951.0(11)	6191.9(5)	15.8(3)
C10	5184(2)	7700.1(11)	6501.7(6)	20.9(3)
C11	5199(3)	7559.4(12)	7031.9(6)	24.4(3)
C12	5884(2)	6703.4(12)	7242.9(6)	23.6(3)
C13	6513(2)	6021.8(11)	6893.2(6)	19.4(3)
O3	7704.9(15)	5312.7(8)	5142.6(5)	22.4(2)

Table 3 Anisotropic Displacement Parameters ($Å^2×10^3$) for 22mv_MLB10_LikhopotsoLCM_37_2f. The Anisotropic displacement factor exponent takes the form: $-2π^2[h^2a^{*2}U_{11}+2hka^*b^*U_{12}+…]$.

Atom	U_{11}	U_{22}	U_{33}	U_{23}	U_{13}	U_{12}
Br1	41.66(12)	22.28(11)	20.94(10)	6.32(6)	-2.92(7)	7.84(7)
O1	27.7(6)	14.4(5)	17.0(5)	-0.2(4)	-0.6(4)	2.2(4)
N1	22.8(6)	13.0(6)	13.2(6)	0.0(5)	0.8(5)	2.9(5)
C1	14.9(7)	15.8(7)	15.5(7)	1.5(5)	0.1(5)	-1.4(5)
O2	41.8(7)	20.5(6)	13.3(5)	1.3(4)	3.1(5)	-1.5(5)
N2	20.8(6)	15.3(6)	15.7(6)	1.4(5)	-0.6(5)	0.5(5)
C2	14.5(7)	15.9(6)	15.1(6)	0.2(5)	-1.1(5)	1.8(5)
C3	18.6(7)	14.6(6)	14.8(7)	0.0(5)	-0.3(5)	0.6(5)
C4	20.5(7)	18.9(7)	16.0(7)	0.8(6)	0.8(5)	2.4(6)
C5	28.2(8)	23.2(8)	15.3(7)	-4.9(6)	-3.3(6)	2.0(6)
C6	23.1(8)	18.3(7)	23.3(7)	-5.7(6)	-4.0(6)	-0.2(6)
C7	17.8(7)	16.2(7)	20.4(7)	1.3(6)	-0.8(5)	-0.2(5)
C8	48.4(11)	20.2(8)	20.9(8)	3.4(6)	4.8(7)	-2.9(8)
C9	16.9(7)	16.1(7)	14.4(6)	0.9(5)	0.2(5)	-2.3(5)
C10	28.0(8)	15.5(7)	19.3(7)	0.9(5)	2.7(6)	2.0(6)
C11	34.3(9)	19.2(7)	19.8(7)	-3.4(6)	4.4(7)	1.4(7)
C12	34.4(9)	22.5(8)	13.9(7)	0.6(6)	1.0(6)	-1.1(7)
C13	23.8(8)	16.0(7)	18.4(7)	3.8(6)	-1.3(6)	-0.9(6)
O3	23.9(6)	17.3(5)	25.9(6)	3.0(4)	2.3(4)	0.1(4)

Table 4 Bond Lengths for 22mv_MLB10_LikhopotsoLCM_37_2f.

Atom	Atom	Length/Å	Atom	Atom	Length/Å
Br1	C13	1.9102(15)	C2	C7	1.392(2)
O1	C1	1.2339(18)	C3	C4	1.387(2)
N1	C1	1.3599(18)	C4	C5	1.399(2)
N1	C9	1.3999(18)	C5	C6	1.382(2)

Table 4 Bond Lengths for 22mv_MLB10_LikhopotsoLCM_37_2f.

Atom	Atom	Length/Å	Atom	Atom	Length/Å
C1	C2	1.495(2)	C6	C7	1.395(2)
O2	C4	1.3663(18)	C9	C10	1.393(2)
O2	C8	1.426(2)	C10	C11	1.386(2)
N2	C9	1.3444(19)	C11	C12	1.388(2)
N2	C13	1.3216(19)	C12	C13	1.380(2)
C2	C3	1.402(2)			

Table 5 Bond Angles for 22mv_MLB10_LikhopotsoLCM_37_2f.

Atom	Atom	Atom	Angle/˚	Atom	Atom	Atom	Angle/˚
C1	N1	C9	127.96(13)	C6	C5	C4	120.15(14)
O1	C1	N1	123.86(13)	C5	C6	C7	120.43(14)
O1	C1	C2	121.15(13)	C2	C7	C6	119.28(14)
N1	C1	C2	114.99(12)	N2	C9	N1	112.12(13)
C4	O2	C8	117.19(12)	N2	C9	C10	122.99(13)
C13	N2	C9	116.68(13)	C10	C9	N1	124.87(14)
C3	C2	C1	117.74(13)	C11	C10	C9	117.67(14)
C7	C2	C1	121.44(13)	C10	C11	C12	120.69(15)
C7	C2	C3	120.67(14)	C13	C12	C11	115.78(14)
C4	C3	C2	119.35(14)	N2	C13	Br1	114.83(11)
O2	C4	C3	124.24(14)	N2	C13	C12	126.18(14)
O2	C4	C5	115.66(13)	C12	C13	Br1	118.99(11)
C3	C4	C5	120.11(14)				

Table 6 Torsion Angles for 22mv_MLB10_LikhopotsoLCM_37_2f.

A	B	C	D	Angle/˚	A	B	C	D	Angle/˚
O1	C1	C2	C3	32.4(2)	C4	C5	C6	C7	-0.4(2)
O1	C1	C2	C7	-143.11(15)	C5	C6	C7	C2	0.8(2)

Table 6 Torsion Angles for 22mv_MLB10_LikhopotsoLCM_37_2f.

A	B	C	D	Angle/˚	A	B	C	D	Angle/˚
N1	C1	C2	C3	-148.56(14)	C7	C2	C3	C4	-0.3(2)
N1	C1	C2	C7	35.94(19)	C8	O2	C4	C3	-5.3(2)
N1	C9	C10	C11	177.84(15)	C8	O2	C4	C5	174.25(16)
C1	N1	C9	N2	-173.99(14)	C9	N1	C1	O1	4.4(2)
C1	N1	C9	C10	7.9(2)	C9	N1	C1	C2	-174.64(13)
C1	C2	C3	C4	-175.83(13)	C9	N2	C13	Br1	-179.50(10)
C1	C2	C7	C6	174.92(14)	C9	N2	C13	C12	1.0(2)
O2	C4	C5	C6	-179.90(15)	C9	C10	C11	C12	0.8(3)
N2	C9	C10	C11	-0.1(2)	C10	C11	C12	C13	-0.6(3)
C2	C3	C4	O2	-179.78(14)	C11	C12	C13	Br1	-179.84(13)
C2	C3	C4	C5	0.7(2)	C11	C12	C13	N2	-0.4(3)
C3	C2	C7	C6	-0.4(2)	C13	N2	C9	N1	-178.91(13)
C3	C4	C5	C6	-0.3(2)	C13	N2	C9	C10	-0.8(2)

Table 7 Hydrogen Atom Coordinates (Å×10^4) and Isotropic Displacement Parameters (Å^2×10^3) for 22mv_MLB10_LikhopotsoLCM_37_2f.

Atom	*X*	*Y*	*z*	U(eq)
H3	6380.86	8821.29	4542.14	19
H5	5168.84	7001.01	3352.92	27
H6	4308.4	5794.32	3936.84	26
H7	4522.17	6075.14	4829.44	22
H8A	7874.74	9609.72	3914.44	45
H8B	5773.23	9930.93	3873.26	45
H8C	7098.36	10046.7	3384.64	45
H10	4730.48	8287.02	6354.72	25
H11	4736.22	8053.75	7253.28	29
H12	5918.22	6593.81	7605.25	28

Table 7 Hydrogen Atom Coordinates (Å×10^4) and Isotropic Displacement Parameters (Å^2×10^3) for 22mv_MLB10_LikhopotsoLCM_37_2f.

Atom	*X*	*Y*	*z*	U(eq)
H3A	8433.95	5658.2	4949.68	34
H3B	8344.53	4898.48	5322.19	34
H1	6300(30)	6453(15)	5520(7)	23(5)

6. Crystallographic data for *N*-(6-chloropyridin-2-yl)-3-methoxybenzamide 158m

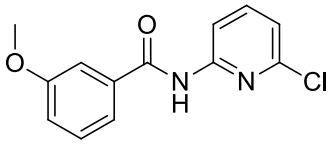

Table 1 Crystal data and structure refinement for 22mv_MLB7_Likhopotso_LCM_47_2f.

Identification code	22mv_MLB7_Likhopotso_LCM_47_2f
Empirical formula	$C_{13}H_{13}ClN_2O_3$
Formula weight	280.70
Temperature/K	173.00
Crystal system	Orthorhombic
Space group	Pbca
a/Å	7.2499(2)
b/Å	13.6609(3)
c/Å	25.8473(5)
α/°	90
β/°	90
γ/°	90
Volume/Å^3	2559.92(10)
Z	8
ρ_{calc}g/cm^3	1.457
μ/mm^{-1}	0.304
F(000)	1168.0

Crystal size/mm^3	0.266 × 0.246 × 0.238
Radiation	MoKα (λ = 0.71073)
2Θ range for data collection/°	6.17 to 56.594
Index ranges	-9 ≤ h ≤ 9, -18 ≤ k ≤ 18, -34 ≤ l ≤ 29
Reflections collected	45432
Independent reflections	3185 [R_{int} = 0.0363, R_{sigma} = 0.0156]
Data/restraints/parameters	3185/0/180
Goodness-of-fit on F^2	1.061
Final R indexes [I>=2σ (I)]	R_1 = 0.0375, wR_2 = 0.0948
Final R indexes [all data]	R_1 = 0.0452, wR_2 = 0.0992
Largest diff. peak/hole / e Å^{-3}	0.32/-0.29

Table 2 Fractional Atomic Coordinates (×10^4) and Equivalent Isotropic Displacement Parameters (Å^2×10^3) for 22mv_MLB7_Likhopotso_LCM_47_2f. U_{eq} is defined as 1/3 of the trace of the orthogonalised U_{IJ} tensor.

Atom	*X*	*Y*	*z*	U(eq)
Cl1	2686.2(7)	4897.8(3)	2865.1(2)	38.71(13)
O1	4890.6(14)	8553.3(7)	4516.7(4)	20.4(2)
N1	4100.5(16)	6964.5(8)	4344.3(4)	17.7(2)
C1	4518.1(17)	7717.7(9)	4667.3(5)	16.3(2)
O2	3655.0(16)	8661.1(7)	6485.5(4)	27.2(2)
N2	3507.7(16)	6104.3(8)	3608.1(4)	20.2(2)
C2	4525.3(17)	7464.4(9)	5231.2(5)	16.6(3)
C3	4019.6(18)	8197.4(9)	5582.6(5)	17.4(3)
C4	4116.6(19)	8003.2(10)	6109.5(5)	19.6(3)
C5	4730(2)	7091.5(10)	6283.9(5)	23.4(3)
C6	5245(2)	6378.4(10)	5933.1(5)	22.7(3)
C7	5132.1(18)	6556.3(10)	5403.5(5)	19.4(3)

Table 2 Fractional Atomic Coordinates (×10^4) and Equivalent Isotropic Displacement Parameters (Å^2×10^3) for 22mv_MLB7_Likhopotso_LCM_47_2f. U_{eq} is defined as 1/3 of the trace of the orthogonalised U_{IJ} tensor.

Atom	*X*	*Y*	*z*	U(eq)
C8	3254(3)	9637.5(11)	6326.2(6)	33.2(4)
C9	4112.6(18)	6959.6(9)	3801.5(5)	17.1(3)
C10	4707(2)	7733.8(10)	3493.6(5)	22.8(3)
C11	4668(2)	7599.4(11)	2961.3(6)	28.0(3)
C12	4042(2)	6726.3(11)	2750.6(5)	28.2(3)
C13	3488(2)	6022.7(10)	3099.4(5)	23.7(3)
O3	7287.9(14)	9690.9(8)	5146.4(4)	25.5(2)

Table 3 Anisotropic Displacement Parameters (Å^2×10^3) for 22mv_MLB7_Likhopotso_LCM_47_2f. The Anisotropic displacement factor exponent takes the form: $-2\pi^2[h^2a^{*2}U_{11}+2hka^*b^*U_{12}+\ldots]$.

Atom	U_{11}	U_{22}	U_{33}	U_{23}	U_{13}	U_{12}
Cl1	64.5(3)	26.8(2)	24.81(19)	-8.10(14)	-4.72(18)	-13.28(18)
O1	27.9(5)	14.9(4)	18.4(4)	0.1(3)	-0.2(4)	-2.3(4)
N1	23.2(6)	14.3(5)	15.8(5)	-0.1(4)	1.3(4)	-2.5(4)
C1	15.8(6)	16.2(6)	16.9(6)	-1.6(4)	-0.1(5)	0.8(4)
O2	45.2(6)	21.5(5)	15.0(5)	-1.8(4)	3.1(4)	2.0(4)
N2	25.9(6)	16.8(5)	17.9(5)	-1.9(4)	-1.3(4)	-1.0(4)
C2	15.9(6)	17.3(6)	16.6(6)	0.0(5)	-1.1(5)	-2.1(5)
C3	20.1(6)	15.1(6)	17.1(6)	0.7(5)	-0.8(5)	-0.7(5)
C4	22.6(6)	19.4(6)	16.8(6)	-0.6(5)	1.0(5)	-2.6(5)
C5	29.4(7)	23.9(7)	16.9(6)	4.7(5)	-1.9(5)	-2.0(6)
C6	24.0(7)	18.0(6)	26.1(7)	5.1(5)	-2.9(5)	0.8(5)
C7	18.6(6)	17.4(6)	22.2(6)	-1.5(5)	-0.5(5)	-0.3(5)
C8	55.2(10)	20.2(7)	24.3(7)	-3.3(6)	5.8(7)	4.8(7)
C9	17.7(6)	17.2(6)	16.5(6)	-1.3(5)	0.2(5)	1.5(5)
C10	30.1(7)	17.8(6)	20.7(6)	-0.7(5)	2.8(6)	-2.4(5)

Table 3 Anisotropic Displacement Parameters ($Å^2×10^3$) for 22mv_MLB7_Likhopotso_LCM_47_2f. The Anisotropic displacement factor exponent takes the form: $-2π^2[h^2a^{*2}U_{11}+2hka^*b^*U_{12}+…]$.

Atom	U_{11}	U_{22}	U_{33}	U_{23}	U_{13}	U_{12}
C11	42.1(9)	22.3(7)	19.6(7)	3.7(5)	4.5(6)	-1.7(6)
C12	41.6(9)	26.8(7)	16.3(6)	-0.2(5)	-0.1(6)	0.8(6)
C13	31.4(7)	19.3(6)	20.2(6)	-4.5(5)	-3.3(6)	-0.9(5)
O3	26.3(5)	19.8(5)	30.5(5)	-3.2(4)	-2.6(4)	0.7(4)

Table 4 Bond Lengths for 22mv_MLB7_Likhopotso_LCM_47_2f.

Atom	Atom	Length/Å	Atom	Atom	Length/Å
Cl1	C13	1.7510(14)	C2	C7	1.3895(18)
O1	C1	1.2359(15)	C3	C4	1.3894(18)
N1	C1	1.3591(16)	C4	C5	1.3972(19)
N1	C9	1.4029(16)	C5	C6	1.382(2)
C1	C2	1.4981(17)	C6	C7	1.3929(19)
O2	C4	1.3654(16)	C9	C10	1.3919(18)
O2	C8	1.4260(18)	C10	C11	1.3883(19)
N2	C9	1.3444(17)	C11	C12	1.388(2)
N2	C13	1.3197(17)	C12	C13	1.378(2)
C2	C3	1.4007(18)			

Table 5 Bond Angles for 22mv_MLB7_Likhopotso_LCM_47_2f.

Atom	Atom	Atom	Angle/˚	Atom	Atom	Atom	Angle/˚
C1	N1	C9	128.06(11)	C6	C5	C4	120.17(12)
O1	C1	N1	123.68(12)	C5	C6	C7	120.39(12)
O1	C1	C2	121.26(11)	C2	C7	C6	119.30(12)
N1	C1	C2	115.06(11)	N2	C9	N1	111.96(11)
C4	O2	C8	117.40(11)	N2	C9	C10	123.27(12)
C13	N2	C9	116.58(12)	C10	C9	N1	124.76(12)

Table 5 Bond Angles for 22mv_MLB7_Likhopotso_LCM_47_2f.

Atom	Atom	Atom	Angle/˚	Atom	Atom	Atom	Angle/˚
C3	C2	C1	117.70(11)	C11	C10	C9	117.39(13)
C7	C2	C1	121.27(11)	C12	C11	C10	120.61(13)
C7	C2	C3	120.89(12)	C13	C12	C11	115.99(13)
C4	C3	C2	119.07(12)	N2	C13	Cl1	114.98(11)
O2	C4	C3	124.03(12)	N2	C13	C12	126.16(13)
O2	C4	C5	115.79(12)	C12	C13	Cl1	118.87(11)
C3	C4	C5	120.18(12)				

Table 6 Torsion Angles for 22mv_MLB7_Likhopotso_LCM_47_2f.

A	B	C	D	Angle/˚	A	B	C	D	Angle/˚
O1	C1	C2	C3	32.24(18)	C4	C5	C6	C7	-0.9(2)
O1	C1	C2	C7	-143.45(13)	C5	C6	C7	C2	1.1(2)
N1	C1	C2	C3	-148.56(12)	C7	C2	C3	C4	-0.55(19)
N1	C1	C2	C7	35.75(17)	C8	O2	C4	C3	-7.5(2)
N1	C9	C10	C11	178.51(13)	C8	O2	C4	C5	172.02(14)
C1	N1	C9	N2	-175.98(13)	C9	N1	C1	O1	4.0(2)
C1	N1	C9	C10	5.1(2)	C9	N1	C1	C2	-175.13(12)
C1	C2	C3	C4	-176.25(12)	C9	N2	C13	Cl1	-179.88(10)
C1	C2	C7	C6	175.23(12)	C9	N2	C13	C12	0.6(2)
O2	C4	C5	C6	-179.46(13)	C9	C10	C11	C12	0.6(2)
N2	C9	C10	C11	-0.3(2)	C10	C11	C12	C13	-0.3(2)
C2	C3	C4	O2	-179.86(12)	C11	C12	C13	Cl1	-179.80(12)
C2	C3	C4	C5	0.7(2)	C11	C12	C13	N2	-0.3(2)
C3	C2	C7	C6	-0.3(2)	C13	N2	C9	N1	-179.20(12)
C3	C4	C5	C6	0.0(2)	C13	N2	C9	C10	-0.3(2)

Table 7 Hydrogen Atom Coordinates (Å×10^4) and Isotropic Displacement Parameters (Å^2×10^3) for 22mv_MLB7_Likhopotso_LCM_47_2f.

Atom	*X*	*Y*	*z*	U(eq)
H3	3615.93	8818.61	5462.27	21
H5	4794.25	6961.53	6644.57	28
H6	5678.68	5763.24	6053.98	27
H7	5466.43	6062.04	5162.52	23
H8A	2203.83	9632.41	6087.64	50
H8B	4333.46	9915.87	6151.57	50
H8C	2950.44	10035.43	6629.97	50
H10	5122.37	8330.63	3641.87	27
H11	5074.37	8110.01	2739.28	34
H12	3998.27	6620.04	2387.55	34
H3A	6483.32	9369.15	4963.99	38
H3B	6635.89	10111.09	5321.16	38
H1	3670(20)	6413(13)	4480(7)	23(4)

7. Crystallographic data for *N*-(3-bromopyridin-2-yl)-3-methoxybenzamide 158n

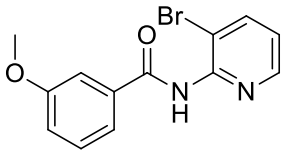

Table 1 Crystal data and structure refinement for 22mv_MLB9_likhopotso_LCM_48_0f.

Identification code	22mv_MLB9_likhopotso_LCM_48_0f
Empirical formula	$C_{13}H_{11}BrN_2O_2$
Formula weight	307.15
Temperature/K	173.00
Crystal system	orthorhombic
Space group	$Pna2_1$

a/Å	9.3622(3)
b/Å	12.4712(6)
c/Å	10.7949(4)
α/°	90
β/°	90
γ/°	90
Volume/$Å^3$	1260.39(9)
Z	4
$\rho_{calc}g/cm^3$	1.619
μ/mm^{-1}	3.256
F(000)	616.0
Crystal size/mm^3	0.302 × 0.076 × 0.065
Radiation	MoKα (λ = 0.71073)
2Θ range for data collection/°	6.534 to 56.592
Index ranges	-12 ≤ h ≤ 12, -16 ≤ k ≤ 16, -14 ≤ l ≤ 14
Reflections collected	36955
Independent reflections	3116 [R_{int} = 0.0717, R_{sigma} = 0.0305]
Data/restraints/parameters	3116/1/168
Goodness-of-fit on F^2	1.014
Final R indexes [I>=2σ (I)]	R_1 = 0.0293, wR_2 = 0.0441
Final R indexes [all data]	R_1 = 0.0422, wR_2 = 0.0478
Largest diff. peak/hole / e $Å^{-3}$	0.25/-0.31
Flack parameter	0.008(5)

Table 2 Fractional Atomic Coordinates (×10^4) and Equivalent Isotropic Displacement Parameters (Å^2×10^3) for 22mv_MLB9_likhopotso_LCM_48_0f. U_{eq} is defined as 1/3 of the trace of the orthogonalised U_{IJ} tensor.

Atom	*X*	*Y*	*z*	U(eq)
Br1	6980.4(3)	2564.6(3)	1568.3(5)	30.37(9)
O1	7486(3)	3199.2(19)	4502(2)	16.3(5)
N1	5224(3)	2670(3)	4094(3)	18.3(7)
C1	6472(3)	2599(3)	4720(3)	14.2(6)
O2	8466(3)	1428(2)	8688(3)	31.6(7)
N2	3900(3)	4168(3)	3578(3)	25.3(7)
C2	6523(4)	1787(3)	5742(3)	15.7(7)
C3	7498(3)	1988(3)	6696(4)	17.7(7)
C4	7578(4)	1289(3)	7695(3)	22.2(8)
C5	6711(4)	388(3)	7735(4)	29.3(9)
C6	5759(4)	192(3)	6779(5)	31.9(13)
C7	5648(4)	891(3)	5778(4)	23.3(8)
C8	9315(5)	2371(4)	8706(5)	35.7(13)
C9	4936(4)	3501(3)	3228(3)	17.0(7)
C10	5604(4)	3579(3)	2086(3)	21.1(8)
C11	5215(5)	4386(3)	1283(3)	29.1(10)
C12	4111(4)	5064(3)	1632(6)	37.5(11)
C13	3496(5)	4923(3)	2779(4)	35.0(11)

Table 3 Anisotropic Displacement Parameters (Å^2×10^3) for 22mv_MLB9_likhopotso_LCM_48_0f. The Anisotropic displacement factor exponent takes the form: $-2\pi^2[h^2a^{*2}U_{11}+2hka^*b^*U_{12}+\ldots]$.

Atom	U_{11}	U_{22}	U_{33}	U_{23}	U_{13}	U_{12}
Br1	28.64(15)	40.8(2)	21.66(13)	0.8(3)	2.4(3)	7.97(18)
O1	13.8(11)	16.5(13)	18.7(12)	3.1(10)	0.2(10)	-0.4(10)
N1	13.6(15)	22.8(19)	18.6(14)	7.1(13)	-1.5(12)	-2.3(12)
C1	15.5(14)	15.0(17)	12.1(13)	-2.7(15)	-0.9(12)	3.4(14)

Table 3 Anisotropic Displacement Parameters ($Å^2×10^3$) for 22mv_MLB9_likhopotso_LCM_48_0f. The Anisotropic displacement factor exponent takes the form: $-2π^2[h^2a^{*2}U_{11}+2hka^*b^*U_{12}+…]$.

Atom	U_{11}	U_{22}	U_{33}	U_{23}	U_{13}	U_{12}
O2	29.4(15)	44.8(19)	20.8(14)	14.4(13)	-6.4(13)	1.0(14)
N2	24.6(17)	25.2(18)	26.2(17)	-2.1(14)	-5.0(15)	5.6(14)
C2	16.7(17)	14.9(18)	15.6(16)	1.1(14)	0.5(14)	3.5(14)
C3	16.5(14)	18.8(15)	17.8(19)	2.0(18)	0.4(18)	2.9(11)
C4	18.6(18)	27(2)	21.0(19)	6.4(16)	0.4(15)	8.1(16)
C5	26(2)	29(2)	33(2)	17.0(18)	5.0(18)	6.5(17)
C6	28(2)	22.1(19)	46(4)	14(2)	4(2)	-0.5(15)
C7	21.8(19)	21(2)	26.9(19)	3.9(16)	-4.9(17)	0.7(16)
C8	36(3)	49(3)	22(2)	8(2)	-8.8(18)	0(2)
C9	16.3(17)	17.0(18)	17.7(17)	0.9(15)	-7.7(14)	-2.8(14)
C10	22.0(18)	19(2)	22.4(16)	-0.5(15)	-5.2(17)	-0.9(16)
C11	39(2)	30(2)	19(2)	7.5(15)	-8.9(16)	-6.5(17)
C12	51(3)	23.4(19)	38(2)	9(3)	-18(3)	5.3(17)
C13	40(3)	25(2)	40(3)	-4(2)	-11(2)	12.9(19)

Table 4 Bond Lengths for 22mv_MLB9_likhopotso_LCM_48_0f.

Atom	Atom	Length/Å	Atom	Atom	Length/Å
Br1	C10	1.890(4)	C2	C7	1.387(5)
O1	C1	1.232(4)	C3	C4	1.388(5)
N1	C1	1.353(4)	C4	C5	1.387(6)
N1	C9	1.421(5)	C5	C6	1.385(6)
C1	C2	1.498(5)	C6	C7	1.392(6)
O2	C4	1.367(4)	C9	C10	1.387(5)
O2	C8	1.420(6)	C10	C11	1.377(5)
N2	C9	1.332(5)	C11	C12	1.388(6)
N2	C13	1.332(5)	C12	C13	1.376(8)

Table 4 Bond Lengths for 22mv_MLB9_likhopotso_LCM_48_0f.

Atom	Atom	Length/Å	Atom	Atom	Length/Å
C2	C3	1.399(5)			

Table 5 Bond Angles for 22mv_MLB9_likhopotso_LCM_48_0f.

Atom	Atom	Atom	Angle/˚	Atom	Atom	Atom	Angle/˚
C1	N1	C9	122.7(3)	C6	C5	C4	119.8(4)
O1	C1	N1	122.0(3)	C5	C6	C7	121.1(4)
O1	C1	C2	121.8(3)	C2	C7	C6	118.8(4)
N1	C1	C2	116.1(3)	N2	C9	N1	114.1(3)
C4	O2	C8	117.1(3)	N2	C9	C10	122.4(3)
C9	N2	C13	117.8(4)	C10	C9	N1	123.4(3)
C3	C2	C1	116.3(3)	C9	C10	Br1	121.6(3)
C7	C2	C1	123.1(3)	C11	C10	Br1	118.9(3)
C7	C2	C3	120.6(3)	C11	C10	C9	119.4(3)
C4	C3	C2	119.7(3)	C10	C11	C12	118.1(4)
O2	C4	C3	124.2(4)	C13	C12	C11	118.6(4)
O2	C4	C5	115.8(3)	N2	C13	C12	123.6(4)
C5	C4	C3	120.0(4)				

Table 6 Torsion Angles for 22mv_MLB9_likhopotso_LCM_48_0f.

A	B	C	D	Angle/˚	A	B	C	D	Angle/˚
Br1	C10	C11	C12	174.2(3)	C3	C2	C7	C6	-0.1(6)
O1	C1	C2	C3	22.5(5)	C3	C4	C5	C6	-0.4(6)
O1	C1	C2	C7	-158.7(4)	C4	C5	C6	C7	-0.5(7)
N1	C1	C2	C3	-154.2(3)	C5	C6	C7	C2	0.8(6)
N1	C1	C2	C7	24.6(5)	C7	C2	C3	C4	-0.8(5)
N1	C9	C10	Br1	0.2(5)	C8	O2	C4	C3	2.4(6)
N1	C9	C10	C11	177.3(3)	C8	O2	C4	C5	-176.9(4)

Table 6 Torsion Angles for 22mv_MLB9_likhopotso_LCM_48_0f.

A	B	C	D	Angle/˚	A	B	C	D	Angle/˚
C1	N1	C9	N2	-113.6(4)	C9	N1	C1	O1	-6.2(5)
C1	N1	C9	C10	70.1(5)	C9	N1	C1	C2	170.5(3)
C1	C2	C3	C4	178.1(3)	C9	N2	C13	C12	-1.6(6)
C1	C2	C7	C6	-178.9(4)	C9	C10	C11	C12	-3.0(6)
O2	C4	C5	C6	178.9(4)	C10	C11	C12	C13	2.4(6)
N2	C9	C10	Br1	-175.7(3)	C11	C12	C13	N2	-0.1(7)
N2	C9	C10	C11	1.4(5)	C13	N2	C9	N1	-175.3(3)
C2	C3	C4	O2	-178.2(3)	C13	N2	C9	C10	0.9(5)
C2	C3	C4	C5	1.0(6)					

Table 7 Hydrogen Atom Coordinates (Å×10^4) and Isotropic Displacement Parameters (Å^2×10^3) for 22mv_MLB9_likhopotso_LCM_48_0f.

Atom	*X*	*Y*	*z*	U(eq)
H3	8102.55	2598.87	6661	21
H5	6769.23	-92.87	8415.13	35
H6	5172.72	-428.82	6807.51	38
H7	4984.81	755.46	5130.5	28
H8A	9920.02	2390.52	7965.19	54
H8B	9918.17	2371.09	9447.51	54
H8C	8692.46	3002.87	8716.08	54
H11	5688.47	4475.79	511.84	35
H12	3786.14	5613.47	1091.65	45
H13	2741.32	5390.42	3013.48	42
H1	4420(50)	2370(50)	4470(60)	51(19)

8. **Crystallographic data for 3-methoxy-*N*-(3-methoxybenzoyl)-*N*-(5-methylpyridin-2-yl)benzamide 165i**

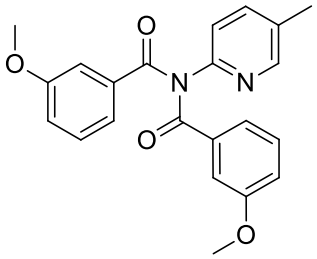

Table 1 Crystal data and structure refinement for 22mvMLB5_Likhopotso_LCM_39_2_s.

Identification code	22mvMLB5_Likhopotso_LCM_39_2_s
Empirical formula	$C_{22}H_{20}N_2O_4$
Formula weight	376.40
Temperature/K	173.00
Crystal system	Monoclinic
Space group	C2/c
a/Å	26.5528(9)
b/Å	9.0587(3)
c/Å	15.9522(4)
α/°	90
β/°	93.8870(10)
γ/°	90
Volume/Å^3	3828.2(2)
Z	8
ρ_{calc}g/cm^3	1.306
μ/mm^{-1}	0.091
F(000)	1584.0
Crystal size/mm^3	0.332 × 0.284 × 0.088
Radiation	MoKα (λ = 0.71073)
2Θ range for data collection/°	5.448 to 56.64
Index ranges	-35 ≤ h ≤ 35, -12 ≤ k ≤ 12, -21 ≤ l ≤ 21

Reflections collected	53945
Independent reflections	4762 [R_{int} = 0.0646, R_{sigma} = 0.0271]
Data/restraints/parameters	4762/0/256
Goodness-of-fit on F^2	1.067
Final R indexes [I>=2σ (I)]	R_1 = 0.0491, wR_2 = 0.1129
Final R indexes [all data]	R_1 = 0.0701, wR_2 = 0.1240
Largest diff. peak/hole / e $Å^{-3}$	0.21/-0.19

Table 2 Fractional Atomic Coordinates (×10^4) and Equivalent Isotropic Displacement Parameters ($Å^2$×10^3) for 22mvMLB5_Likhopotso_LCM_39_2_s. U_{eq} is defined as 1/3 of the trace of the orthogonalised U_{IJ} tensor.

Atom	*X*	*Y*	*z*	U(eq)
O1	2797.0(4)	228.3(14)	5688.2(7)	38.9(3)
N1	3578.5(5)	1258.9(15)	5904.4(8)	28.4(3)
C1	3129.8(6)	668.0(17)	6185.3(9)	28.3(3)
O2	3427.2(4)	2972.9(13)	8912.8(7)	36.0(3)
N2	3894.3(5)	1031.0(15)	4560.6(8)	30.9(3)
C2	3058.5(5)	727.6(17)	7102.2(9)	25.5(3)
O3	4117.7(5)	-43.2(14)	6809.4(8)	43.3(3)
C3	3285.1(5)	1810.5(16)	7617.6(9)	26.0(3)
O4	4510.8(5)	6101.1(15)	5949.7(9)	52.3(4)
C4	3182.3(5)	1879.9(17)	8460.3(9)	27.0(3)
C5	2849.1(6)	883.3(19)	8784.4(9)	31.6(3)
C6	2624.1(6)	-188(2)	8262.4(10)	35.3(4)
C7	2724.3(6)	-277.2(18)	7425.2(10)	31.4(3)
C8	3387.3(8)	2978(2)	9802.3(11)	48.5(5)
C9	3576.1(6)	1725.1(17)	5038.9(9)	26.7(3)
C10	3262.8(6)	2852.3(17)	4765.5(10)	31.0(3)

Table 2 Fractional Atomic Coordinates (×10^4) and Equivalent Isotropic Displacement Parameters (Å^2×10^3) for 22mvMLB5_Likhopotso_LCM_39_2_s. U_{eq} is defined as 1/3 of the trace of the orthogonalised U_{IJ} tensor.

Atom	*X*	*Y*	*z*	U(eq)
C11	3291.9(6)	3336.1(18)	3953.7(10)	35.0(4)
C12	3627.2(6)	2688.2(18)	3431.4(9)	31.1(3)
C13	3913.1(6)	1519.7(18)	3761.1(9)	30.6(3)
C14	3675.6(8)	3241(2)	2546.6(11)	46.6(5)
C15	4052.8(6)	1020.6(18)	6355.9(9)	30.3(3)
C16	4443.5(6)	2163.5(19)	6267.5(9)	31.8(3)
C17	4314.3(6)	3627.6(19)	6121.2(9)	31.3(3)
C18	4686.4(6)	4704(2)	6095.9(10)	38.5(4)
C19	5192.0(7)	4299(3)	6209.1(12)	51.2(5)
C20	5317.7(7)	2840(3)	6357.7(14)	58.5(6)
C21	4951.2(6)	1767(2)	6395.4(12)	47.0(5)
C22	4873.6(9)	7272(3)	5953.9(17)	70.6(7)

Table 3 Anisotropic Displacement Parameters (Å^2×10^3) for 22mvMLB5_Likhopotso_LCM_39_2_s. The Anisotropic displacement factor exponent takes the form: -2π^2[h^{2}a*^{2}U$_{11}$+2hka*b*U$_{12}$+…].

Atom	U_{11}	U_{22}	U_{33}	U_{23}	U_{13}	U_{12}
O1	32.8(6)	54.8(8)	29.6(6)	-9.1(5)	5.1(5)	-14.0(5)
N1	24.0(6)	35.8(7)	25.8(6)	1.1(5)	5.0(5)	-3.1(5)
C1	25.6(7)	29.8(8)	30.0(7)	-2.4(6)	5.2(6)	-2.7(6)
O2	37.5(6)	40.2(6)	30.5(6)	-7.4(5)	3.4(5)	-0.4(5)
N2	27.6(7)	33.2(7)	32.1(6)	-1.7(5)	4.4(5)	-3.7(5)
C2	20.1(7)	29.7(7)	26.7(7)	2.6(6)	2.1(5)	1.7(6)
O3	34.8(6)	46.9(7)	49.3(7)	17.4(6)	11.8(5)	11.3(6)
C3	21.0(7)	28.6(7)	28.8(7)	3.4(6)	4.0(5)	2.0(6)
O4	44.9(8)	42.1(7)	72.0(9)	-13.8(7)	19.3(7)	-18.3(6)
C4	22.5(7)	31.0(8)	27.2(7)	0.2(6)	0.1(5)	7.6(6)

Table 3 Anisotropic Displacement Parameters ($Å^2×10^3$) for 22mvMLB5_Likhopotso_LCM_39_2_s. The Anisotropic displacement factor exponent takes the form: $-2π^2[h^2a^{*2}U_{11}+2hka*b*U_{12}+…]$.

Atom	U_{11}	U_{22}	U_{33}	U_{23}	U_{13}	U_{12}
C5	25.6(7)	44.5(9)	25.1(7)	7.7(6)	3.8(6)	6.1(7)
C6	27.6(8)	43.9(9)	34.5(8)	12.1(7)	3.6(6)	-5.7(7)
C7	26.3(8)	35.0(8)	32.8(8)	4.1(6)	1.1(6)	-4.7(6)
C8	58.7(12)	55.8(12)	30.6(9)	-9.7(8)	1.7(8)	0.3(10)
C9	24.9(7)	30.8(8)	24.7(7)	-2.8(6)	3.9(5)	-6.2(6)
C10	29.9(8)	31.6(8)	32.4(8)	-5.9(6)	9.3(6)	1.1(6)
C11	35.9(9)	30.4(8)	38.9(9)	-1.3(7)	3.0(7)	1.7(7)
C12	34.6(8)	32.0(8)	27.1(7)	-0.4(6)	3.3(6)	-6.6(7)
C13	28.5(8)	33.5(8)	30.6(7)	-3.0(6)	7.7(6)	-3.5(6)
C14	62.0(12)	44.9(10)	33.4(9)	6.1(8)	7.0(8)	-4.4(9)
C15	25.6(7)	38.1(9)	28.1(7)	2.3(6)	7.4(6)	5.4(6)
C16	21.7(7)	47.8(10)	26.0(7)	3.1(7)	2.8(5)	0.7(7)
C17	21.3(7)	45.2(9)	27.5(7)	-4.5(7)	3.3(5)	-5.5(6)
C18	32.7(9)	50.8(11)	32.9(8)	-10.0(7)	7.8(7)	-13.8(8)
C19	27.4(9)	81.2(15)	45.3(10)	-5.4(10)	4.5(7)	-22.2(9)
C20	21.5(9)	94.3(18)	59.4(12)	13.1(12)	0.1(8)	-1.5(10)
C21	24.3(8)	68.3(13)	48.6(10)	13.2(9)	3.0(7)	6.2(8)
C22	69.3(15)	56.0(13)	90.2(17)	-28.4(13)	33.4(13)	-37.4(12)

Table 4 Bond Lengths for 22mvMLB5_Likhopotso_LCM_39_2_s.

Atom	Atom	Length/Å	Atom	Atom	Length/Å
O1	C1	1.2138(18)	C4	C5	1.388(2)
N1	C1	1.4068(19)	C5	C6	1.387(2)
N1	C9	1.4434(18)	C6	C7	1.382(2)
N1	C15	1.424(2)	C9	C10	1.370(2)
C1	C2	1.488(2)	C10	C11	1.374(2)

Table 4 Bond Lengths for 22mvMLB5_Likhopotso_LCM_39_2_s.

Atom	Atom	Length/Å	Atom	Atom	Length/Å
O2	C4	1.3641(19)	C11	C12	1.390(2)
O2	C8	1.430(2)	C12	C13	1.385(2)
N2	C9	1.3336(19)	C12	C14	1.511(2)
N2	C13	1.354(2)	C15	C16	1.479(2)
C2	C3	1.390(2)	C16	C17	1.386(2)
C2	C7	1.394(2)	C16	C21	1.397(2)
O3	C15	1.2103(19)	C17	C18	1.391(2)
C3	C4	1.391(2)	C18	C19	1.392(3)
O4	C18	1.363(2)	C19	C20	1.380(3)
O4	C22	1.432(2)	C20	C21	1.380(3)

Table 5 Bond Angles for 22mvMLB5_Likhopotso_LCM_39_2_s.

Atom	Atom	Atom	Angle/˚	Atom	Atom	Atom	Angle/˚
C1	N1	C9	117.85(12)	C10	C9	N1	119.07(13)
C1	N1	C15	121.33(12)	C9	C10	C11	117.78(14)
C15	N1	C9	118.33(12)	C10	C11	C12	120.63(15)
O1	C1	N1	120.76(13)	C11	C12	C14	121.21(16)
O1	C1	C2	121.23(13)	C13	C12	C11	116.86(14)
N1	C1	C2	117.78(13)	C13	C12	C14	121.93(15)
C4	O2	C8	117.56(13)	N2	C13	C12	123.59(14)
C9	N2	C13	116.74(14)	N1	C15	C16	116.58(13)
C3	C2	C1	121.87(13)	O3	C15	N1	120.55(15)
C3	C2	C7	120.19(13)	O3	C15	C16	122.81(15)
C7	C2	C1	117.78(13)	C17	C16	C15	121.24(14)
C2	C3	C4	119.86(14)	C17	C16	C21	119.78(16)
C18	O4	C22	117.67(17)	C21	C16	C15	118.82(16)
O2	C4	C3	115.24(13)	C16	C17	C18	120.51(15)

Table 5 Bond Angles for 22mvMLB5_Likhopotso_LCM_39_2_s.

Atom	Atom	Atom	Angle/˚	Atom	Atom	Atom	Angle/˚
O2	C4	C5	124.61(13)	O4	C18	C17	114.87(15)
C5	C4	C3	120.15(14)	O4	C18	C19	125.63(17)
C6	C5	C4	119.40(14)	C17	C18	C19	119.49(18)
C7	C6	C5	121.18(15)	C20	C19	C18	119.66(18)
C6	C7	C2	119.22(15)	C19	C20	C21	121.28(18)
N2	C9	N1	116.58(13)	C20	C21	C16	119.3(2)
N2	C9	C10	124.33(14)				

Table 6 Torsion Angles for 22mvMLB5_Likhopotso_LCM_39_2_s.

A	B	C	D	Angle/˚	A	B	C	D	Angle/˚
O1	C1	C2	C3	-147.26(16)	C9	N1	C1	O1	17.7(2)
O1	C1	C2	C7	28.0(2)	C9	N1	C1	C2	-156.79(13)
N1	C1	C2	C3	27.3(2)	C9	N1	C15	O3	-137.04(15)
N1	C1	C2	C7	-157.46(14)	C9	N1	C15	C16	45.60(19)
N1	C9	C10	C11	175.91(14)	C9	N2	C13	C12	0.7(2)
N1	C15	C16	C17	29.9(2)	C9	C10	C11	C12	0.4(2)
N1	C15	C16	C21	-154.77(15)	C10	C11	C12	C13	1.9(2)
C1	N1	C9	N2	-118.45(15)	C10	C11	C12	C14	-177.99(16)
C1	N1	C9	C10	62.97(19)	C11	C12	C13	N2	-2.6(2)
C1	N1	C15	O3	24.7(2)	C13	N2	C9	N1	-176.48(13)
C1	N1	C15	C16	-152.67(14)	C13	N2	C9	C10	2.0(2)
C1	C2	C3	C4	175.92(13)	C14	C12	C13	N2	177.36(15)
C1	C2	C7	C6	-175.74(14)	C15	N1	C1	O1	-144.06(16)
O2	C4	C5	C6	-179.68(14)	C15	N1	C1	C2	41.4(2)
N2	C9	C10	C11	-2.6(2)	C15	N1	C9	N2	43.92(19)
C2	C3	C4	O2	179.40(13)	C15	N1	C9	C10	-134.66(15)
C2	C3	C4	C5	-0.9(2)	C15	C16	C17	C18	175.65(14)

Table 6 Torsion Angles for 22mvMLB5_Likhopotso_LCM_39_2_s.

A	B	C	D	Angle/˚	A	B	C	D	Angle/˚
O3	C15	C16	C17	-147.38(16)	C15	C16	C21	C20	-176.64(17)
O3	C15	C16	C21	27.9(2)	C16	C17	C18	O4	-179.82(14)
C3	C2	C7	C6	-0.4(2)	C16	C17	C18	C19	0.8(2)
C3	C4	C5	C6	0.6(2)	C17	C16	C21	C20	-1.3(3)
O4	C18	C19	C20	179.64(18)	C17	C18	C19	C20	-1.0(3)
C4	C5	C6	C7	-0.2(2)	C18	C19	C20	C21	0.1(3)
C5	C6	C7	C2	0.1(2)	C19	C20	C21	C16	1.0(3)
C7	C2	C3	C4	0.7(2)	C21	C16	C17	C18	0.4(2)
C8	O2	C4	C3	-172.08(14)	C22	O4	C18	C17	177.23(16)
C8	O2	C4	C5	8.2(2)	C22	O4	C18	C19	-3.4(3)

Table 7 Hydrogen Atom Coordinates (Å×10^4) and Isotropic Displacement Parameters (Å^2×10^3) for 22mvMLB5_Likhopotso_LCM_39_2_s.

Atom	*X*	*Y*	*z*	U(eq)
H3	3509.66	2501.55	7394.82	31
H5	2775.76	934.47	9358.32	38
H6	2397.01	-872.51	8484.6	42
H7	2567.31	-1014.63	7073.83	38
H8A	3037.23	3179.71	9924.74	73
H8B	3608.08	3744.63	10058.4	73
H8C	3489.38	2012.57	10033.46	73
H10	3032.93	3285.17	5124.99	37
H11	3080.86	4120.91	3747.61	42
H13	4134.4	1034.78	3407.03	37
H14A	3797.7	4262.34	2565.29	70
H14B	3345.17	3201.26	2233.9	70
H14C	3915.15	2618.65	2266.86	70

Table 7 Hydrogen Atom Coordinates (Å×10^4) and Isotropic Displacement Parameters (Å^2×10^3) for 22mvMLB5_Likhopotso_LCM_39_2_s.

Atom	*X*	*Y*	*z*	U(eq)
H17	3968.84	3897.95	6037.57	38
H19	5449.27	5023.56	6184.11	61
H20	5663.39	2569.03	6435.48	70
H21	5043.09	768.69	6507.23	56
H22A	5114.49	7076.07	5528.27	106
H22B	5054.44	7331.35	6509.14	106
H22C	4700.08	8208.2	5827.15	106

9. Crystallographic data for *N*-(5-bromopyridin-2-yl)-3-methoxy-N-(3-methoxybenzoyl)benzamide 165j

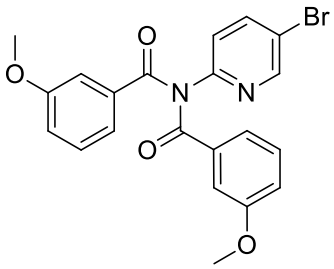

Table 1 Crystal data and structure refinement for 22mv_MLB2Likhopotso_LCM_26_2_f.

Identification code	22mv_MLB2Likhopotso_LCM_26_2_f
Empirical formula	$C_{21}H_{17}BrN_2O_4$
Formula weight	441.27
Temperature/K	173.0
Crystal system	monoclinic
Space group	C2/c
a/Å	21.3612(9)
b/Å	7.9993(4)
c/Å	22.9711(8)
α/°	90

β/°	102.2740(10)
γ/°	90
Volume/Å^3	3835.5(3)
Z	8
ρ_{calc}g/cm^3	1.528
μ/mm^{-1}	2.174
F(000)	1792.0
Crystal size/mm^3	0.225 × 0.151 × 0.074
Radiation	MoKα (λ = 0.71073)
2Θ range for data collection/°	5.454 to 56.64
Index ranges	-28 ≤ h ≤ 28, -10 ≤ k ≤ 10, -29 ≤ l ≤ 30
Reflections collected	59065
Independent reflections	4768 [R_{int} = 0.0395, R_{sigma} = 0.0207]
Data/restraints/parameters	4768/71/349
Goodness-of-fit on F^2	1.110
Final R indexes [I>=2σ (I)]	R_1 = 0.0412, wR_2 = 0.0867
Final R indexes [all data]	R_1 = 0.0558, wR_2 = 0.0922
Largest diff. peak/hole / e Å^{-3}	0.28/-0.31

Table 2 Fractional Atomic Coordinates (×10^4) and Equivalent Isotropic Displacement Parameters (Å^2×10^3) for 22mv_MLB2Likhopotso_LCM_26_2_f. U_{eq} is defined as 1/3 of of the trace of the orthogonalised U_{IJ} tensor.

Atom	*X*	*Y*	*z*	U(eq)
Br1	5156.9(3)	7790.0(10)	505.0(2)	47.87(15)
O1	7433.9(9)	8779(2)	2922.4(8)	32.9(4)
O2	8040.8(10)	3655(3)	4781.0(8)	37.8(5)
O3	6223.2(8)	6731(2)	3780.3(7)	28.1(4)
O4	4891.0(10)	1317(3)	3528.2(10)	41.3(5)

Table 2 Fractional Atomic Coordinates (×10^4) and Equivalent Isotropic Displacement Parameters (Å^2×10^3) for 22mv_MLB2Likhopotso_LCM_26_2_f. U_{eq} is defined as 1/3 of of the trace of the orthogonalised U_{IJ} tensor.

Atom	*X*	*Y*	*z*	U(eq)
N1	5748.5(9)	7154(3)	2310.9(10)	22.2(5)
N2	6710.8(9)	6724(2)	2976.1(8)	21.0(4)
C1	6380.9(10)	6986(3)	2374.5(10)	20.7(4)
C2	6699.2(11)	7046(4)	1906.5(10)	25.5(5)
C3	6337(2)	7322(13)	1339.2(16)	28.3(14)
C4	5681(2)	7442(16)	1270.9(14)	25.9(8)
C5	5401(2)	7380(20)	1758.9(17)	24.1(5)
C6	7250.2(16)	7673(4)	3215.5(14)	24.2(7)
C7	7615.9(17)	7250(3)	3825.3(12)	24.8(5)
C8	7668.7(11)	5623(3)	4039.5(10)	24.7(5)
C9	8030.4(11)	5288(4)	4609.3(11)	28.6(5)
C10	8339.7(14)	6586(4)	4958.5(12)	35.7(7)
C11	8283.5(15)	8177(4)	4735.6(13)	40.2(8)
C12	7929.0(12)	8538(4)	4176.5(12)	32.5(6)
C13	8394.8(18)	3243(5)	5364.5(12)	47.2(8)
C14	6324.0(10)	5978(3)	3354.4(9)	20.2(5)
C15	6094.5(10)	4259(3)	3194.9(10)	20.3(5)
C16	5585.9(11)	3656(3)	3434.2(10)	22.0(5)
C17	5383.7(12)	2023(3)	3323.4(11)	27.6(5)
C18	5701.1(14)	978(3)	2992.4(12)	33.8(6)
C19	6201.2(14)	1588(3)	2759.6(14)	31.4(7)
C20	6399.3(12)	3235(3)	2852.4(11)	24.0(5)
C21	4498.2(19)	2363(5)	3796.8(15)	40.1(9)
Br1A	5160.6(17)	6997(5)	502.7(14)	43.3(8)
O1A	7423(5)	6181(12)	2934(4)	30.5(9)

Table 2 Fractional Atomic Coordinates (×10^4) and Equivalent Isotropic Displacement Parameters (Å^2×10^3) for 22mv_MLB2Likhopotso_LCM_26_2_f. U_{eq} is defined as 1/3 of of the trace of the orthogonalised U_{IJ} tensor.

Atom	*X*	*Y*	*z*	U(eq)
O2A	8058(5)	11331(10)	4782(4)	30.5(9)
O3A	6228(5)	8268(12)	3771(4)	30.5(9)
O4A	4870(4)	13667(12)	3485(4)	30.5(9)
N1A	5736(5)	7770(20)	2296(7)	30.5(9)
N2A	6707(4)	8248(14)	2964(4)	30.5(9)
C1A	6367(5)	7970(20)	2366(4)	30.5(9)
C2A	6685(6)	7960(20)	1898(5)	30.5(9)
C3A	6329(11)	7530(100)	1341(9)	30.5(9)
C4A	5670(11)	7530(110)	1260(8)	30.5(9)
C5A	5395(15)	7410(130)	1750(9)	30.5(9)
C6A	7260(10)	7360(40)	3209(7)	30.5(9)
C7A	7600(13)	7705(15)	3834(6)	30.5(9)
C8A	7680(7)	9339(15)	4039(5)	30.5(9)
C9A	8032(7)	9696(11)	4611(5)	30.5(9)
C10A	8335(9)	8367(15)	4946(6)	30.5(9)
C11A	8268(9)	6760(17)	4739(6)	30.5(9)
C12A	7897(7)	6399(16)	4186(5)	30.5(9)
C13A	8412(7)	11751(19)	5365(4)	30.5(9)
C14A	6325(6)	9017(12)	3342(5)	30.5(9)
C15A	6099(6)	10733(12)	3173(6)	30.5(9)
C16A	5592(6)	11357(15)	3409(7)	30.5(9)
C17A	5368(6)	12967(15)	3286(7)	30.5(9)
C18A	5653(6)	14012(16)	2929(6)	30.5(9)
C19A	6160(7)	13400(18)	2708(7)	30.5(9)
C20A	6377(9)	11772(18)	2814(9)	30.5(9)

Table 2 Fractional Atomic Coordinates (×10^4) and Equivalent Isotropic Displacement Parameters (Å^2×10^3) for 22mv_MLB2Likhopotso_LCM_26_2_f. U_{eq} is defined as 1/3 of of the trace of the orthogonalised U_{IJ} tensor.

Atom	*X*	*Y*	*z*	U(eq)
C21A	4587(11)	12750(30)	3890(8)	30.5(9)

Table 3 Anisotropic Displacement Parameters (Å^2×10^3) for 22mv_MLB2Likhopotso_LCM_26_2_f. The Anisotropic displacement factor exponent takes the form: $-2\pi^2[h^2a^{*2}U_{11}+2hka^*b^*U_{12}+\ldots]$.

Atom	U_{11}	U_{22}	U_{33}	U_{23}	U_{13}	U_{12}
Br1	41.4(2)	74.4(4)	23.69(16)	4.2(3)	-2.39(12)	9.5(3)
O1	32.7(10)	29.3(10)	36.4(10)	2.3(8)	6.9(8)	-10.2(8)
O2	44.3(11)	41.4(12)	23.9(9)	3.9(8)	-1.4(8)	6.1(9)
O3	25.8(9)	33.3(10)	26.4(8)	-10.0(7)	8.3(7)	-6.7(7)
O4	43.8(11)	30.5(11)	55.0(13)	2.3(9)	22.9(10)	-10.6(9)
N1	18.9(9)	23.7(11)	23.7(9)	-0.8(10)	3.7(7)	0.5(9)
N2	19.7(9)	22.7(10)	20.2(9)	1.0(7)	3.4(7)	-3.4(8)
C1	22.0(11)	17.9(12)	22.1(11)	-0.7(9)	4.0(8)	-0.4(9)
C2	23.0(11)	28.8(14)	26.0(11)	1.7(10)	7.8(9)	4.5(10)
C3	32.0(12)	31(4)	23.9(11)	2.2(11)	10.5(9)	2.4(13)
C4	30.1(12)	25(2)	20.3(10)	0.7(10)	-0.7(9)	3.4(11)
C5	19.9(10)	24.2(13)	27.5(11)	-1.7(10)	3.2(9)	2.0(9)
C6	19.4(10)	25(2)	28.9(11)	-4.9(11)	6.5(9)	-0.7(11)
C7	17.5(10)	31.7(15)	25.3(11)	-4.1(12)	4.5(8)	-2.0(14)
C8	21.4(11)	29.5(13)	21.8(11)	-5.3(10)	1.4(9)	-0.6(10)
C9	22.0(11)	39.3(15)	24.2(12)	-3.8(11)	4.2(9)	3.5(10)
C10	24.6(13)	57(2)	23.2(12)	-11.0(13)	0.2(11)	-0.8(12)
C11	32.2(15)	51(2)	34.9(15)	-21.1(14)	2.3(13)	-11.7(13)
C12	28.8(13)	33.4(15)	35.5(14)	-9.2(12)	7.1(11)	-9.8(12)
C13	48.8(18)	63(2)	25.5(13)	9.9(14)	-1.0(12)	15.8(16)
C14	16.2(10)	23.8(12)	20.0(10)	1.1(9)	2.5(8)	-1.2(9)

Table 3 Anisotropic Displacement Parameters ($Å^2×10^3$) for 22mv_MLB2Likhopotso_LCM_26_2_f. The Anisotropic displacement factor exponent takes the form: $-2π^2[h^2a^{*2}U_{11}+2hka^*b^*U_{12}+…]$.

Atom	U_{11}	U_{22}	U_{33}	U_{23}	U_{13}	U_{12}
C15	21.5(11)	18.5(11)	20.2(10)	2.6(8)	3.0(8)	0.5(9)
C16	22.4(11)	22.8(12)	21.3(11)	2.1(9)	5.7(9)	0.6(10)
C17	28.1(13)	25.4(14)	29.5(12)	4.2(11)	6.3(10)	-4.1(11)
C18	43.0(16)	18.5(13)	40.4(15)	-2.2(11)	10.1(12)	-4.2(11)
C19	38.1(18)	21.9(13)	35.9(15)	-2.8(11)	11.7(15)	4.5(12)
C20	24.7(12)	20.9(13)	27.1(12)	1.8(9)	6.9(9)	1.1(10)
C21	40.1(18)	41(2)	44.7(18)	-7.4(14)	21.8(15)	-15.2(14)
Br1A	44.2(12)	55.6(19)	27.4(10)	-4.1(14)	1.5(7)	-2.6(15)

Table 4 Bond Lengths for 22mv_MLB2Likhopotso_LCM_26_2_f.

Atom	Atom	Length/Å	Atom	Atom	Length/Å
Br1	C4	1.894(4)	Br1A	C4A	1.894(5)
O1	C6	1.226(5)	O1A	C6A	1.226(5)
O2	C9	1.363(3)	O2A	C9A	1.363(4)
O2	C13	1.430(3)	O2A	C13A	1.431(4)
O3	C14	1.207(3)	O3A	C14A	1.207(3)
O4	C17	1.363(3)	O4A	C17A	1.363(4)
O4	C21	1.416(4)	O4A	C21A	1.416(5)
N1	C1	1.334(3)	N1A	C1A	1.334(3)
N1	C5	1.339(6)	N1A	C5A	1.339(6)
N2	C1	1.427(3)	N2A	C1A	1.427(3)
N2	C6	1.392(4)	N2A	C6A	1.392(4)
N2	C14	1.449(3)	N2A	C14A	1.449(3)
C1	C2	1.390(3)	C1A	C2A	1.390(4)
C2	C3	1.384(5)	C2A	C3A	1.384(5)

Table 4 Bond Lengths for 22mv_MLB2Likhopotso_LCM_26_2_f.

Atom	Atom	Length/Å	Atom	Atom	Length/Å
C3	C4	1.380(3)	C3A	C4A	1.380(4)
C4	C5	1.379(3)	C4A	C5A	1.379(3)
C6	C7	1.491(3)	C6A	C7A	1.491(4)
C7	C8	1.387(4)	C7A	C8A	1.387(4)
C7	C12	1.389(4)	C7A	C12A	1.389(4)
C8	C9	1.397(3)	C8A	C9A	1.397(4)
C9	C10	1.390(4)	C9A	C10A	1.390(4)
C10	C11	1.367(4)	C10A	C11A	1.368(5)
C11	C12	1.376(4)	C11A	C12A	1.376(4)
C14	C15	1.479(3)	C14A	C15A	1.479(4)
C15	C16	1.403(3)	C15A	C16A	1.403(4)
C15	C20	1.390(3)	C15A	C20A	1.390(4)
C16	C17	1.383(4)	C16A	C17A	1.383(4)
C17	C18	1.399(4)	C17A	C18A	1.398(4)
C18	C19	1.381(4)	C18A	C19A	1.381(4)
C19	C20	1.386(3)	C19A	C20A	1.386(4)

Table 5 Bond Angles for 22mv_MLB2Likhopotso_LCM_26_2_f.

Atom	Atom	Atom	Angle/˚	Atom	Atom	Atom	Angle/˚
C9	O2	C13	117.7(2)	C9A	O2A	C13A	118.4(9)
C17	O4	C21	118.6(2)	C17A	O4A	C21A	118.7(13)
C1	N1	C5	117.5(3)	C1A	N1A	C5A	118.3(15)
C1	N2	C14	114.48(17)	C1A	N2A	C14A	114.1(9)
C6	N2	C1	119.9(2)	C6A	N2A	C1A	121.6(9)
C6	N2	C14	121.2(2)	C6A	N2A	C14A	120.8(10)
N1	C1	N2	113.63(19)	N1A	C1A	N2A	115.4(10)
N1	C1	C2	124.2(2)	N1A	C1A	C2A	123.6(10)

Table 5 Bond Angles for 22mv_MLB2Likhopotso_LCM_26_2_f.

Atom	Atom	Atom	Angle/˚	Atom	Atom	Atom	Angle/˚
C2	C1	N2	122.2(2)	C2A	C1A	N2A	121.0(9)
C3	C2	C1	117.8(3)	C3A	C2A	C1A	117.0(15)
C4	C3	C2	118.0(4)	C4A	C3A	C2A	118.0(14)
C3	C4	Br1	120.1(3)	C3A	C4A	Br1A	119.6(12)
C5	C4	Br1	119.2(4)	C5A	C4A	Br1A	118.3(13)
C5	C4	C3	120.7(4)	C5A	C4A	C3A	119(2)
N1	C5	C4	121.7(5)	N1A	C5A	C4A	120.6(17)
O1	C6	N2	120.8(2)	O1A	C6A	N2A	119.6(9)
O1	C6	C7	121.0(3)	O1A	C6A	C7A	120.4(11)
N2	C6	C7	118.1(4)	N2A	C6A	C7A	119.5(10)
C8	C7	C6	122.2(2)	C8A	C7A	C6A	120.1(12)
C8	C7	C12	119.8(2)	C8A	C7A	C12A	120.2(10)
C12	C7	C6	117.9(3)	C12A	C7A	C6A	119.3(13)
C7	C8	C9	120.0(2)	C7A	C8A	C9A	121.0(10)
O2	C9	C8	115.3(2)	O2A	C9A	C8A	116.6(8)
O2	C9	C10	124.9(2)	O2A	C9A	C10A	126.1(9)
C10	C9	C8	119.8(3)	C10A	C9A	C8A	117.3(10)
C11	C10	C9	119.1(2)	C11A	C10A	C9A	121.6(12)
C10	C11	C12	122.1(3)	C10A	C11A	C12A	121.0(13)
C11	C12	C7	119.2(3)	C11A	C12A	C7A	118.8(12)
O3	C14	N2	120.2(2)	O3A	C14A	N2A	119.6(9)
O3	C14	C15	123.9(2)	O3A	C14A	C15A	124.9(9)
N2	C14	C15	115.82(19)	N2A	C14A	C15A	115.4(8)
C16	C15	C14	117.8(2)	C16A	C15A	C14A	117.6(8)
C20	C15	C14	121.2(2)	C20A	C15A	C14A	123.7(9)
C20	C15	C16	120.9(2)	C20A	C15A	C16A	118.6(10)
C17	C16	C15	119.4(2)	C17A	C16A	C15A	121.0(9)

Table 5 Bond Angles for 22mv_MLB2Likhopotso_LCM_26_2_f.

Atom	Atom	Atom	Angle/˚	Atom	Atom	Atom	Angle/˚
O4	C17	C16	124.2(2)	O4A	C17A	C16A	125.1(9)
O4	C17	C18	116.1(2)	O4A	C17A	C18A	114.8(9)
C16	C17	C18	119.7(2)	C16A	C17A	C18A	120.1(9)
C19	C18	C17	120.2(2)	C19A	C18A	C17A	118.6(11)
C18	C19	C20	120.8(3)	C18A	C19A	C20A	121.8(14)
C19	C20	C15	118.9(3)	C19A	C20A	C15A	119.9(13)

Table 6 Torsion Angles for 22mv_MLB2Likhopotso_LCM_26_2_f.

A	B	C	D	Angle/˚	A	B	C	D	Angle/˚
Br1	C4	C5	N1	-179.5(10)	Br1A	C4A	C5A	N1A	180(7)
O1	C6	C7	C8	-143.9(3)	O1A	C6A	C7A	C8A	146(3)
O1	C6	C7	C12	33.9(4)	O1A	C6A	C7A	C12A	-27(5)
O2	C9	C10	C11	-179.1(3)	O2A	C9A	C10A	C11A	178.7(17)
O3	C14	C15	C16	19.4(3)	O3A	C14A	C15A	C16A	-19(2)
O3	C14	C15	C20	-156.3(2)	O3A	C14A	C15A	C20A	157.9(18)
O4	C17	C18	C19	179.1(3)	O4A	C17A	C18A	C19A	-180.0(14)
N1	C1	C2	C3	1.0(6)	N1A	C1A	C2A	C3A	-7(4)
N2	C1	C2	C3	-179.4(5)	N2A	C1A	C2A	C3A	174(4)
N2	C6	C7	C8	33.0(5)	N2A	C6A	C7A	C8A	-42(4)
N2	C6	C7	C12	-149.2(3)	N2A	C6A	C7A	C12A	145(3)
N2	C14	C15	C16	-162.91(19)	N2A	C14A	C15A	C16A	162.6(13)
N2	C14	C15	C20	21.3(3)	N2A	C14A	C15A	C20A	-20(2)
C1	N1	C5	C4	0.2(15)	C1A	N1A	C5A	C4A	-11(10)
C1	N2	C6	O1	2.6(4)	C1A	N2A	C6A	O1A	-8(4)
C1	N2	C6	C7	-174.3(2)	C1A	N2A	C6A	C7A	180(2)
C1	N2	C14	O3	-117.8(2)	C1A	N2A	C14A	O3A	117.4(15)
C1	N2	C14	C15	64.5(3)	C1A	N2A	C14A	C15A	-64.5(17)

Table 6 Torsion Angles for 22mv_MLB2Likhopotso_LCM_26_2_f.

A	B	C	D	Angle/˚	A	B	C	D	Angle/˚
C1	C2	C3	C4	-3.0(10)	C1A	C2A	C3A	C4A	15(8)
C2	C3	C4	Br1	-179.2(7)	C2A	C3A	C4A	Br1A	179(5)
C2	C3	C4	C5	3.7(14)	C2A	C3A	C4A	C5A	-21(10)
C3	C4	C5	N1	-2.3(18)	C3A	C4A	C5A	N1A	19(11)
C5	N1	C1	N2	-179.2(8)	C5A	N1A	C1A	N2A	-176(5)
C5	N1	C1	C2	0.4(8)	C5A	N1A	C1A	C2A	5(6)
C6	N2	C1	N1	-131.1(2)	C6A	N2A	C1A	N1A	132(2)
C6	N2	C1	C2	49.3(3)	C6A	N2A	C1A	C2A	-50(3)
C6	N2	C14	O3	38.6(3)	C6A	N2A	C14A	O3A	-42(3)
C6	N2	C14	C15	-139.1(2)	C6A	N2A	C14A	C15A	136(2)
C6	C7	C8	C9	178.4(3)	C6A	C7A	C8A	C9A	-176(2)
C6	C7	C12	C11	-178.4(3)	C6A	C7A	C12A	C11A	173(2)
C7	C8	C9	O2	178.8(3)	C7A	C8A	C9A	O2A	-177(2)
C7	C8	C9	C10	-0.4(4)	C7A	C8A	C9A	C10A	5(3)
C8	C7	C12	C11	-0.5(5)	C8A	C7A	C12A	C11A	0(4)
C8	C9	C10	C11	0.0(4)	C8A	C9A	C10A	C11A	-3(3)
C9	C10	C11	C12	0.2(5)	C9A	C10A	C11A	C12A	0(3)
C10	C11	C12	C7	0.1(5)	C10A	C11A	C12A	C7A	1(3)
C12	C7	C8	C9	0.7(5)	C12A	C7A	C8A	C9A	-3(4)
C13	O2	C9	C8	-179.0(2)	C13A	O2A	C9A	C8A	179.8(13)
C13	O2	C9	C10	0.2(4)	C13A	O2A	C9A	C10A	-2(2)
C14	N2	C1	N1	25.6(3)	C14A	N2A	C1A	N1A	-27(2)
C14	N2	C1	C2	-154.0(2)	C14A	N2A	C1A	C2A	151.3(15)
C14	N2	C6	O1	-152.5(2)	C14A	N2A	C6A	O1A	149(2)
C14	N2	C6	C7	30.6(3)	C14A	N2A	C6A	C7A	-23(4)
C14	C15	C16	C17	-176.2(2)	C14A	C15A	C16A	C17A	178.0(15)
C14	C15	C20	C19	174.3(2)	C14A	C15A	C20A	C19A	-175.9(17)

Table 6 Torsion Angles for 22mv_MLB2Likhopotso_LCM_26_2_f.

A	B	C	D	Angle/˚	A	B	C	D	Angle/˚
C15	C16	C17	O4	-179.3(2)	C15A	C16A	C17A	O4A	178.6(16)
C15	C16	C17	C18	2.1(4)	C15A	C16A	C17A	C18A	-1(3)
C16	C15	C20	C19	-1.3(4)	C16A	C15A	C20A	C19A	1(3)
C16	C17	C18	C19	-2.2(4)	C16A	C17A	C18A	C19A	0(3)
C17	C18	C19	C20	0.4(4)	C17A	C18A	C19A	C20A	2(3)
C18	C19	C20	C15	1.3(4)	C18A	C19A	C20A	C15A	-3(3)
C20	C15	C16	C17	-0.4(3)	C20A	C15A	C16A	C17A	0(3)
C21	O4	C17	C16	9.6(4)	C21A	O4A	C17A	C16A	6(3)
C21	O4	C17	C18	-171.7(3)	C21A	O4A	C17A	C18A	-174.8(15)

Table 7 Hydrogen Atom Coordinates (Å×10^4) and Isotropic Displacement Parameters (Å^2×10^3) for 22mv_MLB2Likhopotso_LCM_26_2_f.

Atom	*X*	*Y*	*z*	U(eq)
H2	7150.28	6901.87	1973.51	31
H3	6534.09	7426.24	1007.16	34
H5	4949.78	7511.09	1702.02	29
H8	7459.11	4737.35	3798.93	30
H10	8586.63	6370.81	5346.57	43
H11	8496.11	9061.41	4974.55	48
H12	7898.68	9654.13	4032.25	39
H13A	8852.24	3434.78	5385.6	71
H13B	8324.78	2064.4	5448.39	71
H13C	8250.12	3947.17	5659.21	71
H16	5382.53	4363.65	3670.09	26
H18	5572.35	-155.25	2927.36	41
H19	6411.94	870.21	2533.16	38
H20	6737.56	3656.36	2684.71	29

Table 7 Hydrogen Atom Coordinates (Å×10^4) and Isotropic Displacement Parameters (Å^2×10^3) for 22mv_MLB2Likhopotso_LCM_26_2_f.

Atom	*X*	*Y*	*z*	U(eq)
H21A	4327.2	3272.28	3522.87	60
H21B	4752.47	2833.43	4166.11	60
H21C	4143.07	1707.89	3887.2	60
H2A	7126.52	8235.89	1956.08	37
H3A	6532.05	7242	1025.07	37
H5A	4961.16	7068.75	1700.73	37
H8A	7492.56	10227.61	3787.12	37
H10A	8595.43	8579.26	5328.54	37
H11A	8481.38	5879.13	4979.77	37
H12A	7845.04	5277.44	4048.53	37
H13D	8843.9	11277.67	5423.78	46
H13E	8193.53	11292.54	5664.12	46
H13F	8440.22	12969.18	5405.95	46
H16A	5400.16	10662.99	3657.75	37
H18A	5500.41	15118.07	2839.75	37
H19A	6366.87	14114.55	2476.77	37
H20A	6714.04	11367.54	2641.05	37
H21D	4283.88	11936.91	3670.64	46
H21E	4360.58	13520.13	4105.96	46
H21F	4922.12	12163.43	4174.69	46

Table 8 Atomic Occupancy for 22mv_MLB2Likhopotso_LCM_26_2_f.

Atom	*Occupancy*	Atom	*Occupancy*	Atom	*Occupancy*
Br1	0.8527(15)	O1	0.8527(15)	O2	0.8527(15)
O3	0.8527(15)	O4	0.8527(15)	N1	0.8527(15)
N2	0.8527(15)	C1	0.8527(15)	C2	0.8527(15)

Table 8 Atomic Occupancy for 22mv_MLB2Likhopotso_LCM_26_2_f.

Atom	*Occupancy*	Atom	*Occupancy*	Atom	*Occupancy*
H2	0.8527(15)	C3	0.8527(15)	H3	0.8527(15)
C4	0.8527(15)	C5	0.8527(15)	H5	0.8527(15)
C6	0.8527(15)	C7	0.8527(15)	C8	0.8527(15)
H8	0.8527(15)	C9	0.8527(15)	C10	0.8527(15)
H10	0.8527(15)	C11	0.8527(15)	H11	0.8527(15)
C12	0.8527(15)	H12	0.8527(15)	C13	0.8527(15)
H13A	0.8527(15)	H13B	0.8527(15)	H13C	0.8527(15)
C14	0.8527(15)	C15	0.8527(15)	C16	0.8527(15)
H16	0.8527(15)	C17	0.8527(15)	C18	0.8527(15)
H18	0.8527(15)	C19	0.8527(15)	H19	0.8527(15)
C20	0.8527(15)	H20	0.8527(15)	C21	0.8527(15)
H21A	0.8527(15)	H21B	0.8527(15)	H21C	0.8527(15)
Br1A	0.1473(15)	O1A	0.1473(15)	O2A	0.1473(15)
O3A	0.1473(15)	O4A	0.1473(15)	N1A	0.1473(15)
N2A	0.1473(15)	C1A	0.1473(15)	C2A	0.1473(15)
H2A	0.1473(15)	C3A	0.1473(15)	H3A	0.1473(15)
C4A	0.1473(15)	C5A	0.1473(15)	H5A	0.1473(15)
C6A	0.1473(15)	C7A	0.1473(15)	C8A	0.1473(15)
H8A	0.1473(15)	C9A	0.1473(15)	C10A	0.1473(15)
H10A	0.1473(15)	C11A	0.1473(15)	H11A	0.1473(15)
C12A	0.1473(15)	H12A	0.1473(15)	C13A	0.1473(15)
H13D	0.1473(15)	H13E	0.1473(15)	H13F	0.1473(15)
C14A	0.1473(15)	C15A	0.1473(15)	C16A	0.1473(15)
H16A	0.1473(15)	C17A	0.1473(15)	C18A	0.1473(15)
H18A	0.1473(15)	C19A	0.1473(15)	H19A	0.1473(15)
C20A	0.1473(15)	H20A	0.1473(15)	C21A	0.1473(15)
H21D	0.1473(15)	H21E	0.1473(15)	H21F	0.1473(15)

10. Crystallographic data for 3-((6-chloro-2-(propylamino)pyrimidin-4-yl)oxy)-*N*-(p-tolyl)benzamide 184d

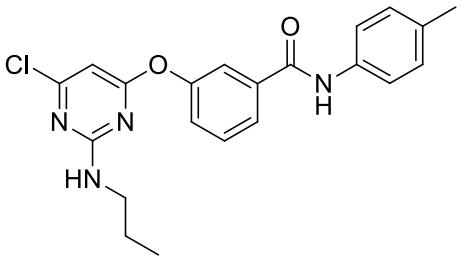

Table 1 Crystal data and structure refinement for 22mbB_MLB2_LCM_58_2_0f.

Identification code	22mbB_MLB2_LCM_58_2_0f
Empirical formula	$C_{42}H_{40}Cl_2N_8O_4$
Formula weight	791.72
Temperature/K	173.00
Crystal system	triclinic
Space group	P-1
a/Å	9.9951(12)
b/Å	11.5794(14)
c/Å	18.459(2)
α/°	92.121(6)
β/°	99.267(6)
γ/°	90.313(5)
Volume/Å^3	2106.9(5)
Z	2
ρ_{calc}g/cm^3	1.248
μ/mm^{-1}	1.792
F(000)	828.0
Crystal size/mm^3	0.139 × 0.028 × 0.016
Radiation	CuKα (λ = 1.54178)
2Θ range for data collection/°	4.854 to 135.82
Index ranges	-10 ≤ h ≤ 11, -13 ≤ k ≤ 13, -21 ≤ l ≤ 22

Reflections collected	46976
Independent reflections	7430 [R_{int} = 0.2423, R_{sigma} = 0.2322]
Data/restraints/parameters	7430/0/509
Goodness-of-fit on F^2	0.934
Final R indexes [I>=2σ (I)]	R_1 = 0.1015, wR_2 = 0.2212
Final R indexes [all data]	R_1 = 0.2804, wR_2 = 0.3269
Largest diff. peak/hole / e Å^{-3}	0.40/-0.60

Table 2 Fractional Atomic Coordinates (×10^4) and Equivalent Isotropic Displacement Parameters (Å^2×10^3) for 22mbB_MLB2_LCM_58_2_0f. U_{eq} is defined as 1/3 of the trace of the orthogonalised U_{IJ} tensor.

Atom	*X*	*y*	*z*	U(eq)
Cl01	5116(2)	8398.4(15)	-1034.0(10)	67.8(7)
Cl02	148(2)	8423.7(16)	-1072.1(11)	70.7(7)
O003	-540(6)	5628(4)	849(3)	62.2(15)
O004	4432(6)	5592(4)	883(3)	62.8(16)
O005	634(6)	6272(4)	3638(3)	64.9(16)
N006	3306(7)	7311(5)	874(3)	53.4(17)
N007	-1421(7)	8707(5)	-91(3)	54.0(18)
N008	2189(7)	9052(5)	832(3)	58.0(18)
N009	3599(7)	6162(5)	4023(3)	55.4(18)
N00A	3586(7)	8702(5)	-29(3)	52.2(17)
N00B	-1691(7)	7342(5)	826(3)	51.6(17)
N00C	-2825(7)	9054(5)	765(3)	55.5(17)
O00D	5670(7)	6219(5)	3643(3)	77.7(19)
N00G	-1485(7)	6329(5)	3940(4)	61.3(19)
C00H	-1185(8)	5540(5)	2751(4)	45.1(19)
C00I	3050(9)	8346(6)	555(4)	51(2)
C00J	-557(8)	7983(6)	-328(4)	51(2)

Table 2 Fractional Atomic Coordinates ($\times 10^4$) and Equivalent Isotropic Displacement Parameters ($Å^2 \times 10^3$) for 22mbB_MLB2_LCM_58_2_0f. U_{eq} is defined as 1/3 of the trace of the orthogonalised U_{IJ} tensor.

Atom	*X*	*y*	*z*	U(eq)
C00K	3833(8)	5342(6)	1505(5)	51(2)
C00L	-607(10)	6074(6)	3479(5)	57(2)
C00M	-840(9)	6671(6)	549(4)	51(2)
C00N	-3403(8)	8831(5)	1415(4)	52(2)
C00O	1583(8)	8784(6)	1460(4)	57(2)
C00P	-613(8)	5834(5)	2142(4)	52(2)
C00Q	-1133(8)	5365(6)	1466(4)	51(2)
C00R	-2171(9)	4585(6)	1373(5)	63(2)
C00S	-1966(8)	8355(6)	492(4)	53(2)
C00T	4137(9)	6641(6)	585(4)	55(2)
C00U	4383(9)	5798(6)	2182(5)	60(2)
C00V	3991(9)	6546(6)	4755(4)	53(2)
C00W	3802(8)	5511(6)	2791(4)	52(2)
C00X	-202(8)	6925(6)	-42(4)	56(2)
C00Z	4564(11)	7355(6)	6239(4)	64(2)
C010	4761(8)	6895(6)	-8(4)	58(2)
C011	5310(10)	6602(6)	5135(5)	68(2)
C012	4405(8)	7966(6)	-290(4)	50(2)
C013	-2243(9)	4755(6)	2669(4)	63(2)
C014	2186(9)	4291(6)	2006(5)	68(2)
C015	2978(9)	6874(6)	5150(4)	63(2)
C016	2713(9)	4751(6)	2692(4)	61(2)
C017	5577(10)	6996(7)	5857(5)	68(2)
C018	4427(11)	5993(6)	3515(5)	61(3)
C019	3246(10)	7263(6)	5864(5)	70(3)

Table 2 Fractional Atomic Coordinates (×10^4) and Equivalent Isotropic Displacement Parameters (Å^2×10^3) for 22mbB_MLB2_LCM_58_2_0f. U_{eq} is defined as 1/3 of the trace of the orthogonalised U_{IJ} tensor.

Atom	*X*	*y*	*z*	U(eq)
C01A	-1041(9)	6843(6)	4666(4)	59(2)
C01B	2771(9)	4575(6)	1401(5)	63(2)
C01C	-985(8)	6207(6)	5273(4)	63(2)
C01D	-2736(9)	4273(6)	1978(5)	69(3)
C01E	-590(9)	6695(7)	5959(5)	67(3)
C01F	-2495(9)	9231(7)	2114(5)	76(3)
C01G	2459(10)	9113(7)	2178(4)	78(3)
C01H	-299(9)	7838(7)	6059(4)	72(3)
C01I	-3111(10)	8977(7)	2796(4)	93(3)
C01J	4896(10)	7803(7)	7022(4)	85(3)
C01K	121(11)	8366(8)	6827(5)	105(4)
C01L	1819(10)	8715(8)	2833(4)	94(3)
C01M	-323(13)	8464(7)	5451(5)	133(5)
C01N	-694(12)	7985(7)	4756(5)	112(4)

Table 3 Anisotropic Displacement Parameters (Å^2×10^3) for 22mbB_MLB2_LCM_58_2_0f. The Anisotropic displacement factor exponent takes the form: $-2\pi^2[h^2a^{*2}U_{11}+2hka^*b^*U_{12}+\ldots]$.

Atom	U_{11}	U_{22}	U_{33}	U_{23}	U_{13}	U_{12}
Cl01	76.0(18)	56.7(12)	73.8(13)	9.2(10)	20.1(12)	3.1(11)
Cl02	80.1(19)	58.3(12)	77.5(14)	13.3(10)	21.6(12)	5.2(11)
O003	80(5)	41(3)	67(3)	13(3)	15(3)	13(3)
O004	84(5)	39(3)	68(3)	9(3)	17(3)	13(3)
O005	56(5)	65(3)	71(4)	2(3)	4(3)	-7(3)
N006	56(5)	39(4)	63(4)	11(3)	3(4)	2(3)
N007	51(5)	45(4)	65(4)	8(3)	7(4)	-3(3)
N008	56(5)	49(4)	75(4)	7(3)	25(4)	9(3)

Table 3 Anisotropic Displacement Parameters ($Å^2×10^3$) for 22mbB_MLB2_LCM_58_2_0f. The Anisotropic displacement factor exponent takes the form: $-2π^2[h^2a^{*2}U_{11}+2hka*b*U_{12}+…]$.

Atom	U_{11}	U_{22}	U_{33}	U_{23}	U_{13}	U_{12}
N009	65(6)	52(4)	52(4)	4(3)	16(4)	-2(3)
N00A	48(5)	39(4)	70(4)	1(3)	11(4)	4(3)
N00B	51(5)	33(4)	69(4)	12(3)	2(3)	5(3)
N00C	59(5)	44(4)	68(4)	11(3)	20(4)	5(3)
O00D	68(5)	90(4)	71(4)	-5(3)	2(4)	-12(4)
N00G	57(6)	63(4)	65(5)	5(4)	13(4)	1(4)
C00H	40(6)	33(4)	61(5)	5(4)	3(4)	-3(4)
C00I	47(6)	50(5)	56(5)	10(4)	2(4)	-13(4)
C00J	54(7)	45(5)	54(5)	1(4)	13(4)	-4(4)
C00K	48(6)	34(4)	72(6)	11(4)	11(5)	7(4)
C00L	42(7)	45(5)	80(6)	21(4)	-3(5)	-9(4)
C00M	50(6)	41(5)	61(5)	9(4)	-2(4)	-2(4)
C00N	46(6)	40(4)	70(5)	10(4)	7(4)	-4(4)
C00O	65(7)	43(4)	67(5)	1(4)	21(5)	-3(4)
C00P	49(6)	40(4)	66(5)	13(4)	6(4)	2(4)
C00Q	51(6)	39(4)	61(5)	8(4)	0(4)	2(4)
C00R	66(7)	51(5)	70(6)	-1(4)	2(5)	7(5)
C00S	42(6)	42(5)	73(6)	7(4)	4(4)	3(4)
C00T	62(7)	37(5)	64(5)	4(4)	2(5)	0(4)
C00U	60(7)	41(4)	78(6)	4(4)	7(5)	0(4)
C00V	57(7)	43(4)	62(6)	13(4)	19(5)	0(4)
C00W	43(6)	40(4)	73(6)	13(4)	8(5)	7(4)
C00X	66(7)	38(4)	63(5)	3(4)	7(5)	5(4)
C00Z	80(8)	51(5)	60(6)	9(4)	4(5)	-6(5)
C010	65(7)	44(5)	61(5)	0(4)	1(5)	6(4)
C011	65(8)	72(6)	69(6)	9(5)	12(5)	11(5)

Table 3 Anisotropic Displacement Parameters ($Å^2×10^3$) for 22mbB_MLB2_LCM_58_2_0f. The Anisotropic displacement factor exponent takes the form: $-2π^2[h^2a^{*2}U_{11}+2hka*b*U_{12}+…]$.

Atom	U_{11}	U_{22}	U_{33}	U_{23}	U_{13}	U_{12}
C012	50(6)	44(5)	54(5)	2(4)	5(4)	-10(4)
C013	66(7)	48(5)	73(6)	6(4)	5(5)	0(4)
C014	57(7)	49(5)	96(7)	-3(5)	8(6)	-1(4)
C015	55(7)	70(5)	60(5)	-6(4)	1(5)	-9(5)
C016	61(7)	49(5)	74(6)	10(4)	11(5)	2(4)
C017	68(8)	67(6)	70(6)	5(4)	11(5)	-1(5)
C018	60(8)	51(5)	64(6)	6(4)	-12(6)	-3(5)
C019	57(8)	68(6)	85(7)	0(5)	11(5)	-9(5)
C01A	61(7)	47(5)	71(6)	9(4)	13(5)	-1(4)
C01B	63(7)	53(5)	72(6)	0(4)	10(5)	-1(4)
C01C	64(7)	46(5)	80(6)	17(4)	9(5)	-6(4)
C01D	69(7)	45(5)	91(7)	4(5)	10(6)	-15(4)
C01E	66(7)	61(5)	72(6)	15(4)	2(5)	-15(5)
C01F	67(8)	67(6)	94(7)	-3(5)	9(6)	-4(5)
C01G	89(8)	71(6)	77(6)	4(5)	28(6)	-12(5)
C01H	78(8)	63(6)	73(6)	7(5)	3(5)	3(5)
C01I	111(10)	93(7)	78(6)	17(5)	25(6)	-4(6)
C01J	96(9)	83(6)	73(6)	5(5)	2(5)	1(6)
C01K	139(11)	86(7)	87(7)	-8(5)	8(7)	8(7)
C01L	85(9)	111(8)	84(6)	3(6)	6(6)	-9(6)
C01M	269(17)	44(5)	75(7)	8(5)	-12(8)	-21(7)
C01N	196(13)	53(6)	78(7)	11(5)	-6(7)	-15(7)

Table 4 Bond Lengths for 22mbB_MLB2_LCM_58_2_0f.

Atom	Atom	Length/Å	Atom	Atom	Length/Å
Cl01	C012	1.734(7)	C00M	C00X	1.389(10)

Table 4 Bond Lengths for 22mbB_MLB2_LCM_58_2_0f.

Atom	Atom	Length/Å	Atom	Atom	Length/Å
Cl02	C00J	1.734(7)	C00N	C01F	1.508(10)
O003	C00M	1.362(8)	C00O	C01G	1.501(10)
O003	C00Q	1.407(9)	C00P	C00Q	1.364(9)
O004	C00K	1.414(8)	C00Q	C00R	1.358(10)
O004	C00T	1.366(8)	C00R	C01D	1.389(10)
O005	C00L	1.246(9)	C00T	C010	1.384(10)
N006	C00I	1.363(8)	C00U	C00W	1.397(10)
N006	C00T	1.303(9)	C00V	C011	1.390(11)
N007	C00J	1.320(9)	C00V	C015	1.387(10)
N007	C00S	1.357(9)	C00W	C016	1.381(10)
N008	C00I	1.338(9)	C00W	C018	1.470(10)
N008	C00O	1.434(8)	C00Z	C017	1.381(11)
N009	C00V	1.400(9)	C00Z	C019	1.387(11)
N009	C018	1.355(10)	C00Z	C01J	1.502(10)
N00A	C00I	1.354(9)	C010	C012	1.388(9)
N00A	C012	1.316(9)	C011	C017	1.376(10)
N00B	C00M	1.307(9)	C013	C01D	1.388(10)
N00B	C00S	1.353(8)	C014	C016	1.378(10)
N00C	C00N	1.444(8)	C014	C01B	1.390(10)
N00C	C00S	1.327(9)	C015	C019	1.360(10)
O00D	C018	1.252(9)	C01A	C01C	1.358(9)
N00G	C00L	1.343(10)	C01A	C01N	1.363(10)
N00G	C01A	1.447(9)	C01C	C01E	1.365(10)
C00H	C00L	1.485(10)	C01E	C01H	1.353(10)
C00H	C00P	1.392(9)	C01F	C01I	1.527(10)
C00H	C013	1.377(10)	C01G	C01L	1.539(10)
C00J	C00X	1.377(9)	C01H	C01K	1.517(10)

Table 4 Bond Lengths for 22mbB_MLB2_LCM_58_2_0f.

Atom	Atom	Length/Å	Atom	Atom	Length/Å
C00K	C00U	1.368(9)	C01H	C01M	1.356(11)
C00K	C01B	1.366(10)	C01M	C01N	1.372(11)

Table 5 Bond Angles for 22mbB_MLB2_LCM_58_2_0f.

Atom	Atom	Atom	Angle/˚	Atom	Atom	Atom	Angle/˚
C00M	O003	C00Q	117.0(6)	N006	C00T	C010	125.6(7)
C00T	O004	C00K	116.4(6)	C00K	C00U	C00W	119.0(8)
C00T	N006	C00I	115.7(7)	C011	C00V	N009	126.0(8)
C00J	N007	C00S	115.1(6)	C015	C00V	N009	117.7(8)
C00I	N008	C00O	123.0(6)	C015	C00V	C011	116.2(8)
C018	N009	C00V	126.4(7)	C00U	C00W	C018	118.0(8)
C012	N00A	C00I	115.3(6)	C016	C00W	C00U	118.8(8)
C00M	N00B	C00S	115.9(7)	C016	C00W	C018	123.2(8)
C00S	N00C	C00N	124.0(6)	C00J	C00X	C00M	113.1(7)
C00L	N00G	C01A	121.8(7)	C017	C00Z	C019	116.5(8)
C00P	C00H	C00L	118.4(7)	C017	C00Z	C01J	120.8(9)
C013	C00H	C00L	121.8(7)	C019	C00Z	C01J	122.7(9)
C013	C00H	C00P	119.8(7)	C00T	C010	C012	113.1(7)
N008	C00I	N006	117.4(7)	C017	C011	C00V	121.0(9)
N008	C00I	N00A	117.8(7)	N00A	C012	Cl01	116.5(6)
N00A	C00I	N006	124.8(8)	N00A	C012	C010	125.4(7)
N007	C00J	Cl02	115.6(6)	C010	C012	Cl01	118.0(7)
N007	C00J	C00X	125.6(7)	C00H	C013	C01D	119.4(8)
C00X	C00J	Cl02	118.7(7)	C016	C014	C01B	119.8(8)
C00U	C00K	O004	119.9(7)	C019	C015	C00V	122.6(8)
C01B	C00K	O004	117.2(8)	C014	C016	C00W	121.2(8)
C01B	C00K	C00U	122.7(8)	C011	C017	C00Z	122.3(9)

Table 5 Bond Angles for 22mbB_MLB2_LCM_58_2_0f.

Atom	Atom	Atom	Angle/˚	Atom	Atom	Atom	Angle/˚
O005	C00L	N00G	123.0(8)	N009	C018	C00W	116.9(8)
O005	C00L	C00H	120.3(9)	O00D	C018	N009	122.9(8)
N00G	C00L	C00H	116.8(8)	O00D	C018	C00W	120.2(9)
O003	C00M	C00X	115.8(8)	C015	C019	C00Z	121.4(9)
N00B	C00M	O003	118.9(7)	C01C	C01A	N00G	120.9(7)
N00B	C00M	C00X	125.3(7)	C01C	C01A	C01N	118.4(8)
N00C	C00N	C01F	112.8(7)	C01N	C01A	N00G	120.6(7)
N008	C00O	C01G	113.4(7)	C00K	C01B	C014	118.4(8)
C00Q	C00P	C00H	119.6(7)	C01A	C01C	C01E	121.0(7)
C00P	C00Q	O003	120.2(7)	C013	C01D	C00R	120.2(8)
C00R	C00Q	O003	118.1(7)	C01H	C01E	C01C	121.2(7)
C00R	C00Q	C00P	121.6(8)	C00N	C01F	C01I	112.2(7)
C00Q	C00R	C01D	119.3(8)	C00O	C01G	C01L	111.4(7)
N00B	C00S	N007	124.9(8)	C01E	C01H	C01K	120.4(8)
N00C	C00S	N007	118.0(7)	C01E	C01H	C01M	117.5(8)
N00C	C00S	N00B	117.0(8)	C01M	C01H	C01K	122.0(8)
O004	C00T	C010	116.1(8)	C01H	C01M	C01N	122.1(8)
N006	C00T	O004	118.2(8)	C01A	C01N	C01M	119.7(8)

Table 6 Torsion Angles for 22mbB_MLB2_LCM_58_2_0f.

A	B	C	D	Angle/˚	A	B	C	D	Angle/˚
Cl02	C00J	C00X	C00M	-179.7(6)	C00S	N007	C00J	Cl02	-179.9(5)
O003	C00M	C00X	C00J	179.3(6)	C00S	N007	C00J	C00X	1.1(11)
O003	C00Q	C00R	C01D	177.3(7)	C00S	N00B	C00M	O003	-178.7(6)
O004	C00K	C00U	C00W	-178.0(6)	C00S	N00B	C00M	C00X	0.9(11)
O004	C00K	C01B	C014	178.4(6)	C00S	N00C	C00N	C01F	85.0(9)
O004	C00T	C010	C012	179.2(6)	C00T	O004	C00K	C00U	-79.5(8)

Table 6 Torsion Angles for 22mbB_MLB2_LCM_58_2_0f.

A	B	C	D	Angle/˚	A	B	C	D	Angle/˚
N006	C00T	C010	C012	-0.6(12)	C00T	O004	C00K	C01B	105.2(7)
N007	C00J	C00X	C00M	-0.8(11)	C00T	N006	C00I	N008	179.3(7)
N008	C00O	C01G	C01L	-175.1(7)	C00T	N006	C00I	N00A	0.4(11)
N009	C00V	C011	C017	180.0(7)	C00T	C010	C012	Cl01	179.8(6)
N009	C00V	C015	C019	-179.8(6)	C00T	C010	C012	N00A	1.3(11)
N00B	C00M	C00X	C00J	-0.3(11)	C00U	C00K	C01B	C014	3.2(12)
N00C	C00N	C01F	C01I	-179.3(6)	C00U	C00W	C016	C014	-1.0(11)
N00G	C01A	C01C	C01E	-178.8(8)	C00U	C00W	C018	N009	151.3(7)
N00G	C01A	C01N	C01M	177.7(10)	C00U	C00W	C018	O00D	-29.3(11)
C00H	C00P	C00Q	O003	-178.1(6)	C00V	N009	C018	O00D	-3.3(12)
C00H	C00P	C00Q	C00R	-2.3(11)	C00V	N009	C018	C00W	176.1(6)
C00H	C013	C01D	C00R	-0.3(12)	C00V	C011	C017	C00Z	0.0(12)
C00I	N006	C00T	O004	180.0(6)	C00V	C015	C019	C00Z	0.0(11)
C00I	N006	C00T	C010	-0.1(12)	C011	C00V	C015	C019	2.0(11)
C00I	N008	C00O	C01G	85.0(9)	C012	N00A	C00I	N006	0.2(11)
C00I	N00A	C012	Cl01	-179.6(5)	C012	N00A	C00I	N008	-178.7(7)
C00I	N00A	C012	C010	-1.1(11)	C013	C00H	C00L	O005	143.3(7)
C00J	N007	C00S	N00B	-0.5(11)	C013	C00H	C00L	N00G	-37.0(10)
C00J	N007	C00S	N00C	178.8(7)	C013	C00H	C00P	C00Q	1.9(11)
C00K	O004	C00T	N006	-2.1(10)	C015	C00V	C011	C017	-1.9(10)
C00K	O004	C00T	C010	178.0(7)	C016	C00W	C018	N009	-31.8(11)
C00K	C00U	C00W	C016	1.8(11)	C016	C00W	C018	O00D	147.6(8)
C00K	C00U	C00W	C018	178.8(7)	C016	C014	C01B	C00K	-2.2(12)
C00L	N00G	C01A	C01C	-105.3(9)	C017	C00Z	C019	C015	-2.0(11)
C00L	N00G	C01A	C01N	75.9(11)	C018	N009	C00V	C011	-13.9(11)
C00L	C00H	C00P	C00Q	-179.3(6)	C018	N009	C00V	C015	168.1(7)
C00L	C00H	C013	C01D	-179.4(7)	C018	C00W	C016	C014	-177.9(7)

Table 6 Torsion Angles for 22mbB_MLB2_LCM_58_2_0f.

A	B	C	D	Angle/˚	A	B	C	D	Angle/˚
C00M	O003	C00Q	C00P	-78.2(9)	C019	C00Z	C017	C011	2.0(11)
C00M	O003	C00Q	C00R	105.8(8)	C01A	N00G	C00L	O005	-0.8(11)
C00M	N00B	C00S	N007	-0.5(11)	C01A	N00G	C00L	C00H	179.5(6)
C00M	N00B	C00S	N00C	-179.8(7)	C01A	C01C	C01E	C01H	2.9(14)
C00N	N00C	C00S	N007	-175.2(6)	C01B	C00K	C00U	C00W	-2.9(12)
C00N	N00C	C00S	N00B	4.1(11)	C01B	C014	C016	C00W	1.2(12)
C00O	N008	C00I	N006	2.6(11)	C01C	C01A	C01N	C01M	-1.1(16)
C00O	N008	C00I	N00A	-178.4(6)	C01C	C01E	C01H	C01K	179.2(9)
C00P	C00H	C00L	O005	-35.4(10)	C01C	C01E	C01H	C01M	-4.5(15)
C00P	C00H	C00L	N00G	144.2(7)	C01E	C01H	C01M	C01N	3.4(18)
C00P	C00H	C013	C01D	-0.6(11)	C01H	C01M	C01N	C01A	-0.6(19)
C00P	C00Q	C00R	C01D	1.3(12)	C01J	C00Z	C017	C011	-178.7(7)
C00Q	O003	C00M	N00B	-2.7(10)	C01J	C00Z	C019	C015	178.7(7)
C00Q	O003	C00M	C00X	177.7(7)	C01K	C01H	C01M	C01N	179.6(11)
C00Q	C00R	C01D	C013	0.0(12)	C01N	C01A	C01C	C01E	0.0(14)

Table 7 Hydrogen Atom Coordinates (Å×10^4) and Isotropic Displacement Parameters (Å^2×10^3) for 22mbB_MLB2_LCM_58_2_0f.

Atom	*X*	*y*	*z*	U(eq)
H008	1985.8	9710.3	619.6	70
H00C	-3056.27	9692.61	534.9	67
H00D	-3578.36	7990.64	1431.76	62
H00E	-4282.91	9228.85	1384.92	62
H00A	1386.19	7944.18	1444.59	69
H00B	710.21	9193.18	1432.24	69
H00P	134.83	6357.01	2197.34	62
H00R	-2506.19	4256	898.57	76

Table 7 Hydrogen Atom Coordinates (Å×10^4) and Isotropic Displacement Parameters (Å^2×10^3) for 22mbB_MLB2_LCM_58_2_0f.

Atom	*X*	*y*	*z*	U(eq)
H00U	5149.1	6301.92	2236.64	72
H00X	417.03	6420.71	-230.5	67
H010	5370.02	6388.41	-202.75	69
H011	6037.92	6363.55	4893.62	82
H013	-2632.09	4544.7	3083.25	75
H014	1425	3780.55	1945.99	82
H015	2061.03	6824.5	4913.67	76
H016	2319.26	4541.5	3104.53	74
H017	6489.4	7022.59	6101.41	82
H019	2515.36	7476.62	6110.54	84
H01B	2439.32	4243.99	927.2	75
H01J	-1223.34	5409.13	5219.65	76
H01K	-3462.99	3727.26	1917.83	83
H01L	-518.52	6224.24	6373.96	81
H01M	-2328.04	10072.82	2101.01	92
H01N	-1610.47	8839.26	2142.41	92
H01A	2588.64	9962.38	2217.46	93
H01C	3360.35	8756.38	2193.06	93
H01O	-3397.58	8164.04	2775.5	139
H01P	-3897.46	9472.03	2815.9	139
H01Q	-2433.63	9131.84	3236.18	139
H01D	5313.7	7189.16	7330.03	128
H01E	4062.12	8053.64	7194.16	128
H01F	5527.84	8459.8	7052.33	128
H01R	752.61	9011.59	6811.03	158
H01S	564.51	7779.99	7149.77	158

Table 7 Hydrogen Atom Coordinates (Å×10^4) and Isotropic Displacement Parameters (Å^2×10^3) for 22mbB_MLB2_LCM_58_2_0f.

Atom	*X*	*y*	*z*	U(eq)
H01T	-683.2	8648.83	7016.82	158
H01G	909.19	9038.05	2806.34	141
H01H	2383.52	8984.09	3292.94	141
H01I	1757.68	7869.07	2816.72	141
H01U	-74.32	9259.29	5507.88	160
H01V	-709.59	8447.54	4340.62	135

Table 8 Solvent masks information for 22mbB_MLB2_LCM_58_2_0f.

Number	X	Y	Z	Volume	Electron count	Content
1	0.500	1.000	0.500	162.3	59.4	?

Appendix 2: ^{1}H and ^{13}C NMR data for a selected number of compounds

Compound 157a

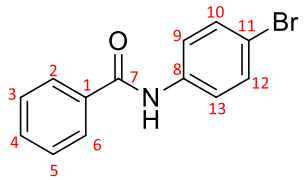

^{1}H NMR spectrum

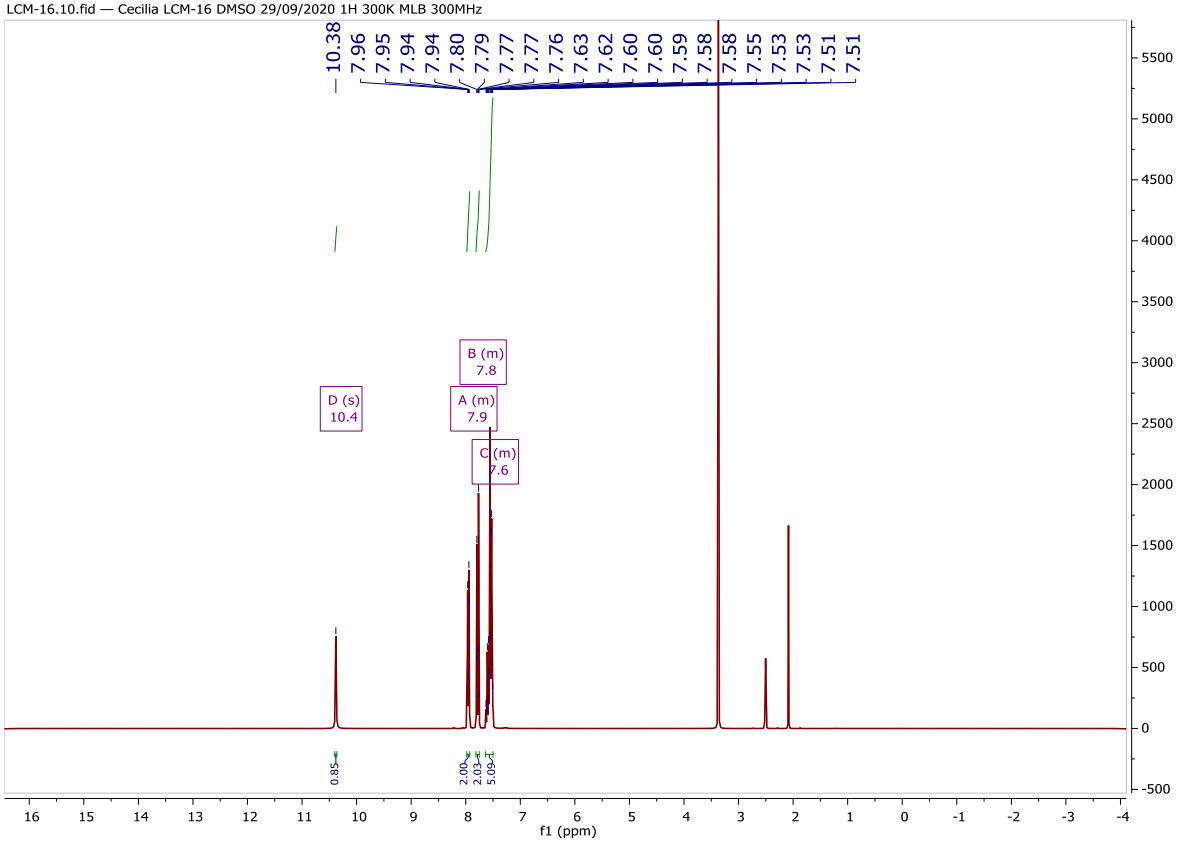

^{13}C NMR spectrum

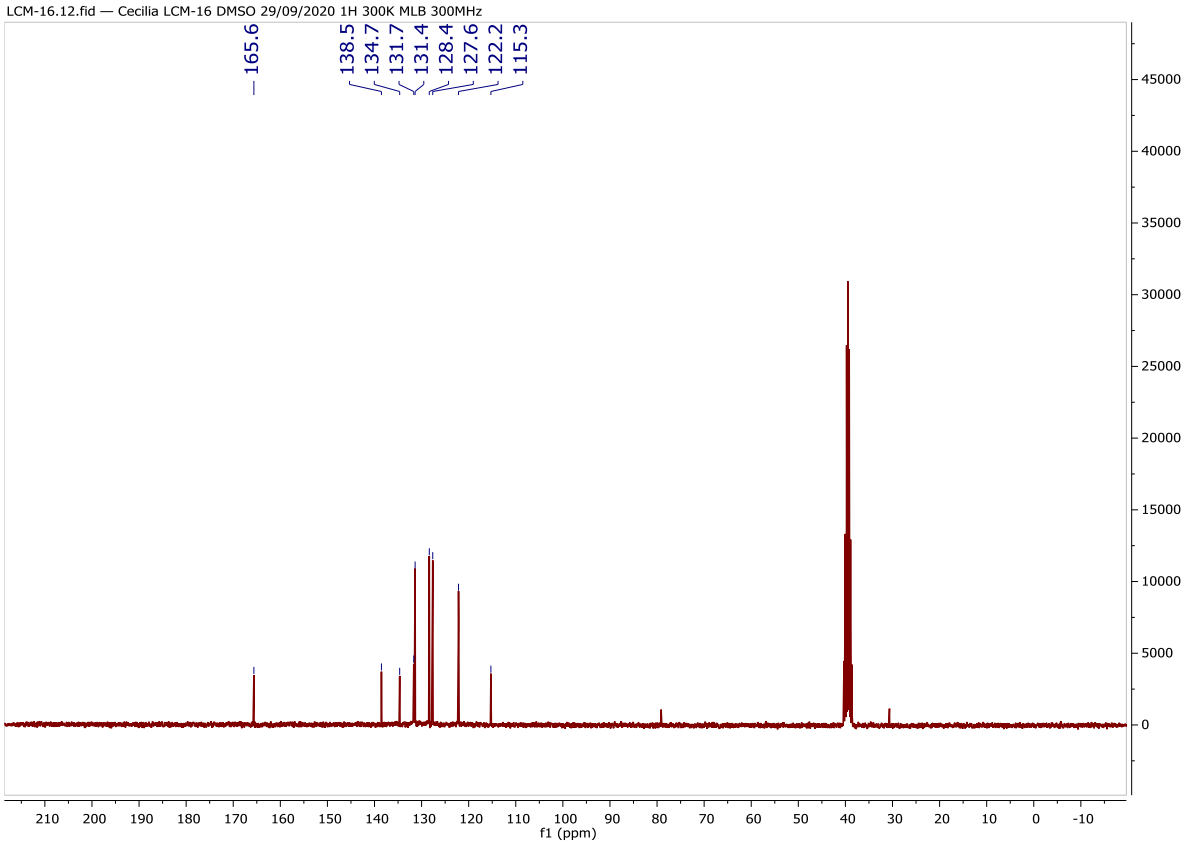

Compound 157c

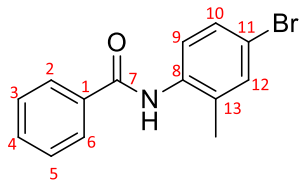

^{1}H NMR spectrum

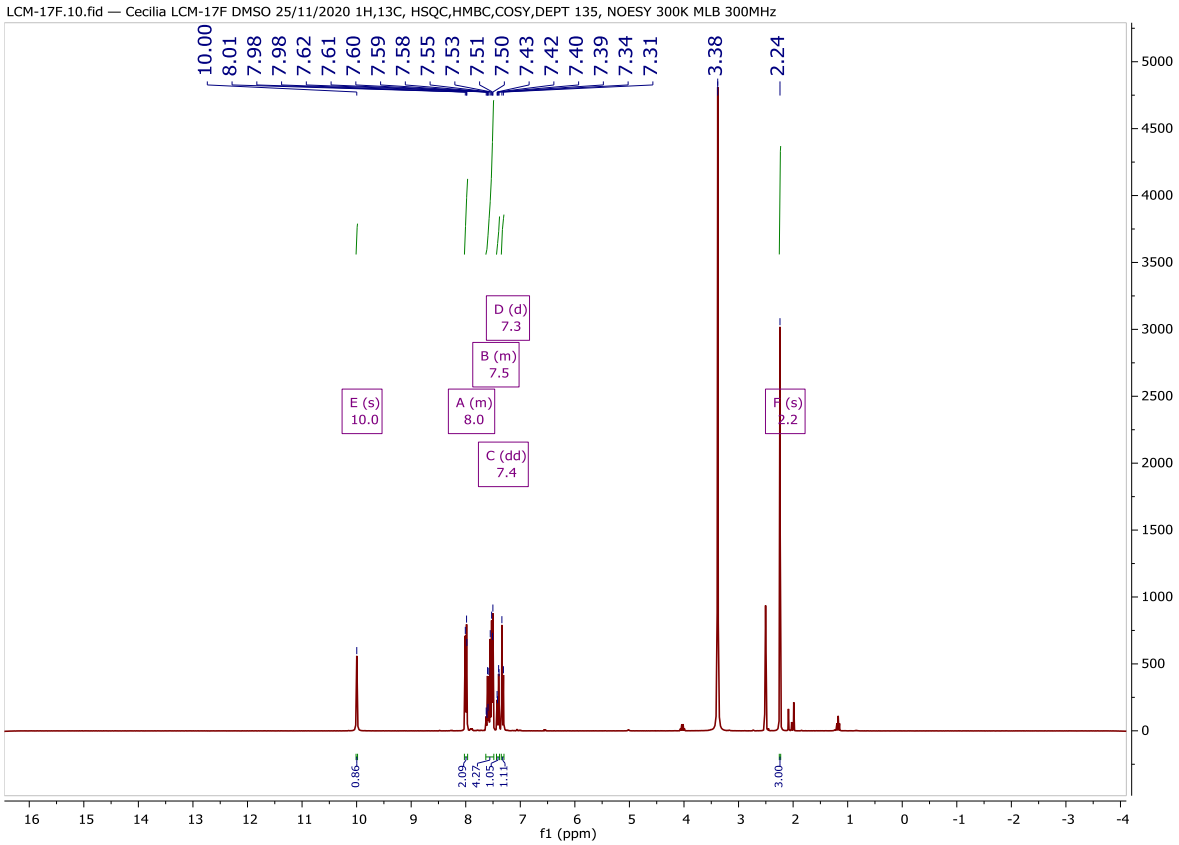

^{13}C NMR spectrum

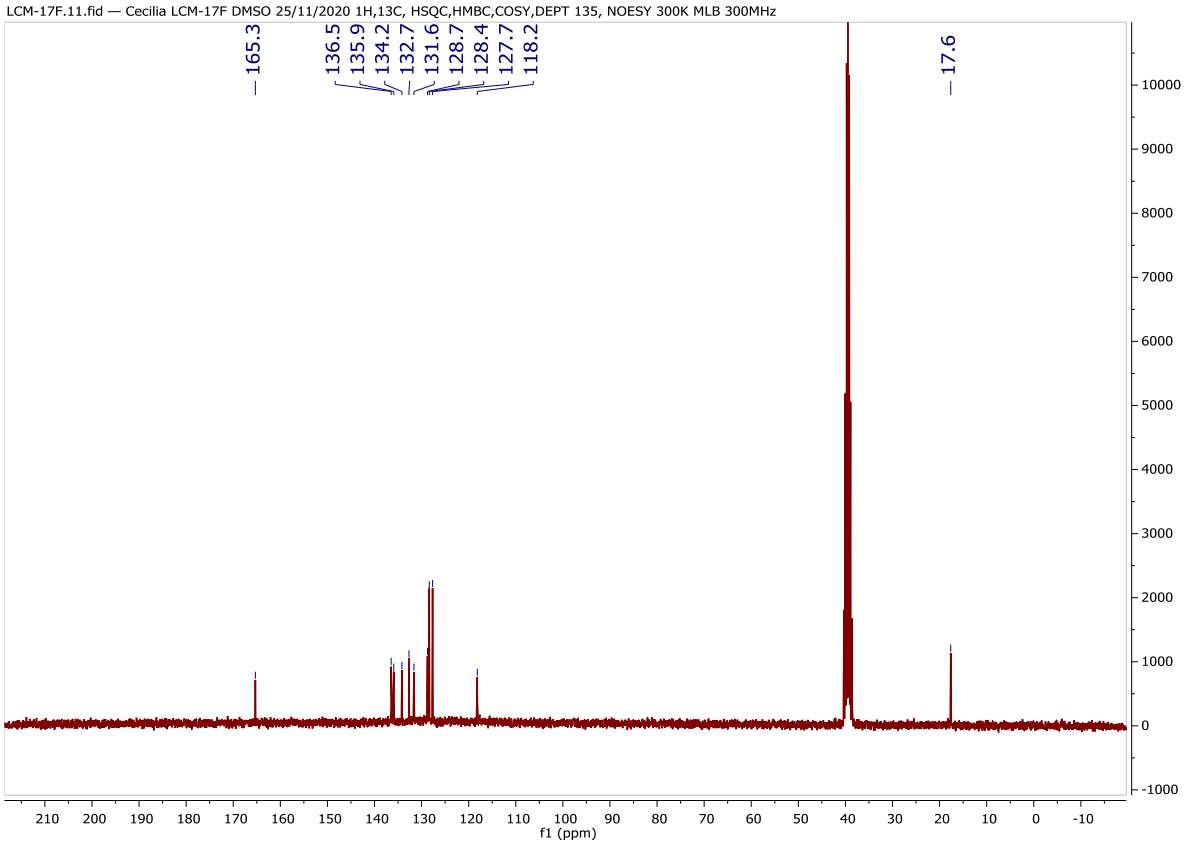

Compound 157d

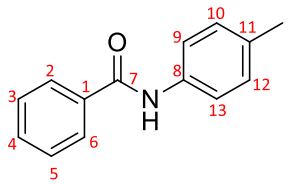

^{1}H NMR spectrum

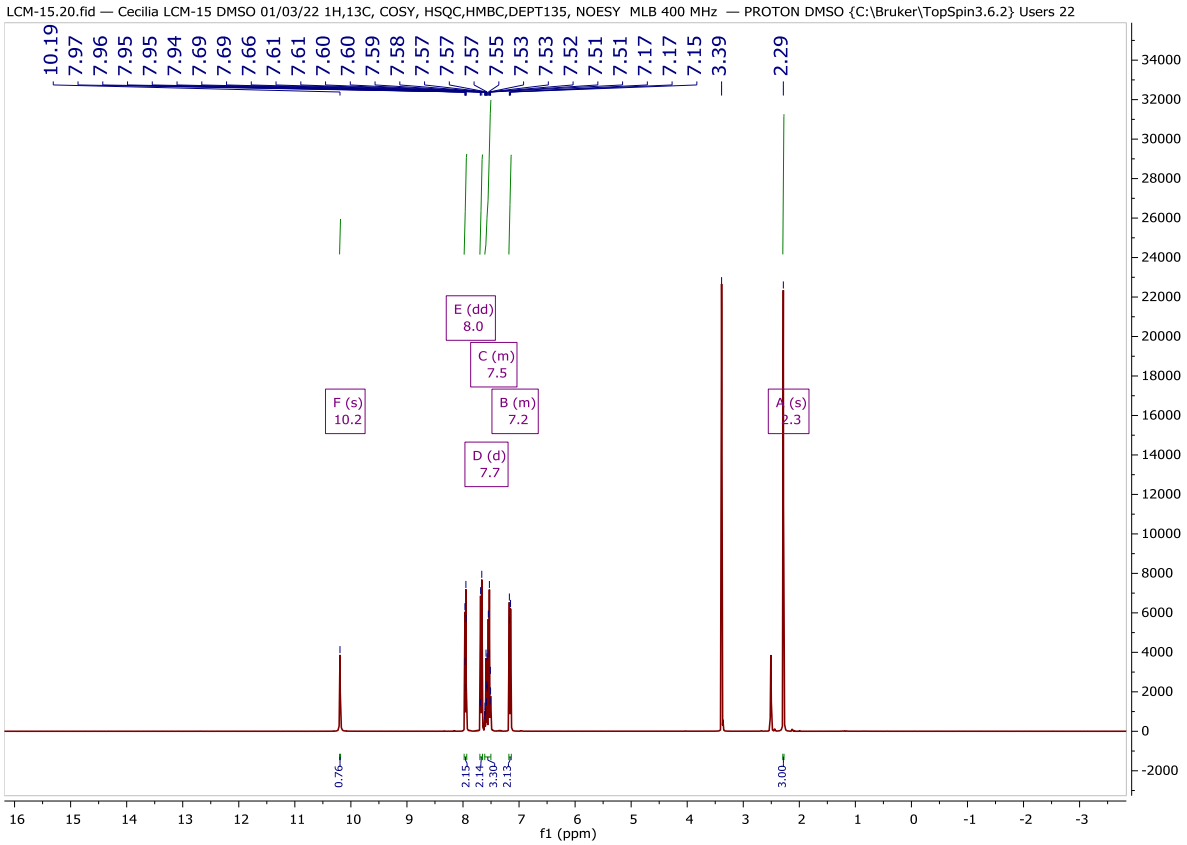

^{13}C NMR spectrum

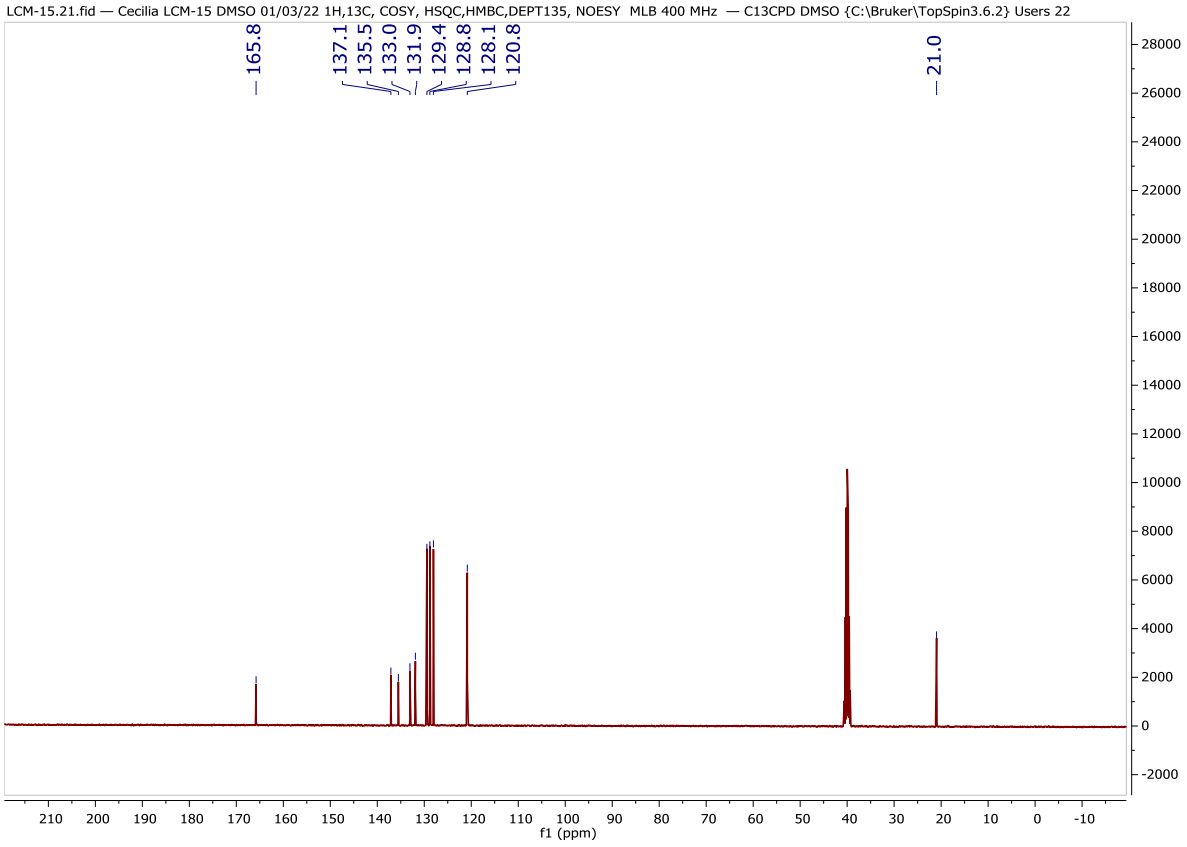

Compound 157e

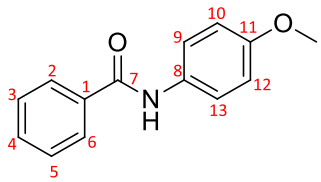

^{1}H NMR spectrum

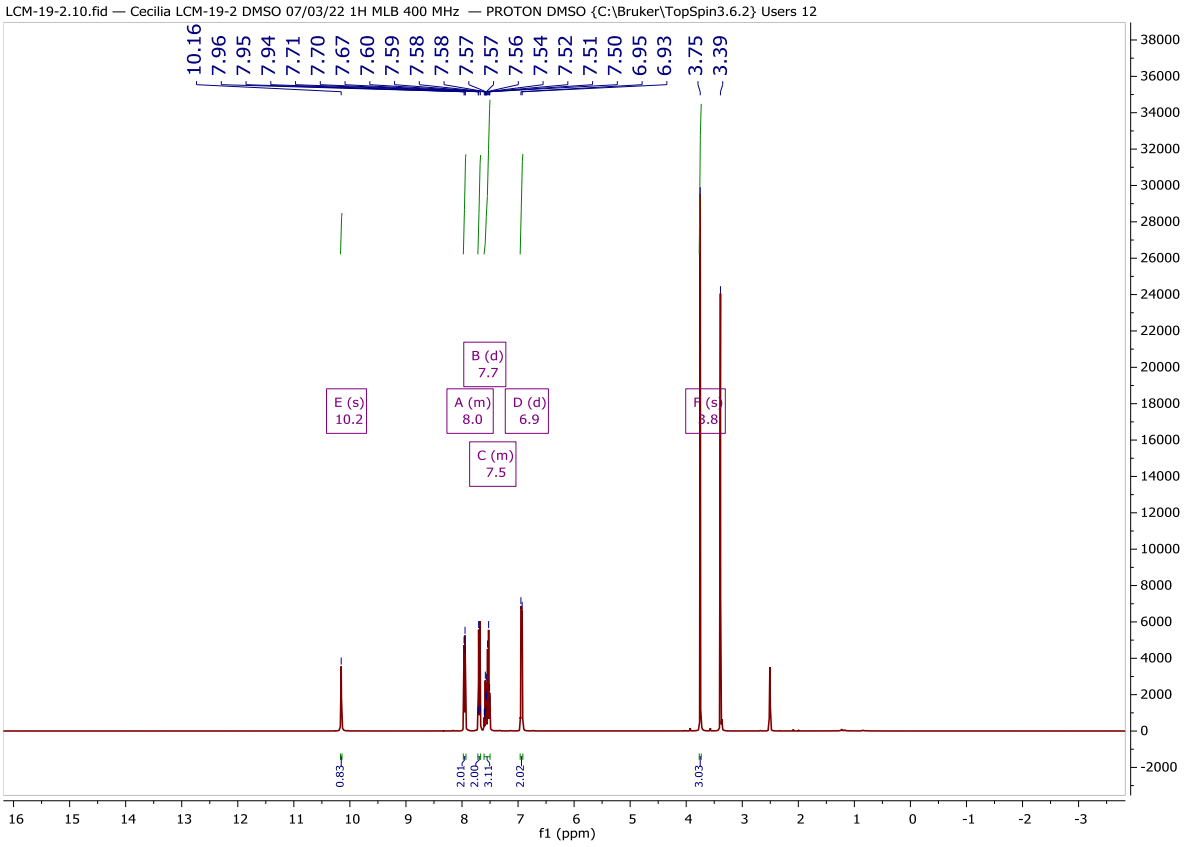

^{13}C NMR spectrum

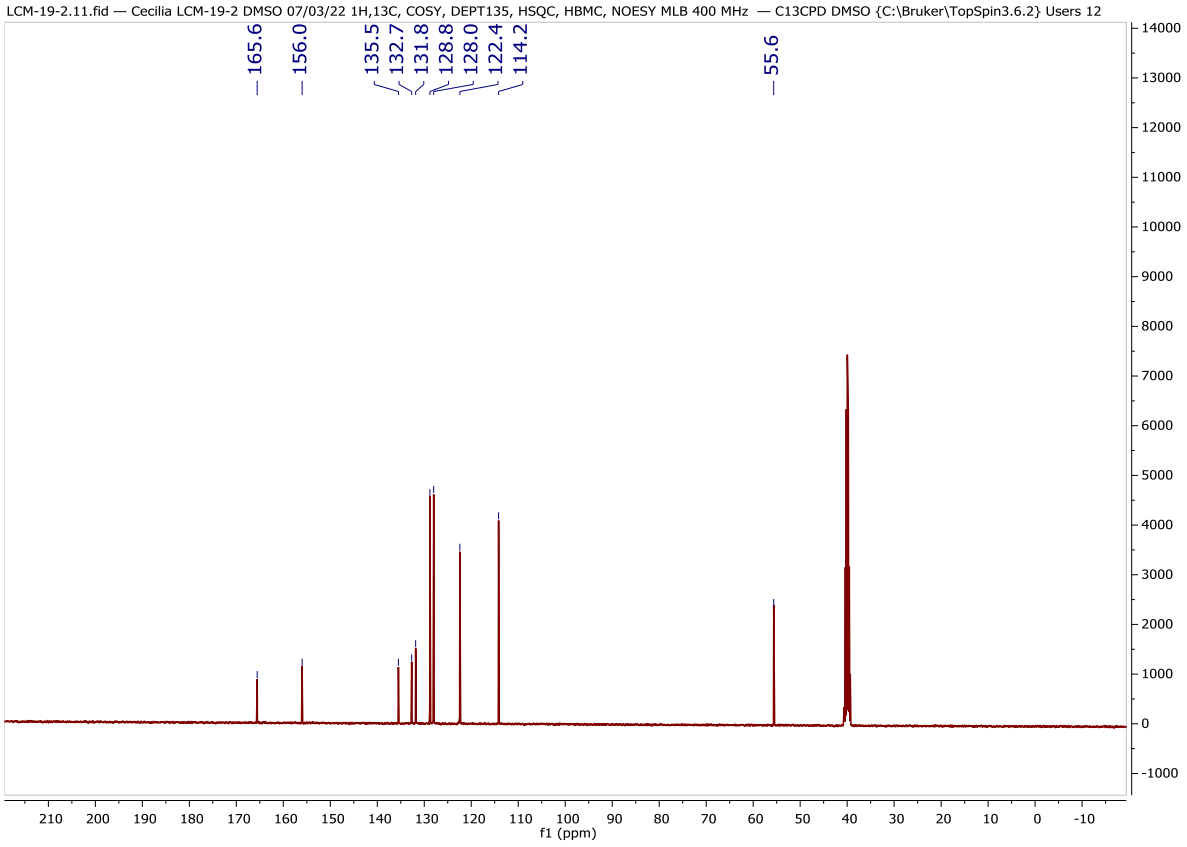

Compound 157f

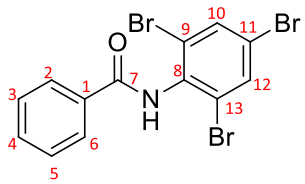

^{1}H NMR spectrum

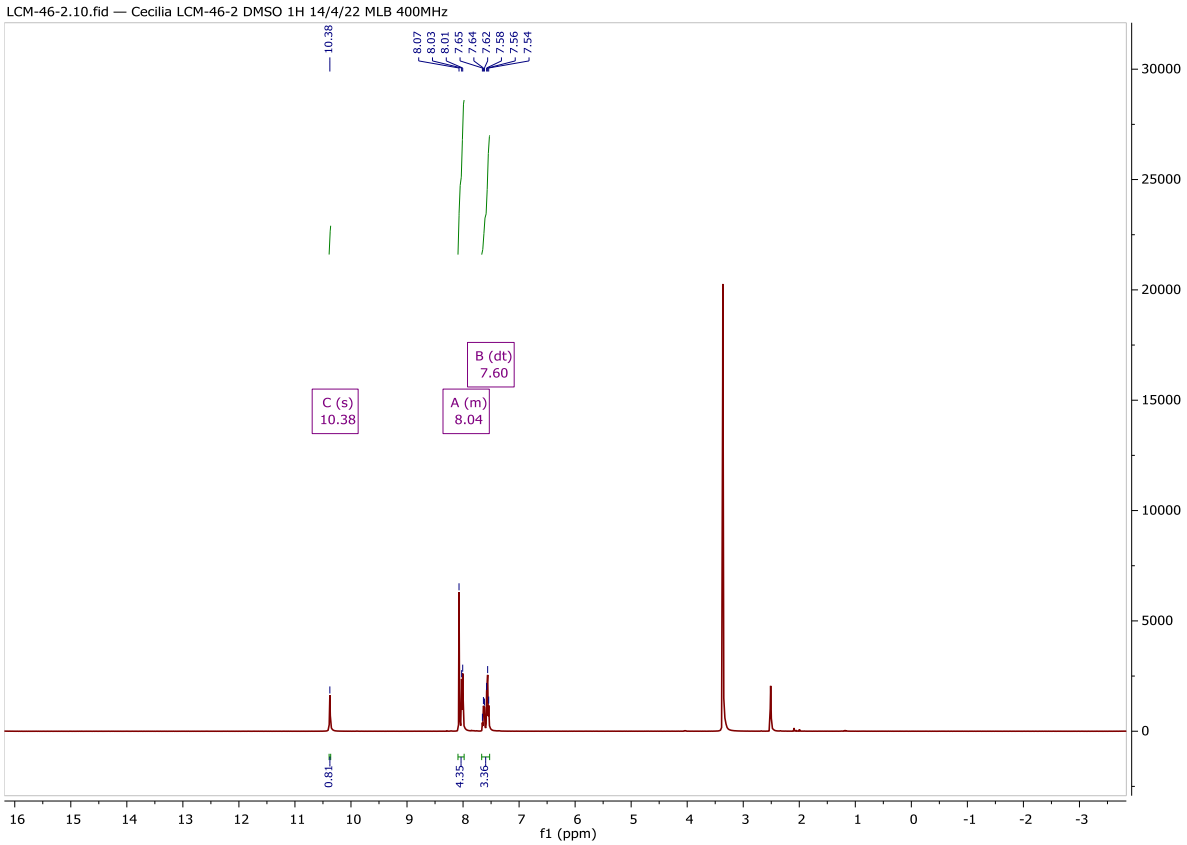

^{13}C NMR spectrum

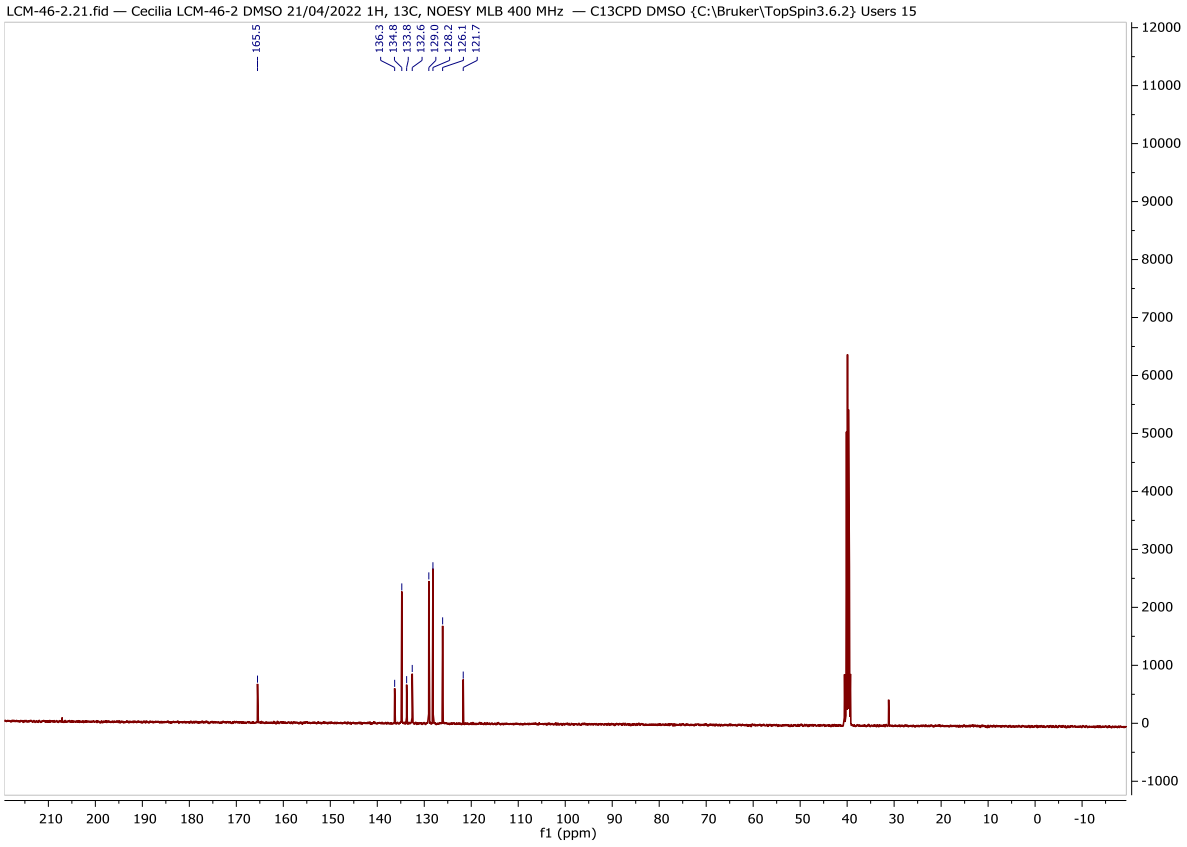

Compound 157h

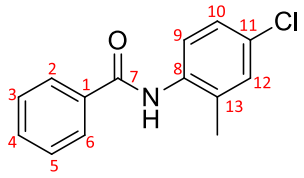

^{1}H NMR spectrum

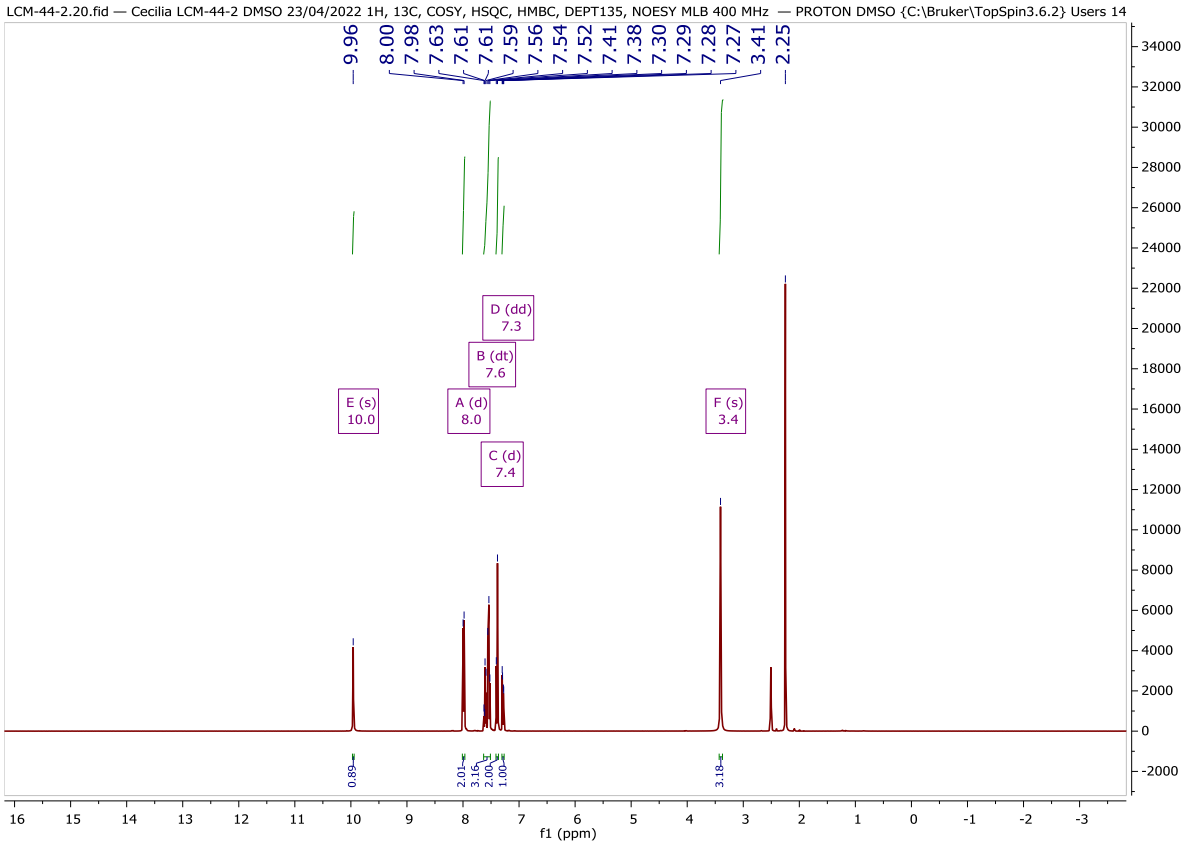

^{13}C NMR spectrum

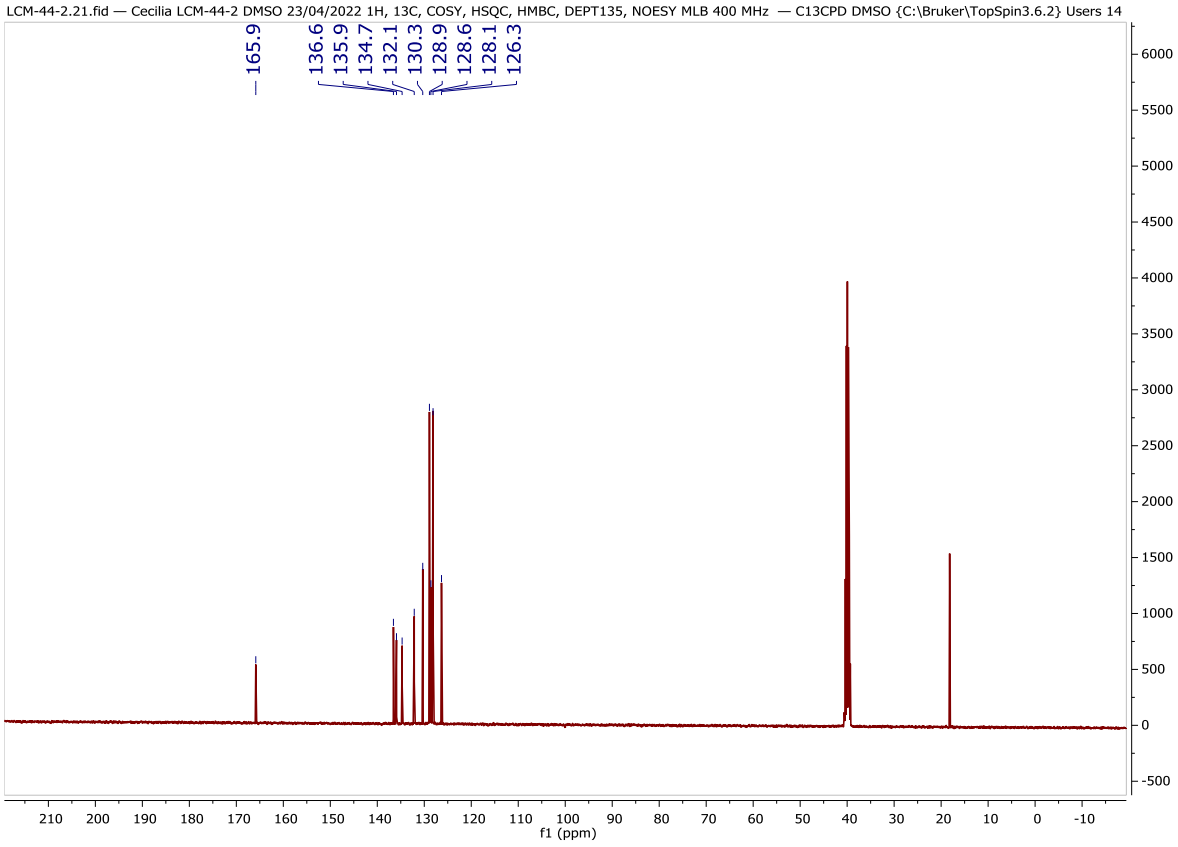

Compound 157n

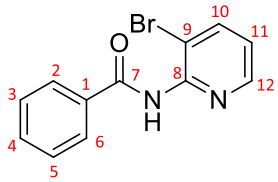

^{1}H NMR spectrum

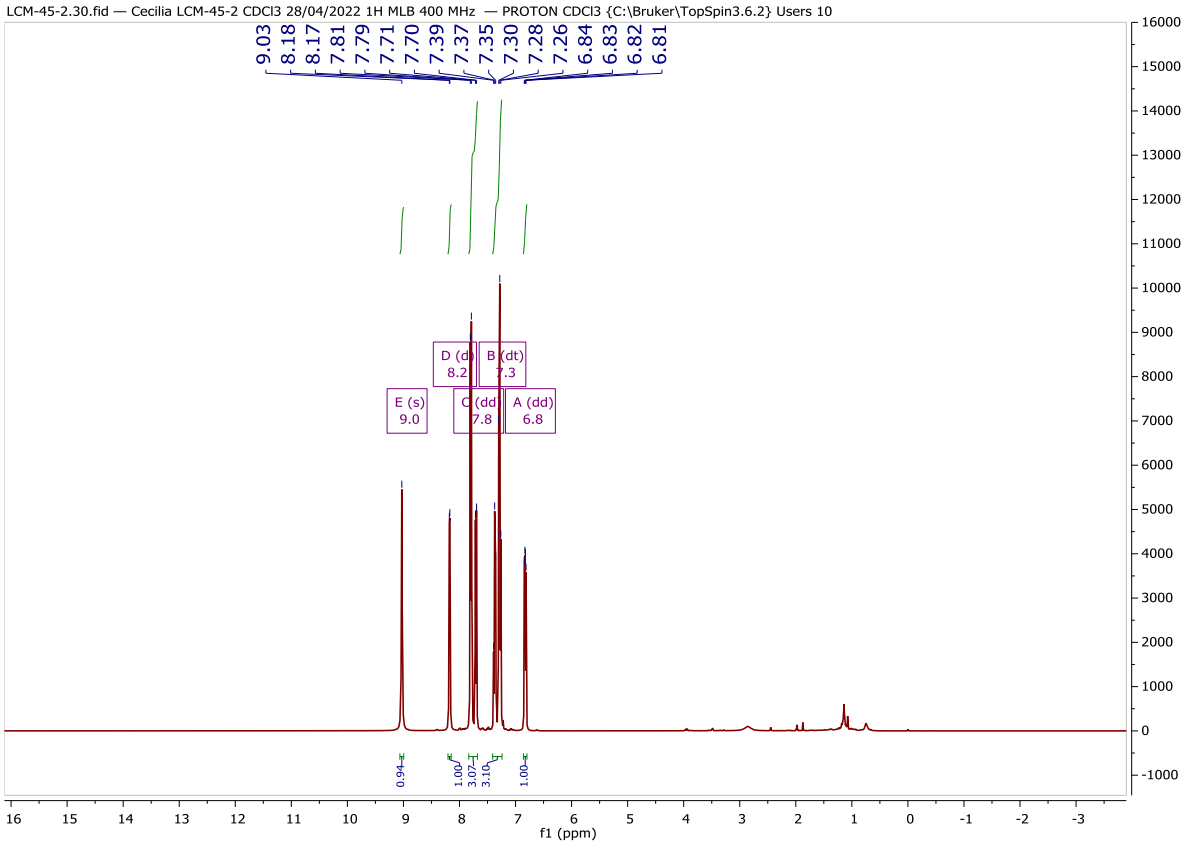

^{13}C NMR spectrum

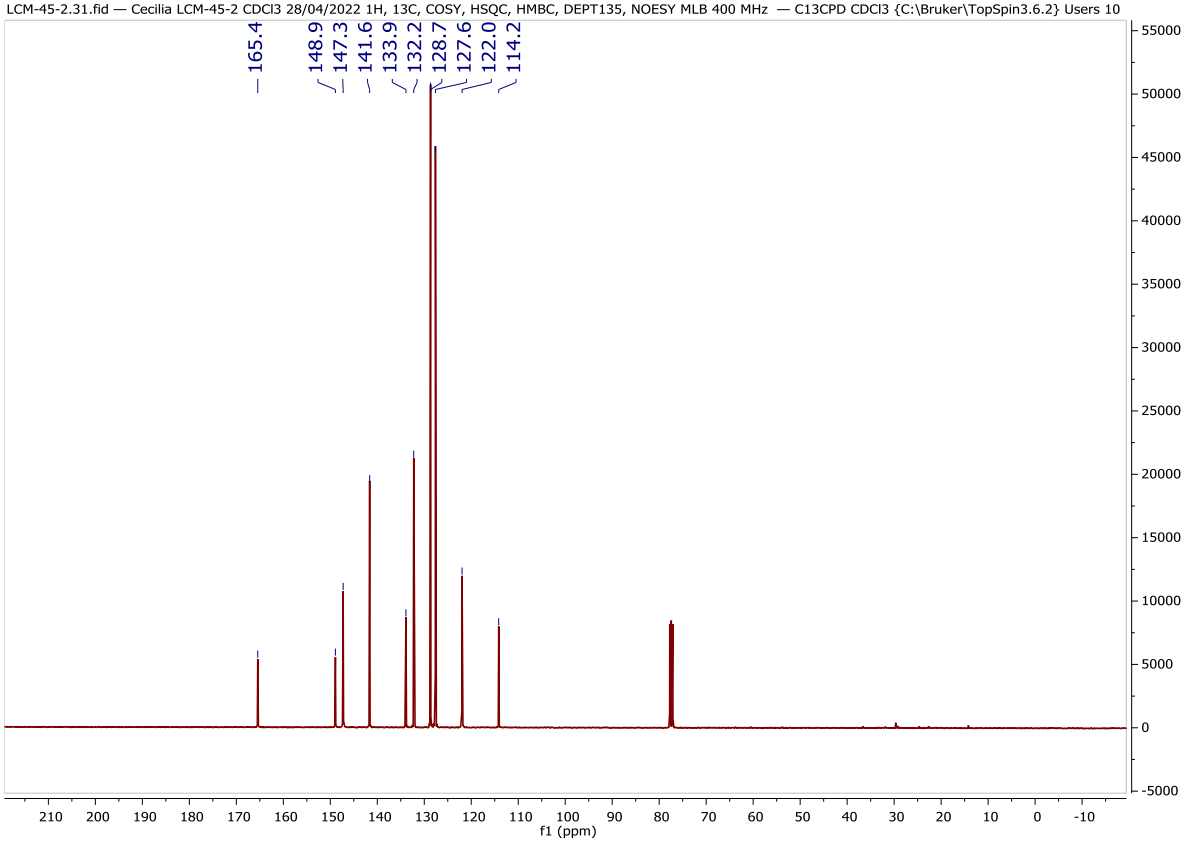

Compound 158a

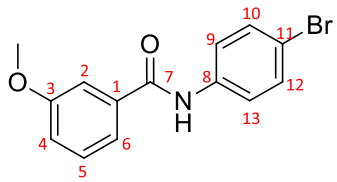

^{1}H NMR spectrum

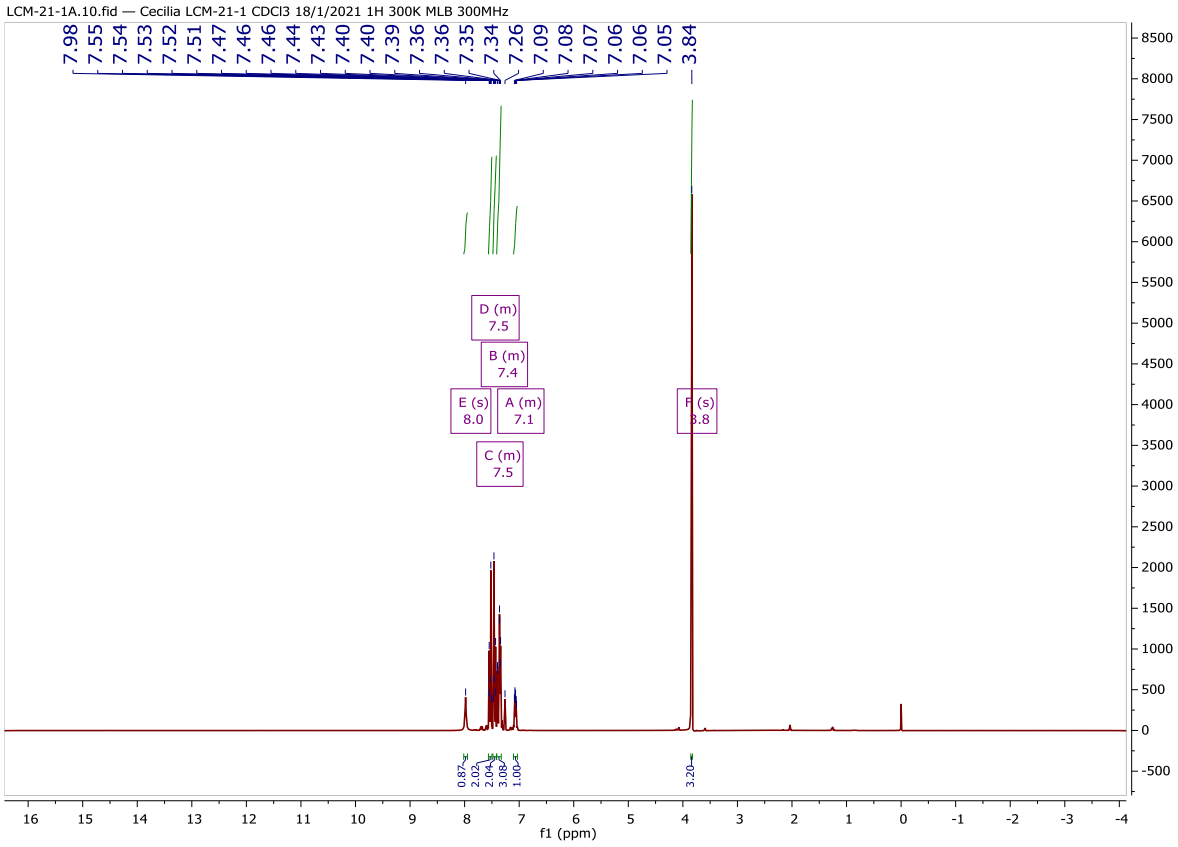

^{13}C NMR spectrum

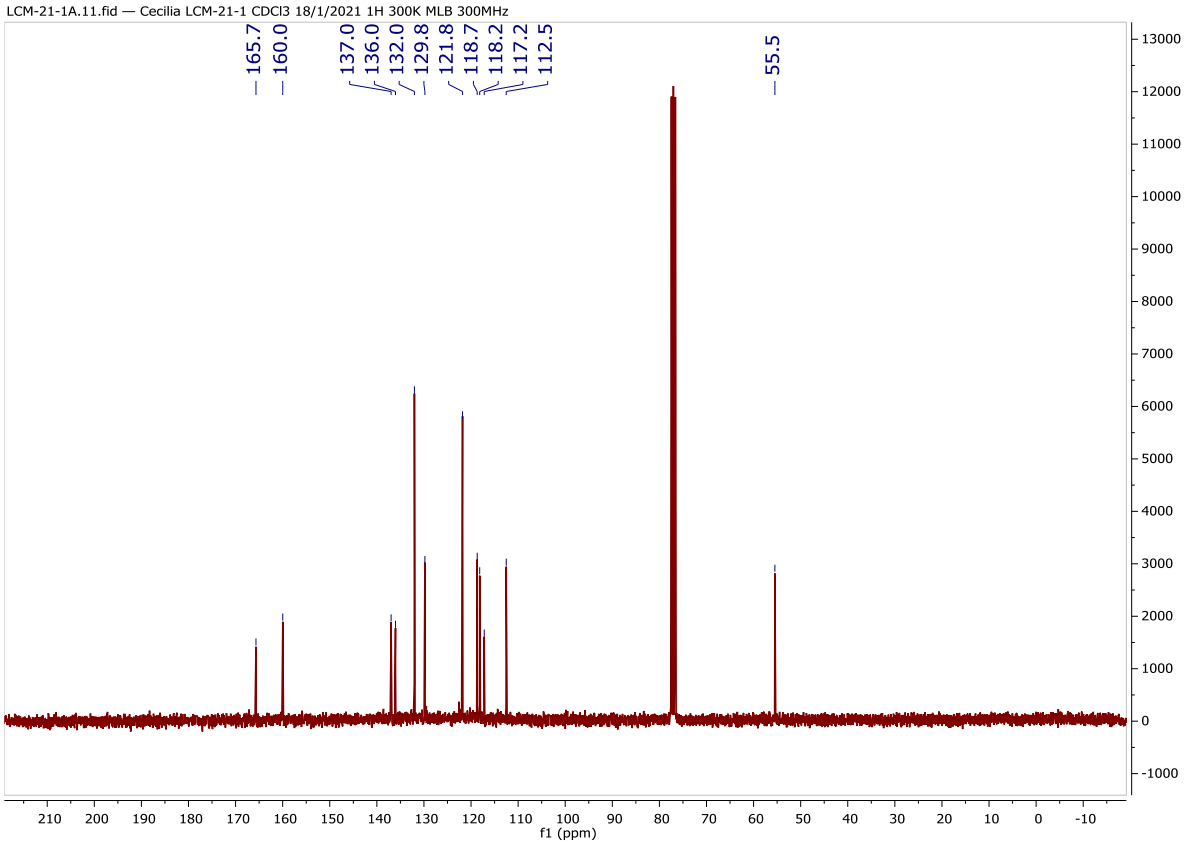

Compound 158b

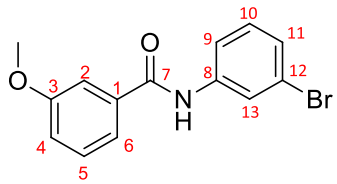

^{1}H NMR spectrum

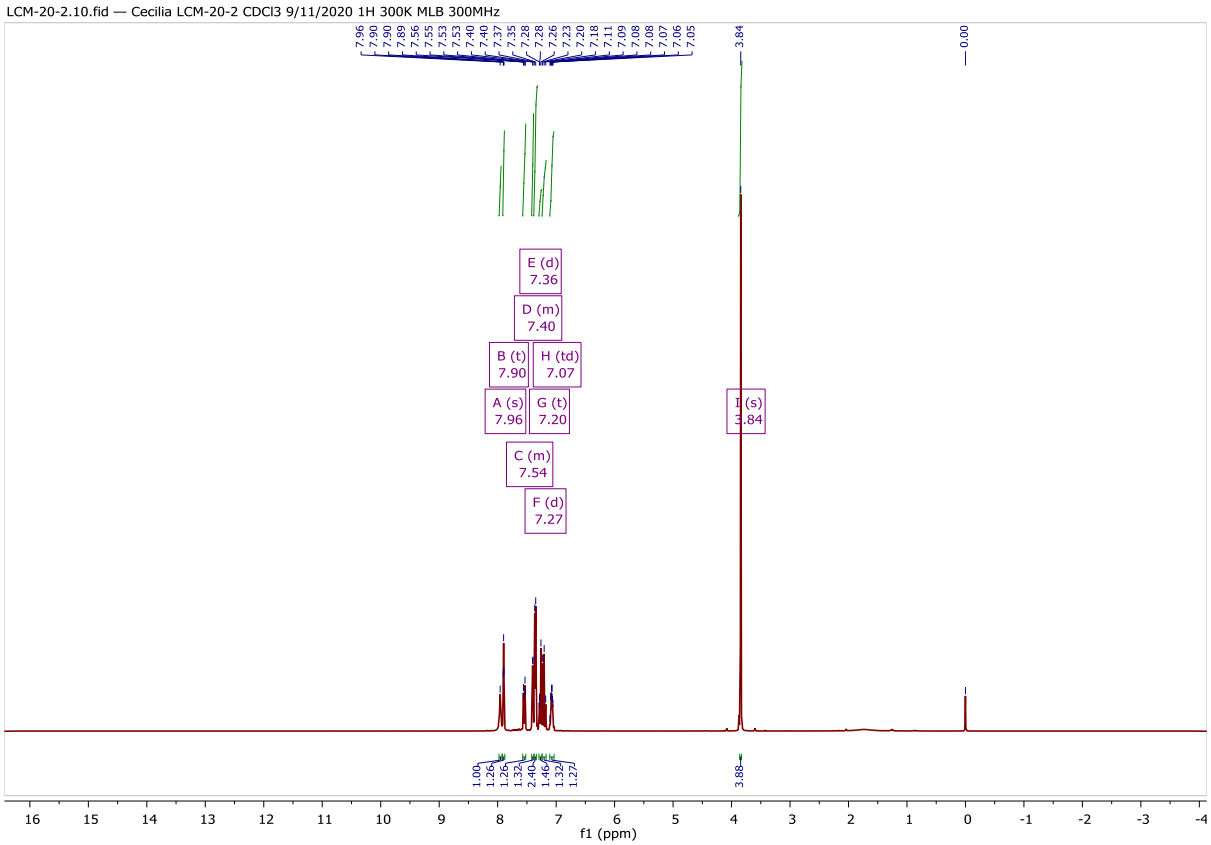

^{13}C NMR spectrum

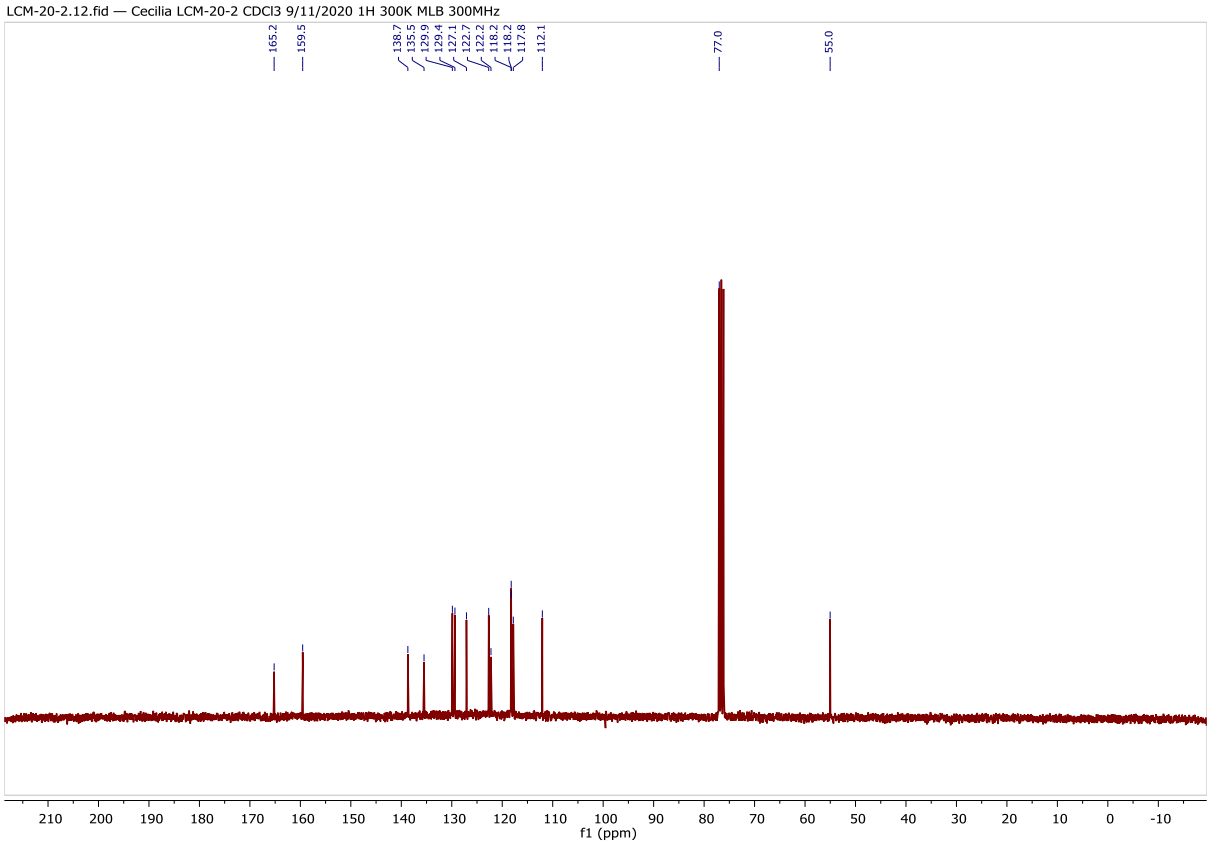

Compound 158d

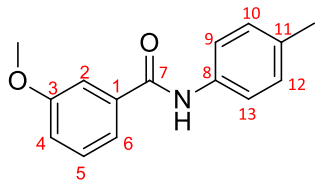

^{1}H NMR spectrum

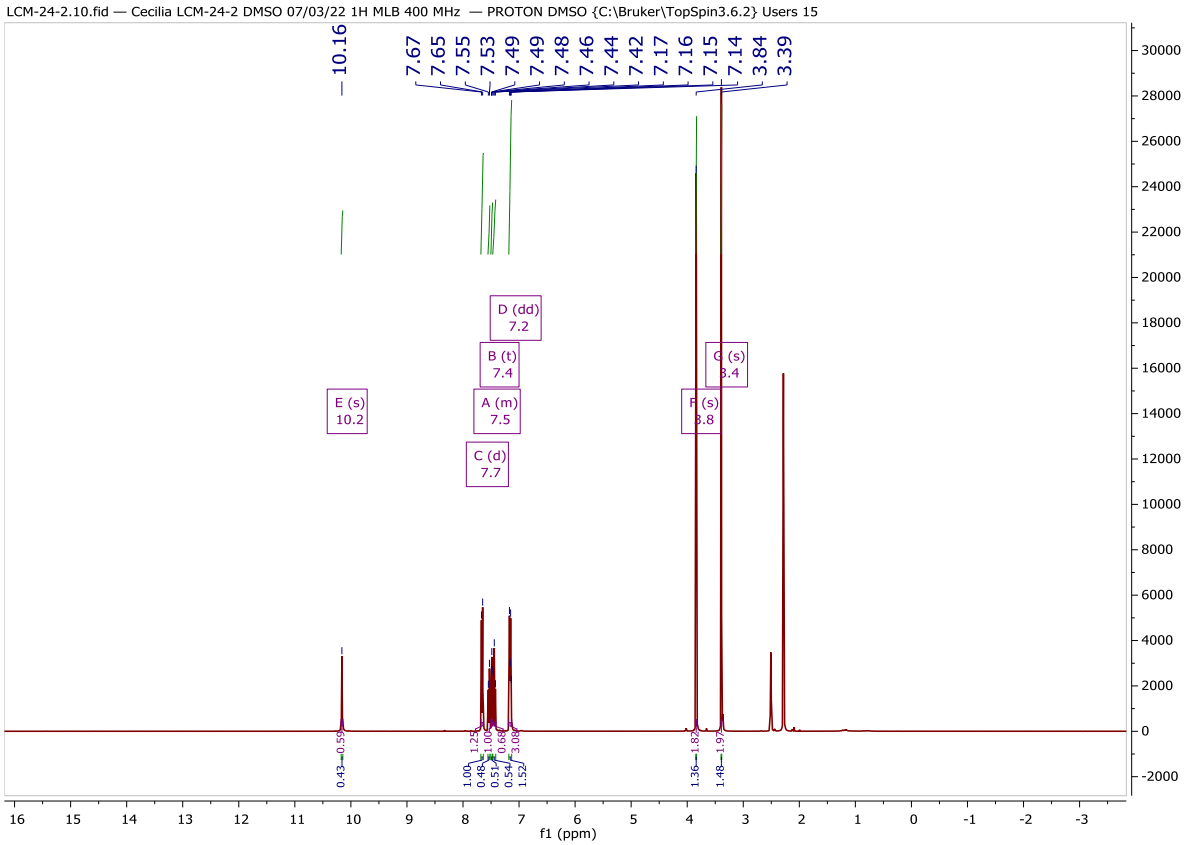

^{13}C NMR spectrum

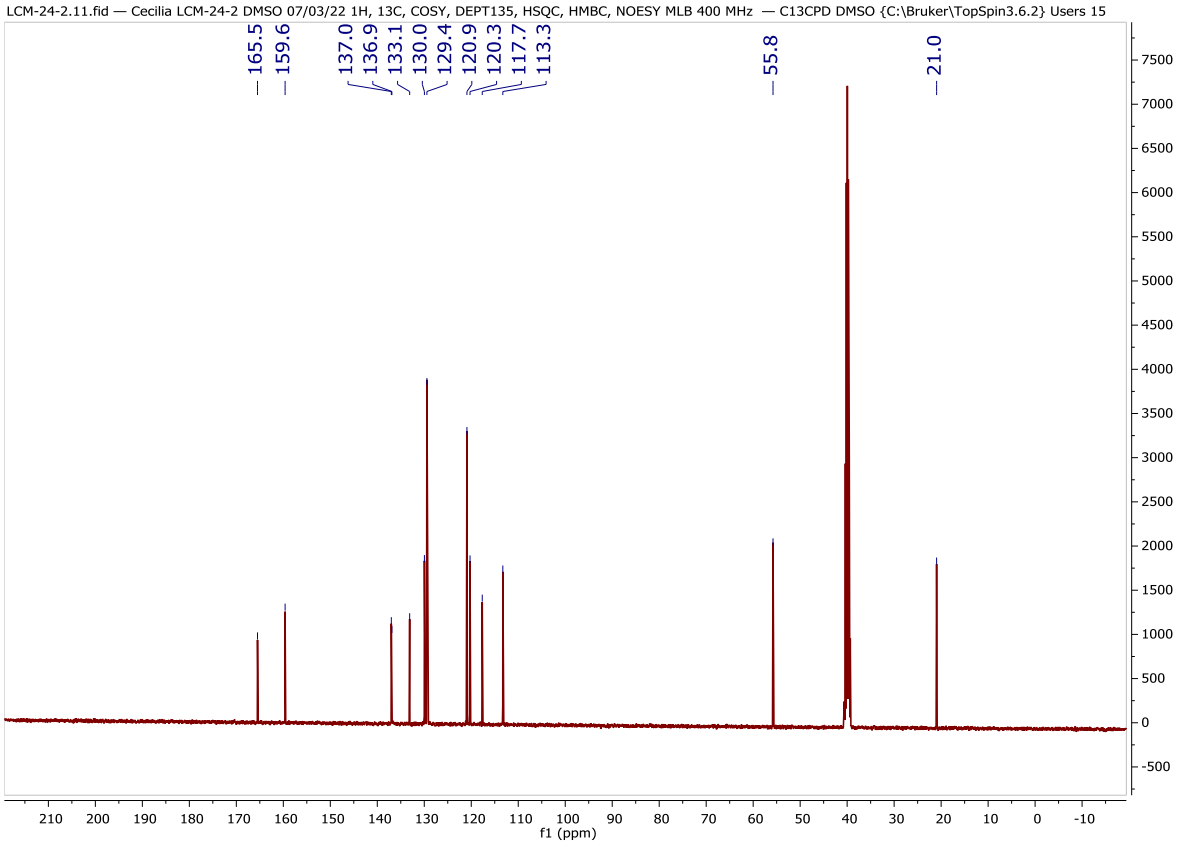

Compound 158e

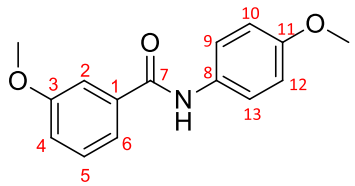

^{1}H NMR spectrum

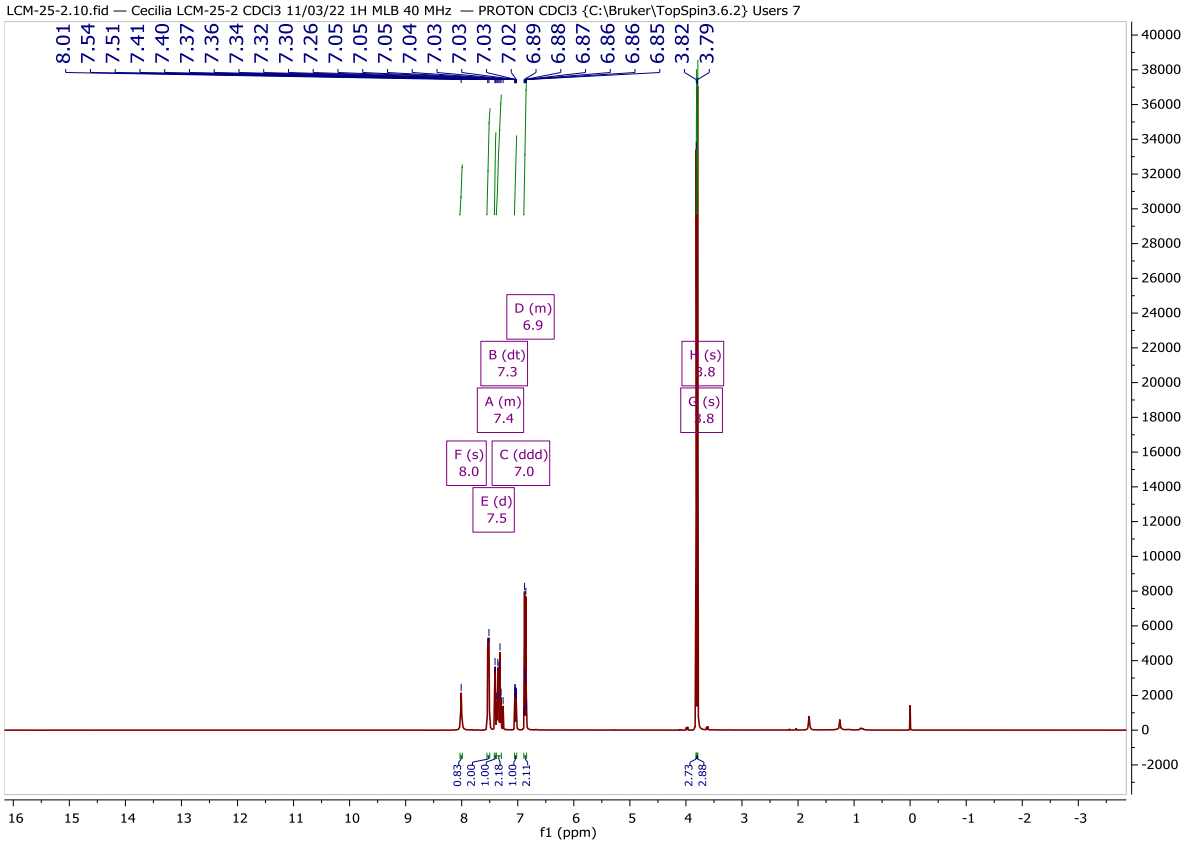

^{13}C NMR spectrum

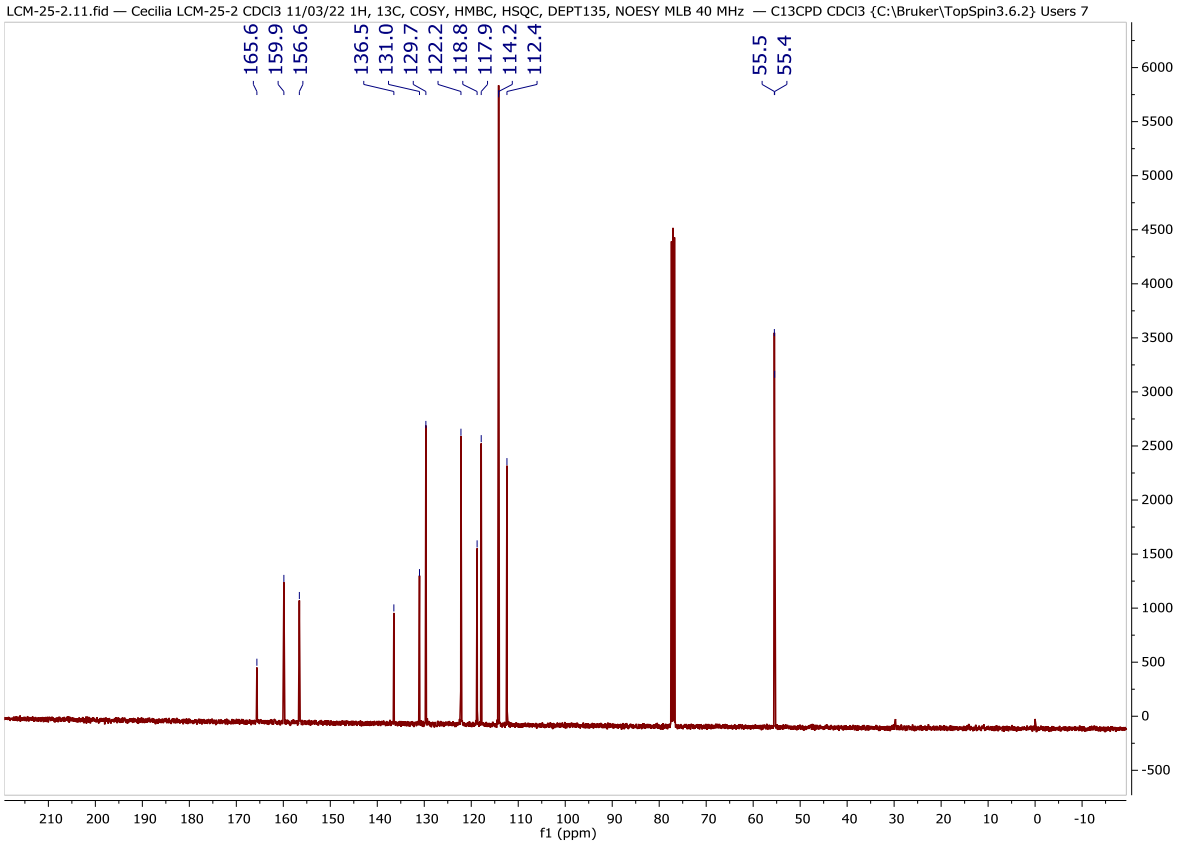

Compound 158h

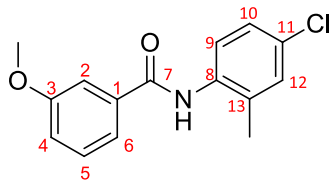

^{1}H NMR spectrum

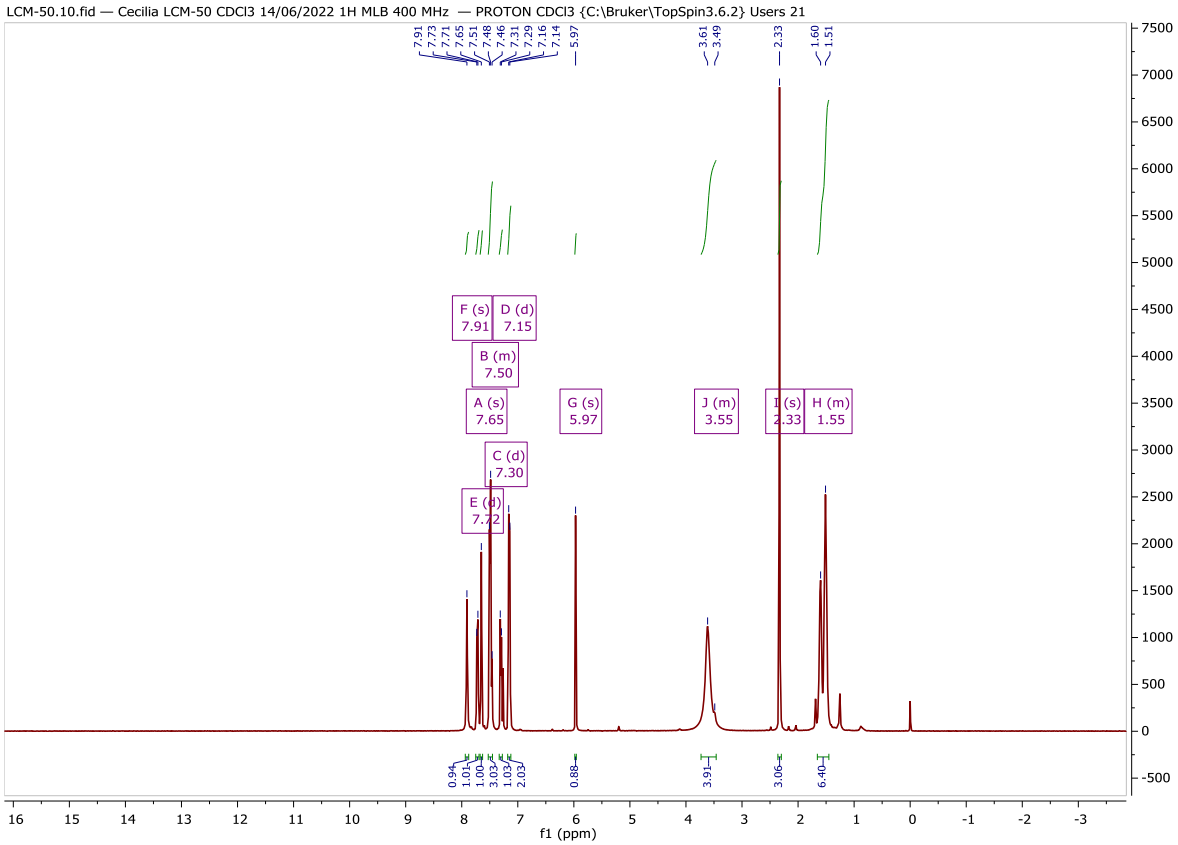

^{13}C NMR spectrum

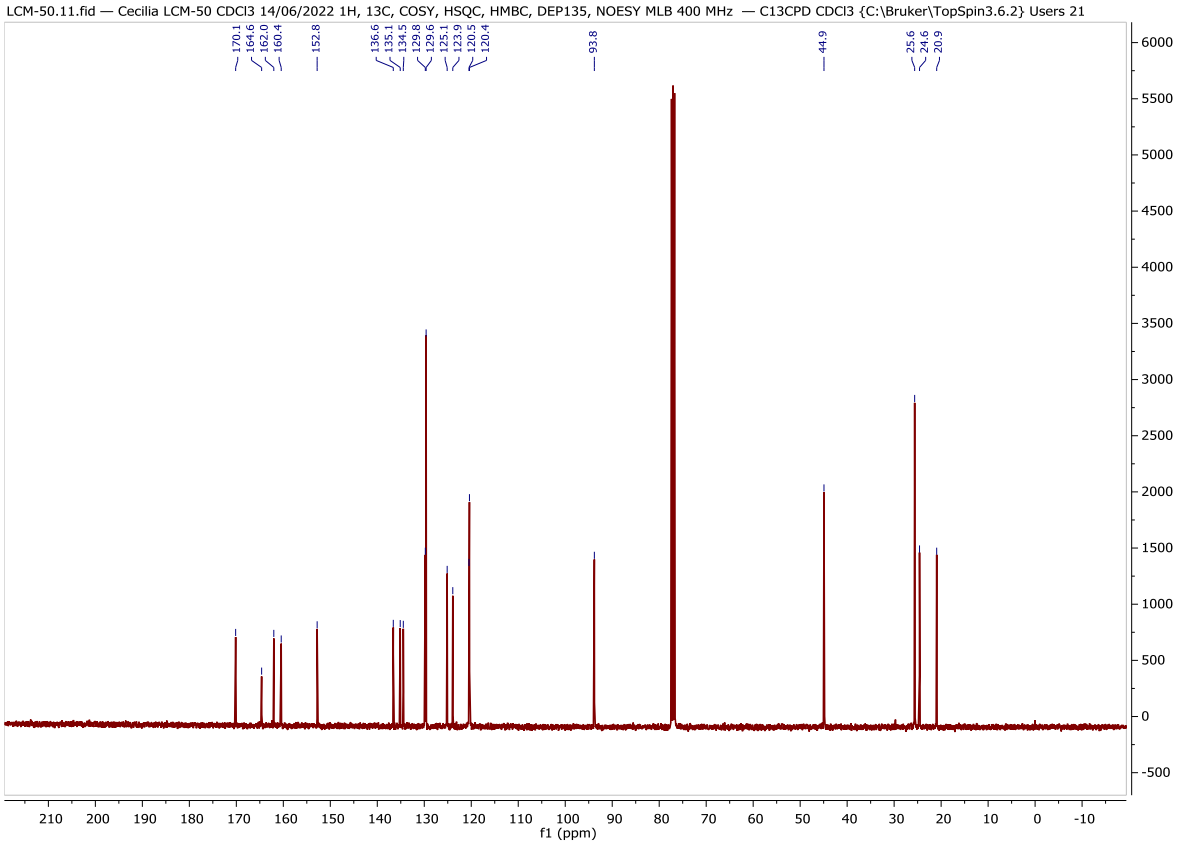

Compound 158k

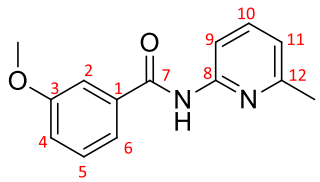

^{1}H NMR spectrum

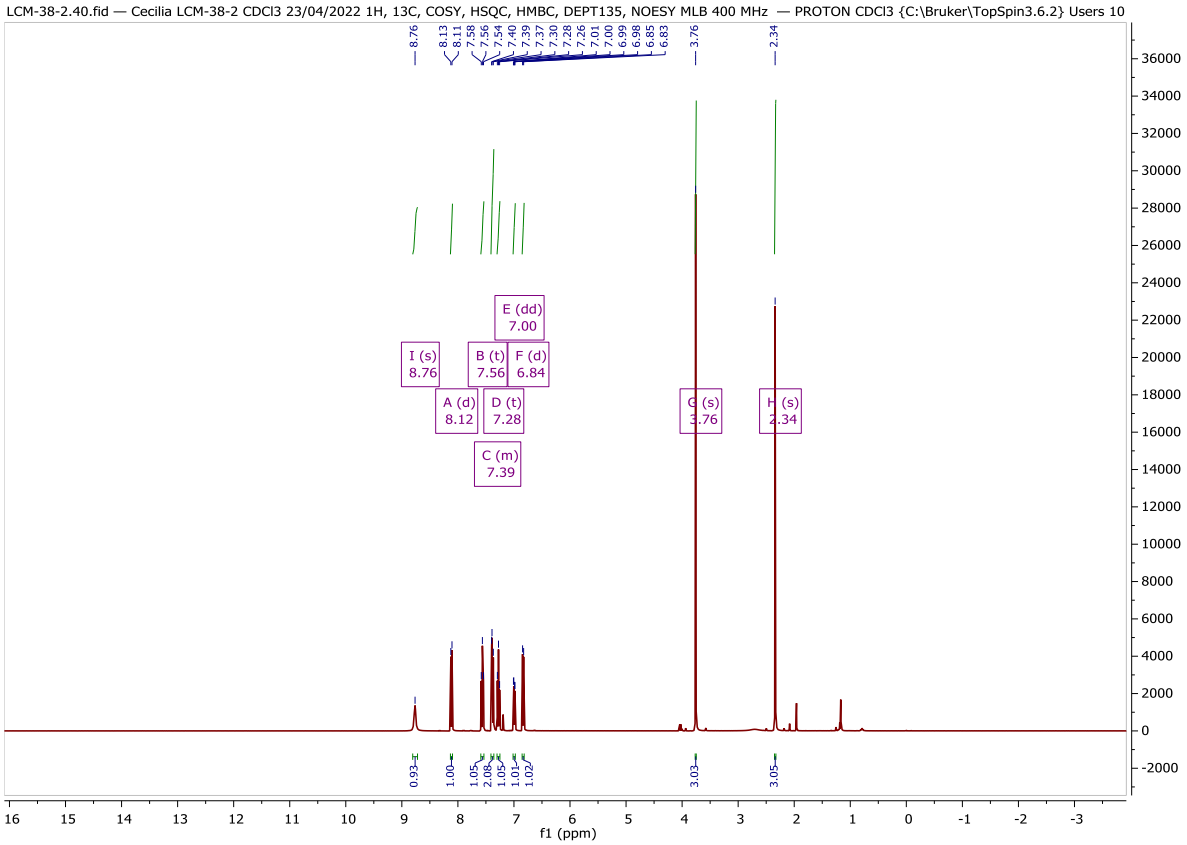

^{13}C NMR spectrum

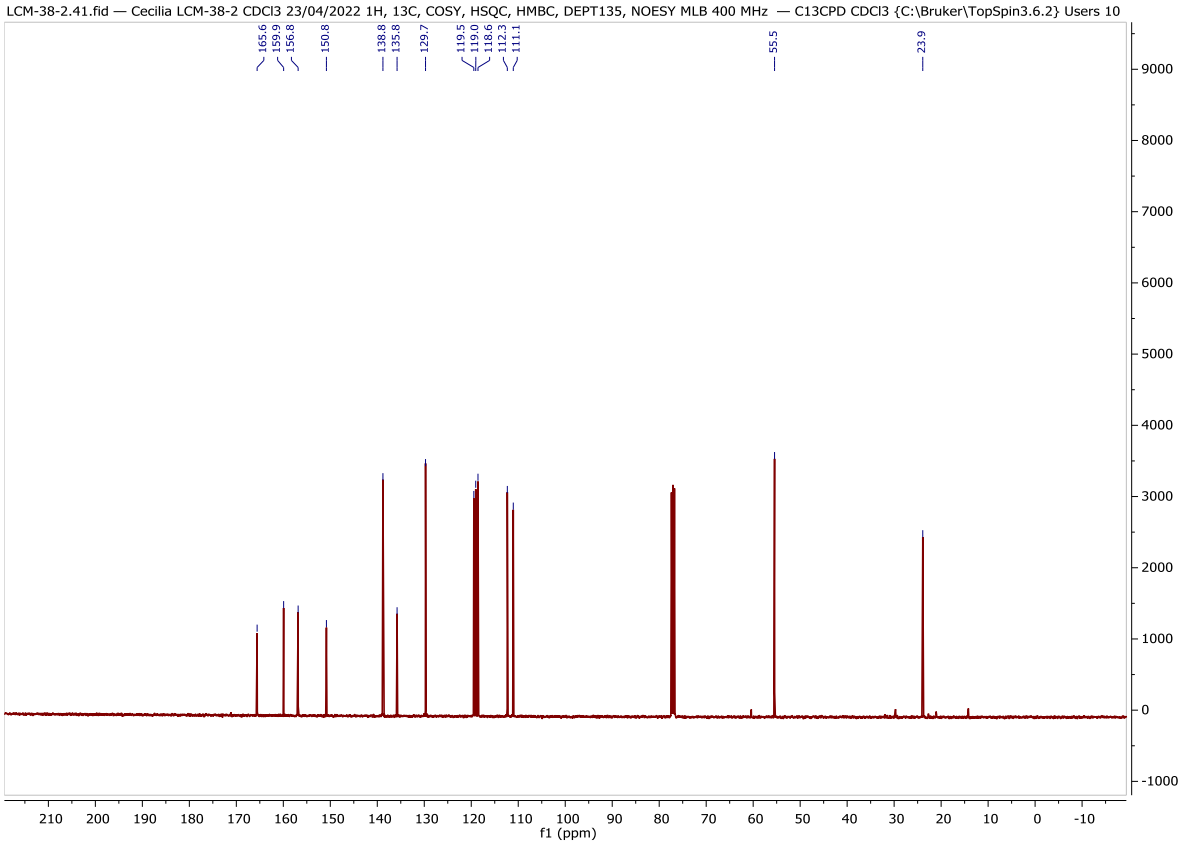

Compound 158l

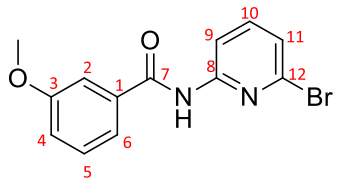

^{1}H NMR spectrum

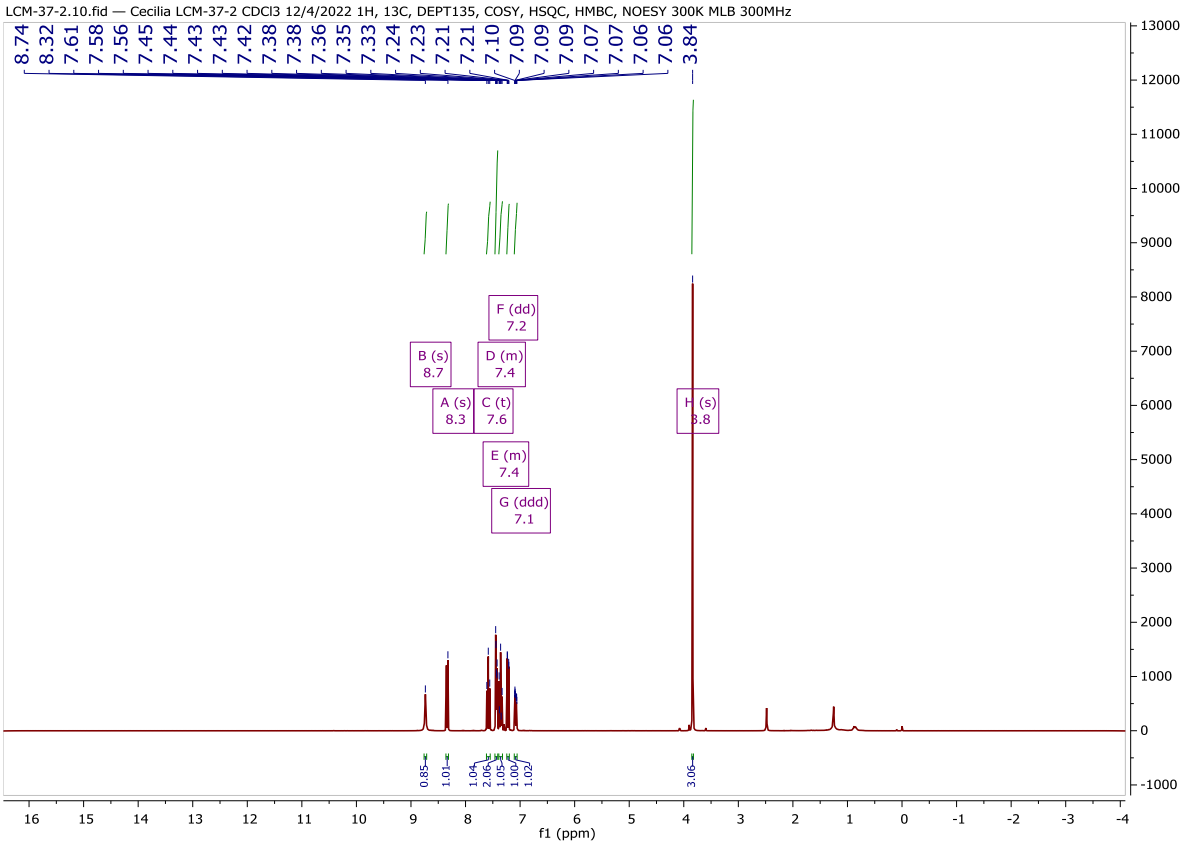

^{13}C NMR spectrum

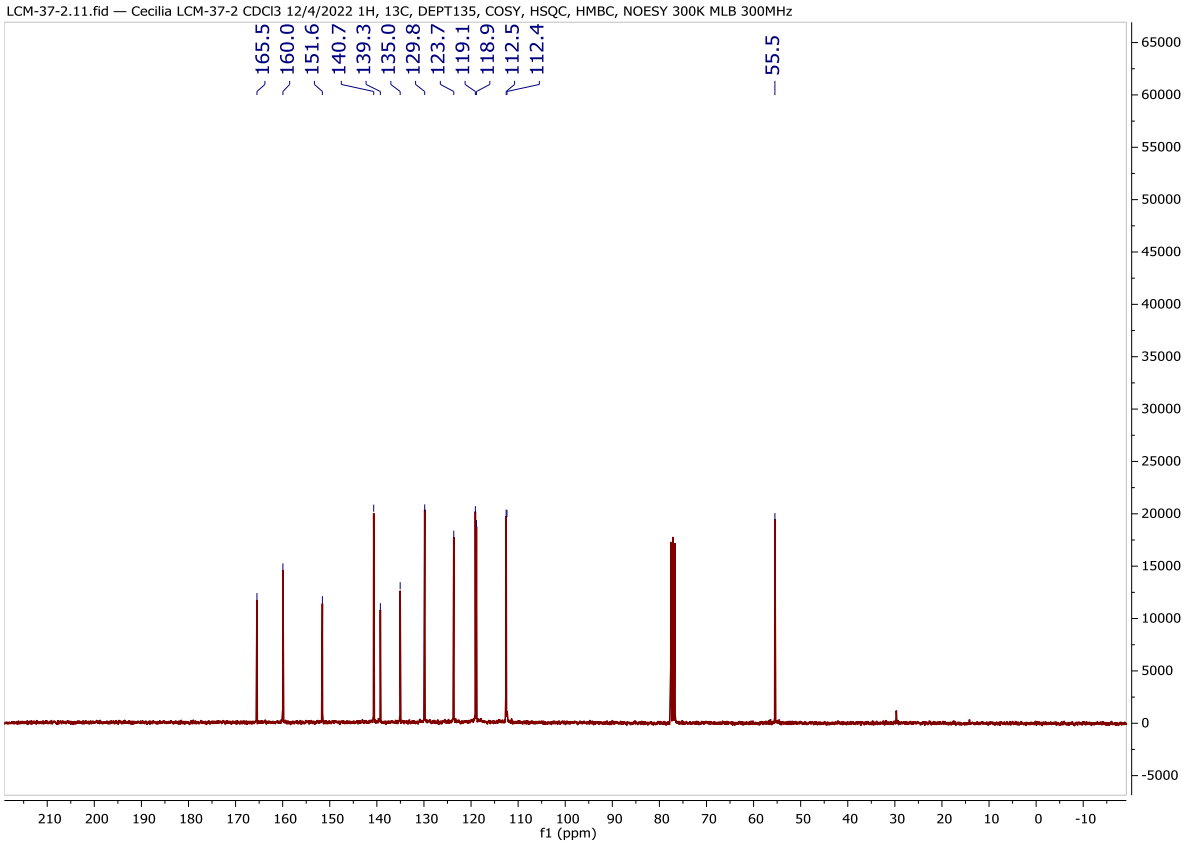

Compound 158m

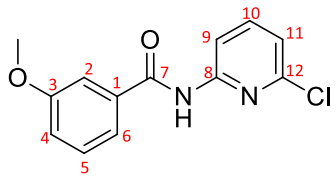

^{1}H NMR spectrum

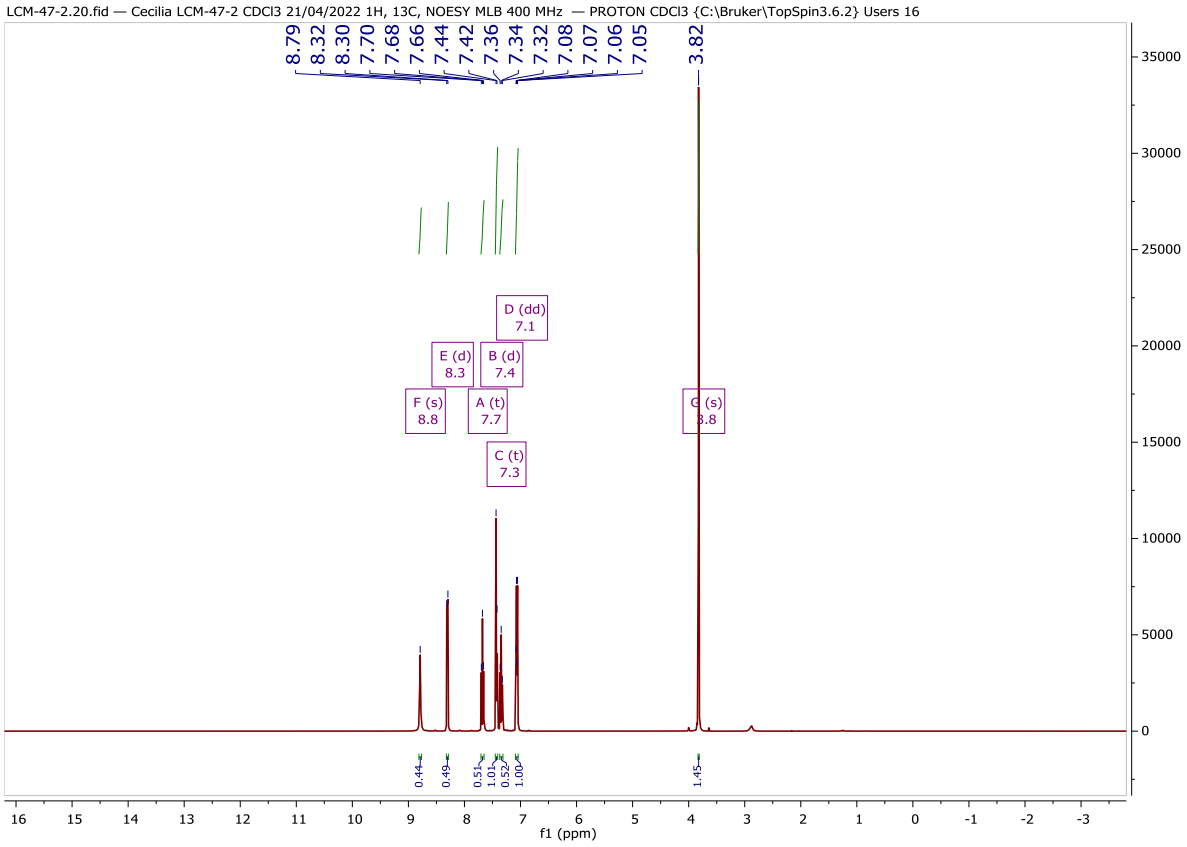

^{13}C NMR spectrum

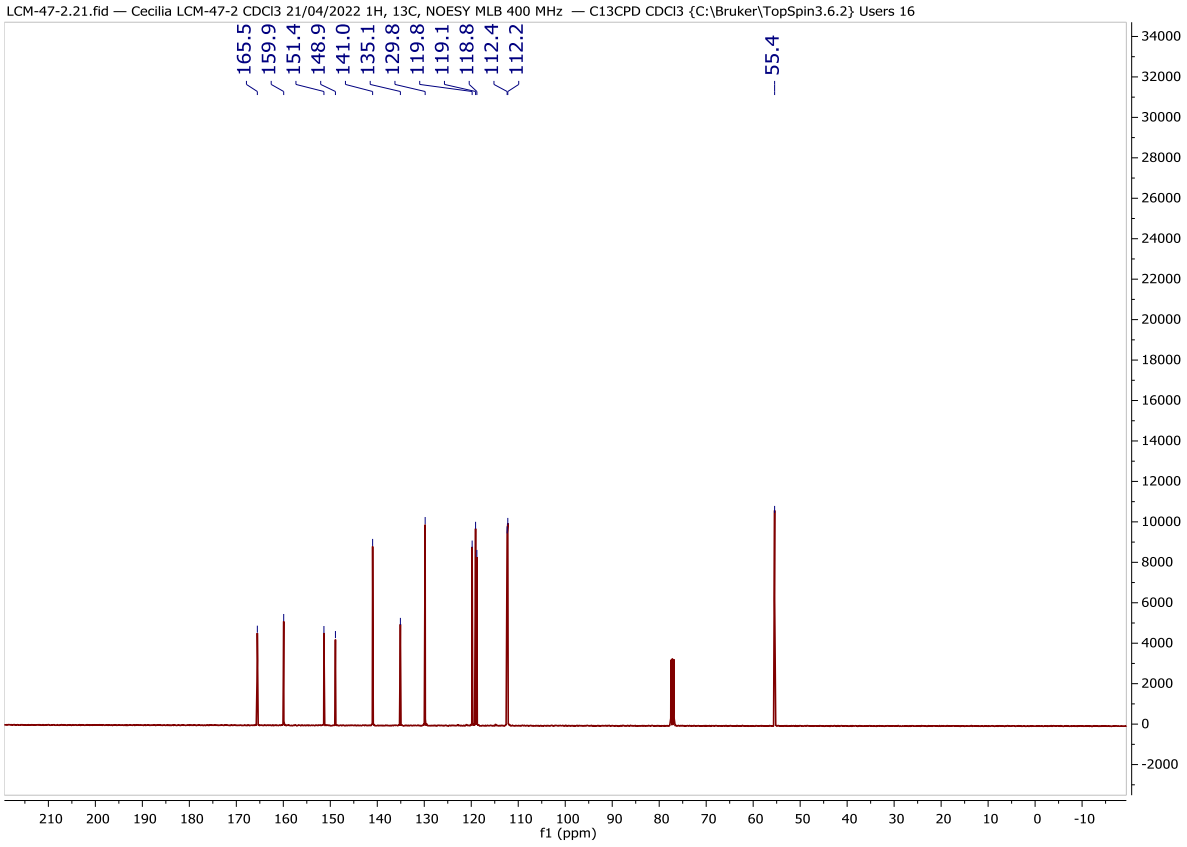

Compound 158o

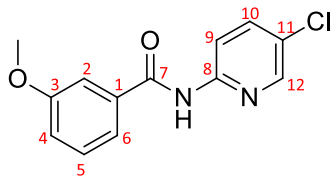

^{1}H NMR spectrum

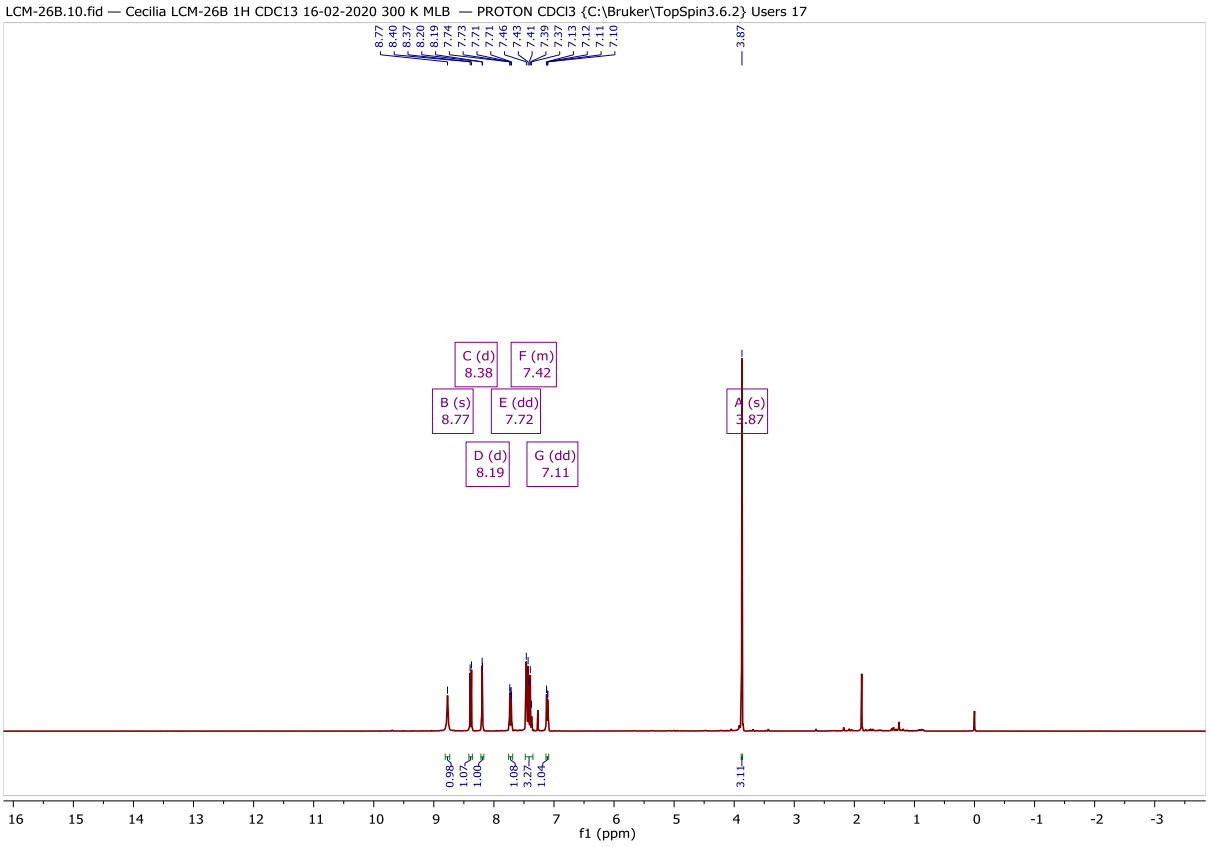

^{13}C NMR spectrum

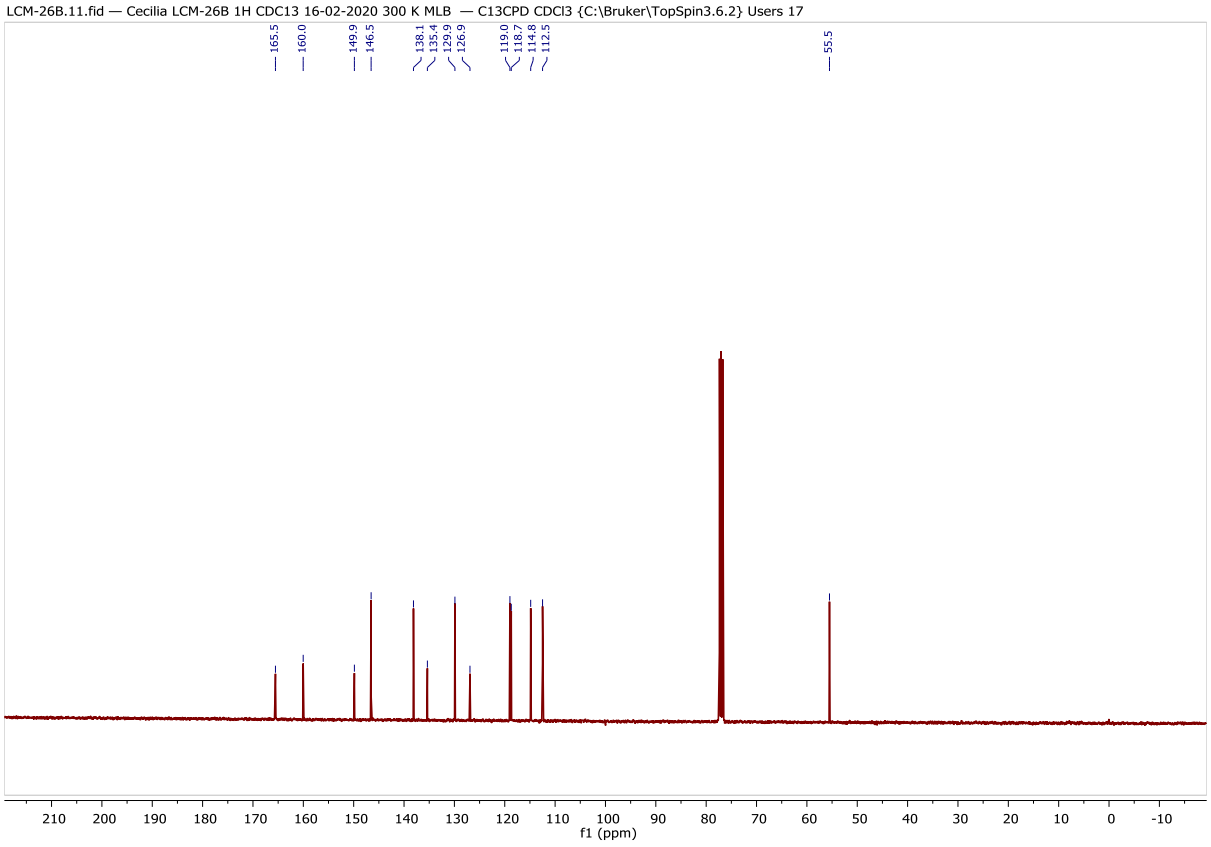

Compound 160i

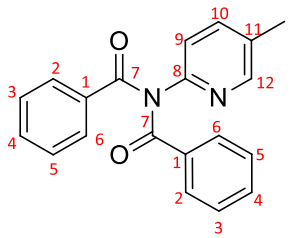

^{1}H NMR spectrum

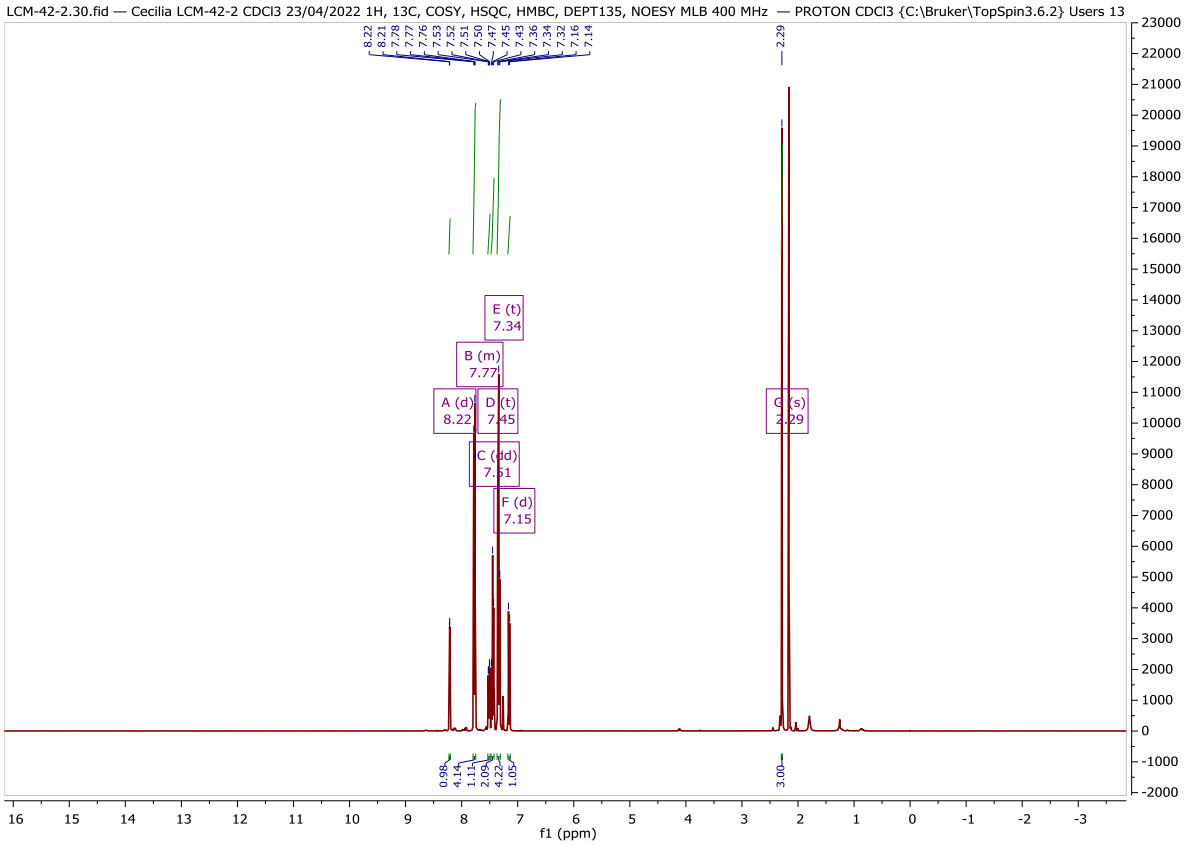

^{13}C NMR spectrum

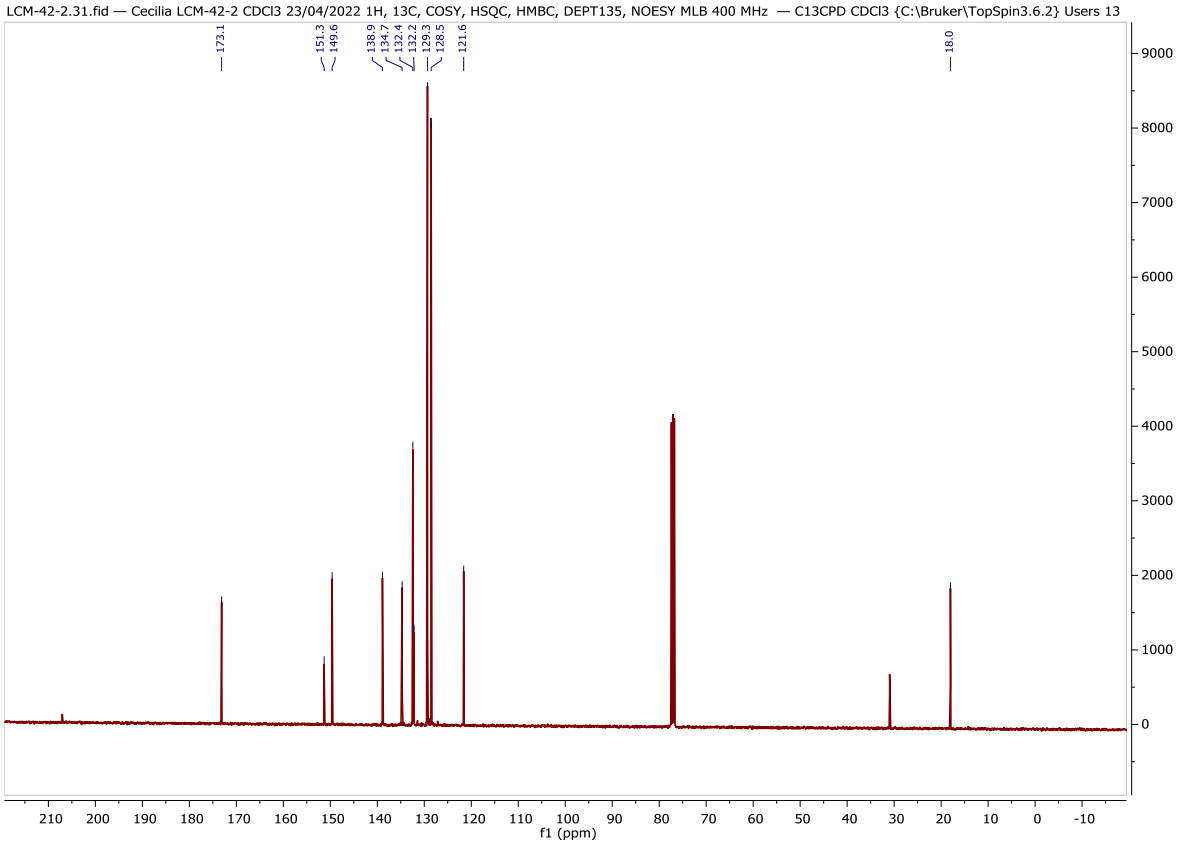

Compound 160n

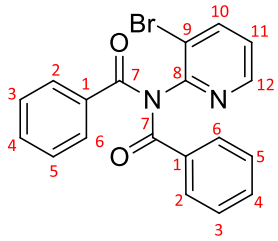

^{1}H NMR spectrum

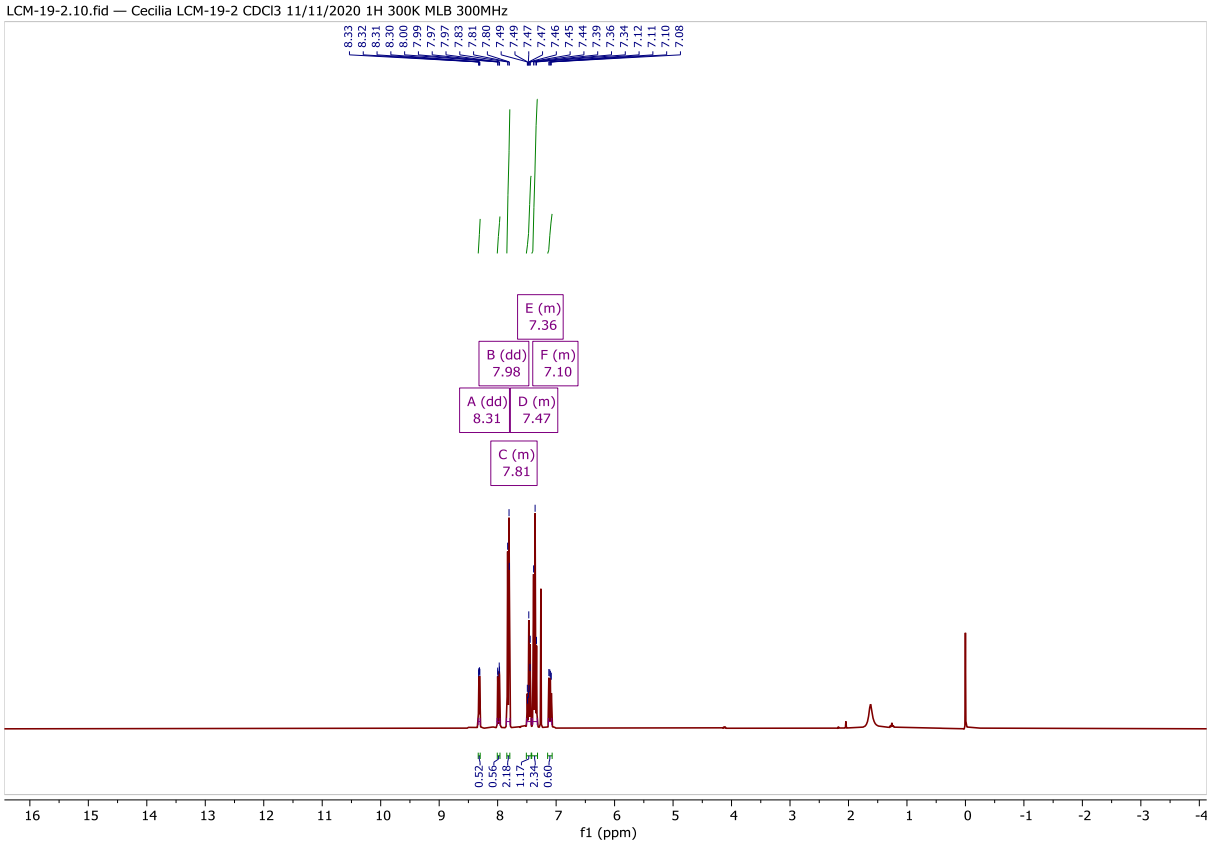

^{13}C NMR spectrum

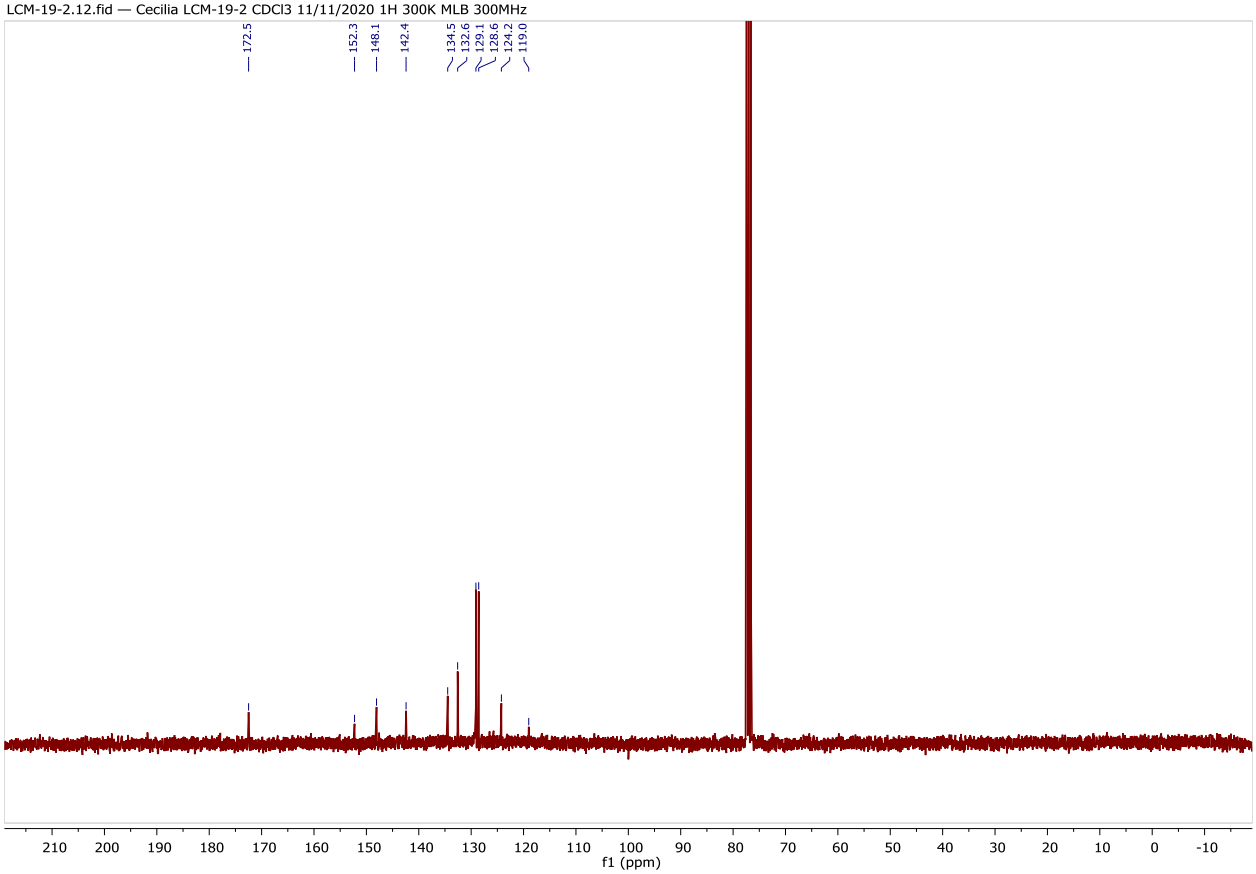

Compound 165i

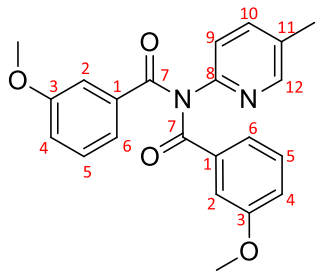

^{1}H NMR spectrum

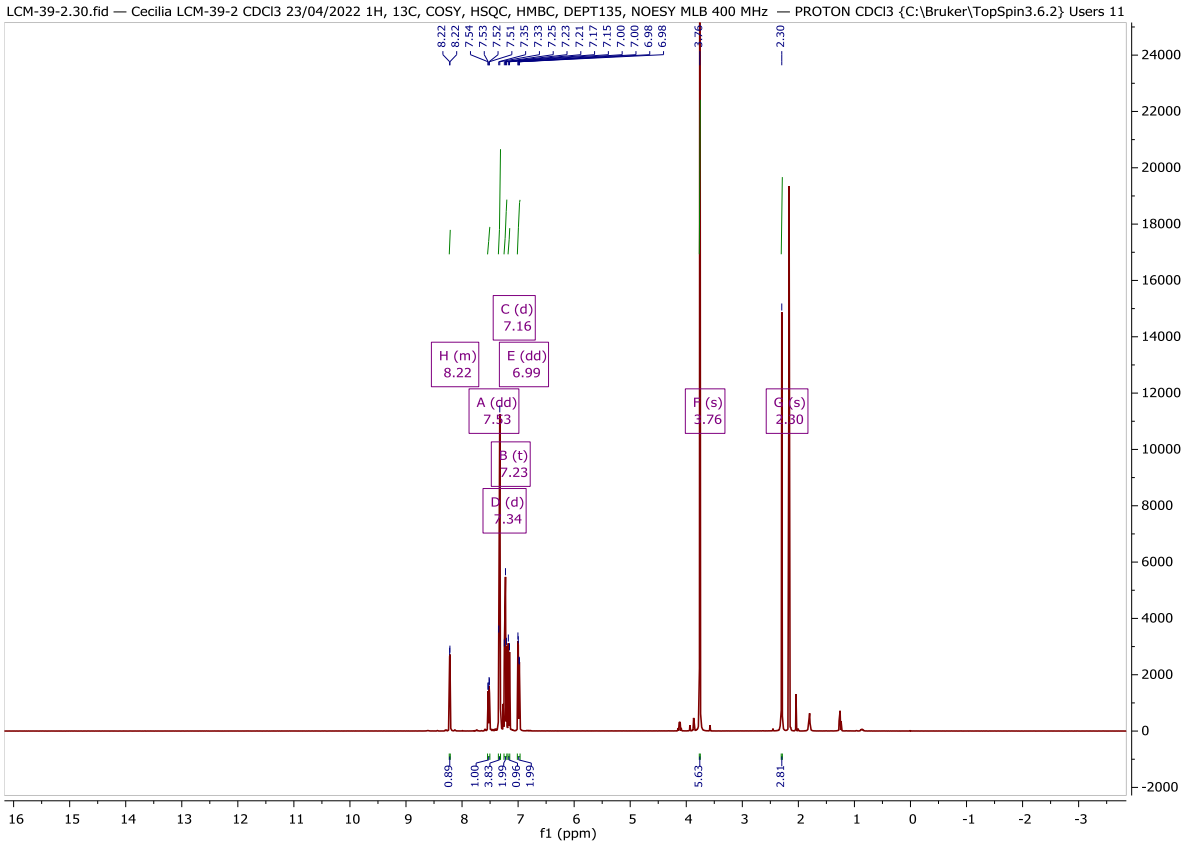

^{13}C NMR spectrum

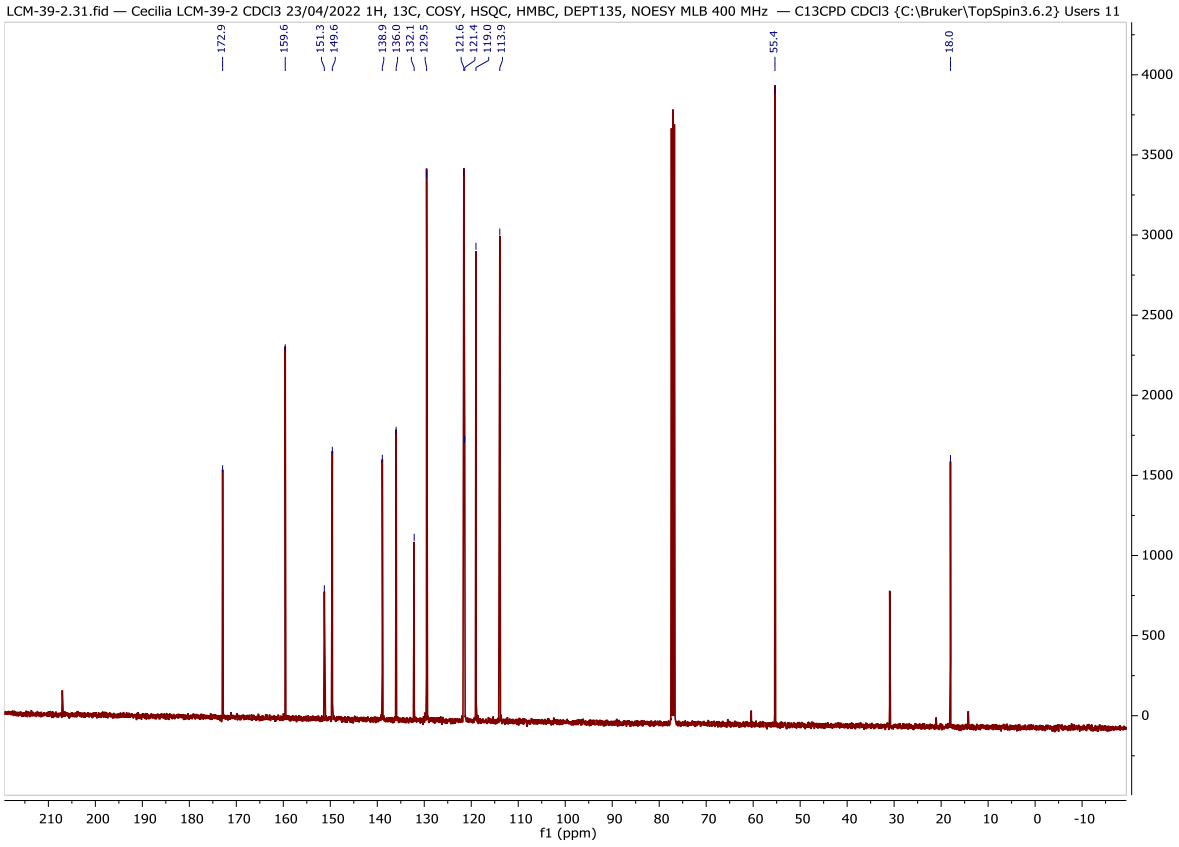

Compound 166j

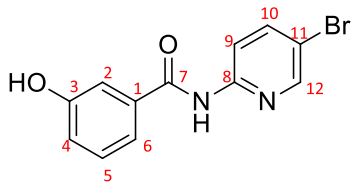

^{1}H NMR spectrum

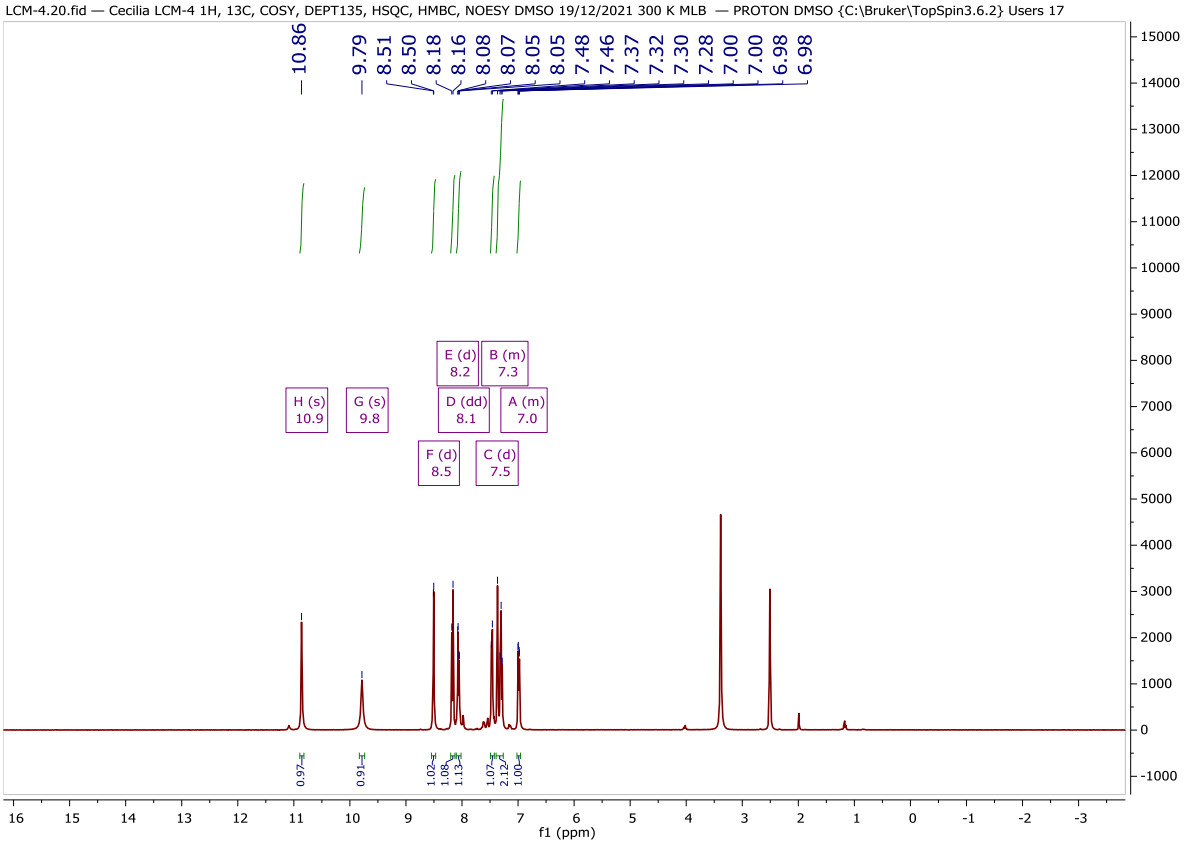

^{13}C NMR spectrum

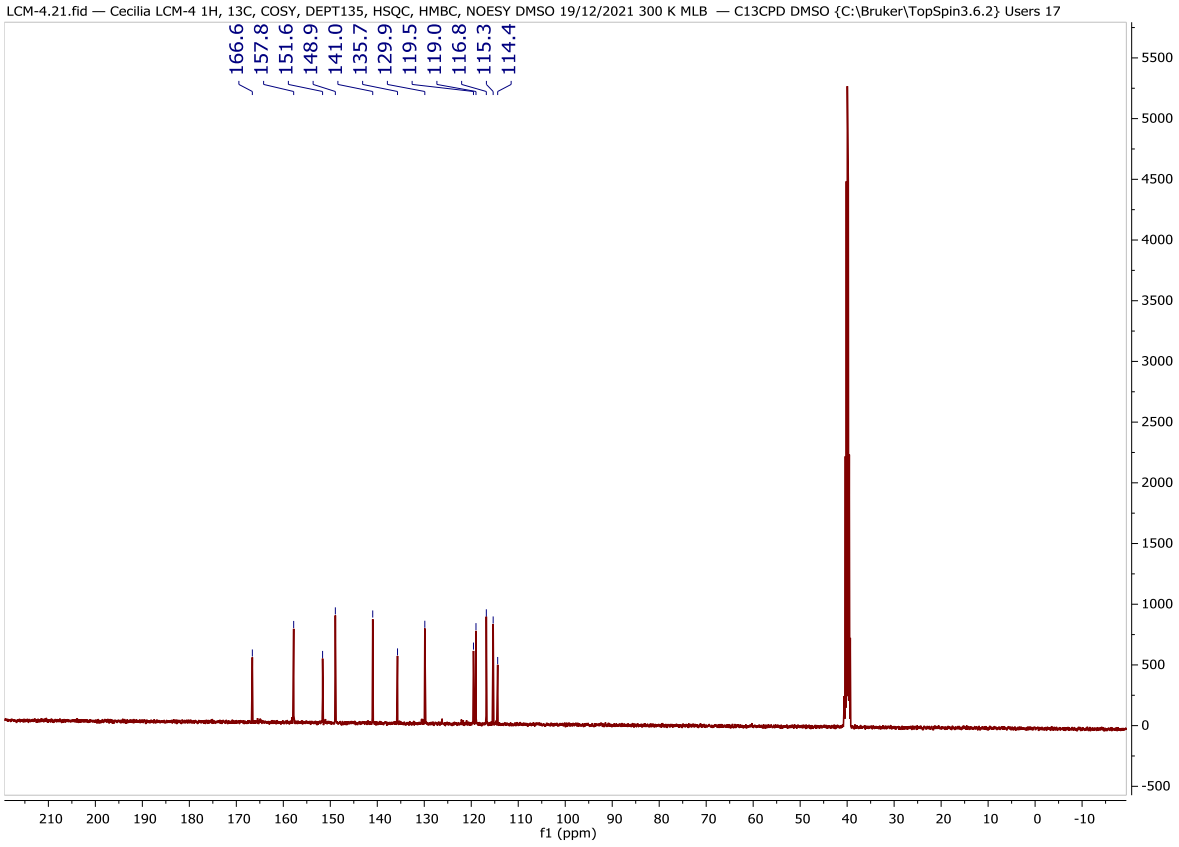

Compound 166l

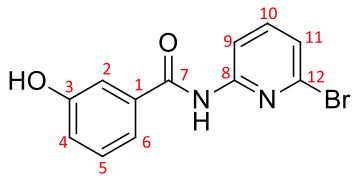

^{1}H NMR spectrum

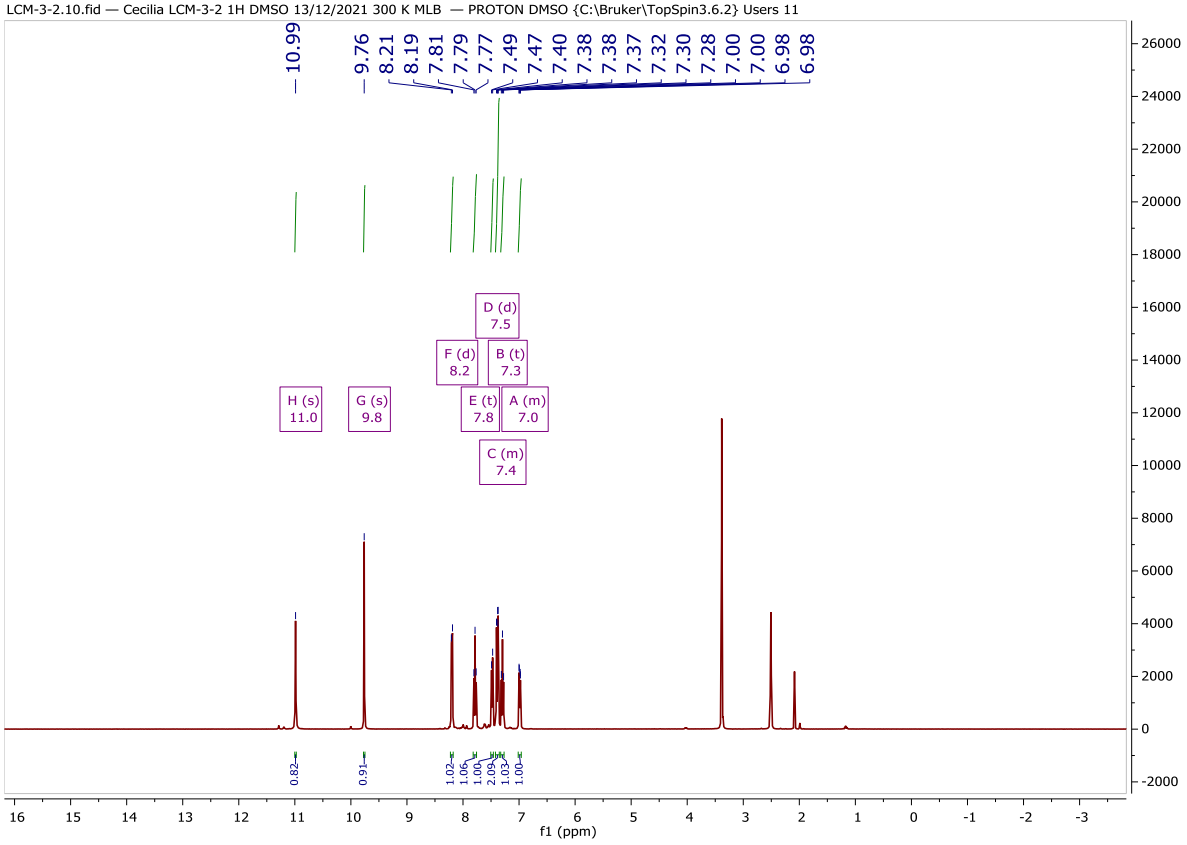

^{13}C NMR spectrum

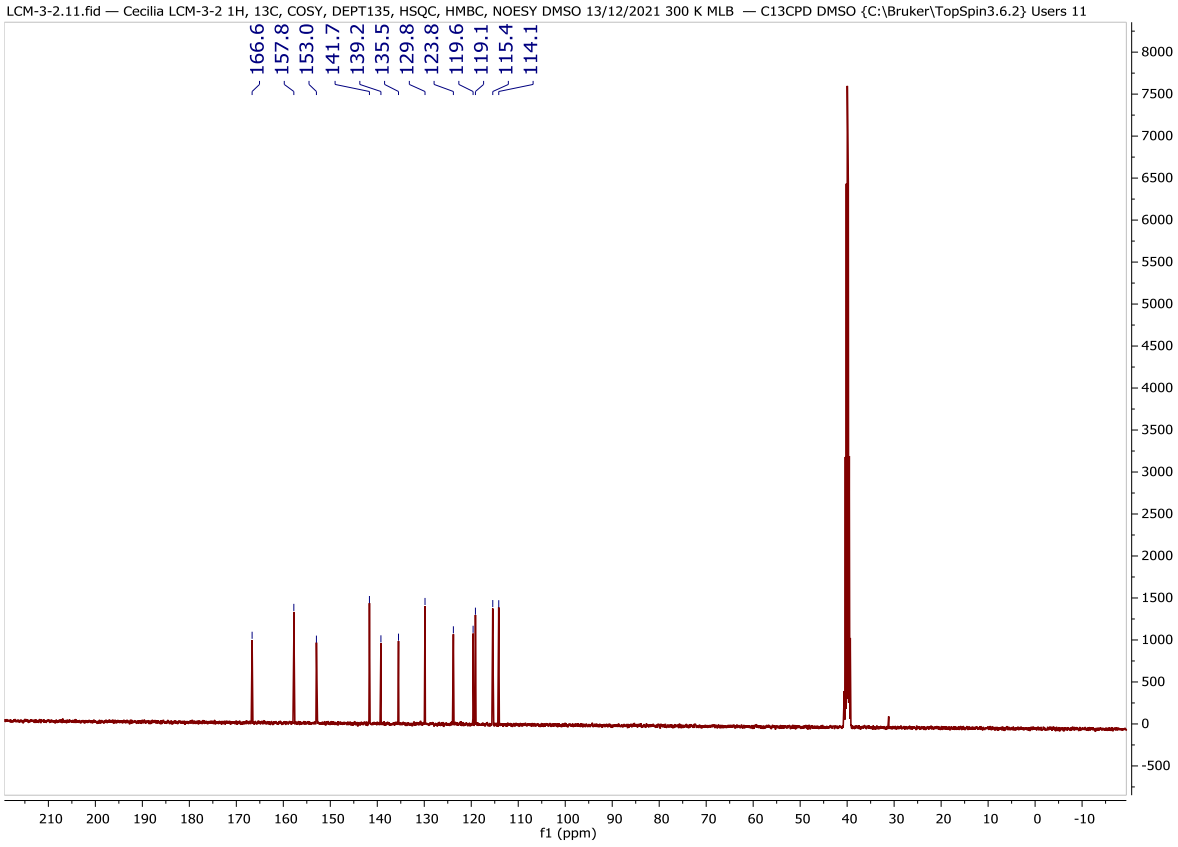

Compound 166m

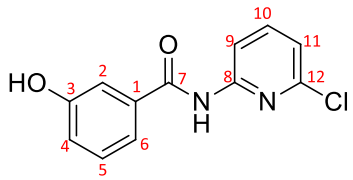

^{1}H NMR spectrum

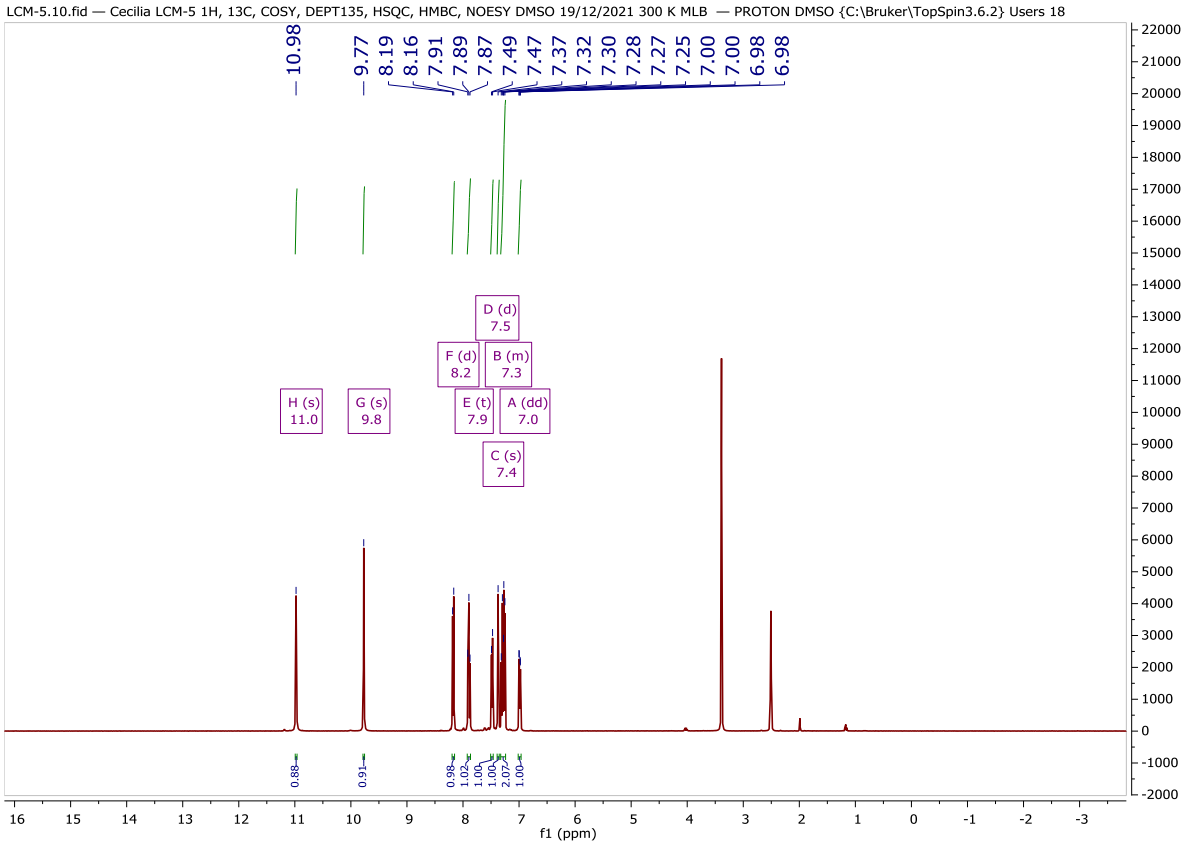

^{13}C NMR spectrum

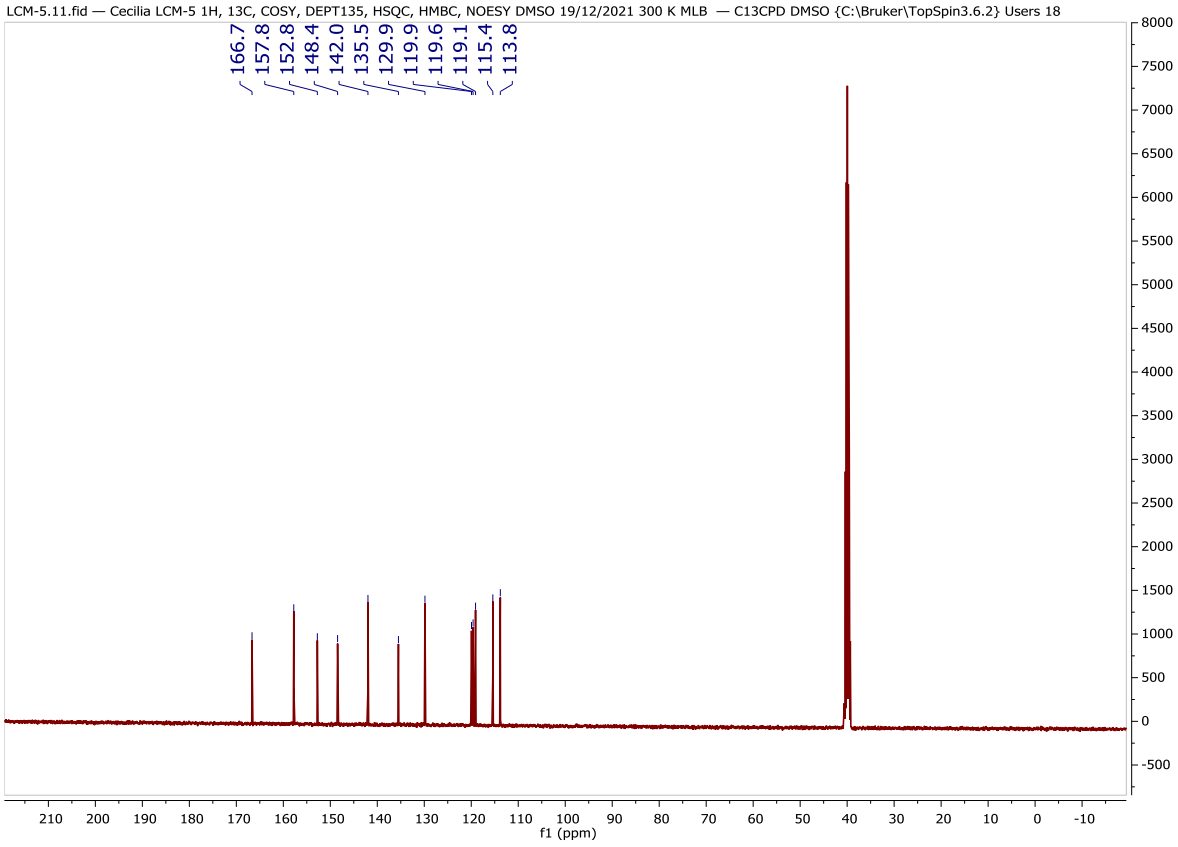

Compound 168d

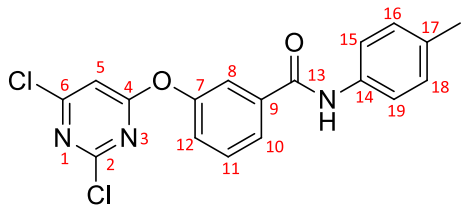

^{1}H NMR spectrum

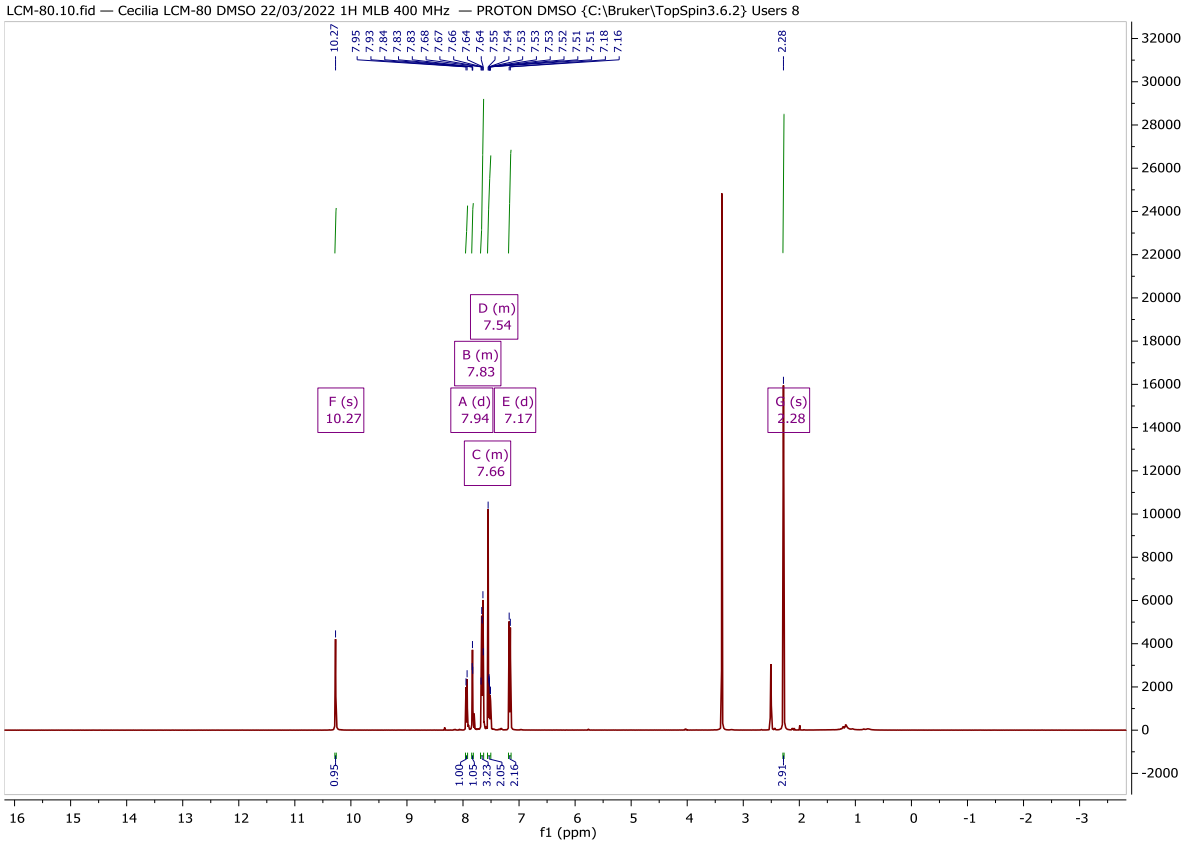

^{13}C NMR spectrum

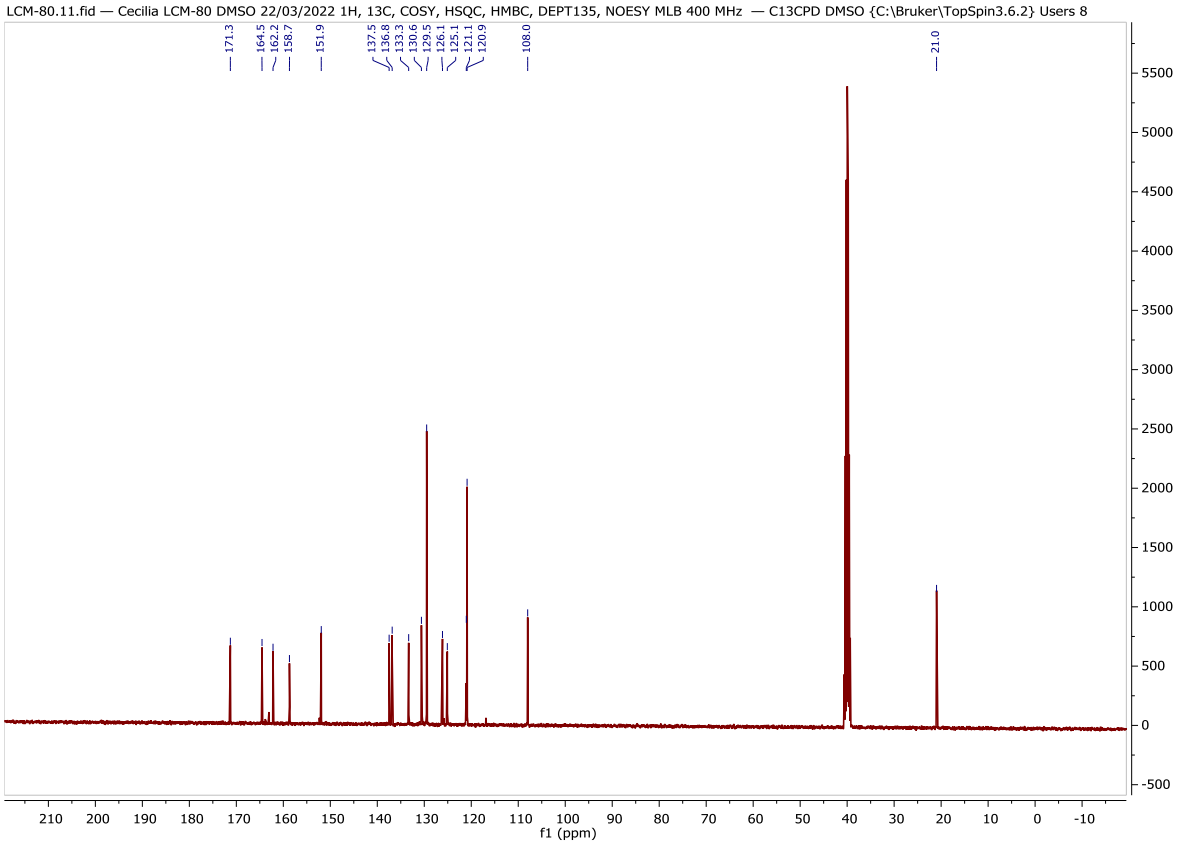

Compound 168e

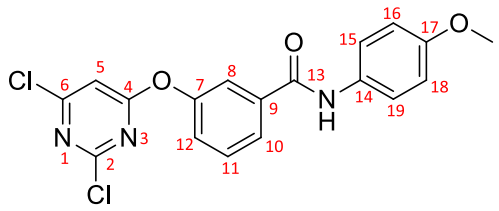

^{1}H NMR spectrum

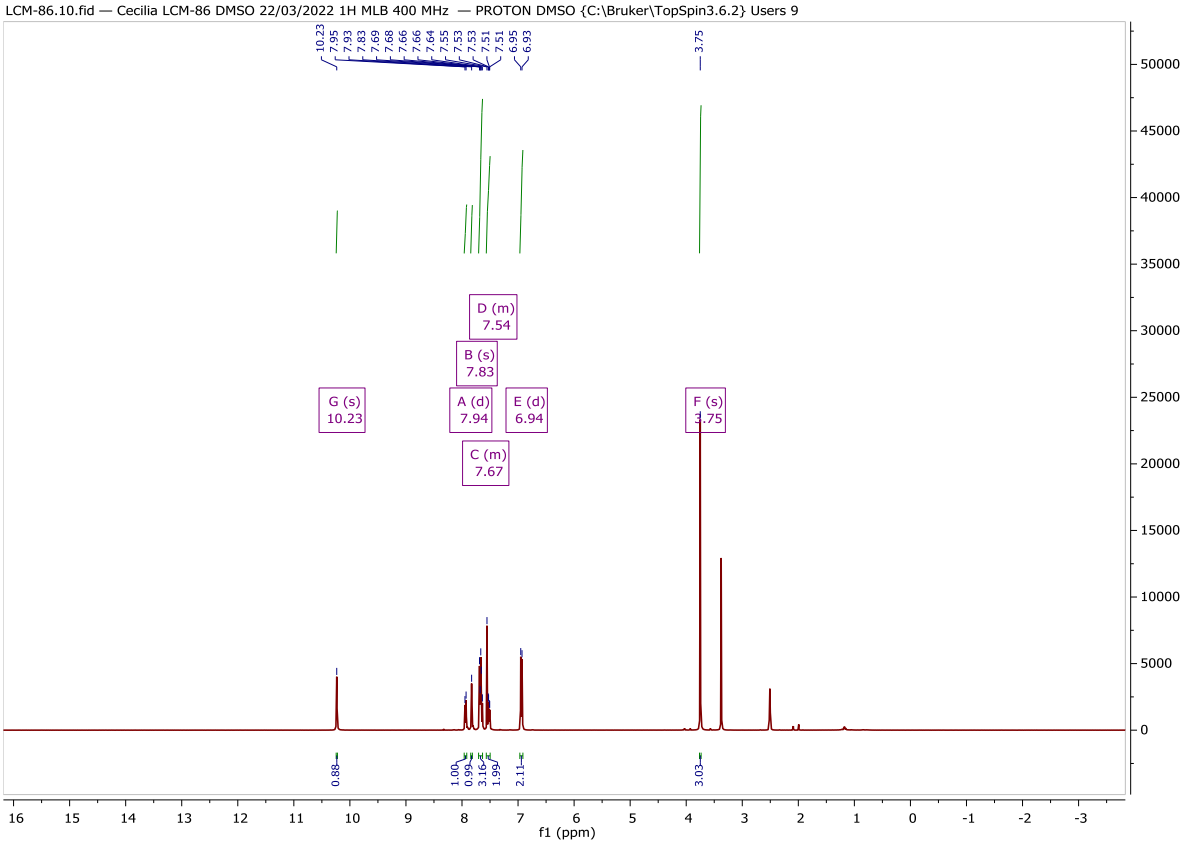

^{13}C NMR spectrum

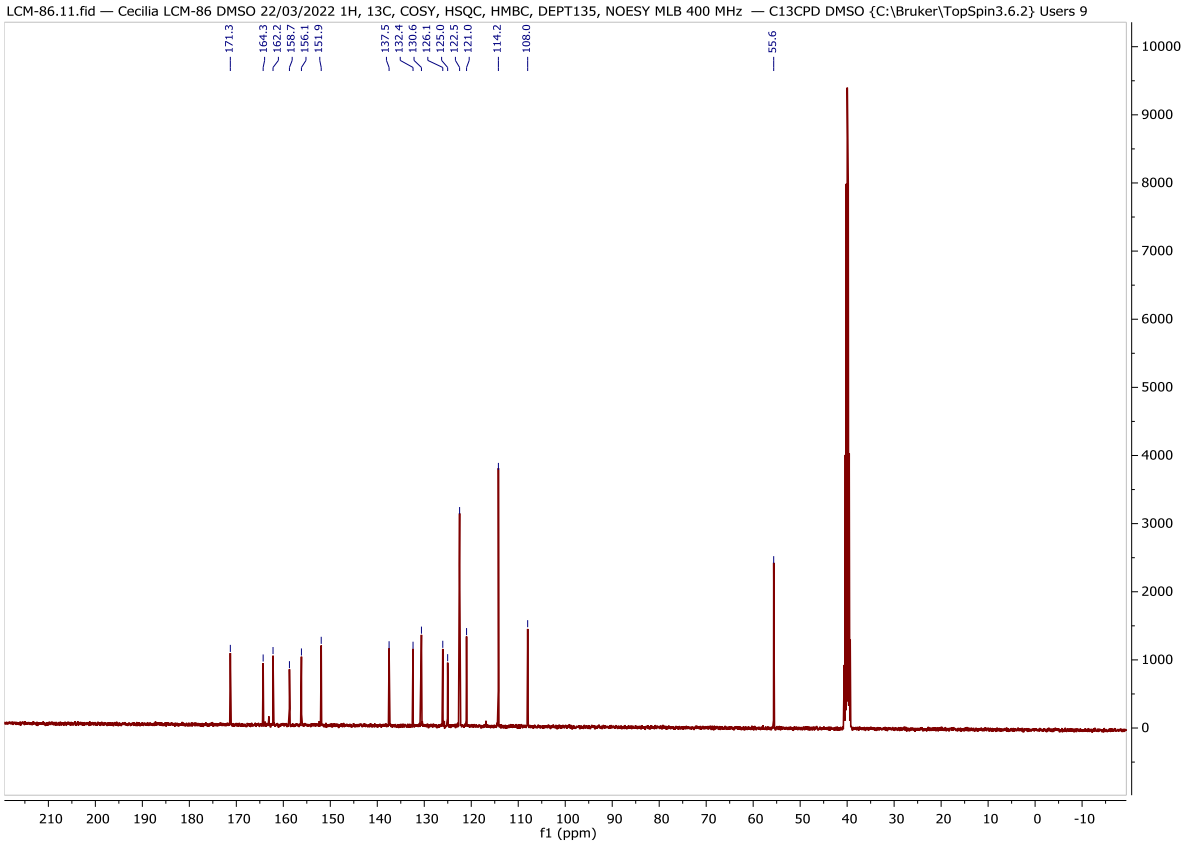

Compound 168j

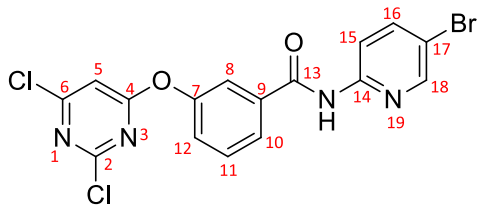

^{1}H NMR spectrum

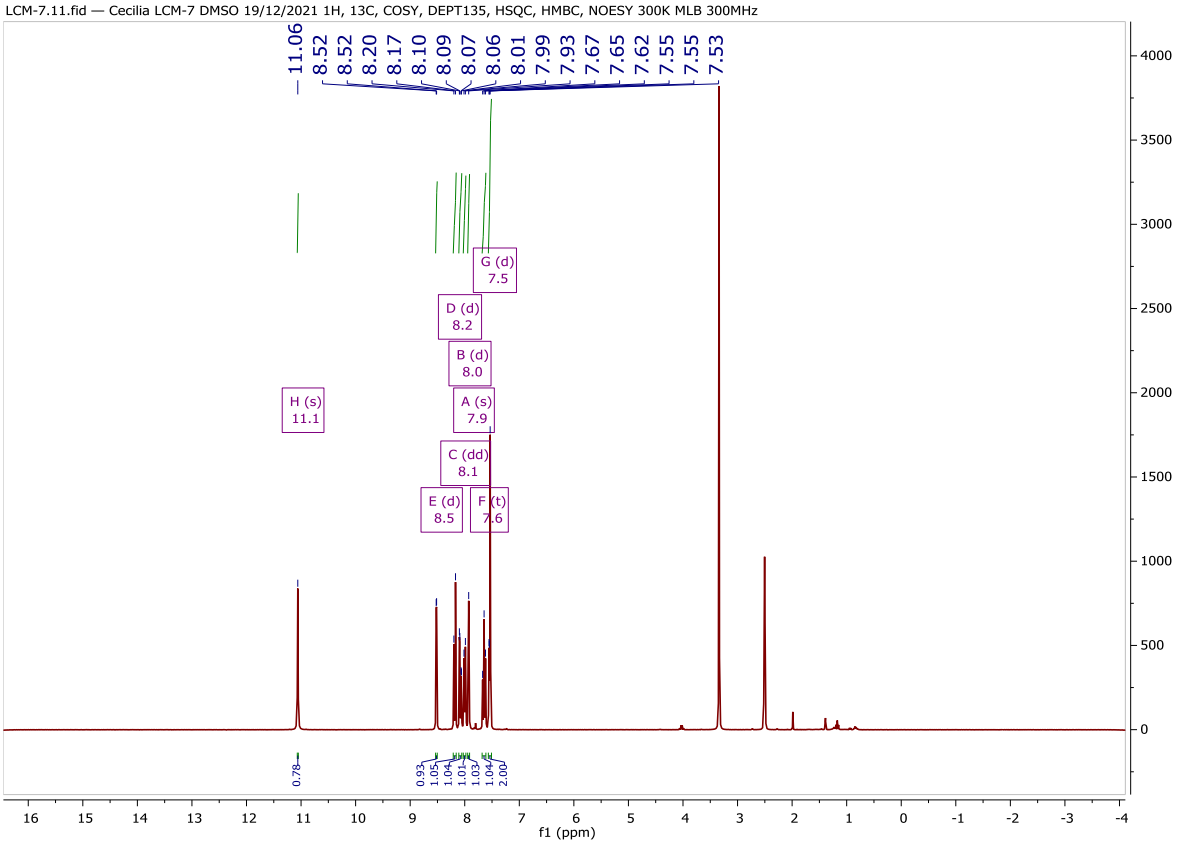

^{13}C NMR spectrum

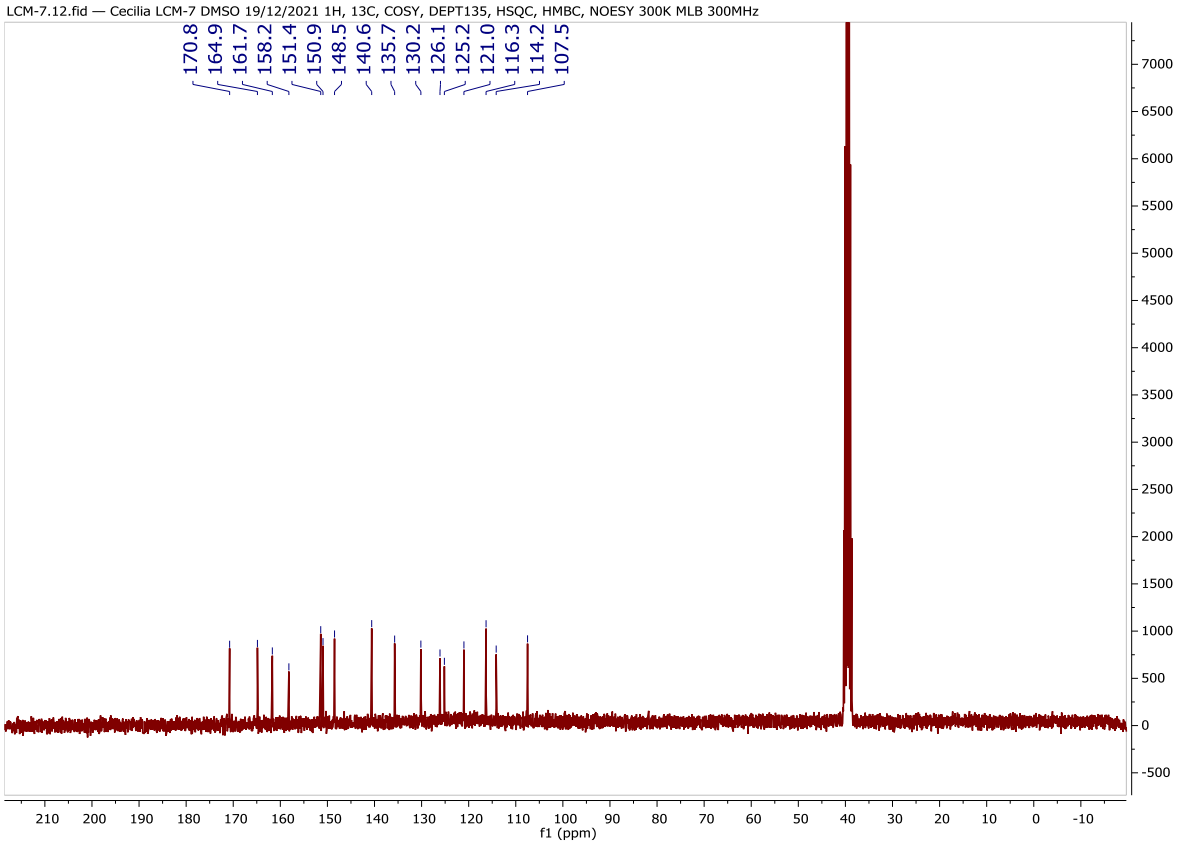

Compound 168k

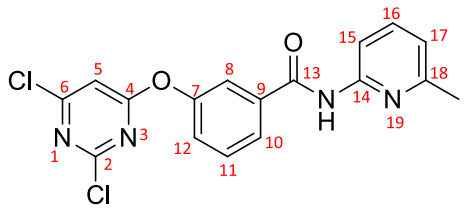

^{1}H NMR spectrum

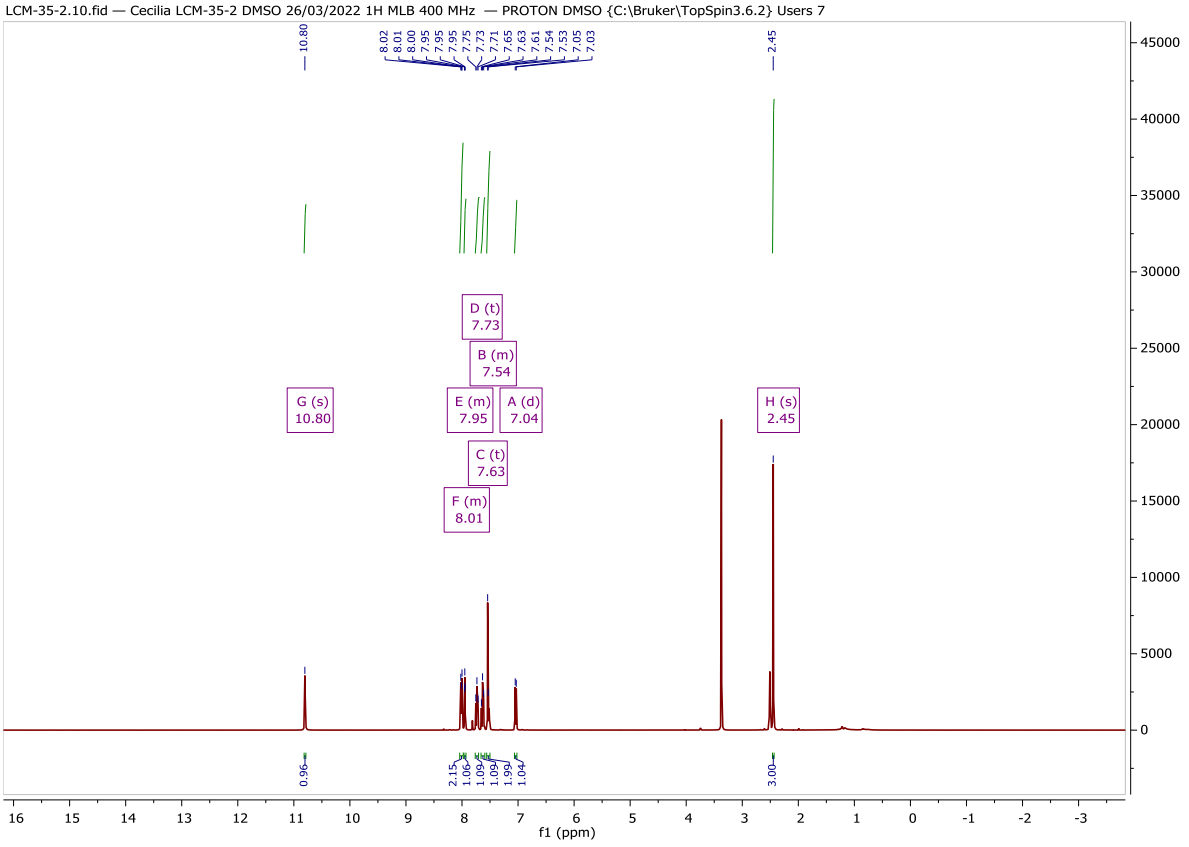

^{13}C NMR spectrum

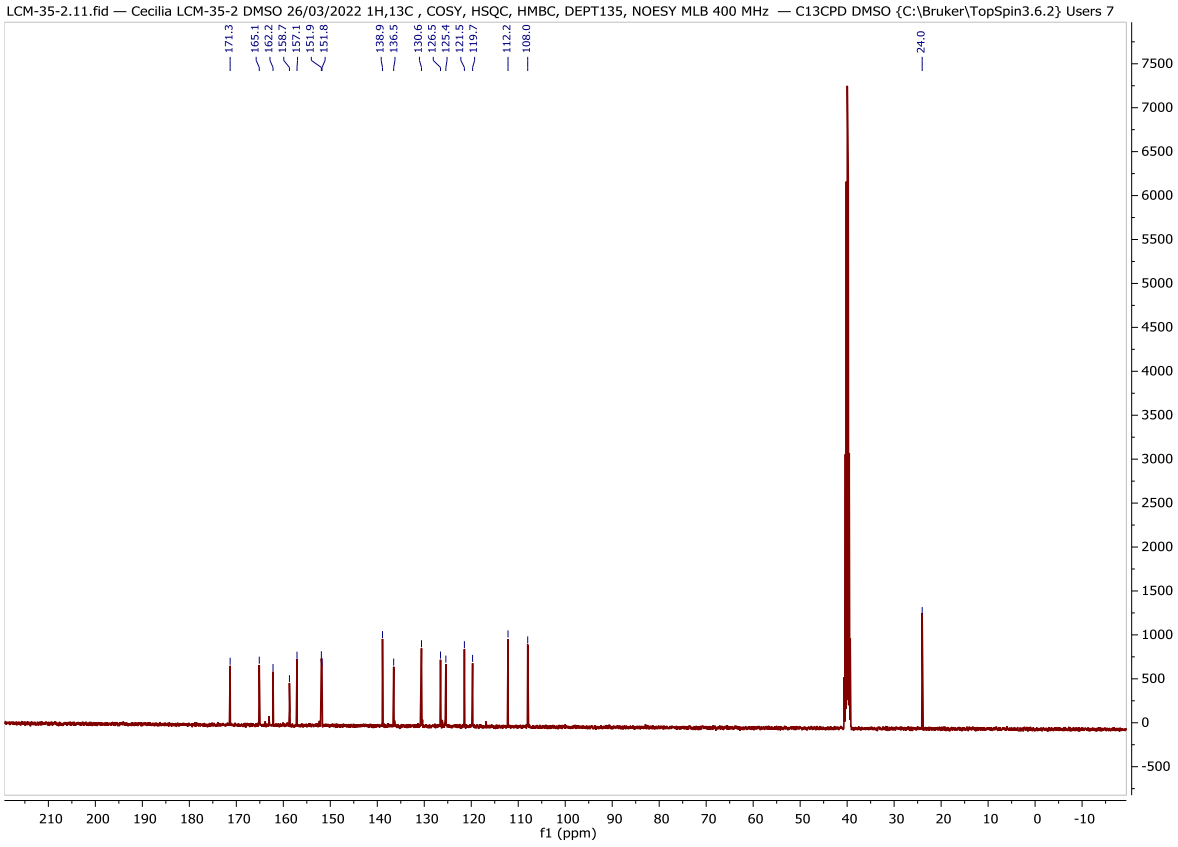

Compound 168l

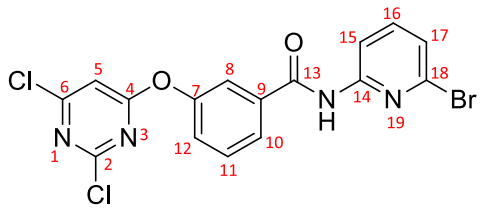

^{1}H NMR spectrum

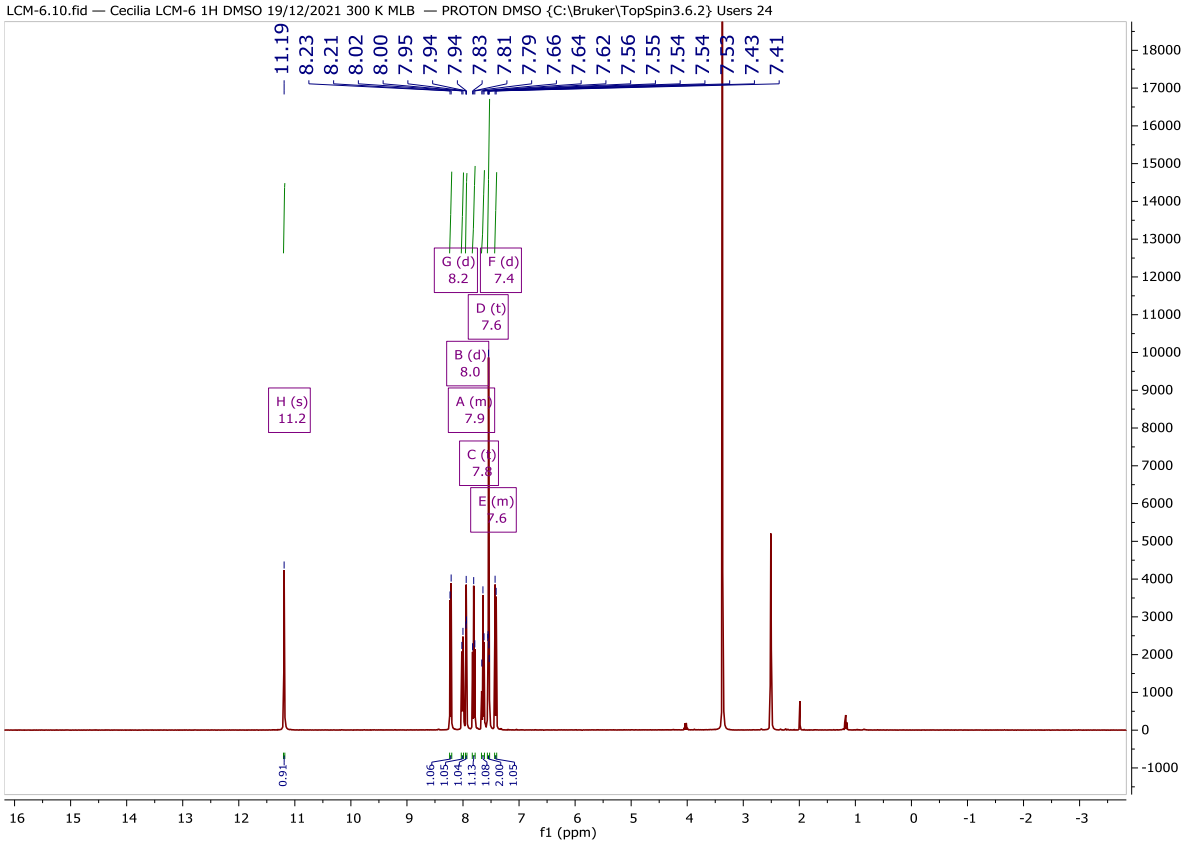

^{13}C NMR spectrum

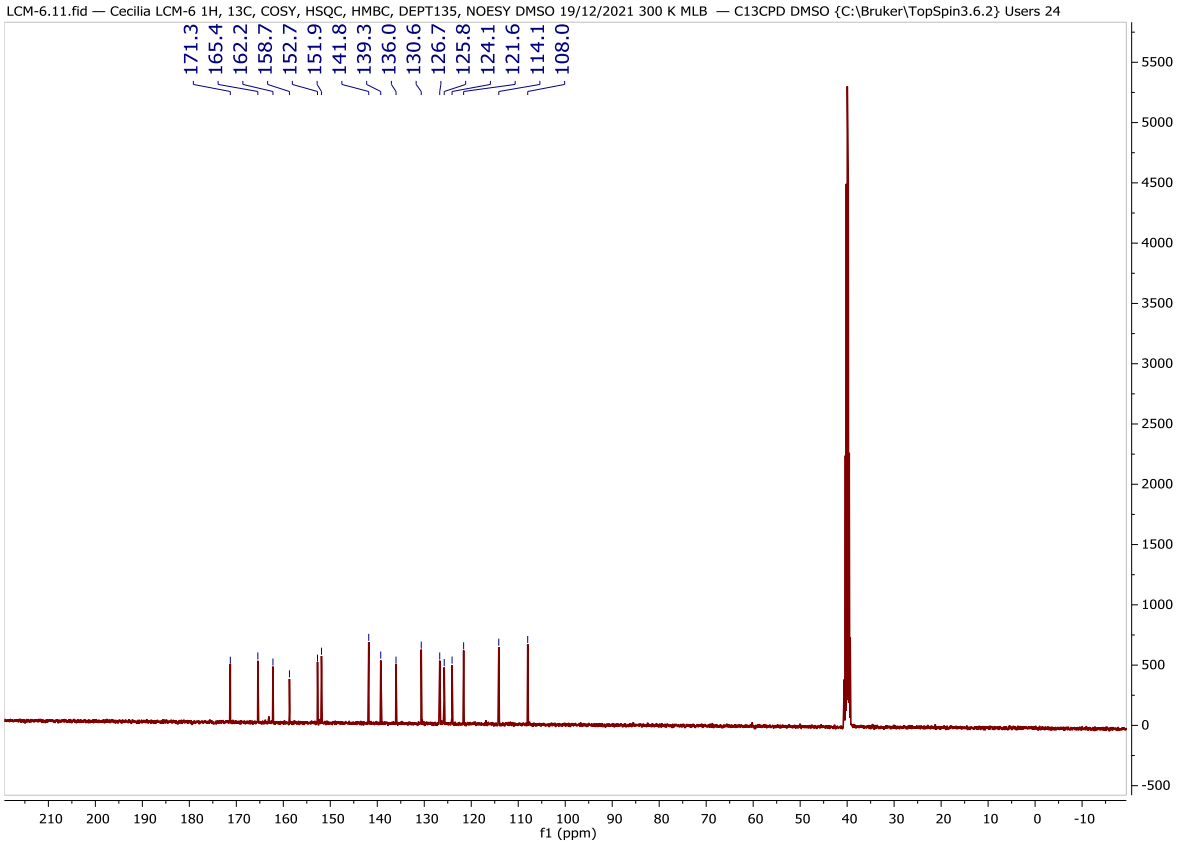

Compound 168m

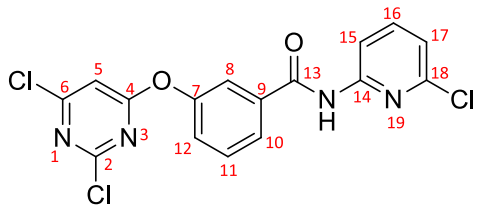

^{1}H NMR spectrum

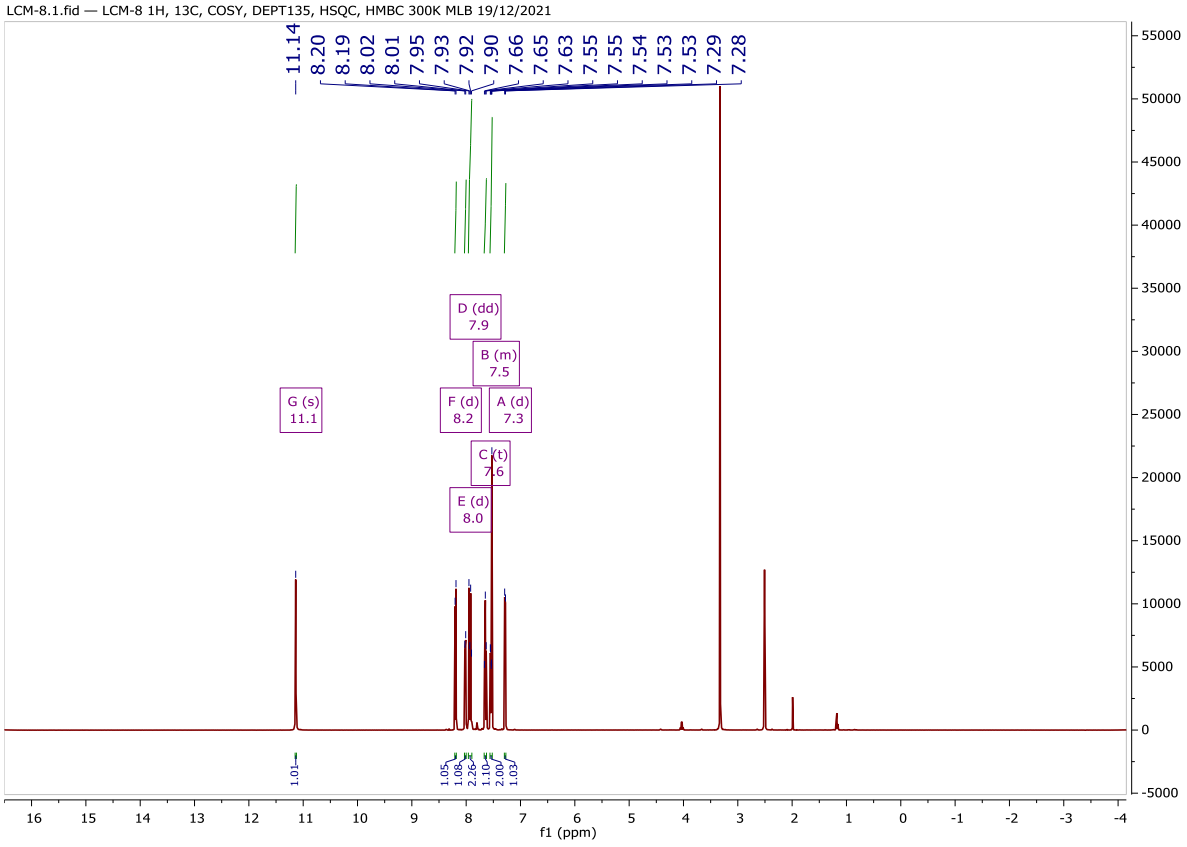

^{13}C NMR spectrum

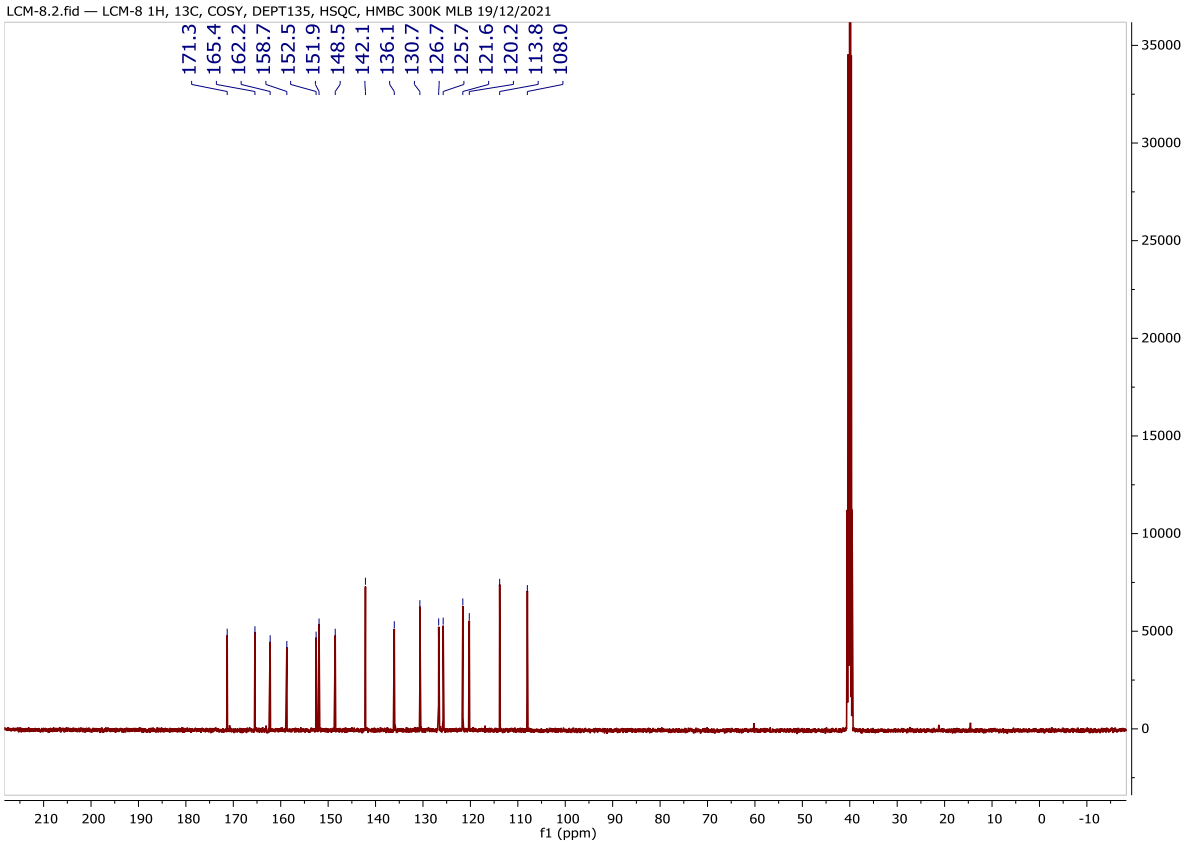

Compound 168o

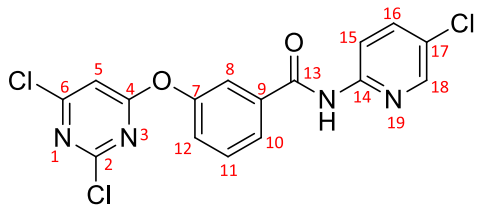

^{1}H NMR spectrum

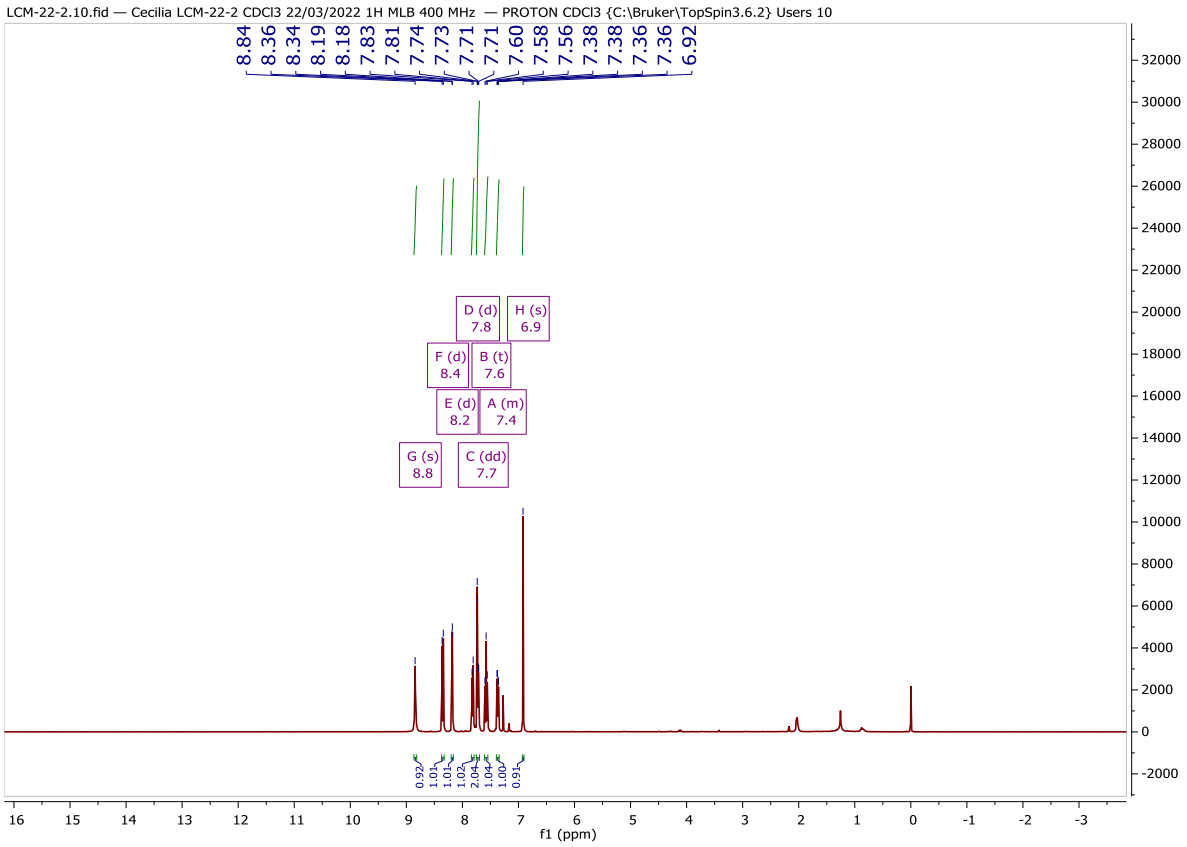

^{13}C NMR spectrum

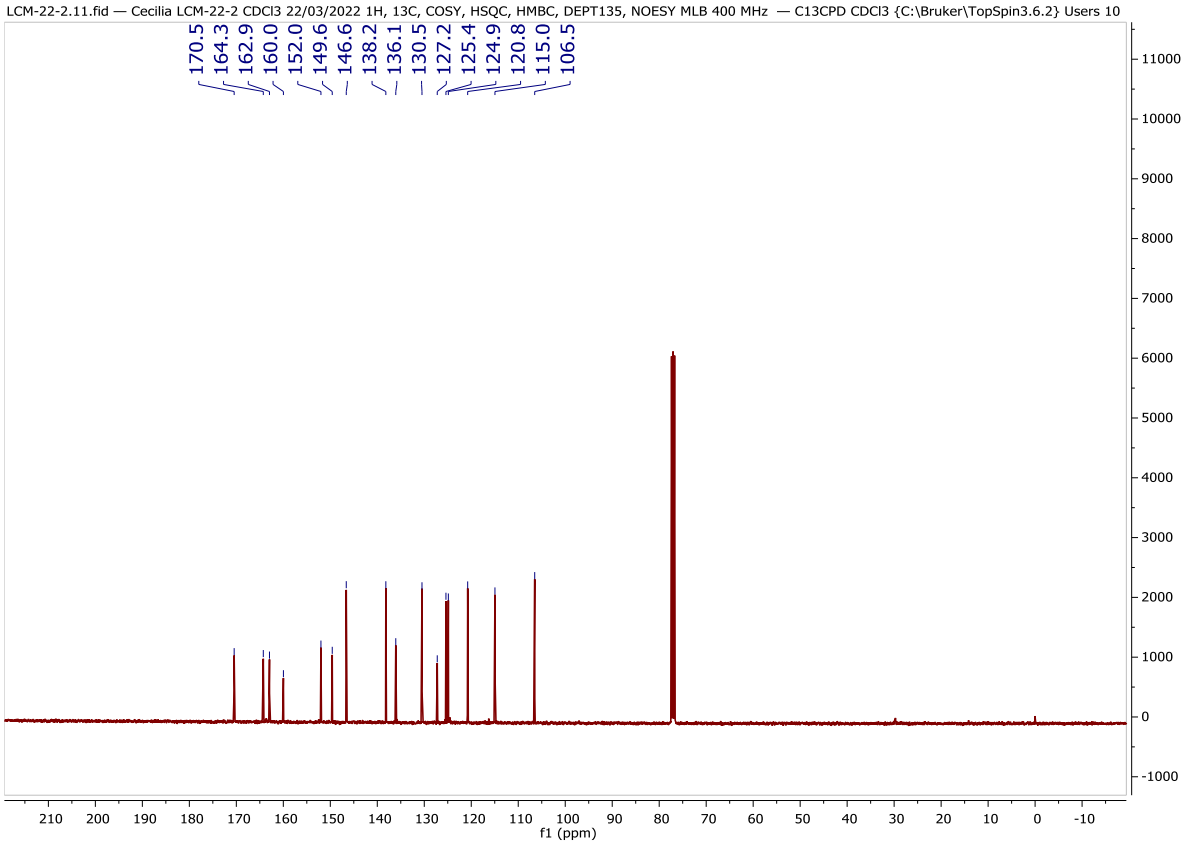

Compound 180a

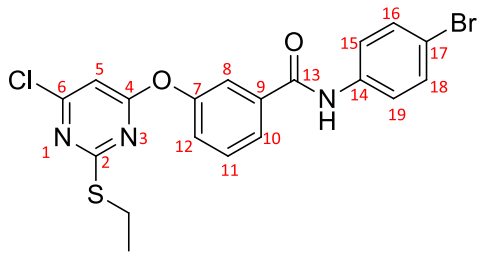

^{1}H NMR spectrum

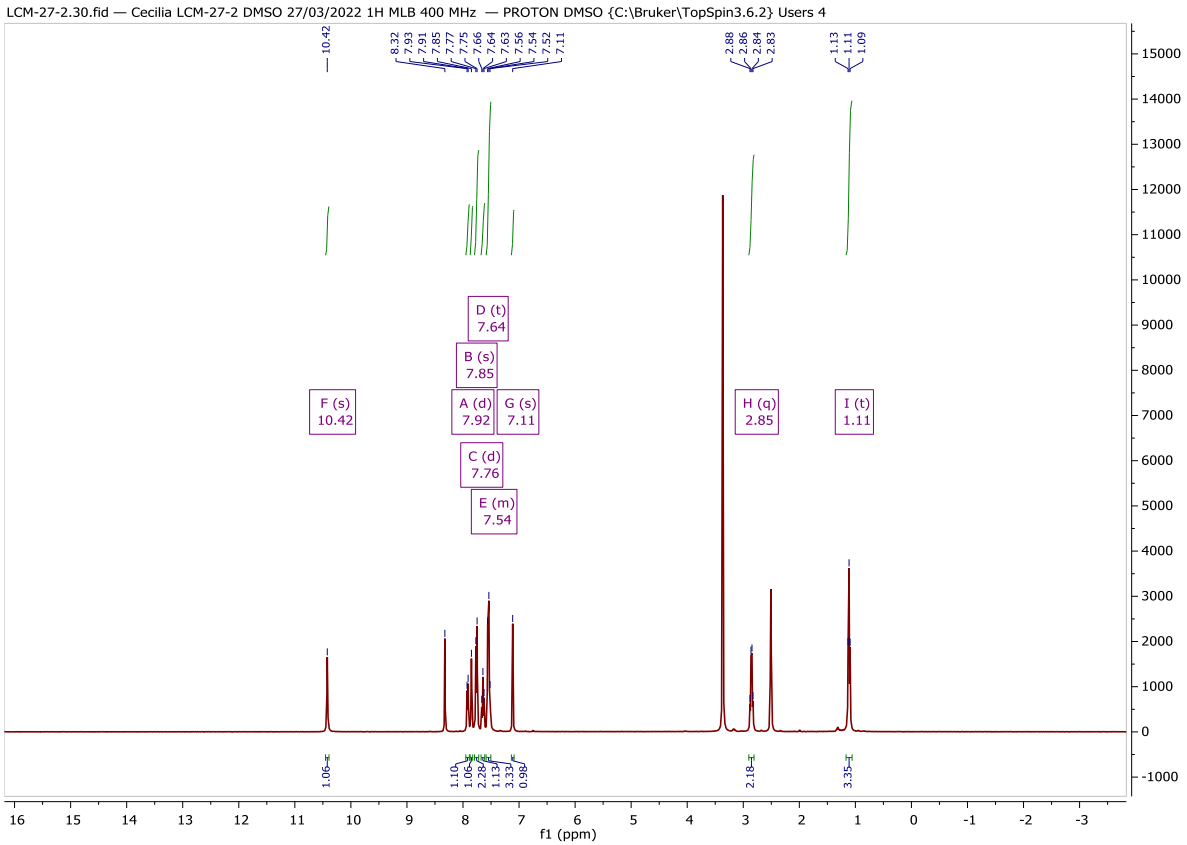

^{13}C NMR spectrum

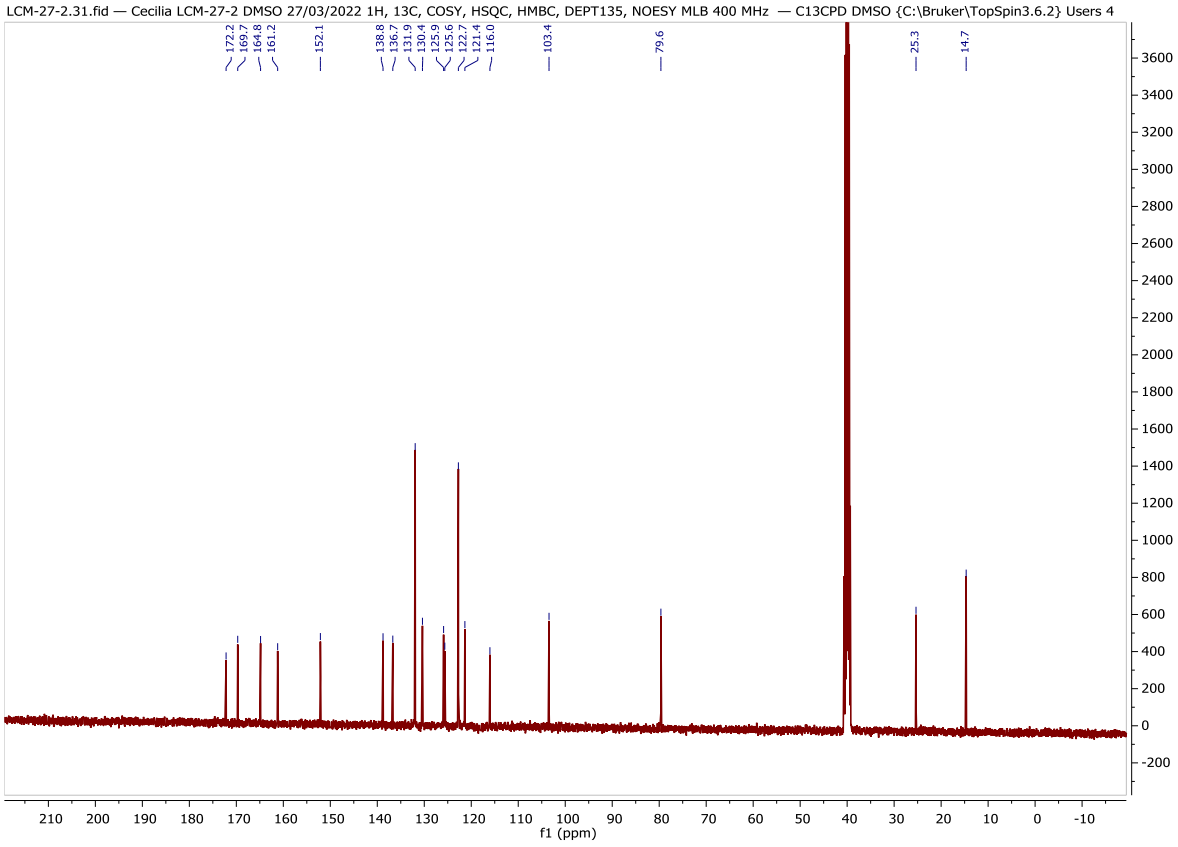

Compound 180d

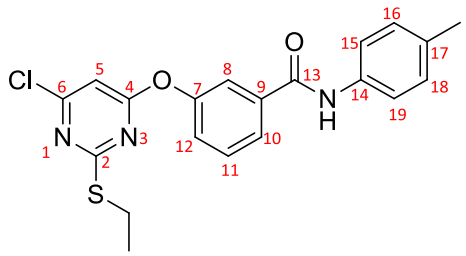

^{1}H NMR spectrum

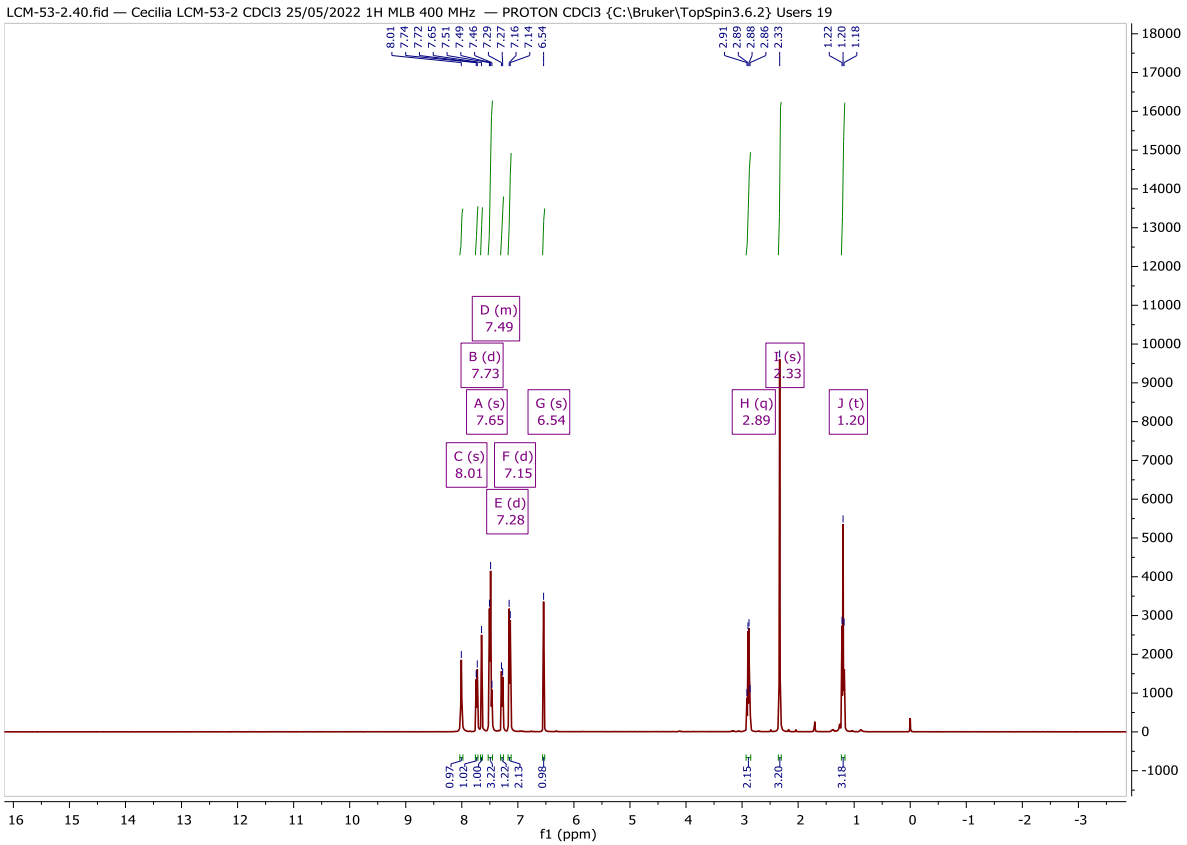

^{13}C NMR spectrum

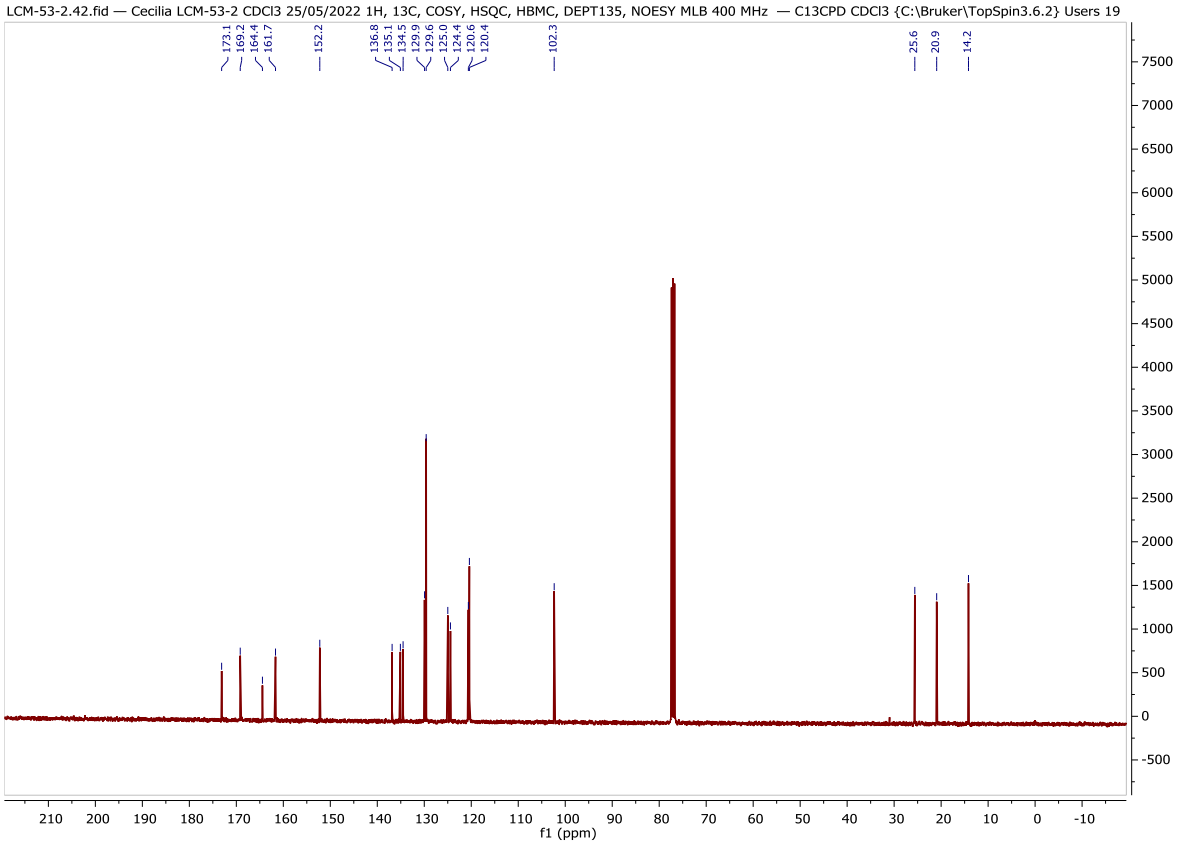

Compound 187d

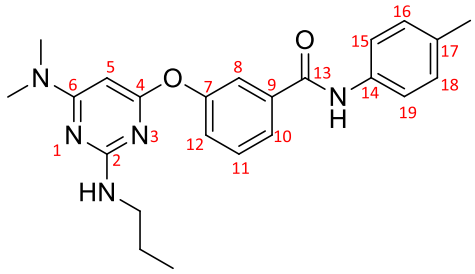

^{1}H NMR spectrum

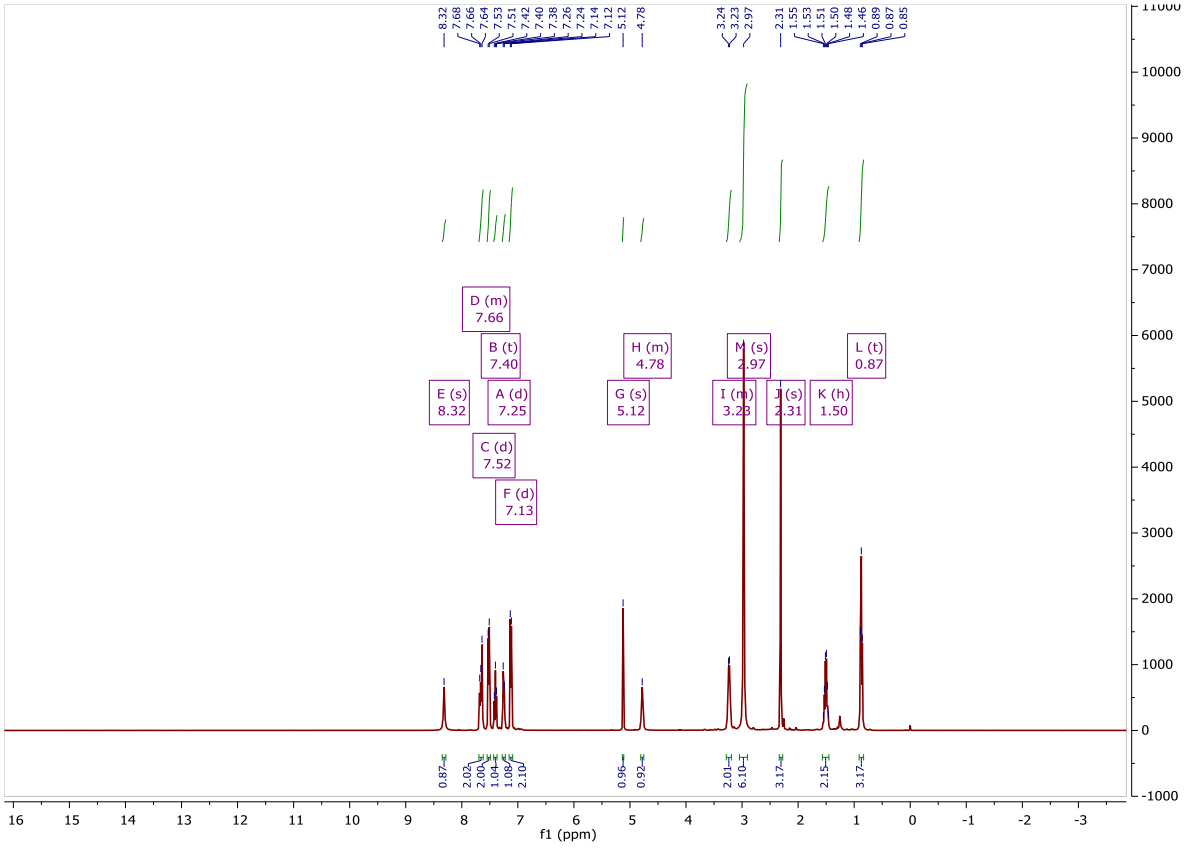

^{13}C NMR spectrum